Abstract and Applied Analysis

Analytical and Numerical Methods for Solving Partial Differential Equations and Integral Equations Arising in Physical Models

Guest Editors: Santanu Saha Ray, Om P. Agrawal, R. K. Bera, Shantanu Das, and T. Raja Sekhar

Analytical and Numerical Methods for Solving Partial Differential Equations and Integral Equations Arising in Physical Models

Abstract and Applied Analysis

Analytical and Numerical Methods for Solving Partial Differential Equations and Integral Equations Arising in Physical Models

Guest Editors: Santanu Saha Ray, Om P. Agrawal, R. K. Bera, Shantanu Das, and T. Raja Sekhar

Editorial Board

Contents

Hindawi Publishing Corporation
Abstract and Applied Analysis
Volume 2014, Article ID 635235, 3 pages
http://dx.doi.org/10.1155/2014/635235

Editorial

Analytical and Numerical Methods for Solving Partial Differential Equations and Integral Equations Arising in Physical Models

Santanu Saha Ray,[1] Om P. Agrawal,[2] R. K. Bera,[3] Shantanu Das,[4] and T. Raja Sekhar[5]

[1] *Department of Mathematics, National Institute of Technology, Rourkela 769008, India*
[2] *Department of Mechanical Engineering and Energy Processes, Southern Illinois University, Carbondale, IL 62901, USA*
[3] *Department of Science, National Institute of Technical Teachers' Training and Research, Kolkata 700106, India*
[4] *Bhabha Atomic Research Centre, Trombay, Mumbai 400085, India*
[5] *Department of Mathematics, Indian Institute of Technology, Kharagpur 721302, India*

Correspondence should be addressed to Santanu Saha Ray; santanusaharay@yahoo.com

Received 15 December 2013; Accepted 15 December 2013; Published 9 January 2014

Mathematical modelling of real-life problems usually results in functional equations, like ordinary or partial differential equations, integral and integrodifferential equations, and stochastic equations. Many mathematical formulations of physical phenomena contain integrodifferential equations; these equations arise in many fields like fluid dynamics, biological models, and chemical kinetics. Partial differential equations (PDEs) have become a useful tool for describing the natural phenomena of science and engineering models. In addition, most physical phenomena of fluid dynamics, quantum mechanics, electricity, ecological systems, and many other models are controlled within their domain of validity by PDEs. Therefore, it becomes increasingly important to be familiar with all traditional and recently developed methods for solving PDEs and the implementations of these methods. Leaving aside quantum mechanics, which remains to date an inherently linear theory, most real-world physical systems, including gas dynamics, fluid mechanics, elasticity, relativity, ecology, neurology, and thermodynamics, are modelled by nonlinear partial differential equations.

The aim of this special issue is to bring together the leading researchers of dynamics, quantum mechanics, ecology, and neurology area including applied mathematicians and allow them to share their original research work. Analytical and numerical methods with advanced mathematical and real physical modelling, recent developments of PDEs, and integral equations in physical systems are included in the main focus of the issue.

Accordingly, various papers on partial differential equations and integral equations have been included in this special issue after completing a heedful, rigorous, and peer-review process. In particular, the nonlinear hydroelastic waves propagating beneath an infinite ice sheet floating on an inviscid fluid of finite depth are investigated analytically in one of the papers. In this paper, the approximate series solutions for the velocity potential and the wave surface elevation are derived, respectively, by an analytic approximation technique named homotopy analysis method (HAM) and are presented for the second-order components.

In another paper, a domain decomposition method is proposed for the coupled stationary Navier-Stokes and Darcy equations with the Beavers-Joseph-Saffman interface condition in order to improve the efficiency of the finite element method. The physical interface conditions are directly utilized to construct the boundary conditions on the interface and then decouple the Navier-Stokes and Darcy equations. Newton iteration is used to deal with the nonlinear systems.

Another paper proposes a pressure-stabilized Lagrange-Galerkin method in a parallel domain decomposition system in which the new stabilization strategy is proved to be effective for large Reynolds number and Rayleigh number simulations. The symmetry of the stiffness matrix enables the interface problems of the linear system to be solved by the preconditioned conjugate method, and an incomplete balanced domain preconditioner is applied to the flow-thermal coupled problems.

One of the papers is of use of Sumudu transform on fractional derivatives for solving some interesting nonhomogeneous fractional ordinary differential equations. Then spectral and spectral element methods have been discussed with Legendre-Gauss-Lobatto nodal basis for general 2nd-order elliptic eigenvalue problems. A priori and a posteriori error estimates for spectral and spectral element methods have been proposed. In the another paper, a generalized double sinh-Gordon equation has many more applications in various fields such as fluid dynamics, integrable quantum field theory, and kink dynamics has been solved by Exp-function method to obtain new exact solutions for this generalized double sinh-Gordon equation. A semianalytical method called the optimal homotopy asymptotic method has been also applied for solving the linear Fredholm integral equations of the first kind in another paper. In one of the papers, two strategies for inverting the open boundary conditions with adjoint method are compared by carrying out semi-idealized numerical experiments. In the first strategy, the open boundary curves are assumed to be partly space varying and are generated by linearly interpolating the values at feature points and, in the second strategy, the open boundary conditions are assumed to be fully space varying and the values at every open boundary points are taken as control variables. Another paper contains the use of a relatively new analytical method like homotopy decomposition method to solve the 2D and 3D Poisson equations and biharmonic equations. The method does not require the linearization or assumptions of weak nonlinearity, the solutions are generated in the form of general solution, and it is more realistic compared to the method of simplifying the physical problems.

One of the papers has shown that a strong solution of the Degasperis-Procesi equation possesses persistence property in the sense that the solution with algebraically decaying initial data and its spatial derivative must retain this property. In another paper, the fractional complex transformation has been used to transform nonlinear partial differential equations to nonlinear ordinary differential equations. The improved (G'/G)-expansion method has suggested solving the space and time fractional foam drainage and KdV equations. Integral equation has been one of the essential tools for various areas of applied mathematics. For solving nonlinear Fredholm integrodifferential equations, the method based on hybrid functions approximate has been proposed in one of the papers. The properties of hybrid of block pulse functions and orthonormal Bernstein polynomials have been presented and utilized to reduce the problem to the solution of nonlinear algebraic equations. Another paper contains many numerical methods, namely, B-Spline wavelet method, Wavelet Galerkin method, and quadrature method, for solving Fredholm integral equations of second kind. A peer-review of different numerical methods for solving both linear and nonlinear Fredholm integral equations of second kind has been presented. This paper has more emphasized on the importance of interdisciplinary effort for advancing the study on numerical methods for solving integral equations. Also one of the papers has used a numerical method like function approximation to determine the numerical solution of system of linear Volterra integrodifferential equations using Bezier curves. Two-dimensional Volterra integral equations have also been solved using more recent semianalytic method like the reduced differential transform method and also compared with the differential transform method. One of the papers has presented a numerical method to achieve the approximate solutions in a generalized expansion form of two-dimensional fractional-order Legendre functions (2D-FLFs). The operational matrices of integration and derivative for 2D-FLFs have been derived.

Then a mixed finite element method has been introduced for an elliptic equation modelling of Darcy flow in porous media. In present mixed finite element, the approximate velocity is continuous and the conservation law holds locally. In order to assess the rotational potential vorticity-conserved equation with topography effect and dissipation effect, the multiple-scale method has been studied to describe the Rossby solitary waves in deep rotational fluids. A one step optimal homotopy analysis method has been applied numerically to harmonic wave propagation in a nonlinear thermoelasticity under influence of rotation, thermal relaxation times, and magnetic field. The problem has been solved in one-dimensional elastic half-space model subjected initially to a prescribed harmonic displacement and the temperature of the medium. In one of the papers, the analytical and multishaped solitary wave solutions have been presented for extended reduced Ostrovsky equation. The exact solitary (traveling) wave solutions are also expressed by three types of functions which are hyperbolic function solution, trigonometric function solution, and rational solution. In order to classify the exact solutions, including solitons and elliptic solutions, of the generalized $K(m,n)$ equation by the complete discrimination system a polynomial method has been obtained. To examine the possible approximate solutions of both integer and noninteger systems of nonlinear differential equations which describe tuberculosis disease population dynamics, the relatively new analytical technique like homotopy decomposition method has been proposed. In one of the papers, a relatively new operator called the triple Laplace transform has been introduced and to make use of the operator some kind of third-order differential equation called Mboctara equations has been solved.

Another paper investigates the effect of boundary slip on the transient pulsatile fluid flow through a vessel with body acceleration. To describe the non-Newtonian behavior, the modified second-grade fluid model has been analyzed in which the viscosity and the normal stresses have been represented in terms of the shear rate. One of the papers proves the existence of global solutions for nonlinear wave equations with damping and source terms by constructing a stable set and also obtaining the asymptotic stability of global solutions through the use of a difference inequality. In order to assess the spatial dynamical behavior of a predator-prey system with Allee effect, the bifurcation analyses have been used in which the exact Turing domain has been found in the parameters space. According to the operator theory, the temperature dependence of the solution to the BCS gap equation has been connected with superconductivity. When the potential is a positive constant, the BCS gap equation reduces to the simple gap equation. The solution to the BCS gap equation has been indeed continuous with respect to both the temperature and the energy under a certain condition when the potential is not a constant. This study represents that there is a unique nonnegative solution to the simple gap equation, which is continuous and strictly decreasing and is of class C^2 with respect to the temperature.

At present, the use of partial differential equation and integral equation in real physical systems is commonly encountered in the fields of science and engineering. Analysis and numerical approximate of such physical models are required for efficient computational tools. The present issue has addressed recent trends and developments regarding the analytical and numerical methods that may be used in the dynamical system. Eventually, it may be expected that the present special issue would certainly helpful to explore the researchers with their new arising problems and elevate the efficiency and accuracy of the solution methods in use nowadays.

Santanu Saha Ray
Om P. Agrawal
R. K. Bera
Shantanu Das
T. Raja Sekhar

Hindawi Publishing Corporation
Abstract and Applied Analysis
Volume 2013, Article ID 426916, 17 pages
http://dx.doi.org/10.1155/2013/426916

Research Article

Numerical Methods for Solving Fredholm Integral Equations of Second Kind

S. Saha Ray and P. K. Sahu

Department of Mathematics, National Institute of Technology, Rourkela 769008, India

Correspondence should be addressed to S. Saha Ray; santanusaharay@yahoo.com

Received 3 September 2013; Accepted 3 October 2013

Academic Editor: Rasajit Bera

Integral equation has been one of the essential tools for various areas of applied mathematics. In this paper, we review different numerical methods for solving both linear and nonlinear Fredholm integral equations of second kind. The goal is to categorize the selected methods and assess their accuracy and efficiency. We discuss challenges faced by researchers in this field, and we emphasize the importance of interdisciplinary effort for advancing the study on numerical methods for solving integral equations.

1. Introduction

Integral equations occur naturally in many fields of science and engineering [1]. A computational approach to solve integral equation is an essential work in scientific research.

Integral equation is encountered in a variety of applications in many fields including continuum mechanics, potential theory, geophysics, electricity and magnetism, kinetic theory of gases, hereditary phenomena in physics and biology, renewal theory, quantum mechanics, radiation, optimization, optimal control systems, communication theory, mathematical economics, population genetics, queuing theory, medicine, mathematical problems of radiative equilibrium, the particle transport problems of astrophysics and reactor theory, acoustics, fluid mechanics, steady state heat conduction, fracture mechanics, and radiative heat transfer problems. Fredholm integral equation is one of the most important integral equations.

Integral equations can be viewed as equations which are results of transformation of points in a given vector spaces of integrable functions by the use of certain specific integral operators to points in the same space. If, in particular, one is concerned with function spaces spanned by polynomials for which the kernel of the corresponding transforming integral operator is separable being comprised of polynomial functions only, then several approximate methods of solution of integral equations can be developed.

A computational approach to solving integral equation is an essential work in scientific research. Some methods for solving second kind Fredholm integral equation are available in the open literature. The B-spline wavelet method, the method of moments based on B-spline wavelets by Maleknejad and Sahlan [2], and variational iteration method (VIM) by He [3–5] have been applied to solve second kind Fredholm linear integral equations. The learned researchers Maleknejad et al. proposed some numerical methods for solving linear Fredholm integral equations system of second kind using Rationalized Haar functions method, Block-Pulse functions, and Taylor series expansion method [6–8]. Haar wavelet method with operational matrices of integration [9] has been applied to solve system of linear Fredholm integral equations of second kind. Quadrature method [10], B-spline wavelet method [11], wavelet Galerkin method [12], and also VIM [13] can be applied to solve nonlinear Fredholm integral equation of second kind. Some iterative methods like Homotopy perturbation method (HPM) [14–16] and Adomian decomposition method (ADM) [16–18] have been applied to solve nonlinear Fredholm integral equation of second kind.

2. Fredholm Integral Equation

The general form of linear Fredholm integral equation is defined as follows:

$$g(x)\,y(x) = f(x) + \lambda \int_a^b K(x,t)\,y(t)\,dt, \quad (1)$$

where a and b are both constants. $f(x)$, $g(x)$, and $K(x,t)$ are known functions while $y(x)$ is unknown function. λ (nonzero parameter) is called eigenvalue of the integral equation. The function $K(x,t)$ is known as kernel of the integral equation.

2.1. Fredholm Integral Equation of First Kind. The linear integral equation is of form (by setting $g(x) = 0$ in (1))

$$f(x) + \lambda \int_a^b K(x,t)\,y(t)\,dt = 0. \quad (2)$$

Equation (2) is known as Fredholm integral equation of first kind.

2.2. Fredholm Integral Equation of Second Kind. The linear integral equation is of form (by setting $g(x) = 1$ in (1))

$$y(x) = f(x) + \int_a^b K(x,t)\,y(t)\,dt. \quad (3)$$

Equation (3) is known as Fredholm integral equation of second kind.

2.3. System of Linear Fredholm Integral Equations. The general form of system of linear Fredholm integral equations of second kind is defined as follows:

$$\sum_{j=1}^{n} g_{i,j} y_j(x) = f_i(x) + \sum_{j=1}^{n} \int_a^b K_{i,j}(x,t)\,y_j(t)\,dt, \quad i = 1,2,\ldots,n, \quad (4)$$

where $f_i(x)$ and $K_{i,j}(x,t)$ are known functions and $y_j(x)$ are the unknown functions for $i, j = 1,2,\ldots,n$.

2.4. Nonlinear Fredholm-Hammerstein Integral Equation of Second Kind. Nonlinear Fredholm-Hammerstein integral equation of second kind is defined as follows:

$$y(x) = f(x) + \int_a^b K(x,t)\,F(y(t))\,dt, \quad (5)$$

where $K(x,t)$ is the kernel of the integral equation, $f(x)$ and $K(x,t)$ are known functions, and $y(x)$ is the unknown function that is to be determined.

2.5. System of Nonlinear Fredholm Integral Equations. System of nonlinear Fredholm integral equations of second kind is defined as follows:

$$\sum_{j=1}^{n} g_{i,j} y_j(x) = f_i(x) + \sum_{j=1}^{n} \int_a^b K_{i,j}(x,t)\,F_{i,j}(t, y_j(t))\,dt, \quad i = 1,2,\ldots,n, \quad (6)$$

where $f_i(x)$ and $K_{i,j}(x,t)$ are known functions and $y_j(x)$ are the unknown functions for $i, j = 1,2,\ldots,n$.

3. Numerical Methods for Linear Fredholm Integral Equation of Second Kind

Consider the following Fredholm integral equation of second kind defined in (3)

$$y(x) = f(x) + \int_a^b K(x,t)\,y(t)\,dt, \quad a \le x \le b, \quad (7)$$

where $K(x,t)$ and $g(x)$ are known functions and $y(x)$ is unknown function to be determined.

3.1. B-Spline Wavelet Method

3.1.1. B-Spline Scaling and Wavelet Functions on the Interval $[0,1]$. Semiorthogonal wavelets using B-spline are specially constructed for the bounded interval and this wavelet can be represented in a closed form. This provides a compact support. Semiorthogonal wavelets form the basis in the space $L^2(R)$.

Using this basis, an arbitrary function in $L^2(R)$ can be expressed as the wavelet series. For the finite interval $[0,1]$, the wavelet series cannot be completely presented by using this basis. This is because supports of some basis are truncated at the left or right end points of the interval. Hence, a special basis has to be introduced into the wavelet expansion on the finite interval. These functions are referred to as the boundary scaling functions and boundary wavelet functions.

Let m and n be two positive integers and let

$$\begin{aligned} a &= x_{-m+1} = \cdots = x_0 < x_1 \\ &< \cdots < x_n = x_{n+1} \\ &= \cdots = x_{n+m-1} = b \end{aligned} \quad (8)$$

be an equally spaced knots sequence. The functions

$$\begin{aligned} B_{m,j,X}(x) &= \frac{x - x_j}{x_{j+m-1} - x_j} B_{m-1,j,X}(x) \\ &\quad + \frac{x_{j+m} - x}{x_{j+m} - x_{j+1}} B_{m-1,j+1,X}(x), \\ &\qquad j = -m+1,\ldots,n-1, \end{aligned} \quad (9)$$

$$B_{1,j,X}(x) = \begin{cases} 1, & x \in [x_j, x_{j+1}), \\ 0, & \text{otherwise}, \end{cases}$$

are called cardinal B-spline functions of order $m \geq 2$ for the knot sequence $X = \{x_i\}_{i=-m+1}^{n+m-1}$ and $\mathrm{Supp}B_{m,j,X}(x) = [x_j, x_{j+m}] \cap [a,b]$.

By considering the interval $[a,b] = [0,1]$, at any level $j \in Z^+$, the discretization step is 2^{-j}, and this generates $n = 2^j$ number of segments in $[0,1]$ with knot sequence

$$X^{(j)} = \begin{cases} x_{-m+1}^{(j)} = \cdots = x_0^{(j)} = 0, \\ x_k^{(j)} = \dfrac{k}{2^j}, \quad k = 1,\dots,n-1, \\ x_n^{(j)} = \cdots = x_{n+m-1}^{(j)} = 1. \end{cases} \tag{10}$$

Let j_0 be the level for which $2^{j_0} \geq 2m-1$; for each level, $j \geq j_0$, the scaling functions of order m can be defined as follows in [2]:

$$\varphi_{m,j,i}(x) = \begin{cases} B_{m,j_0,i}\left(2^{j-j_0}x\right) & i = -m+1,\dots,-1, \\ B_{m,j_0,2^j-m-i}\left(1-2^{j-j_0}x\right) & i = 2^j-m+1,\dots,2^j-1, \\ B_{m,j_0,0}\left(2^{j-j_0}x - 2^{-j_0}i\right) & i = 0,\dots,2^j-m. \end{cases} \tag{11}$$

And the two scale relations for the m-order semiorthogonal compactly supported B-wavelet functions are defined as follows:

$$\psi_{m,j,i-m} = \sum_{k=i}^{2i+2m-2} q_{i,k} B_{m,j,k-m}, \quad i = 1,\dots,m-1,$$
$$\psi_{m,j,i-m} = \sum_{k=2i-m}^{2i+2m-2} q_{i,k} B_{m,j,k-m}, \quad i = m,\dots,n-m+1,$$
$$\psi_{m,j,i-m} = \sum_{k=2i-m}^{n+i+m-1} q_{i,k} B_{m,j,k-m}, \quad i = n-m+2,\dots,n, \tag{12}$$

where $q_{i,k} = q_{k-2i}$.

Hence, there are $2(m-1)$ boundary wavelets and $(n-2m+2)$ inner wavelets in the bounded interval $[a,b]$. Finally, by considering the level j with $j \geq j_0$, the B-wavelet functions in $[0,1]$ can be expressed as follows:

$$\psi_{m,j,i}(x) = \begin{cases} \psi_{m,j_0,i}\left(2^{j-j_0}x\right) & i = -m+1,\dots,-1, \\ \psi_{m,2^j-2m+1-i,i}\left(1-2^{j-j_0}x\right) & i = 2^j-2m+2,\dots,2^j-m, \\ \psi_{m,j_0,0}\left(2^{j-j_0}x - 2^{-j_0}i\right) & i = 0,\dots,2^j-2m+1. \end{cases} \tag{13}$$

The scaling functions $\varphi_{m,j,i}(x)$ occupy m segments and the wavelet functions $\psi_{m,j,i}(x)$ occupy $2m-1$ segments.

When the semiorthogonal wavelets are constructed from B-spline of order m, the lowest octave level $j = j_0$ is determined in [19, 20] by

$$2^{j_0} \geq 2m-1, \tag{14}$$

so as to have a minimum of one complete wavelet on the interval $[0,1]$.

3.1.2. Function Approximation. A function $f(x)$ defined over $[0,1]$ may be approximated by B-spline wavelets as [21, 22]

$$f(x) = \sum_{k=1-m}^{2^{j_0}-1} c_{j_0,k}\varphi_{j_0,k}(x) + \sum_{j=j_0}^{\infty}\sum_{k=1-m}^{2^j-m} d_{j,k}\psi_{j,k}(x). \tag{15}$$

If the infinite series in (15) is truncated at M, then (15) can be written as [2]

$$f(x) \cong \sum_{k=1-m}^{2^{j_0}-1} c_{j_0,k}\varphi_{j_0,k}(x) + \sum_{j=j_0}^{M}\sum_{k=1-m}^{2^j-m} d_{j,k}\psi_{j,k}(x), \tag{16}$$

where $\varphi_{2,k}$ and $\psi_{j,k}$ are scaling and wavelets functions, respectively, and C and Ψ are $(2^{M+1}+m-1)\times 1$ vectors given by

$$C = \left[c_{j_0,1-m},\dots,c_{j_0,2^{j_0}-1}, d_{j_0,1-m},\dots, d_{j_0,2^{j_0}-m},\dots,d_{M,1-m},\dots,d_{M,2^M-m}\right]^T, \tag{17}$$

$$\Psi = \left[\varphi_{j_0,1-m},\dots,\varphi_{j_0,2^{j_0}-1},\psi_{j_0,1-m},\dots, \psi_{j_0,2^{j_0}-m},\dots,\psi_{M,1-m},\dots,\psi_{M,2^M-m}\right]^T, \tag{18}$$

with

$$c_{j_0,k} = \int_0^1 f(x)\,\widetilde{\varphi}_{j_0,k}(x)\,dx, \quad k = 1-m,\dots,2^{j_0}-1,$$
$$d_{j,k} = \int_0^1 f(x)\,\widetilde{\psi}_{j,k}(x)\,dx,$$
$$j = j_0,\dots,M, \quad k = 1-m,\dots,2^M-m, \tag{19}$$

where $\widetilde{\varphi}_{j_0,k}(x)$ and $\widetilde{\psi}_{j,k}(x)$ are dual functions of $\varphi_{j_0,k}$ and $\psi_{j,k}$, respectively. These can be obtained by linear combinations of $\varphi_{j_0,k}$, $k = 1-m,\dots,2^{j_0}-1$, and $\psi_{j,k}$, $j = j_0,\dots,M$, $k = 1-m,\dots,2^M-m$, as follows. Let

$$\Phi = \left[\varphi_{j_0,1-m},\dots,\varphi_{j_0,2^{j_0}-1}\right]^T, \tag{20}$$

$$\overline{\Psi} = \left[\psi_{j_0,1-m},\dots,\psi_{j_0,2^{j_0}-m},\dots,\psi_{M,1-m},\dots,\psi_{M,2^M-m}\right]^T. \tag{21}$$

Using (11), (20), (12)-(13), and (21), we get

$$\int_0^1 \Phi\Phi^T dx = P_1,$$
$$\int_0^1 \overline{\Psi}\,\overline{\Psi}^T dx = P_2. \tag{22}$$

Suppose that $\widetilde{\Phi}$ and $\widetilde{\overline{\Psi}}$ are the dual functions of Φ and $\overline{\Psi}$, respectively; then

$$\int_0^1 \widetilde{\Phi}\Phi^T dx = I_1,$$
$$\int_0^1 \widetilde{\overline{\Psi}}\,\overline{\Psi}^T dx = I_2, \tag{23}$$

$$\widetilde{\Phi} = P_1^{-1}\Phi,$$
$$\widetilde{\overline{\Psi}} = P_2^{-1}\overline{\Psi}. \tag{24}$$

3.1.3. Application of B-Spline Wavelet Method. In this section, linear Fredholm integral equation of the second kind of form (7) has been solved by using B-spline wavelets. For this, we use (16) to approximate $y(x)$ as

$$y(x) = C^T\Psi(x), \tag{25}$$

where $\Psi(x)$ is defined in (18) and C is $(2^{M+1}+m-1)\times 1$ unknown vector defined similarly as in (17). We also expand $f(x)$ and $K(x,t)$ by B-spline dual wavelets $\widetilde{\Psi}$ defined in (24) as

$$f(x) = C_1{}^T\widetilde{\Psi}(x),$$
$$K(x,t) = \widetilde{\Psi}^T(t)\,\Theta\widetilde{\Psi}(x), \tag{26}$$

where

$$\Theta_{i,j} = \int_0^1\left[\int_0^1 K(x,t)\Psi_i(t)\,dt\right]\Psi_j(x)\,dx. \tag{27}$$

From (26) and (25), we get

$$\begin{aligned}\int_0^1 K(x,t)\,y(t)\,dt &= \int_0^1 C^T\Psi(t)\,\widetilde{\Psi}^T(t)\,\Theta\widetilde{\Psi}(x)\,dt\\ &= C^T\Theta\widetilde{\Psi}(x)\end{aligned} \tag{28}$$

since

$$\int_0^1 \Psi(t)\,\widetilde{\Psi}^T(t)\,dt = I. \tag{29}$$

By applying (25)–(28) in (7) we have

$$C^T\Psi(x) - C^T\Theta\widetilde{\Psi}(x) = C_1^T\widetilde{\Psi}(x). \tag{30}$$

By multiplying both sides of (30) with $\Psi^T(x)$ from the right and integrating both sides with respect to x from 0 to 1, we get

$$C^TP - C^T\Theta = C_1^T, \tag{31}$$

since

$$\int_0^1 \widetilde{\Psi}(x)\,\Psi^T(x)\,dx = I, \tag{32}$$

and P is a $(2^{M+1}+m-1)\times(2^{M+1}+m-1)$ square matrix given by

$$P = \int_0^1 \Psi(x)\,\Psi^T(x)\,dx = \begin{pmatrix} P_1 & 0\\ 0 & P_2\end{pmatrix}. \tag{33}$$

Consequently, from (31), we get $C^T = C_1^T(P-\Theta)^{-1}$. Hence, we can calculate the solution for $y(x) = C^T\Psi(x)$.

3.2. Method of Moments

3.2.1. Multiresolution Analysis (MRA) and Wavelets [2]. A set of subspaces $\{V_j\}_{j\in Z}$ is said to be MRA of $L^2(R)$ if it possesses the following properties:

$$V_j \subset V_{j+1}, \quad \forall j\in Z, \tag{34}$$

$$\bigcup_{j\in Z} V_j \text{ is dense in } L^2(R), \tag{35}$$

$$\bigcap_{j\in Z} V_j = \phi, \tag{36}$$

$$f(x)\in V_j \Longleftrightarrow f(2x)\in V_{j+1}, \quad \forall j\in Z, \tag{37}$$

where Z denotes the set of integers. Properties (34)–(36) state that $\{V_j\}_{j\in Z}$ is a nested sequence of subspaces that effectively covers $L^2(R)$. That is, every square integrable function can be approximated as closely as desired by a function that belongs to at least one of the subspaces V_j. A function $\varphi\in L^2(R)$ is called a scaling function if it generates the nested sequence of subspaces V_j and satisfies the dilation equation; namely,

$$\varphi(x) = \sum_k p_k\varphi(ax-k), \tag{38}$$

with $p_k\in l^2$ and a being any rational number.

For each scale j, since $V_j\subset V_{j+1}$, there exists a unique orthogonal complementary subspace W_j of V_j in V_{j+1}. This subspace W_j is called wavelet subspace and is generated by $\psi_{j,k} = \psi(2^jx-k)$, where $\psi\in L^2$ is called the wavelet. From the above discussion, these results follow easily:

$$\begin{aligned} V_{j_1}\cap V_{j_2} &= V_{j_2}, \quad j_1 > j_2,\\ W_{j_1}\cap W_{j_2} &= 0, \quad j_1\neq j_2,\\ V_{j_1}\cap W_{j_2} &= 0, \quad j_1\leq j_2.\end{aligned} \tag{39}$$

Some of the important properties relevant to the present analysis are given below [2, 19].

(1) Vanishing Moment. A wavelet is said to have a vanishing moment of order m if

$$\int_{-\infty}^{\infty} x^p\psi(x)\,dx = 0; \quad p = 0,\dots,m-1. \tag{40}$$

All wavelets must satisfy the previously mentioned condition for $p = 0$.

(2) Semiorthogonality. The wavelets $\psi_{j,k}$ form a semiorthogonal basis if

$$\left\langle \psi_{j,k}, \psi_{s,i} \right\rangle = 0; \quad j \neq s; \ \forall j, k, s, i \in \mathbb{Z}. \tag{41}$$

3.2.2. Method of Moments for the Solution of Fredholm Integral Equation. In this section, we solve the integral equation of form (7) in interval $[0, 1]$ by using linear B-spline wavelets [2]. The unknown function in (7) can be expanded in terms of the scaling and wavelet functions as follows:

$$\begin{aligned} y(x) &\approx \sum_{k=-1}^{2^{j_0}-1} c_k \varphi_{j_0,k}(x) \\ &\quad + \sum_{j=j_0}^{M} \sum_{k=-1}^{2^j-2} d_{j,k} \psi_{j,k}(x) \\ &= C^T \Psi(x). \end{aligned} \tag{42}$$

By substituting this expression into (7) and employing the Galerkin method, the following set of linear system of order $(2^M + 1)$ is generated. The scaling and wavelet functions are used as testing and weighting functions:

$$\begin{pmatrix} \langle \varphi, \varphi \rangle - \langle K\varphi, \varphi \rangle & \langle \psi, \varphi \rangle - \langle K\psi, \varphi \rangle \\ \langle \varphi, \psi \rangle - \langle K\varphi, \psi \rangle & \langle \psi, \psi \rangle - \langle K\psi, \psi \rangle \end{pmatrix} \begin{pmatrix} C \\ D \end{pmatrix} = \begin{pmatrix} F_1 \\ F_2 \end{pmatrix}, \tag{43}$$

where

$$\begin{aligned} C &= \left[c_{-1}, c_0, \ldots, c_3\right]^T, \\ D &= \left[d_{2,-1}, \ldots, d_{2,2}, d_{3,-1}, \ldots, d_{3,6}, \ldots, \right. \\ &\qquad \left. d_{M,-1}, \ldots, d_{M,2^M-2}\right]^T, \\ &\langle \varphi, \varphi \rangle - \langle K\varphi, \varphi \rangle \\ &= \left(\int_0^1 \varphi_{j_0,r}(x) \varphi_{j_0,i}(x) \, dx \right. \\ &\qquad \left. - \int_0^1 \varphi_{j_0,r}(x) \int_0^1 K(x,t) \varphi_{j_0,i}(t) dt \, dx \right)_{i,r}, \\ &\langle \psi, \varphi \rangle - \langle K\psi, \varphi \rangle \\ &= \left(\int_0^1 \varphi_{j_0,r}(x) \psi_{k,j}(x) \, dx \right. \\ &\qquad \left. - \int_0^1 \varphi_{j_0,r}(x) \int_0^1 K(x,t) \psi_{k,j}(t) dt \, dx \right)_{r,k,j}, \\ &\langle \varphi, \psi \rangle - \langle K\varphi, \psi \rangle \\ &= \left(\int_0^1 \psi_{s,l}(x) \varphi_{j_0,i}(x) \, dx \right. \\ &\qquad \left. - \int_0^1 \psi_{s,l}(x) \int_0^1 K(x,t) \varphi_{j_0,i}(t) dt \, dx \right)_{i,l,s}, \\ &\langle \psi, \psi \rangle - \langle K\psi, \psi \rangle \\ &= \left(\int_0^1 \psi_{s,l}(x) \psi_{k,j}(x) \, dx \right. \\ &\qquad \left. - \int_0^1 \psi_{s,l}(x) \int_0^1 K(x,t) \psi_{k,j}(t) dt \, dx \right)_{l,s,k,j}, \\ F_1 &= \int_0^1 f(x) \varphi_{j_0,r}(x) \, dx, \\ F_2 &= \int_0^1 f(x) \psi_{s,l}(x) \, dx, \end{aligned} \tag{44}$$

and the subscripts i, r, k, j, l, and s assume values as given below:

$$\begin{aligned} i, r &= -1, \ldots, 2^{j_0} - 1, \\ l, k &= j_0, \ldots, M, \\ s, j &= -1, \ldots, 2^M - 2. \end{aligned} \tag{45}$$

In fact, the entries with significant magnitude are in the $\langle K\varphi, \varphi \rangle - \langle \varphi, \varphi \rangle$ and $\langle K\psi, \psi \rangle - \langle \psi, \psi \rangle$ submatrices which are of order $(2^{j_0} + 1)$ and $(2^{M+1} + 1)$, respectively.

3.3. Variational Iteration Method [3–5]. In this section, Fredholm integral equation of second kind given in (7) has been considered for solving (7) by variational iteration method. First, we have to take the partial derivative of (7) with respect to x yielding

$$Y'(x) = f'(x) + \int_0^1 K'(x,t) \, y(t) \, dt. \tag{46}$$

We apply variation iteration method for (46). According to this method, correction functional can be defined as

$$\begin{aligned} &y_{n+1}(x) \\ &\quad = y_n(x) \\ &\qquad + \int_0^x \lambda(\xi) \left(y_n'(\xi) - f'(\xi) - \int_a^b K'(\xi,t) \, \tilde{y}_n(t) \, dt \right) d\xi, \end{aligned} \tag{47}$$

where $\lambda(\xi)$ is a general Lagrange multiplier which can be identified optimally by the variational theory, the subscript n denotes the nth order approximation, and $\tilde{y}_n$ is considered as a restricted variation; that is, $\delta\tilde{y}_n = 0$. The successive approximations $y_n(x)$, $n \geq 1$ for the solution $y(x)$ can be readily obtained after determining the Lagrange multiplier and selecting an appropriate initial function $y_0(x)$. Consequently the approximate solution may be obtained by using

$$y(x) = \lim_{n \to \infty} y_n(x). \tag{48}$$

To make the above correction functional stationary, we have

$$\begin{aligned}\delta y_{n+1}(x) = \delta y_n(x) &+ \delta\int_0^x \lambda(\xi)\left(y_n'(\xi) - f'(\xi) - \int_a^b K'(\xi,t)\,\tilde{y}_n(t)\,dt\right)d\xi \\ &= \delta y_n(x) + \int_0^x \lambda(\xi)\,\delta\left(y_n'(\xi)\right)d\xi \\ &= \delta y_n(x) + \lambda\delta y_n\big|_{\xi=x} - \int_0^x \lambda'(\xi)\,\delta y_n(\xi)\,d\xi.\end{aligned} \tag{49}$$

Under stationary condition,

$$\delta y_{n+1} = 0 \tag{50}$$

implies the following Euler Lagrange equation:

$$\lambda'(\xi) = 0, \tag{51}$$

with the following natural boundary condition:

$$1 + \lambda(\xi)\big|_{\xi=x} = 0. \tag{52}$$

Solving (51), along with boundary condition (52), we get the general Lagrange multiplier

$$\lambda = -1. \tag{53}$$

Substituting the identified Lagrange multiplier into (47) results in the following iterative scheme:

$$y_{n+1}(x) = y_n(x) - \int_0^x \left(y_n'(\xi) - f'(\xi) - \int_a^b K'(\xi,t)\,\tilde{y}_n(t)\,dt\right)d\xi, \quad n \ge 0. \tag{54}$$

By starting with initial approximate function $y_0(x) = f(x)$ (say), we can determine the approximate solution $y(x)$ of (7).

4. Numerical Methods for System of Linear Fredholm Integral Equations of Second Kind

Consider the system of linear Fredholm integral equations of second kind of the following form:

$$\sum_{j=1}^{n} y_j(x) = f_i(x) + \sum_{j=1}^{n}\int_0^1 K_{i,j}(x,t)\,y_j(t)\,dt, \quad i = 1,2,\ldots,n, \tag{55}$$

where $f_i(x)$ and $K_{i,j}(x,t)$ are known functions and $y_j(x)$ are the unknown functions for $i, j = 1,2,\ldots,n$.

4.1. Application of Haar Wavelet Method [9]

4.1. Application of Haar Wavelet Method [9]. In this section, an efficient algorithm for solving Fredholm integral equations with Haar wavelets is analyzed. The present algorithm takes the following essential strategy. The Haar wavelet is first used to decompose integral equations into algebraic systems of linear equations, which are then solved by collocation methods.

4.1.1. Haar Wavelets. The compact set of scale functions is chosen as

$$h_0 = \begin{cases} 1, & 0 \le x < 1, \\ 0, & \text{others}. \end{cases} \tag{56}$$

The mother wavelet function is defined as

$$h_1(x) = \begin{cases} 1, & 0 \le x < \dfrac{1}{2}, \\ -1, & \dfrac{1}{2} \le x < 1, \\ 0, & \text{others}. \end{cases} \tag{57}$$

The family of wavelet functions generated by translation and dilation of $h_1(x)$ are given by

$$h_n(x) = h_1\left(2^j x - k\right), \tag{58}$$

where $n = 2^j + k$, $j \ge 0$, $0 \le k < 2^j$.

Mutual orthogonalities of all Haar wavelets can be expressed as

$$\int_0^1 h_m(x)\,h_n(x)\,dx = 2^{-j}\delta_{mn} = \begin{cases} 2^{-j}, & m = n = 2^j + k, \\ 0, & m \ne n. \end{cases} \tag{59}$$

4.1.2. Function Approximation. An arbitrary function $y(x) \in L^2[0,1)$ can be expanded into the following Haar series:

$$y(x) = \sum_{n=0}^{+\infty} c_n h_n(x), \tag{60}$$

where the coefficients c_n are given by

$$c_n = 2^j \int_0^1 y(x)\,h_n(x)\,dx, \quad n = 2^j + k, \quad j \ge 0, \quad 0 \le k < 2^j. \tag{61}$$

In particular, $c_0 = \int_0^1 y(x)dx$.

The previously mentioned expression in (60) can be approximately represented with finite terms as follows:

$$y(x) \approx \sum_{n=0}^{m-1} c_n h_n(x) = C_{(m)}^T h_{(m)}(x), \tag{62}$$

where the coefficient vector $C_{(m)}^T$ and the Haar function vector $h_{(m)}(x)$ are, respectively, defined as

$$\begin{aligned} C_{(m)}^T &= \left[c_0, c_1, \ldots, c_{m-1}\right], \quad m = 2^j, \\ h_{(m)}(x) &= \left[h_0(x), h_1(x), \ldots, h_{m-1}(x)\right]^T, \quad m = 2^j. \end{aligned} \tag{63}$$

The Haar expansion for function $K(x,t)$ of order m is defined as follows:

$$K(x,t) \approx \sum_{u=0}^{m-1}\sum_{v=0}^{m-1} a_{uv} h_v(x) h_u(t), \tag{64}$$

where $a_{uv} = 2^{i+q}\iint_0^1 K(x,t)h_v(x)h_u(t)dx\,dt$, $u = 2^i + j$, $v = 2^q + r$, $i, q \ge 0$.

From (62) and (64), we obtain

$$K(x,t) \approx h_{(m)}^T(t)\, K h_{(m)}(x), \tag{65}$$

where

$$K = (a_{uv})_{m\times m}^T. \tag{66}$$

4.1.3. Operational Matrices of Integration. We define

$$H_{(m)} = \left[h_{(m)}\left(\frac{1}{2m}\right), h_{(m)}\left(\frac{3}{2m}\right), \dots, h_{(m)}\left(\frac{2m-1}{2m}\right)\right], \tag{67}$$

where $H_{(1)} = [1]$, $H_{(2)} = \left[\begin{smallmatrix}1 & 1\\ 1 & -1\end{smallmatrix}\right]$.

Then, for $m = 4$, the corresponding matrix can be represented as

$$\begin{aligned} H_{(4)} &= \left[h_{(4)}\left(\frac{1}{8}\right), h_{(4)}\left(\frac{3}{8}\right), \dots, h_{(4)}\left(\frac{7}{8}\right)\right] \\ &= \begin{bmatrix} 1 & 1 & 1 & 1\\ 1 & 1 & -1 & -1\\ 1 & -1 & 0 & 0\\ 0 & 0 & 1 & -1 \end{bmatrix}. \end{aligned} \tag{68}$$

The integration of the Haar function vector $h_{(m)}(t)$ is

$$\int_0^x h_{(m)}(t)\,dt = P_{(m)} h_{(m)}(x), \quad x \in [0,1), \tag{69}$$

where $P_{(m)}$ is the operational matrix of order m, and

$$\begin{aligned} P_{(1)} &= \left[\frac{1}{2}\right], \\ P_{(m)} &= \frac{1}{2m}\begin{bmatrix} 2mP_{(m/2)} & -H_{(m/2)} \\ H_{(m/2)}^{-1} & 0 \end{bmatrix}. \end{aligned} \tag{70}$$

By recursion of the above formula, we obtain

$$\begin{aligned} P_{(2)} &= \frac{1}{4}\begin{bmatrix} 2 & -1\\ 1 & 0\end{bmatrix}, \\ P_{(4)} &= \frac{1}{16}\begin{bmatrix} 8 & -4 & -2 & -2\\ 4 & 0 & -2 & 2\\ 1 & 1 & 0 & 0\\ 1 & -1 & 0 & 0\end{bmatrix}, \\ P_{(8)} &= \frac{1}{64}\begin{bmatrix} 32 & -16 & -8 & -8 & -4 & -4 & -4 & -4\\ 16 & 0 & -8 & 8 & -4 & -4 & 4 & 4\\ 4 & 4 & 0 & 0 & -4 & 4 & 0 & 0\\ 4 & 4 & 0 & 0 & 0 & 0 & -4 & 4\\ 1 & 1 & 2 & 0 & 0 & 0 & 0 & 0\\ 1 & 1 & -2 & 0 & 0 & 0 & 0 & 0\\ 1 & -1 & 0 & 2 & 0 & 0 & 0 & 0\\ 1 & -1 & 0 & -2 & 0 & 0 & 0 & 0 \end{bmatrix}. \end{aligned} \tag{71}$$

Therefore, we get

$$\begin{aligned} H_{(m)}^{-1} &= \left(\frac{1}{m}\right) H_{(m)}^T \\ &\quad \times \operatorname{diag}\Big(1, 1, 2, 2, \underbrace{2^2, \dots, 2^2}_{2^2}, \dots, \underbrace{2^{\alpha-1}, \dots, 2^{\alpha-1}}_{2^{\alpha-1}}\Big), \end{aligned} \tag{72}$$

where $m = 2^\alpha$ and α is a positive integer.

The inner product of two Haar functions can be represented as

$$\int_0^1 h_{(m)}(t)\, h_{(m)}^T(t)\,dt = D, \tag{73}$$

where

$$\begin{aligned} D = \operatorname{diag}\Big(& 1, 1, 1/2, 1/2, \underbrace{1/2^2, \dots, 1/2^2}_{2^2}, \dots, \\ & \underbrace{1/2^{\alpha-1}, \dots, 1/2^{\alpha-1}}_{2^{\alpha-1}}\Big). \end{aligned} \tag{74}$$

4.1.4. Haar Wavelet Solution for Fredholm Integral Equations System [9]. Consider the following Fredholm integral equations system defined in (55):

$$\sum_{j=1}^m y_j(x) = f_i(x) + \sum_{j=1}^m \int_0^1 K_{i,j}(x,t)\, y_j(t)\,dt, \quad i = 1, 2, \dots, m. \tag{75}$$

The Haar series of $y_j(x)$ and $K_{i,j}(x,t)$, $i = 1, 2, \dots, m$; $j = 1, 2, \dots, m$ are, respectively, expanded as

$$\begin{aligned} y_j(x) &\approx Y_j^T h_{(m)}(x), \quad j = 1, 2, \dots, m, \\ K_{i,j}(x,t) &\approx h_{(m)}^T(t)\, K_{i,j} h_{(m)}(x), \quad i, j = 1, 2, \dots, m. \end{aligned} \tag{76}$$

Substituting (76) into (75), we get

$$\sum_{j=1}^{m} Y_j^T h_{(m)}(x) = f_i(x) + \sum_{j=1}^{m} \int_0^1 Y_j^T h_{(m)}(t)\, h_{(m)}^T(t)\, K_{i,j} h_{(m)}(x)\, dt, \quad i = 1, 2, \ldots, m. \tag{77}$$

From (77) and (73), we get

$$\sum_{j=1}^{m} Y_j^T h_{(m)}(x) = f_i(x) + \sum_{j=1}^{m} Y_j^T D K_{i,j} h_{(m)}(x), \quad i = 1, 2, \ldots, m. \tag{78}$$

Interpolating m collocation points, that is, $\{x_i\}_{i=1}^{m}$, in the interval $[0,1]$ leads to the following algebraic system of equations:

$$\sum_{j=1}^{m} Y_j^T h_{(m)}(x_i) = f_i(x_i) + \sum_{j=1}^{m} Y_j^T D K_{i,j} h_{(m)}(x_i), \quad i = 1, 2, \ldots, m. \tag{79}$$

Hence, Y_j, $j = 1, 2, \ldots, m$ can be computed by solving the above algebraic system of equations and consequently the solutions $y_j(x) \approx Y_j^T h_{(m)}(x)$, $j = 1, 2, \ldots, m$.

4.2. Taylor Series Expansion Method. In this section, we present Taylor series expansion method for solving Fredholm integral equations system of second kind [7]. This method reduces the system of integral equations to a linear system of ordinary differential equation. After including boundary conditions, this system reduces to a system of equations that can be solved easily by any usual methods.

Consider the second kind Fredholm integral equations system defined in (55) as follows:

$$y_i(x) = f_i(x) + \sum_{j=1}^{n} \int_0^1 K_{i,j}(x,t)\, y_j(t)\, dt, \quad i = 1, 2, \ldots, n, \quad 0 \le x \le 1. \tag{80}$$

A Taylor series expansion can be made for the solution of $y_j(t)$ in the integral equation (80):

$$y_j(t) = y_j(x) + y_j'(x)(t-x) + \cdots + \frac{1}{m!} y_j^{(m)}(x)(t-x)^m + E(t), \tag{81}$$

where $E(t)$ denotes the error between $y_j(t)$ and its Taylor series expansion in (81).

If we use the first m term of Taylor series expansion and neglect the term containing $E(t)$, that is, $\int_0^1 \sum_{j=1}^{n} K_{i,j}(x,t) E(t) dt$, then, substituting (81) for $y_j(t)$ into the integral in (80), we have

$$\begin{aligned} y_i(x) &\approx f_i(x) + \sum_{j=1}^{n} \int_0^1 K_{i,j}(x,t) \sum_{r=0}^{m} \frac{1}{r!}(t-x)^r y_j^{(r)}(x)\, dt, \quad i = 1, 2, \ldots, n, \\ y_i(x) &\approx f_i(x) + \sum_{j=1}^{n} \sum_{r=0}^{m} \frac{1}{r!} y_j^{(r)}(x) \int_0^1 K_{i,j}(x,t)(t-x)^r dt, \quad i = 1, 2, \ldots, n, \end{aligned} \tag{82}$$

$$y_i(x) - \sum_{j=1}^{n} \sum_{r=0}^{m} \frac{1}{r!} y_j^{(r)}(x) \left[\int_0^1 K_{i,j}(x,t)(t-x)^r dt \right] \approx f_i(x), \quad i = 1, 2, \ldots, n. \tag{83}$$

Equation (83) becomes a linear system of ordinary differential equations that we have to solve. For solving the linear system of ordinary differential equations (83), we require an appropriate number of boundary conditions.

In order to construct boundary conditions, we first differentiate s times both sides of (80) with respect to x; that is,

$$y_i^{(s)}(x) = f_i^{(s)}(x) + \sum_{j=1}^{n} \int_0^1 K_{i,j}^{(s)}(x,t)\, y_j(t)\, dt, \quad i = 1, 2, \ldots, n, \quad s = 1, 2, \ldots, m, \tag{84}$$

where $K_{i,j}^{(s)}(x,t) = \partial^{(s)} K_{i,j}(x,t)/\partial x^{(s)}$, $s = 1, 2, \ldots, m$.

Applying the mean value theorem for integral in (84), we have

$$y_i^{(s)}(x) - \left[\sum_{j=1}^{n} \int_0^1 K_{i,j}^{(s)}(x,t)\, dt \right] y_j(x) \approx f_i^{(s)}(x), \quad i = 1, 2, \ldots, n, \quad s = 1, 2, \ldots, m. \tag{85}$$

Now (83) combined with (85) becomes a linear system of algebraic equations that can be solved analytically or numerically.

4.3. Block-Pulse Functions for the Solution of Fredholm Integral Equation. In this section, Block-Pulse functions (BPF) have been utilized for the solution of system of Fredholm integral equations [6].

An m-set of BPF is defined as follows:

$$\Phi_i(t) = \begin{cases} 1, & (i-1)\dfrac{T}{m} \le t < i\dfrac{T}{m}, \\ 0, & \text{otherwise} \end{cases} \tag{86}$$

with $t \in [0, T)$, $T/m = h$ and $i = 1, 2, \ldots, m$.

4.3.1. Properties of BPF

(1) Disjointness. One has

$$\Phi_i(t)\,\Phi_j(t) = \begin{cases}\Phi_i(t), & i = j;\\ 0, & i \neq j,\end{cases} \tag{87}$$

, $i, j = 1, 2, \ldots, m$. This property is obtained from definition of BPF.

(2) Orthogonality. One has

$$\int_0^T \Phi_i(t)\,\Phi_j(t)\,dt = \begin{cases}h, & i = j;\\ 0, & i \neq j,\end{cases} \tag{88}$$

$t \in [0, T)$, $i, j = 1, 2, \ldots, m$. This property is obtained from the disjointness property.

(3) Completeness. For every $f \in L^2$, $\{\Phi\}$ is complete; if $\int \Phi f = 0$ then $f = 0$ almost everywhere. Because of completeness of $\{\Phi\}$, we have

$$\int_0^T f^2(t)\,dt = \sum_{i=1}^{\infty} f_i^2 \left\|\Phi_i(t)\right\|^2 \tag{89}$$

for every real bounded function $f(t)$ which is square integrable in the interval $t \in [0, T)$ and $f_i = (1/h) f(t)\Phi_i(t)dt$.

4.3.2. Function Approximation. The orthogonality property of BPF is the basis of expanding functions into their Block-Pulse series. For every $f(t) \in L^2(R)$,

$$f(t) = \sum_{i=1}^{m} f_i \Phi_i(t), \tag{90}$$

where f_i is the coefficient of Block-Pulse function, with respect to ith Block-Pulse function $\Phi_i(t)$.

The criterion of this approximation is that mean square error between $f(t)$ and its expansion is minimum

$$\varepsilon = \frac{1}{T}\int_0^T \left(f(t) - \sum_{j=1}^{m} f_j \Phi_j(t)\right)^2 dt \tag{91}$$

so that we can evaluate Block-Pulse coefficients.

$$\text{Now } \frac{\partial \varepsilon}{\partial f_i} = -\frac{2}{T}\int_0^T \left(f(t) - \sum_{j=1}^{m} f_j \Phi_j(t)\right)\Phi_i(t)\,dt = 0,$$
$$\Longrightarrow f_i = \frac{1}{h}\int_0^T f(t)\,\Phi_i(t)\,dt \quad \text{(using orthogonal property)}. \tag{92}$$

In the matrix form, we obtain the following from (90) as follow:

$$f(t) = \sum_{i=1}^{m} f_i \Phi_i(t) = F^T \Phi(t) = \Phi^T F$$
$$\text{where } F = \left[f_1, f_2, \ldots, f_m\right]^T, \tag{93}$$
$$\Phi(t) = \left[\Phi_1(t), \Phi_2(t), \ldots, \Phi_m(t)\right]^T.$$

Now let $K(t, s)$ be two-variable function defined on $t \in [0, T)$ and $s \in [0, 1)$; then $K(t, s)$ can be expanded to BPF as

$$K(t, s) = \Phi^T(t)\,K\Psi(s), \tag{94}$$

where $\Phi(t)$ and $\Psi(s)$ are m_1 and m_2 dimensional Block-Pulse function vectors and k is a $m_1 \times m_2$ Block-Pulse coefficient matrix.

There are two different cases of multiplication of two BPF. The first case is

$$\Phi(t)\,\Phi^T(t) = \begin{pmatrix}\Phi_1(t) & 0 & \cdots & 0\\ 0 & \Phi_2(t) & \cdots & 0\\ \vdots & \vdots & \ddots & \vdots\\ 0 & 0 & \cdots & \Phi_m(t)\end{pmatrix}. \tag{95}$$

It is obtained from disjointness property of BPF. It is a diagonal matrix with m Block-Pulse functions.

The second case is

$$\Phi^T(t)\,\Phi(t) = 1 \tag{96}$$

because $\sum_{i=1}^{m}(\Phi_i(t))^2 = \sum_{i=1}^{m}\Phi_i(t) = 1$.

Operational Matrix of Integration. BPF integration property can be expressed by an operational equation as

$$\int_0^T \Phi(t)\,dt = P\Phi(t), \tag{97}$$

where

$$\Phi(t) = \left[\Phi_1(t), \Phi_2(t), \ldots, \Phi_m(t)\right]^T. \tag{98}$$

A general formula for $P_{m\times m}$ can be written as

$$P = \frac{1}{2}\begin{pmatrix}1 & 2 & 2 & \cdots & 2\\ 0 & 1 & 2 & \cdots & 2\\ 0 & 0 & 1 & \cdots & 2\\ \vdots & \vdots & \vdots & \ddots & \vdots\\ 0 & 0 & 0 & \cdots & 1\end{pmatrix}. \tag{99}$$

By using this matrix, we can express the integral of a function $f(t)$ into its Block-Pulse series

$$\int_0^t f(t)\,dt = \int_0^t F^T\Phi(t)\,dt = F^T P\Phi(t). \tag{100}$$

4.3.3. Solution for Linear Integral Equations System. Consider the integral equations system from (55) as follows:

$$\sum_{j=1}^{n} y_j(x) = f_i(x) + \sum_{j=1}^{n}\int_\alpha^\beta K_{i,j}(x,t)\,y_j(t)\,dt, \qquad i = 1, 2, \ldots, n. \tag{101}$$

Block-Pulse coefficients of $y_j(x)$, $j = 1, 2, \ldots, n$ in the interval $x \in [\alpha, \beta)$ can be determined from the known functions $f_i(x)$, $i = 1, 2, \ldots, n$ and the kernels $K_{i,j}(x,t)$, $i, j = 1, 2, \ldots n$. Usually, we consider $\alpha = 0$ to facilitie the use of Block-Pulse functions. In case $\alpha \neq 0$, we set $X = ((x-\alpha)/(\beta-\alpha))T$, where $T = mh$.

We approximate $f_i(x)$, $y_j(x)$, $K_{i,j}(x,t)$ by its BPF as follows:

$$\begin{gathered} f_i(x) \approx F_i^T \Phi(x), \\ y_j(x) \approx Y_j^T \Phi(x), \\ K_{i,j}(x,t) \approx \Phi^T(t) K_{i,j} \Phi(x), \end{gathered} \tag{102}$$

where F_i, Y_j, and $K_{i,j}$ are defined in Section 4.3.2, and substituting (102) into (101), we have

$$\begin{gathered} \sum_{j=1}^{n} Y_j^T \Phi(x) = F_i^T \Phi(x) \\ + \sum_{j=1}^{n} \int_0^{mh} Y_j^T \Phi(t) \Phi^T(t) K_{i,j} \Phi(x)\, dt, \\ i = 1, 2, \ldots, n, \end{gathered} \tag{103}$$

$$\begin{gathered} \sum_{j=1}^{n} Y_j^T \Phi(x) = F_i^T \Phi(x) + \sum_{j=1}^{n} Y_j^T hIK_{i,j} \Phi(x), \\ i = 1, 2, \ldots, n, \end{gathered} \tag{104}$$

since

$$\int_0^{mh} \Phi(t) \Phi^T(t)\, dt = hI. \tag{105}$$

From (104), we get

$$\sum_{j=1}^{n} \left(I - hK_{i,j}^T\right) Y_j = F_i, \quad i = 1, 2, \ldots, n. \tag{106}$$

Set $A_{i,j} = I - hK_{i,j}^T$; then we have from (106)

$$\sum_{j=1}^{n} A_{i,j} Y_j = F_i, \quad i = 1, 2, \ldots, n \tag{107}$$

which is a linear system

$$\begin{pmatrix} A_{11} & A_{12} & \cdots & A_{1n} \\ A_{21} & A_{22} & \cdots & A_{2n} \\ \vdots & \vdots & & \vdots \\ A_{n1} & A_{n2} & \cdots & A_{nn} \end{pmatrix} \begin{pmatrix} Y_1 \\ Y_2 \\ \vdots \\ Y_n \end{pmatrix} = \begin{pmatrix} F_1 \\ F_2 \\ \vdots \\ F_n \end{pmatrix}. \tag{108}$$

After solving the above system we can find Y_j, $j = 1, 2, \ldots, n$ and hence obtain the solutions $y_j = \Phi^T Y_j$, $j = 1, 2, \ldots, n$.

5. Numerical Methods for Nonlinear Fredholm-Hammerstein Integral Equation

We consider the second kind nonlinear Fredholm integral equation of the following form:

$$\begin{gathered} u(x) = f(x) + \int_0^1 K(x,t) F(t, u(t))\, dt, \\ 0 \le x \le 1, \end{gathered} \tag{109}$$

where $K(x,t)$ is the kernel of the integral equation, $f(x)$ and $K(x,t)$ are known functions, and $u(x)$ is the unknown function that is to be determined.

5.1. B-Spline Wavelet Method. In this section, nonlinear Fredholm integral equation of second kind of the form given in (109) has been solved by using B-spline wavelets [11].

B-spline scaling and wavelet functions in the interval $[0,1]$ and function approximation have been defined in Sections 3.1.1 and 3.1.2, respectively.

First, we assume that

$$\begin{gathered} y(x) = F(x, u(x)), \\ 0 \le x \le 1. \end{gathered} \tag{110}$$

Now, from (16), we can approximate the functions $u(x)$ and $y(x)$ as

$$\begin{gathered} u(x) = A^T \Psi(x), \\ y(x) = B^T \Psi(x), \end{gathered} \tag{111}$$

where A and B are $(2^{M+1} + m - 1) \times 1$ column vectors similar to C defined in (17).

Again, by using dual of the wavelet functions, we can approximate the functions $f(x)$ and $K(x,t)$ as follows:

$$\begin{gathered} F(x) = D^T \widetilde{\Psi}(x), \\ K(x,t) = \widetilde{\Psi}^T(t) \Theta \widetilde{\Psi}(x), \end{gathered} \tag{112}$$

where

$$\Theta_{(i,j)} = \int_0^1 \left[\int_0^1 K(x,t) \Psi_i(t)\, dt\right] \Psi_j(x)\, dx. \tag{113}$$

From (110)–(112), we get

$$\begin{aligned} &\int_0^1 K(x,t) F(t, u(t))\, dt \\ &\quad = \int_0^1 B^T \Psi(t) \widetilde{\Psi}^T(t) \Theta \widetilde{\Psi}(x)\, dt \\ &\quad = B^T \left[\int_0^1 \Psi(t) \widetilde{\Psi}^T(t)\, dt\right] \Theta \widetilde{\Psi}(x) \\ &\quad = B^T \Theta \widetilde{\Psi}(x), \quad \text{since } \int_0^1 \Psi(t) \widetilde{\Psi}^T(t)\, dt = I. \end{aligned} \tag{114}$$

Applying (110)–(114) in (109), we get

$$A^T \Psi(x) = D^T \widetilde{\Psi}(x) + B^T \Theta \widetilde{\Psi}(x). \tag{115}$$

Multiplying (115) by $\Psi^T(x)$ both sides from the right and integrating both sides with respect to x from 0 to 1, we have

$$\begin{gathered} A^T P = D^T + B^T \Theta, \\ A^T P - D^T - B^T \Theta = 0, \end{gathered} \tag{116}$$

where P is a $(2^{M+1} + m - 1) \times (2^{M+1} + m - 1)$ square matrix given by

$$\begin{gathered} P = \int_0^1 \Psi(x) \Psi^T(x)\, dx = \begin{bmatrix} P_1 & \\ & P_2 \end{bmatrix}, \\ \int_0^1 \widetilde{\Psi}(x) \Psi^T(x)\, dx = I. \end{gathered} \tag{117}$$

Equation (116) gives a system of $(2^{M+1} + m - 1)$ algebraic equations with $2(2^{M+1} + m - 1)$ unknowns for A and B vectors given in (111).

To find the solution $u(x)$ in (111), we first utilize the following equation:

$$F\left(x, A^T \Psi(x)\right) = B^T \Psi(x), \tag{118}$$

with the collocation points $x_i = (i-1)/(2^{M+1} + m - 2)$, where $i = 1, 2, \ldots, 2^{M+1} + m - 1$.

Equation (118) gives a system of $(2^{M+1} + m - 1)$ algebraic equations with $2(2^{M+1} + m - 1)$ unknowns, for A and B vectors given in (111).

Combining (116) and (118), we have a total of $2(2^{M+1} + m - 1)$ system of algebraic equations with $2(2^{M+1} + m - 1)$ unknowns for A and B. Solving those equations for the unknown coefficients in the vectors A and B, we can obtain the solution $u(x) = A^T \Psi(x)$.

5.2. Quadrature Method Applied to Fredholm Integral Equation. In this section, Quadrature method has been applied to solve nonlinear Fredholm-Hammerstein integral equation [10].

The quadrature methods like Simpson rule and modified trapezoid method are applied for solving a definite integral as follows.

5.2.1. Simpson's Rule. One has

$$\begin{aligned} \int_a^b f(x)\, dx &= \sum_{i=1}^{n-1} \int_{x_{i-1}}^{x_{i+1}} f(x)\, dx \\ &= \frac{h}{3} f(a) + \frac{4h}{3} \sum_{i=1}^{n/2} f(x_{2i-1}) \\ &\quad + \frac{2h}{3} \sum_{i=1}^{(n-1)/2} f(x_{2i}) \\ &\quad + \frac{h}{3} f(b) \\ &\quad - \frac{(b-a)}{180} h^4 f^{(4)}(\eta). \end{aligned} \tag{119}$$

5.2.2. Modified Trapezoid Rule. One has

$$\begin{aligned} \int_a^b f(x)\, dx = \sum_{i=1}^{n} \int_{x_{i-1}}^{x_i} f(x)\, dx \\ = \frac{h}{2} f(a) + h \sum_{i=1}^{n-1} f(x_i) \\ + \frac{h}{2} f(b) \\ + \frac{h^2}{12} \left[f'(a) - f'(b) \right]. \end{aligned} \tag{120}$$

Consider the nonlinear Fredholm integral equation of second kind defined in (109) as follows:

$$\begin{gathered} u(x) = f(x) + \int_a^b K(x,t) F(u(t))\, dt, \\ a \le x \le b. \end{gathered} \tag{121}$$

For solving (121), we approximate the right-hand integral of (121) with Simpson's rule and modified trapezoid rule; then we get the following.

5.2.3. Simpson's Rule. One has

$$\begin{aligned} u(x) = f(x) & \\ + \frac{h}{3} \Bigg[& K(x, t_0) F(u_0) \\ & + 4 \sum_{j=1}^{n/2} K\left(x, t_{2j-1}\right) F\left(u_{2j-1}\right) \\ & + 2 \sum_{j=1}^{(n/2)-1} K\left(x, t_{2j}\right) F\left(u_{2j}\right) \\ & + K\left(x, t_n\right) F\left(u_n\right) \Bigg]. \end{aligned} \tag{122}$$

Hence, for $x = x_0, x_1, \ldots, x_n$ and $t = t_0, t_1, \ldots, t_n$ in (122), we have

$$\begin{aligned} u(x_i) = f(x_i) & \\ + \frac{h}{3} \Bigg[& K(x_i, t_0) F(u_0) \\ & + 4 \sum_{j=1}^{n/2} K\left(x_i, t_{2j-1}\right) F\left(u_{2j-1}\right) \end{aligned}$$

$$+2\sum_{j=1}^{(n/2)-1} K\left(x_i, t_{2j}\right) F\left(u_{2j}\right) + K\left(x_i, t_n\right) F\left(u_n\right) \Bigg]. \tag{123}$$

Equation (123) is a nonlinear system of equations and, by solving (123), we obtain the unknowns $u(x_i)$ for $i = 0, 1, \ldots, n$.

5.2.4. Modified Trapezoid Rule. One has

$$\begin{aligned} u(x) = f(x) &+ \frac{h}{2} K(x, t_0) F(u_0) \\ &+ h\sum_{j=1}^{n-1} K\left(x, t_j\right) F\left(u_j\right) \\ &+ \frac{h}{2} K(x, t_n) F(u_n) \\ &+ \frac{h^2}{12}\left[J(x, t_0) F(u_0) \right. \\ &\qquad + K(x, t_0) u_0' F'(u_0) \\ &\qquad - J(x, t_n) F(u_n) \\ &\qquad \left. - K(x, t_n) u_n' F'(u_n)\right], \end{aligned} \tag{124}$$

where $J(x, t) = \partial K(x, t)/\partial t$.

For $x = x_0, x_1, \ldots, x_n$ and $t = t_0, t_1, \ldots, t_n$ in (124), we have

$$\begin{aligned} u(x_i) = f(x_i) &+ \frac{h}{2} K(x_i, t_0) F(u_0) \\ &+ h\sum_{j=1}^{n-1} K\left(x_i, t_j\right) F\left(u_j\right) \\ &+ \frac{h}{2} K(x_i, t_n) F(u_n) \\ &+ \frac{h^2}{12}\left[J(x_i, t_0) F(u_0) \right. \\ &\qquad + K(x_i, t_0) u_0' F'(u_0) \\ &\qquad - J(x_i, t_n) F(u_n) \\ &\qquad \left. - K(x_i, t_n) u_n' F'(u_n)\right], \end{aligned} \tag{125}$$

for $i = 0, 1, \ldots, n$.

This is a system of $(n+1)$ equations and $(n+3)$ unknowns. By taking derivative from (121) and setting $H(x, t) = \partial K(x, t)/\partial x$, we obtain

$$u'(x) = f'(x) + \int_a^b H(x, t) F(u(t))\, dt, \qquad a \le x \le b. \tag{126}$$

If u is a solution of (121), then it is also solution of (126). By using trapezoid rule for (126) and replacing $x = x_i$, we get

$$\begin{aligned} u'(x_i) = f'(x_i) &+ \frac{h}{2} H(x_i, t_0) F(u_0) \\ &+ h\sum_{j=1}^{n-1} H\left(x_i, t_j\right) F\left(u_j\right) \\ &+ \frac{h}{2} H(x_i, t_n) F(u_n), \end{aligned} \tag{127}$$

for $i = 0, 1, \ldots, n$. In case of $i = 0, n$ from system (127), we obtain two equations.

Now (127) combined with (125) generates the nonlinear system of equations as follows:

$$\begin{aligned} u(x_i) = {} & \left(\frac{h}{2} K(x_i, t_0) + \frac{h^2}{12} J(x_i, t_0)\right) F(u_0) \\ &+ h\sum_{j=1}^{n-1} K\left(x_i, t_j\right) F\left(u_j\right) \\ &+ \left(\frac{h}{2} K(x_i, t_n) - \frac{h^2}{12} J(x_i, t_n)\right) F(u_n) \\ &+ \frac{h^2}{12}\left(K(x_i, t_0) u_0' F'(u_0) \right. \\ &\qquad \left. - K(x_i, t_n) u_n' F'(u_n)\right), \\ u'(x_0) = f'(x_0) &+ \frac{h}{2} H(x_0, t_0) F(u_0) \\ &+ h\sum_{j=1}^{n-1} H\left(x_0, t_j\right) F\left(u_j\right) \\ &+ \frac{h}{2} H(x_0, t_n) F(u_n), \end{aligned}$$

$$u'(x_n) = f'(x_n) + \frac{h}{2}H(x_n, t_0)F(u_0) + h\sum_{j=1}^{n-1} H(x_n, t_j)F(u_j) + \frac{h}{2}H(x_n, t_n)F(u_n). \quad (128)$$

By solving this system with $(n+3)$ nonlinear equations and $(n+3)$ unknowns, we can obtain the solution of (109).

5.3. Wavelet Galerkin Method. In this section, the continuous Legendre wavelets [12], constructed on the interval [0, 1], are applied to solve the nonlinear Fredholm integral equation of the second kind. The nonlinear part of the integral equation is approximated by Legendre wavelets, and the nonlinear integral equation is reduced to a system of nonlinear equations.

We have the following family of continuous wavelets with dilation parameter a and the translation parameter b

$$\psi_{a,b}(t) = |a|^{-1/2}\psi\left(\frac{t-b}{a}\right), \quad a, b \in R, \quad a \neq 0. \quad (129)$$

Legendre wavelets $\psi_{m,n}(t) = \psi(k, \hat{n}, m, t)$ have four arguments; $k = 2, 3, \ldots$, $\hat{n} = 2n - 1$, $n = 1, 2, \ldots, 2^{k-1}$, m is the order for Legendre polynomials and t is the normalized time.

Legendre wavelets are defined on [0, 1) by

$$\psi_{m,n}(t) = \begin{cases} \left(m+\frac{1}{2}\right)^{1/2} 2^{k/2} L_m\left(2^k t - \hat{n}\right), & \frac{\hat{n}-1}{2^k} \leq t < \frac{\hat{n}+1}{2^k}, \\ 0, & \text{otherwise}, \end{cases} \quad (130)$$

where $L_m(t)$ are the well-known Legendre polynomials of order m, which are orthogonal with respect to the weight function $w(t) = 1$ and satisfy the following recursive formula:

$$\begin{aligned} L_0(t) &= 1, \\ L_1(t) &= t, \\ L_{m+1}(t) &= \frac{2m+1}{m+1} t L_m(t) - \frac{m}{m+1} L_{m-1}(t), \quad m = 1, 2, 3, \ldots. \end{aligned} \quad (131)$$

The set of Legendre wavelets are an orthonormal set.

5.3.1. Function Approximation. A function $f(x) \in L^2[0, 1]$ can be expanded as

$$f(x) = \sum_{n=1}^{\infty}\sum_{m=0}^{\infty} c_{n,m}\psi_{n,m}(x), \quad (132)$$

where

$$c_{n,m} = \langle f(x), \psi_{n,m}(x)\rangle. \quad (133)$$

If the infinite series in (132) is truncated, then (132) can be written as

$$f(x) \approx \sum_{n=1}^{2^{k-1}}\sum_{m=0}^{M-1} c_{n,m}\psi_{n,m}(x) = C^T\Psi(x), \quad (134)$$

where C and $\Psi(x)$ are $2^{k-1}M \times 1$ matrices given by

$$C = [c_{1,0}, c_{1,1}, \ldots, c_{1,M-1}, c_{2,0}, \ldots, c_{2,M-1}, \ldots, c_{2^{k-1},0}, \ldots, c_{2^{k-1},M-1}]^T, \quad (135)$$

$$\Psi(x) = [\psi_{1,0}(x), \ldots, \psi_{1,M-1}(x), \psi_{2,0}(x), \ldots, \psi_{2,M-1}(x), \ldots, \psi_{2^{k-1},0}(x), \ldots, \psi_{2^{k-1},M-1}(x)]^T. \quad (136)$$

Similarly, a function $k(x,t) \in L^2([0,1] \times [0,1])$ can be approximated as

$$k(x,t) \approx \Psi^T(t) K \Psi(x), \quad (137)$$

where K is $(2^{k-1}M \times 2^{k-1}M)$ matrix, with

$$K_{i,j} = \langle\psi_i(t), \langle k(x,t), \psi_j(x)\rangle\rangle. \quad (138)$$

Also, the integer power of a function can be approximated as

$$[y(x)]^p = [Y^T\Psi(x)]^p = Y_p^{*T}\Psi(x), \quad (139)$$

where Y_p^* is a column vector, whose elements are nonlinear combinations of the elements of the vector Y. Y_p^* is called the operational vector of the pth power of the function $y(x)$.

5.3.2. The Operational Matrices. The integration of the vector $\Psi(x)$ defined in (136) can be obtained as

$$\int_0^t \Psi(t')\,dt' = P\Psi(t), \quad (140)$$

where P is the $(2^{k-1}M \times 2^{k-1}M)$ operational matrix for integration and is given in [23] as

$$P = \begin{bmatrix} L & H & \cdots & H & H \\ 0 & L & \cdots & H & H \\ \vdots & \vdots & \ddots & \vdots & \vdots \\ 0 & 0 & \cdots & L & H \\ 0 & 0 & \cdots & 0 & L \end{bmatrix}. \quad (141)$$

In (141), H and L are $(M \times M)$ matrices given in [23] as

$$H = \frac{1}{2^k}\begin{bmatrix} 2 & 0 & \cdots & 0 \\ 0 & 0 & \cdots & 0 \\ \vdots & \vdots & \ddots & \vdots \\ 0 & 0 & \cdots & 0 \end{bmatrix},$$

$$L = \frac{1}{2^k}\begin{bmatrix} 1 & \frac{1}{\sqrt{3}} & 0 & 0 & \cdots & 0 & 0 \\ -\frac{\sqrt{3}}{3} & 0 & \frac{\sqrt{3}}{3\sqrt{5}} & 0 & \cdots & 0 & 0 \\ 0 & -\frac{\sqrt{5}}{5\sqrt{3}} & 0 & \frac{\sqrt{5}}{5\sqrt{7}} & \cdots & 0 & 0 \\ 0 & 0 & -\frac{\sqrt{7}}{7\sqrt{5}} & 0 & \cdots & 0 & 0 \\ \vdots & \vdots & \vdots & \vdots & \ddots & & \vdots \\ 0 & 0 & 0 & 0 & \cdots & 0 & \frac{\sqrt{2M-3}}{(2M-3)\sqrt{2M-1}} \\ 0 & 0 & 0 & 0 & \cdots & \frac{-\sqrt{2M-1}}{(2M-1)\sqrt{2M-3}} & 0 \end{bmatrix}. \tag{142}$$

The integration of the product of two Legendre wavelets vector functions is obtained as

$$\int_0^1 \Psi(t)\Psi^T(t)\,dt = I, \tag{143}$$

where I is an identity matrix.

The product of two Legendre wavelet vector functions is defined as

$$\Psi(t)\Psi^T(t)C = \widetilde{C}^T\Psi(t), \tag{144}$$

where C is a vector given in (135) and $\widetilde{C}$ is $(2^{k-1}M \times 2^{k-1}M)$ matrix, which is called the product operation of Legendre wavelet vector functions [23, 24].

5.3.3. Solution of Fredholm Integral Equation of Second Kind. Consider the nonlinear Fredholm-Hammerstein integral equation of second kind of the form

$$y(x) = f(x) + \int_0^1 k(x,t)[y(t)]^p dt, \tag{145}$$

where $f \in L^2[0,1]$, $k \in L^2([0,1]\times[0,1])$, y is an unknown function, and p is a positive integer.

We can approximate the following functions as

$$\begin{aligned} f(x) &\approx F^T\Psi(x), \\ y(x) &\approx Y^T\Psi(x), \\ k(x,t) &\approx \Psi^T(t)K\Psi(x), \\ [y(x)]^p &\approx Y^{*T}\Psi(x). \end{aligned} \tag{146}$$

Substituting (146) into (145), we have

$$\begin{aligned} Y^T\Psi(x) &= F^T\Psi(x) \\ &\quad + \int_0^1 Y^{*T}\Psi(t)\Psi^T(t)K\Psi(x)\,dt \\ &= F^T\Psi(x) \\ &\quad + Y^{*T}\left(\int_0^1 \Psi(t)\Psi^T(t)\,dt\right)K\Psi(x) \\ &= F^T\Psi(x) + Y^{*T}K\Psi(x) \\ &= \left(F^T + Y^{*T}K\right)\Psi(x) \\ &\Longrightarrow Y^T - Y^{*T}K - F^T = 0. \end{aligned} \tag{147}$$

Equation (147) is a system of algebraic equations. Solving (147), we can obtain the solution $y(x) \approx Y^T\Psi(x)$.

5.4. Homotopy Perturbation Method. Consider the following nonlinear Fredholm integral equation of second kind of the form

$$u(x) = f(x) + \int_0^1 K(x,t)F(u(t))\,dt, \quad 0 \le x \le 1. \tag{148}$$

For solving (148) by Homotopy perturbation method (HPM) [14–16], we consider (148) as

$$L(u) = u(x) - f(x) - \int_0^1 K(x,t)F(u(t))\,dt = 0. \tag{149}$$

As a possible remedy, we can define $H(u,p)$ by

$$\begin{aligned} H(u,0) &= N(u), \\ H(u,1) &= L(u), \end{aligned} \tag{150}$$

where $N(u)$ is an integral operator with known solution u_0.

We may choose a convex homotopy by

$$H(u,p) = (1-p)N(u) + pL(u) = 0 \tag{151}$$

and continuously trace an implicitly defined curve from a starting point $H(u_0,0)$ to a solution function $H(U,1)$. The embedding parameter p monotonically increases from zero to unit as the trivial problem $L(u) = 0$. The embedding parameter $p \in (0,1]$ can be considered as an expanding parameter. The HPM uses the homotopy parameter p as an expanding parameter; that is,

$$u = u_0 + pu_1 + p^2u_2 + \cdots. \tag{152a}$$

When $p \to 1$, (152a) corresponding to (151) become the approximate solution of (149) as follows:

$$U = \lim_{p\to 1} u = u_0 + u_1 + u_2 + \cdots. \tag{152b}$$

The series in (152b) converges in most cases, and the rate of convergence depends on $L(u)$ [14].

Consider

$$N(u) = u(x) - f(x). \tag{153}$$

The nonlinear term $F(u)$ can be expressed in He polynomials [25] as

$$\begin{aligned} F(u) &= \sum_{m=0}^{\infty} p^m H_m(u_0,u_1,\ldots,u_m) \\ &= H_0(u_0) + pH_1(u_0,u_1) \\ &\quad + \cdots + p^m H_m(u_0,u_1,\ldots u_m) + \cdots, \end{aligned} \tag{154}$$

where

$$\begin{aligned} &H_m(u_0,u_1,\ldots,u_m) \\ &\quad = \frac{1}{m!}\frac{\partial^m}{\partial p^m}\left(F\left(\sum_{k=0}^{m} p^k u_k\right)\right)\Bigg|_{p=0}, \quad m \geq 0. \end{aligned} \tag{155}$$

Substituting (152a), (153), and (154) into (151), we have

$$\begin{aligned} &(1-p)((u_0 + pu_1 + \cdots) - f(x)) \\ &\quad + p\Bigg((u_0 + pu_1 + \cdots) - f(x) \\ &\qquad - \int_0^1 K(x,t)\sum_{m=0}^{\infty} p^m H_m(u_0,u_1,\ldots,u_m)\,dt\Bigg) = 0 \\ &\Longrightarrow (u_0 + pu_1 + \cdots) - f(x) \\ &\qquad - p\int_0^1 K(x,t)\sum_{m=0}^{\infty} p^m H_m(u_0,u_1,\ldots,u_m)\,dt = 0. \end{aligned} \tag{156}$$

Equating the terms with identical power of p in (156), we have

$$\begin{aligned} p^0 &: u_0(x) - f(x) = 0 \Longrightarrow u_0(x) = f(x) \\ p^1 &: u_1(x) - \int_0^1 K(x,t)H_0\,dt = 0 \Longrightarrow u_1(x) \\ &\quad = \int_0^1 K(x,t)H_0\,dt \\ p^2 &: u_2(x) - \int_0^1 K(x,t)H_1\,dt = 0 \Longrightarrow u_2(x) \\ &\quad = \int_0^1 K(x,t)H_1\,dt \\ &\ \ \vdots \end{aligned} \tag{157}$$

and in general form we have

$$\begin{aligned} u_0(x) &= f(x), \\ u_{n+1}(x) &= \int_0^1 K(x,t)H_n\,dt, \quad n = 0,1,2,\ldots. \end{aligned} \tag{158}$$

Hence, we can obtain the approximate solution of aforesaid equation (148) from (152b).

5.5. Adomian Decomposition Method. Adomian decomposition method (ADM) [16–18] has been applied to a wide class of functional equations. This method gives the solution as an infinite series usually converging to an accurate solution. Let us consider the nonlinear Fredholm integral equation of second kind as follows:

$$\begin{aligned} u(x) = f(x) + \int_a^b K(x,t)(Lu(t) + Nu(t))\,dt, \\ a \leq x \leq b, \end{aligned} \tag{159}$$

where $L(u(t))$ and $N(u(t))$ are the linear and nonlinear terms, respectively.

The Adomian decomposition method (ADM) consists of representing $u(x)$ as a series

$$u(x) = \sum_{m=0}^{\infty} u_m(x). \tag{160}$$

In the view of ADM, the nonlinear term Nu can be represented as

$$Nu = \sum_{n=0}^{\infty} A_n, \tag{161}$$

$$\text{where } A_n = \frac{1}{n!}\left(\frac{\partial^n}{\partial\lambda^n}N\left(\sum_{k=0}^{\infty}\lambda^k u_k\right)\right)\Bigg|_{\lambda=0}. \tag{162}$$

Now substituting (160) and (161) into (159), we have

$$\sum_{m=0}^{\infty} u_m(x) = f(x) + \int_a^b K(x,t)\left(L\left(\sum_{m=0}^{\infty} u_m(t)\right) + \sum_{m=0}^{\infty} A_m\right) dt, \tag{163}$$

and, then, ADM uses the recursive relations

$$u_0(x) = f(x),$$
$$u_m(x) = \int_a^b K(x,t)\left(L\left(u_{m-1}(t)\right) + A_{m-1}(t)\right) dt, \quad m \geq 1, \tag{164}$$

where A_m is so-called Adomian polynomial.

Therefore, we obtain the n-terms approximate solution as

$$\varphi_n = u_0 + u_1 + \cdots + u_n \tag{165}$$

with

$$u(x) = \lim_{n\to\infty} \varphi_n. \tag{166}$$

6. Conclusion and Discussion

In this work, we have examined many numerical methods to solve Fredholm integral equations. Using these methods except variational iteration method, the Fredholm integral equations have been reduced to a system of algebraic equations and this system can be easily solved by any usual methods. In this work, we have applied compactly supported semiorthogonal B-spline wavelets along with their dual wavelets for solving both linear and nonlinear Fredholm integral equations of second kind. The problem has been reduced to solve a system of algebraic equations. In order to increase the accuracy of the approximate solution, it is necessary to apply higher-order B-spline wavelet method. The method of moments based on compactly supported semiorthogonal B-spline wavelets via Galerkin method has been used to solve Fredholm integral equation of second kind. This method determines a strong reduction in the computation time and memory requirement in inverting the matrix. Variational iteration method has been successfully applied to find the approximate solution of Fredholm integral equation of both linear and nonlinear types. Taylor series expansion method reduces the system of integral equations to a linear system of ordinary differential equation. After including the required boundary conditions, this system reduces to a system of algebraic equations that can be solved easily. Block-Pulse functions and Haar wavelet method can be applied to the system of Fredholm integral equations by reducing into a system of algebraic equations. These methods give more accuracy if we increase their order. Quadrature method can be applied to solve the nonlinear Fredholm-Hammerstein integral equation of second kind by reducing it to a system of algebraic equations. Homotopy perturbation method (HPM) and Adomian decomposition method (ADM) can be also applied to approximate the solution of nonlinear Fredholm integral equation of second kind. The solutions obtained by HPM and ADM are applicable for not only weakly nonlinear equations, but also strong ones. The approximate solutions by these aforesaid methods highly agree with exact solutions.

References

[1] A.-M. Wazwaz, *Linear and Nonlinear Integral Equations: Methods and Applications*, Springer, New York, NY, USA, 2011.

[2] K. Maleknejad and M. N. Sahlan, “The method of moments for solution of second kind Fredholm integral equations based on B-spline wavelets,” *International Journal of Computer Mathematics*, vol. 87, no. 7, pp. 1602–1616, 2010.

[3] J.-H. He, “Variational iteration method—a kind of non-linear analytical technique: some examples,” *International Journal of Non-Linear Mechanics*, vol. 34, no. 4, pp. 699–708, 1999.

[4] J.-H. He, “Some asymptotic methods for strongly nonlinear equations,” *International Journal of Modern Physics B*, vol. 20, no. 10, pp. 1141–1199, 2006.

[5] J.-H. He, “Variational iteration method—some recent results and new interpretations,” *Journal of Computational and Applied Mathematics*, vol. 207, no. 1, pp. 3–17, 2007.

[6] K. Maleknejad, M. Shahrezaee, and H. Khatami, “Numerical solution of integral equations system of the second kind by block-pulse functions,” *Applied Mathematics and Computation*, vol. 166, no. 1, pp. 15–24, 2005.

[7] K. Maleknejad, N. Aghazadeh, and M. Rabbani, “Numerical solution of second kind Fredholm integral equations system by using a Taylor-series expansion method,” *Applied Mathematics and Computation*, vol. 175, no. 2, pp. 1229–1234, 2006.

[8] K. Maleknejad and F. Mirzaee, “Numerical solution of linear Fredholm integral equations system by rationalized Haar functions method,” *International Journal of Computer Mathematics*, vol. 80, no. 11, pp. 1397–1405, 2003.

[9] X.-Y. Lin, J.-S. Leng, and Y.-J. Lu, “A Haar wavelet solution to Fredholm equations,” in *Proceedings of the International Conference on Computational Intelligence and Software Engineering (CiSE ’09)*, pp. 1–4, Wuhan, China, December 2009.

[10] M. J. Emamzadeh and M. T. Kajani, “Nonlinear Fredholm integral equation of the second kind with quadrature methods,” *Journal of Mathematical Extension*, vol. 4, no. 2, pp. 51–58, 2010.

[11] M. Lakestani, M. Razzaghi, and M. Dehghan, “Solution of nonlinear Fredholm-Hammerstein integral equations by using semiorthogonal spline wavelets,” *Mathematical Problems in Engineering*, vol. 2005, no. 1, pp. 113–121, 2005.

[12] Y. Mahmoudi, “Wavelet Galerkin method for numerical solution of nonlinear integral equation,” *Applied Mathematics and Computation*, vol. 167, no. 2, pp. 1119–1129, 2005.

[13] J. Biazar and H. Ebrahimi, “Iteration method for Fredholm integral equations of second kind,” *Iranian Journal of Optimization*, vol. 1, pp. 13–23, 2009.

[14] D. D. Ganji, G. A. Afrouzi, H. Hosseinzadeh, and R. A. Talarposhti, “Application of homotopy-perturbation method to the second kind of nonlinear integral equations,” *Physics Letters A*, vol. 371, no. 1-2, pp. 20–25, 2007.

[15] M. Javidi and A. Golbabai, “Modified homotopy perturbation method for solving non-linear Fredholm integral equations,” *Chaos, Solitons and Fractals*, vol. 40, no. 3, pp. 1408–1412, 2009.

[16] S. Abbasbandy, "Numerical solutions of the integral equations: homotopy perturbation method and Adomian's decomposition method," *Applied Mathematics and Computation*, vol. 173, no. 1, pp. 493–500, 2006.

[17] E. Babolian, J. Biazar, and A. R. Vahidi, "The decomposition method applied to systems of Fredholm integral equations of the second kind," *Applied Mathematics and Computation*, vol. 148, no. 2, pp. 443–452, 2004.

[18] S. Abbasbandy and E. Shivanian, "A new analytical technique to solve Fredholm's integral equations," *Numerical Algorithms*, vol. 56, no. 1, pp. 27–43, 2011.

[19] J. C. Goswami, A. K. Chan, and C. K. Chui, "On solving first-kind integral equations using wavelets on a bounded interval," *IEEE Transactions on Antennas and Propagation*, vol. 43, no. 6, pp. 614–622, 1995.

[20] M. Lakestani, M. Razzaghi, and M. Dehghan, "Semiorthogonal spline wavelets approximation for fredholm integro-differential equations," *Mathematical Problems in Engineering*, vol. 2006, Article ID 96184, 12 pages, 2006.

[21] C. K. Chui, *An Introduction to Wavelets*, vol. 1 of *Wavelet Analysis and its Applications*, Academic Press, Boston, Mass, USA, 1992.

[22] J. C. Goswami and A. K. Chan, *Fundamentals of Wavelets*, John Wiley &; Sons, Hoboken, NJ, USA, 2nd edition, 2011.

[23] M. Razzaghi and S. Yousefi, "The Legendre wavelets operational matrix of integration," *International Journal of Systems Science*, vol. 32, no. 4, pp. 495–502, 2001.

[24] M. Razzaghi and S. Yousefi, "Legendre wavelets direct method for variational problems," *Mathematics and Computers in Simulation*, vol. 53, no. 3, pp. 185–192, 2000.

[25] A. Ghorbani, "Beyond Adomian polynomials: He polynomials," *Chaos, Solitons and Fractals*, vol. 39, no. 3, pp. 1486–1492, 2009.

Hindawi Publishing Corporation
Abstract and Applied Analysis
Volume 2013, Article ID 742643, 11 pages
http://dx.doi.org/10.1155/2013/742643

Research Article

Classification of Exact Solutions for Generalized Form of $K(m,n)$ Equation

Hasan Bulut

Department of Mathematics, Faculty of Science, Firat University, 23119 Elazig, Turkey

Correspondence should be addressed to Hasan Bulut; hbulut@firat.edu.tr

Received 24 May 2013; Revised 1 August 2013; Accepted 18 August 2013

Academic Editor: Santanu Saha Ray

The classification of exact solutions, including solitons and elliptic solutions, to the generalized $K(m,n)$ equation by the complete discrimination system for polynomial method has been obtained. From here, we find some interesting results for nonlinear partial differential equations with generalized evolution.

1. Introduction

In science and engineering applications, it is often very difficult to obtain analytical solutions of partial differential equations. Recently, many exact solutions of partial differential equations have been examined by the use of trial equation method. Also there are a lot of important methods that have been defined such as Hirota method, tanh-coth method, sine-cosine method, the trial equation method, and the extended trial equation method [1–15] to find exact solutions to nonlinear partial differential equations. There are a lot of nonlinear evolution equations that are solved by the use of various mathematical methods. Soliton solutions, singular solitons, and other solutions have been found by using these approaches. These obtained solutions have been encountered in various areas of applied mathematics and are very important.

In Section 2, we introduce an extended trial equation method for nonlinear evolution equations with higher order nonlinearity. In Section 3, as applications, we procure some exact solutions to nonlinear partial differential equations such as the generalized form of $K(m,n)$ equation [16–18]:

$$\left(q^l\right)_t + aq^m q_x + b(q^n)_{xxx} = 0, \tag{1}$$

where $a, b \in R$ are constants since l, m, and $n \in Z^+$. Here, the first term is the generalized evolution term, while the second term represents the nonlinear term and the third term is the dispersion term. This equation is the generalized form of the KdV equation, where, in particular, the case $l = m = n = 1$ leads to the KdV equation. The Korteweg de Vries equation is one of the most important equations in applied mathematics and physics. There have been several kinds of solutions, such as compactons, that are studied in the context of $K(m,n)$ equation, for various situations. We now offer a more general trial equation method for discussion as follows.

2. The Extended Trial Equation Method

Step 1. For a given nonlinear partial differential equation

$$P\left(u, u_t, u_x, u_{xx}, \ldots\right) = 0, \tag{2}$$

take the general wave transformation

$$u\left(x_1, x_2, \ldots, x_N, t\right) = u\left(\eta\right), \qquad \eta = \lambda\left(\sum_{j=1}^{N} x_j - ct\right), \tag{3}$$

where $\lambda \neq 0$ and $c \neq 0$. Substituting (3) into (2) yields a nonlinear ordinary differential equation:

$$N\left(u, u', u'', \ldots\right) = 0. \tag{4}$$

Step 2. Take the finite series and trial equation as follows:

$$u = \sum_{i=0}^{\delta} \tau_i \Gamma^i, \tag{5}$$

where

$$(\Gamma')^2 = \Lambda(\Gamma) = \frac{\Phi(\Gamma)}{\Psi(\Gamma)} = \frac{\xi_\theta\Gamma^\theta + \cdots + \xi_1\Gamma + \xi_0}{\zeta_\epsilon\Gamma^\epsilon + \cdots + \zeta_1\Gamma + \zeta_0}. \quad (6)$$

Using (5) and (6), we can write

$$\begin{aligned}(u')^2 &= \frac{\Phi(\Gamma)}{\Psi(\Gamma)}\left(\sum_{i=0}^{\delta} i\tau_i\Gamma^{i-1}\right)^2,\\ u'' &= \frac{\Phi'(\Gamma)\Psi(\Gamma) - \Phi(\Gamma)\Psi'(\Gamma)}{2\Psi^2(\Gamma)}\left(\sum_{i=0}^{\delta} i\tau_i\Gamma^{i-1}\right)\\ &\quad + \frac{\Phi(\Gamma)}{\Psi(\Gamma)}\left(\sum_{i=0}^{\delta} i(i-1)\tau_i\Gamma^{i-2}\right),\end{aligned} \quad (7)$$

where $\Phi(\Gamma)$ and $\Psi(\Gamma)$ are polynomials. Substituting these relations into (4) yields an equation of polynomial $\Omega(\Gamma)$ of Γ:

$$\Omega(\Gamma) = \varrho_s\Gamma^s + \cdots + \varrho_1\Gamma + \varrho_0 = 0. \quad (8)$$

According to the balance principle, we can find a relation of θ, ϵ, and δ. We can calculate some values of θ, ϵ, and δ.

Step 3. Letting the coefficients of $\Omega(\Gamma)$ all be zero will yield an algebraic equations system:

$$\varrho_i = 0, \quad i = 0, \ldots, s. \quad (9)$$

Solving this system, we will determine the values of $\xi_0, \ldots, \xi_\theta$; $\zeta_0, \ldots, \zeta_\epsilon$; and $\tau_0, \ldots, \tau_\delta$.

Step 4. Reduce (6) to the elementary integral form

$$\pm(\eta - \eta_0) = \int \frac{d\Gamma}{\sqrt{\Lambda(\Gamma)}} = \int \sqrt{\frac{\Psi(\Gamma)}{\Phi(\Gamma)}}d\Gamma. \quad (10)$$

Using a complete discrimination system for polynomial to classify the roots of $\Phi(\Gamma)$, we solve (10) and obtain the exact solutions to (4). Furthermore, we can write the exact traveling wave solutions to (2), respectively.

3. Application to the Generalized Form of $K(m,n)$ Equation

In order to look for travelling wave solutions of (1), we make the transformation $q(x,t) = u(\eta)$, $\eta = x - ct$, where c is the wave speed. Therefore it can be converted to the ODE

$$-c(u^l(\eta))' + \frac{a}{m+1}(u^{m+1}(\eta))' + b(u^n(\eta))''' = 0, \quad (11)$$

where prime denotes the derivative with respect to η. Then, integrating this equation with respect to η one time and setting the integration constant to zero, we obtain

$$-cu^l(\eta) + \frac{a}{m+1}u^{m+1}(\eta) + b(u^n(\eta))'' = 0. \quad (12)$$

Let $l = n$, applying balance and using the following transformation:

$$u = v^{1/(m-n+1)}. \quad (13)$$

Equation (12) turns into the following equation:

$$\begin{aligned}&-c(m+1)(m+1-n)^2v^2 + a(m+1-n)^2v^3\\ &\quad + bn(m+1)(2n-m-1)(v')^2\\ &\quad + bn(m+1)(m+1-n)vv'' = 0.\end{aligned} \quad (14)$$

Substituting (7) into (14) and using balance principle yield

$$\theta = \epsilon + \delta + 2. \quad (15)$$

After this solution procedure, we obtain the results as follows.

Case 1. If we take $\epsilon = 0$, $\delta = 1$, and $\theta = 3$, then

$$\begin{aligned}(v')^2 &= \frac{(\tau_1)^2(\xi_3\Gamma^3 + \xi_2\Gamma^2 + \xi_1\Gamma + \xi_0)}{\zeta_0},\\ v'' &= \frac{\tau_1(3\xi_3\Gamma^2 + 2\xi_2\Gamma + \xi_1)}{2\zeta_0},\end{aligned} \quad (16)$$

where $\xi_3 \neq 0$ and $\zeta_0 \neq 0$. Respectively, solving the algebraic equation system (9) yields

$$\begin{aligned}\xi_0 &= -\frac{\xi_1^2(3+3m-5n)(1+m+n)}{16\xi_2(1+m-2n)^2},\\ \xi_1 &= \xi_1, \qquad \xi_2 = \xi_2,\\ \xi_3 &= -\frac{8\xi_2^2(1+m-2n)(1+m-n)}{\xi_1(1+m+n)^2},\\ \tau_0 &= \tau_0, \qquad \tau_1 = -\frac{4(1+m-2n)\xi_2\tau_0}{(1+m+n)\xi_1},\\ \zeta_0 &= -\frac{bn\xi_2(1+m)}{a(1+m-n)\tau_0},\\ c &= \frac{an(5+5m-7n)\tau_0}{(1+m)(1+m-n)(1+m+n)}.\end{aligned} \quad (17)$$

Substituting these results into (6) and (10), we have

$$\pm(\eta-\eta_0)=\frac{A}{2}\int\frac{d\Gamma}{\sqrt{\Gamma^3-\dfrac{\xi_1(1+m+n)^2}{8\xi_2(1+m-2n)(1+m-n)}\Gamma^2-\dfrac{\xi_1^2(1+m+n)^2}{8\xi_2^2(1+m-2n)(1+m-n)}\Gamma+\dfrac{\xi_1^3(3+3m-5n)(1+m+n)^3}{128\xi_2^2(1+m-2n)^3(1+m-n)}}},\tag{18}$$

where

$$A=\sqrt{\frac{bn\xi_1(1+m)(1+m+n)^2}{2a\xi_2\tau_0(1+m-n)^2(1+m-2n)}}.\tag{19}$$

Integrating (18), we obtain the solutions to (1) as follows:

$$\begin{gathered}\pm(\eta-\eta_0)=-\frac{A}{\sqrt{\Gamma-\alpha_1}},\\ \pm(\eta-\eta_0)=\frac{A}{\sqrt{\alpha_2-\alpha_1}}\arctan\sqrt{\frac{\Gamma-\alpha_2}{\alpha_2-\alpha_1}},\quad \alpha_2>\alpha_1,\\ \pm(\eta-\eta_0)=\frac{A}{\sqrt{\alpha_1-\alpha_2}}\ln\left|\frac{\sqrt{\Gamma-\alpha_2}-\sqrt{\alpha_1-\alpha_2}}{\sqrt{\Gamma-\alpha_2}+\sqrt{\alpha_1-\alpha_2}}\right|,\quad \alpha_1>\alpha_2,\\ \pm(\eta-\eta_0)=-\frac{A}{\sqrt{\alpha_1-\alpha_3}}F(\varphi,l),\quad \alpha_1>\alpha_2>\alpha_3,\end{gathered}\tag{20}$$

where

$$F(\varphi,l)=\int_0^{\varphi}\frac{d\psi}{\sqrt{1-l^2\sin^2\psi}},\qquad \varphi=\arcsin\sqrt{\frac{\Gamma-\alpha_3}{\alpha_2-\alpha_3}},$$
$$l^2=\frac{\alpha_2-\alpha_3}{\alpha_1-\alpha_3}.\tag{21}$$

Also α_1, α_2, and α_3 are the roots of the polynomial equation

$$\Gamma^3+\frac{\xi_2}{\xi_3}\Gamma^2+\frac{\xi_1}{\xi_3}\Gamma+\frac{\xi_0}{\xi_3}=0.\tag{22}$$

Substituting solutions (20) into (5) and (13), we have

$$\begin{aligned}u(x,t)&=\Big[\tau_0+\tau_1\alpha_1+\Big(A^2\tau_1\Big(\Big(x-(an(5+5m-7n)\tau_0)\\&\qquad\times((1+m)(1+m-n)(1+m+n))^{-1}\\&\qquad\times t-\eta_0\Big)^2\Big)^{-1}\Big)\Big]^{1/(m-n+1)},\\
u(x,t)&=\Big[\tau_0+\tau_1\alpha_1+\tau_1(\alpha_2-\alpha_1)\\&\qquad\times\operatorname{sech}^2\Big(\frac{\sqrt{\alpha_2-\alpha_1}}{A}\Big(x-(an(5+5m-7n)\tau_0)\\&\qquad\times((1+m)(1+m-n)\\&\qquad\times(1+m+n))^{-1}\\&\qquad\times t-\eta_0\Big)\Big)\Big]^{1/(m-n+1)},\\
u(x,t)&=\Big[\tau_0+\tau_1\alpha_1+\tau_1(\alpha_1-\alpha_2)\\&\qquad\times\operatorname{cosech}^2\Big(\frac{\sqrt{\alpha_1-\alpha_2}}{2A}\Big(x-(an(5+5m-7n)\tau_0)\\&\qquad\times((1+m)(1+m-n)\\&\qquad\times(1+m+n))^{-1}\\&\qquad\times t-\eta_0\Big)\Big)\Big]^{1/(m-n+1)},\\
u(x,t)&=\Big[\tau_0+\tau_1\alpha_1+(\tau_1(\alpha_2-\alpha_1))\\&\qquad\times\Big(sn^2\Big(\pm\frac{\sqrt{\alpha_2-\alpha_1}}{A}\\&\qquad\times\Big(x-\frac{an(5+5m-7n)\tau_0}{(1+m)(1+m-n)(1+m+n)}\\&\qquad\times t-\eta_0\Big),\\&\qquad\frac{\alpha_1-\alpha_3}{\alpha_1-\alpha_2}\Big)\Big)^{-1}\Big]^{1/(m-n+1)}.\end{aligned}\tag{23}$$

If we take $\tau_0=-\tau_1\alpha_1$ and $\eta_0=0$, then solutions (23) can reduce to rational function solution

$$u(x,t)=\left(\frac{\widetilde{A}}{x-ct}\right)^{2/(m-n+1)},\tag{24}$$

1-soliton wave solution

$$u(x,t) = \frac{\widetilde{B}}{\cosh^{2/(m-n+1)}(B(x-ct))}, \tag{25}$$

singular soliton solution

$$u(x,t) = \frac{\widetilde{C}}{\sinh^{2/(m-n+1)}(C(x-ct))}, \tag{26}$$

and elliptic soliton solution

$$u(x,t) = \frac{\widetilde{B}}{sn^{2/(m-n+1)}(\varphi,l)}, \tag{27}$$

where $\widetilde{A} = A\sqrt{\tau_1}$, $\widetilde{B} = (\tau_1(\alpha_2-\alpha_1))^{1/(m-n+1)}$, $B = \sqrt{\alpha_2-\alpha_1}/A$, $\widetilde{C} = (\tau_1(\alpha_1-\alpha_2))^{1/(m-n+1)}$, $C = \sqrt{\alpha_1-\alpha_2}/2A$, $\varphi = \pm(\sqrt{\alpha_2-\alpha_1}/A)(x-ct)$, $l^2 = (\alpha_1-\alpha_3)/(\alpha_1-\alpha_2)$, and $c = an(5+5m-7n)\tau_1\alpha_1/(1+m)(1+m-n)(1+m+n)$. Here, $\widetilde{B}$ and $\widetilde{C}$ are the amplitudes of the solitons, while B and C are the inverse widths of the solitons and c is the velocity. Thus, we can say that the solitons exist for $\tau_1 > 0$.

Remark 1. If we choose the corresponding values for some parameters, solution (25) is in full agreement with solution (21) mentioned in [17].

Case 2. If we take $\epsilon = 0$, $\delta = 2$, and $\theta = 4$, then

$$(v')^2 = \frac{(\tau_1+2\tau_2\Gamma)^2(\xi_4\Gamma^4+\xi_3\Gamma^3+\xi_2\Gamma^2+\xi_1\Gamma+\xi_0)}{\zeta_0}, \tag{28}$$

where $\xi_4 \neq 0$ and $\zeta_0 \neq 0$. Respectively, solving the algebraic equation system (9) yields

$$\begin{gathered} \xi_0 = \xi_0, \qquad \xi_1 = \xi_1, \qquad \xi_2 = \frac{\xi_1^2}{3\xi_0}, \qquad \xi_3 = \frac{\xi_1^3}{24\xi_0^2}, \\ \xi_4 = \frac{\xi_1^4}{576\xi_0^3}, \qquad \zeta_0 = -\frac{bn(m+1)(m+n+1)\xi_1^3}{24a(m-n+1)^2\xi_0^2\tau_1}, \\ \tau_0 = \frac{2\xi_0\tau_1}{\xi_1}, \qquad \tau_1 = \tau_1, \qquad \tau_2 = \frac{\xi_1\tau_1}{12\xi_0}, \\ c = -\frac{2an\xi_0\tau_1}{(m+1)(m+n+1)\xi_1}. \end{gathered} \tag{29}$$

Substituting these resultss into (6) and (10), we get

$$\begin{aligned} &\pm(\eta-\eta_0) \\ &\quad = 2A_1 \int \Bigg((d\Gamma) \\ &\qquad \times \left(\Gamma^4 + \left(\frac{24\xi_0}{\xi_1}\right)\Gamma^3 + \left(\frac{192\xi_0^2}{\xi_1^2}\right)\Gamma^2 \right. \\ &\qquad \left. + \left(\frac{576\xi_0^3}{\xi_1^3}\right)\Gamma + \left(\frac{576\xi_0^4}{\xi_1^4}\right)\right)^{-1/2}\Bigg), \end{aligned} \tag{30}$$

where $A_1 = \sqrt{-6bn\xi_0(1+m)(1+m+n)/a\xi_1\tau_1(1+m-n)^2}$. Integrating (30), we obtain the solutions to (1) as follows:

$$\begin{aligned} \pm(\eta-\eta_0) &= -\frac{2A_1}{\Gamma-\alpha_1}, \\ \pm(\eta-\eta_0) &= \frac{4A_1}{\alpha_1-\alpha_2}\sqrt{\frac{\Gamma-\alpha_2}{\Gamma-\alpha_1}}, \quad \alpha_1 > \alpha_2, \\ \pm(\eta-\eta_0) &= \frac{2A_1}{\alpha_1-\alpha_2}\ln\left|\frac{\Gamma-\alpha_1}{\Gamma-\alpha_2}\right|, \\ \pm(\eta-\eta_0) & \\ &= \frac{4A_1}{\sqrt{(\alpha_1-\alpha_2)(\alpha_1-\alpha_3)}} \\ &\quad \times \ln\left|\frac{\sqrt{(\Gamma-\alpha_2)(\alpha_1-\alpha_3)}-\sqrt{(\Gamma-\alpha_3)(\alpha_1-\alpha_2)}}{\sqrt{(\Gamma-\alpha_2)(\alpha_1-\alpha_3)}+\sqrt{(\Gamma-\alpha_3)(\alpha_1-\alpha_2)}}\right|, \\ &\qquad \alpha_1 > \alpha_2 > \alpha_3, \\ \pm(\eta-\eta_0) &= \frac{4A_1}{\sqrt{(\alpha_1-\alpha_4)(\alpha_2-\alpha_3)}}F(\varphi,l), \\ &\qquad \alpha_1 > \alpha_2 > \alpha_3 > \alpha_4, \end{aligned} \tag{31}$$

where

$$\begin{aligned} \varphi_1 &= \arcsin\sqrt{\frac{(\Gamma-\alpha_2)(\alpha_1-\alpha_4)}{(\Gamma-\alpha_1)(\alpha_2-\alpha_4)}}, \\ l_1^2 &= \frac{(\alpha_1-\alpha_3)(\alpha_2-\alpha_4)}{(\alpha_2-\alpha_3)(\alpha_1-\alpha_4)}. \end{aligned} \tag{32}$$

Also α_1, α_2, α_3, and α_4 are the roots of the polynomial equation

$$\Gamma^4 + \frac{\xi_3}{\xi_4}\Gamma^3 + \frac{\xi_2}{\xi_4}\Gamma^2 + \frac{\xi_1}{\xi_4}\Gamma + \frac{\xi_0}{\xi_4} = 0. \tag{33}$$

Substituting solutions (31) into (5) and (13), we have

$$\begin{aligned} &u(x,t) \\ &\quad = \Bigg[\tau_0 + \tau_1\alpha_1 \pm (2\tau_1 A_1) \\ &\qquad \times \left(x + \frac{2an\xi_0\tau_1}{(m+1)(m+n+1)\xi_1}t - \eta_0\right)^{-1} \end{aligned}$$

$$+\tau_2\left(\alpha_1 \pm (2A_1) \times\left(x+\frac{2an\xi_0\tau_1}{(m+1)(m+n+1)\xi_1} \times t-\eta_0\right)^{-1}\right)^2\Bigg]^{1/(m-n+1)},$$

$$u(x,t) = \Bigg[\tau_0+\tau_1\alpha_1 + \left(16A_1^2(\alpha_2-\alpha_1)\tau_1\right) \times\left(16A_1^2-\left[(\alpha_1-\alpha_2) \times\left(x+\frac{2an\xi_0\tau_1}{(m+1)(m+n+1)\xi_1}t-\eta_0\right)\right]^2\right)^{-1}$$

$$+\tau_2\left(\alpha_1+\left(16A_1^2(\alpha_2-\alpha_1)\right) \times\left(16A_1^2-\left[(\alpha_1-\alpha_2) \times\left(x+\frac{2an\xi_0\tau_1}{(m+1)(m+n+1)\xi_1} \times t-\eta_0\right)\right]^2\right)^{-1}\right)^2\Bigg]^{1/(m-n+1)},$$

$$u(x,t) = \Bigg[\tau_0+\tau_1\alpha_2+\left((\alpha_2-\alpha_1)\tau_1\right) \times\left(\exp\left[\frac{\alpha_1-\alpha_2}{2A_1} \times\left(x+\frac{2an\xi_0\tau_1}{(m+1)(m+n+1)\xi_1}t-\eta_0\right)\right]-1\right)^{-1}$$

$$+\tau_2\left(\alpha_2+(\alpha_2-\alpha_1) \times\left(\exp\left[\frac{\alpha_1-\alpha_2}{2A_1} \times\left(x+\frac{2an\xi_0\tau_1}{(m+1)(m+n+1)\xi_1} \times t-\eta_0\right)\right]-1\right)^{-1}\right)^2\Bigg]^{1/(m-n+1)},$$

$$u(x,t) = \Bigg[\tau_0+\tau_1\alpha_1+\left((\alpha_1-\alpha_2)\tau_1\right) \times\left(\exp\left[\frac{\alpha_1-\alpha_2}{2A_1} \times\left(x+(2an\xi_0\tau_1) \times\left((m+1)(m+n+1)\xi_1\right)^{-1} \times t-\eta_0\right)\right]-1\right)^{-1}$$

$$+\tau_2\left(\alpha_1+(\alpha_1-\alpha_2) \times\left(\exp\left[\frac{\alpha_1-\alpha_2}{2A_1} \times\left(x+(2an\xi_0\tau_1) \times\left((m+1)(m+n+1)\xi_1\right)^{-1} \times t-\eta_0\right)\right]-1\right)^{-1}\right)^2\Bigg]^{1/(m-n+1)},$$

$$u(x,t) = \Bigg[\tau_0+\tau_1\alpha_1-\left(2(\alpha_1-\alpha_2)(\alpha_1-\alpha_3)\tau_1\right) \times\Bigg(2\alpha_1-\alpha_2-\alpha_3+(\alpha_3-\alpha_2) \times\cosh\left[\frac{\sqrt{(\alpha_1-\alpha_2)(\alpha_1-\alpha_3)}}{2A_1} \times\left(x+\frac{2an\xi_0\tau_1}{(m+1)(m+n+1)\xi_1} \times t-\eta_0\right)\right]\Bigg)^{-1}$$

$$+\tau_2\Bigg(\alpha_1-\left(2(\alpha_1-\alpha_2)(\alpha_1-\alpha_3)\right) \times\Bigg(2\alpha_1-\alpha_2-\alpha_3+(\alpha_3-\alpha_2)$$

$$
\begin{aligned}
&\times \cosh \left[\frac{\sqrt{(\alpha_1-\alpha_2)(\alpha_1-\alpha_3)}}{2A_1} \right. \\
&\quad \times \left(x + \frac{2an\xi_0\tau_1}{(m+1)(m+n+1)\xi_1} \right. \\
&\quad \left. \left. \left. \left. \left. \times t - \eta_0 \right) \right] \right) ^{-1} \right) ^{2} \right] ^{1/(m-n+1)},
\end{aligned}
$$

$$
\begin{aligned}
u(x,t) &= \left[\tau_0 + \tau_1\alpha_2 + \left((\alpha_1-\alpha_2)(\alpha_4-\alpha_2)\tau_1 \right) \right. \\
&\quad \times \left((\alpha_1-\alpha_4) \right. \\
&\quad \times sn^2 \left(\frac{\sqrt{(\alpha_1-\alpha_3)(\alpha_2-\alpha_4)}}{4A_1} \right. \\
&\quad \times \left(x + \frac{2an\xi_0\tau_1}{(m+1)(m+n+1)\xi_1} \times t - \eta_0 \right), \\
&\quad \left. \frac{(\alpha_2-\alpha_3)(\alpha_1-\alpha_4)}{(\alpha_1-\alpha_3)(\alpha_2-\alpha_4)} \right) \\
&\quad \left. + \alpha_4 - \alpha_2 \right)^{-1} \\
&\quad + \tau_2 \left(\alpha_2 + \left((\alpha_1-\alpha_2)(\alpha_4-\alpha_2)\tau_1 \right) \right. \\
&\quad \times \left((\alpha_1-\alpha_4) \right. \\
&\quad \times sn^2 \left(\frac{\sqrt{(\alpha_1-\alpha_3)(\alpha_2-\alpha_4)}}{4A_1} \right. \\
&\quad \times \left(x + \frac{2an\xi_0\tau_1}{(m+1)(m+n+1)\xi_1} \times t - \eta_0 \right), \\
&\quad \left. \frac{(\alpha_2-\alpha_3)(\alpha_1-\alpha_4)}{(\alpha_1-\alpha_3)(\alpha_2-\alpha_4)} \right) \\
&\quad \left. \left. \left. + \alpha_4 - \alpha_2 \right)^{-1} \right)^{2} \right]^{1/(m-n+1)}.
\end{aligned}
\tag{34}
$$

For simplicity, if we take $\eta_0 = 0$, then we can write solutions (34) as follows:

$$
\begin{aligned}
u(x,t) &= \left[\sum_{i=0}^{2} \tau_i \left(\alpha_1 \pm \frac{2A_1}{x-ct} \right)^i \right]^{1/(m-n+1)}, \\
u(x,t) &= \left[\sum_{i=0}^{2} \tau_i \left(\alpha_1 + \left(16A_1^2 (\alpha_1-\alpha_2) \right) \right. \right. \\
&\quad \left. \left. \times \left(16A_1^2 - \left[(\alpha_1-\alpha_2)(x-ct) \right]^2 \right)^{-1} \right)^i \right]^{1/(m-n+1)}, \\
u(x,t) &= \left[\sum_{i=0}^{2} \tau_i \left(\alpha_2 + \frac{\alpha_2-\alpha_1}{\exp\left[B_1(x-ct) \right] - 1} \right)^i \right]^{1/(m-n+1)}, \\
u(x,t) &= \left[\sum_{i=0}^{2} \tau_i \left(\alpha_1 + \frac{\alpha_1-\alpha_2}{\exp\left[B_1(x-ct) \right] - 1} \right)^i \right]^{1/(m-n+1)}, \\
u(x,t) &= \left[\sum_{i=0}^{2} \tau_i \left(\alpha_1 - \left(2(\alpha_1-\alpha_2)(\alpha_1-\alpha_3) \right) \right. \right. \\
&\quad \times \left(2\alpha_1 - \alpha_2 - \alpha_3 + (\alpha_3-\alpha_2) \right. \\
&\quad \left. \left. \left. \times \cosh\left[C_1 (x-ct) \right] \right)^{-1} \right)^i \right]^{1/(m-n+1)}, \\
u(x,t) &= \left[\sum_{i=0}^{2} \tau_i \left(\alpha_2 + \left((\alpha_1-\alpha_2)(\alpha_4-\alpha_2) \right) \right. \right. \\
&\quad \times \left((\alpha_1-\alpha_4)\, sn^2(\varphi, l) \right. \\
&\quad \left. \left. \left. + \alpha_4 - \alpha_2 \right)^{-1} \right)^i \right]^{1/(m-n+1)},
\end{aligned}
\tag{35}
$$

where $B_1 = (\alpha_1-\alpha_2)/2A_1$, $C_1 = \sqrt{(\alpha_1-\alpha_2)(\alpha_1-\alpha_3)}/2A_1$, $\varphi_1 = (\sqrt{(\alpha_1-\alpha_3)(\alpha_2-\alpha_4)}/4A_1)(x-ct)$, $l_1^2 = (\alpha_2-\alpha_3)(\alpha_1-\alpha_4)/(\alpha_1-\alpha_3)(\alpha_2-\alpha_4)$, and $c = -2an\xi_0\tau_1/(m+1)(m+n+1)\xi_1$. Here, A_1 is the amplitude of the soliton, while c is the velocity and B_1 and C_1 are the inverse widths of the solitons. Thus, we can say that the solitons exist for $\tau_1 > 0$.

Case 3. If we take $\epsilon = 0$, $\delta = 3$, and $\theta = 5$, then

$$\begin{aligned}(v')^2 &= \left(\tau_1 + 2\tau_2\Gamma + 3\tau_3\Gamma^2\right)^2 \\ &\quad\times\left(\xi_5\Gamma^5 + \xi_4\Gamma^4 + \xi_3\Gamma^3 + \xi_2\Gamma^2 + \xi_1\Gamma + \xi_0\right) \\ &\quad\times(\zeta_0)^{-1},\end{aligned} \tag{36}$$

where $\xi_5 \neq 0$ and $\zeta_0 \neq 0$. Respectively, solving the algebraic equation system (9) yields

$$\begin{gathered}\xi_0 = \frac{\xi_5\left(\tau_2^2 - 4\tau_1\tau_3\right)\left(2\tau_2^3 - 9\tau_1\tau_2\tau_3 + 2\sqrt{(\tau_2^2 - 3\tau_1\tau_3)^3}\right)}{81\tau_3^5}, \\ \xi_1 = \frac{\xi_5\left(4\tau_2^4 + 9\tau_1\tau_2^2\tau_3 - 108\tau_1^2\tau_3^2 + 4\tau_2\sqrt{(\tau_2^2 - 3\tau_1\tau_3)^3}\right)}{81\tau_3^4}, \\ \xi_2 = \frac{\xi_5\left(-11\tau_2^3 + 63\tau_1\tau_2\tau_3 - 2\sqrt{(\tau_2^2 - 3\tau_1\tau_3)^3}\right)}{27\tau_3^3}, \\ \xi_3 = \frac{\xi_5\left(\tau_2^2 + 7\tau_1\tau_3\right)}{3\tau_3^2}, \qquad \xi_4 = \frac{5\xi_5\tau_2}{3\tau_3}, \\ \zeta_0 = -\frac{9bn(m+1)(m+n+1)\xi_5}{2a\tau_3(m-n+1)^2}, \\ \tau_0 = -\frac{2\tau_2^3 - 9\tau_1\tau_2\tau_3 + 2\sqrt{(\tau_2^2 - 3\tau_1\tau_3)^3}}{27\tau_3^2}, \\ \tau_1 = \tau_1, \qquad \tau_2 = \tau_2, \\ \tau_3 = \tau_3, \qquad \xi_5 = \xi_5, \\ c = -\frac{8an\sqrt{(\tau_2^2 - 3\tau_1\tau_3)^3}}{27(m+1)(m+n+1)\tau_3^2}.\end{gathered} \tag{37}$$

Substituting these results into (6) and (10), we get

$$\begin{aligned}&\pm(\eta - \eta_0) \\ &= 3A_2\int\left((d\Gamma)\right. \\ &\qquad\times\left(\Gamma^5 + \frac{\xi_4}{\xi_5}\Gamma^4 + \frac{\xi_3}{\xi_5}\Gamma^3\right. \\ &\qquad\left.\left.+\frac{\xi_2}{\xi_5}\Gamma^2 + \frac{\xi_1}{\xi_5}\Gamma + \frac{\xi_0}{\xi_5}\right)^{-1/2}\right),\end{aligned} \tag{38}$$

where $A_2 = \sqrt{-bn(1+m)(1+m+n)/2a\tau_3(1+m-n)^2}$. Integrating (38), we obtain the solutions to (1) as follows:

$$\begin{aligned}\pm(\eta - \eta_0) &= -\frac{2A_2}{\sqrt{(\Gamma - \alpha_1)^3}}, \\ \pm(\eta - \eta_0) &= \frac{3A_2\operatorname{arctanh}\left[\sqrt{(\Gamma - \alpha_2)/(\alpha_1 - \alpha_2)}\right]}{(\alpha_1 - \alpha_2)^{3/2}} \\ &\quad - \frac{3A_2\sqrt{\Gamma - \alpha_2}}{(\alpha_1 - \alpha_2)(\Gamma - \alpha_1)}, \quad \alpha_1 > \alpha_2, \\ \pm(\eta - \eta_0) &= -\frac{6A_2\arctan\left[\sqrt{(\Gamma - \alpha_1)/(\alpha_1 - \alpha_2)}\right]}{(\alpha_1 - \alpha_2)^{3/2}} \\ &\quad - \frac{6A_2}{\sqrt{\Gamma - \alpha_1}(\alpha_1 - \alpha_2)}, \\ \pm(\eta - \eta_0) &= \frac{6A_2\operatorname{arctanh}\left[\sqrt{(\Gamma - \alpha_3)/(\alpha_2 - \alpha_3)}\right]}{\alpha_1 - \alpha_2} \\ &\quad\times\left(\frac{1}{\sqrt{\alpha_2 - \alpha_3}} - \frac{1}{\sqrt{\alpha_1 - \alpha_3}}\right), \\ &\qquad \alpha_1 > \alpha_2 > \alpha_3, \\ &\pm(\eta - \eta_0) \\ &\quad = \frac{-6A_2}{\sqrt{\Gamma - \alpha_1}(\alpha_1 - \alpha_2)(\alpha_1 - \alpha_3)} \\ &\quad\times\left[\sqrt{(\Gamma - \alpha_2)(\Gamma - \alpha_3)} + i\left(E(\varphi, l) - F(\varphi, l)\right)\right],\end{aligned} \tag{39}$$

where

$$\begin{gathered}E(\varphi, l) = \int_0^{\varphi}\sqrt{1 - l^2\sin^2\psi}\,d\psi, \\ \varphi_2 = -\arcsin\sqrt{\frac{\Gamma - \alpha_1}{\alpha_2 - \alpha_1}}, \\ l_2^2 = \frac{\alpha_1 - \alpha_2}{\alpha_1 - \alpha_3},\end{gathered} \tag{40}$$

$$\begin{aligned}&\pm(\eta - \eta_0) \\ &\quad = \frac{-6iA_2}{\sqrt{\alpha_2 - \alpha_3}(\alpha_1 - \alpha_2)}\left(F(\varphi, l) - \pi(\varphi, n, l)\right), \\ &\qquad \alpha_1 > \alpha_2 > \alpha_3 > \alpha_4,\end{aligned}$$

where

$$\begin{gathered}\varphi_3 = -\arcsin\sqrt{\frac{\alpha_3 - \alpha_2}{\Gamma - \alpha_2}}, \qquad l_3^2 = \frac{\alpha_2 - \alpha_4}{\alpha_2 - \alpha_3}, \\ n = \frac{\alpha_2 - \alpha_1}{\alpha_2 - \alpha_3}.\end{gathered} \tag{41}$$

Also α_1, α_2, α_3, α_4, and α_5 are the roots of the polynomial equation

$$\Gamma^5+\frac{\xi_4}{\xi_5}\Gamma^4+\frac{\xi_3}{\xi_5}\Gamma^3+\frac{\xi_2}{\xi_5}\Gamma^2+\frac{\xi_1}{\xi_5}\Gamma+\frac{\xi_0}{\xi_5}=0. \tag{42}$$

Case 4. If we take $\epsilon=1$, $\delta=1$, and $\theta=4$, then

$$\left(v'\right)^2=\frac{\tau_1^2\left(\xi_4\Gamma^4+\xi_3\Gamma^3+\xi_2\Gamma^2+\xi_1\Gamma+\xi_0\right)}{\zeta_0+\zeta_1\Gamma}, \tag{43}$$

where $\xi_4\neq 0$ and $\zeta_1\neq 0$. Respectively, solving the algebraic equation system (9) yields

$$\begin{aligned}
\xi_0&=\frac{\zeta_0\tau_0^2\left(M+2a(1+m-n)^2\left(2\zeta_1\tau_0+\zeta_0\tau_1\right)\right)}{bn\,(1+m)\,(1+m+n)\,\zeta_1\tau_1^2},\\
\xi_3&=\xi_3,\\
\xi_4&=-\frac{2a(1+m-n)^2\zeta_1\tau_1}{bn\,(1+m)\,(1+m+n)},\\
\xi_1&=\left(\tau_0\left(4a(1+m-n)^2\zeta_1^2\tau_0^2\right.\right.\\
&\qquad+2\zeta_0\tau_1\left(M+2a(1+m-n)^2\zeta_0\tau_1\right)\\
&\qquad\left.\left.+\zeta_1\tau_0\left(M+8a(1+m-n)^2\zeta_0\tau_1\right)\right)\right)\\
&\quad\times\left(bn\,(1+m)\,(1+m+n)\,\zeta_1\tau_1^2\right)^{-1},\\
\xi_2&=\left(6a(1+m-n)^2\zeta_1^2\tau_0^2\right.\\
&\quad+2\zeta_1\tau_0\left(M+2a(1+m-n)^2\zeta_0\tau_1\right)\\
&\quad\left.+\zeta_0\tau_1\left(M+2a(1+m-n)^2\zeta_0\tau_1\right)\right)\\
&\quad\times\left(bn\,(1+m)\,(1+m+n)\,\zeta_1\tau_1^2\right)^{-1},\\
\zeta_0&=\zeta_0,\qquad \zeta_1=\zeta_1,\\
\tau_0&=\tau_0,\qquad \tau_1=\tau_1,\\
c&=\frac{n\left(M+2a(1+m-n)^2\left(3\zeta_1\tau_0+\zeta_0\tau_1\right)\right)}{(1+m)\,(1+m+n)\,(1+m-n)^2\zeta_1},
\end{aligned} \tag{44}$$

where $M=bn(1+m)(1+m+n)\xi_3$. Substituting these results into (6) and (10), we get

$$\begin{aligned}
&\pm\left(\eta-\eta_0\right)\\
&\quad=A_3\int\left(\left(\Gamma+\frac{\zeta_0}{\zeta_1}\right)\right.\\
&\qquad\times\left(\Gamma^4+\left(\frac{\xi_3}{\xi_4}\right)\Gamma^3+\left(\frac{\xi_2}{\xi_4}\right)\Gamma^2\right.\\
&\qquad\left.\left.+\left(\frac{\xi_1}{\xi_4}\right)\Gamma+\left(\frac{\xi_0}{\xi_4}\right)\right)^{-1}\right)^{1/2}d\Gamma,
\end{aligned} \tag{45}$$

where $A_3=\sqrt{bn(1+m)(1+m+n)/2a\tau_1(1+m-n)^2}$. Integrating (45), we obtain the solution to (1) as follows:

$$\begin{aligned}
\pm\left(\eta-\eta_0\right)&=-A_3\sqrt{\frac{\zeta_1}{\zeta_0+\zeta_1\alpha_1}}\\
&\quad\times\operatorname{arctanh}\left[\sqrt{\frac{\zeta_0+\zeta_1\Gamma}{\zeta_0+\zeta_1\alpha_1}}\right]\\
&\quad-\frac{A_3}{\Gamma-\alpha_1}\sqrt{\frac{\zeta_0+\zeta_1\,\Gamma}{\zeta_1}},\\
\pm\left(\eta-\eta_0\right)&=\frac{2A_3}{\alpha_1-\alpha_2}\\
&\quad\times\left(-\sqrt{\frac{\zeta_0+\zeta_1\,\alpha_1}{\zeta_1}}\right.\\
&\qquad\times\operatorname{arctanh}\left[\sqrt{\frac{\zeta_0+\zeta_1\,\Gamma}{\zeta_0+\zeta_1\,\alpha_1}}\right]\\
&\qquad+\sqrt{\zeta_0+\zeta_1\alpha_2}\\
&\qquad\left.\times\operatorname{arctanh}\left[\sqrt{\frac{\zeta_0+\zeta_1\,\Gamma}{\zeta_0+\zeta_1\,\alpha_2}}\right]\right),\\
\pm\left(\eta-\eta_0\right)&=2A_3\\
&\quad\times\left(\sqrt{\frac{\left(\Gamma-\alpha_1\right)\left(\zeta_0+\zeta_1\quad\Gamma\right)}{\zeta_1(\Gamma-\alpha_2\ )^2}}\right.\\
&\qquad\left.+i\sqrt{\alpha_1-\alpha_2}\left(E\left(\varphi,l\right)-F\left(\varphi,l\right)\right)\right),
\end{aligned} \tag{46}$$

where

$$\begin{aligned}
\varphi_4&=-\arcsin\sqrt{\frac{\zeta_1\left(\alpha_1-\Gamma\right)}{\zeta_0+\zeta_1\alpha_1}},\\
l_4^2&=\frac{\zeta_0+\zeta_1\alpha_1}{\zeta_1\left(\alpha_1-\alpha_2\right)},\\
\pm\left(\eta-\eta_0\right)&=\frac{-2A_3}{\sqrt{\alpha_2-\alpha_1}}E\left(\varphi,l\right),
\end{aligned} \tag{47}$$

where

$$\begin{aligned}
\varphi_5&=\arcsin\left[\sqrt{\frac{\alpha_2-\alpha_1}{\Gamma-\alpha_1}}\right],\\
l_5^2&=\frac{\zeta_0+\zeta_1\alpha_1}{\zeta_1\left(\alpha_1-\alpha_2\right)},\\
\pm\left(\eta-\eta_0\right)&=\frac{-2iA_3}{\left(\alpha_1-\alpha_2\right)\sqrt{\zeta_1\left(\zeta_0+\zeta_1\alpha_2\right)}}
\end{aligned}$$

$$\times\left(\zeta_0\left(F(\varphi,l)-\pi(\varphi,n,l)\right)+\zeta_1\left(\alpha_2F(\varphi,l)-\alpha_2\pi(\varphi,n,l)\right)\right), \tag{48}$$

where

$$\varphi_6=-\arcsin\sqrt{\frac{\zeta_0+\zeta_1\alpha_2}{\zeta_1(\alpha_2-\Gamma)}},$$
$$l_6^2=\frac{\zeta_1(\alpha_2-\alpha_3)}{\zeta_0+\zeta_1\alpha_2},\qquad n_1=\frac{\zeta_1(\alpha_2-\alpha_1)}{\zeta_0+\zeta_1\alpha_2}. \tag{49}$$

Case 5. If we take $\epsilon=1$, $\delta=2$, and $\theta=5$, then

$$(v')^2=\frac{(\tau_1+2\tau_2\Gamma)^2\left(\xi_5\Gamma^5+\xi_4\Gamma^4+\xi_3\Gamma^3+\xi_2\Gamma^2+\xi_1\Gamma+\xi_0\right)}{\zeta_0+\zeta_1\Gamma}, \tag{50}$$

where $\xi_5\neq0$ and $\zeta_1\neq0$. Respectively, solving the algebraic equation system (9) yields

$$\begin{gathered}
\xi_0=\frac{\tau_0^2(-2\xi_5\tau_1+\xi_4\tau_2)}{\tau_2^3},\\
\xi_1=\frac{\tau_0\left(2\xi_4\tau_1\tau_2+\xi_5\left(-4\tau_1^2+\tau_0\tau_2\right)\right)}{\tau_2^3},\\
\xi_2=\frac{\xi_4\tau_2\left(\tau_1^2+2\tau_0\tau_2\right)-2\xi_5\left(\tau_1^3+\tau_0\tau_1\tau_2\right)}{\tau_2^3},\\
\xi_3=\frac{-3\xi_5\tau_1^2+2\tau_2(\xi_5\tau_0+\xi_4\tau_1)}{\tau_2^2},\\
\zeta_0=\frac{-2bn(1+m)(1+m+n)(\xi_4\tau_2-2\xi_5\tau_1)}{a(1+m-n)^2\tau_2^2},\\
\zeta_1=\frac{-2bn(1+m)(1+m+n)\xi_5}{a(1+m-n)^2\tau_2^2},\\
\xi_4=\xi_4,\qquad \xi_5=\xi_5,\\
\tau_0=\tau_0,\qquad \tau_1=\tau_1,\qquad \tau_2=\tau_2,\\
c=-\frac{an\left(\tau_1^2-4\tau_0\tau_2\right)}{2(1+m)(1+m+n)\tau_2}.
\end{gathered} \tag{51}$$

Substituting these results into (6) and (10), we get

$$\pm(\eta-\eta_0)=A_4\times\int\left(\left(\Gamma+\frac{\zeta_0}{\zeta_1}\right)\times\left(\Gamma^5+\frac{\xi_4}{\xi_5}\Gamma^4+\frac{\xi_3}{\xi_5}\Gamma^3+\frac{\xi_2}{\xi_5}\Gamma^2+\frac{\xi_1}{\xi_5}\Gamma+\frac{\xi_0}{\xi_5}\right)^{-1}\right)^{1/2}d\Gamma, \tag{52}$$

where $A_4=\sqrt{-2bn(1+m)(1+m+n)/a\tau_2^2(1+m-n)^2}$. Integrating (52), we obtain the solution to (1) as follows:

$$\pm(\eta-\eta_0)=\frac{-2A_4}{3\sqrt{\zeta_1}(\zeta_0+\zeta_1\alpha_1)}\left(\frac{\zeta_0+\zeta_1\Gamma}{\Gamma-\alpha_1}\right)^{3/2},$$

$$\begin{aligned}
\pm(\eta-\eta_0)&=\frac{-A_4(\zeta_0+\zeta_1\alpha_2)}{2(\alpha_1-\alpha_2)^{3/2}\sqrt{\zeta_1(\zeta_0+\zeta_1\alpha_1)}}\\
&\quad\times\ln\Big|(\Gamma-\alpha_1)\\
&\quad\times\Big(\zeta_0(\Gamma+\alpha_1-2\alpha_2)+2\sqrt{(\zeta_0+\zeta_1\Gamma)(\zeta_0+\zeta_1\alpha_1)(\Gamma-\alpha_2)(\alpha_1-\alpha_2)}\\
&\quad+\zeta_1(2\Gamma\alpha_1-\alpha_2(\Gamma+\alpha_1))\Big)^{-1}\Big|\\
&\quad-\frac{A_4}{(\alpha_1-\alpha_2)(\Gamma-\alpha_1)}\sqrt{\frac{(\zeta_0+\zeta_1\Gamma)(\Gamma-\alpha_2)}{\zeta_1}},\qquad\alpha_1>\alpha_2,
\end{aligned}$$

$$\begin{aligned}
\pm(\eta-\eta_0)&=\frac{-2A_4}{(\alpha_1-\alpha_2)}\sqrt{\frac{\zeta_0+\zeta_1\Gamma}{\zeta_1(\Gamma-\alpha_1)}}\\
&\quad-\frac{2A_4}{(\alpha_1-\alpha_2)^{3/2}}\sqrt{\frac{\zeta_0+\zeta_1\alpha_2}{\zeta_1}}\\
&\quad\times\arctan\left[\sqrt{\frac{(\Gamma-\alpha_1)(\zeta_0+\zeta_1\alpha_2)}{(\alpha_1-\alpha_2)(\zeta_0+\zeta_1\Gamma)}}\right],
\end{aligned}$$

$$\begin{aligned}
\pm(\eta-\eta_0)&=\frac{-A_4}{\alpha_1-\alpha_3}\sqrt{\frac{\zeta_0+\zeta_1\alpha_2}{\zeta_1(\alpha_2-\alpha_3)}}\\
&\quad\times\ln\Big|(\alpha_2-\Gamma)\\
&\quad\times\Big(\zeta_0(\Gamma+\alpha_2-2\alpha_3)+2\sqrt{(\zeta_0+\zeta_1\Gamma)(\zeta_0+\zeta_1\alpha_2)(\Gamma-\alpha_3)(\alpha_2-\alpha_3)}\\
&\quad+\zeta_1(2\Gamma\alpha_2-\alpha_3(\Gamma+\alpha_2))\Big)^{-1}\Big|\\
&\quad-\frac{A_4}{\alpha_1-\alpha_3}\\
&\quad\times\sqrt{\frac{\zeta_0+\zeta_1\alpha_1}{\zeta_1(\alpha_1-\alpha_3)}}\\
&\quad\times\ln\Big|\Big(\zeta_0(\Gamma+\alpha_1-2\alpha_3)\\
&\quad+2\sqrt{(\zeta_0+\zeta_1\Gamma)(\zeta_0+\zeta_1\alpha_1)(\Gamma-\alpha_3)(\alpha_1-\alpha_3)}
\end{aligned}$$

$$
\begin{aligned}
&+\zeta_1\left(2\Gamma\alpha_1-\alpha_3\left(\Gamma+\alpha_1\right)\right)) \\
&\times\left(\Gamma-\alpha_2\right)^{-1}\Big|, \quad \alpha_1>\alpha_2>\alpha_3, \\
\pm\left(\eta-\eta_0\right) &= \frac{-2A_4}{\alpha_1-\alpha_3} \\
&\times\sqrt{\frac{\zeta_0+\zeta_1\alpha_3}{\zeta_1\left(\alpha_1-\alpha_2\right)}}E\left(\varphi,l\right), \\
&\alpha_1>\alpha_2>\alpha_3,
\end{aligned} \tag{53}
$$

where

$$
\begin{aligned}
\varphi_7 &= \arcsin\sqrt{\frac{\left(\Gamma-\alpha_3\right)\left(\alpha_2-\alpha_1\right)}{\left(\Gamma-\alpha_1\right)\left(\alpha_2-\alpha_3\right)}}, \\
l_7^2 &= \frac{\left(\alpha_3-\alpha_2\right)\left(\zeta_0+\zeta_1\alpha_1\right)}{\left(\alpha_1-\alpha_2\right)\left(\zeta_0+\zeta_1\alpha_3\right)}, \\
\pm&\left(\eta-\eta_0\right) \\
&= \frac{2A_4\left(\alpha_2-\alpha_4\right)}{\left(\alpha_1-\alpha_2\right)\left(\alpha_3-\alpha_4\right)\sqrt{\zeta_1\left(\alpha_2-\alpha_3\right)\left(\zeta_0+\zeta_1\alpha_4\right)}} \\
&\times\left(\frac{\left(\zeta_0+\zeta_1\Gamma\right)\left(\alpha_3-\alpha_4\right)}{\alpha_1-\alpha_2}\pi\left(\varphi,n,l\right)\right. \\
&\left.+\frac{\left(\zeta_0+\zeta_1\alpha_2\right)\left(\alpha_4-\alpha_3\right)}{\alpha_2-\alpha_4}F\left(\varphi,l\right)\right),
\end{aligned} \tag{54}
$$

where

$$
\begin{aligned}
\varphi_8 &= \arcsin\sqrt{\frac{\left(\Gamma-\alpha_3\right)\left(\alpha_2-\alpha_1\right)}{\left(\Gamma-\alpha_1\right)\left(\alpha_2-\alpha_3\right)}}, \\
l_8^2 &= \frac{\left(\alpha_3-\alpha_2\right)\left(\zeta_0+\zeta_1\alpha_1\right)}{\left(\alpha_1-\alpha_2\right)\left(\zeta_0+\zeta_1\alpha_3\right)}, \\
n_2 &= -\frac{\left(\alpha_1-\alpha_2\right)\left(\alpha_3-\alpha_4\right)}{\left(\alpha_2-\alpha_3\right)\left(\alpha_1-\alpha_4\right)}, \\
&\alpha_1>\alpha_2>\alpha_3>\alpha_4.
\end{aligned} \tag{55}
$$

4. Discussion

Thus we introduce a more general extended trial equation method for nonlinear partial differential equations as follows.

Step 1. Extended trial equation (6) can be reduced to the following more general form:

$$
u=\frac{A\left(\Gamma\right)}{B\left(\Gamma\right)}=\frac{\sum_{i=0}^{\delta}\tau_i\Gamma^i}{\sum_{j=0}^{\mu}\omega_j\Gamma^j}, \tag{56}
$$

where

$$
\left(\Gamma'\right)^2=\Lambda\left(\Gamma\right)=\frac{\Phi\left(\Gamma\right)}{\Psi\left(\Gamma\right)}=\frac{\xi_\theta\Gamma^\theta+\cdots+\xi_1\Gamma+\xi_0}{\zeta_\epsilon\Gamma^\epsilon+\cdots+\zeta_1\Gamma+\zeta_0}. \tag{57}
$$

Here, τ_i $(i=0,\ldots,\delta)$, ω_j $(j=0,\ldots,\mu)$, ξ_ς $(\varsigma=0,\ldots,\theta)$, and ζ_σ $(\sigma=0,\ldots,\epsilon)$ are the constants to be specified.

Step 2. Taking trial equations (56) and (57), we derive the following equations:

$$
\left(u'\right)^2=\frac{\Phi\left(\Gamma\right)}{\Psi\left(\Gamma\right)}\frac{\left(A'\left(\Gamma\right)B\left(\Gamma\right)-A\left(\Gamma\right)B'\left(\Gamma\right)\right)^2}{B^4\left(\Gamma\right)}, \tag{58}
$$

$$
\begin{aligned}
u'' &= \left(A'\left(\Gamma\right)B\left(\Gamma\right)-A\left(\Gamma\right)B'\left(\Gamma\right)\right) \\
&\times\left\{\left(\Phi'\left(\Gamma\right)\Psi\left(\Gamma\right)-\Phi\left(\Gamma\right)\Psi'\left(\Gamma\right)\right)B\left(\Gamma\right)\right. \\
&\quad\left.-4\Phi\left(\Gamma\right)\Psi\left(\Gamma\right)B'\left(\Gamma\right)\right\} \\
&+2\Phi\left(\Gamma\right)\Psi\left(\Gamma\right)B\left(\Gamma\right)\left(A''\left(\Gamma\right)B\left(\Gamma\right)-A\left(\Gamma\right)B''\left(\Gamma\right)\right) \\
&\times\left(2B^3\left(\Gamma\right)\Psi^2\left(\Gamma\right)\right)^{-1}
\end{aligned} \tag{59}
$$

and other derivation terms such as u'''.

Step 3. Substituting u', u'', and other derivation terms into (5) yields the following equation:

$$
\Omega\left(\Gamma\right)=\varrho_s\Gamma^s+\cdots+\varrho_1\Gamma+\varrho_0=0. \tag{60}
$$

According to the balance principle we can determine a relation of θ, ϵ, δ, and μ.

Step 4. Letting the coefficients of $\Omega(\Gamma)$ all be zero will yield an algebraic equations system $\varrho_i=0$ $(i=0,\ldots,s)$. Solving this equations system, we will determine the values $\tau_0,\ldots\tau_\delta$; $\omega_0,\ldots,\omega_\mu$; $\xi_0,\ldots,\xi_\theta$; and $\zeta_0,\ldots,\zeta_\epsilon$.

Step 5. Substituting the results obtained in Step 4 into (57) and integrating (57), we can find the exact solutions of (3).

5. Conclusions and Remarks

In this study, we proposed an extended trial equation method and used it to obtain some soliton and elliptic function solutions to the generalized $K(m,n)$ equation. Otherwise, we discussed a more general trial equation method. The proposed method can also be applied to other nonlinear differential equations with nonlinear evolution.

References

[1] R. Hirota, "Exact solutions of the Korteweg-de-Vries equation for multiple collisions of solitons," *Physics Letters A*, vol. 27, pp. 1192–1194, 1971.

[2] W. Malfliet and W. Hereman, "The tanh method: exact solutions of nonlinear evolution and wave equations," *Physica Scripta*, vol. 54, no. 6, pp. 563–568, 1996.

[3] M. Naja, S. Arbabi, and M. Naja, "New application of sine-cosine method for the generalized $(2+1)$-dimensional nonlinear evolution equations," *International Journal of Advanced Mathematical Sciences*, vol. 1, no. 2, pp. 45–49, 2013.

[4] Y. Gurefe, A. Sonmezoglu, and E. Misirli, "Application of the trial equation method for solving some nonlinear evolution equations arising in mathematical physics," *Pramana Journal of Physics*, vol. 77, pp. 1023–1029, 2011.

[5] Y. Gurefe, A. Sonmezoglu, and E. Misirli, "Application of an irrational trial equation method to high-dimensional nonlinear evolution equations," *Journal of Advanced Mathematical Studies*, vol. 5, no. 1, pp. 41–47, 2012.

[6] C. S. Liu, "Trial equation method and its applications to nonlinear evolution equations," *Acta Physica Sinica*, vol. 54, no. 6, pp. 2505–2509, 2005.

[7] C. S. Liu, "Trial equation method for nonlinear evolution equations with rank inhomogeneous: mathematical discussions and applications," *Communications in Theoretical Physics*, vol. 45, pp. 219–223, 2006.

[8] Y. Pandir, Y. Gurefe, U. Kadak, and E. Misirli, "Classification of exact solutions for some nonlinear partial differential equations with generalized evolution," *Abstract and Applied Analysis*, vol. 2012, Article ID 478531, 16 pages, 2012.

[9] Y. Gurefe, E. Misirli, A. Sonmezoglu, and M. Ekici, "Extended trial equation method to generalized partial differential equations," *Applied Mathematics and Computation*, vol. 219, no. 10, pp. 5253–5260, 2013.

[10] Y. Pandir, Y. Gurefe, and E. Misirli, "Classification of exact solutions to the generalized KadomtsevPetviashvili equation," *Physica Scripta*, vol. 87, Article ID 025003, 12 pages, 2013.

[11] Y. Pandir, Y. Gurefe, and E. Misirli, "The extended trial equation method for some time fractional differential equations," *Discrete Dynamics in Nature and Society*, vol. 2013, Article ID 491359, 13 pages, 2013.

[12] C. S. Liu, "A new trial equation method and its applications," *Communications in Theoretical Physics*, vol. 45, pp. 395–397, 2006.

[13] C. Y. Jun, "Classification of traveling wave solutions to the Vakhnenko equations," *Computational and Applied Mathematics*, vol. 62, no. 10, pp. 3987–3996, 2011.

[14] C. Y. Jun, "Classification of traveling wave solutions to the modified form of the Degasperis-Procesi equation," *Mathematical and Computer Modelling*, vol. 56, no. 1-2, pp. 43–48, 2012.

[15] C.-S. Liu, "Applications of complete discrimination system for polynomial for classifications of traveling wave solutions to nonlinear differential equations," *Computer Physics Communications*, vol. 181, no. 2, pp. 317–324, 2010.

[16] G. Ebadi and A. Biswas, "The G'/G method and topological soliton solution of the K(m,n) equation," *Communications in Nonlinear Science and Numerical Simulation*, vol. 16, no. 6, pp. 2377–2382, 2011.

[17] M. S. Bruzon and M. L. Gandarias, "Classical potential symmetries of the K(m,n) equation with generalized evolution term," *WSEAS Transactions on Mathematics*, vol. 9, no. 4, pp. 275–284, 2010.

[18] M. S. Bruzon, M. L. Gandarias, G. A. Gonzalez, and R. Hansen, "The K(m,n) equation with generalized evolution term studied by symmetry reductions and qualitative analysis," *Applied Mathematics and Computation*, vol. 218, no. 20, pp. 10094–10105, 2012.

Hindawi Publishing Corporation
Abstract and Applied Analysis
Volume 2013, Article ID 562140, 13 pages
http://dx.doi.org/10.1155/2013/562140

Research Article

Numerical Solution of the Fractional Partial Differential Equations by the Two-Dimensional Fractional-Order Legendre Functions

Fukang Yin, Junqiang Song, Yongwen Wu, and Lilun Zhang

College of Computer, National University of Defense Technology, Changsha 410073, China

Correspondence should be addressed to Fukang Yin; yinfukang@nudt.edu.cn

Received 13 May 2013; Revised 8 September 2013; Accepted 8 September 2013

Academic Editor: Santanu Saha Ray

A numerical method is presented to obtain the approximate solutions of the fractional partial differential equations (FPDEs). The basic idea of this method is to achieve the approximate solutions in a generalized expansion form of two-dimensional fractional-order Legendre functions (2D-FLFs). The operational matrices of integration and derivative for 2D-FLFs are first derived. Then, by these matrices, a system of algebraic equations is obtained from FPDEs. Hence, by solving this system, the unknown 2D-FLFs coefficients can be computed. Three examples are discussed to demonstrate the validity and applicability of the proposed method.

1. Introduction

Fractional partial differential equations play a significant role in modeling physical and engineering processes. Therefore, there is an urgent need to develop efficient and fast convergent methods for FPDEs. Recently, several different techniques, including Adomian's decomposition method (ADM) [1, 2], homotopy perturbation method (HPM) [3–5], variational iteration method (VIM) [6–8], spectral methods [9–13], orthogonal polynomials method [14–17], and wavelets method [18–21] have been presented and applied to solve FPDEs.

The method based on the orthogonal functions is a wonderful and powerful tool for solving the FDEs and has enjoyed many successes in this realm. The operational matrix of fractional integration has been determined for some types of orthogonal polynomials, such as Chebyshev polynomials [16], Legendre polynomials [22], Laguerre polynomials [23–25], and Jacobi polynomials [26]. Moreover, the operational matrix of fractional derivative for Chebyshev polynomials [9] and Legendre polynomials [9, 14] also has been derived. However, since these polynomials using integer power series to approximate fractional ones, it cannot accurately represent properties of fractional calculus. Recently, Rida and Yousef [27] presented a fractional extension of the classical Legendre polynomials by replacing the integer order derivative in Rodrigues formula with fractional order derivatives. The defect is that the complexity of these functions made them unsuitable for solving FDEs. Subsequently, Kazem et al. [28] presented the orthogonal fractional order Legendre functions based on shifted Legendre polynomials to find the numerical solution of FDEs and drew a conclusion that their method is accurate, effective, and easy to implement.

Benefiting from their "exponential-convergence" property when smooth solutions are involved, spectral methods have been widely and effectively used for the numerical solution of partial differential equations. The basic idea of spectral methods is to expand a function into sets of smooth global functions, called the trial functions. Because of their special properties, the orthogonal polynomials are usually chosen to be trial functions. Spectral methods can obtain very accurate approximations for a smooth solution while only need a few degrees of freedom. Recently, Chebyshev spectral method [9], Legendre spectral method [10], and adaptive pseudospectral method [11] were proposed for solving fractional boundary value problems. Moreover, generalized Laguerre spectral algorithms and Legendre spectral Galerkin method were developed by Baleanu et al. [12] and Bhrawy and Alghamdi [13] for fractional initial value problems, respectively.

Motivated and inspired by the ongoing research in orthogonal polynomials methods and spectral methods, we construct two-dimensional fractional-order Legendre functions and derive the operational matrices of integration and derivative for the solution of FPDEs. To the best of the authors' knowledge, such approach has not been employed for solving FPDEs.

The rest of the paper is organized as follows. In Section 2, we introduce some mathematical preliminaries of the fractional calculus theory and fractional-order Legendre functions. In Section 3, a basis of 2D-FLFs is defined and some properties are given. Section 4 is devoted to the operational matrices of fractional derivative and integration for 2D-FLFs. Some numerical examples are presented in Section 5. Finally, we conclude the paper with some remarks.

2. Preliminaries and Notations

2.1. Fractional Calculus Theory. Some necessary definitions and Lemma of the fractional calculus theory [29, 30] are listed here for our subsequent development.

Definition 1. A real function $h(t)$, $t > 0$, is said to be in the space C_μ, $\mu \in R$, if there exists a real number $p > \mu$, such that $h(t) = t^p h_1(t)$, where $h_1(t) \in C(0, \infty)$, and it is said to be in the space C_μ^n if and only if $h^{(n)} \in C_\mu$, $n \in N$.

Definition 2. Riemann-Liouville fractional integral operator (J^α) of order $\alpha \geq 0$, of a function $f \in C_\mu$, $\mu \geq -1$ is defined as

$$J^\alpha f(t) = \frac{1}{\Gamma(\alpha)} \int_0^t (t-\tau)^{\alpha-1} f(\tau)\, d\tau, \quad t > 0, \qquad J^0 f(t) = f(t), \tag{1}$$

where $\Gamma(\alpha)$ is the well-known Gamma function. Some properties of the operator J^α can be found, for example, in [29, 30].

Definition 3. The fractional derivative of $f(x)$ in the Caputo sense is defined as

$$(D^\alpha f)(x) = \begin{cases} \dfrac{1}{\Gamma(m-\alpha)} \times \displaystyle\int_0^x \frac{f^{(m)}(\xi)}{(x-\xi)^{\alpha-m+1}} d\xi, & (\alpha > 0,\ m-1 < \alpha < m), \\ \dfrac{d^m f(x)}{dx^m}, & \alpha = m, \end{cases} \tag{2}$$

where $f : R \to R$, $x \to f(x)$ denotes a continuous (but not necessarily differentiable) function.

Lemma 4. *Let $n-1 < \alpha \leq n$, $n \in N$, $t > 0$, $h \in C_\mu^n$, $\mu \geq -1$. Then*

$$(J^\alpha D^\alpha) h(t) = h(t) - \sum_{k=0}^{n-1} h^{(k)}(0^+) \frac{t^k}{k!}. \tag{3}$$

2.2. Fractional-Order Legendre Functions. In this section, we introduce the fractional-order Legendre functions which were first proposed by Kazem et al. [28]. The normalized eigenfunctions problem for FLFs is

$$\left(\left(x - x^{1+\alpha}\right) L_i'^{\alpha}(x)\right)' + \alpha^2 i (i+1) x^{\alpha-1} L_i^\alpha(x) = 0, \quad x \in (0,1), \tag{4}$$

which is a singular Sturm-Liouville problem. The fractional-order Legendre polynomials, denoted by $\mathrm{FL}_i^\alpha(x)$, are defined on the interval $[0,1]$ and can be determined with the aid of following recurrence formulae:

$$\begin{aligned} &\mathrm{FL}_0^\alpha(x) = 1, \qquad \mathrm{FL}_1^\alpha(x) = 2x^\alpha - 1, \\ &\mathrm{FL}_{i+1}^\alpha(x) = \frac{(2i+1)(2x^\alpha - 1)}{i+1} \mathrm{FL}_i^\alpha(x) - \frac{i}{i+1} \mathrm{FL}_{i-1}^\alpha(x), \quad i = 1, 2, \ldots, \end{aligned} \tag{5}$$

and the analytic form of $\mathrm{FL}_i^\alpha(x)$ of degree i is given by

$$\mathrm{FL}_i^\alpha(x) = \sum_{s=0}^{i} b_{s,i} x^{s\alpha}, \qquad b_{s,i} = \frac{(-1)^{i+s}(i+s)!}{(i-s)!(s!)^2}, \tag{6}$$

where $\mathrm{FL}_i^\alpha(0) = (-1)^i$ and $\mathrm{FL}_i^\alpha(1) = 1$. The orthogonality condition is

$$\int_0^1 \mathrm{FL}_n^\alpha(x)\, \mathrm{FL}_m^\alpha(x)\, \omega(x)\, dx = \frac{1}{(2n+1)\alpha} \delta_{nm}, \tag{7}$$

where $\omega(x) = x^{\alpha-1}$ is the weight function and δ is the Kronecker delta. For more details, please see [28].

3. 2D-FLFs

In this section, the definitions and theorems of 2D-FLFs are given by Liu's method described in [31].

3.1. Definitions and Properties of the 2D-FLFs

Definition 5. Let $\{\mathrm{FL}_n^\alpha(x)\}_{n=0}^\infty$ be the fractional Legendre polynomials on $[0,1]$; we call $\{\mathrm{FL}_i^\alpha(x)\mathrm{FL}_j^\beta(y)\}_{i,j=0}^\infty$ the two-dimensional fractional Legendre polynomials on $[0,1] \times [0,1]$.

Theorem 6. *The basis $\{FL_i^\alpha(x) FL_j^\beta(y)\}_{i,j=0}^\infty$ is orthogonal on $[0,1] \times [0,1]$ with the weight function $\omega(x,y) = \omega(x)\omega(y) = x^{\alpha-1} y^{\beta-1}$.*

Proof. Let $i \neq m$ or $j \neq n$

$$\int_0^1 \int_0^1 \omega(x,y) \mathrm{FL}_i^{\alpha}(x) \mathrm{FL}_j^{\beta}(y) \mathrm{FL}_m^{\alpha}(x) \mathrm{FL}_n^{\beta}(y)\, dx\, dy = \int_0^1 \omega(x) \mathrm{FL}_i^{\alpha}(x) \mathrm{FL}_m^{\alpha}(x)\, dx \times \int_0^1 \omega(y) \mathrm{FL}_j^{\beta}(y) \mathrm{FL}_n^{\beta}(y)\, dy = 0. \tag{8}$$

□

Theorem 7. *Consider*

$$\begin{aligned} &\int_0^1 \int_0^1 \omega(x,y) \left[FL_i^{\alpha}(x) FL_j^{\beta}(y)\right]^2 dx\, dy = \frac{1}{(2i+1)\alpha} \frac{1}{(2j+1)\beta}, \\ &\int_0^1 \int_0^1 \omega(x,y) \left[FL_i^{\alpha}(x) FL_j^{\beta}(y)\right]^2 dx\, dy = \int_0^1 \omega(x) \left[FL_i^{\alpha}(x)\right]^2 dx \int_0^1 \omega(y) \left[FL_j^{\beta}(y)\right]^2 dy = \frac{1}{(2i+1)\alpha} \frac{1}{(2j+1)\beta}. \end{aligned} \tag{9}$$

3.2. 2D-FLFs Expansion

Definition 8. A function of two independent variables $f(x,y)$ which is integrable in square $[0,1] \times [0,1]$ can be expanded as

$$f(x,y) = \sum_{i=0}^{\infty}\sum_{j=0}^{\infty} a_{ij} \mathrm{FL}_i^{\alpha}(x) \mathrm{FL}_j^{\beta}(y), \tag{10}$$

where

$$a_{ij} = (2i+1)(2j+1)\alpha\beta \times \int_0^1 \int_0^1 f(x,y)\, \omega(x,y) \mathrm{FL}_i^{\alpha}(x) \mathrm{FL}_j^{\beta}(y)\, dx\, dy. \tag{11}$$

Theorem 9. *If the series $\sum_{i=0}^{\infty}\sum_{j=0}^{\infty} a_{ij} FL_i^{\alpha}(x) FL_j^{\beta}(y)$ converges uniformly to $f(x,y)$ on the square $[0,1] \times [0,1]$, then we have*

$$a_{ij} = (2i+1)(2j+1)\alpha\beta \times \int_0^1 \int_0^1 f(x,y)\, \omega(x,y)\, FL_i^{\alpha}(x)\, FL_j^{\beta}(y)\, dx\, dy. \tag{12}$$

Proof. By multiplying $\omega(x,y)\mathrm{FL}_n^{\alpha}(x)\mathrm{FL}_m^{\beta}(y)$ on both sides of (10), where n and m are fixed and integrating termwise with regard to x and y on $[0,1] \times [0,1]$, then

$$\begin{aligned} &\int_0^1 \int_0^1 f(x,y)\, \omega(x,y) \mathrm{FL}_n^{\alpha}(x) \mathrm{FL}_m^{\beta}(y)\, dx\, dy \\ &= \sum_{i=0}^{\infty}\sum_{j=0}^{\infty} a_{ij} \int_0^1 \int_0^1 \omega(x,y) \mathrm{FL}_i^{\alpha}(x) \mathrm{FL}_j^{\beta}(y) \times \mathrm{FL}_n^{\alpha}(x) \mathrm{FL}_m^{\beta}(y)\, dx\, dy \\ &= \sum_{i=0}^{\infty}\sum_{j=0}^{\infty} a_{ij} \int_0^1 \omega(x) \mathrm{FL}_i^{\alpha}(x) \mathrm{FL}_n^{\alpha}(x)\, dx \times \int_0^1 \omega(y) \mathrm{FL}_j^{\beta}(y) \mathrm{FL}_m^{\beta}(y)\, dy \\ &= a_{nm} \int_0^1 \omega(x) \left[\mathrm{FL}_n^{\alpha}(x)\right]^2 dx \int_0^1 \omega(y) \left[\mathrm{FL}_m^{\beta}(y)\right]^2 dy \\ &= a_{nm} \frac{1}{(2n+1)\alpha} \frac{1}{(2m+1)\beta}. \end{aligned} \tag{13}$$

Finally one can get (11). □

If the infinite series in (10) is truncated, then it can be written as

$$f(x,y) \approx \sum_{i=0}^{m}\sum_{j=0}^{m'} a_{ij} \mathrm{FL}_i^{\alpha}(x) \mathrm{FL}_j^{\beta}(y) = C^T \Psi(x^{\alpha}, y^{\alpha}), \tag{14}$$

where C and $\Psi(x^{\alpha}, y^{\beta})$ are given by

$$C = \left[c_{0,0}, c_{0,1}, \ldots, c_{0,m'-1}, c_{1,0}, c_{1,1}, \ldots, c_{1,m'-1}, \ldots, c_{m-1,0}, c_{m-1,1}, \ldots, c_{m-1,m'-1}\right]^T, \tag{15}$$

$$\Psi(x^{\alpha}, y^{\beta}) = \left[\psi_{0,0}, \psi_{0,1}, \ldots, \psi_{0,m'-1}, \psi_{1,0}, \psi_{1,1}, \ldots, \psi_{1,m'-1}, \ldots, \psi_{m-1,0}, \psi_{m-1,1}, \ldots, \psi_{m-1,m'-1}\right]^T, \tag{16}$$

where $\psi_{ij} = \mathrm{FL}_i^{\alpha}(x)\mathrm{FL}_j^{\beta}(y)$, $i = 0, 1, \ldots, m$, and $j = 0, 1, \ldots, m'$.

According to the definition of FLFs, one can find that fractional Legendre polynomials are identical to Legendre polynomials shifted to $[0,1]$ when using the transform $x^{\alpha} \to x$, $y^{\beta} \to y$. Therefore, in a similar method described in [31], we can easily get the convergence and stability theorems of proposed method.

Lemma 10. *If the function $f(x,y)$ is a continuous function on $[0,1] \times [0,1]$ and the series $\sum_{i=0}^{\infty}\sum_{j=0}^{\infty} a_{ij} FL_i^{\alpha}(x) FL_j^{\beta}(y)$ converges uniformly to $f(x,y)$, then $\sum_{i=0}^{\infty}\sum_{j=0}^{\infty} a_{ij} FL_i^{\alpha}(x) FL_j^{\beta}(y)$ is the 2D-FLFs expansion of $f(x,y)$.*

Proof (by contradiction). Let

$$f(x,y) = \sum_{i=0}^{\infty}\sum_{j=0}^{\infty} b_{ij}\mathrm{FL}_i^{\alpha}(x)\,\mathrm{FL}_j^{\beta}(y),$$
$$f(x,y) \sim \sum_{i=0}^{\infty}\sum_{j=0}^{\infty} a_{ij}\mathrm{FL}_i^{\alpha}(x)\,\mathrm{FL}_j^{\beta}(y). \tag{17}$$

Then there is at least one coefficient such that $a_{nm} \neq b_{nm}$. However,

$$\begin{aligned} b_{nm} &= (2n+1)(2m+1)\alpha\beta \\ &\quad \times \int_0^1\int_0^1 f(x,y)\,\omega(x,y)\,\mathrm{FL}_n^{\alpha}(x)\,\mathrm{FL}_m^{\beta}(y)\,dx\,dy \\ &= a_{nm}. \end{aligned} \tag{18}$$

□

Lemma 11. *If two continuous functions defined on* $[0,1]\times[0,1]$ *have the identical 2D-FLFs expansions, then these two functions are identical.*

Proof. Suppose that $f(x,y)$ and $g(x,y)$ can be expanded by 2D-FLFs as follows:

$$f(x,y) \sim \sum_{i=0}^{\infty}\sum_{j=0}^{\infty} a_{ij}\mathrm{FL}_i^{\alpha}(x)\,\mathrm{FL}_j^{\beta}(y),$$
$$g(x,y) \sim \sum_{i=0}^{\infty}\sum_{j=0}^{\infty} a_{ij}\mathrm{FL}_i^{\alpha}(x)\,\mathrm{FL}_j^{\beta}(y). \tag{19}$$

By subtracting the above two equations with each other, one has

$$\begin{aligned} f(x,y) - g(x,y) &\sim \sum_{i=0}^{\infty}\sum_{j=0}^{\infty}\left(a_{ij}-a_{ij}\right)\mathrm{FL}_i^{\alpha}(x)\,\mathrm{FL}_j^{\beta}(y) \\ &= 0 = \sum_{i=0}^{\infty}\sum_{j=0}^{\infty} 0\times\mathrm{FL}_i^{\alpha}(x)\,\mathrm{FL}_j^{\beta}(y). \end{aligned} \tag{20}$$

Then Lemma 11 can be proved. □

Theorem 12. *If the 2D-FLFs expansion of a continuous function* $f(x,y)$ *converges uniformly, then the 2D-FLFs expansion converges to the function* $f(x,y)$.

Proof. Theorem 12 can be proved by Theorems 7 and 9. □

Theorem 13. *If the sum of the absolute values of the 2D-FLFs coefficients of a continuous function* $f(x,y)$ *forms a convergent series, then the 2D-FLFs expansion is absolutely uniformly convergent, and converges to the function* $f(x,y)$.

Proof. Consider

$$\begin{aligned} \left|\sum_{i=0}^{\infty}\sum_{j=0}^{\infty} a_{ij}\mathrm{FL}_i^{\alpha}(x)\,\mathrm{FL}_j^{\beta}(y)\right| &\le \sum_{i=0}^{\infty}\sum_{j=0}^{\infty}\left|a_{ij}\right|\left|\mathrm{FL}_i^{\alpha}(x)\right|\left|\mathrm{FL}_j^{\beta}(y)\right| \\ &\le \sum_{i=0}^{\infty}\sum_{j=0}^{\infty}\left|a_{ij}\right|. \end{aligned} \tag{21}$$

Then $\sum_{i=0}^{\infty}\sum_{j=0}^{\infty} a_{ij}\mathrm{FL}_i^{\alpha}(x)\mathrm{FL}_j^{\beta}(y)$ converges uniformly to the function $f(x,y)$. □

Theorem 14. *If a continuous function* $f(x,y)$*, defined on* $[0,1]\times[0,1]$*, has bounded mixed partial derivative* $D_x^{2\alpha}D_y^{2\beta}f(x,y)$*, then the 2D-FLFs expansion of the function converges uniformly to the function.*

Proof. Let $f(x,y)$ be a function defined on $[0,1]\times[0,1]$ such that

$$\left|D_x^{2\alpha}D_y^{2\beta}f(x,y)\right| \le M, \tag{22}$$

where M is a positive constant and

$$\begin{aligned} a_{ij} &= (2i+1)(2j+1)\alpha\beta \\ &\quad \times \int_0^1\int_0^1 f(x,y)\,\omega(x,y)\,\mathrm{FL}_i^{\alpha}(x)\,\mathrm{FL}_j^{\beta}(y)\,dx\,dy. \end{aligned} \tag{23}$$

By employing the transform $X = 2x^{\alpha}-1$ and $Y = 2y^{\beta}-1$, one can obtain

$$a_{ij} = \frac{2i+1}{2}\frac{2j+1}{2}\int_{-1}^{1}\int_{-1}^{1} f(X,Y)\,p_i(X)\,p_j(Y)\,dX\,dY. \tag{24}$$

Consequently, in a similar method described in [31], Theorem 14 can be proved. □

4. Operational Matrices of 2D-FLFs

4.1. Integration Operational Matrices of 2D-FLFs

Lemma 15. *The Riemann-Liouville fractional integration of order* $\gamma > 0$ *of the 2D-FLFs* ψ_{ij} *can be obtained in the form of*

$$J_x^{\gamma}\left\{\psi_{ij}\left(x^{\alpha},y^{\beta}\right)\right\} = FL_j^{\beta}(y)\sum_{s=0}^{i} b_{si}\frac{\Gamma(1+s\alpha)}{\Gamma(1+s\alpha+\gamma)}x^{s\alpha+\gamma}. \tag{25}$$

Proof. Consider

$$\begin{aligned} J_x^{\gamma}\left\{\psi_{ij}\left(x^{\alpha},y^{\beta}\right)\right\} &= J_x^{\gamma}\left\{\mathrm{FL}_i^{\alpha}(x)\,\mathrm{FL}_j^{\beta}(y)\right\} \\ &= J_x^{\gamma}\left\{\mathrm{FL}_i^{\alpha}(x)\right\}\mathrm{FL}_j^{\beta}(y) \\ &= J_x^{\gamma}\left\{\sum_{s=0}^{i} b_{si}x^{s\alpha}\right\}\mathrm{FL}_j^{\beta}(y) \\ &= \mathrm{FL}_j^{\beta}(y)\sum_{s=0}^{i} b_{si}\frac{\Gamma(1+s\alpha)}{\Gamma(1+s\alpha+\gamma)}x^{s\alpha+\gamma}. \end{aligned} \tag{26}$$

□

Lemma 16. *Let $\gamma > 0$; then one has*

$$\int_0^1 \int_0^1 J_x^\gamma \{\psi_{ij}\} \psi_{i'j'} \omega(x,y)\, dx\, dy = \begin{cases} \displaystyle\sum_{s=0}^{i}\sum_{s'=0}^{i'} \frac{b_{si} b_{s'i'}}{(s+s'+1)\alpha+\gamma} \\ \qquad \times \dfrac{\Gamma(1+s\alpha)}{\Gamma(1+s\alpha+\gamma)} \dfrac{1}{(2j+1)\beta}, & j = j' \\ 0, & j \neq j'. \end{cases} \tag{27}$$

Proof. Using previous Lemma 15 and (6), one can have

$$\begin{aligned} &\int_0^1 \int_0^1 J_x^\gamma \{\psi_{ij}(x^\alpha, y^\beta)\} \psi_{i'j'}(x^\alpha, y^\beta) \omega(x,y)\, dx\, dy \\ &= \int_0^1 \int_0^1 \omega(x,y) \mathrm{FL}_{i'}^\alpha(x^\alpha) \mathrm{FL}_{j'}^\beta(y^\beta) \mathrm{FL}_j^\beta(y^\beta) \\ &\qquad \times \sum_{s=0}^{i} b_{si} \frac{\Gamma(1+s\alpha)}{\Gamma(1+s\alpha+\gamma)} x^{s\alpha+\gamma} dx\, dy \\ &= \int_0^1 \int_0^1 \omega(y) \mathrm{FL}_j^\beta(y^\beta) \mathrm{FL}_{j'}^\beta(y^\beta) \\ &\qquad \times \sum_{s=0}^{i}\sum_{s'=0}^{i'} b_{si} b_{s'i'} \frac{\Gamma(1+s\alpha)}{\Gamma(1+s\alpha+\gamma)} \\ &\qquad \times x^{(s+s'+1)\alpha+\gamma-1} dx\, dy \\ &= \int_0^1 \omega(y) \mathrm{FL}_j^\beta(y^\beta) \mathrm{FL}_{j'}^\beta(y^\beta) \\ &\quad \times \left(\int_0^1 \sum_{s=0}^{i}\sum_{s'=0}^{i'} b_{si} b_{s'i'} \frac{\Gamma(1+s\alpha)}{\Gamma(1+s\alpha+\gamma)} \right. \\ &\qquad \left. \times\, x^{(s+s'+1)\alpha+\gamma-1} dx \right) dy \\ &= \sum_{s=0}^{i}\sum_{s'=0}^{i'} \frac{b_{si} b_{s'i'}}{(s+s'+1)\alpha+\gamma} \frac{\Gamma(1+s\alpha)}{\Gamma(1+s\alpha+\gamma)} \\ &\qquad \times \int_0^1 \omega(y) \mathrm{FL}_j^\beta(y^\beta) \mathrm{FL}_{j'}^\beta(y^\beta)\, dy \\ &= \begin{cases} \displaystyle\sum_{s=0}^{i}\sum_{s'=0}^{i'} \frac{b_{si} b_{s'i'}}{(s+s'+1)\alpha+\gamma} \\ \qquad \times \dfrac{\Gamma(1+s\alpha)}{\Gamma(1+s\alpha+\gamma)} \dfrac{1}{(2j+1)\beta}, & j = j' \\ 0, & j \neq j'. \end{cases} \end{aligned} \tag{28}$$

□

Theorem 17. *Let $\Psi(x^\alpha, y^\beta)$ be the 2D-FLFs vector defined in* (16)*; then one has*

$$J_x^\gamma \Psi(x^\alpha, y^\beta) \simeq \mathbf{P}_x^\gamma \Psi(x^\alpha, y^\beta), \tag{29}$$

where $\mathbf{P}_x^\gamma$ is the $mm' \times mm'$ operational matrix of Riemann-Liouville fractional integration of order $\gamma > 0$, and has the form as follows:

$$\mathbf{P}_x^\gamma = \begin{bmatrix} E_{0,0} & E_{0,1} & \cdots & E_{0,m-1} \\ E_{1,0} & E_{1,1} & \cdots & E_{1,m-1} \\ \vdots & \vdots & \ddots & \vdots \\ E_{m-1,0} & E_{m-1,1} & \cdots & E_{m-1,m-1} \end{bmatrix}, \tag{30}$$

in which $E_{i,i'}$ is $m' \times m'$ matrix and the elements are defined as follows:

$$E_{i,i'} = I \sum_{s=0}^{i}\sum_{s'=0}^{i'} \frac{b_{si} b_{s'i'} (2i'+1)\alpha}{(s+s'+1)\alpha+\gamma} \frac{\Gamma(1+s\alpha)}{\Gamma(1+s\alpha+\gamma)}, \qquad i, i' = 0, 1, \ldots, m-1, \tag{31}$$

and I is $m' \times m'$ identity matrix.

Proof. Using (29) and orthogonality property of FLFs, one can get

$$\mathbf{P}_x^\gamma = \left\langle J_x^\gamma \Psi(x^\alpha, y^\beta), \Psi^T(x^\alpha, y^\beta) \right\rangle H^{-1}, \tag{32}$$

where $\langle J_x^\gamma \Psi(x^\alpha, y^\beta), \Psi^T(x^\alpha, y^\beta) \rangle$ and H^{-1} are two $m' \times m'$ matrices defined as

$$\begin{aligned} &\left\langle J_x^\gamma \Psi(x^\alpha, y^\beta), \Psi^T(x^\alpha, y^\beta) \right\rangle \\ &= \left\{ \int_0^1 \int_0^1 J_x^\gamma \{\Psi_k(x^\alpha, y^\beta)\} \right. \\ &\qquad \left. \times\, \Psi_{k'}(x^\alpha, y^\beta) \omega(x,y)\, dx\, dy \right\}_{k,k'}^{mm'} \\ &= \left\{ \sum_{s=0}^{i}\sum_{s'=0}^{i'} b_{si} b_{s'i'} \frac{\Gamma(1+s\alpha)}{\Gamma(1+s\alpha+\gamma)} \right. \\ &\qquad \left. \times \frac{1}{(s+s'+1)\alpha+\gamma} \frac{1}{(2j+1)\beta} \right\}_{i,i';j=j'}^{m;m'}, \\ &H^{-1} = \left\{ (2i'+1)(2j+1)\alpha\beta \right\}_{i,i';j=j'}^{m;m'}. \end{aligned} \tag{33}$$

Now by substituting above equations in (32), Theorem 12 can be proved. □

In a similar way as previous, one can obtain the operational matrix of Riemann-Liouville fractional integration with respect to variable y.

Theorem 18. *Let $\Psi(x^\alpha, y^\beta)$ be the 2D-FLFs vector defined in* (16)*; one has*

$$J_y^\gamma \Psi(x^\alpha, y^\beta) \simeq \mathbf{P}_y^\gamma \Psi(x^\alpha, y^\beta), \tag{34}$$

where $\mathbf{P}_y^{\gamma}$ *is the* $mm' \times mm'$ *operational matrix of Riemann-Liouville fractional integration of order* $\gamma > 0$*, and has the form as follows:*

$$\mathbf{P}_y^{\gamma} = \begin{bmatrix} E & O & \cdots & O \\ O & E & \cdots & O \\ \vdots & \vdots & \ddots & \vdots \\ O & O & \cdots & E \end{bmatrix}, \tag{35}$$

in which E *is* $m' \times m'$ *matrix and the elements are defined as follows:*

$$E_{j,j'} = \sum_{r=0}^{j} \sum_{r'=0}^{j'} \frac{b_{rj} b_{r'j'} (2j'+1)\beta}{(r+r'+1)\beta + \gamma} \frac{\Gamma(1+r\beta)}{\Gamma(1+r\beta+\gamma)}, \quad j, j' = 0, 1, \ldots, m'-1. \tag{36}$$

4.2. Derivative Operational Matrices of 2D-FLFs

Lemma 19. *The FLFs Caputo fractional derivative of* $\gamma > 0$ *can be obtained in the form of*

$$D_x^{\gamma} \{\psi_{ij}(x^{\alpha}, y^{\beta})\} = FL_j^{\beta}(y^{\beta}) \sum_{s=0}^{i} b'_{si} \frac{\Gamma(1+s\alpha)}{\Gamma(1+s\alpha-\gamma)} x^{s\alpha-\gamma}, \tag{37}$$

where $b'_{s,i} = 0$ *when* $s\alpha \in N_0$ *and* $s\alpha < \gamma$ *in other case* $b'_{s,i} = b_{s,i}$.

Proof. Consider

$$\begin{aligned} D_x^{\gamma} \{\psi_{ij}(x^{\alpha}, y^{\beta})\} &= D_x^{\gamma} \{\mathrm{FL}_i^{\alpha}(x^{\alpha}) \mathrm{FL}_j^{\beta}(y^{\beta})\} \\ &= \mathrm{FL}_j^{\beta}(y^{\beta}) D_x^{\gamma} \{\mathrm{FL}_i^{\alpha}(x^{\alpha})\} \\ &= D_x^{\gamma} \left\{ \sum_{s=0}^{i} b_{si} x^{s\alpha} \right\} \mathrm{FL}_j^{\beta}(y^{\beta}) \\ &= \mathrm{FL}_j^{\beta}(y^{\beta}) \sum_{s=0}^{i} b'_{si} \frac{\Gamma(1+s\alpha)}{\Gamma(1+s\alpha-\gamma)} x^{s\alpha-\gamma}. \end{aligned} \tag{38}$$

□

Lemma 20. *Let* $\gamma > 0$, $\alpha \notin N$*; then one has*

$$\int_0^1 \int_0^1 D_x^{\gamma} \{\psi_{ij}\} \psi_{i'j'} \omega(x,y)\, dx\, dy = \begin{cases} \displaystyle\sum_{s=0}^{i} \sum_{s'=0}^{i'} \frac{b_{si} b_{s'i'}}{(s+s'+1)\alpha - \gamma} \times \frac{\Gamma(1+s\alpha)}{\Gamma(1+s\alpha-\gamma)} \frac{1}{(2j+1)\beta}, & j = j' \\ 0, & j \neq j'. \end{cases} \tag{39}$$

Proof. Using previous Lemma 19 and (6), one can have

$$\begin{aligned} &\int_0^1 \int_0^1 D_x^{\gamma} \{\psi_{ij}(x^{\alpha}, y^{\beta})\} \psi_{i'j'}(x^{\alpha}, y^{\beta}) \omega(x,y)\, dx\, dy \\ &= \int_0^1 \int_0^1 \omega(x,y) \mathrm{FL}_{i'}^{\alpha}(x^{\alpha}) \mathrm{FL}_{j'}^{\beta}(y^{\beta}) \mathrm{FL}_j^{\beta}(y^{\beta}) \times \sum_{s=0}^{i} b'_{si} \frac{\Gamma(1+s\alpha)}{\Gamma(1+s\alpha-\gamma)} x^{s\alpha-\gamma} dx\, dy \\ &= \int_0^1 \int_0^1 \omega(y) \mathrm{FL}_j^{\beta}(y^{\beta}) \mathrm{FL}_{j'}^{\beta}(y^{\beta}) \times \sum_{s=0}^{i} \sum_{s'=0}^{i'} b'_{si} b_{s'i'} \frac{\Gamma(1+s\alpha)}{\Gamma(1+s\alpha-\gamma)} \times x^{(s+s'+1)\alpha-\gamma-1} dx\, dy \\ &= \int_0^1 \omega(y) \mathrm{FL}_j^{\beta}(y^{\beta}) \mathrm{FL}_{j'}^{\beta}(y^{\beta}) \times \left(\int_0^1 \sum_{s=0}^{i} \sum_{s'=0}^{i'} b'_{si} b_{s'i'} \frac{\Gamma(1+s\alpha)}{\Gamma(1+s\alpha-\gamma)} \times x^{(s+s'+1)\alpha-\gamma-1} dx \right) dy \\ &= \sum_{s=0}^{i} \sum_{s'=0}^{i'} \frac{b'_{si} b_{s'i'}}{(s+s'+1)\alpha-\gamma} \frac{\Gamma(1+s\alpha)}{\Gamma(1+s\alpha-\gamma)} \times \int_0^1 \omega(y) \mathrm{FL}_j^{\beta}(y^{\beta}) \mathrm{FL}_{j'}^{\beta}(y^{\beta})\, dy \\ &= \begin{cases} \displaystyle\sum_{s=0}^{i} \sum_{s'=0}^{i'} \frac{b'_{si} b_{s'i'}}{(s+s'+1)\alpha-\gamma} \times \frac{\Gamma(1+s\alpha)}{\Gamma(1+s\alpha-\gamma)} \frac{1}{(2j+1)\beta}, & j = j' \\ 0, & j \neq j'. \end{cases} \end{aligned} \tag{40}$$

□

Theorem 21. *Let* $\Psi(x^{\alpha}, y^{\beta})$ *be the 2D-FLFs vector defined in* (16)*; one has*

$$D_x^{\gamma} \Psi(x^{\alpha}, y^{\beta}) \simeq \mathbf{D}_x^{\gamma} \Psi(x^{\alpha}, y^{\beta}), \tag{41}$$

where $\mathbf{D}_x^{\gamma}$ *is the* $mm' \times mm'$ *operational matrix of Caputo fractional derivative of order* $\gamma > 0$*, and has the form as follows:*

$$\mathbf{D}_x^{\gamma} = \begin{bmatrix} O & O & \cdots & O \\ F_{1,0} & O & \cdots & O \\ \vdots & \vdots & \ddots & \vdots \\ F_{m-1,0} & F_{m-1,1} & \cdots & O \end{bmatrix} \tag{42}$$

in which $F_{i,i'}$ is $m' \times m'$ matrix and the elements are defined as follows:

$$F_{i,i'} = I \sum_{s=0}^{i} \sum_{s'=0}^{i'} \frac{b'_{si} b_{s'i'} \left(2i'+1\right) \alpha}{\left(s+s'+1\right)\alpha - \gamma} \frac{\Gamma\left(1+s\alpha\right)}{\Gamma\left(1+s\alpha-\gamma\right)}, \quad i, i' = 0, 1, \ldots, m-1, \tag{43}$$

and I is a $m' \times m'$ identity matrix.

Proof. Using (41) and the orthogonality property of FLFs, one can have

$$\mathbf{D}_x^{\gamma} = \left\langle D_x^{\gamma} \Psi\left(x^{\alpha}, y^{\beta}\right), \Psi^T\left(x^{\alpha}, y^{\beta}\right)\right\rangle H^{-1}, \tag{44}$$

where $\langle D_x^{\gamma}\Psi(x^{\alpha}, y^{\beta}), \Psi^T(x^{\alpha}, y^{\beta})\rangle$ and H^{-1} are two $mm' \times mm'$ matrices defined as

$$\begin{aligned}
&\left\langle D_x^{\gamma} \Psi\left(x^{\alpha}, y^{\beta}\right), \Psi^T\left(x^{\alpha}, y^{\beta}\right)\right\rangle \\
&= \left\{\int_0^1 \int_0^1 D_x^{\gamma}\left\{\Psi_k\left(x^{\alpha}, y^{\beta}\right)\right\} \times \Psi_{k'}\left(x^{\alpha}, y^{\beta}\right) \omega\left(x, y\right) dx\, dy \right\}_{k,k'}^{mm'} \\
&= \left\{\sum_{s=0}^{i} \sum_{s'=0}^{i'} \frac{b'_{si} b_{s'i'}}{\left(s+s'+1\right)\alpha - \gamma} \times \frac{\Gamma\left(1+s\alpha\right)}{\Gamma\left(1+s\alpha-\gamma\right)} \frac{1}{\left(2j+1\right)\beta}\right\}_{i,i';j=j'}^{m;m'}
\end{aligned} \tag{45}$$

$$H^{-1} = \left\{\left(2i'+1\right)\left(2j+1\right)\alpha\beta\right\}_{i,i';j=j'}^{m;m'}.$$

Now by substituting above equations in (44), Theorem 21 can be proved. □

In a similar way as above, one can get Caputo fractional derivative of order $\gamma > 0$ with respect to variable y.

Theorem 22. *Let $\Psi(x^{\alpha}, y^{\beta})$ be the 2D-FLFs vector defined in* (16)*; one can have*

$$D_y^{\gamma} \Psi\left(x^{\alpha}, y^{\beta}\right) \simeq \mathbf{D}_y^{\gamma} \Psi\left(x^{\alpha}, y^{\beta}\right), \tag{46}$$

where $\mathbf{D}_y^{\gamma}$ is the $mm' \times mm'$ operational matrix of Caputo fractional derivative of order $\gamma > 0$, and has the form as follows:

$$\mathbf{D}_y^{\gamma} = \begin{bmatrix} F & O & \cdots & O \\ O & F & \cdots & O \\ \vdots & \vdots & \ddots & \vdots \\ O & O & \cdots & F \end{bmatrix}, \tag{47}$$

in which F is $m' \times m'$ matrix and the elements are defined as follows:

$$F_{j,j'} = \sum_{r=0}^{j} \sum_{r'=0}^{j'} \frac{b'_{rj} b_{r'j'} \left(2j'+1\right) \beta}{\left(r+r'+1\right)\beta + \gamma} \frac{\Gamma\left(1+r\beta\right)}{\Gamma\left(1+r\beta+\gamma\right)}, \quad j, j' = 0, 1, \ldots, m'-1. \tag{48}$$

5. Applications and Results

Consider the following FPDEs:

$$\begin{aligned}
&D_x^{\alpha} u\left(x, t\right) + D_t^{\beta} u\left(x, t\right) \\
&\quad + N\left[u\left(x, t\right)\right] + L\left[u\left(x, t\right)\right] = g\left(x, t\right), \quad \alpha, \beta \in (0, 1],
\end{aligned} \tag{49}$$

where L and N are linear operator and nonlinear operator; respectively. D^{α} and D^{β} are the Caputo fractional derivatives of order α and β, respectively; g is a known analytic function.

By employing operator J_t^{β} on both sides of (49) and then using the Lemma 4, one can have

$$\begin{aligned}
&u\left(x, t\right) + J_t^{\beta}\left\{D_x^{\alpha} u\left(x, t\right) + Nu\left(x, t\right) + Lu\left(x, t\right)\right\} \\
&\quad - \sum_{k=0}^{m-1} u^{(k)}\left(x, 0\right) \frac{x^k}{k!} - J_t^{\beta} g\left(x, t\right) = 0.
\end{aligned} \tag{50}$$

We first express unknown function $u(x, t)$ and derivative term $D_x^{\alpha} u(x, t)$ as

$$u\left(x, t\right) = C^T \Psi\left(x^{\alpha}, t^{\beta}\right), \qquad D_x^{\alpha} u\left(x, t\right) = C^T \mathbf{D}_x^{\alpha} \Psi\left(x^{\alpha}, t^{\beta}\right). \tag{51}$$

Now for the nonlinear part, by employing the nonlinear term approximation method described in [32] and then by using transform $x \rightarrow x^{\alpha}$, $t \rightarrow t^{\beta}$, one can get the 2D-FLFs expansion of nonlinear term as

$$Nu\left(x, t\right) = N^T \Psi\left(x^{\alpha}, t^{\beta}\right), \tag{52}$$

where N^T is coefficient matrix of nonlinear term which must be computed and its order is $mm' \times mm'$.

For the linear part, we have

$$Lu\left(x, t\right) = L^T \Psi\left(x^{\alpha}, t^{\beta}\right), \tag{53}$$

where L is a matrix of order $mm' \times mm'$.

After substituting (51)–(53) into (50), one can obtain

$$C^T + \left(C^T \mathbf{D}_x^{\alpha} + N^T + L^T\right) \mathbf{P}_y^{\beta} - C_{\text{guess}}^T = 0. \tag{54}$$

According to the Wu's [33] technology for determining the initial iteration value, the initial iteration value is chosen as $u_{\text{guess}} = \sum_{k=0}^{m-1} u^{(k)}(x, 0)(x^k/k!) + J_t^{\beta}\{g(x, t)\} = C_{\text{guess}}^T \Psi(x^{\alpha}, t^{\beta})$. The coefficient matrix C^T can be computed by using the MATLAB function fsolve( ) or the method described in [34].

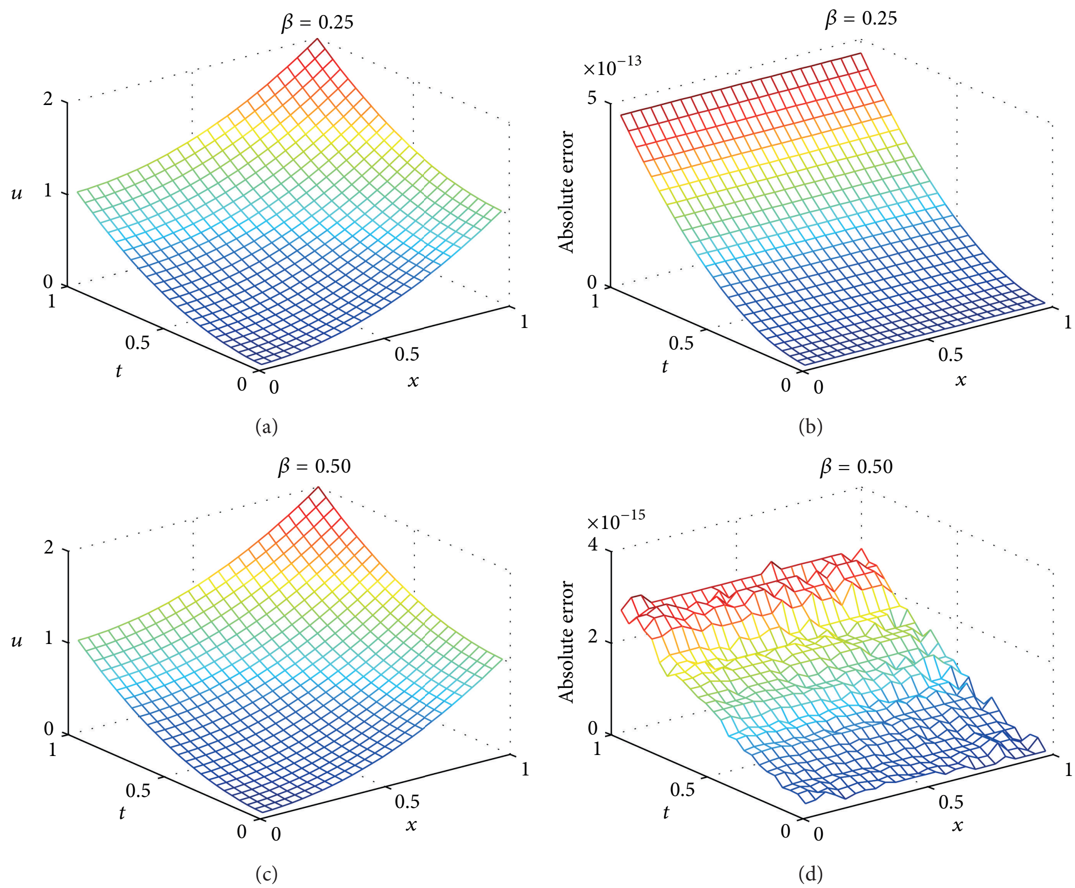

Figure 1: Numerical results for Example 23 when $\beta = 0.25, 0.50$.

Now, the present method is applied to solve the linear and nonlinear FPDEs, and their results are compared with the solution of other methods. The accuracy of our approach is estimated by the following error functions:

$$e_j = (u_{\text{exact}})_j - (u_{\text{approx}})_j, \qquad e = u_{\text{exact}} - u_{\text{approx}},$$
$$\|e\|_{L_\infty} = \max_{1\le j\le N} |e_j|, \qquad \|e\|_{L_2} = \sqrt{\sum_{j=1}^{N} \left|(e_j)^2\right|}, \tag{55}$$
$$\|e\|_{\text{RMS}} = \sqrt{\frac{1}{N}\sum_{j=1}^{N} \left|(e_j)^2\right|}.$$

Example 23. Consider the one-dimensional linear inhomogeneous fractional Burger's equation [35]:

$$\frac{\partial^\beta u(x,t)}{\partial t^\beta} + \frac{\partial u(x,t)}{\partial x} - \frac{\partial^2 u(x,t)}{\partial x^2} = \frac{2t^{2-\beta}}{\Gamma(3-\beta)} + 2x - 2, \quad 0 < \beta \le 1, \tag{56}$$

with the initial condition $u(x,0) = x^2$ and the exact solution being $u(x,t) = x^2 + t^2$.

By employing 2D-FLFs method, one can get

$$C^T \left[I + \left(\mathbf{D}_x^\alpha - (\mathbf{D}_x^\alpha)^2\right)\mathbf{P}_t^\beta\right] = C_{\text{guess}}^T, \tag{57}$$

where $\alpha = 1$. Then we can get $C^T = C_{\text{guess}}^T \text{inv}(I + (\mathbf{D}_x^\alpha - (\mathbf{D}_x^\alpha)^2)\mathbf{P}_t^\beta)$.

Figures 1(a) and 1(b) show the numerical results for $\beta = 0.25$ with $m = 3$, $m' = 9$ and $\beta = 0.5$ with $m = 3$, $m' = 5$, respectively. It should be found that the accuracy of 2D-FLFs method is very high while only a small number of 2D-FLFs are needed.

Example 24. Consider nonlinear fractional Klein-Gordon equation [36, 37]:

$$D_t^\beta u(x,t) - D_x^\alpha u(x) + u^3(x) = g(x,t), \quad x \ge 0, \quad t > 0, \quad \alpha, \beta \in (1,2], \tag{58}$$

subject to the initial conditions

$$u(x,0) = 0, \qquad u_t(x,0) = 0, \tag{59}$$

and $g(x,t) = \Gamma(\beta+1)x^\alpha - \Gamma(\alpha+1)t^\beta + x^{3\alpha}t^{3\beta}$. The exact solution of (58) is $u(x,t) = x^\alpha t^\beta$.

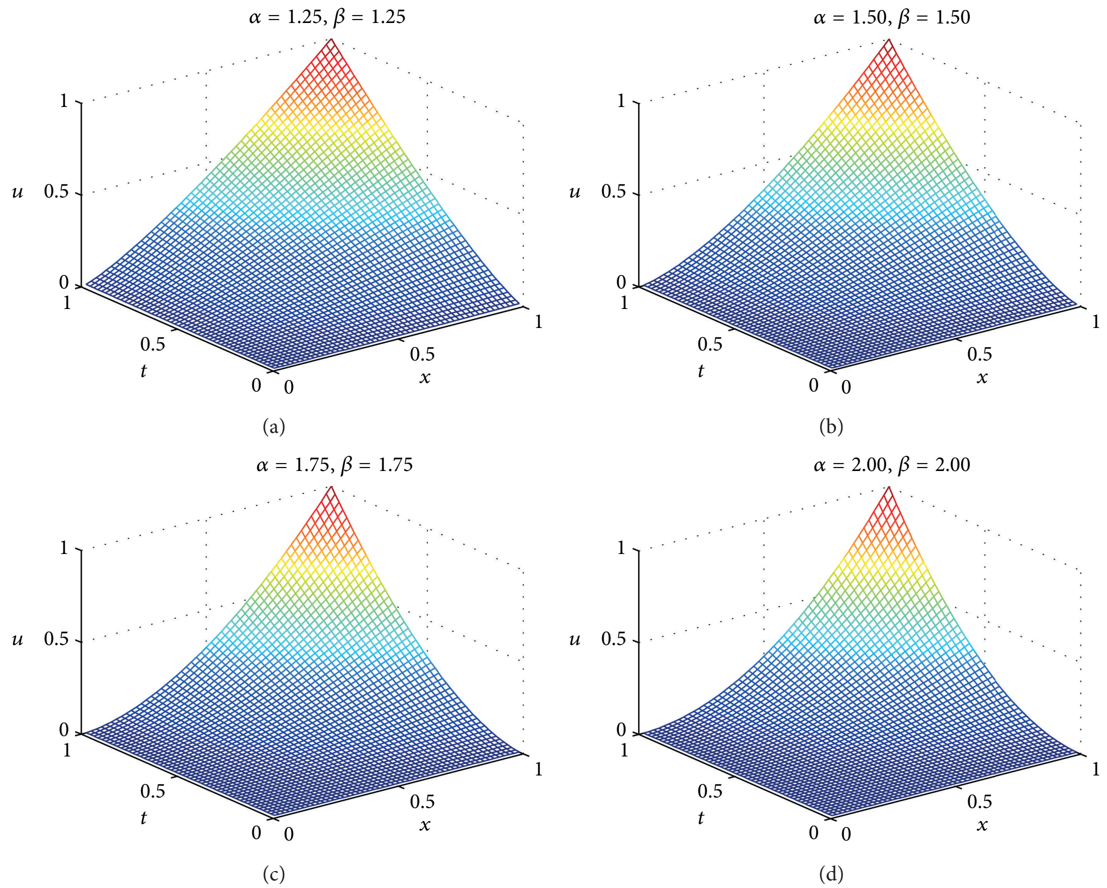

FIGURE 2: Numerical results of Example 24 for different values of α and β.

By employing 2D-FLFs method with $m = 3$ and $m' = 3$, one can have

$$C^T + \left(-C^T \mathbf{D}_x^{\alpha} + N^T\right) \mathbf{P}_t^{\beta} - C_{\text{guess}}^T = 0. \tag{60}$$

The numerical results of Example 24 for different values of α and β are shown in Figure 2. In addition, L_2 and L_∞ errors are presented in Table 1. From Table 1, one can conclude that the solutions of 2D-FLFs method are in good agreement with the exact results. Compared with homotopy analysis method (HAM) [36] and homotopy perturbation method (HPM) [37], 2D-FLFs method can get high accuracy solution while only need a few terms of 2D-FLFs.

Example 25. Consider the nonlinear time-fractional advection partial differential equation [37–39]

$$D_t^{\beta} u(x,t) + u(x,t) u_x(x,t) = x + xt^2, \quad t > 0, \quad x \in R, \quad 0 < \beta \leq 1, \tag{61}$$

subject to the initial condition

$$u(x,0) = 0. \tag{62}$$

Figure 3 gives the approximation solutions of (61) for $\beta = 0.50$ with $m = 4$, $m' = 5$ and $\beta = 0.75$ with $m = 4$, $m' = 9$. Moreover, Table 2 shows the approximate solutions for (61) obtained for different values of β using the fractional variational iteration method (FVIM) [39] and 2D-FLFs method. The values of $\beta = 1$ are the only case for which we know the exact solution $u(x,t) = xt$. It should be noted that only the fourth-order term of the FVIM was used in evaluating the approximate solutions for Table 2. From Table 2, it clearly appears that 2D-FLFs method is more accurate than FVIM and the obtained results are in good agreement with exact solution.

Example 26. We finally consider the linear time-fractional wave equation:

$$\frac{\partial^{2\beta} u}{\partial t^{2\beta}} = \frac{1}{2} x^2 \frac{\partial^2 u}{\partial x^2}, \quad t > 0, \; x \in R, \; 0.5 < \beta \leq 1, \tag{63}$$

subject to the initial conditions

$$u(x,0) = x, \qquad \frac{\partial u(x,0)}{\partial t} = x^2. \tag{64}$$

Table 3 gives a comparison of the approximate solutions at different values of β using the FVIM [39] and 2D-FLFs method. Figure 4 shows the numerical solutions of 2D-FLFs method for (63) at different values of β with $m = 3$, $m' = 9$. The values of $\beta = 1$ are the only case for which we know

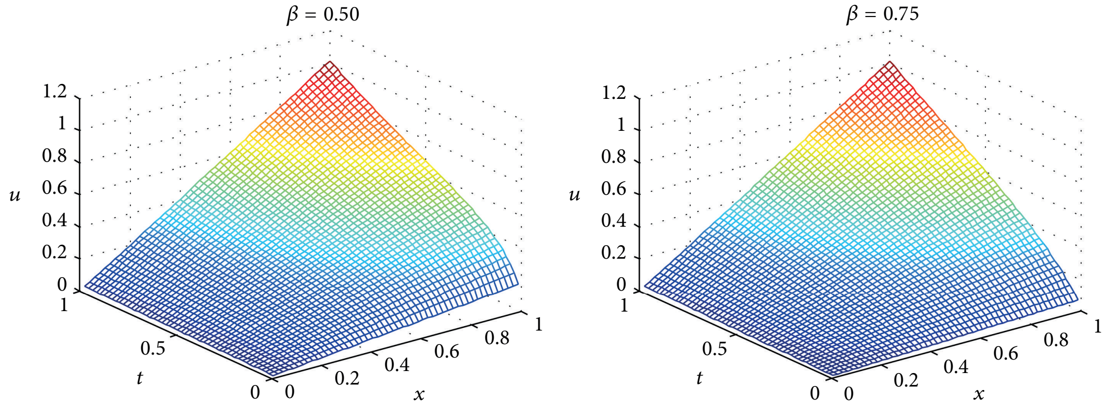

(a) (b)

FIGURE 3: Numerical results of Example 25 for different value of β.

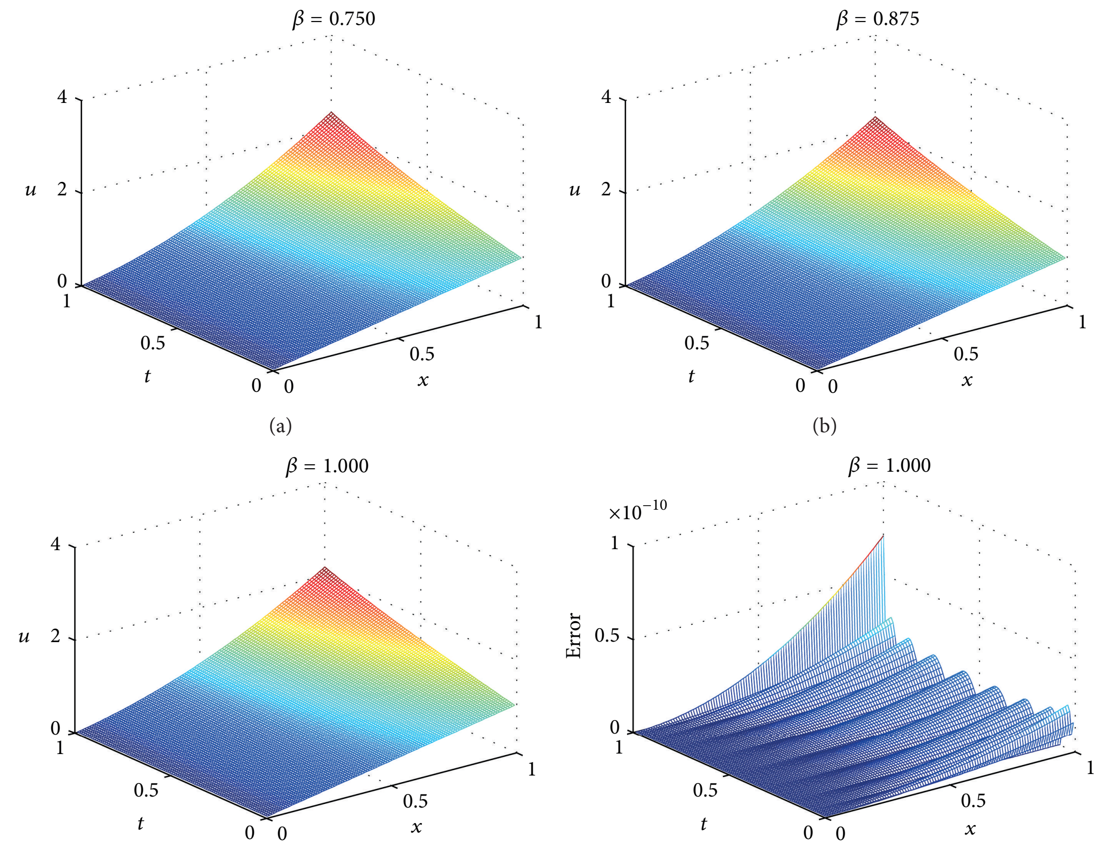

(a) (b) (c) (d)

FIGURE 4: Numerical results of Example 26 for different value of β.

TABLE 1: Errors of Example 24 for different values of α and β with $M = M' = 4$.

Error	$\alpha = \beta = 1.25$	$\alpha = \beta = 1.50$	$\alpha = \beta = 1.75$	$\alpha = \beta = 2.00$
L_2	$5.6437e - 015$	$1.2075e - 015$	$3.4584e - 015$	$8.9917e - 016$
L_∞	$4.4409e - 016$	$1.1102e - 016$	$3.3307e - 016$	$1.1102e - 016$

Table 2: Numerical values when $\beta = 0.50$, 0.75, and 1.0 for (61).

t	x	$\beta = 0.50$ FVIM	$\beta = 0.50$ 2D-FLFs	$\beta = 0.75$ FVIM	$\beta = 0.75$ 2D-FLFs	$\beta = 1.00$ FVIM	$\beta = 1.00$ 2D-FLFs	Exact
0.25	0.25	0.12422501	0.12225461	0.09230374	0.09224583	0.06250058	0.062500	0.062500
	0.50	0.24845002	0.24450922	0.18460748	0.18449165	0.12500117	0.125000	0.125000
	0.75	0.37267504	0.36676383	0.27691122	0.27673748	0.18750175	0.187500	0.187500
	1.00	0.49690005	0.48901844	0.36921496	0.36898331	0.25000234	0.250000	0.250000
0.50	0.25	0.18377520	0.16584130	0.15148283	0.14985508	0.12507592	0.125000	0.125000
	0.50	0.36755040	0.33168259	0.30296566	0.29971016	0.25015184	0.250000	0.250000
	0.75	0.55132559	0.49752389	0.45444848	0.44956524	0.37522776	0.375000	0.375000
	1.00	0.73510079	0.66336518	0.60593131	0.59942032	0.50030368	0.500000	0.500000
0.75	0.25	0.27227270	0.20678964	0.21407798	0.20119503	0.18881843	0.187500	0.187500
	0.50	0.54454540	0.41357929	0.42815596	0.40239005	0.37763687	0.375000	0.375000
	0.75	0.81681810	0.62036893	0.64223394	0.60358508	0.56645530	0.562500	0.562500
	1.00	1.08909080	0.82715857	0.85631192	0.80478011	0.75527373	0.750000	0.750000

Table 3: Numerical values when $\beta = 0.750$, 0.875, and 1.000 for (63).

t	x	$\beta = 0.750$ FVIM	$\beta = 0.750$ 2D-FLFs	$\beta = 0.875$ FVIM	$\beta = 0.875$ 2D-FLFs	$\beta = 1.000$ FVIM	$\beta = 1.000$ Exact
0.25	0.25	0.26622298	0.26622021	0.26593959	0.26594005	0.26578827	0.26578827
	0.50	0.56489190	0.56488083	0.56375836	0.56376020	0.56315308	0.56315308
	0.75	0.89600678	0.89598187	0.89345630	0.89346046	0.89209443	0.89209443
	1.00	1.25956762	1.25952332	1.25503343	1.25504082	1.25261232	1.25261232
0.50	0.25	0.28474208	0.28474415	0.28340402	0.28340659	0.28256846	0.28256846
	0.50	0.63896831	0.63897662	0.63361610	0.63362636	0.63027383	0.63027383
	0.75	1.06267869	1.06269739	1.05063622	1.05065931	1.04311611	1.04311611
	1.00	1.55587323	1.55590647	1.53446439	1.53450544	1.52109530	1.52109531
0.75	0.25	0.30690489	0.30690747	0.30361709	0.30361656	0.30139478	0.30139480
	0.50	0.72761955	0.72762986	0.71446834	0.71446625	0.70557913	0.70557918
	0.75	1.26214400	1.26216719	1.23255378	1.23254905	1.21255304	1.21255316
	1.00	1.91047821	1.91051944	1.85787338	1.85786498	1.82231652	1.82231673

the exact solution $u(x,t) = x + x^2 \sinh(t)$. As previous, only the fourth-order term of the FVIM was used in evaluating the numerical solutions for Table 3. In the case of $\beta = 1$, it can be found that absolute error of 2D-FLFs is not bigger than $1.0e-10$ which is very small compared with that obtained by FVIM.

6. Conclusion

We define a basis of 2D-FLFs and derived its operational matrices of fractional derivative and integration, which are used to approximate the numerical solution of FPDEs. Compared with other numerical methods, 2D-FLFs method can accurately represent properties of fractional calculus. Moreover, only a small number of 2D-FLFs are needed to obtain a satisfactory result. The obtained results demonstrate the validity and applicability of proposed method for solving the FPFEs.

Acknowledgments

This work is supported by the National Natural Science Foundation of China (Grant no. 11272352). The authors are grateful to the anonymous referees for their comments which substantially improved the quality of this paper.

References

[1] Z. Odibat and S. Momani, “Numerical methods for nonlinear partial differential equations of fractional order,” *Applied Mathematical Modelling*, vol. 32, no. 1, pp. 28–39, 2008.

[2] S. Momani and Z. Odibat, “Analytical approach to linear fractional partial differential equations arising in fluid mechanics,” *Physics Letters A*, vol. 355, no. 4-5, pp. 271–279, 2006.

[3] Z. Odibat and S. Momani, “Modified homotopy perturbation method: application to quadratic Riccati differential equation of fractional order,” *Chaos, Solitons & Fractals*, vol. 36, no. 1, pp. 167–174, 2008.

[4] S. H. Hosseinnia, A. Ranjbar, and S. Momani, "Using an enhanced homotopy perturbation method in fractional differential equations via deforming the linear part," *Computers & Mathematics with Applications*, vol. 56, no. 12, pp. 3138–3149, 2008.

[5] O. Abdulaziz, I. Hashim, and S. Momani, "Solving systems of fractional differential equations by homotopy-perturbation method," *Physics Letters A*, vol. 372, no. 4, pp. 451–459, 2008.

[6] J. H. He, "Approximate analytical solution for seepage flow with fractional derivatives in porous media," *Computer Methods in Applied Mechanics and Engineering*, vol. 167, no. 1-2, pp. 57–68, 1998.

[7] J. H. He, "Variational iteration method—a kind of non-linear analytical technique: some examples," *International Journal of Non-Linear Mechanics*, vol. 34, no. 4, pp. 699–708, 1999.

[8] J. H. He, "Variational iteration method—some recent results and new interpretations," *Journal of Computational and Applied Mathematics*, vol. 207, no. 1, pp. 3–17, 2007.

[9] E. H. Doha, A. H. Bhrawy, and S. S. Ezz-Eldien, "A Chebyshev spectral method based on operational matrix for initial and boundary value problems of fractional order," *Computers & Mathematics with Applications*, vol. 62, no. 5, pp. 2364–2373, 2011.

[10] A. H. Bhrawy and M. M. Al-Shomrani, "A shifted Legendre spectral method for fractional-order multi-point boundary value problems," *Advances in Difference Equations*, vol. 2012, article 8, 19 pages, 2012.

[11] M. Maleki, I. Hashim, M. Tavassoli Kajani, and S. Abbasbandy, "An adaptive pseudospectral method for fractional order boundary value problems," *Abstract and Applied Analysis*, vol. 2012, Article ID 381708, 19 pages, 2012.

[12] D. Baleanu, A. H. Bhrawy, and T. M. Taha, "Two efficient generalized Laguerre spectral algorithms for fractional initial value problems," *Abstract and Applied Analysis*, vol. 2013, Article ID 546502, 10 pages, 2013.

[13] A. H. Bhrawy and M. A. Alghamdi, "A new legendre spectral galerkin and pseudo-spectral approximations for fractional initial value problems," *Abstract and Applied Analysis*, vol. 2013, Article ID 306746, 10 pages, 2013.

[14] A. Saadatmandi and M. Dehghan, "A new operational matrix for solving fractional-order differential equations," *Computers & Mathematics with Applications*, vol. 59, no. 3, pp. 1326–1336, 2010.

[15] A. H. Bhrawy, A. S. Alofi, and S. S. Ezz-Eldien, "A quadrature tau method for fractional differential equations with variable coefficients," *Applied Mathematics Letters*, vol. 24, no. 12, pp. 2146–2152, 2011.

[16] A. H. Bhrawy and A. S. Alofi, "The operational matrix of fractional integration for shifted Chebyshev polynomials," *Applied Mathematics Letters*, vol. 26, no. 1, pp. 25–31, 2013.

[17] S. Yüzbasi, "Numerical solution of the Bagley-Torvik equation by the Bessel collocation method," *Mathematical Methods in the Applied Sciences*, vol. 36, no. 3, pp. 300–312, 2013.

[18] J. L. Wu, "A wavelet operational method for solving fractional partial differential equations numerically," *Applied Mathematics and Computation*, vol. 214, no. 1, pp. 31–40, 2009.

[19] A. Saadatmandi and M. Dehghan, "A new operational matrix for solving fractional-order differential equations," *Computers & Mathematics with Applications*, vol. 59, no. 3, pp. 1326–1336, 2010.

[20] H. Jafari, S. A. Yousefi, M. A. Firoozjaee, S. Momani, and C. M. Khalique, "Application of Legendre wavelets for solving fractional differential equations," *Computers & Mathematics with Applications*, vol. 62, no. 3, pp. 1038–1045, 2011.

[21] Y. Li, "Solving a nonlinear fractional differential equation using Chebyshev wavelets," *Communications in Nonlinear Science and Numerical Simulation*, vol. 15, no. 9, pp. 2284–2292, 2010.

[22] A. Ahmadian, M. Suleiman, and S. Salahshour, "An operational matrix based on Legendre polynomials for solving fuzzy fractional-order differential equations," *Abstract and Applied Analysis*, vol. 2013, Article ID 505903, 29 pages, 2013.

[23] A. H. Bhrawy, D. Baleanu, L. M. Assas, and J. A. T. Machado, "On a generalized Laguerre operational matrix of fractional integration," *Mathematical Problems in Engineering*, Article ID 569286, 7 pages, 2013.

[24] A. H. Bhrawy and T. M. Taha, "An operational matrix of fractional integration of the Laguerre polynomials and its application on a semi-infinite interval," *Mathematical Sciences*, vol. 6, article 41, 7 pages, 2012.

[25] A. H. Bhrawy, M. M. Alghamdi, and T. M. Taha, "A new modified generalized Laguerre operational matrix of fractional integration for solving fractional differential equations on the half line," *Advances in Difference Equations*, p. 2012:179, 12, 2012.

[26] S. Kazem, "An integral operational matrix based on Jacobi polynomials for solving fractional-order differential equations," *Applied Mathematical Modelling*, vol. 37, no. 3, pp. 1126–1136, 2013.

[27] S. Z. Rida and A. M. Yousef, "On the fractional order Rodrigues formula for the Legendre polynomials," *Advances and Applications in Mathematical Sciences*, vol. 10, no. 5, pp. 509–517, 2011.

[28] S. Kazem, S. Abbasbandy, and S. Kumar, "Fractional-order Legendre functions for solving fractional-order differential equations," *Applied Mathematical Modelling*, vol. 37, no. 7, pp. 5498–5510, 2013.

[29] I. Podlubny, *Fractional Differential Equations*, vol. 198, Academic Press, San Diego, Calif, USA, 1999.

[30] I. Podlubny, "Geometric and physical interpretation of fractional integration and fractional differentiation," *Fractional Calculus & Applied Analysis*, vol. 5, no. 4, pp. 367–386, 2002.

[31] N. Liu and E. B. Lin, "Legendre wavelet method for numerical solutions of partial differential equations," *Numerical Methods for Partial Differential Equations*, vol. 26, no. 1, pp. 81–94, 2010.

[32] F. Yin, J. Song, X. Cao, and F. Lu, "Couple of the variational iteration method and Legendre wavelets for nonlinear partial differential equations," *Journal of Applied Mathematics*, vol. 2013, Article ID 157956, 11 pages, 2013.

[33] G. C. Wu, "Challenge in the variational iteration method—a new approach to identification of the Lagrange multipliers," *Journal of King Saud University*, vol. 25, pp. 175–178, 2013.

[34] F. Yin, J. Song, and F. Lu, "A coupled method of Laplace transform and Legendre wavelets for nonlinear Klein-Gordon equations," *Mathematical Methods in the Applied Sciences*, 2013.

[35] N. Imran and S. T. Mohyud-Din, "Decomposition method for fractional partial differential equation (PDEs) using Laplace transformation," *International Journal of Physical Sciences*, vol. 8, no. 16, pp. 684–688, 2013.

[36] K. A. Gepreel and M. S. Mohamed, "Analytical approximate solution for nonlinear space-time fractional Klein Gordon equation," *Chinese Physics B*, vol. 22, no. 1, Article ID 010201, 2013.

[37] A. M. A. El-Sayed, A. Elsaid, and D. Hammad, "A reliable treatment of homotopy perturbation method for solving the nonlinear Klein-Gordon equation of arbitrary (fractional) orders," *Journal of Applied Mathematics*, vol. 2012, Article ID 581481, 13 pages, 2012.

[38] S. Momani and Z. Odibat, "A novel method for nonlinear fractional partial differential equations: combination of DTM and generalized Taylor's formula," *Journal of Computational and Applied Mathematics*, vol. 220, no. 1-2, pp. 85–95, 2008.

[39] J. Song, F. Yin, X. Cao, and F. Lu, "Fractional variational iteration method versus Adomian's decomposition method in some fractional partial differential equations," *Journal of Applied Mathematics*, vol. 2013, Article ID 392567, 10 pages, 2013.

Hindawi Publishing Corporation
Abstract and Applied Analysis
Volume 2013, Article ID 390132, 7 pages
http://dx.doi.org/10.1155/2013/390132

Research Article

Persistence Property and Estimate on Momentum Support for the Integrable Degasperis-Procesi Equation

Zhengguang Guo[1] and Liangbing Jin[2]

[1] *College of Mathematics and Information Science, Wenzhou University, Wenzhou, Zhejiang 325035, China*
[2] *Department of Mathematics, Zhejiang Normal University, Jinhua, Zhejiang 321004, China*

Correspondence should be addressed to Zhengguang Guo; gzgmath@gmail.com

Received 24 April 2013; Accepted 4 October 2013

Academic Editor: T. Raja Sekhar

It is shown that a strong solution of the Degasperis-Procesi equation possesses persistence property in the sense that the solution with algebraically decaying initial data and its spatial derivative must retain this property. Moreover, we give estimates of measure for the momentum support.

1. Introduction

Recently, Degasperis and Procesi [1] consider the following family of third order dispersive conservation laws:

$$u_t + c_0 u_x + \gamma u_{xxx} - \alpha^2 u_{xxt} = \left(c_1 u^2 + c_2 u_x^2 + c_3 u u_{xx}\right)_x, \quad (1)$$

where α, γ, c_0, c_1, c_2, and c_3 are real constants. Within this family, only three equations that satisfy asymptotic integrability condition up to third order are singled out, namely, the KdV equation

$$u_t + u_x + u u_x + u_{xxx} = 0, \quad (2)$$

the Camassa-Holm equation

$$u_t - u_{xxt} + 3 u u_x = 2 u_x u_{xx} + u u_{xxx}, \quad (3)$$

and a new equation (the Degasperis-Procesi equation, the DP equation, for simplicity) which can be written as (after rescaling) the dispersionless form [1]

$$u_t - u_{xxt} + 4 u u_x = 3 u_x u_{xx} + u u_{xxx}. \quad (4)$$

It is worth noting that in [2] both the Camassa-Holm and DP equations are derived as members of a one-parameter family of asymptotic shallow water approximations to the Euler equations: this is important because it shows that (after the addition of linear dispersion terms) both the Camassa-Holm and DP equations are physically relevant; otherwise the DP equation would be of purely theoretical interest.

When $c_1 = -3c_3/2\alpha^2$ and $c_2 = c_3/2$ in (1), we recover the Camassa-Holm equation derived physically by Camassa and Holm in [3] by approximating directly the Hamiltonian for Euler's equations in the shallow water regime, where $u(x,t)$ represents the free surface above a flat bottom. There is also a geometric approach which is used to prove the least action principle holding for the Camassa-Holm equation, compared with [4]. It is worth pointing out that a fundamental aspect of the Camassa-Holm equation, the fact that it is a completely integrable system, was shown in [5, 6]. Some satisfactory results have been obtained for this shallow water equation recently, we refer the readers to see [7–19].

Although, the DP equation (4) has a similar form to the Camassa-Holm equation and admits exact peakon solutions analogous to the Camassa-Holm peakons [20], these two equations are pretty different. The isospectral problem for equation (4) is

$$\Psi_x - \Psi_{xxx} - \lambda y \Psi = 0, \quad (5)$$

while for Camassa-Holm equation it is

$$\Psi_{xx} - \frac{1}{4}\Psi - \lambda y \Psi = 0, \quad (6)$$

where $y = u - u_{xx}$ for both cases. This implies that the inside structures of the DP equation (4) and the Camassa-Holm equation are truly different. However, we not only have some similar results [21–23], but also have considerable differences in the scattering/inverse scattering approach, compared with the discussion in [5, 6] and in the paper [24].

Analogous to the Camassa-Holm equation, (4) can be written in Hamiltonian form and has infinitely many conservation laws. Here we list some of the simplest conserved quantities [20]:

$$H_{-1} = \int_{\mathbb{R}} u^3 dx, \qquad H_0 = \int_{\mathbb{R}} y\, dx, \qquad H_1 = \int_{\mathbb{R}} yv\, dx,$$
$$H_5 = \int_{\mathbb{R}} y^{1/3} dx, \qquad H_7 = \int_{\mathbb{R}} \left(y_x^2 y^{-7/3} + 9y^{-1/3}\right) dx, \tag{7}$$

where $v = (4-\partial_x^2)^{-1}u$. So they are different from the invariants of the Camassa-Holm equation

$$E(u) = \int_{\mathbb{R}} \left(u^2 + u_x^2\right) dx, \quad F(u) = \int_{\mathbb{R}} \left(u^3 + uu_x^2\right) dx. \tag{8}$$

Set $Q = (1 - \partial_x^2)$; then the operator Q^{-1} in $\mathbb{R}$ can be expressed by

$$Q^{-1} f = G * f = \frac{1}{2} \int_{\mathbb{R}} e^{-|x-y|} f(y)\, dy. \tag{9}$$

Equation (4) can be written as

$$u_t + uu_x + \partial_x G * \left(\frac{3}{2}u^2\right) = 0, \tag{10}$$

while the Camassa-Holm equation can be written as

$$u_t + uu_x + \partial_x G * \left(u^2 + \frac{1}{2}u_x^2\right) = 0. \tag{11}$$

On the other hand, the DP equation can also be expressed in the following momentum form:

$$\begin{gathered} y_t + y_x u = -3yu_x \\ y = \left(1 - \partial_x^2\right) u. \end{gathered} \tag{12}$$

This formulation is important to motivate us to consider the measure of momentum support which is the second object of this paper, since we found that (12) is similar to the vorticity equation of the three-dimensional Euler equation for incompressible perfect fluids (U is the speed, and ω is its vorticity)

$$\begin{gathered} \omega_t + (U \cdot \nabla)\, \omega = (\omega \cdot \nabla)\, U, \\ \operatorname{div} U = 0, \\ \operatorname{curl} U = \omega. \end{gathered} \tag{13}$$

The stretching term $(\omega \cdot \nabla)U$ in (13) is similar to the term $-3yu_x$ in (12).

One can follow the argument for the Camassa-Holm equation [8] to establish the following well posedness theorem for the Degasperis-Procesi equation.

Theorem 1 (see [23]). *Given $u(x, t = 0) = u_0 \in H^s(\mathbb{R})$, $s > 3/2$, then there exist a T and a unique solution u to* (4) *(also* (10)*) such that*

$$u(x,t) \in C\left([0,T); H^s(\mathbb{R})\right) \cap C^1\left([0,T); H^{s-1}(\mathbb{R})\right). \tag{14}$$

It should be mentioned that due to the form of (10) (no derivative appears in the convolution term), Coclite and Karlsen [25] established global existence and uniqueness result for entropy weak solutions belonging to the class $L^1(\mathbb{R}) \cap BV(\mathbb{R})$.

2. Unique Continuation

The purpose of this section is to show that the solution to (10) and its first-order spatial derivative retain algebraic decay at infinity as their initial values do. Precisely, we prove.

Theorem 2. *Assume that for some $T > 0$ and $s > 3/2$, $u \in C([0,T]; H^s(\mathbb{R}))$ is a strong solution of the initial value problem associated with* (10)*, and that $u_0(x) = u(x,0)$ satisfies that for some $\theta > 1$*

$$|u_0(x)|, \qquad |\partial_x u_0(x)| = O\left(x^{-\theta}\right) \quad \text{as } x \uparrow \infty. \tag{15}$$

Then

$$|u(x,t)|, \qquad |\partial_x u(x,t)| = O\left(x^{-\theta}\right) \quad \text{as } x \uparrow \infty, \tag{16}$$

uniformly in the time interval $[0, T]$.

Notation. We will say that

$$|f(x)| = O\left(x^{-\theta}\right) \quad \text{as } x \uparrow \infty \quad \text{if } \lim_{x\to\infty} \frac{|f(x)|}{x^{-\theta}} = L, \tag{17}$$

where L is a nonnegative constant.

Proof. We introduce the following notations:

$$F(u) = \frac{3}{2}u^2, \tag{18}$$

$$M = \sup_{t\in[0,T]} \|u(t)\|_{H^s}. \tag{19}$$

Multiplying (10) by u^{2p-1} with $p \in Z^+$ and integrating the result in the x-variable, one gets

$$\int_{-\infty}^{\infty} u^{2p-1}\left(u_t + uu_x + \partial_x G * F(u)\right) dx = 0. \tag{20}$$

The first term in (20) is

$$\begin{aligned} \int_{-\infty}^{\infty} u^{2p-1} u_t dx &= \int_{-\infty}^{\infty} \frac{1}{2p} \frac{du^{2p}}{dt} dx \\ &= \frac{1}{2p} \frac{d}{dt} \int_{-\infty}^{\infty} u^{2p} dx = \|u(t)\|_{2p}^{2p-1} \frac{d}{dt} \|u(t)\|_{2p}, \end{aligned} \tag{21}$$

and for the rest, we have

$$\left|\int_{-\infty}^{\infty} u^{2p-1} u u_x dx\right| = \left|\int_{-\infty}^{\infty} u^{2p} u_x dx\right| \le \|u_x(t)\|_\infty \|u(t)\|_{2p}^{2p},$$
$$\left|\int_{-\infty}^{\infty} u^{2p-1} \partial_x G * F(u)\, dx\right| \le \|u(t)\|_{2p}^{2p-1} \left\|\partial_x G * F(u)(t)\right\|_{2p}. \tag{22}$$

From the above inequalities, we get

$$\frac{d}{dt}\|u(t)\|_{2p} \le \|u_x(t)\|_\infty \|u(t)\|_{2p} + \left\|\partial_x G * F(u)\right\|_{2p}, \tag{23}$$

and therefore, by Sobolev embedding theorem and Gronwall's inequality, there exists a constant M such that

$$\|u(t)\|_{2p} \le \left(\|u(0)\|_{2p} + \int_0^t \left\|\partial_x G * F(u)\right\|_{2p} d\tau\right) e^{Mt}. \tag{24}$$

Since $f \in L^1(\mathbb{R}) \cap L^\infty(\mathbb{R})$ implies

$$\lim_{q\to\infty} \|f\|_q = \|f\|_\infty, \tag{25}$$

taking the limits in (24) (note that $\partial_x G \in L^1$ and $F(u) \in L^1 \cap L^\infty$) from (25) we get

$$\|u(t)\|_\infty \le \left(\|u(0)\|_\infty + \int_0^t \left\|\partial_x G * F(u)\right\|_\infty d\tau\right) e^{Mt}. \tag{26}$$

We will now repeat the above arguments using the barrier function

$$\varphi_N(x) = \begin{cases} 1, & x \le 1, \\ x^\theta, & x \in (1, N), \\ N^\theta, & x \ge N, \end{cases} \tag{27}$$

where $N \in \mathbb{Z}^+$. Observe that for all N we have

$$0 \le \varphi_N'(x) \le \theta \varphi_N(x) \quad \text{a.e. } x \in \mathbb{R}. \tag{28}$$

Using notation in (18), from (10) we obtain

$$(u\varphi_N)_t + (u\varphi_N) u_x + \varphi_N \partial_x G * F(u) = 0. \tag{29}$$

Hence, as in the weightless case (26), we get

$$\begin{aligned}\|u(t)\varphi_N\|_\infty &\le e^{Mt}\|u(0)\varphi_N\|_\infty \\ &\quad + e^{Mt}\int_0^t \left\|\varphi_N \partial_x G * F(u)\right\|_\infty d\tau.\end{aligned} \tag{30}$$

A simple calculation shows that there exists $C_0 > 0$ depending only on θ such that, for any $N \in \mathbb{Z}^+$,

$$\frac{1}{2}\varphi_N(x)\int_{-\infty}^{\infty} e^{-|x-y|}\frac{1}{\varphi_N(y)} dy \le C_0. \tag{31}$$

Thus, for any appropriate function f one finds that

$$\begin{aligned}&\left|\varphi_N \partial_x G * f^2(x)\right| \\ &\quad = \left|\frac{1}{2}\varphi_N(x)\int_{-\infty}^{\infty} \operatorname{sgn}(x-y)\, e^{-|x-y|} f^2(y)\, dy\right| \\ &\quad \le \frac{\varphi_N(x)}{2}\int_{-\infty}^{\infty} e^{-|x-y|}\frac{1}{\varphi_N(y)}\varphi_N(y) f(y) f(y)\, dy \\ &\quad \le \left(\frac{\varphi_N(x)}{2}\int_{-\infty}^{\infty}\frac{e^{-|x-y|}}{\varphi_N(y)} dy\right)\|\varphi_N f\|_\infty \|f\|_\infty \\ &\quad \le C_0 \|\varphi_N f\|_\infty \|f\|_\infty.\end{aligned} \tag{32}$$

Combining with (30), we get

$$\|u(t)\varphi_N\|_\infty \le C_1\left(\|u_0\varphi_N\|_\infty + \int_0^t \|\varphi_N u\|_\infty d\tau\right), \tag{33}$$

where $C_1 = C_1(M; T,) > 0$. By Gronwall's inequality, there exists a constant $\widetilde{C}$ for any $t \in [0, T]$ such that

$$\|\varphi_N u\|_\infty \le \widetilde{C}\|u_0\varphi_N\|_\infty \le \widetilde{C}\left\|u_0 \cdot \max\left(1, x^\theta\right)\right\|_\infty. \tag{34}$$

Finally, taking the limit as N goes to infinity in (34) we find that for any $t \in [0, T]$

$$\left|u(x,t)\, x^\theta\right| \le \widetilde{C}\left\|u_0 \cdot \max\left(1, x^\theta\right)\right\|_\infty. \tag{35}$$

From (15), we get $|u(x,t)| = O(x^{-\theta})$ as $x \uparrow \infty$.

Next, differentiating (10) in the x-variable produces the equation

$$u_{xt} + u u_{xx} + u_x^2 + \partial_x^2 G * \left(\frac{3}{2}u^2\right) = 0. \tag{36}$$

Again, multiplying (36) by u_x^{2p-1}, $(p \in \mathbb{Z}^+)$, integrating the result in the x-variable, and using integration by parts

$$\begin{aligned}\int_{-\infty}^{\infty} u u_{xx} (u_x)^{2p-1} dx &= \int_{-\infty}^{\infty} u \frac{(u_x)^{2p}}{2p} dx \\ &= -\frac{1}{2p}\int_{-\infty}^{\infty} u_x (u_x)^{2p} dx,\end{aligned} \tag{37}$$

one gets the inequality

$$\frac{d}{dt}\|u_x(t)\|_{2p} \le 2\|u_x(t)\|_\infty \|u_x(t)\|_{2p} + \left\|\partial_x^2 G * F(u)\right\|_{2p}, \tag{38}$$

and therefore as before

$$\|u_x(t)\|_{2p} \le \left(\|u_x(0)\|_{2p} + \int_0^t \left\|\partial_x^2 G * F(u)\right\|_{2p} d\tau\right) e^{2Mt}. \tag{39}$$

Since $\partial_x^2 G = G - \delta$, we can use (25) and pass to the limit in (39) to obtain

$$\|u_x(t)\|_\infty \le \left(\|u_x(0)\|_\infty + \int_0^t \left\|\partial_x^2 G * F(u)\right\|_\infty d\tau\right) e^{2Mt}; \tag{40}$$

from (36) we get

$$\partial_t(u_x\varphi_N) + uu_{xx}\varphi_N + (u_x\varphi_N)u_x + \varphi_N\partial_x^2 G * F(u) = 0. \tag{41}$$

We need to eliminate the second derivatives in the second term in (41). Thus, combining integration by parts and (28), we find

$$\begin{aligned}
&\left|\int_{-\infty}^{\infty} uu_{xx}\varphi_N(u_x\varphi_N)^{2p-1}dx\right| \\
&\quad = \left|\int_{-\infty}^{\infty} u(u_x\varphi_N)^{2p-1}\left(\partial_x(u_x\varphi_N) - u_x\varphi_N'\right)dx\right| \\
&\quad = \left|\int_{-\infty}^{\infty} u\left(\partial_x\left(\frac{(u_x\varphi_N)^{2p}}{2p}\right) - u_x\varphi_N'(u_x\varphi_N)^{2p-1}\right)dx\right| \\
&\quad \le \kappa\cdot\left(\|u(t)\|_\infty + \|\partial_x u(t)\|_\infty\right)\|\partial_x u\varphi_N\|_{2p}^{2p}.
\end{aligned} \tag{42}$$

Since $\partial_x^2 G = G - \delta$, the argument in (32) also shows that

$$\left|\varphi_N\partial_x^2 G * f^2(x)\right| \le C_0\|\varphi_N f\|_\infty\|f\|_\infty. \tag{43}$$

Similarly, we get

$$\begin{aligned}
&\|u_x(t)\varphi_N\|_\infty \\
&\quad \le C_2\left(\|u_x(0)\varphi_N\|_\infty + \int_0^t \|u(\tau)\varphi_N\|_\infty d\tau\right),
\end{aligned} \tag{44}$$

where $C_2 = C_2(M;T)$.

Then, taking the limit as N goes to infinity, we find that for any $t \in [0,T]$

$$\left|u_x(t)x^\theta\right| \le C_2\left(\left\|u_x(0)x^\theta\right\|_\infty + \int_0^t \left\|u(\tau)x^\theta\right\|_\infty d\tau\right). \tag{45}$$

Since $|u(x,t)| = O(x^{-\theta})$ as $x \uparrow \infty$ and (15), we get

$$\left|\partial_x u(x,t)\right| = O\left(x^{-\theta}\right), \quad \text{as } x \uparrow \infty. \tag{46}$$

This completes the proof. □

3. Measure of Momentum Support

It is known that, for the Degasperis-Procesi equation, the momentum density $y(x,t)$ with compactly supported initial data $y_0(x)$ will retain this property; that is, $y(x,t)$ is also compactly supported [21]. However, the same argument for $u(x,t)$ is false [21]. Note that a detailed description of solution $u(x,t)$ outside of the support of $y(x,t)$ is given in [26, 27]. Moreover, the exponential behavior of u in x outside this support is obvious. The comparison of the DP equation and the incompressible Euler equation above implies that the momentum $y(x,t)$ in (12) plays a similar role as the vorticity does in (13). This motivates us to estimate the size of supp $y(t,\cdot)$ for strong solutions. The approach is inspired by the work of Kim [28] and the recent work [29].

We first introduce the particle trajectory method. Let $u \in C([0,T],H^3(\mathbb{R})) \cap C^1([0,T],H^2(\mathbb{R}))$ be a strong solution of (4) guaranteed by the well posedness Theorem 1. Let $s \in [0,T]$, $q(t;\alpha,s)$ be the solution of the following initial value problem:

$$\begin{aligned}
&\frac{dq(t;\alpha,s)}{dt} = u(s+t, q(t;\alpha,s)), s, s+t \in [0,T], \quad \alpha \in \mathbb{R}, \\
&q(0;\alpha,s) = \alpha, \quad \alpha \in \mathbb{R}.
\end{aligned} \tag{47}$$

Then, $q(t;\cdot,s) : \mathbb{R} \to \mathbb{R}$ is an increasing diffeomorphism. It is shown [21, 23] that

$$y(q(t;x,0),t)\, q_x^3(t;x,0) = y(x,0); \tag{48}$$

this implies that the support of y propagates along the flow. Set $D(t)$ to be the support of $y(\cdot,t)$. Let $\psi \in L^2(D(s))$, and let $\psi^t \in L^2(D(s+t))$ be given by the following:

$$\psi^t(q(t;\alpha,s)) = \psi(\alpha). \tag{49}$$

Moreover, we also want to mention the standard argument on the first Dirichlet eigenvalue problem. Let Ω be an open interval in $\mathbb{R}$, and, $\lambda_1(\Omega)$ be the first Dirichlet eigenvalue of the Laplacian on Ω. Then we have

$$\lambda_1(\Omega) = \inf\left\{\left\|\phi'\right\|^2_{L^2(\Omega)} \mid \phi \in H_0^1(\Omega) \text{ with } \|\phi\|_{L^2(\Omega)} = 1\right\}. \tag{50}$$

It is just $(\pi/|\Omega|)^2$ and the normalized eigenfunctions are the suitable translations of

$$\pm\left(\frac{2}{|\Omega|}\right)^{1/2}\sin\left(\frac{\pi x}{|\Omega|}\right). \tag{51}$$

Theorem 3. *Let $y \in C([0,T];H^1(\mathbb{R})) \cap C^1([0,T];L^2(\mathbb{R}))$ be a strong solution of* (12). *Let $D(t)$ be the support of $y(\cdot,t)$ for $t \in [0,T]$ with its initial $D(0)$ being connected.*

(I) *Suppose there exists a positive constant K such that $u_x(x,k) > -K$ for $(x,t) \in \mathbb{R}\times[0,T]$. Then*

$$\begin{aligned}
&|D(0)|\, e^{-(\exp(5KT/2)\|y_0\|_{L^2(\mathbb{R})})t} \\
&\quad \le |D(t)| \le |D(0)|\, e^{(\exp(5KT/2)\|y_0\|_{L^2(\mathbb{R})})t}.
\end{aligned} \tag{52}$$

(II) y_0 *does not change sign or*

$$\begin{aligned}
&y_0(x) \le 0, \qquad x \in (-\infty, x_0), \\
&y_0(x) \ge 0, \qquad x \in (x_0, \infty),
\end{aligned} \tag{53}$$

and $y_0 \in H^1(\mathbb{R}) \cap L^1(\mathbb{R})$*; then, for all* $t \geq 0$

$$\begin{aligned} |D(0)| e^{-\|y_0\|_{L^1(\mathbb{R})} t} &\leq |D(t)| \\ &\leq |D(0)| e^{\|y_0\|_{L^1(\mathbb{R})} t}. \end{aligned} \tag{54}$$

Proof. (I) The relation of momenta y and u gives

$$u(x,t) = \frac{1}{2} \int_{\mathbb{R}} e^{-|x-\xi|} y(\xi,t)\, d\xi, \tag{55}$$

$$u_x(x,t) = \frac{1}{2} \int_{\mathbb{R}} \operatorname{sgn}(\xi - x) e^{-|x-\xi|} y(\xi,t)\, d\xi. \tag{56}$$

Then, we have by (12) and the lower bound of u_x

$$\begin{aligned} &\frac{d}{dt} \int_{\mathbb{R}} y^2(x,t)\, dx \\ &\quad = -5 \int_{\mathbb{R}} u_x(x,t) y^2(x,t)\, dx \leq 5K \int_{\mathbb{R}} y^2(x,t)\, dx. \end{aligned} \tag{57}$$

Thus

$$\frac{d}{dt} \|y(x,t)\|_{L^2}^2 \leq 5K \|y(x,t)\|_{L^2}^2. \tag{58}$$

Therefore, (56), (58), and Gronwall inequality imply that

$$|u_x(x,t)| \leq \frac{1}{2} \|y(x,t)\|_{L^2} \leq \frac{1}{2} e^{5KT/2} \|y_0\|_{L^2}. \tag{59}$$

On the other hand, due to Propositions A.2 and A.3, $\lambda_1(D(s))$ is Lipschitz and differentiable almost everywhere. Moreover, we have

$$-4M_1 \lambda_1(D(s)) \leq \frac{d}{ds} \lambda_1(D(s)) \leq 4M_1 \lambda_1(D(s)). \tag{60}$$

Then, it follows that

$$e^{-4M_1 s} \lambda_1(D(0)) \leq \lambda_1(D(s)) \leq e^{4M_1 s} \lambda_1(D(0)) \tag{61}$$

with $\lambda_1(D(s)) = \pi^2/|D(s)|^2$. So (52) follows from (61) and (59).

(II) If $y_0 \in H^1(\mathbb{R}) \cap L^1(\mathbb{R})$ does not change sign, we conclude that solutions of (10) exist globally in time. Equality (56) and the conservation of $\int_{\mathbb{R}} y(x,t) dx$ yield

$$|u_x(x,t)| \leq \frac{1}{2} \|y(x,t)\|_{L^1(\mathbb{R})} = \frac{1}{2} \|y_0(x)\|_{L^1(\mathbb{R})}. \tag{62}$$

By similar arguments of (I), constant M_1 in (61) can be replaced by $\|y_0(x)\|_{L^1(\mathbb{R})}/2$; then (54) follows. If (53) is satisfied, we know that the solution of (10) exists globally in time [21, 30]. From (53) and (48), it is easy to get

$$\begin{aligned} y(x,t) &\leq 0, \qquad x \in (-\infty, q(x_0,t)), \\ y(x,t) &\geq 0, \qquad x \in (q(x_0,t), \infty), \end{aligned} \tag{63}$$

where we denote $q(t; x, s)$ with $s = 0$ by $q(x,t)$. By direct computation, we have

$$\int_{\mathbb{R}} |y(x,t)|\, dx = \int_{q(x_0,t)}^{\infty} y(x,t)\, dx - \int_{-\infty}^{q(x_0,t)} y(x,t)\, dx. \tag{64}$$

Next, we prove that $\|y(x,t)\|_{L^1(\mathbb{R})}$ is decreasing with respect to time. To this end, one gets, by differentiating (64) with respect to t and integrating by parts,

$$\begin{aligned} \frac{d}{dt} \int_{\mathbb{R}} |y(x,t)|\, dx &= \int_{q(x_0,t)}^{\infty} y_t(x,t)\, dx \\ &\quad - \int_{-\infty}^{q(x_0,t)} y_t(x,t)\, dx \\ &\quad - 2(yu)(q(x_0,t),t) \\ &= -\int_{q(x_0,t)}^{\infty} (y_x u + 3yu_x)\, dx \\ &\quad + \int_{-\infty}^{q(x_0,t)} (y_x u + 3yu_x)\, dx \\ &\quad - 2(yu)(q(x_0,t),t) \\ &= -2 \int_{q(x_0,t)}^{\infty} yu_x dx + 2 \int_{-\infty}^{q(x_0,t)} yu_x dx \\ &= u^2(q(x_0,t),t) - u_x^2(q(x_0,t),t) \\ &= \int_{q(x_0,t)}^{\infty} e^{-\xi} y(\xi,t)\, dx \int_{-\infty}^{q(x_0,t)} e^{\xi} y(\xi,t)\, dx \\ &\leq 0. \end{aligned} \tag{65}$$

This implies that

$$|u_x(x,t)| \leq \frac{1}{2} \|y(x,t)\|_{L^1(\mathbb{R})} \leq \frac{1}{2} \|y_0(x)\|_{L^1(\mathbb{R})}. \tag{66}$$

Therefore, (54) follows by replacing M_1 with $\|y_0(x)\|_{L^1(\mathbb{R})}/2$ in (61). □

Appendix

The following propositions with standard proofs are known in [29]; we list them here only for convenience of readers.

Proposition A.1. *Let* $s, s+t \in [0,T], \alpha \in D(s)$*, and* $\psi \in H_0^1(D(s))$*;* u_x *can be bounded by a constant* M_1*; then*

(a)

$$e^{-M_1|t|} \leq q_\alpha(t; \alpha, s) \leq e^{M_1|t|}, \tag{A.1}$$

(b)

$$\begin{aligned} |\psi'(\alpha)| e^{-M_1|t|} &\leq \left| (\psi^t)'(q(t;\alpha,s)) \right| \\ &\leq |\psi'(\alpha)| e^{M_1|t|}, \end{aligned} \tag{A.2}$$

(c)

$$\|\psi\|_{L^2(D(s))}e^{-M_1|t|/2} \leq \left\|\psi^t\right\|_{L^2(D(s+t))} \leq \|\psi\|_{L^2(D(s))}e^{M_1|t|/2}. \quad (A.3)$$

Proof. (a) Differentiating (47) with respect to α, we obtain

$$\frac{dq_t}{d\alpha} = u_q q_\alpha. \quad (A.4)$$

Since $q(t;\cdot,s) : \mathbb{R} \to \mathbb{R}$ is an increasing diffeomorphism, then $q_\alpha > 0$. Combining the bound of u_x, there holds

$$-M_1 q_\alpha \leq q_{\alpha t} \leq M_1 q_\alpha. \quad (A.5)$$

This can be solved as (a).

(b) Differentiating (49) with respect to α to get

$$\psi_q^t q_\alpha = \psi'(\alpha), \quad (A.6)$$

then (A.2) is a direct consequence of (A.1).

(c) Equation (49) and the definition of Sobolev norm give that

$$\left\|\psi^t\right\|^2_{L^2(D(s+t))} = \int_{D(s+t)} \psi^t(x)^2 dx = \int_{D(s)} \psi^2(\alpha)\, q_\alpha d\alpha, \quad (A.7)$$

where we have used the change of variable $x = q(t;\alpha,s)$. So (A.3) follows from (A.1). □

Proposition A.2. *Under the hypothesis of Theorem 3, for $s, s+t \in [0,T]$,*

$$\limsup_{t\to 0^+} \frac{\lambda_1(D(s+t)) - \lambda_1(D(s))}{t} \leq 4M_1\lambda_1(D(s)),$$
$$\liminf_{t\to 0^-} \frac{\lambda_1(D(s+t)) - \lambda_1(D(s))}{t} \geq -4M_1\lambda_1(D(s)). \quad (A.8)$$

Proof. Let $t > 0$, $\phi_1 \in H_0^1(D(s))$ with $\|\phi_1\|_{L^2(D(s))} = 1$ be a first normalized eigenfunction on $D(s)$. Then, for $\varphi \in H_0^1(D(s+t))$ with $\|\varphi\|_{L^2(D(s+t))} = 1$, we have

$$\begin{aligned}\lambda_1(D(s+t)) - \lambda_1(D(s)) &= \inf \left\|\varphi'\right\|^2_{L^2(D(s+t))} - \left\|\phi_1'\right\|^2_{L^2(D(s))} \\ &\leq \left\|\phi_1^t\right\|^{-2}_{L^2(D(s+t))}\left\|\left(\phi_1^t\right)'\right\|^2_{L^2(D(s+t))} \\ &\quad - \left\|\phi_1'\right\|^2_{L^2(D(s))}.\end{aligned} \quad (A.9)$$

Furthermore

$$\begin{aligned}&\left\|\phi_1^t\right\|^{-2}_{L^2(D(s+t))}\left\|\left(\phi_1^t\right)'\right\|^2_{L^2(D(s+t))} \\ &\quad = \left\|\phi_1^t\right\|^{-2}_{L^2(D(s+t))} \int_{D(s)} \left[\left(\phi_1^t\right)'\right]^2 q_\alpha d\alpha \\ &\quad \leq \left\|\phi_1^t\right\|^{-2}_{L^2(D(s+t))} e^{3M_1 t}\left\|\phi_1'\right\|^2_{L^2(D(s))} \\ &\quad \leq e^{4M_1 t}\left\|\phi_1'\right\|^2_{L^2(D(s))}.\end{aligned} \quad (A.10)$$

Combing (A.9) and (A.10) together yields

$$\begin{aligned}&\limsup_{t\to 0^+} \frac{\lambda_1(D(s+t)) - \lambda_1(D(s))}{t} \\ &\quad \leq \limsup_{t\to 0^+} \frac{e^{4M_1 t}\left\|\phi_1'\right\|^2_{L^2(D(s))} - \left\|\phi_1'\right\|^2_{L^2(D(s))}}{t} \\ &\quad = 4M_1\lambda_1(D(s)).\end{aligned} \quad (A.11)$$

The second one follows by similar arguments for $t < 0$. □

Proposition A.3. *Under the hypothesis of Theorem 3, for $s, s+t \in [0,T]$,*

$$\limsup_{t\to 0^-} \frac{\lambda_1(D(s+t)) - \lambda_1(D(s))}{t} \leq 4M_1\lambda_1(D(s)),$$
$$\liminf_{t\to 0^+} \frac{\lambda_1(D(s+t)) - \lambda_1(D(s))}{t} \geq -4M_1\lambda_1(D(s)). \quad (A.12)$$

Proof. Let $\phi_1 \in H_0^1(D(s))$ with $\|\phi_1\|_{L^2(D(s))} = 1$ be a first normalized eigenfunction on $D(s)$, and let $\phi_2 \in L^2(D(s))$ be such that its t-transport is a normalized first eigenfunction on $D(s+t)$. For $t > 0$, using the left halves of (A.1) and (A.2) and then the right half of (A.3) we get

$$\begin{aligned}\left\|\left(\phi_2^t\right)'\right\|^2_{L^2(D(s+t))} &= \int_{D(s+t)} \left[\left(\phi_2^t(x)\right)'\right]^2 dx \\ &= \int_{D(s)} \left[\left(\phi_2^t\right)'\right]^2 q_\alpha d\alpha \\ &\geq e^{-3M_1 t}\int_{D(s)} \left[\phi_2'(\alpha)\right]^2 d\alpha \\ &= e^{-3M_1 t}\left\|\phi_2\right\|^2_{L^2(D(s))}\left\|\left(\frac{\phi_2}{\left\|\phi_2\right\|^2_{L^2(D(s))}}\right)'\right\|^2_{L^2(D(s))} \\ &\geq e^{-4M_1 t}\left\|\phi_2^t\right\|^2_{L^2(D(s+t))}\lambda_1(D(s)) \\ &= e^{-4M_1 t}\lambda_1(D(s)).\end{aligned} \quad (A.13)$$

Hence

$$\begin{aligned}&\liminf_{t\to 0^+} \frac{\lambda_1(D(s+t)) - \lambda_1(D(s))}{t} \\ &\quad \geq \liminf_{t\to 0^+} \frac{e^{-4M_1 t} - 1}{t}\lambda_1(D(s)) \\ &\quad = -4M_1\lambda_1(D(s)).\end{aligned} \quad (A.14)$$

The other part is similar. □

Acknowledgments

This work was partially supported by ZJNSF, under Grant nos. LQ12A01009 and LQ13A010008, and NSFC, under Grant nos. 11301394,11226176, and 11226172.

References

[1] A. Degasperis and M. Procesi, "Asymptotic integrability," in *Symmetry and Perturbation Theory*, pp. 23–37, World Science Publisher, River Edge, NJ, USA, 1999.

[2] H. R. Dullin, G. A. Gottwald, and D. D. Holm, "Camassa-Holm, Korteweg-de Vries-5 and other asymptotically equivalent equations for shallow water waves," *Fluid Dynamics Research*, vol. 33, no. 1-2, pp. 73–95, 2003.

[3] R. Camassa and D. D. Holm, "An integrable shallow water equation with peaked solitons," *Physical Review Letters*, vol. 71, no. 11, pp. 1661–1664, 1993.

[4] A. Constantin and B. Kolev, "On the geometric approach to the motion of inertial mechanical systems," *Journal of Physics A*, vol. 35, no. 32, pp. R51–R79, 2002.

[5] A. Constantin, "On the inverse spectral problem for the Camassa-Holm equation," *Journal of Functional Analysis*, vol. 155, no. 2, pp. 352–363, 1998.

[6] A. Constantin and H. P. McKean, "A shallow water equation on the circle," *Communications on Pure and Applied Mathematics*, vol. 52, no. 8, pp. 949–982, 1999.

[7] A. Bressan and A. Constantin, "Global conservative solutions of the Camassa-Holm equation," *Archive for Rational Mechanics and Analysis*, vol. 183, no. 2, pp. 215–239, 2007.

[8] A. Constantin and J. Escher, "Well-posedness, global existence, and blowup phenomena for a periodic quasi-linear hyperbolic equation," *Communications on Pure and Applied Mathematics*, vol. 51, no. 5, pp. 475–504, 1998.

[9] A. Constantin and W. A. Strauss, "Stability of the Camassa-Holm solitons," *Journal of Nonlinear Science*, vol. 12, no. 4, pp. 415–422, 2002.

[10] Z. Guo, "Blow up, global existence, and infinite propagation speed for the weakly dissipative Camassa-Holm equation," *Journal of Mathematical Physics*, vol. 49, no. 3, Article ID 033516, 2008.

[11] A. A. Himonas, G. Misiołek, G. Ponce, and Y. Zhou, "Persistence properties and unique continuation of solutions of the Camassa-Holm equation," *Communications in Mathematical Physics*, vol. 271, no. 2, pp. 511–522, 2007.

[12] Y. A. Li and P. J. Olver, "Well-posedness and blow-up solutions for an integrable nonlinearly dispersive model wave equation," *Journal of Differential Equations*, vol. 162, no. 1, pp. 27–63, 2000.

[13] H. P. McKean, "Breakdown of a shallow water equation," *The Asian Journal of Mathematics*, vol. 2, no. 4, pp. 867–874, 1998.

[14] H. P. McKean, "Breakdown of the Camassa-Holm equation," *Communications on Pure and Applied Mathematics*, vol. 57, no. 3, pp. 416–418, 2004.

[15] G. Misiołek, "Classical solutions of the periodic Camassa-Holm equation," *Geometric and Functional Analysis*, vol. 12, no. 5, pp. 1080–1104, 2002.

[16] S. Shkoller, "Geometry and curvature of diffeomorphism groups with H^1 metric and mean hydrodynamics," *Journal of Functional Analysis*, vol. 160, no. 1, pp. 337–365, 1998.

[17] Z. Xin and P. Zhang, "On the weak solutions to a shallow water equation," *Communications on Pure and Applied Mathematics*, vol. 53, no. 11, pp. 1411–1433, 2000.

[18] Z. Yin, "On the Cauchy problem for an integrable equation with peakon solutions," *Illinois Journal of Mathematics*, vol. 47, no. 3, pp. 649–666, 2003.

[19] Y. Zhou, "Wave breaking for a periodic shallow water equation," *Journal of Mathematical Analysis and Applications*, vol. 290, no. 2, pp. 591–604, 2004.

[20] A. Degasperis, D. D. Holm, and A. N. I. Hone, "A new integrable equation with peakon solutions," *Theoretical and Mathematical Physics*, vol. 133, no. 2, pp. 1463–1474, 2002.

[21] Z. Guo, "Some properties of solutions to the weakly dissipative Degasperis-Procesi equation," *Journal of Differential Equations*, vol. 246, no. 11, pp. 4332–4344, 2009.

[22] D. Henry, "Persistence properties for the Degasperis-Procesi equation," *Journal of Hyperbolic Differential Equations*, vol. 5, no. 1, pp. 99–111, 2008.

[23] Y. Zhou, "Blow-up phenomenon for the integrable Degasperis-Procesi equation," *Physics Letters. A*, vol. 328, no. 2-3, pp. 157–162, 2004.

[24] A. Constantin, "On the scattering problem for the Camassa-Holm equation," *Proceedings of the Royal Society London A*, vol. 457, no. 2008, pp. 953–970, 2001.

[25] G. M. Coclite and K. H. Karlsen, "On the well-posedness of the Degasperis-Procesi equation," *Journal of Functional Analysis*, vol. 233, no. 1, pp. 60–91, 2006.

[26] D. Henry, "Infinite propagation speed for the Degasperis-Procesi equation," *Journal of Mathematical Analysis and Applications*, vol. 311, no. 2, pp. 755–759, 2005.

[27] O. G. Mustafa, "A note on the Degasperis-Procesi equation," *Journal of Nonlinear Mathematical Physics*, vol. 12, no. 1, pp. 10–14, 2005.

[28] N. Kim, "Eigenvalues associated with the vortex patch in 2-D Euler equations," *Mathematische Annalen*, vol. 330, no. 4, pp. 747–758, 2004.

[29] S.-G. Kang and T.-M. Tang, "The support of the momentum density of the Camassa-Holm equation," *Applied Mathematics Letters*, vol. 24, no. 12, pp. 2128–2132, 2011.

[30] Y. Liu and Z. Yin, "Global existence and blow-up phenomena for the Degasperis-Procesi equation," *Communications in Mathematical Physics*, vol. 267, no. 3, pp. 801–820, 2006.

Hindawi Publishing Corporation
Abstract and Applied Analysis
Volume 2013, Article ID 903625, 9 pages
http://dx.doi.org/10.1155/2013/903625

Research Article

Existence and Decay Estimate of Global Solutions to Systems of Nonlinear Wave Equations with Damping and Source Terms

Yaojun Ye

Department of Mathematics and Information Science, Zhejiang University of Science and Technology, Hangzhou 310023, China

Correspondence should be addressed to Yaojun Ye; yeyaojun@zust.edu.cn

Received 30 April 2013; Revised 1 September 2013; Accepted 2 September 2013

Academic Editor: T. Raja Sekhar

The initial-boundary value problem for a class of nonlinear wave equations system in bounded domain is studied. The existence of global solutions for this problem is proved by constructing a stable set and obtain the asymptotic stability of global solutions through the use of a difference inequality.

1. Introduction

In this paper, we are concerned with the global solvability and decay stabilization for the following nonlinear wave equations system:

$$u_{tt} - \operatorname{div}\left(|\nabla u|^{p-2}\nabla u\right) + |u_t|^{q-2}u_t - \Delta u_t = |v|^{r+2}|u|^r u, \quad (x,t) \in \Omega \times R^+, \tag{1}$$

$$v_{tt} - \operatorname{div}\left(|\nabla v|^{p-2}\nabla v\right) + |v_t|^{q-2}v_t - \Delta v_t = |u|^{r+2}|v|^r v, \quad (x,t) \in \Omega \times R^+ \tag{2}$$

with the initial-boundary value conditions

$$u(x,0) = u_0(x) \in W_0^{1,p}(\Omega), \qquad u_t(x,0) = u_1(x) \in L^2(\Omega) \quad x \in \Omega, \tag{3}$$

$$v(x,0) = v_0(x) \in W_0^{1,p}(\Omega), \qquad v_t(x,0) = v_1(x) \in L^2(\Omega) \quad x \in \Omega, \tag{4}$$

$$u(x,t) = 0, \quad v(x,t) = 0, \quad (x,t) \in \partial\Omega \times R^+, \tag{5}$$

where Ω is a bounded open domain in R^n with a smooth boundary $\partial\Omega$, $p, q \geq 2$, $r > 0$ and $p < 2(r+2) \leq np/(n-p)$ for $n \geq p$ and $p < 2(r+2) < +\infty$ for $n < p$.

When $p = 2$, Medeiros and Miranda [1] proved the existence and uniqueness of global weak solutions. Cavalcanti et al. in [2–4] considered the asymptotic behavior for wave equation and an analogous hyperbolic-parabolic system with boundary damping and boundary source term. In paper [5, 6], the authors dealt with the existence, uniform decay rates, and blowup for solutions of systems of nonlinear wave equations with damping and source terms.

Rammaha and Wilstein [7] and Yang [8] are concerned with the initial boundary value problem for a class of quasilinear evolution equations with nonlinear damping and source terms. Under appropriate conditions, by a Galerkin approximation scheme combined with the potential well method, they proved the existence and asymptotic behavior of global weak solutions when $m < p$, where $m \geq 0$ and p are, respectively, the growth orders of the nonlinear strain terms and the source term.

Ono [9] considers the following initial-boundary value problem for nonlinear wave equations with nonlinear dissipative terms:

$$\begin{gathered} u_{tt} - \Delta u + \delta_1 u_t + \delta_2 |u_t|^{\beta} u_t - \delta_3 \Delta u_t = |u|^{\alpha} u, \quad (x,t) \in \Omega \times R^+, \\ u(x,0) = u_0(x), \quad u_t(x,0) = u_1(x), \quad x \in \Omega, \\ u(x,t) = 0, \quad x \in \partial\Omega, \ t \geq 0, \end{gathered} \tag{6}$$

where $\delta_i \geq 0$, $i = 1, 2, 3$, and $\alpha, \beta > 0$ are constants. The author mainly investigates on the blowup phenomenon to problem (6). On the other hand, in the case of $\delta_1+\delta_2+\delta_3 > 0$, he shows that the problem (6) admits a unique global solution, and its energy has some decay properties under some assumptions on u_0 and initial energy $E(0) \equiv E(u_0, u_1)$. In particular, when $\delta_2 > 0$ and $\delta_1 + \delta_3 > 0$ in (6), the energy $E(t) \equiv E(u(t), u_t(t))$ has some polynomial and exponential decay rates, respectively.

For the following strongly damped nonlinear wave equation

$$u_{tt} - \Delta u_t - \Delta u + f(u_t) + g(u) = h, \tag{7}$$

Dell'Oro and Pata [10] obtain the long-time behavior of the related solution semigroup, which is shown to possess the global attractor in the natural weak energy space. In addition, the existence of global and local solutions, decay estimates, and blowup for solutions of nonlinear wave equation with source and damping terms and exponential nonlinearities are studied in [11–14].

In this paper, we prove the global existence for the problem (1)–(5) by applying the potential well theory introduced by Sattinger [15] and Payne and Sattinger [16]. Meanwhile, we obtain the asymptotic stabilization of global solutions by using a difference inequality [17].

For simplicity of notations, hereafter we denote by $\|\cdot\|_p$ the norm of $L^p(\Omega)$; $\|\cdot\|$ denotes $L^2(\Omega)$ norm, and we write equivalent norm $\|\cdot\nabla\|_p$ instead of $W_0^{1,p}(\Omega)$ norm $\|\cdot\|_{W_0^{1,p}(\Omega)}$. Moreover, C denotes various positive constants depending on the known constants and may be different at each appearance.

2. Local Existence

In this section, we investigate the local existence and uniqueness of the solutions of the problem (1)–(5). For this purpose, we list up two useful lemmas which will be used later and give the definition of weak solutions.

Lemma 1. *Let $u \in W_0^{1,p}(\Omega)$, then $u \in L^s(\Omega)$; and the inequality $\|u\|_s \leq C\|u\|_{W_0^{1,p}(\Omega)}$ holds with a constant $C > 0$ depending on Ω, p, and s, provided that $2 \leq s < +\infty$, $2 \leq n \leq p$ and $2 \leq s \leq np/(n-p)$, $2 < p < n$.*

Lemma 2 (Young inequality). *Let $a, b \geq 0$ and $1/p + 1/q = 1$ for $1 < p, q < +\infty$; then one has the inequality*

$$ab \leq \delta a^p + C(\delta) b^q, \tag{8}$$

where $\delta > 0$ is an arbitrary constant, and $C(\delta)$ is a positive constant depending on δ.

Definition 3. A pair of functions (u, v) is said to be a weak solution of (1)–(5) on $[0, T]$ if $u, v \in C([0,T], W_0^{1,p}(\Omega))$, $u_t, v_t \in C([0,T], L^2(\Omega))$, $[u(0), v(0)] = [u_0, v_0] \in W_0^{1,p}(\Omega) \times W_0^{1,p}(\Omega)$, $[u_t(0), v_t(0)] = [u_1, v_1] \in L^2(\Omega) \times L^2(\Omega)$, and $[u, v]$ satisfies

$$\begin{aligned}
&\langle u_t(t), \phi\rangle_{L^2(\Omega)} - \langle u_1, \phi\rangle_{L^2(\Omega)} \\
&\quad + \int_0^t \left\langle \left(|\nabla u|^{p-2}\nabla u\right), \nabla\phi\right\rangle_{L^2(\Omega)} d\tau \\
&\quad + \int_0^t \left\langle |u_t|^{q-2} u_t, \phi\right\rangle_{L^2(\Omega)} d\tau + \int_0^t \langle \nabla u_t, \nabla\phi\rangle_{L^2(\Omega)} \\
&= \int_0^t \left\langle |v|^{r+2}|u|^r u, \phi\right\rangle_{L^2(\Omega)} d\tau, \\
&\langle v_t(t), \psi\rangle_{L^2(\Omega)} - \langle v_1, \psi\rangle_{L^2(\Omega)} \\
&\quad + \int_0^t \left\langle \left(|\nabla v|^{p-2}\nabla v\right), \nabla\psi\right\rangle_{L^2(\Omega)} d\tau \\
&\quad + \int_0^t \left\langle |v_t|^{q-2} v_t, \psi\right\rangle_{L^2(\Omega)} d\tau + \int_0^t \langle \nabla v_t, \nabla\psi\rangle_{L^2(\Omega)} \\
&= \int_0^t \left\langle |u|^{r+2}|v|^r v, \psi\right\rangle_{L^2(\Omega)} d\tau,
\end{aligned} \tag{9}$$

for all test functions $\phi, \psi \in W_0^{1,p}(\Omega)$ and for almost all $t \in [0, T]$.

The local existence and uniqueness of solutions for problem (1)–(5) can be proved through the use of Galerkin method. The result reads as follows.

Theorem 4 (local solution). *Supposed that $[u_0, v_0] \in W_0^{1,p}(\Omega) \times W_0^{1,p}(\Omega)$, $[u_1, v_1] \in L^2(\Omega) \times L^2(\Omega)$, and $p < 2(r+2) \leq np/(n-p)$ if $n \geq p$ and $p < 2(r+2) < +\infty$ for $n < p$, then there exists $T > 0$ such that the problem (1)–(5) has a unique local solution $[u(t), v(t)]$ satisfying*

$$\begin{aligned}
&[u, v] \in L^\infty\left([0, T);\ W_0^{1,p}(\Omega) \times W_0^{1,p}(\Omega)\right); \\
&[u_t, v_t] \in L^\infty\left([0, T);\ L^2(\Omega) \times L^2(\Omega)\right),
\end{aligned} \tag{10}$$

$$\begin{aligned}
E(t) + \int_0^t &\left(\|\nabla u_\tau(\tau)\|^2 + \|\nabla v_\tau(\tau)\|^2\right. \\
&\left. + \|u(\tau)\|_q^q + \|v(\tau)\|_q^q\right) d\tau = E(0),
\end{aligned} \tag{11}$$

where

$$\begin{aligned}
E(t) = &\frac{1}{2}\left(\|u_t\|^2 + \|v_t\|^2\right) + \frac{1}{p}\left(\|\nabla u\|_p^p + \|\nabla v\|_p^p\right) \\
&- \frac{1}{r+2}\|uv\|_{r+2}^{r+2}.
\end{aligned} \tag{12}$$

Proof. Let $\{\omega_i\}_{i=1}^\infty$ be a basis for $W_0^{1,p}(\Omega)$. Supposed that V_k is the subspace of $W_0^{1,p}(\Omega)$ generated by $\{\omega_1, \omega_2, \ldots, \omega_k\}$, $k \in N$. We are going to look for the approximate solution

$$u_k(t) = \sum_{i=1}^k g_{ik}(t)\,\omega_i, \qquad v_k(t) = \sum_{i=1}^k h_{ik}(t)\,\omega_i \tag{13}$$

which satisfies the following Cauchy problem:

$$\begin{aligned}\int_\Omega \left(u_k'' - \operatorname{div}\left(\left|\nabla u_k\right|^{p-2}\nabla u_k\right) + \left|u_k'\right|^{q-2}u_k' - \Delta u_k'\right)\omega_i dx \\ = \int_\Omega \left|v_k\right|^{r+2}\left|u_k\right|^r u_k \omega_i dx,\end{aligned} \tag{14}$$

$$\begin{aligned}\int_\Omega \left(v_k'' - \operatorname{div}\left(\left|\nabla v_k\right|^{p-2}\nabla v_k\right) + \left|v_k'\right|^{q-2}v_k' - \Delta v_k'\right)\omega_i dx \\ = \int_\Omega \left|u_k\right|^{r+2}\left|v_k\right|^r v_k \omega_i dx,\end{aligned} \tag{15}$$

$$u_k(0) = u_{0k} = \sum_{i=1}^{k}(u_0, \omega_i)\,\omega_i \longrightarrow u_0, \quad \text{in } W_0^{1,p}(\Omega), \quad k \longrightarrow \infty, \tag{16}$$

$$v_k(0) = v_{0k} = \sum_{i=1}^{k}(v_0, \omega_i)\,\omega_i \longrightarrow v_0 \quad \text{in } W_0^{1,p}(\Omega), \quad k \longrightarrow \infty, \tag{17}$$

$$u_k'(0) = u_{1k} = \sum_{i=1}^{k}(u_1, \omega_i)\,\omega_i \longrightarrow u_1 \quad \text{in } L^2(\Omega), \quad k \longrightarrow \infty, \tag{18}$$

$$v_k'(0) = v_{1k} = \sum_{i=1}^{k}(v_1, \omega_i)\,\omega_i \longrightarrow v_1 \quad \text{in } L^2(\Omega), \quad k \longrightarrow \infty. \tag{19}$$

Note that, we can solve the problem (14)–(19) by a Picard's iteration method in ordinary differential equations. Hence, there exists a solution in $[0, T_k)$ for some $T_k > 0$, and we can extend this solution to the whole interval $[0, T]$ for any given $T > 0$ by making use of the a priori estimates below.

Multiplying (14) by $g_{ik}'(t)$ and (15) by $h_{ik}'(t)$ and summing over i from 1 to k, we obtain

$$\begin{aligned}\frac{1}{2}\frac{d}{dt}\left(\left\|u_k'(t)\right\|^2 + \left\|\nabla u_k\right\|_p^p\right) + \left\|u_k'(t)\right\|_q^q + \left\|\nabla u_k'(t)\right\|^2 \\ = \int_\Omega \left|v_k\right|^{r+2}\left|u_k\right|^r u_k u_k'\, dx,\end{aligned} \tag{20}$$

$$\begin{aligned}\frac{1}{2}\frac{d}{dt}\left(\left\|v_k'(t)\right\|^2 + \left\|\nabla v_k\right\|_p^p\right) + \left\|v_k'(t)\right\|_q^q + \left\|\nabla v_k'(t)\right\|^2 \\ = \int_\Omega \left|u_k\right|^{r+2}\left|v_k\right|^r v_k v_k'\, dx.\end{aligned} \tag{21}$$

By summing (20) and (21) and integrating the resulting identity over $[0, t]$, we have

$$\begin{aligned}&\frac{1}{2}\left(\left\|u_k'(t)\right\|^2 + \left\|v_k'(t)\right\|^2 + \left\|\nabla u_k\right\|_p^p + \left\|\nabla v_k\right\|_p^p\right) \\ &\quad + \int_0^t \left(\left\|\nabla u_k'(t)\right\|^2 + \left\|\nabla v_k'(t)\right\|^2 + \left\|u_k'(\tau)\right\|_q^q + \left\|v_k'(\tau)\right\|_q^q\right) d\tau \\ &\quad \le C_0 + \int_0^t \int_\Omega \left(\left|v_k\right|^{r+2}\left|u_k\right|^r u_k u_k' + \left|u_k\right|^{r+2}\left|v_k\right|^r v_k v_k'\right) dx\, d\tau.\end{aligned} \tag{22}$$

We estimate the right-hand terms of (22) as follows: we get from Hölder inequality and Lemmas 1 and 2 that

$$\begin{aligned}&\left|\int_0^t \int_\Omega \left(\left|v_k\right|^{r+2}\left|u_k\right|^r u_k u_k' + \left|u_k\right|^{r+2}\left|v_k\right|^r v_k v_k'\right) dx\, d\tau\right| \\ &\quad \le \int_0^t \left(\left\|u_k'(\tau)\right\|^2 + \left\|v_k'(\tau)\right\|^2\right) d\tau + \int_0^t \int_\Omega \left|u_k v_k\right|^{2(r+1)}\left(\left|u_k\right|^2 + \left|v_k\right|^2\right) dx\, d\tau \\ &\quad \le \int_0^t \left(\left\|u_k'(\tau)\right\|^2 + \left\|v_k'(\tau)\right\|^2\right) d\tau + C\int_0^t \left(\left\|u_k\right\|_{2(r+2)}^{2(r+2)} + \left\|v_k\right\|_{2(r+2)}^{2(r+2)}\right) d\tau \\ &\quad \le C\int_0^t \left(\left\|u_k'(\tau)\right\|^2 + \left\|v_k'(\tau)\right\|^2 + \left\|\nabla u_k\right\|_p^{2(r+2)} + \left\|\nabla v_k\right\|_p^{2(r+2)}\right) d\tau \\ &\quad \le C\int_0^t \left(\left\|u_k'(\tau)\right\|^2 + \left\|v_k'(\tau)\right\|^2 + \left\|\nabla u_k\right\|_p^p + \left\|\nabla v_k\right\|_p^p\right)^{2(r+2)/p} d\tau.\end{aligned} \tag{23}$$

It follows from (22) and (23) that

$$\begin{aligned}&\left\|u_k'(t)\right\|^2 + \left\|v_k'(t)\right\|^2 + \left\|\nabla u_k\right\|_p^p + \left\|\nabla v_k\right\|_p^p \\ &\quad + 2\int_0^t \left(\left\|u_k'(\tau)\right\|_q^q \| + \left\|v_k'(\tau)\right\|_q^q + \left\|\nabla u_k'(t)\right\|^2 + \left\|\nabla v_k'(t)\right\|^2\right) d\tau \\ &\quad \le 2C_0 + C\int_0^t \left(\left\|u_k'(\tau)\right\|^2 + \left\|v_k'(\tau)\right\|^2 + \left\|\nabla u_k\right\|_p^p + \left\|\nabla v_k\right\|_p^p\right)^{2(r+2)/p} d\tau,\end{aligned} \tag{24}$$

which implies that

$$\begin{aligned}&\left\|u_k'(t)\right\|^2 + \left\|v_k'(t)\right\|^2 + \left\|\nabla u_k\right\|_p^p + \left\|\nabla v_k\right\|_p^p \\ &\quad \le 2C_0 + C\int_0^t \left(\left\|u_k'(\tau)\right\|^2 + \left\|v_k'(\tau)\right\|^2 + \left\|\nabla u_k\right\|_p^p + \left\|\nabla v_k\right\|_p^p\right)^{2(r+2)/p} d\tau.\end{aligned} \tag{25}$$

We get from (25) and Gronwall type inequality that

$$\begin{aligned}&\left\|u_k'(t)\right\|^2 + \left\|v_k'(t)\right\|^2 + \left\|\nabla u_k\right\|_p^p + \left\|\nabla v_k\right\|_p^p \\ &\quad \le \left[2C_0 - \frac{2(r+2)-p}{p}Ct\right]^{-p/(2(r+2)-p)}.\end{aligned} \tag{26}$$

Thus, we deduce from (26) that there exists a time $T > 0$ such that

$$\left\|u_k'(t)\right\|^2 + \left\|v_k'(t)\right\|^2 + \|\nabla u_k\|_p^p + \|\nabla v_k\|_p^p \le C_1, \quad \forall t \in [0,T], \tag{27}$$

where C_1 is a positive constant independent of k.

We have from (24) and (26) that

$$2\int_0^t \left(\left\|u_k'(\tau)\right\|_q^q + \left\|v_k'(\tau)\right\|_q^q + \left\|\nabla u_k'(\tau)\right\|^2 + \left\|\nabla v_k'(\tau)\right\|^2\right) d\tau \le C_2, \quad \forall t \in [0,T]. \tag{28}$$

It follows from (27) and (28) that

$$\begin{gathered} \left\|u_k'(t)\right\|^2 \le C_1, \qquad \left\|v_k'(t)\right\|^2 \le C_1, \\ \|\nabla u_k\|_p^p \le C_1, \qquad \|\nabla v_k\|_p^p \le C_1. \\ u_k'(t) \text{ and } v_k'(t) \text{ are bounded in } L^2([0,T];\ L^q(\Omega)) \\ \text{and } L^2\left([0,T];\ H_0^1(\Omega)\right). \end{gathered} \tag{29}$$

Using the same process as the proof of Theorem 2.1 in paper [18], we derive that $[u(t), v(t)]$ is a local solution of the problem (1)–(5). By (20) and (21), we conclude that (11) is valid. □

3. Global Existence

In order to state our main results, we first introduce the following functionals:

$$J([u,v]) = \frac{1}{p}\left(\|\nabla u\|_p^p + \|\nabla v\|_p^p\right) - \frac{1}{r+2}\|uv\|_{r+2}^{r+2}, \tag{30}$$

$$K([u,v]) = \left(\|\nabla u\|_p^p + \|\nabla v\|_p^p\right) - 2\|uv\|_{r+2}^{r+2} \tag{31}$$

for $[u,v] \in W_0^{1,p}(\Omega) \times W_0^{1,p}(\Omega)$.

We put that

$$d = \inf\left\{\sup_{\lambda \ge 0} J(\lambda[u,v]) : [u,v] \in W_0^{1,p}(\Omega) \times W_0^{1,p}(\Omega) / \{[0,0]\}\right\}. \tag{32}$$

Then, we are able to define the stable set as follows for problem (1)–(5):

$$W = \left\{[u,v] \in W_0^{1,p}(\Omega) \times W_0^{1,p}(\Omega) \mid K([u,v]) > 0, J([u,v]) < d\right\} \cup \{[0,0]\}. \tag{33}$$

We denote the total energy related to (1) and (2) by (12), and

$$E(0) = \frac{1}{2}\left(\|u_1\|^2 + \|v_1\|^2\right) + \frac{1}{p}\left(\|\nabla u_0\|_p^p + \|\nabla v_0\|_p^p\right) - \frac{1}{r+2}\|u_0 v_0\|_{r+2}^{r+2} \tag{34}$$

is the total energy of the initial data.

Lemma 5. *Let $[u,v]$ be a solution to problem (1)–(5); then, $E(t)$ is a nonincreasing function for $t > 0$ and*

$$\frac{d}{dt}E(t) = -\left(\|u_t\|_q^q + \|v_t\|_q^q + \|\nabla u_t\|_2^2 + \|\nabla v_t\|_2^2\right). \tag{35}$$

We have from (11) that $E(t)$ is the primitive of an integrable function. Therefore, $E(t)$ is absolutely continuous, and equality (35) is satisfied.

Lemma 6. *Supposed that $[u,v] \in W_0^{1,p}(\Omega) \times W_0^{1,p}(\Omega)$, and $p < 2(r+2) \le np/(n-p)$ if $n \ge p$; $p < 2(r+2) < +\infty$ if $n < p$, then $d > 0$.*

Proof. Since

$$J(\lambda[u,v]) = \frac{\lambda^p}{p}\left(\|\nabla u\|_p^p + \|\nabla v\|_p^p\right) - \frac{\lambda^{2(r+2)}}{r+2}\|uv\|_{r+2}^{r+2}, \tag{36}$$

so we get

$$\frac{d}{d\lambda}J(\lambda[u,v]) = \lambda^{p-1}\left(\|\nabla u\|_p^p + \|\nabla v\|_p^p\right) - 2\lambda^{2r+3}\|uv\|_{r+2}^{r+2}. \tag{37}$$

In case $uv \ne 0$, let $(d/d\lambda)J(\lambda[u,v]) = 0$, which implies that

$$\lambda_1 = \left(\frac{\|\nabla u\|_p^p + \|\nabla v\|_p^p}{2\|uv\|_{r+2}^{r+2}}\right)^{1/(2r-p+4)}. \tag{38}$$

As $\lambda = \lambda_1$, an elementary calculation shows that $(d^2/d\lambda^2)J(\lambda[u,v])|_{\lambda=\lambda_1} < 0$. Therefore, we have that

$$\begin{aligned} \sup_{\lambda \ge 0} J(\lambda[u,v]) &= J(\lambda_1[u,v]) \\ &= \frac{2(r+2)-p}{2p(r+2)}\left(\frac{\|\nabla u\|_p^p + \|\nabla v\|_p^p}{2^{p/(2r+4)}\|uv\|_{r+2}^{p/2}}\right)^{(2r+4)/(2r-p+4)}. \end{aligned} \tag{39}$$

It follows from Hölder inequality and Lemma 1 that

$$\begin{aligned} \|uv\|_{r+2}^{p/2} &\le \|u\|_{2(r+2)}^{p/2}\|v\|_{2(r+2)}^{p/2} \\ &\le \frac{1}{2}\left(\|u\|_{2(r+2)}^p + \|v\|_{2(r+2)}^p\right) \\ &\le C\left(\|\nabla u\|_p^p + \|\nabla v\|_p^p\right). \end{aligned} \tag{40}$$

We get from (39) and (40) that

$$\sup_{\lambda \ge 0} J(\lambda[u,v]) \ge \frac{2(r+2)-p}{2p(r+2)}\left(2^{p/(2r+4)}C\right)^{-(2r+4)/(2r-p+4)} > 0. \tag{41}$$

In case $uv = 0$ and $u = 0$ or $v = 0$, then

$$J(\lambda[u,v]) = \frac{\lambda^p}{p}\left(\|\nabla u\|_p^p + \|\nabla v\|_p^p\right). \tag{42}$$

Therefore, we have

$$J(\lambda[u,v]) = +\infty. \tag{43}$$

We conclude from (41) and (43) that

$$d \geq \frac{2(r+2)-p}{2p(r+2)}\left(2^{p/(2r+4)}C\right)^{-(2r+4)/(2r-p+4)} > 0. \tag{44}$$

Thus, we complete the proof of Lemma 6. □

Lemma 7. *Supposed that $p < 2(r+2) \leq np/(n-p)$ for $n \geq p$ and $p < 2(r+2) < +\infty$ for $n < p$, if $[u_0, v_0] \in W$, $[u_1, v_1] \in L^2(\Omega) \times L^2(\Omega)$ and $E(0) < d$, then $[u,v] \in W$ for $\forall t \in [0,T)$.*

Proof. Assume that there exists a number $t^* \in (0,T)$ such that $[u(t), v(t)] \in W$ on $[0,t^*)$ and $u(t^*) \notin W$. Then, in virtue of the continuity of $u(t)$, we see $u(t^*) \in \partial W$, where ∂W denotes the boundary of domain W. From the definition of W and the continuity of $J([u(t), v(t)])$ and $K([u(t), v(t)])$ in t, we have either

$$J([u(t^*), v(t^*)]) = d \tag{45}$$

or

$$K([u(t^*), v(t^*)]) = 0. \tag{46}$$

It follows from (12) and (30) that

$$J([u(t^*), v(t^*)]) \leq E(t^*) \leq E(0) < d. \tag{47}$$

So, case (45) is impossible.

Assume that (46) holds; then, we get that

$$\begin{aligned} &\frac{d}{d\lambda}J(\lambda[u(t^*), v(t^*)]) \\ &\quad = \lambda^{p-1}\left(1-\lambda^{2r-p+4}\right)\left(\|\nabla u\|_p^p + \|\nabla v\|_p^p\right). \end{aligned} \tag{48}$$

We obtain from $(d/d\lambda)J(\lambda[u(t^*), v(t^*)]) = 0$ that $\lambda = 1$. Since

$$\begin{aligned} &\left.\frac{d^2}{d\lambda^2}J(\lambda[u(t^*), v(t^*)])\right|_{\lambda=1} \\ &\quad = -\left[(2(r+2)-p) + (2r+3)\right] < 0. \end{aligned} \tag{49}$$

Consequently, we get from (47) that

$$\sup_{\lambda\geq 0} J(\lambda[u(t^*), v(t^*)]) = J([u(t^*), v(t^*)]) < d, \tag{50}$$

which contradicts the definition of d. Hence, case (46) is impossible as well. Thus we conclude that $[u(t), v(t)] \in W$ on $[0,T)$. □

Theorem 8 (global solution). *Supposed that $p < 2(r+2) \leq np/(n-p)$ as $n \geq p$ and $p < 2(r+2) < +\infty$ as $n < p$, and $[u(t), v(t)]$ is a local solution of problem* (1)–(5) *on $[0,T)$. If $[u_0, v_0] \in W$, $[u_1, v_1] \in L^2(\Omega) \times L^2(\Omega)$ and $E(0) < d$, then $[u(t), v(t)]$ is a global solution of problem* (1)–(5).

Proof. It suffices to show that $\|u_t\|^2 + \|v_t\|^2 + \|\nabla u\|_p^p + \|\nabla v\|_p^p$ is bounded uniformly with respect to t. Under the hypotheses in Theorem 8, we get from Lemma 7 that $[u,v] \in W$ on $[0,T)$. So the following formula holds on $[0,T)$:

$$\begin{aligned} J([u,v]) &= \frac{1}{p}\left(\|\nabla u\|_p^p + \|\nabla v\|_p^p\right) - \frac{1}{r+2}\|uv\|_{r+2}^{r+2} \\ &\geq \frac{2(r+2)-p}{2p(r+2)}\left(\|\nabla u\|_p^p + \|\nabla v\|_p^p\right). \end{aligned} \tag{51}$$

We have from (51) that

$$\begin{aligned} &\frac{1}{2}\left(\|u_t\|^2 + \|v_t\|^2\right) + \frac{2(r+2)-p}{2p(r+2)}\left(\|\nabla u\|_p^p + \|\nabla v\|_p^p\right) \\ &\quad \leq \frac{1}{2}\left(\|u_t\|^2 + \|v_t\|^2\right) + J([u(t), v(t)]) \\ &\quad = E(t) \leq E(0) < d. \end{aligned} \tag{52}$$

Hence, we get

$$\begin{aligned} &\left(\|u_t\|^2 + \|v_t\|^2\right) + \left(\|\nabla u\|_p^p + \|\nabla v\|_p^p\right) \\ &\quad \leq \max\left(2, \frac{2p(r+2)}{2(r+2)-p}\right)d < +\infty. \end{aligned} \tag{53}$$

The above inequality and the continuation principle lead to the global existence of the solution $[u,v]$ for problem (1)–(5). □

4. Asymptotic Behavior of Global Solutions

The following lemma plays an important role in studying the decay estimate of global solutions for the problem (1)–(5).

Lemma 9 (see [9]). *Suppose that $\varphi(t)$ is a nonincreasing nonnegative function on $[0,+\infty)$ and satisfies*

$$\varphi(t)^{r+1} \leq k\left(\varphi(t) - \varphi(t+1)\right), \quad \forall t \geq 0. \tag{54}$$

Then, $\varphi(t)$ has the decay property

$$\varphi(t) \leq \left[\frac{r}{k}(t-1) + M^{-r}\right]^{-1/r}, \quad \forall t \geq 1, \tag{55}$$

where $k, r > 0$ are constants and $M = \max_{t\in[0,1]}\varphi(t)$.

Lemma 10. *Under the assumptions of Theorem 8, if initial value $[u_0, v_0] \in W$ and $[u_1, v_1] \in L^2(\Omega)\times L^2(\Omega)$ are sufficiently small such that*

$$C^{2(r+2)}\left(\frac{2p(r+2)}{2p(r+2)-p}E(0)\right)^{(2(r+2)-p)/p} < 1, \tag{56}$$

then

$$\left(\|\nabla u\|_p^p + \|\nabla v\|_p^p\right) \leq \frac{1}{\theta}K([u,v]), \tag{57}$$

where $\theta = 1 - C^{2(r+2)}((2p(r+2)/(2p(r+2)-p))E(0))^{(2(r+2)-p)/p} > 0$ is a positive constant and C is the optimal Sobolev's constant from $W_0^{1,p}(\Omega)$ to $L^{2(r+2)}(\Omega)$.

Proof. We have from Lemma 1 and (52) that

$$\begin{aligned}
2\|uv\|_{r+2}^{r+2} &\le 2\|u\|_{2(r+2)}^{r+2}\|v\|_{2(r+2)}^{r+2} \\
&\le \|u\|_{2(r+2)}^{2(r+2)} + \|v\|_{2(r+2)}^{2(r+2)} \\
&\le C^{2(r+2)}\left(\|\nabla u\|_p^{2(r+2)} + \|\nabla v\|_p^{2(r+2)}\right) \\
&\le C^{2(r+2)}\left(\|\nabla u\|_p^{2(r+2)-p}\|\nabla u\|_p^p \right. \\
&\qquad \left. + \|\nabla v\|_p^{2(r+2)-p}\|\nabla v\|_p^p\right) \\
&\le C^{2(r+2)}\left(\frac{2p(r+2)}{2p(r+2)-p}E(0)\right)^{(2(r+2)-p)/p} \\
&\quad \times \left(\|\nabla u\|_p^p + \|\nabla v\|_p^p\right).
\end{aligned} \tag{58}$$

Therefore, we get from (58) and (31) that

$$\begin{aligned}
&\left[1 - C^{2(r+2)}\left(\frac{2p(r+2)}{2p(r+2)-p}E(0)\right)^{(2(r+2)-p)/p}\right] \\
&\quad \times \left(\|\nabla u\|_p^p + \|\nabla v\|_p^p\right) \le K([u,v]).
\end{aligned} \tag{59}$$

Let

$$\theta = 1 - C^{2(r+2)}\left(\frac{2p(r+2)}{2p(r+2)-p}E(0)\right)^{(2(r+2)-p)/p} > 0; \tag{60}$$

then, we have from (59) that

$$\|\nabla u\|_p^p + \|\nabla v\|_p^p \le \frac{1}{\theta}K([u,v]). \tag{61}$$

□

Theorem 11. *Under the assumptions of Theorem 8, if $p < q < r+2$ and (56) hold, then the global solution $[u, v]$ in W of the problem (1)–(5) has the following decay property:*

$$E(t) \le \left[\frac{p-2}{pC}(t-1) + M^{(p+q-pq)/p}\right]^{p/(p+q-pq)}, \quad \forall t > 1, \tag{62}$$

where $M = \max_{t\in[0,1]}E(t) > 0$ is some constant depending only on $[u_0, v_0]$ and $[u_1, v_1]$.

Proof. Multiplying (1) by u_t and (2) by v_t and integrating over $\Omega \times [t, t+1]$, and summing up together, we get

$$\begin{aligned}
&\int_t^{t+1}\left(\|u_t(s)\|_q^q + \|v_t(s)\|_q^q + \|\nabla u_t(s)\|_2^2\right. \\
&\qquad \left. + \|\nabla v_t(s)\|_2^2\right) ds = E(t) - E(t+1).
\end{aligned} \tag{63}$$

Thus, there exists $t_1 \in [t, t+1/4]$, $t_2 \in [t+3/4, t+1]$ such that

$$\begin{aligned}
&4\left(\|u_t(t_i)\|_q^q + \|v_t(t_i)\|_q^q + \|\nabla u_t(t_i)\|_2^2 + \|\nabla v_t(t_i)\|_2^2\right) \\
&\quad = E(t) - E(t+1), \quad i = 1, 2.
\end{aligned} \tag{64}$$

On the other hand, we multiply (1) by u and (2) by v and integrate over $\Omega \times [t_1, t_2]$. Adding them together, we obtain

$$\begin{aligned}
\int_{t_1}^{t_2} K([u,v])\,ds &= \int_{t_1}^{t_2}\|u_t\|^2 ds + \int_{t_1}^{t_2}\|v_t\|^2 ds \\
&\quad + (u_t(t_1), u(t_1)) - (u_t(t_2), u(t_2)) \\
&\quad + (v_t(t_1), v(t_2)) - (v_t(t_2)\, v(t_2)) \\
&\quad - \left(\int_{t_1}^{t_2}\int_\Omega |u_t|^{q-2}u_t u\,dx\,ds \right. \\
&\qquad \left. + \int_{t_1}^{t_2}\int_\Omega |v_t|^{q-2}v_t v\,dx\,ds\right) \\
&\quad - \int_{t_1}^{t_2}\int_\Omega \nabla u_t \nabla u\,dx\,ds - \int_{t_1}^{t_2}\int_\Omega \nabla v_t \nabla v\,dx\,ds.
\end{aligned} \tag{65}$$

From (63), Sobolev inequality, and Hölder inequality, we have

$$\begin{aligned}
\int_{t_1}^{t_2}\|u_t\|^2 ds &\le C\int_{t_1}^{t_2}\|\nabla u_t\|^2 ds \le C(E(t) - E(t+1)), \\
\int_{t_1}^{t_2}\|v_t\|^2 ds &\le C\int_{t_1}^{t_2}\|\nabla v_t\|^2 ds \le C(E(t) - E(t+1)).
\end{aligned} \tag{66}$$

We get from (52), (64), and Lemmas 1 and 2 that

$$\begin{aligned}
|u_t(t_i), u(t_i)| &\le \|u_t(t_i)\| \cdot \|u(t_i)\| \le C\|\nabla u_t(t_i)\| \cdot \|\nabla u(t_i)\|_p \\
&\le C(E(t) - E(t+1))^{1/2}\sup_{t\le s\le t+1}E(s)^{1/p} \\
&\le C(\varepsilon)(E(t) - E(t+1))^{p/2(p-1)} \\
&\quad + \varepsilon\sup_{t\le s\le t+1}E(s), \quad i = 1, 2, \\
|(v_t(t_i), v(t_i))| &\le \|v_t(t_i)\| \cdot \|v(t_i)\| \le C\|\nabla v_t(t_i)\| \cdot \|\nabla v(t_i)\|_p \\
&\le C(E(t) - E(t+1))^{1/2}\sup_{t\le s\le t+1}E(s)^{1/p} \\
&\le C(\varepsilon)(E(t) - E(t+1))^{p/2(p-1)} \\
&\quad + \varepsilon\sup_{t\le s\le t+1}E(s), \quad i = 1, 2.
\end{aligned} \tag{67}$$

From Hölder inequality and Lemma 2,we get

$$\begin{aligned}
\left|\int_{t_1}^{t_2}\int_\Omega |u_t|^{q-2}u_t u\,dx\,ds\right| &\le \int_{t_1}^{t_2}\|u_t\|_q^{q-1}\|u\|_q ds \\
&\le \left(\int_{t_1}^{t_2}\|u_t\|_q^q ds\right)^{(q-1)/q}\left(\int_{t_1}^{t_2}\|u\|_q^q ds\right)^{1/q} \\
&\le C(\varepsilon)\int_{t_1}^{t_2}\|u_t\|_q^q ds + \varepsilon\int_{t_1}^{t_2}\|u\|_q^q ds,
\end{aligned} \tag{68}$$

$$\left|\int_{t_1}^{t_2}\int_\Omega |v_t|^{q-2}v_t v\,dx\,ds\right| \le \int_{t_1}^{t_2}\|v_t\|_q^{q-1}\|v\|_q ds$$
$$\le \left(\int_{t_1}^{t_2}\|v_t\|_q^q ds\right)^{(q-1)/q}\left(\int_{t_1}^{t_2}\|v\|_q^q ds\right)^{1/q}$$
$$\le C(\varepsilon)\int_{t_1}^{t_2}\|v_t\|_q^q ds + \varepsilon\int_{t_1}^{t_2}\|v\|_q^q ds. \tag{69}$$

Since $p < q < r+2$ and the property of the function $f(x)=\alpha^x/x$, $\alpha\ge 0$, $x>0$, we obtain

$$\frac{\|u\|_q^q}{q} \le C\frac{\|u\|_p^p}{p} + C\frac{\|u\|_{r+2}^{r+2}}{r+2}, \qquad \frac{\|v\|_q^q}{q} \le C\frac{\|v\|_p^p}{p} + C\frac{\|v\|_{r+2}^{r+2}}{r+2}. \tag{70}$$

We conclude from (69), (70), $[u,v]\in W$, and Lemma 1 that

$$\|u\|_q^q + \|v\|_q^q \le C\left(\|u\|_p^p + \|u\|_{r+2}^{r+2} + \|v\|_p^p + \|v\|_{r+2}^{r+2}\right)$$
$$\le C\left(\|u\|_p^p + \|\nabla u\|_p^p + \|v\|_p^p + \|\nabla v\|_p^p\right) \tag{71}$$
$$\le C\left(\|\nabla u\|_p^p + \|\nabla v\|_p^p\right) \le CE(t).$$

It follows from (63), (68), (69), and (71) that

$$\left|-\left(\int_{t_1}^{t_2}\int_\Omega |u_t|^{q-2}u_t u\,dx\,ds + \int_{t_1}^{t_2}\int_\Omega |v_t|^{q-2}v_t v\,dx\,ds\right)\right|$$
$$\le C(\varepsilon)(E(t)-E(t+1)) + \varepsilon C\int_{t_1}^{t_2}E(s)\,ds, \tag{72}$$

and we obtain from (63), Sobolev inequality, Hölder inequality, and Lemma 2 that

$$\left|-\int_{t_1}^{t_2}\int_\Omega \nabla u_t\nabla u ds\right| \le \int_{t_1}^{t_2}\|\nabla u_t\|\cdot\|\nabla u\|\,ds$$
$$\le \left(\int_{t_1}^{t_2}\|\nabla u_t\|^2 ds\right)^{1/2}\left(\int_{t_1}^{t_2}\|\nabla u\|^2 ds\right)^{1/2}$$
$$\le C(E(t)-E(t+1))^{1/2}\left(\int_{t_1}^{t_2}\|\nabla u\|_p^2 ds\right)^{1/2}$$
$$\le C(E(t)-E(t+1))^{1/2}\left(\int_{t_1}^{t_2}\|\nabla u\|_p^p ds\right)^{1/p}$$
$$\le C(E(t)-E(t+1))^{p/2(p-1)} + \varepsilon\int_{t_1}^{t_2}\|\nabla u\|_p^p ds. \tag{73}$$

Similarly, we have the following formula:

$$\left|-\int_{t_1}^{t_2}\int_\Omega \nabla v_t\nabla v ds\right| \le \int_{t_1}^{t_2}\|\nabla v_t\|\cdot\|\nabla v\|\,ds$$
$$\le \left(\int_{t_1}^{t_2}\|\nabla v_t\|^2 ds\right)^{1/2}\left(\int_{t_1}^{t_2}\|\nabla v\|^2 ds\right)^{1/2}$$
$$\le C(E(t)-E(t+1))^{1/2}\left(\int_{t_1}^{t_2}\|\nabla v\|_p^2 ds\right)^{1/2}$$
$$\le C(E(t)-E(t+1))^{1/2}\left(\int_{t_1}^{t_2}\|\nabla v\|_p^p ds\right)^{1/p}$$
$$\le C(E(t)-E(t+1))^{p/2(p-1)} + \varepsilon\int_{t_1}^{t_2}\|\nabla v\|_p^p ds. \tag{74}$$

We get from (57), (73), and (74) that

$$\left|\int_{t_1}^{t_2}\int_\Omega (\nabla u_t\nabla u + \nabla v_t\nabla v)\,ds\right|$$
$$\le C(E(t)-E(t+1))^{p/2(p-1)} + \varepsilon\int_{t_1}^{t_2}\left(\|\nabla u\|_p^p + \|\nabla v\|_p^p\right)ds$$
$$\le C(E(t)-E(t+1))^{p/2(p-1)} + \frac{\varepsilon}{\theta}\int_{t_1}^{t_2}K([u,v])\,ds. \tag{75}$$

Choosing small enough ε, we have from (65), (66), (67), (72), and (75) that

$$\int_{t_1}^{t_2}K([u,v])\,ds \le C\Big[(E(t)-E(t+1)) + (E(t)-E(t+1))^{p/2(p-1)}\Big] + \varepsilon\sup_{t\le s\le t+1}E(s) + \varepsilon\int_{t_1}^{t_2}E(s)\,ds. \tag{76}$$

It follows from (30) and (31) that

$$J([u,v]) = \frac{2(r+2)-p}{2p(r+2)}\left(\|\nabla u\|_p^p + \|\nabla v\|_p^p\right) + \frac{1}{2(r+2)}K([u,v]). \tag{77}$$

On the other hand, from (12) and using (57) and (77), we deduce that

$$E(t) = \frac{1}{2}\left(\|u_t\|^2 + \|v_t\|^2\right) + J([u,v])$$
$$= \frac{1}{2}\left(\|u_t\|^2 + \|v_t\|^2\right) + \frac{2(r+2)-p}{2p(r+2)} \times\left(\|\nabla u\|_p^p + \|\nabla v\|_p^p\right) + \frac{1}{2(r+2)}K([u,v])$$
$$\le \frac{1}{2}\left(\|u_t\|^2 + \|v_t\|^2\right) + \left(\frac{2(r+2)-p}{2\theta p(r+2)} + \frac{1}{2(r+2)}\right) \times K([u,v]). \tag{78}$$

By integrating (78) over $[t_1, t_2]$, we obtain

$$\int_{t_1}^{t_2} E(s)\,ds \le \frac{1}{2}\int_{t_1}^{t_2} \left(\|u_t\|^2 + \|v_t\|^2\right) ds + \left(\frac{2(r+2)-p}{2\theta p(r+2)} + \frac{1}{2(r+2)}\right)\int_{t_1}^{t_2} K([u,v])\,ds. \tag{79}$$

For small enough ε, we have from (76) and (79) that

$$\int_{t_1}^{t_2} E(s)\,ds \le C\left[(E(t)-E(t+1)) + (E(t)-E(t+1))^{p/(2(p-1))}\right] + \varepsilon \sup_{t\le s\le t+1} E(s). \tag{80}$$

Thus, there exists $t^* \in [t_1, t_2]$, such that

$$E(t^*) \le C\left[(E(t)-E(t+1)) + (E(t)-E(t+1))^{p/2(p-1)}\right] + \varepsilon \sup_{t\le s\le t+1} E(s). \tag{81}$$

Multiplying (1) by u_t and (2) by v_t and integrating over $\Omega \times [t^*, t_2]$, and summing up, we get

$$E(t_2) = E(t^*) - \int_{t^*}^{t_2} \left(\|u_t\|_q^q + \|v_t\|_q^q + \|\nabla u_t\|^2 + \|\nabla v_t\|^2\right) ds. \tag{82}$$

Therefore, we obtain from (63), (81), and (82) that

$$\sup_{t\le s\le t+1} E(s) \le C\left[(E(t)-E(t+1)) + (E(t)-E(t+1))^{p/2(p-1)}\right] + \varepsilon \sup_{t\le s\le t+1} E(s). \tag{83}$$

Choosing small enough ε, we have from (83) that

$$\sup_{t\le s\le t+1} E(s) \le C\left[(E(t)-E(t+1)) + (E(t)-E(t+1))^{p/2(p-1)}\right]. \tag{84}$$

Since $p > 2$ and $E(t) < E(0)$, we get

$$\sup_{t\le s\le t+1} E(s) \le C(E(t)-E(t+1))^{p/2(p-1)}. \tag{85}$$

Consequently,

$$\sup_{t\le s\le t+1} E(s)^{(2(p-1))/p} \le C(E(t)-E(t+1)). \tag{86}$$

Thus, applying Lemma 9 to (86), we get

$$E(t) \le \left[\frac{p-2}{pC}(t-1) + M^{(p-2)/p}\right]^{p/(2-p)}, \quad \forall t > 1, \tag{87}$$

where $M = \max_{t\in[0,1]} E(t) > 0$ is some constant depending only on $[u_0, v_0]$ and $[u_1, v_1]$. □

Acknowledgments

This research was supported by the National Natural Science Foundation of China (no. 61273016), The Natural Science Foundation of Zhejiang Province (no. Y6100016), The Middle-aged and Young Leader in Zhejiang University of Science and Technology (2008–2012), and the Interdisciplinary Pre-research Project of Zhejiang University of Science and Technology (2010–2012).

References

[1] L. A. Medeiros and M. M. Miranda, "Weak solutions for a system of nonlinear Klein-Gordon equations," *Annali di Matematica Pura ed Applicata*, vol. 146, pp. 173–183, 1987.

[2] M. M. Cavalcanti, V. N. D. Cavalcanti, J. S. P. Filho, and J. A. Soriano, "Existence and uniform decay of solutions of a parabolic-hyperbolic equation with nonlinear boundary damping and boundary source term," *Communications in Analysis and Geometry*, vol. 10, no. 3, pp. 451–466, 2002.

[3] M. M. Cavalcanti, V. N. Domingos Cavalcanti, and P. Martinez, "Existence and decay rate estimates for the wave equation with nonlinear boundary damping and source term," *Journal of Differential Equations*, vol. 203, no. 1, pp. 119–158, 2004.

[4] M. M. Cavalcanti and V. N. Domingos Cavalcanti, "Existence and asymptotic stability for evolution problems on manifolds with damping and source terms," *Journal of Mathematical Analysis and Applications*, vol. 291, no. 1, pp. 109–127, 2004.

[5] K. Agre and M. A. Rammaha, "Systems of nonlinear wave equations with damping and source terms," *Differential and Integral Equations*, vol. 19, no. 11, pp. 1235–1270, 2006.

[6] C. O. Alves, M. M. Cavalcanti, V. N. Domingos Cavalcanti, M. A. Rammaha, and D. Toundykov, "On existence, uniform decay rates and blow up for solutions of systems of nonlinear wave equations with damping and source terms," *Discrete and Continuous Dynamical Systems*, vol. 2, no. 3, pp. 583–608, 2009.

[7] M. A. Rammaha and Z. Wilstein, "Hadamard well-posedness for wave equations with p-Laplacian damping and supercritical sources," *Advances in Differential Equations*, vol. 17, no. 1-2, pp. 105–150, 2012.

[8] Z. Yang, "Existence and asymptotic behaviour of solutions for a class of quasi-linear evolution equations with non-linear damping and source terms," *Mathematical Methods in the Applied Sciences*, vol. 25, no. 10, pp. 795–814, 2002.

[9] K. Ono, "Blow up phenomenon for nonlinear dissipative wave equatins," *Journal of Mathematics, Tokushima University*, vol. 30, pp. 19–43, 1996.

[10] F. Dell'Oro and V. Pata, "Long-term analysis of strongly damped nonlinear wave equations," *Nonlinearity*, vol. 24, no. 12, pp. 3413–3435, 2011.

[11] T. F. Ma and J. A. Soriano, "On weak solutions for an evolution equation with exponential nonlinearities," *Nonlinear Analysis*, vol. 37, no. 8, Ser. A: Theory Methods, pp. 1029–1038, 1999.

[12] M. A. Rammaha, "The influence of damping and source terms on solutions of nonlinear wave equations," *Boletim da Sociedade Paranaense de Matemática*, vol. 25, no. 1-2, pp. 77–90, 2007.

[13] C. O. Alves and M. M. Cavalcanti, "On existence, uniform decay rates and blow up for solutions of the 2-D wave equation with exponential source," *Calculus of Variations and Partial Differential Equations*, vol. 34, no. 3, pp. 377–411, 2009.

[14] L. Bociu, M. Rammaha, and D. Toundykov, "On a wave equation with supercritical interior and boundary sources and damping terms," *Mathematische Nachrichten*, vol. 284, no. 16, pp. 2032–2064, 2011.

[15] D. H. Sattinger, "On global solution of nonlinear hyperbolic equations," *Archive for Rational Mechanics and Analysis*, vol. 30, pp. 148–172, 1968.

[16] L. E. Payne and D. H. Sattinger, "Saddle points and instability of nonlinear hyperbolic equations," *Israel Journal of Mathematics*, vol. 22, no. 3-4, pp. 273–303, 1975.

[17] M. Nakao, "A difference inequality and its application to nonlinear evolution equations," *Journal of the Mathematical Society of Japan*, vol. 30, no. 4, pp. 747–762, 1978.

[18] E. Piskin and N. Polat, "Global existence, decay and blow-up solutions for coupled nonlinear wave equations with damping and source terms," *Turkish Journal of Mathematics*, vol. 30, pp. 1–19, 2013.

Hindawi Publishing Corporation
Abstract and Applied Analysis
Volume 2013, Article ID 262010, 14 pages
http://dx.doi.org/10.1155/2013/262010

Research Article

A Class of Spectral Element Methods and Its A Priori/A Posteriori Error Estimates for 2nd-Order Elliptic Eigenvalue Problems

Jiayu Han and Yidu Yang

School of Mathematics and Computer Science, Guizhou Normal University, Guiyang 550001, China

Correspondence should be addressed to Yidu Yang; ydyang@gznu.edu.cn

Received 24 May 2013; Accepted 1 September 2013

Academic Editor: Rasajit Bera

This paper discusses spectral and spectral element methods with Legendre-Gauss-Lobatto nodal basis for general 2nd-order elliptic eigenvalue problems. The special work of this paper is as follows. (1) We prove a priori and a posteriori error estimates for spectral and spectral element methods. (2) We compare between spectral methods, spectral element methods, finite element methods and their derived p-version, h-version, and hp-version methods from accuracy, degree of freedom, and stability and verify that spectral methods and spectral element methods are highly efficient computational methods.

1. Introduction

As we know, finite element methods are local numerical methods for partial differential equations and particularly well suitable for problems in complex geometries, whereas spectral methods can provide a superior accuracy, at the expense of domain flexibility. Spectral element methods combine the advantages of the above methods (see [1]). So far, spectral and spectral element methods are widely applied to boundary value problems (see [1, 2]), as well as applied to symmetric eigenvalue problems (see [3]). However, it is still a new subject to apply them to nonsymmetric elliptic eigenvalue problems.

A posteriorii error estimates and highly efficient computational methods for finite elements of eigenvalue problems are the subjects focused on by the academia these years; see [3–16], and among them, for nonsymmetric 2nd-order elliptic eigenvalue problems, [5, 15] provide a posteriori error estimates and adaptive algorithms, [9] the function value recovery techniques and [8, 10] two-level discretization schemes.

Based on the work mentioned above, this paper shall further apply spectral and spectral element methods to nonsymmetric elliptic eigenvalue problems. This paper will mainly perform the following work.

(1) We prove a priori and a posteriori error estimates of spectral and spectral element methods with Legendre-Gauss-Lobatto nodal basis, respectively, for the general 2nd-order elliptic eigenvalue problems.

(2) We compare between spectral methods, spectral element methods with Legendre-Gauss-Lobatto nodal basis, finite element methods, and their derived p-version, h-version, and hp-version methods from accuracy, degree of freedom, and stability and verify that spectral methods and spectral element methods are highly efficient computational methods for nonsymmetric 2nd-order elliptic eigenvalue problems.

This paper is organized as follows. Section 2 introduces basic knowledge of second elliptic eigenvalue problems. Sections 3 and 4 are devoted to a priori and a posteriori error estimates of spectral and spectral element methods, respectively. In Section 5, some numerical experiments are performed by the methods mentioned above.

2. Preliminaries

Consider the 2nd-order elliptic boundary value problem

$$\begin{aligned} Lw = -\nabla \cdot (D\nabla w) + \mathbf{b} \cdot \nabla w + cw &= f, \quad \text{in } \Omega, \\ w &= 0, \quad \text{on } \partial\Omega, \end{aligned} \tag{1}$$

where $\Omega \subset R^d$ ($d = 2, 3$) is a bounded domain, $\mathbf{b}$ and c are a real-valued vector function and a real-valued function, respectively, and D is a positive scalar function with $D(x) \geq D_0 > 0$ ($\forall x \in \Omega$).

We denote the complex Sobolev spaces with norm $\|\cdot\|_m$ by $H^m(\Omega)$, $H_0^1(\Omega) = \{v \in H^1(\Omega), v|_{\partial\Omega} = 0\}$. Let $(\cdot,\cdot)$ and $\|\cdot\|_{0,\Omega}$ be a inner product and a norm in the complex space $L^2(\Omega)$, respectively.

In this paper, C denotes a generic positive constant independent of the polynomial degrees and mesh scales, which may not be the same at different occurrences.

Define the bilinear form $a(\cdot,\cdot)$ as follows:

$$a(w, v) = \int_\Omega D\nabla w \nabla \overline{v} + (\mathbf{b} \cdot \nabla w)\overline{v} + cw\overline{v}, \quad \forall w, v \in H_0^1(\Omega). \tag{2}$$

We assume that $f \in L^2(\Omega)$, D, $\mathbf{b}$, and c are bounded functions on Ω, namely $D, c \in L^\infty(\Omega)$, $\mathbf{b} \in (L^\infty(\Omega))^d$. Further more, we assume that $\nabla \cdot \mathbf{b}$ exists and satisfies

$$-\frac{1}{2}\nabla \cdot \mathbf{b} + c \geq 0, \quad \text{in } \Omega. \tag{3}$$

Under these assumptions, the bilinear form $a(\cdot,\cdot)$ is continuous in $H_0^1(\Omega)$ and $H_0^1(\Omega)$-elliptic; that is, there exist two constants $A, B > 0$ independent of w, v such that

$$\begin{aligned} |a(w, v)| &\leq A\|w\|_{1,\Omega}\|v\|_{1,\Omega}, \quad \forall w, v \in H_0^1(\Omega), \\ \operatorname{Re} a(v, v) &\geq B\|v\|_{1,\Omega}^2, \quad \forall v \in H_0^1(\Omega). \end{aligned} \tag{4}$$

The corresponding variational formulation of (1) is given as follows: find $w \in H_0^1(\Omega)$, such that

$$a(w, v) = (f, v), \quad \forall v \in H_0^1(\Omega). \tag{5}$$

The adjoint problem of (5) is as follows: find $w^* \in H_0^1(\Omega)$, such that

$$a(v, w^*) = (v, f), \quad \forall v \in H_0^1(\Omega). \tag{6}$$

As the general 2nd-order elliptic boundary value problems, we assume that the regularity estimates for problem (5) and its adjoint problem (6) hold, respectively. Namely

$$\|w\|_{r_1+1,\Omega} \leq C\|f\|_{0,\Omega}, \quad 0 < r_1 \leq 1, \tag{7}$$

$$\|w^*\|_{r_2+1,\Omega} \leq C\|f\|_{0,\Omega}, \quad 0 < r_2 \leq 1. \tag{8}$$

We assume that $K_h = \{\kappa\}$ is a regular rectangle (resp. cuboid) or simplex partition of the domain Ω and satisfies $\overline{\Omega} = \bigcup \overline{\kappa}$. We associate with the partition a polynomial degree vector $\mathbf{N} = \{N_\kappa\}$, where N_κ is the polynomial degree in κ. Let h_κ be the diameter of the element κ, and let $h = \max_{\kappa\in K_h} h_\kappa$.

We define spectral and spectral element spaces as follows:

$$\begin{aligned} S_N(\Omega) &= \{v \in P_N(\Omega), v|_{\partial\Omega} = 0\}, \\ S_{N,h}(\Omega) &= \{v \in C(\overline{\Omega}) : v|_\kappa \in P_{N_\kappa}(\kappa), \forall \kappa \in K_h, v|_{\partial\Omega} = 0\}, \end{aligned} \tag{9}$$

where $P_N(\Omega)$ and $P_{N_\kappa}(\kappa)$ are polynomial spaces of degree N (resp. degree N in every direction) in Ω and degree N_κ (resp. degree N_κ in every direction) in the element κ, respectively.

The spectral approximation of (5) is as follows: find $w_N \in S_N(\Omega)$, such that

$$a(w_N, v) = (f, v), \quad \forall v \in S_N(\Omega). \tag{10}$$

The spectral element approximation of (5) is as follows: find $w_{N,h} \in S_{N,h}(\Omega)$, such that

$$a(w_{N,h}, v) = (f, v), \quad \forall v \in S_{N,h}(\Omega). \tag{11}$$

We assume that $f \in L^2(\Omega)$ and derive from Lax-Milgram theorem that the variational formations (5), (6), (10), and (11) have a unique solution, respectively.

Define the interpolation operators

$$\begin{aligned} I_{N_\kappa,h_\kappa} &: C(\kappa) \longrightarrow P_{N_\kappa}(\kappa), \\ I_N &: C(\Omega) \longrightarrow S_N(\Omega), \end{aligned} \tag{12}$$

as the interpolations in the element κ and the domain Ω, respectively, with the tensorial Legendre-Gauss-Lobatto (LGL) interpolation nodes.

Define the interpolation operator

$$I_{N,h} : C(\Omega) \longrightarrow S_{N,h}(\Omega), \quad \text{satisfying } I_{N,h}|_\kappa = I_{N_\kappa,h_\kappa}. \tag{13}$$

We quote from [2] (see (5.8.27) therein) the interpolation estimates for spectral and spectral element methods with LGL Nodal-basis as follows.

For all $v \in H^{s_\kappa}(\kappa)$, $s_\kappa \geq (d+1)/2$,

$$\left\|v - I_{N_\kappa,h_\kappa}v\right\|_{1,\kappa} \leq C(s_\kappa)\, h_\kappa^{\min(N_\kappa+1,s_\kappa)-1} N_\kappa^{-s_\kappa+1}\|v\|_{s_\kappa,\kappa}, \tag{14}$$

$$\left\|v - I_{N_\kappa,h_\kappa}v\right\|_{0,\kappa} \leq C(s_\kappa)\, h_\kappa^{\min(N_\kappa+1,s_\kappa)} N_\kappa^{-s_\kappa}\|v\|_{s_\kappa,\kappa}. \tag{15}$$

For all $v \in H^s(\Omega)$, $s \geq (d+1)/2$,

$$\left\|v - I_N v\right\|_{1,\Omega} \leq C(s)\, N^{-s+1}\|v\|_{s,\Omega}, \tag{16}$$

$$\left\|v - I_N v\right\|_{0,\Omega} \leq C(s)\, N^{-s}\|v\|_{s,\Omega}. \tag{17}$$

We assume that the solution of boundary value problem (5) $w \in H_0^1(\Omega) \cap H^m(\Omega)$ ($m > 1$), that w_N and $w_{N,h}$ are the solutions of (10) and (11), respectively; then we derive from Céa lemma and the interpolation estimates that

$$\|w_N - w\|_{1,\Omega} \le C(m) N^{-m+1} \|w\|_{m,\Omega}, \tag{18}$$

$$\|w_{N,h} - w\|_{1,\Omega} \le \left\{ \sum_{\kappa} C(s_\kappa) h_\kappa^{2\{\min(N_\kappa+1,s_\kappa)-1\}} \times N_\kappa^{2(-s_\kappa+1)} \|w\|_{s_\kappa,\kappa}^2 \right\}^{1/2}, \tag{19}$$

where $s_\kappa \ge (d+1)/2, \forall \kappa \in K_h$.

Particularly, if $N_\kappa = N, \forall \kappa \in K_h$, then we have

$$\|w_{N,h} - w\|_{1,\Omega} \le C(m) h^{\min(N+1,m)-1} \times N^{1-m} \|w\|_{m,\Omega}. \tag{20}$$

Note that (18) is also suited to spectral methods with modal basis (see [1, 2]).

Using Aubin-Nitsche technique, we deduce from the regularity estimate (8) and the estimates (18)–(20) the priori estimates of boundary value problem (5) for spectral and spectral element methods; that is,

$$\|w_N - w\|_{0,\Omega} \le CN^{-m-r_2+1} \|w\|_{m,\Omega}, \tag{21}$$

$$\|w_{N,h} - w\|_{0,\Omega} \le CN^{-m-r_2+1} h^{r_2+\min(N+1,m)-1} \|w\|_{m,\Omega}. \tag{22}$$

3. Spectral and Spectral-Element Approximations and Error Estimates for Eigenvalue Problems

3.1. Spectral and Spectral-Element Approximations for Eigenvalue Problems. Consider the following eigenvalue problem corresponding to the boundary value problem (1):

$$\begin{aligned} Lu &= \lambda u, \quad \text{in } \Omega, \\ u &= 0, \quad \text{on } \partial\Omega. \end{aligned} \tag{23}$$

The variational formation of (23) is given by the following: find $\lambda \in \mathbb{C}, 0 \ne u \in H_0^1(\Omega)$, such that

$$a(u,v) = \lambda(u,v), \quad \forall v \in H_0^1(\Omega). \tag{24}$$

The spectral approximation scheme of (24) is given by the following: find $\lambda_N \in \mathbb{C}, 0 \ne u_N \in S_N(\Omega)$, such that

$$a(u_N, v_N) = \lambda_N (u_N, v_N), \quad \forall v_N \in S_N(\Omega). \tag{25}$$

The spectral element approximation scheme of (24) is given by the following: find $\lambda_{N,h} \in \mathbb{C}, 0 \ne u_{N,h} \in S_{N,h}(\Omega)$, such that

$$a(u_{N,h}, v_{N,h}) = \lambda_{N,h} (u_{N,h}, v_{N,h}), \quad \forall v_{N,h} \in S_{N,h}(\Omega), \tag{26}$$

Define the solution operators $T : L^2(\Omega) \to H_0^1(\Omega), T_N : L^2(\Omega) \to S_N(\Omega)$, and $T_{N,h} : L^2(\Omega) \to S_{N,h}(\Omega)$ by

$$\begin{aligned} a(Tf, v) &= (f, v), \quad \forall f \in L^2(\Omega), \ \forall v \in H_0^1(\Omega), \\ a(T_N f, v_N) &= (f, v_N), \quad \forall f \in L^2(\Omega), \ \forall v_N \in S_N(\Omega), \\ a(T_{N,h} f, v_{N,h}) &= (f, v_{N,h}), \quad \forall f \in L^2(\Omega), \ \forall v_{N,h} \in S_{N,h}(\Omega). \end{aligned} \tag{27}$$

Obviously (see [17]), the equivalent operator forms for (24) and (26) are the following.

Find $\lambda \in \mathbb{C}, 0 \ne u \in H_0^1(\Omega)$, such that

$$Tu = \lambda^{-1} u. \tag{28}$$

Find $\lambda_{N,h} \in \mathbb{C}, 0 \ne u_{N,h} \in S_{N,h}(\Omega)$, such that

$$T_{N,h} u_{N,h} = \lambda_{N,h}^{-1} u_{N,h}. \tag{29}$$

The adjoint problem of the eigenvalue problem (23) is

$$\begin{aligned} L^* u^* &= \lambda^* u^*, \quad \text{in } \Omega, \\ u^* &= 0, \quad \text{on } \partial\Omega, \end{aligned} \tag{30}$$

where $L^* u^* = -\nabla \cdot (D \nabla u^*) - \mathbf{b} \cdot \nabla u^* + (c - \nabla \cdot \mathbf{b}) u^*$.

The variational formation of (30) is given by the following: find $\lambda^* \in \mathbb{C}, 0 \ne u^* \in H_0^1(\Omega)$, such that

$$a^*(u^*, v) := \overline{a(v, u^*)} = \lambda^* (u^*, v), \quad \forall v \in H_0^1(\Omega). \tag{31}$$

The spectral element approximation scheme of (31) is given by the following: find $\lambda_{N,h}^* \in \mathbb{C}, 0 \ne u_{N,h}^* \in S_{N,h}(\Omega)$, such that

$$a^*(u_{N,h}^*, v_{N,h}) = \lambda_{N,h}^* (u_{N,h}^*, v_{N,h}), \quad \forall v_{N,h} \in S_{N,h}(\Omega). \tag{32}$$

We can likewise define the equivalent operator forms for the eigenvalue problems (31) and (32) as

$$\begin{aligned} T^* u^* &= \lambda^{*-1} u^*, \\ T_{N,h}^* u_{N,h}^* &= \lambda_{N,h}^{*-1} u_{N,h}^*. \end{aligned} \tag{33}$$

Let λ be an eigenvalue of (23). There exists a smallest integer μ, called the ascent of λ, such that $\ker((\lambda^{-1} - T)^\mu) = \ker((\lambda^{-1} - T)^{\mu+1})$. $q = \dim \ker((\lambda^{-1} - T)^\mu)$ is called the algebraic multiplicity of λ. The functions in $\ker((\lambda^{-1} - T)^\mu)$ are called generalized eigenfunctions of T corresponding to λ. Likewise the ascent, algebraic multiplicity and generalized eigenfunctions of $\lambda_{N,h}$, λ^* and $\lambda_{N,h}^*$ can be defined.

Let λ be an eigenvalue of (23) with the algebraic multiplicity q and the ascent μ. Assume $\|T_{N,h} - T\|_{1,\Omega} \to 0$ $(N \to \infty, h \to 0)$; then there are eigenvalues $\lambda_{j,N,h}$ $(j = 1, 2, \ldots, q)$ of (26) which converge to λ. Let $M(\lambda)$ be the space spanned by all generalized eigenfunctions corresponding to λ of T, and let $M_{N,h}(\lambda)$ be the space spanned by all generalized eigenfunctions corresponding to all eigenvalues of $T_{N,h}$ that converge to λ.

In view of adjoint problems (31) and (32), the definitions of $M^*(\lambda^*)$ and $M^*_{N,h}(\lambda^*)$ are analogous to $M(\lambda)$ and $M_{N,h}(\lambda)$. Let $\widehat{M}(\lambda) = \{v \in M(\lambda) : \|v\|_{1,\Omega} = 1\}$, and let $\widehat{M^*}(\lambda^*) = \{v \in M^*(\lambda^*) : \|v\|_{1,\Omega} = 1\}$.

Note that when $\mathbf{b} = 0$, both (24) and (26) are symmetric. Thus, the ascent $\mu = 1$ of λ, and the ascent $l = 1$ of $\lambda_{N,h}$.

3.2. A Priori Error Estimates. We will analyze a prior error estimates for spectral element methods which are suitable for spectral methods with mesh fineness h not considered.

Assume that R and U are two closed subspace in $H_0^1(\Omega)$. Denote

$$\delta(R,U) = \sup_{\substack{v\in R\\ \|v\|_{1,\Omega}=1}} \operatorname{dist}(v,U),$$
$$\theta(R,U) = \max(\delta(R,U), \delta(U,R)). \tag{34}$$

We say that $\theta(R,U)$ is the gap between R and U.

Denote

$$\varepsilon_{N,h} = \varepsilon_{N,h}(\lambda) = \sup_{u\in\widehat{M}(\lambda)} \inf_{v\in S_{N,h}(\Omega)} \|u-v\|_{1,\Omega},$$
$$\varepsilon^*_{N,h} = \varepsilon^*_{N,h}(\lambda^*) = \sup_{u\in\widehat{M^*}(\lambda^*)} \inf_{v\in S_{N,h}(\Omega)} \|u-v\|_{1,\Omega}. \tag{35}$$

We give the following four lemmas from Theorem 8.1–8.4 in [17], which are applications to spectral element methods.

Lemma 1. *Assume $\|T_{N,h}-T\|_{1,\Omega} \to 0$ $(N\to\infty, h\to 0)$. For small enough h and big enough N, there holds*

$$\theta(M(\lambda), M_{N,h}(\lambda)) \le C\varepsilon_{N,h}. \tag{36}$$

Lemma 2. *Assume $\|T_{N,h}-T\|_{1,\Omega} \to 0$ $(N\to\infty, h\to 0)$; then*

$$\left|\lambda^{-1} - \frac{1}{q}\sum_{j=1}^{q}\lambda_{j,N,h}^{-1}\right| \le C\varepsilon_{N,h}\varepsilon^*_{N,h}. \tag{37}$$

Lemma 3. *Assume that $\|T_{N,h}-T\|_{1,\Omega} \to 0$ $(N\to\infty, h\to 0)$; then there holds*

$$\left|\lambda - \lambda_{j,N,h}\right| \le C\left(\varepsilon_{N,h}\varepsilon^*_{N,h}\right)^{1/\mu} \quad (j=1,2,\ldots,q). \tag{38}$$

Since $\ker((\lambda^{-1}-T)^l)$ $(l\ge 1)$ is a finite dimensional space, there exists a direct-sum decomposition $H_0^1(\Omega) = \ker((\lambda^{-1}-T)^l) \oplus M_l$. We define the operator E_l as a projection along M_l from $H_0^1(\Omega)$ to $\ker((\lambda^{-1}-T)^l)$.

Lemma 4. *Assume $\|T_{N,h}-T\|_{1,\Omega} \to 0$ $(N\to\infty, h\to 0)$. Let $\lambda_{N,h}$ be an eigenvalue of $T_{N,h}$ and $\lim_{N\to\infty,h\to 0}\lambda_{N,h} = \lambda$. $u_{N,h}$ satisfies $(\lambda_{N,h}^{-1} - T_{N,h})^k u_{N,h} = 0$ and $\|u_{N,h}\|_{1,\Omega} = 1$, where $k \le \mu$ is a positive integer. Then, for every integer $l \in [k,\mu]$, there holds*

$$\|u_{N,h} - E_l u_{N,h}\|_{1,\Omega} \le C\varepsilon_{N,h}^{(l-k+1)/\mu}. \tag{39}$$

We assume that in this section, for the sake of simplicity, $N_\kappa = N, \forall\kappa\in K_h$.

Theorem 5. *If $M(\lambda) \subset H^{t_1}(\Omega)$ and $M^*(\lambda^*) \subset H^{t_2}(\Omega)$, then there holds the following error estimates:*

$$\left|\frac{1}{q}\sum_{j=1}^{q}\lambda_{j,N,h} - \lambda\right| \le C\left(\frac{h^{\tau_1+\tau_2-2}}{N^{t_1+t_2-2}}\right) \sup_{u\in\widehat{M}(\lambda)} \|u\|_{t_1,\Omega} \sup_{v\in\widehat{M^*}(\lambda^*)} \|v\|_{t_2,\Omega}, \tag{40}$$

$$\left|\lambda_{j,N,h} - \lambda\right| \le C\left(\left(\frac{h^{\tau_1+\tau_2-2}}{N^{t_1+t_2-2}}\right) \sup_{u\in\widehat{M}(\lambda)} \|u\|_{t_1,\Omega} \sup_{v\in\widehat{M^*}(\lambda^*)} \|v\|_{t_2,\Omega}\right)^{1/\mu} \quad (j=1,2,\ldots,q), \tag{41}$$

$$\theta(M(\lambda), M_{N,h}(\lambda)) \le C\frac{h^{\tau_1-1}}{N^{t_1-1}} \sup_{u\in\widehat{M}(\lambda)} \|u\|_{t_1,\Omega}. \tag{42}$$

Let $\|u_{N,h}\|_{1,\Omega} = 1$, and let $(\lambda_{N,h}^{-1} - T_{N,h})^{l_1} u_{N,h} = 0$, for some $l_1 \le \mu$. Then, for every integer l_2 $(l_1 \le l_2 \le \mu)$, there exists a function u', such that $(\lambda^{-1}-T)^{l_2}u' = 0$ and

$$\left\|u_{N,h} - u'\right\|_{1,\Omega} \le C\left(\left(\frac{h^{\tau_1-1}}{N^{t_1-1}}\right) \sup_{u\in\widehat{M}(\lambda)} \|u\|_{t_1,\Omega}\right)^{(l_2-l_1+1)/\mu}, \tag{43}$$

where $\tau_1 = \min(N+1, t_1)$, $\tau_2 = \min(N+1, t_2)$.

Proof. We derive from the error estimate (20) that

$$\left\|T_{N,h} - T\right\|_{1,\Omega} = \sup_{f\in H_0^1(\Omega)} \frac{\left\|(T-T_{N,h})f\right\|_{1,\Omega}}{\left\|f\right\|_{1,\Omega}} \le C(1+r_1)h^{r_1}N^{-r_1} \longrightarrow 0 \quad (N\longrightarrow\infty, h\longrightarrow 0). \tag{44}$$

By (14),

$$\varepsilon_{N,h} = \varepsilon_{N,h}(\lambda) = \sup_{u\in\widehat{M}(\lambda)} \inf_{v\in S_{N,h}(\Omega)} \|u-v\|_{1,\Omega} \le C\left(\frac{h^{\tau_1-1}}{N^{t_1-1}}\right) \sup_{u\in\widehat{M}(\lambda)} \|u\|_{t_1,\Omega}. \tag{45}$$

Analogically,

$$\varepsilon^*_{N,h} \le C\left(\frac{h^{\tau_2-1}}{N^{t_2-1}}\right) \sup_{u\in\widehat{M^*}(\lambda^*)} \|u\|_{t_2,\Omega}. \tag{46}$$

Plugging the two inequalities above into (36), (38), and (39) yields (42), (41), and (43), respectively. We find from (37) that

$$\begin{aligned}\left|\frac{1}{q}\sum_{j=1}^{q}\lambda_{j,N,h}-\lambda\right| &= \left|\frac{1}{q}\sum_{j=1}^{q}\frac{\lambda_{j,N,h}^{-1}-\lambda^{-1}}{\lambda^{-1}\lambda_{j,N,h}^{-1}}\right| \\ &\leq C\left|\frac{1}{q}\sum_{j=1}^{q}\lambda_{j,N,h}^{-1}-\lambda^{-1}\right| \leq C\varepsilon_{N,h}\varepsilon_{N,h}^{*},\end{aligned} \tag{47}$$

combining with (45) and (46) yields (40). □

Supposing that $\|T_{N,h}-T\|_{0,\Omega} \to 0\,(N \to \infty, h \to 0)$, $\rho(T)$ is a regular set of T, and $\Gamma \subset \rho(T)$ is a closed Jordan curve enclosing λ^{-1}.

Denote

$$\begin{aligned}R(z) &= (T-z)^{-1}, \\ R(T_{N,h},z) &= (T_{N,h}-z)^{-1}.\end{aligned} \tag{48}$$

Define the spectral projection operators

$$\begin{aligned}E &= \frac{-1}{2i\pi}\int_{\Gamma}R(T,z)\,\mathrm{d}z : H_0^1(\Omega) \longrightarrow M(\lambda), \\ E_{N,h} &= \frac{-1}{2i\pi}\int_{\Gamma}R(T_{N,h},z)\,\mathrm{d}z : H_0^1(\Omega) \longrightarrow M_{N,h}(\lambda).\end{aligned} \tag{49}$$

We give the following lemma by referring to [18, 19] (see proposition 5.3 in [18] and theorem 1.3.2 in [19]).

Lemma 6. *If $\|T_{N,h}-T\|_{0,\Omega} \to 0\,(N \to \infty, h \to 0)$, then there holds that $E_{N,h} \to E(p)$, $R(T_{N,h},z)$ is uniformly bounded with N and h, and*

$$\begin{aligned}\|(E_{N,h}-E)\,v\|_{0,\Omega} &\leq C\max_{z\in\Gamma}\|(T-T_{N,h})\,R(z)\,v\|_{0,\Omega}, \\ &\qquad \forall v \in H_0^1(\Omega), \\ \|(E_{N,h}-E)\,v\|_{0,\Omega} &\leq C\max_{z\in\Gamma}\|(T-T_{N,h})\,R(T_{N,h},z)\,v\|_{0,\Omega}, \\ &\qquad \forall v \in H_0^1(\Omega).\end{aligned} \tag{50}$$

Theorem 7. *Under the assumptions of Theorem 5, further assume that the ascent of λ is $\mu = 1$. Let $(\lambda_{N,h}, u_{N,h})$ be an eigenpair of* (26) *with $\|u_{N,h}\|_{0,\Omega} = 1$; then there exists an eigenpair (λ, u) of* (24)*, such that*

$$\|u_{N,h}-u\|_{1,\Omega} \leq \frac{Ch^{\tau_1-1}\|u\|_{t_1,\Omega}}{N^{t_1-1}}, \tag{51}$$

$$\|u_{N,h}-u\|_{0,\Omega} \leq \frac{Ch^{r_2+\tau_1-1}\|u\|_{t_1,\Omega}}{N^{r_2+t_1-1}}, \tag{52}$$

$$\begin{aligned}&|\lambda_{N,h}-\lambda| \\ &\quad \leq C\left(\left(\frac{h^{\tau_1+\tau_2-2}}{N^{t_1+t_2-2}}\right)\sup_{u\in\widehat{M}(\lambda)}\|u\|_{t_1,\Omega}\sup_{v\in\widehat{M^*}(\lambda^*)}\|v\|_{t_2,\Omega}\right),\end{aligned} \tag{53}$$

where $\tau_1 = \min(N+1, t_1)$ and $\tau_2 = \min(N+1, t_2)$.

Let (λ, u) be an eigenpair of (24)*. If $\lambda_{N,h}$ is an eigenvalue of* (26) *convergence to λ, then there exists $u_{N,h} \in \ker(\lambda_{N,h}^{-1}-T_{N,h})$, such that* (51)–(53) *hold.*

Proof. We deduce (53) immediately from (41). We derive from (22) and (7) that

$$\|Tf-T_{N,h}f\|_{0,\Omega} \leq CN^{-r_1-r_2}h^{r_1+r_2}\|f\|_{0,\Omega}; \tag{54}$$

thus,$\|T-T_{N,h}\|_{0,\Omega} \to 0\,(N \to \infty, h \to 0)$. Taking $u = Eu_{N,h}$ and by virtue of $R(T_{N,h},z)u_{N,h} = (\lambda_{N,h}^{-1}-z)^{-1}u_{N,h}$, Lemma 6 and (22), we have

$$\begin{aligned}\|u-u_{N,h}\|_{0,\Omega} &= \|Eu_{N,h}-E_{N,h}u_{N,h}\|_{0,\Omega} \\ &\leq C\|(T-T_{N,h})\,u_{N,h}\|_{0,\Omega} \\ &\leq C\left(\|(T-T_{N,h})\,u\|_{0,\Omega}\right. \\ &\qquad \left.+\|(T-T_{N,h})\,(u_{N,h}-u)\|_{0,\Omega}\right),\end{aligned} \tag{55}$$

from which follows

$$\begin{aligned}\|u-u_{N,h}\|_{0,\Omega} &\leq C\|(T-T_{N,h})\,u\|_{0,\Omega} \\ &\leq \frac{Ch^{r_2+\tau_1-1}\|u\|_{t_1,\Omega}}{N^{r_2+t_1-1}},\end{aligned} \tag{56}$$

which is (52). By direct calculation, we have

$$\begin{aligned}&\|u-u_{N,h}\|_{1,\Omega} \\ &\quad = \|\lambda Tu-\lambda_h T_{N,h}u_{N,h}\|_{1,\Omega} \\ &\quad \leq \|\lambda Tu-\lambda T_{N,h}u\|_{1,\Omega}+\|\lambda T_{N,h}u-\lambda_h T_{N,h}u_{N,h}\|_{1,\Omega} \\ &\quad \leq \|(T-T_{N,h})\,(\lambda u)\|_{1,\Omega}+C\|\lambda u-\lambda_{N,h}u_{N,h}\|_{0,\Omega}.\end{aligned} \tag{57}$$

Plugging (20), (52), and (53) into (57) yields (51).

If (λ, u) is an eigenpair of (24), let $u_{N,h} = E_{N,h}u$; by the same argument we can prove (51) and (52). □

4. A Posteriori Error Estimates

Based on [20], we will discuss a posteriori error estimates. We further assume that $\Omega \subset R^2$, the partition K_h is γ-shape regular, and the polynomial degree of neighboring elements are comparable; that is, there exists $\gamma > 0$, such that for all $\kappa, \kappa' \in K_h$, $\overline{\kappa} \cap \overline{\kappa'} \neq \emptyset$,

$$\begin{aligned}\gamma^{-1}h_\kappa &\leq h_{\kappa'} \leq \gamma h_\kappa, \\ \gamma^{-1}(N_\kappa+1) &\leq N_{\kappa'}+1 \leq \gamma(N_\kappa+1).\end{aligned} \tag{58}$$

We refer to the hp-clément interpolation estimates given by [20, 21] (see theorems 2.2 and 2.3, respectively), which generalize the well-known clément type interpolation operators studied in [22] and [23] to the hp context.

Lemma 8. *Assume that the partition K_h is γ-shape regular and the polynomial distribution* **N** *is comparable. Then there* *exists a positive constant $C = C(\gamma)$ and the clément operator $I: H_0^1(\Omega) \to S_{N,h}(\Omega)$, such that*

$$\|v - Iv\|_{0,\kappa} \le C \frac{h_\kappa}{N_\kappa} \|\nabla v\|_{0,\omega_\kappa}, \tag{59}$$

$$\|v - Iv\|_{0,e} \le C \sqrt{\frac{h_e}{N_e}} \|\nabla v\|_{0,\omega_e}, \tag{60}$$

where h_e is the length of the edge e and $N_e = \max(N_{\kappa_1}, N_{\kappa_2})$, where κ_1, κ_2 are elements sharing the edge e and ω_κ, ω_e are patches covering κ and e with a few layers, respectively.

Define interval $\widehat{I} = (0,1)$ and weight function $\Phi_{\widehat{I}}(x) := x(1-x)$. Denote the reference square and triangle element by $\widehat{\kappa} = (0,1)^2$ and $\widehat{\kappa} = \{(x,y) | 0 < x < 1, 0 < y < \sqrt{3}(1/2 - |1/2 - x|)\}$, respectively. Define weight function $\Phi_{\widehat{\kappa}}(x) := \operatorname{dist}(x, \partial\widehat{\kappa})$.

The following three lemmas are given by [20]. Lemmas 9–10 provide the polynomial inverse estimates in standard interval and element, while Lemma 11 provides a result for the extension from an edge to the element.

Lemma 9. *Let $-1 < \alpha < \beta, \sigma \in [0,1]$. Then there exists $C = C(\alpha, \beta)$, such that for all $N \in \mathbb{N}$ and all univariate polynomials π_N of degree N,*

$$\begin{aligned} &\int_{\widehat{I}} \Phi_{\widehat{I}}^{\alpha}(x) \left|\pi_N(x)\right|^2 dx \\ &\quad \le C N^{2(\beta-\alpha)} \int_{\widehat{I}} \Phi_{\widehat{I}}^{\beta} \left|\pi_N(x)\right|^2 dx. \end{aligned} \tag{61}$$

Lemma 10. *Let $-1 < \alpha < \beta, \sigma \in [0,1]$. Then there exist $C_1 = C(\alpha, \beta), C_2 = C_\sigma > 0$, such that for all $N \in \mathbb{N}$ and all polynomials π_N of degree bi-N,*

$$\begin{aligned} &\int_{\widehat{\kappa}} \Phi_{\widehat{\kappa}}^{\alpha} \left|\pi_N\right|^2 dx dy \\ &\quad \le C_1 N^{2(\beta-\alpha)} \int_{\widehat{\kappa}} \Phi_{\widehat{\kappa}}^{\beta} \left|\pi_N\right|^2 dx dy, \end{aligned} \tag{62}$$

$$\begin{aligned} &\int_{\widehat{\kappa}} \Phi_{\widehat{\kappa}}^{2\sigma} \left|\nabla\pi_N\right|^2 dx dy \\ &\quad \le C_2 N^{2(2-\sigma)} \int_{\widehat{\kappa}} \Phi_{\widehat{\kappa}}^{\sigma} \left|\pi_N\right|^2 dx dy. \end{aligned} \tag{63}$$

Lemma 11. *Let $\alpha \in (1/2, 1]$. $\widehat{e} := (0,1) \times \{0\}$, $\Phi_{\widehat{e}} := x(1-x)$; then there exists $C_\alpha > 0$ such that for all $N \in \mathbb{N}, \varepsilon \in (0,1]$, and all univariate polynomials π of degree N, there exists an extension $v_{\widehat{e}} \in H^1(\widehat{\kappa})$ and holds*

$$v_{\widehat{e}}|_{\widehat{e}} = \pi \cdot \Phi_{\widehat{e}}^{\alpha}, \qquad v_{\widehat{e}}|_{\partial\widehat{\kappa}\setminus\widehat{e}} = 0, \tag{64}$$

$$\left\|v_{\widehat{e}}\right\|_{0,\widehat{\kappa}}^2 \le C_\alpha \varepsilon \left\|\pi \Phi_{\widehat{e}}^{\alpha/2}\right\|_{0,\widehat{e}}^2, \tag{65}$$

$$\left\|\nabla v_{\widehat{e}}\right\|_{0,\widehat{\kappa}}^2 \le C_\alpha \left(\varepsilon N^{2(2-\alpha)} + \varepsilon^{-1}\right) \left\|\pi \Phi_{\widehat{e}}^{\alpha/2}\right\|_{0,\widehat{e}}^2. \tag{66}$$

It is easy to know that the three lemmas above hold for complex-valued polynomials.

Let $D_\kappa, \mathbf{b}_\kappa$, and c_κ be the interpolations of D, $\mathbf{b}$, and c in κ with the polynomial degree N_κ (resp. degree N_κ in every direction), respectively, or the $L^2(\kappa)$-projection on the space of polynomials with degree N_κ. For convenient argument, here and hereafter we assume that (λ, u) and $(\lambda^* = \overline{\lambda}, u^*)$ are the eigenpairs of the eigenvalue problem (24) and its adjoint problem (31), respectively. $(\lambda_{N,h}, u_{N,h})$ and $(\lambda_{N,h}^* = \overline{\lambda_{N,h}}, u_{N,h}^*)$ are the solutions of the corresponding spectral element approximations (26) and (32), respectively.

Denote

$$\begin{aligned} L_\kappa u_{N,h} :&= -\nabla \cdot \left(D_\kappa \nabla u_{N,h}\right) \\ &\quad + \mathbf{b}_\kappa \cdot \nabla u_{N,h} + c_\kappa u_{N,h}, \\ L_\kappa^* u_{N,h}^* :&= -\nabla \cdot \left(D_\kappa \nabla u_{N,h}^*\right) \\ &\quad - \mathbf{b}_\kappa \cdot \nabla u_{N,h}^* + \left(c_\kappa - \nabla \cdot \mathbf{b}_\kappa\right) u_{N,h}^*. \end{aligned} \tag{67}$$

Define the local error indicators

$$\begin{aligned} \eta_{\alpha;\kappa}^2 &:= \eta_{\alpha;B_\kappa}^2 + \eta_{\alpha;E_\kappa}^2, \\ \eta_{\alpha;\kappa}^{*2} &:= \eta_{\alpha;B_\kappa}^{*2} + \eta_{\alpha;E_\kappa}^{*2}. \end{aligned} \tag{68}$$

Their first terms $\eta_{\alpha;B_\kappa}^2, \eta_{\alpha;B_\kappa}^{*2}$ are the weighted element internal residuals given by

$$\begin{aligned} \eta_{\alpha;B_\kappa}^2 &:= \frac{h_\kappa^2}{N_\kappa^2} \left\|\left(-L_\kappa u_{N,h} + \lambda_{N,h} u_{N,h}\right) \Phi_\kappa^{\alpha/2}\right\|_{0,\kappa}^2, \\ \eta_{\alpha;B_\kappa}^{*2} &:= \frac{h_\kappa^2}{N_\kappa^2} \left\|\left(-L_\kappa^* u_{N,h}^* + \lambda_{N,h}^* u_{N,h}^*\right) \Phi_\kappa^{\alpha/2}\right\|_{0,\kappa}^2. \end{aligned} \tag{69}$$

Their second terms $\eta_{\alpha;E_\kappa}^2, \eta_{\alpha;E_\kappa}^{*2}$ are the weighted element boundary residuals given by

$$\begin{aligned} \eta_{\alpha;E_\kappa}^2 &:= \sum_{e \subset \partial\kappa \cap \Omega} \frac{h_e}{2N_e} \left\|D_\kappa \left[\frac{\partial u_{N,h}}{\partial n}\right] \Phi_e^{\alpha/2}\right\|_{0,e}^2, \\ \eta_{\alpha;E_\kappa}^{*2} &:= \sum_{e \subset \partial\kappa \cap \Omega} \frac{h_e}{2N_e} \left\|D_\kappa \left[\frac{\partial u_{N,h}^*}{\partial n}\right] \Phi_e^{\alpha/2}\right\|_{0,e}^2, \end{aligned} \tag{70}$$

where we denote the jump of the normal derivatives of $u_{N,h}$ and $u_{N,h}^*$ across the edges by $[\partial u_{N,h}/\partial n]$ and $[\partial u_{N,h}^*/\partial n]$, respectively. h_e is the length of edge e. The weight functions Φ_κ and Φ_e are scaled transformations of the weight functions $\Phi_{\widehat{\kappa}}$ and $\Phi_{\widehat{e}}$; that is, if F_κ is the element map for element κ and e is the image of the edge $\widehat{e}$ under F_κ, then

$$\Phi_\kappa = C_\kappa \Phi_{\widehat{\kappa}} \circ F_\kappa^{-1}, \qquad \Phi_e = C_e \Phi_{\widehat{e}} \circ F_\kappa^{-1}, \tag{71}$$

where we choose $C_\kappa, C_e > 0$, such that

$$\int_\kappa \Phi_\kappa dx dy = \int_\kappa dx dy, \qquad \int_e \Phi_e ds = \int_e ds. \tag{72}$$

We define the global error indicators as follows:

$$\begin{aligned} \eta_\alpha^2 &:= \sum_{\kappa \in K_h} \eta_{\alpha;\kappa}^2, \\ \eta_\alpha^{*2} &:= \sum_{\kappa \in K_h} \eta_{\alpha;\kappa}^{*2}. \end{aligned} \tag{73}$$

Theorem 12. *Let $\alpha \in [0,1]$. Then there exists a constant $C > 0$ independent of h, $\mathbf{N}$, and κ, such that*

$$\begin{aligned}\|u - u_{N,h}\|_{1,\Omega}^2 \le{}& C \sum_{\kappa\in K_h} N_\kappa^{2\alpha}\eta_{\alpha;\kappa}^2 \\ &+ C \sum_{\kappa\in K_h}\left\{\frac{h_\kappa^2}{N_\kappa^2}\|L_\kappa u_{N,h} - Lu_{N,h}\|_{0,\kappa}^2 \right.\\ &\quad+ \sum_{e\subset\partial\kappa\cap\Omega}\frac{h_e}{N_e}\|D - D_\kappa\|_{0,e}^2 \\ &\quad\left.\times\left\|\frac{\partial u_{N,h}}{\partial n}\right\|_{0,\infty,e}^2\right\} \\ &+ C\|\lambda u - \lambda_{N,h}u_{N,h}\|_{0,\Omega}^2.\end{aligned} \tag{74}$$

Proof. We denote $w := u - u_{N,h} - I(u - u_{N,h})$, where I is hp-clément operator given by Lemma 8. We derive from $H_0^1(\Omega)$-elliptic of $a(\cdot,\cdot)$ that

$$\begin{aligned}C\|u - u_{N,h}\|_{1,\Omega}^2 \le{}& a(u - u_{N,h}, w) \\ &+ a(u - u_{N,h}, I(u - u_{N,h})) \\ ={}& \lambda\int_\Omega u\overline{w} - a(u_{N,h}, w) \\ &+ \int_\Omega(\lambda u - \lambda_{N,h}u_{N,h}) \\ &\times\overline{I(u - u_{N,h})} \\ ={}& \int_\Omega(\lambda_{N,h}u_{N,h})\overline{w} \\ &+ \int_\Omega(\lambda u - \lambda_{N,h}u_{N,h})\overline{u - u_{N,h}} \\ &- a(u_{N,h}, w),\end{aligned} \tag{75}$$

$$\begin{aligned}a(u_{N,h}, w) ={}& \sum_{\kappa\in\kappa_h}\int_\kappa Lu_{N,h}\overline{w} \\ &- \sum_{\kappa\in\kappa_h}\int_{\partial\kappa} D\frac{\partial u_{N,h}}{\partial n}\overline{w} \\ ={}& \sum_{\kappa\in\kappa_h}\int_\kappa Lu_{N,h}\overline{w} \\ &- \frac{1}{2}\sum_{\kappa\in\kappa_h}\sum_{e\subset\partial\kappa\cap\Omega}\int_e D\left[\frac{\partial u_{N,h}}{\partial n}\right]\overline{w}.\end{aligned}$$

Therefore,

$$\begin{aligned}C\|u - u_{N,h}\|_{1,\Omega}^2 \le{}& \sum_{\kappa\in K_h}\int_\kappa(-Lu_{N,h} + \lambda_{N,h}u_{N,h})\overline{w} \\ &+ \frac{1}{2}\sum_{\kappa\in K_h}\sum_{e\subset\partial\kappa\cap\Omega}\int_e D\left[\frac{\partial u_{N,h}}{\partial n}\right]\overline{w} \\ &+ \int_\Omega(\lambda u - \lambda_{N,h}u_{N,h})\overline{(u - u_{N,h})},\end{aligned} \tag{76}$$

which together with

$$\begin{aligned}\int_e D\left[\frac{\partial u_{N,h}}{\partial n}\right]\overline{w} ={}& \int_e(D - D_\kappa)\left[\frac{\partial u_{N,h}}{\partial n}\right]\overline{w} \\ &+ \int_e D_\kappa\left[\frac{\partial u_{N,h}}{\partial n}\right]\overline{w}, \\ \int_\kappa(-Lu_{N,h} + \lambda_{N,h}u_{N,h})\overline{w} ={}& \int_\kappa(-L_\kappa u_{N,h} + \lambda_{N,h}u_{N,h})\overline{w} \\ &+ \int_\kappa(L_\kappa u_{N,h} - Lu_{N,h})\overline{w}\end{aligned} \tag{77}$$

and using Cauchy-Schwartz inequality, the hp-clément interpolation estimates in Lemma 8 then yield

$$\begin{aligned}&\|u - u_{N,h}\|_{1,\Omega}^2 \\ &\le C\left\{\sum_{\kappa\in K_h}\left[\eta_{0;B_\kappa}^2 + \eta_{0;E_\kappa}^2 + \frac{h_\kappa^2}{N_\kappa^2}\|L_\kappa u_{N,h} - Lu_{N,h}\|_{0,\kappa}^2\right.\right. \\ &\qquad\left.\left.+ \sum_{e\subset\partial\kappa\cap\Omega}\frac{h_e}{N_e}\left\|(D - D_\kappa)\left[\frac{\partial u_{N,h}}{\partial n}\right]\right\|_{0,e}^2\right]\right\}^{1/2} \\ &\quad\times\|u - u_{N,h}\|_{1,\Omega} + C\|\lambda u - \lambda_{N,h}u_{N,h}\|_{0,\Omega}\|u - u_{N,h}\|_{0,\Omega}.\end{aligned} \tag{78}$$

Using scaled transformation and setting $\alpha = 0, \beta = \alpha$ in (61) and (62), we get $\eta_{0;E_\kappa} \le CN_\kappa^\alpha\eta_{\alpha;E_\kappa}$ and $\eta_{0;B_\kappa} \le CN_\kappa^\alpha\eta_{\alpha;B_\kappa}$; then this proof concludes. □

For the adjoint eigenvalue problem, we still have the following.

Theorem 13. *Let $\alpha \in [0,1]$. Then there exists a constant $C > 0$ independent of h, $\mathbf{N}$, and κ, such that*

$$\begin{aligned}&\|u^* - u_{N,h}^*\|_{1,\Omega}^2 \\ &\le C\sum_{\kappa\in K_h} N_\kappa^{2\alpha}\eta_{\alpha;\kappa}^{*2} \\ &\quad+ C\sum_{\kappa\in K_h}\left\{\frac{h_\kappa^2}{N_\kappa^2}\|L_\kappa^* u_{N,h}^* - L^* u_{N,h}^*\|^2\right. \\ &\qquad\left.+ \sum_{e\subset\partial\kappa\cap\Omega}\frac{h_e}{N_e}\|D - D_\kappa\|_{0,e}^2\left\|\frac{\partial u_{N,h}^*}{\partial n}\right\|_{0,\infty,e}^2\right\} \\ &\quad+ C\|\lambda^* u^* - \lambda_{N,h}^* u_{N,h}^*\|_{0,\Omega}^2.\end{aligned} \tag{79}$$

Lemma 14. *Let $\alpha \in [0,1], \varepsilon > 0$. Then there exists a constant $C(\varepsilon) > 0$ independent of $h, \mathbf{N}$, and κ, such that*

$$\eta^2_{\alpha;B_\kappa} \le C(\varepsilon)\Big\{N_\kappa^{2(1-\alpha)}\|u-u_{N,h}\|^2_{1,\kappa} + N_\kappa^{\max\{1+2\varepsilon-2\alpha,0\}}\frac{h_\kappa^2}{N_\kappa^2} \times \left(\|\lambda_{N,h}u_{N,h}-\lambda u + Lu_{N,h} - L_\kappa u_{N,h}\|^2_{0,k}\right)\Big\}. \tag{80}$$

Proof. We denote $v_\kappa := (-L_\kappa u_{N,h} + \lambda_{N,h}u_{N,h})\Phi_\kappa^\alpha \in H_0^1(\kappa)$ with $\alpha \in (0,1]$ and extend v_κ to Ω by $v_\kappa = 0$ on $\Omega \setminus \kappa$; then

$$\begin{aligned}
\left\|v_\kappa \Phi_\kappa^{-\alpha/2}\right\|^2_{0,\kappa} &= \int_\kappa (-L_\kappa u_{N,h} + \lambda_{N,h}u_{N,h})\overline{v_\kappa} \\
&= -\int_\kappa (L_\kappa u_{N,h})\overline{v_\kappa} + a(u, v_\kappa) + \int_\kappa (\lambda_{N,h}u_{N,h} - \lambda u)\overline{v_\kappa} \\
&= a(u-u_{N,h}, v_\kappa) + \int_\kappa (\lambda_{N,h}u_{N,h} - \lambda u + Lu_{N,h} - L_\kappa u_{N,h})\overline{v_\kappa} \\
&\le C\|u-u_{N,h}\|_{1,\kappa}|v_\kappa|_{1,\kappa} + \left\|(\lambda_{N,h}u_{N,h} - \lambda u + Lu_{N,h} - L_\kappa u_{N,h})\Phi_\kappa^{\alpha/2}\right\|_{0,\kappa} \times \left\|v_\kappa\Phi_\kappa^{-\alpha/2}\right\|_{0,\kappa}.
\end{aligned} \tag{81}$$

We consider the H^1 semi norm for v_κ. Using the polynomial inverse estimates (62)-(63) in Lemma 10, by transformation between the reference element $\widehat{\kappa}$ and κ, we find for $\alpha > 1/2$ that

$$\begin{aligned}
|v_\kappa|^2_{1,\kappa} &\le 2\int_\kappa \Phi_\kappa^{2\alpha}|\nabla(\lambda_{N,h}u_{N,h} - L_\kappa u_{N,h})|^2 + 2\int_\kappa |\nabla\Phi_\kappa^\alpha|^2|\lambda_{N,h}u_{N,h} - L_\kappa u_{N,h}|^2 \\
&\le C\frac{N_\kappa^{2(2-\alpha)}}{h_\kappa^2}\int_\kappa \Phi_\kappa^\alpha|\lambda_{N,h}u_{N,h} - L_\kappa u_{N,h}|^2 + C\frac{1}{h_\kappa^2}\int_\kappa \Phi_\kappa^{2(\alpha-1)}|\lambda_{N,h}u_{N,h} - L_\kappa u_{N,h}|^2 \\
&\le C\frac{N_\kappa^{2(2-\alpha)}}{h_\kappa^2}\int_\kappa \Phi_\kappa^\alpha|\lambda_{N,h}u_{N,h} - L_\kappa u_{N,h}|^2 \\
&= CN_\kappa^{2(1-\alpha)}\frac{N_\kappa^2}{h_\kappa^2}\|v_\kappa\Phi_\kappa^{-\alpha/2}\|^2_{0,\kappa}.
\end{aligned} \tag{82}$$

Note that (62) is applicable since $\alpha > 1/2$ implies $2(\alpha-1) > -1$; thus, we set $\beta = \alpha, \alpha = 2(\alpha-1)$ in (62); then the third inequality above holds.

Since $\eta_{\alpha;B_\kappa} = h_\kappa/N_\kappa\|v_\kappa\Phi_\kappa^{-\alpha/2}\|_{0,\kappa}$, we obtain

$$\eta_{\alpha;B_\kappa} \le C\left(N_\kappa^{1-\alpha}\|u-u_{N,h}\|_{1,\kappa} + \frac{h_\kappa}{N_\kappa}\|Lu_{N,h} - L_\kappa u_{N,h} + \lambda_{N,h}u_{N,h} - \lambda u\|_{0,\kappa}\right). \tag{83}$$

To obtain an upper bound in the case of $0 \le \alpha \le 1/2$, we use the polynomial inverse estimate (62) in Lemma 10; for $\beta > 1/2$, we derive from (62) that

$$\begin{aligned}
\frac{N_\kappa}{h_\kappa}\eta_{\alpha;B_\kappa} &= \Phi_\kappa^{\alpha/2}\|(\lambda_{N,h}u_{N,h} - L_\kappa u_{N,h})\|_{0,\kappa} \\
&\le CN_\kappa^{\beta-\alpha}\left\|(\lambda_{N,h}u_{N,h} - L_\kappa u_{N,h})\Phi_\kappa^{\beta/2}\right\|_{0,\kappa} \\
&= CN_\kappa^{\beta-\alpha}\frac{N_\kappa}{h_\kappa}\eta_{\beta;B_\kappa} \\
&\le CN_\kappa^{\beta-\alpha}\left(N_\kappa^{1-\beta}\frac{N_\kappa}{h_\kappa}\|u-u_{N,h}\|_{1,\kappa} + \|\lambda_{N,h}u_{N,h} - \lambda u + Lu_{N,h} - L_\kappa u_{N,h}\|_{0,\kappa}\right).
\end{aligned} \tag{84}$$

Setting $\beta = 1/2 + \varepsilon, \varepsilon > 0$,

$$\eta_{\alpha;B_\kappa} \le C(\varepsilon)\Big\{N_\kappa^{1-\alpha}\|u-u_{N,h}\|_{1,\kappa} + N_\kappa^{1/2+\varepsilon-\alpha}\frac{h_\kappa}{N_\kappa} \times \|\lambda_{N,h}u_{N,h} - \lambda u + Lu_{N,h} - L_\kappa u_{N,h}\|_{0,\kappa}\Big\}. \tag{85}$$

We obtain the desired result immediately from (83) and (85). □

In order to obtain a local upper bound for the error indicator $\eta_{\alpha;\kappa}$, we consider the edge residual term $\eta_{\alpha;E_\kappa}$. we introduce the set

$$\omega_\kappa := \cup\left\{\kappa' \,\middle|\, \kappa' \text{ and } \kappa \text{ share at least one edge}\right\}. \tag{86}$$

Lemma 15. *Let $\alpha \in [0,1], \varepsilon > 0$. Then there exists a constant $C(\varepsilon) > 0$ independent of $h, \mathbf{N}$, and κ, such that*

$$\eta^2_{\alpha;E_\kappa} \le C(\varepsilon)N_\kappa^{\max(1-2\alpha+2\varepsilon,0)} \times \left\{N_\kappa\|u-u_{N,h}\|^2_{1,\omega_\kappa} + N_\kappa^{2\varepsilon}\frac{h_\kappa^2}{N_\kappa^2} \times \|\lambda_{N,h}u_{N,h} - \lambda u + Lu_{N,h} - L_\kappa u_{N,h}\|^2_{0,\omega_\kappa}\right\}. \tag{87}$$

Proof. We will use weight functions on edge and a suitable extension operator. For a given element κ with edge e, we choose the element κ_1 so that $\partial\kappa_1 \cap \partial\kappa = e$. Denote $\overline{\kappa_e} := \overline{\kappa_1} \cup \overline{\kappa}$; we construct a function $w_e \in H_0^1(\kappa_e)$ with $w_e|_e = D_\kappa[\partial u_{N,h}/\partial n]\Phi_e^\alpha$ as follows.

Let $v_{\widehat{e}} = C_e D_\kappa[\partial u_{N,h}/\partial n]\Phi_{\widehat{e}}^\alpha$ (C_e is defined by (71)). Using Lemma 11, we extend $v_{\widehat{e}}$ to $\widehat{\kappa}$, where the polynomial π corresponds to $C_e D_\kappa[\partial u_{N,h}/\partial n]$. Define $w_e|_\kappa$ and $w_e|_{\kappa_1}$ as the affine transformation of $v_{\widehat{e}}$ in $\widehat{\kappa}$; Thus, w_e is a piecewise H^1-function. From (64), we know w_e vanishes on $\partial\kappa_e$; Therefore, $w_e \in H_0^1(\kappa_e)$. It is trivial to extend w_e to Ω, such that $w_e = 0$ in $\Omega \setminus \kappa_e$. We find

$$\begin{aligned} \left\| D_\kappa \left[\frac{\partial u_{N,h}}{\partial n} \right] \Phi_e^{\alpha/2} \right\|_{0,e}^2 &= \int_e D \left[\frac{\partial u_{N,h}}{\partial n} \right] \overline{w_e} + \int_e (D_\kappa - D) \left[\frac{\partial u_{N,h}}{\partial n} \right] \overline{w_e} \\ &= \int_{\kappa_e} L u_{N,h} \overline{w_e} - a(u_{N,h}, w_e) \\ &\quad + \int_e (D_\kappa - D) \left[\frac{\partial u_{N,h}}{\partial n} \right] \overline{w_e} \\ &= \int_{\kappa_e} (L u_{N,h} - \lambda u) \overline{w_e} + a(u - u_{N,h}, w_e) \\ &\quad + \int_e (D_\kappa - D) \left[\frac{\partial u_{N,h}}{\partial n} \right] \overline{w_e} \\ &\le \| L u_{N,h} - \lambda u \|_{0,\kappa_e} \| w_e \|_{0,\kappa_e} \\ &\quad + C \| u - u_{N,h} \|_{1,\kappa_e} | w_e |_{1,\kappa_e} \\ &\quad + \left\| \frac{(D_\kappa - D)}{D_\kappa} \right\|_{0,\infty,e} \left\| D_\kappa \left[\frac{\partial u_{N,h}}{\partial n} \right] \Phi_e^{\alpha/2} \right\|_{0,e}^2 . \end{aligned} \tag{88}$$

Therefore,

$$\begin{aligned} \left\| D_\kappa \left[\frac{\partial u_{N,h}}{\partial n} \right] \Phi_e^{\alpha/2} \right\|_{0,e}^2 &\le C \| L u_{N,h} - \lambda u \|_{0,\kappa_e} \| w_e \|_{0,\kappa_e} \\ &\quad + C \| u - u_{N,h} \|_{1,\kappa_e} | w_e |_{1,\kappa_e} . \end{aligned} \tag{89}$$

We consider the case of $\alpha \in (1/2, 1]$ first. Using the affine equivalence and (65)-(66) in Lemma 11, we obtain the upper bounds for $\|w_e\|_{0,\kappa_e}$ and $|w_e|_{1,\kappa_e}$ as follows:

$$\begin{aligned} | w_e |_{1,\kappa_e}^2 &\le C \frac{1}{h_\kappa} \left(\varepsilon N_\kappa^{2(2-\alpha)} + \varepsilon^{-1} \right) \\ &\quad \times \left\| D_\kappa \left[\frac{\partial u_{N,h}}{\partial n} \right] \Phi_e^{\alpha/2} \right\|_{0,e}^2 , \\ \| w_e \|_{0,\kappa_e} &\le C h_\kappa \varepsilon \left\| D_\kappa \left[\frac{\partial u_{N,h}}{\partial n} \right] \Phi_e^{\alpha/2} \right\|_{0,e}^2 . \end{aligned} \tag{90}$$

It follows from (89)-(90) that

$$\begin{aligned} \left\| D_\kappa \left[\frac{\partial u_{N,h}}{\partial n} \right] \Phi_e^{\alpha/2} \right\|_{0,e} &\le C \left\{ \left(\frac{1}{h_\kappa} \left(\varepsilon N_\kappa^{2(2-\alpha)} + \varepsilon^{-1} \right) \right)^{1/2} \right. \\ &\quad \left. \times \| u - u_{N,h} \|_{1,\kappa_e} + (h_\kappa \varepsilon)^{1/2} \parallel \| L u_{N,h} - \lambda u \|_{0,\kappa_e} \right\} . \end{aligned} \tag{91}$$

By the definition of $\eta_{\alpha;E_\kappa}^2$ and setting $\alpha = 0$ in Lemma 14, we get

$$\begin{aligned} \| L_\kappa u_{N,h} - \lambda_{N,h} u_{N,h} \|_{0,k}^2 &\le C(\varepsilon) \left\{ \frac{N_\kappa^4}{h_\kappa^2} \| u - u_{N,h} \|_{1,k}^2 + N_\kappa^{1+2\varepsilon} \right. \\ &\quad \left. \times \| \lambda_{N,h} u_{N,h} - \lambda u + L u_{N,h} - L_\kappa u_{N,h} \|_{0,k}^2 \right\} , \end{aligned} \tag{92}$$

by the triangle inequality

$$\begin{aligned} \| L u_{N,h} - \lambda u \|_{0,\kappa_e} &\le \| L_\kappa u_{N,h} - \lambda_{N,h} u_{N,h} \|_{0,\kappa_e} \\ &\quad + \| \lambda_{N,h} u_{N,h} - \lambda u + L u_{N,h} - L_\kappa u_{N,h} \|_{0,\kappa_e} . \end{aligned} \tag{93}$$

Combining the three inequalities above and summing, we have

$$\begin{aligned} \eta_{\alpha;E_\kappa}^2 &\le C \left\{ \frac{1}{N_\kappa} \left(\varepsilon N_\kappa^{2(2-\alpha)} + \varepsilon^{-1} \right) + N_\kappa^3 \varepsilon \right\} \\ &\quad \times \| u - u_{N,h} \|_{1,\omega_\kappa}^2 + C \varepsilon N_\kappa^{2(1+\varepsilon)} \frac{h_\kappa^2}{N_\kappa^2} \\ &\quad \times \| \lambda_{N,h} u_{N,h} - \lambda u + L u_{N,h} - L_\kappa u_{N,h} \|_{0,\omega_\kappa}^2 . \end{aligned} \tag{94}$$

Setting $\varepsilon = 1/N_\kappa^2$ in the above inequality yields the assertion for $\alpha > 1/2$. For the case of $\alpha \in [0, 1/2]$, we set $\beta = 1/2 + \varepsilon$, use (62) in Lemma 10 to get $\eta_{\alpha;E_\kappa} \le N_\kappa^{\beta-\alpha} \eta_{\beta;E_\kappa}$, and find the desired result. □

Combining Lemmas 14 and 15, we obtain the following theorem.

Theorem 16. *Let $\alpha \in [0, 1]$, $\varepsilon > 0$. Then there exists a constant $C > 0$ independent of h, $\mathbf{N}$, and κ, such that*

$$\begin{aligned} \eta_{\alpha;\kappa}^2 &\le C(\varepsilon) N_\kappa^{\max(1-2\alpha+2\varepsilon,0)} \\ &\quad \times \left\{ N_\kappa \| u - u_{N,h} \|_{1,\omega_\kappa}^2 + N_\kappa^{2\varepsilon} \frac{h_\kappa^2}{N_\kappa^2} \right. \\ &\quad \left. \times \| \lambda_{N,h} u_{N,h} - \lambda u + L u_{N,h} - L_\kappa u_{N,h} \|_{0,\omega_\kappa}^2 \right\} . \end{aligned} \tag{95}$$

Similarly, we have Theorem 17.

Theorem 17. *Let $\alpha \in [0,1], \varepsilon > 0$. Then there exists a constant $C > 0$ independent of $h, \mathbf{N}$, and κ, such that*

$$\begin{aligned}\eta_{\alpha;\kappa}^{*2} &\le C(\varepsilon) N_\kappa^{\max(1-2\alpha+2\varepsilon,0)} \\ &\quad \times \left\{ N_\kappa \left\| u^* - u_{N,h}^* \right\|_{1,\omega_\kappa}^2 + N_\kappa^{2\varepsilon} \frac{h_\kappa^2}{N_\kappa^2} \right. \\ &\quad \left. \times \left\| \lambda_{N,h}^* u_{N,h}^* - \lambda^* u^* + L^* u_{N,h}^* - L_\kappa^* u_{N,h}^* \right\|_{0,\omega_\kappa}^2 \right\}.\end{aligned} \quad (96)$$

In order to estimate bounds of $|\lambda - \lambda_{N,h}|$, we also need Lemma 18 (see [8, 10]).

Lemma 18. *Let (λ, u) be an eigenpair of (24), and let $(\lambda^* = \overline{\lambda}, u^*)$ be the associated eigenpair of the adjoint problem (31). Then for all $w, w^* \in H_0^1(\Omega)$, $(w, w^*) \neq 0$,*

$$\begin{aligned}&\frac{a(w,w^*)}{(w,w^*)} - \lambda \\ &\quad = \frac{a(w-u, w^*-u^*)}{(w,w^*)} - \lambda \frac{(w-u, w^*-u^*)}{(w,w^*)}.\end{aligned} \quad (97)$$

Theorem 19. *Under the assumptions of Theorem 7, we assume that $D, \mathbf{b}$, and c are smooth enough, and let $\alpha \in [0,1]$. Then there exists an eigenpair (λ, u) of (24), such that*

$$\left\| u - u_{N,h} \right\|_{1,\Omega} \le C \left(\sum_{\kappa \in K_h} N_\kappa^{2\alpha} \eta_{\alpha;\kappa}^2 \right)^{1/2}, \quad (98)$$

$$\eta_{\alpha;\kappa}^2 \le C(\varepsilon) N_\kappa^{\max(2-2\alpha+2\varepsilon,1)} \left\| u - u_{N,h} \right\|_{1,\omega_\kappa}^2. \quad (99)$$

Further let the ascent of $\lambda_{N,h}$ be $l = 1$, and let $(\lambda_{N,h}^*, u_{N,h}^*)$ be the corresponding adjoint eigenpair of (32), then there exists an adjoint eigenpair (λ^*, u^*) of (31), such that

$$\left| \lambda_{N,h} - \lambda \right| \le C \left(\sum_{\kappa \in K_h} N_\kappa^{2\alpha} \eta_{\alpha;\kappa}^2 \right)^{1/2} \left(\sum_{\kappa \in K_h} N_\kappa^{2\alpha} \eta_{\alpha;\kappa}^{*2} \right)^{1/2}. \quad (100)$$

Particularly, if the eigenvalue problem (23) is symmetric (i.e., $\mathbf{b} = 0$), then

$$C C(\varepsilon)^{-1} \sum_{\kappa \in K_h} N_\kappa^{\min(2\alpha-2-2\varepsilon,-1)} \eta_{\alpha;\kappa}^2 \le \left| \lambda_{N,h} - \lambda \right|. \quad (101)$$

Proof. We know from the assumption $D, c \in H^{t_1}(\kappa), \mathbf{b} \in (H^{t_1}(\kappa))^2$. By the interpolation error estimates (14) and (15), we have

$$\left\| L_\kappa u_{N,h} - L u_{N,h} \right\|_{0,\kappa} \le C h_\kappa^{\min(N_\kappa+1,t_1)-1} N_\kappa^{-t_1+1}. \quad (102)$$

From $D \in H^{t_1}(\kappa)$, we know that $D \in H^{t_1-1/2}(e)$. By the interpolation error estimate on edge of element (see formula (5.4.42) in [2]), we get

$$\left\| D - D_\kappa \right\|_{0,e} \le C h_e^{\min(N_\kappa+1,t_1-1/2)} N_\kappa^{-t_1+1/2}. \quad (103)$$

Note that the formula (51) gives the optimal orders of convergence; thus, we deduce that the second and third terms on the right side of (74) are higher order infinitesimals. We derive from (52) and (53), and $N = N_\kappa$, that

$$\begin{aligned}&\left\| \lambda u - \lambda_{N,h} u_{N,h} \right\|_{0,\Omega} \\ &\quad \le \left| \lambda - \lambda_{N,h} \right| \left\| u \right\|_{0,\Omega} \\ &\qquad + \left| \lambda_{N,h} \right| \left\| u - u_{N,h} \right\|_{0,\Omega} \\ &\quad \le \frac{C h^{\tau_1+\tau_2-2}}{N^{t_1+t_2-2}} + \frac{C h^{r_2+\tau_1-1}}{N^{r_2+t_1-1}} \le \frac{C h^{r_2+\tau_1-1}}{N^{r_2+t_1-1}}.\end{aligned} \quad (104)$$

Therefore, the fourth term on the right side of (74) is also a higher order infinitesimal. Up to higher order terms, we get (98). We ignore higher order infinitesimals in (95) and get (99). From Lemma 4 in [10], we know that $(u_{N,h}, u_{N,h}^*) = 1$ and $u_{N,h}^*$ is uniformly bounded with h and N. By the same argument of (98), we can deduce that

$$\left\| u^* - u_{N,h}^* \right\|_{1,\Omega}^2 \le C \sum_{\kappa \in K_h} N_\kappa^{2\alpha} \eta_{\alpha;\kappa}^{*2}. \quad (105)$$

From (97), we have

$$\begin{aligned}&\frac{a\left(u_{N,h}, u_{N,h}^*\right)}{\left(u_{N,h}, u_{N,h}^*\right)} - \lambda \\ &\quad = \frac{a\left(u_{N,h} - u, u_{N,h}^* - u^*\right)}{\left(u_{N,h}, u_{N,h}^*\right)} \\ &\qquad - \lambda \frac{\left(u_{N,h} - u, u_{N,h}^* - u^*\right)}{\left(u_{N,h}, u_{N,h}^*\right)};\end{aligned} \quad (106)$$

that is,

$$\begin{aligned}\lambda_{N,h} - \lambda &= a\left(u_{N,h} - u, u_{N,h}^* - u^*\right) \\ &\quad - \lambda \left(u_{N,h} - u, u_{N,h}^* - u^*\right).\end{aligned} \quad (107)$$

Substituting (98) and (105) into the above equality, we obtain (100).

If the eigenvalue problem (23) is symmetric (i.e., $\mathbf{b} = 0$), then

$$\begin{aligned}\lambda_{N,h} - \lambda &= a\left(u_{N,h} - u, u_{N,h} - u\right) \\ &\quad - \lambda \left(u_{N,h} - u, u_{N,h} - u\right).\end{aligned} \quad (108)$$

Up to higher order term $\lambda(u_{N,h} - u, u_{N,h} - u)$, by (99) we get (101). □

Remark 20. Babuška and Osborn [17] have discussed hp finite element approximation with simplex partition for eigenvalue problems. Obviously, the Interpolation estimates (14) and (15) hold for hp finite element with simplex partition (see [24]). Therefore, our theoretical results of spectral methods and spectral methods for eigenvalue problems, which have been discussed in Sections 3 and 4, hold for hp finite element with simplex partition.

Table 1: Errors of LGL-SM, modal, and Eq-SM for 1st eigenvalue.

N	DOF	LGL-SM λ_1	Modal-SM λ_1	Eq-SM λ_1
4	9	$5.19E+00$	$5.19E+00$	$5.19E+00$
5	16	$4.51E-01$	$4.51E-01$	$4.51E-01$
6	25	$7.68E-03$	$7.68E-03$	$7.68E-03$
7	36	$1.07E-05$	$1.07E-05$	$1.07E-05$
8	49	$1.21E-05$	$1.21E-05$	$1.21E-05$
9	64	$9.16E-07$	$9.16E-07$	$9.16E-07$
10	81	$2.46E-08$	$2.46E-08$	$2.48E-08$
11	100	$2.91E-10$	$2.91E-10$	$4.35E-09$
12	121	$9.31E-13$	$1.06E-12$	$2.79E-08$
13	144	$5.68E-14$	$1.28E-13$	$1.41E-07$
14	169	$2.84E-14$	$1.28E-13$	$2.28E-06$
15	196	$7.82E-14$	$2.13E-14$	$3.60E-05$

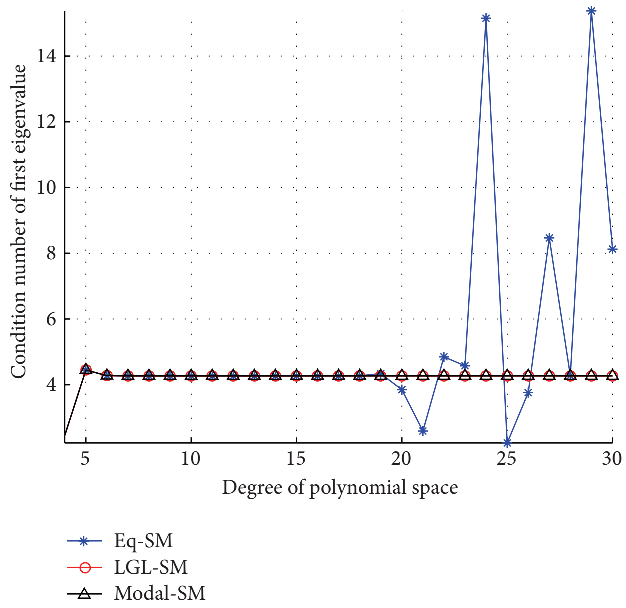

Figure 1: Condition number of first eigenvalue for SM.

5. Numerical Experiments

In this section, we simply denote spectral methods, spectral element methods, and finite element methods with SM, SEM, and FEM, respectively. And spectral methods with equidistant nodal basis, modal basis, and LGL nodal basis are replaced by Eq-SM, Modal-SM, and LGL-SM, respectively. Note that all these methods employ the tensorial basis.

In our experiment, we compute $1/|(u_{N,h}, u^*_{N,h})|$ as condition number for simple eigenvalue (see Remark 2.1 in [25]), where $u_{N,h}$ and $u^*_{N,h}$ are eigenfunctions of eigenvalue problem (25) and its adjoint problem (32) normalized with $\|\cdot\|_{0,\Omega}$, respectively.

5.1. Example 1. Consider the nonsymmetric eigenvalue problem

$$-\Delta u + 10u_x + u_y = \lambda u, \quad \text{in } \Omega = (0,1)^2, \qquad u = 0, \quad \text{on } \partial\Omega. \tag{109}$$

The first eigenvalue of (109) $\lambda_1 = 101/4 + 2\pi^2$ is a simple eigenvalue. And the corresponding eigenfunctions are sufficiently smooth.

5.1.1. Comparisons between LGL-SM, Modal, and Eq-SM. Figure 1 shows that the condition numbers of the first eigenvalue for LGL-SM, Modal-SM, and Eq-SM coincide with each other at the beginning but perform abnormally with $N > 19$ for Eq-SM. Table 1 tells us that when $N > 11$, the accuracy of first eigenvalue obtained by Eq-SM is not as good as obtained that by LGL-SM and Modal-SM. When $N = 15$, the error of the first eigenvalues obtained by Eq-SM is greater than 1E-5; however, the order of the magnitude of errors for LGL-SM and Modal-SM still keeps below 1E-13. The best result of first eigenvalue error for Eq-SM is merely 1E-9 or so.

5.1.2. LGL-SM and Modal-SM versus hp-SEM. Tables 1 and 2 indicate that increasing the polynomial degree N or decreasing the mesh fineness h can decrease the errors of the first eigenvalue. But it is expensive to increase polynomial degree and decrease mesh fineness h at the same time. For $h = 1/4$ and $h = 1/16$, we obtain from Table 2 the first eigenvalue errors $2.8E-14$ and $1.3E-13$ and the corresponding degree of freedom 1225 and 6241 for hp-SEM, respectively, Whereas from Table 1, to reach this accuracy, LGL-SM and Modal-SM should merely perform the interpolation approximations with polynomial degree bi-14 and bi-13 or so, and the corresponding degrees of freedom are merely 169 and 144, respectively. Therefore, we conclude that LGL-SM and Modal-SM are highly accurate and efficient for this kind of nonsymmetric eigenvalue problems.

In Figure 2 from [9], when the degree of freedom is up to 1000, the error of linear FEM is about 1E-2; the function value recovery techniques in [9] obviously improves the accuracy up to 1E-5. Comparing Tables 1 and 2 in this paper with Figure 2 in [9], we can also find the advantages of LGL-SM, Modal-SM, and hp-SEM over the function value recovery techniques for FEM given by [9] from accuracy and degree of freedom.

5.1.3. hp-SEM versus hp-FEM. From Table 4, we find that the condition number of the first eigenvalue for hp-version methods (hp-SEM and hp-FEM) stays at 4.27. It is indicated from Tables 2 and 3 that, when N is greater than 7, compared with hp-SEM, the errors of hp-FEM tend to become large, whereas the errors of hp-SEM still keep stable or even stay a decreasing tendency; however, this phenomenon is not apparent for $h = 1/2$.

Remark 21. Condition numbers of 1st eigenvalue for hp-FEM (not listed in Table 4) are almost the same to those for hp-SEM.

Table 2: Errors and DOF of hp-SEM for the first eigenvalue.

N	$h = 1/2$		$h = 1/4$		$h = 1/8$		$h = 1/16$	
	Error	DOF	Error	DOF	Error	DOF	Error	DOF
2	$5.18E+00$	9	$2.54E-01$	49	$1.50E-02$	225	$9.00E-04$	961
3	$7.00E-03$	25	$6.10E-04$	121	$1.20E-05$	529	$1.90E-07$	2209
4	$8.40E-03$	49	$2.60E-05$	225	$9.70E-08$	961	$3.70E-10$	3969
5	$1.64E-04$	81	$1.60E-07$	361	$1.50E-10$	1521	$1.30E-13$	6241
6	$4.10E-07$	121	$2.30E-11$	529	$9.90E-13$	2209	$3.60E-12$	9025
7	$3.10E-08$	169	$1.70E-12$	729	$3.10E-13$	3025	$1.60E-12$	12321
8	$1.90E-10$	225	$1.90E-13$	961	$2.10E-12$	3969	$4.80E-12$	16129
9	$5.50E-13$	289	$2.80E-14$	1225	$6.00E-13$	5041	$1.10E-12$	20449
10	$3.80E-13$	361	$1.10E-12$	1521	$4.40E-12$	6241	$1.50E-11$	25281

Table 3: Errors of hp-FEM for the first eigenvalue.

N	$h = 1/2$	$h = 1/4$	$h = 1/8$	$h = 1/16$
3	$7.00E-03$	$6.10E-04$	$1.20E-05$	$1.90E-07$
4	$8.40E-03$	$2.60E-05$	$9.70E-08$	$3.70E-10$
5	$1.60E-04$	$1.60E-07$	$1.50E-10$	$1.30E-12$
6	$4.10E-07$	$2.40E-11$	$3.60E-13$	$8.60E-12$
7	$3.10E-08$	$6.10E-12$	$1.30E-11$	$3.00E-11$
8	$1.80E-10$	$3.10E-11$	$2.30E-10$	$2.10E-10$
9	$7.50E-11$	$3.40E-11$	$6.80E-10$	$7.40E-10$
10	$2.50E-11$	$9.90E-10$	$8.70E-09$	$6.60E-09$
11	$2.00E-09$	$9.60E-09$	$8.90E-09$	$5.40E-07$

Table 4: Condition number of first eigenvalue for hp-SEM.

N	$h = 1/2$	$h = 1/4$	$h = 1/8$	$h = 1/16$
3	4.284381324	4.270132842	4.269625046	4.269615821
4	4.267343095	4.269607452	4.269615638	4.26961567
5	4.269636446	4.269615725	4.26961567	4.26961567
6	4.269619135	4.26961567	4.26961567	4.26961567
7	4.269615617	4.26961567	4.26961567	4.26961567
8	4.26961567	4.26961567	4.26961567	4.26961567
9	4.26961567	4.26961567	4.26961567	4.26961567

5.1.4. Validity of the Error Indicator. Denote

$$\psi_\alpha = \left(\sum_{\kappa\in K_h} N_\kappa^{2\alpha}\eta_{\alpha;\kappa}^2\right)^{1/2}\left(\sum_{\kappa\in K_h} N_\kappa^{2\alpha}\eta_{\alpha;\kappa}^{*2}\right)^{1/2}. \quad (110)$$

From Theorem 19, we know that ψ_α is a reliable error indicator for $\lambda_{N,h}$. We choose ψ_0 (setting $\alpha = 0$ in (110)) as a posteriorii error indicator.

In Figures 2 and 3, we denote the true error and est. error with $|\lambda_{N,h} - \lambda|$ and ψ_0, respectively.

As is depicted in Figure 2, when the polynomial degree $N \leq 12$, the error indicator ψ_0 can properly estimate the true errors of LGL-SM for the first eigenvalue, however, also slightly underestimate the true errors. It is easy to see that ψ_0 shows almost the same algebraic decay as the true error with the polynomial degree N ($\leq$12) increasing. Nevertheless, the error indicator ψ_0 cannot approximate the true errors if N is large enough, which is caused by round-off errors derived from the bad condition number of eigenvalue. In Figure 3, we give the comparison between the error indicator ψ_0 and the true errors for hp-SEM.

Table 5: The Approximate eigenvalues and indicator ψ_0 of P-SEM.

N	$\lambda_{N,h}$	ψ_0
3	28.56900	$2.72E+01$
4	31.99175	$3.49E+00$
5	34.82082	$2.25E-01$
6	34.65087	$1.31E-02$
7	34.65057	$3.32E-03$
8	34.64765	$1.92E-03$
9	34.64567	$1.22E-03$
10	34.64432	$8.11E-04$
11	34.64335	$5.62E-04$
12	34.64265	$4.02E-04$
13	34.64212	$2.95E-04$
14	34.64171	$2.22E-04$
15	34.64139	$1.71E-04$
16	34.64114	$1.33E-04$
17	34.64094	$1.06E-04$
18	34.64078	$8.49E-05$

5.2. Example 2. Consider the nonsymmetric eigenvalue problem

$$-\Delta u + 10u_x = \lambda u, \quad \text{in } \Omega = \frac{(-1,1)^2}{(0,1)^2}, \quad u = 0, \quad \text{on } \partial\Omega. \quad (111)$$

A reference value for the first eigenvalue (simple eigenvalue) of (111) is 34.6397 given by [5]. And the corresponding eigenfunctions have the singularity at the origin. Next, we shall compare the relevant numerical results between P-SEM and the other methods adopted in this paper. Note that here and hereafter P-version methods are for the fixed mesh fineness $h = 1$. Table 5 lists part data of the approximate eigenvalues computed by P-SEM and the corresponding error indicator ψ_0 for reference.

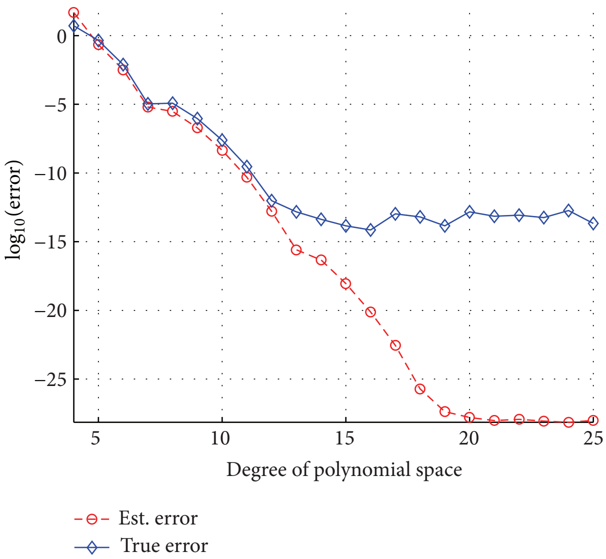

FIGURE 2: The Error indicator ψ_0 of LGL-SM.

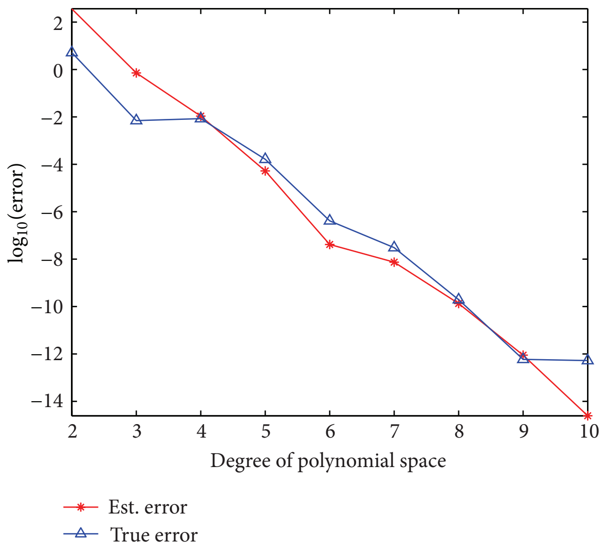

FIGURE 3: The Error indicator ψ_0 of hp-SEM ($h = 1/2$).

5.2.1. *Stability of P-Version Methods.*

Figure 4 indicates that the eigenvalues computed by P-FEM will not seriously deviate from the results computed by P-SEM until the interpolation polynomial degree N is up to 19. This phenomenon coincides with the abnormity of condition number of first eigenvalue for P-FEM (see Figure 5). The reason is that the singularities of the eigenfunctions limit the accuracy of both kinds of methods; this is slightly different from the case of the eigenvalue problem with the sufficiently smooth eigenfunctions.

5.2.2. *P-SEM versus Other Methods.*

By calculations, we find that, in the case of the linear FEM, for fixed mesh fineness $h = 1/256$, the approximate eigenvalue is 34.6403 with degree of freedom up to 195585. But P-SEM with the polynomial degree bi-22 can reach this accuracy, and the corresponding

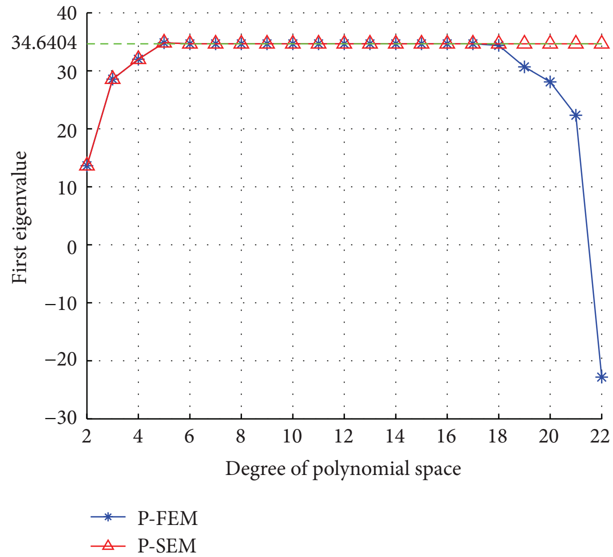

FIGURE 4: The Approximate 1st eigenvalue of P-SEM and P-FEM.

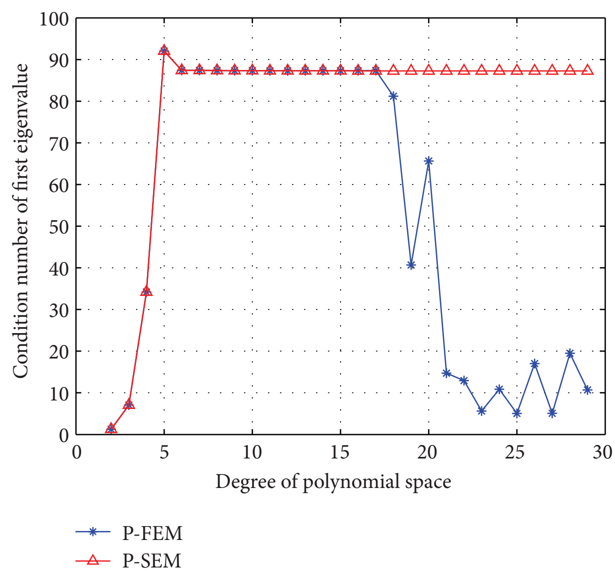

FIGURE 5: Condition number of first eigenvalue for P-SEM and P-FEM.

degree of freedom is merely 1365. Compared with the linear FEM, hp-SEM can obtain a higher accuracy with less degrees of freedom as follows: for fixed $h = 1/16$ and $N = 10$, the approximate eigenvalue is 34.63984 with degree of freedom 76161 but P-SEM with polynomial degree bi-44 can reach this accuracy. Therefore, P-SEM is more efficient for the eigenvalue problems with the singular solutions than the other methods.

Acknowledgments

This work was supported by the National Natural Science Foundation of China (Grant no. 11161012) and the Educational

Administration and Innovation Foundation of Graduate Students of Guizhou Normal University (no. 2012(11)).

References

[1] J. Shen, T. Tang, and L.-L. Wang, *Spectral Methods: Algorithms, Analysis and Applications*, vol. 41 of *Springer Series in Computational Mathematics*, Springer, Heidelberg, Germany, 2011.

[2] C. Canuto, M. Y. Hussaini, A. Quarteroni, and T. A. Zang, *Spectral Methods: Fundamentals in Single Domains*, Scientific Computation, Springer, Heidelberg, Germany, 2006.

[3] M. G. Armentano, C. Padra, R. Rodríguez, and M. Scheble, "An *hp* finite element adaptive scheme to solve the laplace model for fluid-solid vibrations," *Computer Methods in Applied Mechanics and Engineering*, vol. 200, no. 1–4, pp. 178–188, 2011.

[4] H. Bi and Y. Yang, "Multiscale discretization scheme based on the Rayleigh quotient iterative method for the Steklov eigenvalue problem," *Mathematical Problems in Engineering*, vol. 2012, Article ID 487207, 18 pages, 2012.

[5] C. Carstensen, J. Gedicke, V. Mehrmann, and A. Miedlar, "An adaptive homotopy approach for non-selfadjoint eigenvalue problems," *Numerische Mathematik*, vol. 119, no. 3, pp. 557–583, 2011.

[6] X. Dai and A. Zhou, "Three-scale finite element discretizations for quantum eigenvalue problems," *SIAM Journal on Numerical Analysis*, vol. 46, no. 1, pp. 295–324, 2007.

[7] S. Giani and I. G. Graham, "A convergent adaptive method for elliptic eigenvalue problems," *SIAM Journal on Numerical Analysis*, vol. 47, no. 2, pp. 1067–1091, 2009.

[8] K. Kolman, "A two-level method for nonsymmetric eigenvalue problems," *Acta Mathematicae Applicatae Sinica*, vol. 21, no. 1, pp. 1–12, 2005.

[9] A. Naga and Z. Zhang, "Function value recovery and its application in eigenvalue problems," *SIAM Journal on Numerical Analysis*, vol. 50, no. 1, pp. 272–286, 2012.

[10] Y. Yang and X. Fan, "Generalized rayleigh quotient and finite element two-grid discretization schemes," *Science in China A*, vol. 52, no. 9, pp. 1955–1972, 2009.

[11] Y. Yang and H. Bi, "Two-grid finite element discretization schemes based on shifted-inverse power method for elliptic eigenvalue problems," *SIAM Journal on Numerical Analysis*, vol. 49, no. 4, pp. 1602–1624, 2011.

[12] Y. Yang, Y. Zhang, and H. Bi, "Multigrid discretization and iterative algorithm for mixed variational formulation of the eigenvalue problem of electric field," *Abstract and Applied Analysis*, vol. 2012, Article ID 190768, 25 pages, 2012.

[13] Y. Yang, W. Jiang, Y. Zhang, W. Wang, and H. Bi, "A two-scale discretization scheme for mixed variational formulation of eigenvalue problems," *Abstract and Applied Analysis*, vol. 2012, Article ID 812914, 29 pages, 2012.

[14] Y. Zhang, Y. Yang, and J. Liu, "Highly efficient calculation schemes of finite-element filter approach for the eigenvalue problem of electric field," *Mathematical Problems in Engineering*, vol. 2012, Article ID 529498, 21 pages, 2012.

[15] V. Heuveline and R. Rannacher, "A posteriori error control for finite element approximations of elliptic eigenvalue problems," *Advances in Computational Mathematics*, vol. 15, no. 1–4, pp. 107–138, 2001.

[16] Y. Yang and W. Jiang, "Upper spectral bounds and a posteriori error analysis of several mixed finite element approximations for the Stokes eigenvalue problem," *Science China Mathematics*, vol. 56, no. 6, pp. 1313–1330, 2013.

[17] I. Babuška and J. Osborn, "Eigenvalue problems," in *Handbook of Numerical Analysis: Finite Element Methods (Part 1)*, P. G. Ciarlet and J. L. Lions, Eds., vol. 2, pp. 641–787, Elsevier Science North Holland, Amsterdam, The Netherlands, 1991.

[18] F. Chatelin, *Spectral approximation of linear operators*, Computer Science and Applied Mathematics, Academic Press, New York, NY, USA, 1983.

[19] Y. Yang, *Finite Element Methods For Eigenvalue Problems*, Science Press, Beijing, China, 2012, (Chinese).

[20] J. M. Melenk and B. I. Wohlmuth, "On residual-based a posteriori error estimation in *hp*-FEM," *Advances in Computational Mathematics*, vol. 15, no. 1–4, pp. 311–331, 2001.

[21] J. M. Melenk, "*hp*-interpolation of nonsmooth functions and an application to *hp*-a posteriori error estimation," *SIAM Journal on Numerical Analysis*, vol. 43, no. 1, pp. 127–155, 2005.

[22] P. Clément, "Approximation by finite element functions using local regularization," *RAIRO Analyse Numérique*, vol. 9, no. 2, pp. 77–84, 1975.

[23] L. R. Scott and S. Zhang, "Finite element interpolation of nonsmooth functions satisfying boundary conditions," *Mathematics of Computation*, vol. 54, no. 190, pp. 483–493, 1990.

[24] I. Babuška and M. R. Dorr, "Error estimates for the combined h and p versions of the finite element method," *Numerische Mathematik*, vol. 37, no. 2, pp. 257–277, 1981.

[25] J. Gedicke and C. Carstensen, *A Posteriori Error Estimators For Non-Symmetric Eigenvalue Problems*, DFG Research Center Matheon, Berlin, Germany, 2009.

Hindawi Publishing Corporation
Abstract and Applied Analysis
Volume 2013, Article ID 108026, 13 pages
http://dx.doi.org/10.1155/2013/108026

Research Article

Nonlinear Hydroelastic Waves beneath a Floating Ice Sheet in a Fluid of Finite Depth

Ping Wang[1,2] and Zunshui Cheng[1,3]

[1] *School of Mathematics and Physics, Qingdao University of Science and Technology, Qingdao 266061, China*
[2] *Shanghai Institute of Applied Mathematics and Mechanics, Shanghai University, Shanghai 200072, China*
[3] *Research Center for Complex Systems and Network Sciences, Department of Mathematics, Southeast University, Nanjing 210096, China*

Correspondence should be addressed to Ping Wang; pingwang2003@126.com

Received 21 May 2013; Revised 29 August 2013; Accepted 29 August 2013

Academic Editor: Rasajit Bera

The nonlinear hydroelastic waves propagating beneath an infinite ice sheet floating on an inviscid fluid of finite depth are investigated analytically. The approximate series solutions for the velocity potential and the wave surface elevation are derived, respectively, by an analytic approximation technique named homotopy analysis method (HAM) and are presented for the second-order components. Also, homotopy squared residual technique is employed to guarantee the convergence of the series solutions. The present formulas, different from the perturbation solutions, are highly accurate and uniformly valid without assuming that these nonlinear partial differential equations (PDEs) have small parameters necessarily. It is noted that the effects of water depth, the ice sheet thickness, and Young's modulus are analytically expressed in detail. We find that, in different water depths, the hydroelastic waves traveling beneath the thickest ice sheet always contain the largest wave energy. While with an increasing thickness of the sheet, the wave elevation tends to be smoothened at the crest and be sharpened at the trough. The larger Young's modulus of the sheet also causes analogous effects. The results obtained show that the thickness and Young's modulus of the floating ice sheet all greatly affect the wave energy and wave profile in different water depths.

1. Introduction

In recent decades, the ice cover in the polar region has attracted more and more attention in the field of ocean engineering and polar engineering in view of their practical importance and theoretical investigations. The motivations for the research work are to study damage to offshore constructions by floating ice sheets, the transportation systems in the cold region where the ice cover can be considered as roads and aircraft runways and air-cushioned vehicles are used to break the ice, for example. One of the important problems in this field would appear to be the accurate measurement of the characteristics of waves traveling beneath a floating ice sheet. And such wave may have been generated in the ice cover itself by the wind, or it may have originated by a moving load on the ice sheets. Considerable work has been done since the first theoretical model of wave propagation in sea ice was proposed by Greenhill [1] in 1887. A comprehensive summary on mathematical method and modeling for the problem can be found in some review articles such as Squire et al. [2, 3]. In addition to ice sheets, this work can apply to very large floating structures (VLFSs) such as floating airports, mobile offshore bases, offshore port facilities, offshore storage and waste disposal provisions, energy islands including some wave power configurations, and ultralarge ships, where there is an extensive complementary literature [4–6].

Most theoretical works on the problem are still in the scope of linear theory based on the assumption that the wave amplitudes generated are very small in comparison with the wave lengths. So such models are not appropriate to describe waves of arbitrary amplitude considered here. According to hydrodynamics and elasticity, we can construct the nonlinear partial differential equations (PDEs) (1)–(5) to describe nonlinear hydroelastic waves of arbitrary amplitude traveling through water covered by an ice sheet in finite water depth. Unfortunately, it is very difficult to solve analytically the coupled nonlinear PDEs mathematically. Further, most of the most works literature on the nonlinear theory of sea waves ice sheet interaction are necessarily in the context of weakly nonlinear analysis due to the limitation of present mathematical tools. Now the main analytical study on such complex nonlinear PDEs still follows the well-known perturbation technique. For example, Forbes [7] derived nonlinear PDEs to describe two-dimensional periodic waves beneath an elastic sheet floating on the surface of an infinitely deep fluid. The periodic solutions are sought using the Fourier series and perturbation expansions for the Fourier coefficients. And it is found that the solutions have certain features in common with capillary-gravity waves. Following the framework in [7], Forbes continued his study of finite-amplitude surface waves beneath a floating elastic sheet in infinitely deep water [8], and optimized their previous perturbation technology directly by developing the Fourier coefficients as expansions in the wave height. Waves of extremely large amplitude are found to exist, and results are presented for waves belonging to several different nonlinear solution branches. Recently, Vanden-Broeck and Părău [9] further extended the results of Forbes for periodic waves to the arbitrary-amplitude waves. It is noted that perturbation and asymptotic approximations of nonlinear PDEs often break down as nonlinearity becomes strong. So the weakly nonlinear solutions of small-amplitude waves are derived by the perturbation approach, while fully nonlinear solutions of large-amplitude waves have to be calculated numerically by means of the numerical series truncation method in Vanden-Broeck's study.

Furthermore, perturbation and asymptotic techniques depend extremely on the small/large parameters in general, while our nonlinear PDEs have no any small/large parameters. Thus the perturbation techniques are not applicable to the nonlinear problem under consideration. In this paper, we apply a new analytic approximation method known as the homotopy analysis method (HAM) to effectively solve the nonlinear PDEs presented here. Based on the concept of homotopy in algebraic topology, the HAM was proposed by Liao [10] in 1992. Unlike the perturbation method, the HAM is entirely independent of any small/large parameters. Moreover, it provides us with extremely large freedom to choose base functions and initial approximations (16) and (17) of solutions and auxiliary linear operators (21)–(23) only under some basic rules [11, 12]. More importantly, in contrast to all other previous analytic techniques, the HAM provides us a convenient way to control and adjust the convergence of the approximate series solutions by means of introducing an auxiliary parameter c_0. The method has been systematically described by Liao [11, 12]. Recently the HAM has been successfully applied to the study of a number of classical nonlinear differential equations including nonlinear equations arising in fluid mechanics [13–18], heat transfer [19, 20], solitons and integrable models [21–24], and finance [25, 26]. These aforementioned studies show the validity and generality of the HAM for some highly nonlinear PDEs with multiple solutions, singularity, and unknown boundary conditions.

The objective of the present work is to analytically study the nonlinear hydroelastic waves under an ice sheet lying over an incompressible inviscid fluid of finite uniform depth by means of the HAM. According to the potential theory in hydrodynamics and elasticity, the nonlinear partial differential equations (PDEs) (1)–(5) are composed of the Laplace equation taken as the governing equation for inviscid flows, the kinematic and dynamic boundary conditions on the unknown ice sheet-water interface with a zero draft, a simple linear model for the thin sheet that includes the effects of flexural rigidity and vertical inertia, and a bottom boundary condition. The convergent homotopy-series solutions for the velocity potential and the wave surface elevation are formally derived by applying the HAM with the consideration of the minimum of the squared residual, respectively. It should be mentioned that we study the effects of the water depth and two important physical parameters including Young's modulus and the thickness of the ice sheet on the wave energy and its elevation in detail. Discussion and conclusions are made in Sections 4 and 5, respectively. All of results obtained will help enrich our understanding of nonlinear hydroelastic waves propagating under a floating ice sheet on a fluid of finite depth.

2. Mathematical Description

The problem under consideration is a train of nonlinear hydroelastic waves propagating beneath a two-dimensional infinite elastic plate floating on a fluid of finite depth h and a zero draft. A Cartesian coordinate oxz is used in which the z-axis points vertically upward, while $z = 0$ represents the undisturbed surface. We follow Greenhill in [1] assuming that this problem is capable of modeling ocean waves in the presence of sea ice when the fluid is inviscid and incompressible and the flow is irrotational, and the ice sheet is mathematically idealized as a thin elastic plate. Then the governing equations for a velocity potential $\phi(x,z,t)$ can be written as

$$\frac{\partial^2\phi}{\partial x^2} + \frac{\partial^2\phi}{\partial z^2} = 0, \quad (-h \le z \le \zeta(x,t)), \tag{1}$$

where $\zeta(x,t)$ is the wave surface elevation. The bottom boundary condition reads

$$\frac{\partial\phi}{\partial z} = 0, \quad (z = -h). \tag{2}$$

The motion of the fluid and the plate is coupled through the dynamic free-surface condition. We also assume that any particle which is once between the elastic plate and the water surface remains on it. So the kinematic and dynamic boundary conditions on the unknown surface $z = \zeta(x,t)$ are, respectively, modeled as

$$\frac{\partial\zeta}{\partial t} + \frac{\partial\phi}{\partial x}\frac{\partial\zeta}{\partial x} - \frac{\partial\phi}{\partial z} = 0, \tag{3}$$

$$\frac{\partial\phi}{\partial t} + \frac{1}{2}\left|\nabla\phi\right|^2 + \frac{p_e}{\rho} + g\zeta = 0, \tag{4}$$

where p_e is the water-plate interface pressure, ρ is the fluid density, and g is the gravitational acceleration, for a thin homogeneous elastic plate with uniform mass density ρ_e and constant thickness d.

Since we are considering long waves here, the linear Kirchhoff (Euler-Bernoulli) beam theory is applied to the floating elastic plate as follows:

$$p_e = D\frac{\partial^4 \zeta}{\partial x^4} + m_e\left(\frac{\partial^2 \zeta}{\partial t^2} + g\right), \quad (5)$$

where $m_e = \rho_e d$, $D = Ed^3/[12(1-\nu^2)]$ is the flexural rigidity of the plate, E is the effective Young's modulus of the plate, and ν Poisson's ratio. We substitute (5) into (4) to derive a new form of the dynamic boundary condition as follows:

$$\frac{\partial \phi}{\partial t} + \frac{1}{2}|\nabla\phi|^2 + g\zeta + \frac{1}{\rho}\left[D\frac{\partial^4 \zeta}{\partial x^4} + m_e\left(\frac{\partial^2 \zeta}{\partial t^2} + g\right)\right] = 0. \quad (6)$$

Here, we consider a train of nonlinear waves traveling beneath an elastic plate with constant wave number k and constant angular frequency ω of the incident wave. For a general case it should be emphasized that, by means of the traveling-wave method directly, the progressive waves are transferred from the temporal differentiation into the spatial one, which is very different from the mathematical model obtained by simply eliminating the time-dependent terms from the kinematic and dynamic boundary conditions on the unknown free surface [7–9]. Namely, we introduce an independent variable transformation

$$X = kx - \omega t, \quad (7)$$

where the angular frequency ω and the wave number k are given. Thus, we can express the potential function $\phi(x, z, t) = \phi(X, z)$ and the traveling wave profile $\zeta(x, t) = \zeta(X)$.

Then the governing equation and the bottom boundary condition for the velocity potential are transformed, respectively, by

$$k^2\frac{\partial^2 \phi}{\partial X^2} + \frac{\partial^2 \phi}{\partial z^2} = 0, \quad (-h \le z \le \zeta(X)), \quad (8)$$

$$\frac{\partial \phi}{\partial z} = 0, \quad (z = -h). \quad (9)$$

With the transformation (7), (3), and (6) on $z = \zeta(X)$ are given by

$$-\omega\frac{d\zeta}{dX} + k^2\frac{\partial \phi}{\partial X}\frac{d\zeta}{dX} - \frac{\partial \phi}{\partial z} = 0, \quad (10)$$

$$-\omega\frac{\partial \phi}{\partial X} + f + g\zeta + \frac{1}{\rho}\left[Dk^4\frac{d^4 \zeta}{dX^4} + m_e\left(\omega^2\frac{d^2 \zeta}{dX^2} + g\right)\right] = 0, \quad (11)$$

respectively, where

$$f = \frac{1}{2}\left[k^2\left(\frac{\partial \phi}{\partial X}\right)^2 + \left(\frac{\partial \phi}{\partial z}\right)^2\right]. \quad (12)$$

We combine partially (10) and (11) to gain the boundary conditions on $z = \zeta(X)$ as follows:

$$\begin{aligned}\omega^2\frac{\partial^2 \phi}{\partial X^2} + g\frac{\partial \phi}{\partial z} - \omega\frac{\partial f}{\partial X} - \frac{\omega}{\rho}\left(Dk^4\frac{d^5 \zeta}{dX^5} + m_e\omega^2\frac{d^3 \zeta}{dX^3}\right)& \\ - k^2 g\frac{\partial \phi}{\partial X}\frac{d\zeta}{dX} = 0.&\end{aligned} \quad (13)$$

Now the corresponding unknown potential function $\phi(X, z)$ and the wave surface elevation $\zeta(X)$ are governed by (8), (9), (11), and (13).

3. Analytic Approach Based on the Homotopy Analysis Method

3.1. Solution Expression and Initial Approximation. Using the homotopy analysis method, we should first of all start from a set of base functions and solution expression which are very important to approximate the unknown solutions of the nonlinear boundary problem under consideration. Mathematically, it seems impossible to guess the expression forms of the unknown potential function and the wave vertical displacement. Fortunately, considering the physical background of our problem, we may gain proper solution expressions of it. From viewpoints of the physical considerations here, our problem is composed of a train of progressive waves cause by a load moving on the ice sheet, an infinite elastic plate acting as an ice sheet floating on an fluid of finite depth. As is well known, in case of the pure water waves, the progressive wave elevation can be expressed as

$$\zeta(X) = \sum_{n=0}^{+\infty}\beta_n\cos(nX) \quad (14)$$

by a set of base functions $\{\cos(nX), n \ge 0\}$, where β_n are unknown coefficients. In the case of plate-covered surface, since we assume that there is no gap between the bottom surface of the thin elastic plate and the top surface of the fluid layer and a zero draft, the vertical displacement of the thin plate is still periodic in the X direction. Therefore, we clearly know that $\zeta(X)$ can be expressed in the above form (14) too.

Besides, according to the linear wave theory, we can find the solutions of the Laplace equation (8) by the separation of variables method. To acquire those solutions, we have to use kinematic and dynamic boundary conditions of the free surface and the boundary condition in finite water depth, and we consider the solution derived here as the solution expression of potential function

$$\phi(X, z) = \sum_{n=1}^{+\infty}\alpha_n\frac{\cosh[nk(z+h)]}{\cosh(nkh)}\sin(nX) \quad (15)$$

by a set of base functions $\{\cosh[nk(z+h)]/\cosh(nkh)\sin(nX), n \ge 0\}$, where α_n are unknown coefficients. Note that the potential function $\phi(X, z)$ defined by (15) automatically satisfies the governing equation (8) and the bottom boundary condition (9). The above expressions (14) and (15) are called the solution expressions of $\phi(X, z)$ and $\zeta(X)$, respectively, which play important roles in the method of homotopy analysis.

According to the solution expression (15) and the boundary condition (9), we construct the initial approximation of the potential function:

$$\phi_0(X,z) = \alpha_{0,1}\frac{\cosh[k(z+h)]}{\cosh(kh)}\sin(X), \quad (16)$$

where $\alpha_{0,1}$ is an unknown coefficient. We choose

$$\zeta_0(X) = 0. \quad (17)$$

as the initial approximation of wave profile $\zeta(X)$ to simplify the subsequent solution procedure [18, 20]. It should be emphasized that higher order terms can hold the corrections of the analytic series solutions due to the nonlinearity inherent in (11) and (13) although the initial guess $\zeta_0(X)$ is zero.

3.2. Continuous Variation. The HAM is based on a kind of continuous mapping of an initial approximation to the exact solution through a series of deformation equations. For simplicity, based on the nonlinear boundary condition (13) and (11), we define the two following nonlinear operators $\mathcal{N}_1$ and $\mathcal{N}_2$ as follows

$$\begin{aligned}
&\mathcal{N}_1[\Phi(X,z;q),\eta(X;q)] \\
&\quad= \omega^2\frac{\partial^2\Phi(X,z;q)}{\partial X^2} + g\frac{\partial\Phi(X,z;q)}{\partial z} - \omega\frac{\partial F}{\partial X} \\
&\qquad- \frac{\omega}{\rho}\left(Dk^4\frac{\partial^5\eta(X;q)}{\partial X^5} + \omega^2 m_e\frac{\partial^3\eta(X;q)}{\partial X^3}\right) \\
&\qquad- k^2 g\frac{\partial\Phi(X,z;q)}{\partial X}\frac{\partial\eta(X;q)}{\partial X},
\end{aligned} \quad (18)$$

$$\begin{aligned}
&\mathcal{N}_2[\eta(X;q),\Phi(X,z;q)] \\
&\quad= -\omega\frac{\partial\Phi(X,z;q)}{\partial X} + F + g\eta(X;q) \\
&\qquad+ \frac{1}{\rho}\left[Dk^4\frac{\partial^4\eta(X;q)}{\partial X^4} + m_e\left(\omega^2\frac{\partial^2\eta(X;q)}{\partial X^2} + g\right)\right],
\end{aligned} \quad (19)$$

where

$$F = \frac{1}{2}\left[k^2\left(\frac{\partial\Phi}{\partial X}\right)^2 + \left(\frac{\partial\Phi}{\partial z}\right)^2\right] \quad (20)$$

and $q \in [0,1]$ is the embedding parameter of the HAM.

Here, it should be emphasized that, as mentioned by Liao and Cheung and Tao et al. [14, 15], the HAM provides us with extremely large freedom to choose the auxiliary linear operators and the initial guess. Note that both linear terms of $\Phi(X,z;q)$ and linear terms of $\eta(X;q)$ are all contained in (18). If we choose all linear terms, the subsequent iterative procedure will become very complex. Fortunately, based on the HAM, we can completely forget the linear terms in (13) and choose proper auxiliary linear operator of $\Phi(X,z;q)$ by means of the solution expression (15) which is obtained under the physical considerations as

$$\overline{\mathcal{L}}_1[\Phi(X,z;q)] = \omega^2\frac{\partial^2\Phi(X,z;q)}{\partial X^2} + g\frac{\partial\Phi(X,z;q)}{\partial z}. \quad (21)$$

In particular, if the angular frequency ω is given, we can choose such an approximation based on the linear wave theory to simplify the subsequent resolution of the nonlinear PDEs as follows:

$$\omega \approx \sqrt{gk\tanh(kh)}. \quad (22)$$

So we simplify the auxiliary linear operator in (21) as follows:

$$\begin{aligned}
\mathcal{L}_1[\Phi(X,z;q)] = gk\tanh(kh)\frac{\partial^2\Phi(X,z;q)}{\partial X^2} \\
+ g\frac{\partial\Phi(X,z;q)}{\partial z},
\end{aligned} \quad (23)$$

where $\mathcal{L}_1[0] = 0$. Note that, due to the weakly nonlinear effects, the actual frequency ω is often slightly different from the linear dispersion relation $\omega_0 = \sqrt{gk\tanh(kh)}$. In Section 4, $\omega/\omega_0 = 1.01$ is chosen so that the perturbation theory is valid and corresponding results are highly accurate, and then we can compare our results with those obtained by the perturbation method.

Based on the linear operator of the wave profile function $\eta(X;q)$ in the nonlinear operator $\mathcal{N}_2$, for simplicity, we may choose another auxiliary linear operator:

$$\mathcal{L}_2[\eta(X;q)] = \frac{\partial^4\eta(X;q)}{\partial X^4} + \frac{\partial^2\eta(X;q)}{\partial X^2} + \eta(X;q), \quad (24)$$

where $\mathcal{L}_2[0] = 0$.

We let c_0 be an nonzero convergence-control parameter. It is noted that both c_0 and q in the HAM are auxiliary parameters without any physical meaning. Instead of the nonlinear PDEs (8), (9), (11), and (13), we reconstruct the so-called zeroth-order deformation equations as follows:

$$k^2\frac{\partial^2\Phi(X,z;q)}{\partial X^2} + \frac{\partial^2\Phi(X,z;q)}{\partial z^2} = 0, \quad (-h \le z \le \eta(X;q)), \quad (25)$$

$$\frac{\partial\Phi(X,z;q)}{\partial z} = 0, \quad (z = -h), \quad (26)$$

$$\begin{aligned}
&(1-q)\mathcal{L}_1[\Phi(X,z;q) - \phi_0(X,z)] \\
&\quad= qc_0\mathcal{N}_1[\Phi(X,z;q),\eta(X;q)], \quad (z = \eta(X;q)),
\end{aligned} \quad (27)$$

$$\begin{aligned}
&(1-q)\mathcal{L}_2[\eta(X;q) - \zeta_0(X)] \\
&\quad= qc_0\mathcal{N}_2[\eta(X;q),\Phi(X,z;q)], \quad (z = \eta(X;q)).
\end{aligned} \quad (28)$$

Then, from (27) and (28), two mapping functions $\Phi(X,z;q)$ and $\eta(X;q)$ vary respectively continuously from their initial approximation $\phi_0(X,z)$ and $\zeta_0(X)$ to the exact solutions $\phi(X,z)$ and $\zeta(X)$ of the original problem. The Taylor series of $\Phi(X,z;q)$ and $\eta(X;q)$ at $q=0$ are

$$\Phi(X,z;q)=\phi_0(X,z)+\sum_{m=1}^{+\infty}\phi_m(X,z)\,q^m, \tag{29}$$

$$\eta(X;q)=\zeta_0(X)+\sum_{m=1}^{+\infty}\zeta_m(X)\,q^m, \tag{30}$$

where

$$\{\phi_m(X,z),\zeta_m(X)\}=\frac{1}{m!}\frac{\partial^m}{\partial q^m}\{\Phi(X,z;q),\eta(X;q)\}\big|_{q=0}. \tag{31}$$

Assume that c_0 is so properly chosen that the series in (29) and (30) converge at $q=1$; then we have the so-called homotopy-series solutions as follows:

$$\begin{aligned}\phi(X,z)&=\Phi(X,z;\ 1)=\phi_0(X,z)+\sum_{m=1}^{+\infty}\phi_m(X,z),\\ \zeta(X)&=\eta(X;\ 1)=\zeta_0(X)+\sum_{m=1}^{+\infty}\zeta_m(X).\end{aligned} \tag{32}$$

At the nth-order of approximations, we have

$$\begin{aligned}\phi(X,z)&\approx\phi_0(X,z)+\sum_{m=1}^{+n}\phi_m(X,z),\\ \zeta(X)&\approx\zeta_0(X)+\sum_{m=1}^{+n}\zeta_m(X).\end{aligned} \tag{33}$$

As shown later in the following section, the unknown terms $\phi_m(X,z)$ and $\zeta_m(X)$ are governed by the linear PDEs (34)–(36).

3.3. High-Order Deformation Equations. High-order deformation equations for the unknown $\phi_m(X,z)$, $\zeta_m(X)$ can be derived directly from the zeroth-order deformation equations. Firstly, substituting the homotopy-Maclaurin series (29) and (30) into the governing equation (25) and the boundary condition in finite water depth (26) and then equating the like-power of the embedding parameter q, we have

$$\begin{aligned}k^2\frac{\partial^2\phi_m(X,z)}{\partial X^2}+\frac{\partial^2\phi_m(X,z)}{\partial z^2}&=0,\quad(-h\le z\le 0),\\ \frac{\partial\phi_m(X,z)}{\partial z}&=0,\quad(z=-h),\end{aligned} \tag{34}$$

where $m\ge 1$.

Note that, $\Phi(X,z;q)$ at the unknown surface $z=\eta(X;q)$ may be expressed in terms of the Taylor expansion at $z=0$ instead of $z=\eta(X;q)$. The detailed derivation of the expansion of $\Phi(X,z;q)$ at the unknown surface is given in Appendices (A.1)–(A.5). Upon the substitution of appropriate series (A.5) and (30) into the boundary conditions (27) and (28), we have two linear boundary conditions on $z=0$ as follows:

$$\mathscr{L}_1(\phi_m)\big|_{z=0}=c_0\Delta^{\phi}_{m-1}+\chi_m S_{m-1}-\overline{S}_m, \tag{35}$$

$$\mathscr{L}_2(\zeta_m)=c_0\Delta^{\zeta}_{m-1}+\chi_m\left(\frac{d^4\zeta_{m-1}}{dX^4}+\frac{d^2\zeta_{m-1}}{dX^2}+\zeta_{m-1}\right), \tag{36}$$

where

$$\chi_m=\begin{cases}0, & m\leqslant 1\\ 1, & m>1.\end{cases} \tag{37}$$

The detailed derivation of the above equations and the expression for ϕ_m and ζ_m are given in Appendix A. It should be noted that (27) and (28) holds on the unknown boundary $z=\eta(X;q)$, while (35) and (36) hold on $z=0$. Furthermore, the original nonlinear DPEs (1)–(5) are transferred into an infinite number of linear decoupled high-order deformation equations (34)–(36). Namely, given ϕ_{m-1} and ζ_{m-1}, ϕ_m and ζ_m can be obtained easily by means of the inverse operators of the right-hand sides of (35) and (36), respectively, and a computer algebra system such as Mathematica. The resulting expressions for ϕ_m and ζ_m are presented to the second order in the coming subsection.

3.4. First-Order and Second-Order Approximations. Substituting initial approximations (16) and (17) into (36), we can get $\zeta_1(X)$ using the inverse linear operator $\mathscr{L}_2$ in (36) as follows:

$$\begin{aligned}\zeta_1(X)=&\frac{1}{4}\left[4dgc_0+c_0a_{0,1}^2+k^2c_0a_{0,1}^2\tanh^2(hk)\right]\\ &-\omega c_0\alpha_{0,1}\cos(X)\\ &+\frac{1}{52}\left[c_0a_{0,1}^2-k^2c_0a_{0,1}^2\tanh^2(hk)\right]\cos(2X).\end{aligned} \tag{38}$$

But now the coefficient $\alpha_{0,1}$ in the initial approximation of $\phi_0(X,z)$ in (16) is still unknown. So we introduce an additional equation to relate the solutions with the wave height:

$$\zeta_1(m\pi)-\zeta_1(n\pi)=H, \tag{39}$$

in which m is an even integer, n is an odd integer, and H is the wave height to the first order based on the HAM. The relation (39) for the wave height and its vertical displacement can determine the solution of $\alpha_{0,1}$.

Further, in the analogous manner as for the first-order approximation, by using the inverse linear operator $\mathscr{L}_1$ in (35), it is easy to get the solution of $\phi_1(X,z)$, especially by means of the symbolic computation software such as Mathematica:

$$\alpha_{0,1} = -\frac{H}{2\omega c_0},$$

$$\begin{aligned}\phi_1(X,z) &= \alpha_{1,1}\frac{\cosh[k(h+z)]}{\cosh(kh)}\sin(X) \\ &+ \frac{-H^2 + H^2k^2\tanh^2(hk)}{16gk\omega c_0[2\tanh(hk)-\tanh(2hk)]} \\ &\times \frac{\cosh[2k(h+z)]}{\cosh(2kh)}\sin(2X).\end{aligned} \tag{40}$$

We find the common solution $\phi_1(X,z)$ has one unknown coefficient $\alpha_{1,1}$ which can be determined by avoiding the "secular" term $\sin(X)$ in $\phi_2(X,z)$. We note that all subsequent functions occur recursively. Utilizing the linear equations (35) and (36) to continue with the first-order approximations we have

$$\begin{aligned}\zeta_2(X) &= \beta_{2,0} + \beta_{2,1}\cos(X) + \beta_{2,2}\cos(2X) \\ &+ \beta_{2,3}\cos(3X) + \beta_{2,4}\cos(4X), \\ \phi_2(X,z) &= \alpha_{2,1}\frac{\cosh[k(h+z)]}{\cosh(kh)}\sin(X) \\ &+ \alpha_{2,2}\frac{\cosh[2k(h+z)]}{\cosh(2kh)}\sin(2X) \\ &+ \alpha_{2,3}\frac{\cosh[3k(h+z)]}{\cosh(3kh)}\sin(3X) \\ &+ \alpha_{2,4}\frac{\cosh[4k(h+z)]}{\cosh(4kh)}\sin(4X) \\ &+ \alpha_{2,5}\frac{\cosh[5k(h+z)]}{\cosh(5kh)}\sin(5X),\end{aligned} \tag{41}$$

where $\alpha_{i,j}$ is the jth unknown coefficient of $\phi_i(X,z)$ and $\beta_{i,j}$ is the jth unknown coefficient of $\zeta_i(X)$. The detailed expressions of these coefficients for ϕ_2 and ζ_2 are given in Appendix B.

In order to obtain higher-order functions $\phi_m(X,z)$ and $\zeta_m(X)$, we need only to continue this approach. In principle, we can acquire infinite-order solutions for our physical model. It is also worthwhile to mention that these solutions will retain model parameters and the convergence control parameter c_0.

3.5. Optimal Convergence-Control Parameter. If we fix all model parameters in our approximate series solutions, there is still an unknown convergence control parameter c_0 in them, which is used to guarantee the convergence of our approximation solutions. According to Liao [12], it is the convergence control parameter c_0 that essentially differs the HAM from all other analytic methods. And the optimal value of c_0 is determined by the minimum of the total squared-residual ε_m^T of our nonlinear problem, defined by

$$\varepsilon_m^T = \varepsilon_m^\phi + \varepsilon_m^\zeta, \tag{42}$$

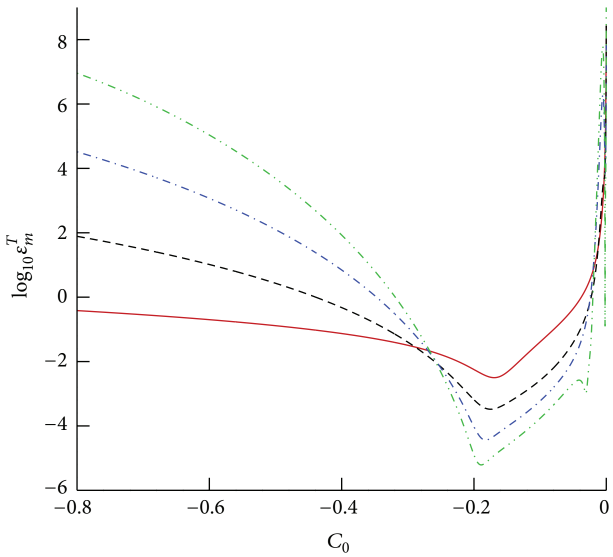

FIGURE 1: Residual squares of $\log_{10}\varepsilon_m^T$ versus c_0. Solid line: first-order approximation; dashed line: third-order approximation; dash-dotted line: fifth-order approximation; dash-dot-dotted line: seventh-order approximation.

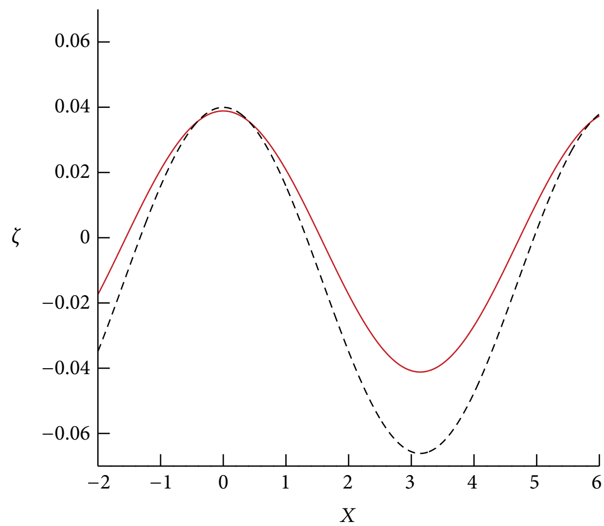

FIGURE 2: Comparison of our present 3rd-order surface elevation ζ with those obtained by the perturbation method. Solid line: perturbation-series solution; dashed line: homotopy-series solution.

where

$$\begin{aligned}\varepsilon_m^\phi &= \frac{1}{1+M}\sum_{i=0}^{M}\left(\mathcal{N}_1[\phi(X,z),\zeta(X)]\big|_{X=i\Delta X}\right)^2, \\ \varepsilon_m^\zeta &= \frac{1}{1+M}\sum_{i=0}^{M}\left(\mathcal{N}_2[\phi(X,z),\zeta(X)]\big|_{X=i\Delta X}\right)^2,\end{aligned} \tag{43}$$

where ε_m^ϕ and ε_m^ζ are two residual square errors of boundary conditions (27) and (28), respectively. M is the number of the discrete points, and $\Delta X = \pi/M$. In this paper, we choose $M = 10$.

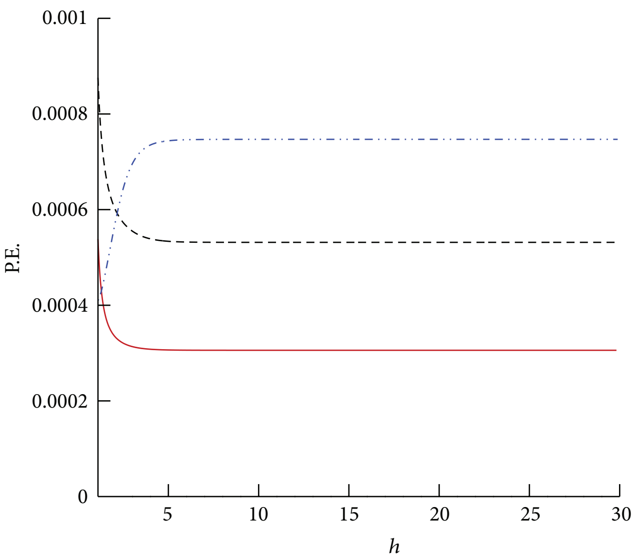

FIGURE 3: P.E. for (44) versus the water depth h for different plate thicknesses d. Solid line: $d = 0.001$; dashed line: $d = 0.005$; dash-dot-dotted line: $d = 0.01$.

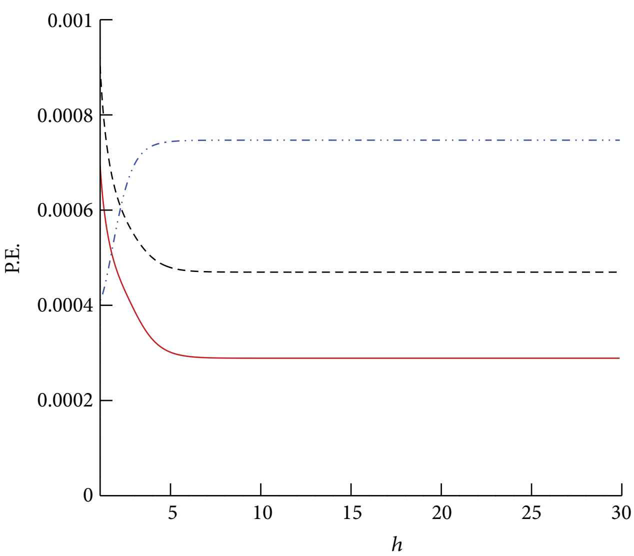

FIGURE 4: P.E. for (44) versus the water depth h for different Young's moduli of the plate E. Solid line: $E = 10^8$; dashed line: $E = 10^9$; dash-dot-dotted line: $E = 10^{10}$.

Theorem 2.1 given by Liao in [12] can guarantee the rationality of (42). So we obtain the optimal convergence control parameter c_0 by the minimum of the squared-residual ε_m^T, generally corresponding to $d\varepsilon_m^T/dc_0 = 0$.

4. Results and Analysis

In order to show the convergence of the analytical series solution to our problems by means of the HAM, we consider the cases of $k = \pi/5\,\mathrm{m}^{-1}$, $d = 0.01$ m, $\rho_e = 900\,\mathrm{kgm}^{-3}$, $\nu = 0.33$, $E = 10^{10}\,\mathrm{Nm}^{-2}$, $h = 5$ m, $H = 0.1$ m, and $\omega/\omega_0 = 1.01$ and take these data hereinafter for computation unless otherwise stated. The total residual square error ε_m^T at several orders of approximation versus the convergence-control parameter c_0 is shown in Figure 1. It is found that ε_m^T at every order has the smallest values which corresponds to the optimal c_0. For example, as $m = 7$, the optimal $c_0 = -0.18$, and the smallest value of $\varepsilon_7^T = 7.910 \times 10^{-6}$. So, let the optimal convergence-control parameter $c_0 = -0.18$, the total residual square error ε_m^T decreases quickly as the order m increases, as shown in Table 1. It is also found that ε_{15}^T is down to 5.382×10^{-11} at the 15th-order of approximation, which indicates the convergence of our series solutions. In this way, we ensure that all our solutions are highly accurate.

TABLE 1: The total residual square error ε_m^T for different approximation order m with $c_0 = -0.18$.

m	ε_m^T
1	3.497×10^{-3}
3	3.404×10^{-4}
5	3.700×10^{-5}
7	7.910×10^{-6}
10	4.803×10^{-8}
15	5.382×10^{-11}

Also, we compare our HAM solutions of waves propagating beneath an elastic plate floating on a fluid of finite depth with those results obtained by perturbation techniques, as shown in Figure 2. It should be noted that the perturbation-series solution is derived by substituting the series expansions (4.5) and (4.6) in [9] into the nonlinear PDEs (8)–(12), and equating power of small parameter ϵ leads to a succession of linear PDEs, and then the linear PDEs can be solved by the separation of variables. In Figure 2. It is seen that our homotopy-series approximation of the surface elevation ζ agrees well with the perturbation-series approximation, and only slight derivations occur at the trough of the wave profile as in Figure 2, which further indicates the validity of our present theory about nonlinear hydroelastic waves beneath a floating ice sheet.

We define quantities which measure how much energy there is in the wave propagating beneath an infinite elastic plate. Let P.E. be the mean potential density per unit length in the X-axis [27]. In terms of the wave surface elevation function, the energy density can be written as

$$\text{P.E.} = \frac{1}{4\pi^2} \int_0^{2\pi} \zeta^2 (X)\, \mathrm{d}X. \quad (44)$$

Different from all research objectives in [7–9], we firstly consider in this paper the effect of water depth on nonlinear hydroelastic waves beneath a floating elastic plate in detail. The energy of hydroelastic waves for different Young's moduli of the plate E and different plate thicknesses h in various water depths are as shown in Figures 3 and 4 and Tables 2 and 3, respectively. We find that, when water depth h is about more than 2, the hydroelastic waves traveling beneath the thickest plate always contain the largest wave energy in different water

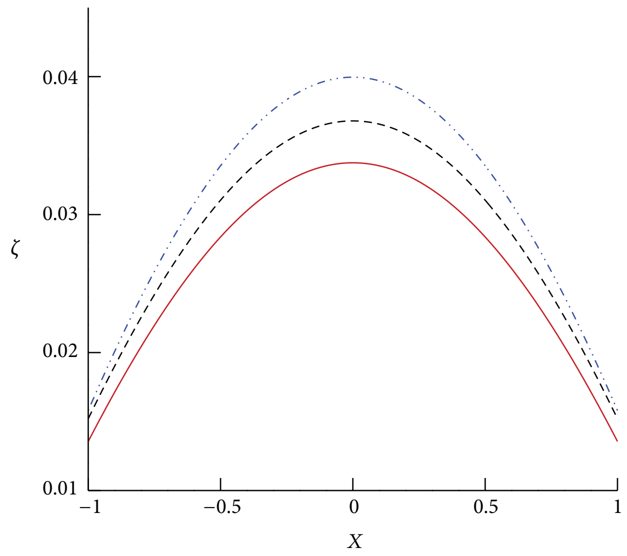

Figure 5: Variation of the plate deflection $\zeta(X)$ near the crest versus X for different Young's moduli of the plate E. Solid line: $E = 10^8$; dashed line: $E = 10^9$; dash-dot-dotted line: $E = 10^{10}$.

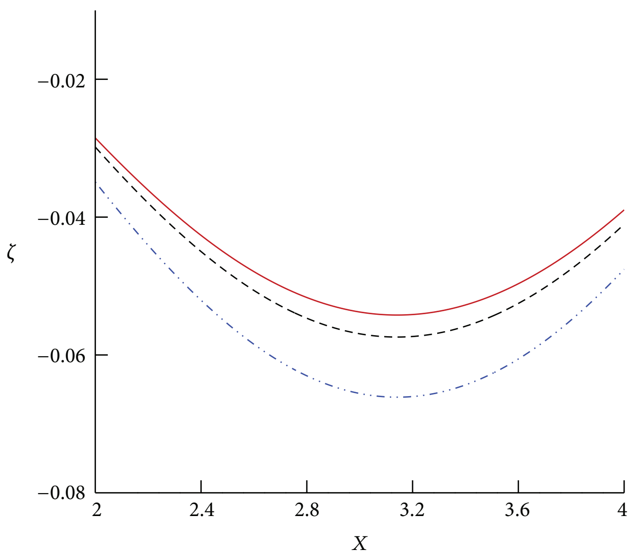

Figure 6: Variation of the plate deflection $\zeta(X)$ near the trough versus X for different Young's moduli of the plate E. Solid line: $E = 10^8$; dashed line: $E = 10^9$; dash-dot-dotted line: $E = 10^{10}$.

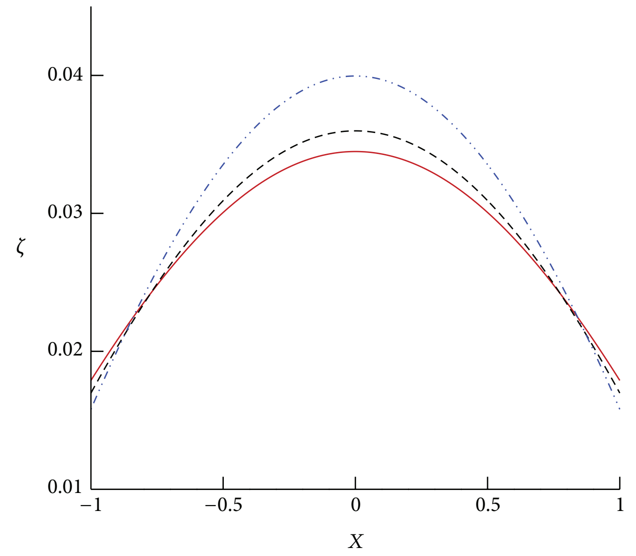

Figure 7: Variation of the plate deflection $\zeta(X)$ near the crest versus X for different plate thicknesses d. Solid line: $d = 0.001$; dashed line: $d = 0.005$; dash-dot-dotted line: $d = 0.01$.

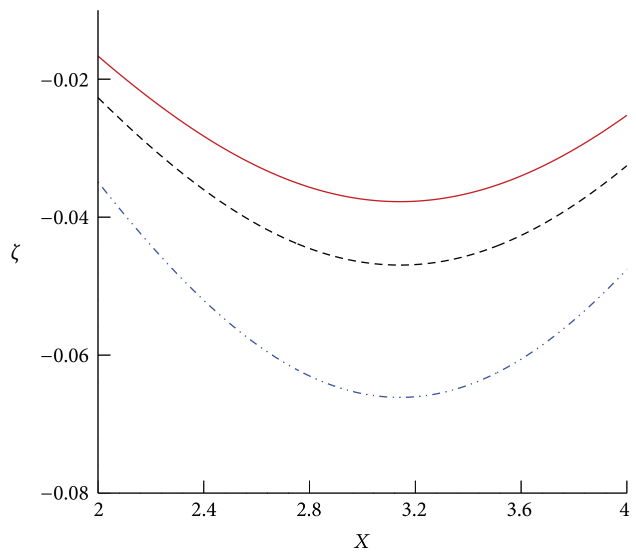

Figure 8: Variation of the plate deflection $\zeta(X)$ near the trough versus X for different plate thicknesses d. Solid line: $d = 0.001$; dashed line: $d = 0.005$; dash-dot-dotted line: $d = 0.01$.

depths. And with an increasing Young's modulus of the plate, the wave energy becomes large too.

The effect of Young's modulus E of the plate on the wave elevation $\zeta(X)$ under a floating elastic plate is studied. Figures 5 and 6 show the differences in $\zeta(X)$ for $E = 10^8$, 10^9, and 10^{10}. According to Figures 5 and 6, respectively, we can see that the nonlinear hydroelastic response of the waves becomes flatter at the crest and steeper at the trough due to the larger value of Young's modulus E. Finally, we consider the impact the plate thickness d by increasing d from 0.001 to 0.01. In Figures 7 and 8, we show several displacements $\zeta(X)$ with $d = 0.001$, $d = 0.005$, and $d = 0.01$, respectively. It indicates that the results are very similar to the effects due to different Young's moduli E of the plate.

5. Conclusions

In this paper, the nonlinear hydroelastic waves propagating beneath a two-dimensional infinite elastic plate floating on a fluid of finite depth are investigated analytically by the HAM. Mathematically, for a train of nonlinear hydroelastic waves traveling at a constant velocity in a fluid of finite or infinite depth, the PDEs in [7–9] were obtained by simply eliminating the time-dependent terms from the kinematic

Table 2: P.E. for (44) with different plate thicknesses and various water depths h.

h	P.E. ($d = 0.001$)	P.E. ($d = 0.005$)	P.E. ($d = 0.01$)
1	0.00067245	0.00100093	0.00040836
3	0.00031356	0.00055509	0.00069567
5	0.00030650	0.00053375	0.00074396
10	0.00030590	0.00053158	0.00074694
15	0.00030592	0.00053159	0.00074694
20	0.00030595	0.00053159	0.00074696
30	0.00030600	0.00053159	0.00074696
∞	0.00030600	0.00053159	0.00074696

Table 3: P.E. for (44) with different values of Young's modulus of the plate E and various water depths h.

h	P.E. ($E = 10^8$)	P.E. ($E = 10^9$)	P.E. ($E = 10^{10}$)
1	0.00076484	0.0009946	0.00040836
3	0.00038884	0.00054698	0.00069567
5	0.00030138	0.00047932	0.00074396
10	0.00028886	0.00046970	0.00074694
15	0.00028884	0.00046969	0.00074694
20	0.00028884	0.00046969	0.00074696
30	0.00028884	0.00046969	0.00074696
∞	0.00028884	0.00046969	0.00074696

and dynamic boundary conditions on the unknown free surface in the frame of reference moving with the wave. Here, for a general case it should be noted that we construct the PDEs by directly applying the traveling-wave method to transfer the temporal differentiation into the spatial one in a fixed Cartesian coordinate oxz. Furthermore, the convergent homotopy-series solutions for the PDES are derived by the HAM with the optimal convergence control parameter.

Physically, we study the effect of the water depth on the nonlinear hydroelastic waves under an elastic plate in detail. It is found that, in different water depths, the wave energy density (P.E.) tends to become larger with an increasing thickness of the sheet. The same conclusions are obtained in various water depths by means of different values of Young's modulus of the plate. Additionally, the influences of Young's modulus and the thickness of the plate on the wave elevation $\zeta(X)$ are investigated, respectively. As Young's modulus of the plate increases, the wave elevation becomes lower. And the increasing thickness of the plate flattens the crest and sharpens the trough of the wave profile. The results obtained here demonstrate that Young's modulus and the thickness of the sheet have important effects on the energy and the profile of nonlinear hydroelastic waves under an ice sheet floating on a fluid of finite depth.

Appendices

A. The Detailed Derivation of (35) and (36) and the Expressions for ϕ_m and ζ_m

Let

$$\eta^n = \left(\sum_{i=1}^{+\infty} \zeta_i q^i\right)^n = \sum_{i=n}^{+\infty} \mu_{n,i} q^i. \tag{A.1}$$

For any z, we have a Maclaurin series as follows:

$$\phi_m(X, z) = \sum_{n=0}^{+\infty} \frac{1}{n!} \frac{\partial^n \phi_m}{\partial z^n}\bigg|_{z=0} z^n. \tag{A.2}$$

For $z = \eta(X; q)$, it follows from (A.1) and (A.2) that

$$\begin{aligned} \phi_m(X, \eta) &= \sum_{n=0}^{+\infty} \left(\frac{1}{n!} \frac{\partial^n \phi_m}{\partial z^n}\bigg|_{z=0} \right) \left(\sum_{i=n}^{+\infty} \mu_{n,i} q^i \right) \\ &= \sum_{i=0}^{+\infty} \psi_{m,i} q^i, \end{aligned} \tag{A.3}$$

where

$$\psi_{m,i} = \sum_{n=0}^{i} \left(\frac{1}{n!} \frac{\partial^n \phi_m}{\partial z^n}\bigg|_{z=0} \right) \mu_{n,i}. \tag{A.4}$$

Thus we have, for $z = \eta(X; q)$,

$$\begin{aligned} \Phi(X, \eta; q) &= \sum_{m=0}^{+\infty} \phi_m(X, \eta) q^m = \sum_{m=0}^{+\infty} \left(\sum_{n=0}^{+\infty} \psi_{m,i} q^i \right) q^m \\ &= \sum_{m=0}^{+\infty} \varphi_m q^m, \end{aligned} \tag{A.5}$$

where

$$\varphi_m = \sum_{i=0}^{m} \psi_{m-i,i}. \tag{A.6}$$

Substituting the series expansions (A.1) and (A.5) into the boundary conditions (27) and (28) and then equating the like-power of the embedding parameter q, we have two linear boundary conditions (35) and (36), respectively. And the explicit expressions for Δ^{ϕ}_{m-1}, S_{m-1}, $\overline{S}_m$, and Δ^{ζ}_{m-1} in these two conditions are given by

$$\begin{aligned}
\Delta^{\phi}_{m-1} &= \omega^2\frac{\mathrm{d}^2\varphi_m}{\mathrm{d}X^2} + g\overline{\varphi}_m \\
&\quad - \omega\sum_{n=0}^{m}\left(\frac{\mathrm{d}\varphi_n}{\mathrm{d}X}\frac{\mathrm{d}^2\varphi_{m-n}}{\mathrm{d}X^2} + \overline{\varphi}_n\frac{\mathrm{d}\overline{\varphi}_{m-n}}{\mathrm{d}X}\right) \\
&\quad - \frac{\omega}{\rho}Dk^4\frac{\mathrm{d}^5\zeta_m}{\mathrm{d}X^5} - \frac{\omega^3 m_e}{\rho}\frac{\mathrm{d}^3\zeta_m}{\mathrm{d}X^3} - k^2 g\sum_{n=0}^{m}\frac{\mathrm{d}\varphi_n}{\mathrm{d}X}\frac{\mathrm{d}\zeta_{m-n}}{\mathrm{d}X}, \\
S_{m-1} &= \sum_{i=0}^{m-2}\left(\frac{\mathrm{d}^2\psi_{m-1-i,i}}{\mathrm{d}X^2} + \gamma_{m-1-i,i}\right), \\
\overline{S}_m &= \sum_{i=1}^{m-1}\left(\frac{\mathrm{d}^2\psi_{m-i,i}}{\mathrm{d}X^2} + \gamma_{m-i,i}\right), \\
\Delta^{\zeta}_{m-1} &= -\omega\frac{\mathrm{d}\varphi_{m-1}}{\mathrm{d}X} \\
&\quad + \frac{1}{2}\sum_{n=0}^{m-1}\left(\frac{\mathrm{d}\varphi_n}{\mathrm{d}X}\frac{\mathrm{d}\varphi_{m-1-n}}{\mathrm{d}X} + \overline{\varphi}_n\overline{\varphi}_{m-1-n}\right) + \zeta_{m-1} \\
&\quad + \frac{Dk^4}{\rho}\frac{\mathrm{d}^4\zeta_{m-1}}{\mathrm{d}X^4} + \frac{m_e\omega^2}{\rho}\frac{\mathrm{d}^2\zeta_{m-1}}{\mathrm{d}X^2}, \quad (m \geq 2), \\
\Delta^{\zeta}_{0} &= \frac{1}{2}\left[\left(\frac{\mathrm{d}\varphi_0}{\mathrm{d}X}\right)^2 + \overline{\varphi}_0^2\right] - \omega\frac{\mathrm{d}\varphi_0}{\mathrm{d}X} + \frac{m_e g}{\rho},
\end{aligned} \tag{A.7}$$

where

$$\begin{aligned}
\overline{\varphi}_m &= \sum_{i=0}^{m}\gamma_{m-i,i}, \\
\gamma_{m-i,i} &= \sum_{n=0}^{i}\frac{1}{n!}\left(\left.\frac{\partial^{n+1}\phi_{m-i}}{\partial z^{n+1}}\right|_{z=0}\right)\mu_{n,i}.
\end{aligned} \tag{A.8}$$

B. Expressions of the Coefficients

$$\begin{aligned}
\beta_{2,0} &= \frac{1}{16\omega^2 c_0}\left[H^2 + gH^2c_0 + 16\mathrm{d}g\omega^2c_0^2\right. \\
&\quad + 16\mathrm{d}g^2\omega^2c_0^3 - 4H\omega c_0\alpha_{1,1} \\
&\quad + H^2k^2\tanh^2(hk) + gH^2k^2c_0\tanh^2(hk) \\
&\quad \left.-4Hk^2\omega c_0\alpha_{1,1}\tanh^2(hk)\right], \\
\beta_{2,1} &= \left(\left[H^3\rho + 32gHk\rho\omega^2c_0\tanh(hk)\right.\right. \\
&\quad + 32DgHk^5\omega^2c_0^2\tanh(hk) \\
&\quad + 32g^2Hk\rho\omega^2c_0^2\tanh(hk) \\
&\quad - 32\mathrm{d}gHk\rho\omega^4c_0^2\tanh(hk) \\
&\quad - 64gk\rho\omega^3c_0^2\alpha_{1,1}\tanh(hk) \\
&\quad - 16gHk\rho\omega^2c_0\tanh(2hk) \\
&\quad - 16DgHk^5\omega^2c_0^2\tanh(2hk) \\
&\quad - 16g^2Hk\rho\omega^2c_0^2\tanh(2hk) \\
&\quad + 16\mathrm{d}gHk\rho\omega^4c_0^2\tanh(2hk) \\
&\quad + 32gk\rho\omega^3c_0^2\alpha_{1,1}\tanh(2hk) \\
&\quad + H^3k^2\rho\tanh(hk)\tanh(2hk) \\
&\quad - H^3k^4\rho\tanh^3(hk)\tanh(2hk) \\
&\quad \left.\left.-H^3k^2\rho\tanh^2(hk)\right]\right) \\
&\quad \times\left(\left[32gk\rho\omega^2c_0\left(2\tanh(hk) - \tanh(2hk)\right)\right]\right)^{-1}, \\
\beta_{2,2} &= \frac{1}{13} - \frac{\mathrm{d}H^2}{52} + \frac{gH^2}{208\omega^2} + \frac{DH^2k^4}{13\rho\omega^2} \\
&\quad + \frac{H^2}{16\omega^2c_0} - \frac{H\alpha_{1,1}}{4\omega} + \frac{1}{52}\mathrm{d}H^2k^2\tanh^2(hk) \\
&\quad - \frac{gH^2k^2\tanh^2(hk)}{208\omega^2} - \frac{DH^2k^6\tanh^2(hk)}{13\rho\omega^2} \\
&\quad - \frac{H^2k^2\tanh^2(hk)}{16\omega^2c_0} \\
&\quad + \frac{Hk^2\alpha_{1,1}\tanh^2(hk)}{4\omega} \\
&\quad + \frac{H^2}{8gk\left(2\tanh(hk) - \tanh(2hk)\right)} \\
&\quad - \frac{H^2k\tanh^2(hk)}{8g\left(2\tanh(hk) - \tanh(2hk)\right)}, \\
\beta_{2,3} &= \left(H^3 - H^3k^2\tanh^2(hk)\right. \\
&\quad - H^3k^2\tanh(hk)\tanh(2hk) \\
&\quad \left.+H^3k^4\tanh^3(hk)\tanh(2hk)\right) \\
&\quad \times\left(2336gk\omega^2c_0\left(2\tanh(hk) - \tanh(2hk)\right)\right)^{-1}, \\
\beta_{2,4} &= 0,
\end{aligned} \tag{B.1}$$

$$\alpha_{1,1} = \Big(\Big[H\Big(-13H^2\left(1+2gk^2\right)\rho\omega^2 - gk\left(gH^2k^2\rho - 208\left(Dk^4\omega^4 - d\rho\omega^6\right)c_0^2\right) \times \tanh(2hk) + H^2k^2\rho\tanh^2(hk) \times \left(13\left(1+2gk^2\right)\omega^2 + g^2k^3\tanh(2hk)\right) + H^2k^4\rho\tanh^3(hk) \times \left(-2g^2k - 13(-1+g)\omega^2\tanh(2hk)\right) + k\tanh(hk) \times \Big(416g\omega^4\left(-Dk^4 + \mathrm{d}\rho\omega^2\right)c_0^2 + H^2k\rho \times \left(2g^2k + 13(-1+g)\omega^2\tanh(2hk)\right) + H^2k\rho\big(2g^2k + 13(-1+g) \times\omega^2\tanh(2hk)\big)\Big)\Big)\Big]\Big) \times \Big(\Big[-416\omega^2c_0^2 \times \Big(\mathrm{d}g^2k^2 + \omega^2gk\rho\omega \times \Big(gH^2k^2\left(-1+\tanh^2(hk)\right) \times \left(25 + 27k^2\tanh^2(hk)\right) - gk\tanh(hk) - \mathrm{d}g^2k^2\tanh^2(hk)\Big)\Big) \times (2\tanh(hk) - \tanh(2hk))\Big]\Big)^{-1},$$

$$\alpha_{2,2} = \frac{1}{-4gk\tanh(hk) + 2gk\tanh(2hk)} \times \Bigg[-\frac{gH^2k^2}{8\omega} + \frac{2DH^2k^4}{13\rho\omega} - \frac{\mathrm{d}H^2\omega}{26} - \frac{H\alpha_{1,1}}{2} - \frac{gHk^2\alpha_{1,1}}{4} - \frac{2DH^2k^6\tanh^2(hk)}{13\rho\omega} + \frac{1}{26}\mathrm{d}H^2k^2\omega\tanh^2(hk) + \frac{1}{2}Hk^2\alpha_{1,1}\tanh^2(hk) + gHk^2\alpha_{1,1}\tanh^2(hk) - \frac{H^2k\omega\tanh^2(hk)}{8g\tanh(hk) - 4g\tanh(2hk)} + \frac{H^2\omega}{8gk\tanh(hk) - 4gk\tanh(2hk)} - \frac{H^2\tanh(2hk)\left(1 + k^2\tanh^2(hk)\right)}{16\omega\tanh(hk) - 8\omega\tanh(2hk)} + \frac{\mathrm{d}gH^2k\left(1 - k^2\tanh^2(hk)\right)}{8\omega\tanh(hk) - 4\omega\tanh(2hk)} + \left(\mathrm{d}gH^2k\tanh(hk)\tanh(2hk) \times \left(-1 + k^2\tanh^2(hk)\right)\right) \times (4\omega\tanh(hk) - 2\omega\tanh(2hk))^{-1} + \frac{-H^2\tanh(2hk)\left(-1 + k^2\tanh^2(hk)\right)}{16\omega c_0\tanh(hk) - 8\omega c_0\tanh(2hk)} + \frac{H^2\tanh(hk)\left(1 - k^2\tanh^2(hk)\tanh(2hk)\right)}{8\omega c_0\tanh(hk) - 4\omega c_0\tanh(2hk)} + \frac{H^4k\left(1 - k^4\tanh^4(hk)\right)}{128\omega^3c_0^2\tanh(hk) - 64\omega^3c_0^2\tanh(2hk)} + \frac{H^4k\tanh(hk)\tanh(2hk)\left(-1 + k^4\tanh^4(hk)\right)}{64\omega^3c_0^2\tanh(hk) - 32\omega^3c_0^2\tanh(2hk)}\Bigg],$$

$$\alpha_{2,3} = \frac{1}{-9gk\tanh(hk) + 3gk\tanh(3hk)} \times \Big[\left(gH^2k^4\alpha_{1,1}\tanh^2(hk) - 9gH^2k^4\alpha_{1,1}\tanh^4(hk)\right) \times \left(416\omega^2c_0\right)^{-1} + \left(-gH^3k^2 - gH^2k^2\alpha_{1,1} + gH^3k^4\tanh^2(hk) + 9gH^2k^2\alpha_{1,1}\tanh^2(hk)\right) \times \left(416\omega^2c_0\right)^{-1} + \frac{5H^3k\tanh(hk)\tanh(2hk)\left(1 - k^2\tanh^2(hk)\right)}{2\left(32\omega c_0\tanh(hk) - 16\omega c_0\tanh(2hk)\right)} + \frac{H^3k\left(1 - k^2\tanh^2(hk)\right)}{2\left(16\omega c_0\tanh(hk) - 8\omega c_0\tanh(2hk)\right)} + \left(H^3k\tanh(hk)\left(-\tanh(hk) - \tanh(2hk) + k^2\tanh^2(hk)\tanh(2hk)\right)\right) \times \left(2\left(32g\omega c_0\tanh(hk) - 16g\omega c_0\tanh(2hk)\right)\right)^{-1}$$

$$
\begin{aligned}
&+\left(H^3 k \tanh(hk)\,(-\tanh(hk)-\tanh(2hk)\right.\\
&\qquad\left.+k^2\tanh^2(hk)\tanh(2hk)\,)\right)\\
&\times\left(2\left(16g\omega c_0\tanh(hk)-8g\omega c_0\tanh(2hk)\right)\right)^{-1}\\
&+\left(3H^3\right)\left(4\left(16gk\omega c_0\tanh(hk)\right.\right.\\
&\qquad\left.\left.-8gk\omega c_0\tanh(2hk)\right)\right)^{-1}\Big],
\end{aligned}
$$

$$
\begin{aligned}
&\alpha_{2,4}\\
&=\frac{1}{-16gk\tanh(hk)+4gk\tanh(4hk)}\\
&\quad\times\left[\frac{H^4k\left(1+k^4\tanh^4(hk)-2k^2\tanh^2(hk)\right)}{4\left(832\omega^3c_0^2\tanh(hk)-416\omega^3c_0^2\tanh(2hk)\right)}\right.\\
&\qquad+\frac{H^3k\tanh(hk)\tanh(2hk)\left(-1+k^2\tanh^2(hk)\right)}{2\left(8\omega c_0\tanh(hk)-4\omega c_0\tanh(2hk)\right)}\\
&\qquad\times\left(H^4k\tanh(hk)\tanh(2hk)\right.\\
&\qquad\qquad\left.\times\left(-1-k^4\tanh^4(hk)+2k^2\tanh^2(hk)\right)\right)\\
&\qquad\times\left(4\left(104\omega^3c_0^2\tanh(hk)\right.\right.\\
&\qquad\qquad\left.\left.\left.-52\omega^3c_0^2\tanh(2hk)\right)\right)^{-1}\right],\\
&\qquad\qquad\alpha_{2,5}=0.
\end{aligned}
\tag{B.2}
$$

Conflict of Interests

There is no conflict of interests in the paper. The authors themselves used the program of the symbolic computation software named Mathematica independently to gain the approximate analytical solutions of the PDEs considered here.

Acknowledgments

This work was supported in part by China Postdoctoral Science Foundation funded Project 20100481088 and in part by the Natural Science Foundation of Shandong Province of China under Grant ZR2010FL016. The authors would like to thank the reviewer for his constructive comments.

References

[1] A. G. Greenhill, "Wave motion in hydrodynamics," *American Journal of Mathematics*, vol. 9, no. 1, pp. 62–96, 1886.

[2] V. A. Squire, J. P. Dugan, P. Wadhams, P. J. Rottier, and A. K. Liu, "Of ocean waves and sea ice," *Annual Review of Fluid Mechanics*, vol. 27, pp. 115–168, 1995.

[3] V. A. Squire, "Of ocean waves and sea-ice revisited," *Cold Regions Science and Technology*, vol. 49, no. 2, pp. 110–133, 2007.

[4] V. A. Squire, "Synergies between VLFS hydroelasticity and sea ice research," *International Journal of Offshore and Polar Engineering*, vol. 18, no. 4, pp. 241–253, 2008.

[5] T. Kakinuma, K. Yamashita, and K. Nakayama, "Surface and internal waves due to a moving load on a very large floating structure," *Journal of Applied Mathematics*, vol. 2012, Article ID 830530, 14 pages, 2012.

[6] F. Xu and D. Q. Lu, "Wave scattering by a thin elastic plate floating on a two-layer fluid," *International Journal of Engineering Science*, vol. 48, no. 9, pp. 809–819, 2010.

[7] L. K. Forbes, "Surface waves of large amplitude beneath an elastic sheet. Part 1. High-order series solution," *Journal of Fluid Mechanics*, vol. 169, pp. 409–428, 1986.

[8] L. K. Forbes, "Surface waves of large amplitude beneath an elastic sheet. Part 2. Galerkin solution," *Journal of Fluid Mechanics*, vol. 188, pp. 491–508, 1988.

[9] J.-M. Vanden-Broeck and E. I. Părău, "Two-dimensional generalized solitary waves and periodic waves under an ice sheet," *Philosophical Transactions of the Royal Society A*, vol. 369, no. 1947, pp. 2957–2972, 2011.

[10] S.-J. Liao, *The proposed homotopy analysis technique for the solution of nonlinear problems [Ph. D. Dissertation]*, Shanghai Jiao Tong University, 1992.

[11] S.-J. Liao, *Beyond Perturbation: Introduction to the Homotopy Analysis Method*, Modern Mechanics and Mathematics, Chapman and Hall/ CRC Press, 1st edition, 2003.

[12] S.-J. Liao, *Homotopy Analysis Method in Nonlinear Differential Equations*, Springer & Higher Education Press, Heidelberg, Germany, 2003.

[13] S.-J. Liao, "On the analytic solution of magnetohydrodynamic flows of non-Newtonian fluids over a stretching sheet," *Journal of Fluid Mechanics*, vol. 488, pp. 189–212, 2003.

[14] S.-J. Liao and K. F. Cheung, "Homotopy analysis of nonlinear progressive waves in deep water," *Journal of Engineering Mathematics*, vol. 45, no. 2, pp. 105–116, 2003.

[15] L. Tao, H. Song, and S. Chakrabarti, "Nonlinear progressive waves in water of finite depth—an analytic approximation," *Coastal Engineering*, vol. 54, no. 11, pp. 825–834, 2007.

[16] S.-J. Liao, "On the homotopy multiple-variable method and its applications in the interactions of nonlinear gravity waves," *Communications in Nonlinear Science and Numerical Simulation*, vol. 16, no. 3, pp. 1274–1303, 2011.

[17] D. Xu, Z. Lin, S.-J. Liao, and M. Stiassnie, "On the steady-state fully resonant progressive waves in water of finite depth," *Journal of Fluid Mechanics*, vol. 710, pp. 379–418, 2012.

[18] J. Cheng and S. Q. Dai, "A uniformly valid series solution to the unsteady stagnation-point flow towards an impulsively stretching surface," *Science China*, vol. 53, no. 3, pp. 521–526, 2010.

[19] S. Abbasbandy, "The application of homotopy analysis method to nonlinear equations arising in heat transfer," *Physics Letters A*, vol. 360, no. 1, pp. 109–113, 2006.

[20] S.-J. Liao and A. Campo, "Analytic solutions of the temperature distribution in Blasius viscous flow problems," *Journal of Fluid Mechanics*, vol. 453, pp. 411–425, 2002.

[21] W. Wu and S.-J. Liao, "Solving solitary waves with discontinuity by means of the homotopy analysis method," *Chaos, Solitons and Fractals*, vol. 26, no. 1, pp. 177–185, 2005.

[22] E. Sweet and R. A. van Gorder, "Analytical solutions to a generalized Drinfel'd-Sokolov equation related to DSSH and KdV," *Applied Mathematics and Computation*, vol. 216, pp. 2783–2791, 2010.

[23] R. A. van Gorder, "Analytical method for the construction of solutions to the Föppl-von Kármán equations governing deflections of a thin flat plate," *International Journal of Non-Linear Mechanics*, vol. 47, pp. 1–6, 2012.

[24] S.-J. Liao, "An optimal homotopy-analysis approach for strongly nonlinear differential equations," *Communications in Nonlinear Science and Numerical Simulation*, vol. 15, no. 8, pp. 2003–2016, 2010.

[25] L. Zou, Z. Zong, Z. Wang, and L. He, "Solving the discrete KdV equation with homotopy analysis method," *Physics Letters A*, vol. 370, no. 3-4, pp. 287–294, 2007.

[26] J. Cheng, S.-P. Zhu, and S.-J. Liao, "An explicit series approximation to the optimal exercise boundary of American put options," *Communications in Nonlinear Science and Numerical Simulation*, vol. 15, no. 5, pp. 1148–1158, 2010.

[27] A. J. Roberts, "Highly nonlinear short-crested water waves," *Journal of Fluid Mechanics*, vol. 135, pp. 301–321, 1983.

Hindawi Publishing Corporation
Abstract and Applied Analysis
Volume 2013, Article ID 416757, 8 pages
http://dx.doi.org/10.1155/2013/416757

Research Article

Numerical Solution of Nonlinear Fredholm Integrodifferential Equations by Hybrid of Block-Pulse Functions and Normalized Bernstein Polynomials

S. H. Behiry

General Required Courses Department, Jeddah Community College, King Abdulaziz University, Jeddah 21589, Saudi Arabia

Correspondence should be addressed to S. H. Behiry; salah_behiry@hotmail.com

Received 24 April 2013; Accepted 1 September 2013

Academic Editor: Santanu Saha Ray

A numerical method for solving nonlinear Fredholm integrodifferential equations is proposed. The method is based on hybrid functions approximate. The properties of hybrid of block pulse functions and orthonormal Bernstein polynomials are presented and utilized to reduce the problem to the solution of nonlinear algebraic equations. Numerical examples are introduced to illustrate the effectiveness and simplicity of the present method.

1. Introduction

Integrodifferential equations are often involved in mathematical formulation of physical phenomena. Fredholm integrodifferential equations play an important role in many fields such as economics, biomechanics, control, elasticity, fluid dynamics, heat and mass transfer, oscillation theory, and airfoil theory; for examples see [1–3] and references cited therein. Finding numerical solutions for Fredholm integrodifferential equations is one of the oldest problems in applied mathematics. Numerous works have been focusing on the development of more advanced and efficient methods for solving integrodifferential equations such as wavelets method [4, 5], Walsh functions method [6], sinc-collocation method [7], homotopy analysis method [8], differential transform method [9], the hybrid Legendre polynomials and block-pulse functions [10], Chebyshev polynomials method [11], and Bernoulli matrix method [12].

Block-pulse functions have been studied and applied extensively as a basic set of functions for signals and functions approximations. All these studies and applications show that block-pulse functions have definite advantages for solving problems involving integrals and derivatives due to their clearness in expressions and their simplicity in formulations; see [13]. Also, Bernstein polynomials play a prominent role in various areas of mathematics. Many authors have used these polynomials in the solution of integral equations, differential equations, and approximation theory; see for instance [14–17].

The purpose of this work is to utilize the hybrid functions consisting of combination of block-pulse functions with normalized Bernstein polynomials for obtaining numerical solution of nonlinear Fredholm integrodifferential equation:

$$\sum_{i=0}^{s} p_i(x)\, y^{(i)}(x) = g(x) + \lambda \int_0^1 k(x,t)\,[y(t)]^q\,dt, \quad 0 \le x,\ t < 1, \tag{1}$$

with the conditions

$$y^{(i)}(0) = \alpha_i, \quad 0 \le i \le s-1, \tag{2}$$

where $y^{(i)}(x)$ is the ith derivative of the unknown function that will be determined, $k(x,t)$ is the kernel of the integral, $g(x)$ and $p_i(x)$ are known analytic functions, q is a positive integer, and λ and α_i are suitable constants. The proposed approach for solving this problem uses few numbers of basis and benefits of the orthogonality of block-pulse functions and the advantages of orthonormal Bernstein polynomials properties to reduce the nonlinear integrodifferential equation to easily solvable nonlinear algebraic equations.

This paper is organized as follows. In the next section, we present Bernstein polynomials and hybrid of block-pulse functions. Also, their useful properties such as functions approximation, convergence analysis, operational matrix of product, and operational matrix of differentiation are given. In Section 3, the numerical scheme for the solution of (1) and (2) is described. In Section 4, the proposed method is applied to some nonlinear Fredholm integrodifferential equations, and comparisons are mad with the existing analytic or numerical solutions that were reported in other published works in the literature. Finally conclusions are given in Section 5.

2. Properties of Hybrid Functions

2.1. Hybrid of Block-Pulse Functions and Orthonormal Bernstein Polynomials. The Bernstein polynomials of nth degree are defined on the interval $[0,1]$ as [16]

$$B_{i,n}(x) = \binom{n}{i} x^i (1-x)^{n-i}, \quad \text{for } i = 0,1,2,\ldots,n, \tag{3}$$

where

$$\binom{n}{i} = \frac{n!}{i!\,(n-i)!}. \tag{4}$$

There are $(n+1)$ nth degree Bernstein polynomials. Using Gram-Schmidt orthonormalization process on $B_{i,n}(x)$, we obtain a class of orthonormal polynomials from the Bernstein polynomials. We call them orthonormal Bernstein polynomials of degree n and denote them by $b_{i,n}(x)$, $0 \le i \le n$. For $n = 3$, the four orthonormal Bernstein polynomials are given by

$$\begin{aligned} b_{0,3}(x) &= -\sqrt{7}\left[x^3 - 3x^2 + 3x - 1\right], \\ b_{1,3}(x) &= \sqrt{5}\left[7x^3 - 15x^2 + 9x - 1\right], \\ b_{2,3}(x) &= -\sqrt{3}\left[21x^3 - 33x^2 + 13x - 1\right], \\ b_{3,3}(x) &= 35x^3 - 45x^2 + 15x - 1. \end{aligned} \tag{5}$$

Hybrid functions $h_{ji}(x)$, $j = 1,2,\ldots,m$ and $i = 0,1,\ldots,n$ are defined on the interval $[0,1)$ as

$$h_{ji}(x) = \begin{cases} \sqrt{m}\, b_{i,n}(mx - j + 1), & \dfrac{j-1}{m} \le x < \dfrac{j}{m}, \\ 0, & \text{otherwise}, \end{cases} \tag{6}$$

where j and n are the order of block-pulse functions and degree of orthonormal Bernstein polynomials, respectively.

It is clear that these sets of hybrid functions in (6) are orthonormal and disjoint.

2.2. Functions Approximation. A function $y(x) \in L^2[0,1)$ may be approximated as

$$y(x) \approx \sum_{j=1}^{m}\sum_{i=0}^{n} c_{ji} h_{ji}(x) = \mathbf{C}^T \mathbf{H}(x), \tag{7}$$

where

$$\begin{gathered} \mathbf{C} = \left[\mathbf{C}_1^T, \mathbf{C}_2^T, \ldots, \mathbf{C}_j^T, \ldots, \mathbf{C}_m^T\right]^T, \\ \mathbf{C}_j = \left[c_{j0}, c_{j1}, c_{j2}, \ldots, c_{jn}\right]^T, \quad j = 1,2,\ldots,m, \end{gathered} \tag{8}$$

$$\mathbf{H}(x) = \left[\mathbf{H}_1^T(x), \mathbf{H}_2^T(x), \ldots, \mathbf{H}_j^T(x), \ldots, \mathbf{H}_m^T(x)\right]^T, \tag{9}$$

and $\mathbf{H}_j(x) = [h_{j0}(x), h_{j1}(x), \ldots, h_{jn}(x)]^T$, $j = 1,2,\ldots,m$. The constant coefficients c_{ji} are $(y(x), h_{ji}(x))$, $i = 0,1,2,\ldots,n$, $j = 1,2,\ldots,m$, and $(\cdot,\cdot)$ is the standard inner product on $L^2[0,1)$.

We can also approximate the function $k(x,t) \in L^2([0,1)\times[0,1))$ by

$$k(x,t) \approx \sum_{i=1}^{m}\sum_{j=1}^{m}\sum_{l=0}^{n}\sum_{r=0}^{n} k_{lr}^{ij} h_{il}(x) h_{jr}(t) = \mathbf{H}^T(x)\mathbf{K}\mathbf{H}(t), \tag{10}$$

where $\mathbf{K} = [\mathbf{K}^{ij}]$ is an $m(n+1)\times m(n+1)$ matrix, such that the elements of the sub matrix $\mathbf{k}^{ij}$ are

$$\begin{gathered} k_{lr}^{ij} = \int_{i-1/m}^{i/m}\int_{j-1/m}^{j/m} k(x,t)\, h_{i(l-1)}(x)\, h_{j(r-1)}(t)\, dx\,dt, \\ l, r = 1,2,\ldots,n+1, \ \ i, j = 1,2,\ldots,m, \end{gathered} \tag{11}$$

utilizing properties of block-pulse function and orthonormal Bernstein polynomials.

2.3. Convergence Analysis. In this section, the error bound and convergence is established by the following lemma.

Lemma 1. *Suppose that $f \in C^{(n+1)}[0,1)$ is $n+1$ times continuously differentiable function such that $f = \sum_{j=1}^{m} f_j$, and let $Y_j = \operatorname{Span}\{h_{j0}(x), h_{j1}(x), \ldots, h_{jn}(x)\}$, $j = 1,2,\ldots,m$. If $\mathbf{C}_j^T\mathbf{H}_j(x)$ is the best approximation to f_j from Y_j, then $\mathbf{C}^T\mathbf{H}(x)$ approximates f with the following error bound:*

$$\begin{gathered} \left\| f - \mathbf{C}^T\mathbf{H}(x)\right\|_2 \le \frac{\gamma}{m^{n+1}(n+1)!\sqrt{2n+3}}, \\ \gamma = \max_{x\in[0.1)} \left| f^{(n+1)}(x)\right|. \end{gathered} \tag{12}$$

Proof. The Taylor expansion for the function $f_j(x)$ is

$$\begin{aligned} \widetilde{f}_j(x) &= f_j\left(\frac{j-1}{m}\right) + f_j'\left(\frac{j-1}{m}\right)\left(x - \frac{j-1}{m}\right) \\ &\quad + \cdots + f_j^{(n)}\left(\frac{j-1}{m}\right)\frac{(x-(j-1/m))^n}{n!}, \\ &\qquad \frac{j-1}{m} \le x < \frac{j}{m}, \end{aligned} \tag{13}$$

for which it is known that

$$\begin{gathered} \left| f_j(x) - \widetilde{f}_j(x)\right| \le \left| f^{(n+1)}(\eta)\right| \frac{(x-(j-1/m))^{n+1}}{(n+1)!}, \\ \eta \in \left[\frac{j-1}{m}, \frac{j}{m}\right), \ j = 1,2,\ldots,m. \end{gathered} \tag{14}$$

Since $\mathbf{C}_j^T\mathbf{H}_j(x)$ is the best approximation to f_j form Y_j and $\tilde{f}_j \in Y_j$, using (14) we have

$$\begin{aligned}\left\|f_j - \mathbf{C}_j^T \mathbf{H}_j(x)\right\|_2^2 &\le \left\|f_j - \tilde{f}_j\right\|^2 \\ &= \int_{j-1/m}^{j/m} \left|f_j(x) - \tilde{f}_j(x)\right|^2 dx \\ &\le \int_{j-1/m}^{j/m} \left[\frac{f^{(n+1)}(\eta)\left(x-(j-1/m)\right)^{n+1}}{(n+1)!}\right]^2 dx \\ &\le \left[\frac{\gamma}{(n+1)!}\right]^2 \int_{j-1/m}^{j/m} \left(x - \frac{j-1}{m}\right)^{2n+2} dx \\ &= \left[\frac{\gamma}{(n+1)!}\right]^2 \frac{1}{m^{2n+3}(2n+3)}.\end{aligned} \tag{15}$$

Now,

$$\begin{aligned}\left\|f - \mathbf{C}^T\mathbf{H}(x)\right\|_2^2 &\le \sum_{j=1}^{m} \left\|f_j - \mathbf{C}_j^T\mathbf{H}_j(x)\right\|_2^2 \\ &\le \frac{\gamma^2}{m^{2n+2}[(n+1)!]^2(2n+3)}.\end{aligned} \tag{16}$$

By taking the square roots we have the above bound. □

2.4. The Operational Matrix of Product. In this section, we present a general formula for finding the $m(n+1)\times m(n+1)$ operational matrix of product $\widetilde{\mathbf{C}}$ whenever

$$\mathbf{C}^T\mathbf{H}(x)\mathbf{H}^T(x) \approx \mathbf{H}^T(x)\widetilde{\mathbf{C}}, \tag{17}$$

where

$$\widetilde{\mathbf{C}} = \operatorname{diag}\left[\widetilde{\mathbf{C}}_1, \widetilde{\mathbf{C}}_2, \ldots, \widetilde{\mathbf{C}}_j, \ldots, \widetilde{\mathbf{C}}_m\right]. \tag{18}$$

In (18), $\widetilde{\mathbf{C}}_j = [c_{lr}^j]$ are $(n+1)\times(n+1)$ symmetric matrices depending on n, where

$$c_{lr}^j = \int_{j-1/m}^{j/m} \left(h_{j(l-1)}(x)\, h_{j(r-1)}(x) \sum_{i=0}^{n} c_{ji} h_{ji}(x)\right) dx, \quad l, r = 1, 2, \ldots, n+1. \tag{19}$$

Furthermore, the integration of cross-product of two hybrid functions vectors is

$$\int_0^1 \mathbf{H}(x)\mathbf{H}^T(x)\, dx = \mathbf{I}, \tag{20}$$

where $\mathbf{I}$ is the $m(n+1)$ identity matrix.

2.5. The Operational Matrix of Differentiation. The operational matrix of derivative of the hybrid functions vector $\mathbf{H}(x)$ is defined by

$$\frac{d}{dx}\mathbf{H}(x) = \mathbf{D}\mathbf{H}(x), \tag{21}$$

where $\mathbf{D}$ is the $m(n+1)\times m(n+1)$ operational matrix of derivative given as

$$\begin{aligned}\mathbf{H}(x) &= \left[\mathbf{H}_1^T(x), \mathbf{H}_2^T(x), \ldots, \mathbf{H}_j^T(x), \ldots, \mathbf{H}_m^T(x)\right]^T \\ &= \widetilde{\mathbf{A}}\widetilde{\mathbf{T}}(x),\end{aligned} \tag{22}$$

where $\widetilde{\mathbf{A}} = \operatorname{diag}[\mathbf{A}_1, \mathbf{A}_2, \ldots, \mathbf{A}_j, \ldots, \mathbf{A}_m]$ is the $m(n+1) \times m(n+1)$ coefficient matrix of the $(n+1)\times(n+1)$ coefficient submatrix $\mathbf{A}_j$, and $\widetilde{\mathbf{T}}(x) = [\mathbf{t}_1(x), \mathbf{t}_2(x), \ldots, \mathbf{t}_j(x), \ldots, \mathbf{t}_m(x)]^T$ is the $m(n+1)$ vector with $\mathbf{t}_j(x) = [1, x, x^2, \ldots, x^n]^T$, such that $\mathbf{H}_j(x) = \mathbf{A}_j\mathbf{t}_j(x)$. Now

$$\frac{d}{dx}\mathbf{H}(x) = \widetilde{\mathbf{A}}\widetilde{\mathbf{Q}}\widetilde{\mathbf{T}}(x) = \widetilde{\mathbf{A}}\widetilde{\mathbf{Q}}\widetilde{\mathbf{A}}^{-1}\mathbf{H}(x), \tag{23}$$

where $\widetilde{\mathbf{Q}} = \operatorname{diag}[\mathbf{Q}, \ldots, \mathbf{Q}]$ is the $m(n+1)\times m(n+1)$ matrix of the $(n+1)\times(n+1)$ sub-matrix $\mathbf{Q}$, such that

$$\mathbf{Q} = \begin{bmatrix} 0 & 0 & 0 & \cdots & 0 & 0 \\ 1 & 0 & 0 & \cdots & 0 & 0 \\ 0 & 2 & 0 & \cdots & 0 & 0 \\ \vdots & \vdots & \vdots & \cdots & \vdots & \vdots \\ 0 & 0 & 0 & \cdots & n & 0 \end{bmatrix}. \tag{24}$$

Hence,

$$\mathbf{D} = \widetilde{\mathbf{A}}\widetilde{\mathbf{Q}}\widetilde{\mathbf{A}}^{-1}. \tag{25}$$

In general, we can have

$$\frac{d^k}{dx^k}\mathbf{H}(x) = \mathbf{D}^k\mathbf{H}(x), \quad k = 1, 2, 3, \ldots. \tag{26}$$

3. Outline of the Solution Method

This section presents the derivation of the method for solving sth-order nonlinear Fredholm integrodifferential equation (1) with the initial conditions (2).

Step 1. The functions $y^{(i)}(x)$, $i = 0, 1, 2, \ldots, s$ are being approximated by

$$y^{(i)}(x) = \mathbf{C}^T(\mathbf{H}(x))^{(i)} = \mathbf{C}^T\mathbf{D}^i\mathbf{H}(x), \quad i = 0, 1, 2, \ldots, s, \tag{27}$$

where $\mathbf{D}$ is given by (25).

Step 2. The function $k(x,t)$ is being approximated by (10).

Step 3. In this step, we present a general formula for approximate $y^q(x)$. By using (7) and (17), we can have

$$y^2(x) = \left[\mathbf{C}^T\mathbf{H}(x)\right]^2 = \mathbf{C}^T\mathbf{H}(x)\mathbf{H}^T(x)\mathbf{C} = \mathbf{H}^T(x)\widetilde{\mathbf{C}}\mathbf{C}, \tag{28}$$

$$\begin{aligned}y^3(x) &= \mathbf{C}^T\mathbf{H}(x)\left[\mathbf{C}^T\mathbf{H}(x)\right]^2 = \mathbf{C}^T\mathbf{H}(x)\mathbf{H}^T(x)\widetilde{\mathbf{C}}\mathbf{C} \\ &= \mathbf{H}^T(x)\widetilde{\mathbf{C}}\widetilde{\mathbf{C}}\mathbf{C} = \mathbf{H}^T(x)\left(\widetilde{\mathbf{C}}\right)^2\mathbf{C},\end{aligned} \tag{29}$$

and so by use of induction, $y^q(x)$ will be approximated as

$$y^q(x) = \mathbf{H}^T(x)\left(\widetilde{\mathbf{C}}\right)^{q-1}\mathbf{C}. \tag{30}$$

Table 1: Numerical comparison of absolute difference errors for Example 3.

x	Method of [17]	The proposed method	
	$n = 7$	$n = 2$, $m = 30$	$n = 3$, $m = 30$
0.0	$3.2038E - 009$	$3.1309E - 007$	$4.0173E - 010$
0.2	$7.1841E - 010$	$3.8241E - 007$	$4.9068E - 010$
0.4	$1.4151E - 010$	$4.6707E - 007$	$5.9932E - 010$
0.6	$4.0671E - 011$	$5.7048E - 007$	$7.3201E - 010$
0.8	$9.1044E - 010$	$6.9679E - 007$	$8.9407E - 010$
1.0	$3.7002E - 009$	$8.2709E - 007$	$1.4907E - 010$

Step 4. Approximate the functions $g(x)$ and $p_i(x)$ by

$$g(x) \approx \mathbf{G}^T \mathbf{H}(x), \tag{31}$$

$$p_i(x) \approx \mathbf{P}_i^T H(x), \quad i = 0, 1, 2, \ldots, s, \tag{32}$$

where $\mathbf{G}$ and $\mathbf{P}_i$ are constant coefficient vectors which are defined similarly to (7).

Now, using (27)–(32) and (10) to substitute into (1), we can obtain

$$\sum_{i=0}^{s} \mathbf{P}_i^T \mathbf{H}(x) \mathbf{H}^T(x) \left(\mathbf{D}^i\right)^T \mathbf{C} = \mathbf{H}^T(x) \mathbf{G} + \lambda \int_0^1 \mathbf{H}^T(x) \mathbf{K} \mathbf{H}(t) \mathbf{H}^T(t) \left(\widetilde{\mathbf{C}}\right)^{q-1} \mathbf{C} dt. \tag{33}$$

Utilizing (17) and (20), we may have

$$\sum_{i=0}^{s} \mathbf{H}^T(x) \widetilde{\mathbf{P}}_i \left(\mathbf{D}^i\right)^T \mathbf{C} = \mathbf{H}^T(x) \mathbf{G} + \lambda \mathbf{H}^T(x) \mathbf{K} \left(\widetilde{\mathbf{C}}\right)^{q-1} \mathbf{C}, \tag{34}$$

and hence we get

$$\sum_{i=0}^{s} \widetilde{\mathbf{P}}_i \left(\mathbf{D}^i\right)^T \mathbf{C} - \lambda \mathbf{K} \left(\widetilde{\mathbf{C}}\right)^{q-1} \mathbf{C} = \mathbf{G}. \tag{35}$$

The matrix (35) gives a system of $m(n+1)$ nonlinear algebraic equations which can be solved utilizing the initial condition for the elements of $\mathbf{C}$. Once $\mathbf{C}$ is known, $y(x)$ can be constructed by using (7).

4. Applications and Numerical Results

In this section, numerical results of some examples are presented to validate accuracy, applicability, and convergence of the proposed method. Absolute difference errors of this method is compared with the existing methods reported in the literature [5, 6, 17, 18]. The computations associated with these examples were performed using MATLAB 9.0.

Example 1. Consider the first-order nonlinear Fredholm integrodifferential equation [17, 18] as follows:

$$y'(x) = 1 - \frac{1}{3}x + \int_0^1 x\, y^2(t)\, dt, \quad 0 \le x < 1, \tag{36}$$

with the initial condition

$$y(0) = 0. \tag{37}$$

In this example, we have $p_0 = 0$, $p_1 = 1$, $g(x) = 1 - (1/3)x$, $\lambda = 1$, $k(x,t) = x$, and $q = 2$.

The matrix (35) for this example is

$$\widetilde{\mathbf{P}}_1 \mathbf{D}^T \mathbf{C} - \mathbf{K}\left(\widetilde{\mathbf{C}}\right) \mathbf{C} = \mathbf{G}, \tag{38}$$

where for $n = 1$ and $m = 2$ we have

$$\widetilde{\mathbf{P}}_1 = \mathbf{I}, \qquad \mathbf{D}^T = \begin{bmatrix} -3 & 3\sqrt{3} & 0 & 0 \\ -\sqrt{3} & 3 & 0 & 0 \\ 0 & 0 & -3 & 3\sqrt{3} \\ 0 & 0 & -\sqrt{3} & 3 \end{bmatrix}, \qquad \mathbf{C} = \begin{bmatrix} c_{10} \\ c_{11} \\ c_{20} \\ c_{21} \end{bmatrix},$$

$$\mathbf{K} = \begin{bmatrix} \frac{1}{16} & \frac{\sqrt{3}}{48} & \frac{1}{16} & \frac{\sqrt{3}}{48} \\ \frac{\sqrt{3}}{16} & \frac{1}{16} & \frac{\sqrt{3}}{16} & \frac{1}{16} \\ \frac{1}{4} & \frac{\sqrt{3}}{12} & \frac{1}{4} & \frac{\sqrt{3}}{12} \\ \frac{\sqrt{3}}{8} & \frac{1}{8} & \frac{\sqrt{3}}{8} & \frac{1}{8} \end{bmatrix},$$

$$\widetilde{\mathbf{C}} = \frac{1}{4} \begin{bmatrix} 3\sqrt{6}c_{10} - \sqrt{2}c_{11} & -\sqrt{2}c_{10} + \sqrt{6}c_{11} & 0 & 0 \\ -\sqrt{2}c_{10} + \sqrt{6}c_{11} & \sqrt{6}c_{10} + 5\sqrt{2}c_{11} & 0 & 0 \\ 0 & 0 & 3\sqrt{6}c_{20} - \sqrt{2}c_{21} & -\sqrt{2}c_{20} + \sqrt{6}c_{21} \\ 0 & 0 & -\sqrt{2}c_{20} + \sqrt{6}c_{21} & \sqrt{6}c_{20} + 5\sqrt{2}c_{21} \end{bmatrix},$$

$$\mathbf{G} = \begin{bmatrix} \frac{17\sqrt{6}}{72} \\ \frac{5\sqrt{2}}{24} \\ \frac{7\sqrt{6}}{36} \\ \frac{\sqrt{2}}{6} \end{bmatrix}. \tag{39}$$

Equation (38) gives a system of nonlinear algebraic equations that can be solved utilizing the initial condition (37); that is, $\sqrt{6}c_{10} - \sqrt{2}c_{11} = 0$, we obtain

$$c_{10} = \frac{\sqrt{6}}{24}, \quad c_{11} = \frac{\sqrt{2}}{8},$$
$$c_{20} = \frac{\sqrt{6}}{6}, \quad c_{21} = \frac{\sqrt{2}}{4}. \tag{40}$$

Substituting these values into (7), the result will be $y(x) = x$, that is, the exact solution. It is noted that the result gives the exact solution as in [17], while in [18] using the sinc method the maximum absolute error is 1.52165×10^{-3}.

Example 2. Consider the first-order nonlinear Fredholm integrodifferential equation [6, 17] as follows:

$$xy'(x) - y(x) = -\frac{1}{6} + \frac{4}{5}x^2 + \int_0^1 \left(x^2 + t\right) y^2(t)\, dt, \quad 0 \le x < 1. \tag{41}$$

with the initial condition

$$y(0) = 0. \tag{42}$$

In this example, we have $p_0 = -1$, $p_1 = x$, $g(x) = -(1/6) + (4/5)x^2$, $\lambda = 1$, $k(x,t) = x^2 + t$, and $q = 2$.

The matrix (35) for this example is

$$\left(\widetilde{\mathbf{P}}_0 + \widetilde{\mathbf{P}}_1\mathbf{D}^T\right)\mathbf{C} - \mathbf{K}\left(\widetilde{\mathbf{C}}\right)\mathbf{C} = \mathbf{G}, \tag{43}$$

where for $n = 2$ and $m = 2$ we have

$$\widetilde{\mathbf{P}}_0 = -\mathbf{I}, \qquad \widetilde{\mathbf{P}}_1 = \begin{bmatrix} \frac{1}{12} & \frac{\sqrt{15}}{60} & \frac{-\sqrt{5}}{120} & 0 & 0 & 0 \\ \frac{\sqrt{15}}{60} & \frac{1}{4} & \frac{\sqrt{3}}{24} & 0 & 0 & 0 \\ \frac{-\sqrt{5}}{120} & \frac{\sqrt{3}}{24} & \frac{5}{12} & 0 & 0 & 0 \\ 0 & 0 & 0 & \frac{7}{12} & \frac{\sqrt{15}}{60} & \frac{-\sqrt{5}}{120} \\ 0 & 0 & 0 & \frac{\sqrt{15}}{60} & \frac{3}{4} & \frac{\sqrt{3}}{24} \\ 0 & 0 & 0 & \frac{-\sqrt{5}}{120} & \frac{\sqrt{3}}{24} & \frac{11}{12} \end{bmatrix},$$

$$\mathbf{D}^T = \begin{bmatrix} -5 & \frac{7\sqrt{15}}{3} & -2\sqrt{5} & 0 & 0 & 0 \\ \frac{-\sqrt{15}}{3} & -3 & \frac{14\sqrt{3}}{3} & 0 & 0 & 0 \\ 0 & \frac{-8\sqrt{3}}{3} & 8 & 0 & 0 & 0 \\ 0 & 0 & 0 & -5 & \frac{7\sqrt{15}}{3} & -2\sqrt{5} \\ 0 & 0 & 0 & \frac{-\sqrt{15}}{3} & -3 & \frac{14\sqrt{3}}{3} \\ 0 & 0 & 0 & 0 & \frac{-8\sqrt{3}}{3} & 8 \end{bmatrix}, \qquad \mathbf{C} = \begin{bmatrix} c_{10} \\ c_{11} \\ c_{12} \\ c_{20} \\ c_{21} \\ c_{22} \end{bmatrix}, \qquad \mathbf{G} = \begin{bmatrix} -\frac{11\sqrt{10}}{450} \\ \frac{-\sqrt{6}}{90} \\ \frac{\sqrt{2}}{180} \\ \frac{23\sqrt{10}}{900} \\ \frac{13\sqrt{6}}{180} \\ \frac{19\sqrt{2}}{180} \end{bmatrix},$$

$$\mathbf{K}=\begin{bmatrix} \frac{1}{24} & \frac{\sqrt{15}}{45} & \frac{7\sqrt{5}}{240} & \frac{13}{72} & \frac{\sqrt{15}}{20} & \frac{41\sqrt{5}}{720} \\ \frac{\sqrt{15}}{72} & \frac{1}{12} & \frac{5\sqrt{3}}{144} & \frac{\sqrt{15}}{24} & \frac{1}{16} & \frac{\sqrt{3}}{16} \\ \frac{\sqrt{5}}{48} & \frac{5\sqrt{3}}{144} & \frac{1}{24} & \frac{7\sqrt{5}}{144} & \frac{\sqrt{3}}{16} & \frac{5}{72} \\ \frac{7}{48} & \frac{31\sqrt{15}}{720} & \frac{\sqrt{15}}{20} & \frac{41}{144} & \frac{17\sqrt{15}}{240} & \frac{7\sqrt{5}}{90} \\ \frac{7\sqrt{15}}{144} & \frac{3}{16} & \frac{5\sqrt{3}}{72} & \frac{11\sqrt{15}}{144} & \frac{13}{48} & \frac{7\sqrt{3}}{72} \\ \frac{\sqrt{5}}{16} & \frac{11\sqrt{3}}{144} & \frac{1}{12} & \frac{13\sqrt{5}}{144} & \frac{5\sqrt{3}}{48} & \frac{1}{9} \end{bmatrix}, \qquad \widetilde{\mathbf{C}}=\begin{bmatrix} \widetilde{\mathbf{c}}_1 & \mathbf{0} \\ \mathbf{0} & \widetilde{\mathbf{c}}_2 \end{bmatrix},$$

$$\widetilde{\mathbf{c}}_j=\begin{bmatrix} \frac{5\sqrt{10}}{7}c_{j0}-\frac{5\sqrt{6}}{21}c_{j1}+\frac{\sqrt{2}}{7}c_{j2} & -\frac{5\sqrt{6}}{21}c_{j0}+\frac{11\sqrt{10}}{35}c_{j1}-\frac{8\sqrt{30}}{105}c_{j2} & \frac{\sqrt{2}}{7}c_{j0}-\frac{8\sqrt{30}}{105}c_{j1}+\frac{3\sqrt{10}}{35}c_{j2} \\ -\frac{5\sqrt{6}}{21}c_{j0}+\frac{11\sqrt{10}}{35}c_{j1}-\frac{8\sqrt{30}}{105}c_{j2} & \frac{11\sqrt{10}}{35}c_{j0}+\frac{3\sqrt{6}}{7}c_{j1}+\frac{\sqrt{2}}{7}c_{j2} & -\frac{8\sqrt{30}}{105}c_{j0}+\frac{\sqrt{2}}{7}c_{j1}+\frac{5\sqrt{6}}{21}c_{j2} \\ \frac{\sqrt{2}}{7}c_{j0}-\frac{8\sqrt{30}}{105}c_{j1}+\frac{3\sqrt{10}}{35}c_{j2} & -\frac{8\sqrt{30}}{105}c_{j0}+\frac{\sqrt{2}}{7}c_{j1}+\frac{5\sqrt{6}}{21}c_{j2} & \frac{3\sqrt{10}}{35}c_{j0}+\frac{5\sqrt{6}}{21}c_{j1}+\frac{13\sqrt{2}}{7}c_{j2} \end{bmatrix},$$
$$j=1,2. \tag{44}$$

Equation (43) gives a system of nonlinear algebraic equations that can be solved utilizing the initial condition (42); that is, $\sqrt{10}c_{10}-\sqrt{6}c_{11}+\sqrt{2}c_{12}=0$, we obtain

$$c_{10}=\frac{\sqrt{10}}{240},\quad c_{11}=\frac{\sqrt{6}}{48},$$
$$c_{12}=\frac{\sqrt{2}}{24},\quad c_{20}=\frac{\sqrt{10}}{15}, \tag{45}$$
$$c_{21}=\frac{\sqrt{6}}{8},\quad c_{22}=\frac{\sqrt{2}}{6}.$$

Substituting these values into (7), the result will be $y(x)=x^2$, that is, the exact solution. It is noted that the result gives the exact solution as in [17], while in [6] approximate solution is obtained with maximum absolute error 1.0000×10^{-5}.

Example 3. Consider the second-order nonlinear Fredholm integrodifferential equation [17] as follows:

$$y''(x)+xy'(x)-xy(x)=e^x\sin x+\int_0^1 \sin x\cdot e^{-2t}y^2(t)\,dt,$$
$$0\le x<1, \tag{46}$$

with the initial conditions

$$y(0)=y'(0)=1. \tag{47}$$

The exact solution is $y(x)=e^x$. We solve this example by using the proposed method with $n=2$, $m=30$ and $n=3$, $m=30$. Comparison among the proposed method and methods in [17] is shown in Table 1. It is clear from this table that the results obtained by the proposed method, using few numbers of basis, are very promising and superior to that of [17].

Example 4. Consider the following nonlinear Fredholm integrodifferential equation [5, 17]:

$$y'(x)+y(x)=\frac{1}{2}\left(e^{-2}-1\right)+\int_0^1 y^2(t)\,dt,\quad 0\le x<1, \tag{48}$$

with the initial conditions

$$y(0)=1. \tag{49}$$

The exact solution of this problem is $y(x)=e^{-x}$. In Table 2 we have compared the absolute difference errors of the proposed method with the collocation method based on Haar wavelets in [5] and method in [17].

Maximum absolute errors of Example 4 for some different values of n and m are shown in Table 3. As it is seen from Table 3, for a certain value of n as m increases the accuracy increases, and for a certain value of m as n increases the accuracy increases as well. In case of $m=1$, the numerical solution obtained is based on orthonormal Bernstein polynomials only, while in case of $n=0$, the numerical solution obtained is based on block-pulse functions only.

Table 2: Numerical comparison of absolute difference errors for Example 4.

x	Method of [5] Number of collocation points $N = 128$	Method of [17] $n = 7$	The proposed method $n = 3$, $m = 35$	$n = 4$, $m = 15$
0.125	$3.7591E-007$	$2.4509E-010$	$5.5200E-011$	$1.6710E-011$
0.250	$6.6413E-007$	$1.0202E-010$	$8.9982E-011$	$3.9705E-012$
0.375	$8.6917E-007$	$1.6139E-010$	$9.4606E-011$	$1.2126E-011$
0.500	$1.0020E-006$	$3.2362E-010$	$9.2457E-011$	$1.8312E-012$
0.625	$1.0757E-006$	$1.9197E-010$	$7.4991E-011$	$8.1299E-012$
0.750	$1.1029E-006$	$6.6120E-011$	$4.9442E-011$	$7.7237E-012$
0.875	$1.0944E-006$	$2.2417E-010$	$2.6083E-011$	$2.5547E-012$

Table 3: Maximum absolute errors for different values of n and m for Example 4.

n \ m	1	5	10	15	20	25	30	35
0	$5.7735E-01$	$1.1547E-01$	$5.7735E-02$	$3.8490E-02$	$2.8868E-02$	$2.3094E-02$	$1.9245E-02$	$1.6496E-02$
1	$2.2361E-01$	$8.9443E-03$	$2.2361E-03$	$9.9381E-04$	$5.5902E-04$	$3.5777E-04$	$2.4845E-04$	$1.8254E-04$
2	$6.2994E-02$	$5.0395E-04$	$6.2994E-05$	$1.8665E-05$	$7.8743E-06$	$4.0316E-06$	$2.3331E-06$	$1.4693E-06$
3	$1.3889E-02$	$2.2222E-05$	$1.3889E-06$	$2.7435E-07$	$8.6806E-08$	$3.5556E-08$	$1.7147E-08$	$9.2554E-09$
4	$2.5126E-03$	$8.0403E-07$	$2.5126E-08$	$3.3088E-09$	$7.8519E-10$	$2.5729E-10$	$1.0340E-10$	$4.7839E-11$
5	$3.8521E-04$	$2.4653E-08$	$3.8521E-10$	$3.3818E-11$	$6.0189E-12$	$1.5778E-12$	$5.2841E-13$	$2.0955E-13$
6	$5.1230E-05$	$6.5574E-10$	$5.1230E-12$	$2.9984E-13$	$4.0023E-14$	$8.3935E-15$	$2.3425E-15$	$7.9625E-16$

5. Conclusion

In this work, we present a numerical method for solving nonlinear Fredholm integrodifferential equations based on hybrid of block-pulse functions and normalized Bernstein polynomials. One of the most important properties of this method is obtaining the analytical solutions if the equation has an exact solution, that is, a polynomial function. Another considerable advantage is this method has high relative accuracy for small numbers of basis n. The matrices $\mathbf{K}$, $\widetilde{\mathbf{C}}$, and $\mathbf{D}$ in (10), (17), and (25), respectively, have large numbers of zero elements, and they are sparse; hence, the present method is very attractive and reduces the CPU time and computer memory. Moreover, satisfactory results of illustrative examples with respect to several other methods (e.g., Haar wavelets method, Walsh functions method, Bernstein polynomials method, and sinc collocation method) are included to demonstrate the validity and applicability of the proposed method.

References

[1] M. Dehghan and A. Saadatmandi, "Chebyshev finite difference method for Fredholm integro-differential equation," *International Journal of Computer Mathematics*, vol. 85, no. 1, pp. 123–130, 2008.

[2] Z. Lackiewicz, M. Rahman, and B. D. Welfert, "Numerical solution of a Fredholm integro-differential equation modelling neural networks," *Applied Numerical Mathematics*, vol. 56, no. 3-4, pp. 423–432, 2006.

[3] M. Lakestani, M. Razzaghi, and M. Dehghan, "Semiorthogonal spline wavelets approximation for Fredholm integro-differential equations," *Mathematical Problems in Engineering*, vol. 2006, Article ID 96184, 12 pages, 2006.

[4] S. H. Behiry and H. Hashish, "Wavelet methods for the numerical solution of Fredholm integro-differential equations," *International Journal of Applied Mathematics*, vol. 11, no. 1, pp. 27–35, 2002.

[5] S. Islam, I. Aziz, and M. Fayyaz, "A new approach for numerical solution of integro-differential equations via Haar wavelets," *International Journal of Computer Mathematics*, 2013.

[6] Y. Ordokhani, "An application of Walsh functions for Fredholm-Hammerstein integro-differential equations," *International Journal of Contemporary Mathematical Sciences*, vol. 5, no. 22, pp. 1055–1063, 2010.

[7] S. Yeganeh, Y. Ordokhani, and A. Saadatmandi, "A sinc-collocation method for second-order boundary value problems of nonlinear integro-differential equation," *Journal of Information and Computing Science*, vol. 7, no. 2, pp. 151–160, 2012.

[8] Sh. S. Behzadi, S. Abbasbandy, T. Allahviranloo, and A. Yildirim, "Application of homotopy analysis method for solving a class of nonlinear Volterra-Fredholm integro-differential equations," *The Journal of Applied Analysis and Computation*, vol. 2, no. 2, pp. 127–136, 2012.

[9] S. H. Behiry and S. I. Mohamed, "Solving high-order nonlinear Volterra-Fredholm integro-differential equations by differential transform method," *Natural Science*, vol. 4, no. 8, pp. 581–587, 2012.

[10] K. Maleknejad, B. Basirat, and E. Hashemizadeh, "Hybrid Legendre polynomials and block-pulse functions approach for nonlinear Volterra-Fredholm integro-differential equations," *Computers & Mathematics with Applications*, vol. 61, no. 9, pp. 2821–2828, 2011.

[11] R. Ezzati and S. Najafalizadeh, "Application of Chebyshev polynomials for solving nonlinear Volterra-Fredholm integral equations system and convergence analysis," *Indian Journal of Science and Technology*, vol. 5, no. 2, pp. 2060–2064, 2012.

[12] A. H. Bhrawy, E. Tohidi, and F. Soleymani, "A new Bernoulli matrix method for solving high-order linear and nonlinear Fredholm integro-differential equations with piecewise intervals," *Applied Mathematics and Computation*, vol. 219, no. 2, pp. 482–497, 2012.

[13] Z. H. Jiang and W. Schaufelberger, *Block Pulse Functions and Their Applications in Control Systems*, Springer, Berlin, Germany, 1992.

[14] S. A. Yousefi, Z. Barikbin, and M. Dehghan, "Ritz-Galerkin method with Bernstein polynomial basis for finding the product solution form of heat equation with non-classic boundary conditions," *International Journal of Numerical Methods for Heat & Fluid Flow*, vol. 22, no. 1, pp. 39–48, 2012.

[15] K. Maleknejad, E. Hashemizadeh, and B. Basirat, "Computational method based on Bernstein operational matrices for nonlinear Volterra-Fredholm-Hammerstein integral equations," *Communications in Nonlinear Science and Numerical Simulation*, vol. 17, no. 1, pp. 52–61, 2012.

[16] G. Tachev, "Pointwise approximation by Bernstein polynomials," *Bulletin of the Australian Mathematical Society*, vol. 85, no. 3, pp. 353–358, 2012.

[17] Y. Ordokhani and S. Davaei far, "Application of the Bernstein polynomials for solving the nonlinear Fredholm integro-differential equations," *Journal of Applied Mathematics and Bioinformatics*, vol. 1, no. 2, pp. 13–31, 2011.

[18] K. Jalaei, M. Zarebnia, and M. M. Chalaki, "Development of the sinc method for nonlinear integro-differential eequations," *Australian Journal of Basic and Applied Sciences*, vol. 4, no. 11, pp. 5508–5515, 2010.

Hindawi Publishing Corporation
Abstract and Applied Analysis
Volume 2013, Article ID 282593, 14 pages
http://dx.doi.org/10.1155/2013/282593

Research Article

Semi-Idealized Study on Estimation of Partly and Fully Space Varying Open Boundary Conditions for Tidal Models

Jicai Zhang[1,2] and Haibo Chen[3,4]

[1] *Institute of Physical Oceanography, Ocean College, Zhejiang University, Hangzhou 310058, China*
[2] *MOE Key Laboratory of Coast and Island Development, Nanjing University, Nanjing 210093, China*
[3] *Laboratory of Physical Oceanography, Ocean University of China, Qingdao 266100, China*
[4] *China Offshore Environmental Services Ltd., Qingdao 266061, China*

Correspondence should be addressed to Jicai Zhang; jicai_zhang@163.com

Received 5 June 2013; Revised 1 September 2013; Accepted 1 September 2013

Academic Editor: Rasajit Bera

Two strategies for estimating open boundary conditions (OBCs) with adjoint method are compared by carrying out semi-idealized numerical experiments. In the first strategy, the OBC is assumed to be partly space varying and generated by linearly interpolating the values at selected feature points. The advantage is that the values at feature points are taken as control variables so that the variations of the curves can be reproduced by the minimum number of points. In the second strategy, the OBC is assumed to be fully space varying and the values at every open boundary points are taken as control variables. A series of semi-idealized experiments are carried out to compare the effectiveness of two inversion strategies. The results demonstrate that the inversion effect is in inverse proportion to the number of feature points which characterize the spatial complexity of open boundary forcing. The effect of ill-posedness of inverse problem will be amplified if the observations contain noises. The parameter estimation problems with more control variables will be much more sensitive to data noises, and the negative effects of noises can be restricted by reducing the number of control variables. This work provides a concrete evidence that ill-posedness of inverse problem can generate wrong parameter inversion results and produce an unreal "good data fitting."

1. Introduction

The tides and tidal currents are the basic motion forms of ocean water and play an important role in the research on other processes, such as the storm surge, the circulation and the estuarine dynamics [1, 2]. For tidal models, open boundary conditions (OBCs) are one of the most important parameters, which are determined by the physics of tides and tidal currents. Therefore, how to obtain reasonable and accurate OBCs for regional tidal models has been a subject of ongoing research. Data assimilation methods have been commonly used to optimize the open boundary conditions [3–7].

Data assimilation methods, especially the complex ones like four-dimensional variational (4DVAR), are developed on the base of rigorous mathematical theories, such as inverse problem theory and optimal control theory. The ultimate purpose of applying data assimilation method is to reduce the data misfit between model results and various observations, by either improving the models or dynamically interpolating the observations. Among all the data assimilation methods, the 4DVAR is one of the most effective and powerful approaches. It is based on the optimal control methods and perturbation theory [8, 9]. This technique allows us to retrieve an optimal data for a given model from heterogeneous observation fields [9]. It is an advanced data assimilation method which involves the adjoint method and has the advantage of directly assimilating various observations distributed in time and space into numerical models while maintaining dynamical and physical consistency with the model. The adjoint method is a powerful tool for parameter estimation. Navon [10] presented an important overview on the state of the art of parameter estimation in meteorology and oceanography in view of application of

4DVAR data assimilation techniques to inverse parameter estimation problems. Zhang and Lu [7] studied the parameter estimation problems with a three-dimensional tidal model with 4DVAR and also summarized relative works. More recently, Kazantsev [9] briefly revealed the history of data assimilation starting from Lorenz's pioneering work and then deeply studied the sensitivity of a shallow-water model to parameters by applying adjoint based technique.

For parameter estimation problems, it is of great importance to reasonably reduce the number of spatially varying control variables because of the ill-posedness of inverse problem. As noted by Yeh in the work of ground water flow parameter estimation, the inverse or parameter estimation problem is often ill-posed and beset by instability and nonuniqueness, particularly if one seeks parameters distributed in space and time domain [11]. The same viewpoint has been put forward by references [12–16]. Consequently, how to reduce the number of parameters to be estimated became an important aspect needing to draw attention to [13–17]. In this work two strategies for inverting the open boundary conditions with adjoint method are compared by carrying out semi-idealized numerical experiments. In the first strategy, the OBC is assumed to be partly space varying and generated by linearly interpolating the values at selected feature points. The feature points are selected by calculating the second-order derivatives of discrete curves and the values at selected feature points are taken as control variables to be estimated. The advantage is that most of the variations of the curves can be reproduced by the minimum number of points. In the second strategy, the OBC is assumed to be fully space varying and the values at every open boundary points are taken as control variables.

This paper is organized as follows. The 2D tidal model with adjoint is briefly described in Section 2. The two inversion strategies are developed in Section 3. A series of semi-idealized numerical experiments are carried out and the results are analyzed and discussed in Section 4. Conclusions in Section 5 complete the paper.

2. The Adjoint Tidal Model

2.1. The 2D Tidal Model. The governing equations for the tides used in the present study are the vertically integrated equations of continuity and momentum:

$$\begin{gathered}\frac{\partial \zeta}{\partial t}+\frac{1}{a}\frac{\partial\left[(h+\zeta)u\right]}{\partial\lambda}+\frac{1}{a}\frac{\partial\left[(h+\zeta)v\cos\phi\right]}{\partial\phi}=0,\\ \frac{\partial u}{\partial t}+\frac{u}{a}\frac{\partial u}{\partial\lambda}+\frac{v}{R}\frac{\partial u}{\partial\phi}-\frac{uv\tan\phi}{R}-fv-A\Delta u+\frac{g}{a}\frac{\partial\left(\zeta-\overline{\zeta}\right)}{\partial\lambda}=F_\lambda,\\ \frac{\partial v}{\partial t}+\frac{u}{a}\frac{\partial v}{\partial\lambda}+\frac{v}{R}\frac{\partial v}{\partial\phi}+\frac{u^2\tan\phi}{R}+fu-A\Delta v+\frac{g}{R}\frac{\partial\left(\zeta-\overline{\zeta}\right)}{\partial\phi}=F_\phi,\end{gathered}\tag{1}$$

where t is time; λ and ϕ are the east longitude and north latitude, respectively; ζ is the sea surface elevation above the undisturbed sea level; u and v are the east and north components of fluid velocity, respectively, $\overline{\zeta}$ is the adjusted height of equilibrium tides; R is the radius of the earth, $a = R\cos\phi$; $f = 2\Omega\sin\phi$, where Ω represents the angular speed of earth rotation; g is the acceleration due to gravity, h is the undisturbed water depth and $H = h+\zeta$ denotes the total water depth; A is the coefficient of horizontal eddy viscosity; Δ is the Laplace operator and $\Delta(u,v) = a^{-1}[a^{-1}\partial_\lambda(\partial_\lambda(u,v))+R^{-1}\partial_\phi(\cos\phi\partial_\phi(u,v))]$; F_λ and F_ϕ are east and north components of bottom friction terms, respectively, and their expressions are given in quadratic form:

$$F_\lambda=-C_Q\frac{\sqrt{u^2+v^2}}{h+\zeta}u,\qquad F_\phi=-C_Q\frac{\sqrt{u^2+v^2}}{h+\zeta}v.\tag{2}$$

2.2. The Adjoint. The general idea of the adjoint method is described as follows. First, a model is defined by an algorithm and its independent variables such as initial conditions, boundary conditions, and empirical parameters. The cost function which measures the data misfit between the modeling results and observations is then minimized through optimizing the control variables. In detail, the cost function decreases along the opposite direction of the gradients with respect to the control variables, and this gradient is calculated by what has become known as the adjoint model. In order to construct the adjoint equations, the cost function is defined as

$$J(\zeta)=\frac{1}{2}K_\zeta\iint_{\Omega_{T,S}}\left(\zeta-\widehat{\zeta}\right)^2 dS\,dT,\tag{3}$$

and the Lagrangian function is defined as

$$\begin{aligned}L=\iint_{\Omega_{T,S}}\Bigg[&\mu\left(\frac{\partial u}{\partial t}+\frac{u}{a}\frac{\partial u}{\partial\lambda}+\frac{v}{R}\frac{\partial u}{\partial\phi}-\frac{uv\tan\phi}{R}-fv-F_\lambda-A\Delta u+\frac{g}{a}\frac{\partial\left(\zeta-\overline{\zeta}\right)}{\partial\lambda}\right)\\ &+v\left(\frac{\partial v}{\partial t}+\frac{u}{a}\frac{\partial v}{\partial\lambda}+\frac{v}{R}\frac{\partial v}{\partial\phi}+\frac{u^2\tan\phi}{R}+fu-F_\phi-A\Delta v+\frac{g}{R}\frac{\partial\left(\zeta-\overline{\zeta}\right)}{\partial\phi}\right)\\ &+\tau\left(\frac{\partial\zeta}{\partial t}+\frac{1}{a}\frac{\partial\left[(h+\zeta)u\right]}{\partial\lambda}+\frac{1}{a}\frac{\partial\left[(h+\zeta)v\cos\phi\right]}{\partial\phi}\right)\Bigg]dS\,dT\\ &+J(\zeta),\end{aligned}\tag{4}$$

where $\widehat{\zeta}$ is the observations of surface elevation; $\Omega_{T,S}$ stands for the whole integration area of time and space; μ, v, and τ are the adjoint variables (namely, Lagrangian multipliers) of u, v, and ζ, respectively. Based on the theory of Lagrangian

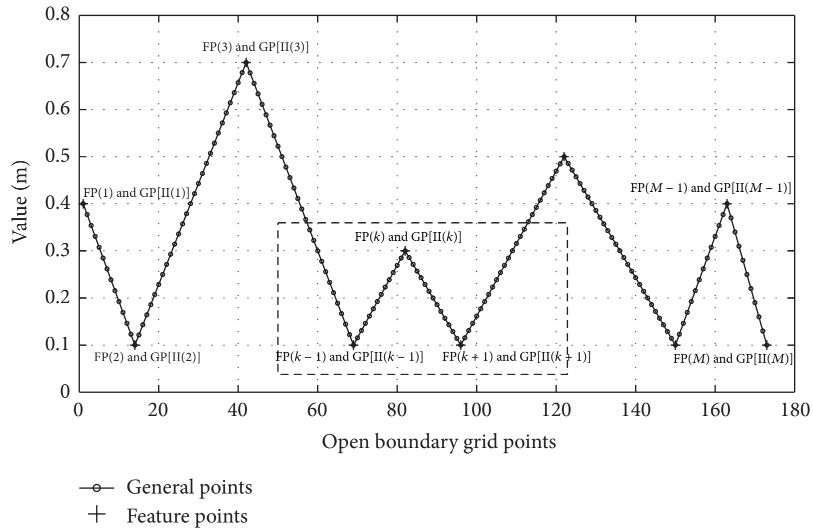

FIGURE 1: Example of discrete curves and their feature points. GP stands for general points and FP indicates feature points.

multiplier method, we have the following first-order derivates of Lagrangian function with respect to all the model variables:

$$\frac{\partial L}{\partial \zeta}=0, \qquad \frac{\partial L}{\partial u}=0, \qquad \frac{\partial L}{\partial v}=0, \tag{5a}$$

$$\frac{\partial L}{\partial \tau}=0, \qquad \frac{\partial L}{\partial \mu}=0, \qquad \frac{\partial L}{\partial \nu}=0, \tag{5b}$$

$$\frac{\partial L}{\partial C_Q}=0, \qquad \frac{\partial L}{\partial a}=0, \qquad \frac{\partial L}{\partial b}=0. \tag{5c}$$

Equations (5b) give the original governing (1) and the adjoint equations can be developed from (5a). In (5c), a and b are the Fourier coefficients along the open boundary and C_Q denotes the bottom friction coefficients. From (5c) we can obtain the optimization formulae of model parameters.

Based on (5a) the adjoint equations can be obtained as

$$\begin{aligned}
&\frac{\partial \tau}{\partial t}+\frac{u}{a}\frac{\partial \tau}{\partial \lambda}+\frac{v}{a}\frac{\partial(\tau\cos\phi)}{\partial\phi}+\frac{g}{a}\frac{\partial\mu}{\partial\lambda}+\frac{g}{a}\frac{\partial\nu}{\partial\phi}-K_\zeta\left(\zeta-\hat{\zeta}\right)\\
&\qquad=\Psi(1,1)+\Psi(1,2),\\
&\frac{\partial\mu}{\partial t}-f\nu-\frac{\mu}{a}\frac{\partial u}{\partial\lambda}-\frac{\nu}{a}\frac{\partial v}{\partial\lambda}+\frac{1}{a}\frac{\partial}{\partial\lambda}(\mu u)+\frac{1}{R}\frac{\partial}{\partial\phi}(\mu v)\\
&\qquad+\frac{h+\zeta}{a}\frac{\partial\tau}{\partial\lambda}+\frac{h+\zeta}{a}\frac{\partial\tau}{\partial\lambda}+A\Delta\mu+\frac{\mu v\tan\phi}{R}\\
&\qquad-\frac{2\nu u\tan\phi}{R}=\Psi(2,1)+\Psi(2,2),\\
&\frac{\partial\nu}{\partial t}+f\mu-\frac{\mu}{R}\frac{\partial u}{\partial\phi}-\frac{\nu}{R}\frac{\partial v}{\partial\phi}+\frac{1}{a}\frac{\partial}{\partial\lambda}(\nu u)+\frac{1}{R}\frac{\partial}{\partial\phi}(\nu v)\\
&\qquad+\frac{h+\zeta}{a}\frac{\partial(\tau\cos\phi)}{\partial\phi}+\frac{h+\zeta}{a}\frac{\partial(\tau\cos\phi)}{\partial\phi}+A\Delta\nu\\
&\qquad+\frac{\mu u\tan\phi}{R}=\Psi(3,1)+\Psi(3,2),
\end{aligned} \tag{6}$$

where $\Psi(i,j)$ $(1\le i\le 3, 1\le j\le 2)$ is a matrix whose components denote the adjoint terms of bottom friction. The components of Ψ for the quadratic parameterizations are given as

$$\Psi=\begin{Bmatrix}
-\mu\dfrac{C_Q u\sqrt{u^2+v^2}}{(h+\zeta)^2} & -\nu\dfrac{C_Q v\sqrt{u^2+v^2}}{(h+\zeta)^2}\\
\mu\dfrac{C_Q\left(2u^2+v^2\right)}{(h+\zeta)\sqrt{u^2+v^2}} & \nu\dfrac{C_Q uv}{(h+\zeta)\sqrt{u^2+v^2}}\\
\mu\dfrac{C_Q uv}{(h+\zeta)\sqrt{u^2+v^2}} & \nu\dfrac{C_Q\left(u^2+2v^2\right)}{(h+\zeta)\sqrt{u^2+v^2}}
\end{Bmatrix}, \tag{7}$$

The numerical schemes for the forward model and the adjoint model in this section are both based on Lu and Zhang [17] and Zhang et al. [18].

3. Methodology

3.1. Feature Points of a Curve. If the values of OBCs are plotted versus the location or index of grid points along open boundaries, they will form a discretized curve. Without loss of generality, the curve can be presented by Figure 1. Assume there are N general (or, computational) points along open boundaries with index of GP(k), $k = 1, 2, \ldots, N$. This type of curve can be approximately linearly expressed by a certain series of points which are defined as feature points in this paper. For the curve shown in Figure 1, one can easily obtain the feature points as indicated by symbol "+." Assume the number of feature points is M with index of FP(j), $j = 1, 2, \ldots, M$. Further assuming the feature point with index of j is coincident with the general point with index of II(j), we can obtain the following relation: II(1) = 1, II(M) = N, II(j) = k, $2 < k < N - 1$.

It is easy to conclude that any general point can be linearly expressed by two adjacent feature points. For example, as shown in Figure 1, an arbitrary general point $\mathrm{GP}(k)$ locates between two adjacent feature points $\mathrm{FP}(j-1)$ and $\mathrm{FP}(j)$, where $\mathrm{II}(j-1) \le k \le \mathrm{II}(j)$. Through linear interpolation, we can obtain the value of $\mathrm{GP}(k)$ as

$$\mathrm{GP}(k) = \frac{\mathrm{II}(j)-k}{\mathrm{II}(j)-\mathrm{II}(j-1)}\mathrm{FP}(j-1) + \frac{k-\mathrm{II}(j-1)}{\mathrm{II}(j)-\mathrm{II}(j-1)}\mathrm{FP}(j). \tag{8}$$

For the whole curve (or the whole boundary), the relation between general points and feature points can be similarly expressed in matrix form as

$$\mathbf{V_{GP}} = \mathbf{W_{FG}} \times \mathbf{V_{FP}}, \tag{9}$$

where $\mathbf{V_{GP}}$ and $\mathbf{V_{FP}}$ are both column vectors with dimensions of N and M, respectively, and $\mathbf{W_{FG}}$ is the weighting matrix of linear interpolation with dimensions of $N \times M$. The detailed forms of three matrixes are given as

$$\mathbf{V_{GP}} = [\mathrm{GP}(1), \mathrm{GP}(2), \ldots, \mathrm{GP}(N)]^T, \tag{10}$$

$$\mathbf{V_{FP}} = [\mathrm{FP}(1), \mathrm{FP}(2), \ldots, \mathrm{FP}(M)]^T, \tag{11}$$

$$\mathbf{W_{FG}} = \underbrace{\begin{pmatrix}
w_{1,1} & 0 & 0 & 0 & 0 & 0 & 0 & 0 \\
w_{2,1} & w_{22} & 0 & 0 & 0 & 0 & 0 & 0 \\
\vdots & \vdots & 0 & 0 & 0 & 0 & 0 & 0 \\
w_{\mathrm{II}(2)-1,1} & w_{\mathrm{II}(2)-1,2} & 0 & 0 & 0 & 0 & 0 & 0 \\
0 & w_{\mathrm{II}(2),2} & 0 & 0 & 0 & 0 & 0 & 0 \\
0 & 0 & \ddots & 0 & 0 & 0 & 0 & 0 \\
0 & 0 & 0 & w_{\mathrm{II}(j-1),j-1} & 0 & 0 & 0 & 0 \\
0 & 0 & 0 & w_{\mathrm{II}(j-1)+1,j-1} & w_{\mathrm{II}(j-1)+1,j} & 0 & 0 & 0 \\
0 & 0 & 0 & \vdots & \vdots & 0 & 0 & 0 \\
0 & 0 & 0 & w_{\mathrm{II}(j)-1,j-1} & w_{\mathrm{II}(j)-1,j} & 0 & 0 & 0 \\
0 & 0 & 0 & 0 & w_{\mathrm{II}(j),j} & 0 & 0 & 0 \\
0 & 0 & 0 & 0 & 0 & \ddots & 0 & 0 \\
0 & 0 & 0 & 0 & 0 & 0 & w_{\mathrm{II}(M-1),M-1} & 0 \\
0 & 0 & 0 & 0 & 0 & 0 & w_{\mathrm{II}(M-1)+1,M-1} & w_{\mathrm{II}(M-1)+1,M} \\
0 & 0 & 0 & 0 & 0 & 0 & \vdots & \vdots \\
0 & 0 & 0 & 0 & 0 & 0 & w_{\mathrm{II}(M)-1,M-1} & w_{\mathrm{II}(M)-1,M} \\
0 & 0 & 0 & 0 & 0 & 0 & & w_{\mathrm{II}(M),M}
\end{pmatrix}}_{M \text{ columns, } N \text{ rows}}, \tag{12}$$

where the nonzero components are the linear interpolation coefficients. Specifically, without loss of generality,

$$w_{\mathrm{II}(j),j} = 1.0, \quad j = 1, 2, \ldots, M, \tag{13a}$$

$$w_{\mathrm{II}(j-1)+m,j-1} = \frac{\mathrm{II}(j)-\mathrm{II}(j-1)-m}{\mathrm{II}(j)-\mathrm{II}(j-1)}, \quad 1 \le m < \mathrm{II}(j)-\mathrm{II}(j-1), \tag{13b}$$

$$w_{\mathrm{II}(j-1)+m,j} = \frac{m}{\mathrm{II}(j)-\mathrm{II}(j-1)}, \quad 1 \le m < \mathrm{II}(j)-\mathrm{II}(j-1). \tag{13c}$$

Using (9), any general points along open boundaries can be highly approximated through the linear interpolation of selected feature points. It indicates that the OBC identification problem can be transformed to seek the values of a few selected feature points, which reduces the number of control variables.

3.2. Selection of Feature Points for Periodic Tidal Open Boundary. Along a certain open boundary, we also assume that there are N general grid points. The height of water level ζ at the nth time step is given by

$$\zeta^n_{\mathrm{GP}(k)} = a_0 + \left[a_{\mathrm{GP}(k)} \cos(\omega n \Delta t) + b_{\mathrm{GP}(k)} \sin(\omega n \Delta t)\right], \tag{14}$$

where $\mathrm{GP}(k)$ stands for the general points of open boundaries and $1 \leqslant k \leqslant N$, ω is the frequency of M_2 constituent, $a_{\mathrm{GP}(k)}$ and $b_{\mathrm{GP}(k)}$ are the Fourier coefficients at $\mathrm{GP}(k)$, Δt is the time step of computation.

For regional tidal models the values of $a_{\mathrm{GP}(k)}$ and $b_{\mathrm{GP}(k)}$ can be obtained from large scale numerical models. It should be noted $a_{\mathrm{GP}(k)}$ and $b_{\mathrm{GP}(k)}$ are space dependent, and therefore the variations of their values versus the grids along the open boundary will constitute two curves (curve_*a* and curve_*b*) similar to the one shown in Figure 1. The feature points for this type of curve can be selected by computing the second-order differential of each general point. The detailed selection procedures are given as follows.

(1) Suppose the absolute values of second-order differentials of general points GP(k) are SD_$a(k)$ for curve_*a* and SD_$b(k)$ for curve_*b*, respectively. For the general points locating in the middle of curve_a and curve_b, that is, $2 \leqslant k \leqslant N-1$, SD_$a(k)$ and SD_$b(k)$ can be computed as

$$\mathrm{SD\_}a(k) = \left|\frac{a_{\mathrm{GP}(k+1)} - 2a_{\mathrm{GP}(k)} + a_{\mathrm{GP}(k-1)}}{2\Delta d}\right|,$$
$$\mathrm{SD\_}b(k) = \left|\frac{b_{\mathrm{GP}(k+1)} - 2b_{\mathrm{GP}(k)} + b_{\mathrm{GP}(k-1)}}{2\Delta d}\right|, \quad (15)$$

where Δd is the size of computation grids and equals Δx or Δy according to the direction of open boundaries (Δx for west-east direction and Δy for north-south direction).

(2) Further define that the "maximum second-order differential" for point GP(k) is SD(k). The value of SD(k) is calculated as

$$\mathrm{SD}(k) = \max\left[\mathrm{SD\_}a(k), \mathrm{SD\_}b(k)\right]. \quad (16)$$

(3) Define a threshold value of SD(k), $2 \leqslant k \leqslant N-1$, to be T_{SD}. The points with larger values of SD(k) than T_{SD} are selected as feature points. The value of T_{SD} is problem dependent and should be determined according to the specific requirement on the number of control variables.

(4) It is easy to understand that the first and the last general points GP(1) and GP(N) are automatically selected as feature points indexed as FP(1) and FP(M).

3.3. Inversion Strategies and Gradients. In this work two strategies for inverting the open boundary conditions with adjoint method are compared by carrying out semi-idealized numerical experiments. In the first strategy the open boundary curves are assumed to be partly space varying and are generated by linearly interpolating the values at feature points. The feature points are selected by calculating the second-order derivatives of discrete curves and the values at selected feature points are taken as control variables to be estimated. The advantage is that most of the variations of the curves can be reproduced by the minimum number of points. In the second strategy, the OBC is assumed to be fully space varying and the values at every open boundary point are taken as control variables.

The Broyden-Fletcher-Goldfarb-Shanno (BFGS) method, which is a quasi-Newton conjugate-gradient algorithm, has been widely used in the unconstrained inverse problems and is famous for its efficiency [19, 20]. The limited-memory BFGS (L-BFGS) algorithm is an adaptation of the BFGS method to large problem. Zou et al. [20] concluded that among the tested quasi-Newton methods, the L-BFGS method had the best performance. In this work L-BFGS method is employed to optimize the control variables, namely, the OBCs. In order to perform inversion with L-BFGS, the gradients of cost function with respect to the control variables in two strategies have to be calculated.

3.3.1. Gradients for Partly Space Varying Inversion Strategy. In the first inversion strategy (partly space varying OBC), feature points for open boundary curves are selected and the OBCs at general points can be linearly interpolated from feature points. Consequently, the gradients of cost function with respect to the Fourier coefficients at feature points $aa_{\mathrm{FP}(j)}$ and $bb_{\mathrm{FP}(j)}$ (aa_j and bb_j for simplicity, $1 \leqslant j \leqslant M$) have to be computed in order to optimize the OBCs with L-BFGS. The gradients are deduced from

$$\frac{\partial L}{\partial aa_j} = 0, \quad \frac{\partial L}{\partial bb_j} = 0, \quad 1 \le j \le M, \quad (17)$$

which yields

$$\frac{\partial J}{\partial aa_1} + \sum_{k=1}^{i(2)-1} w_{k,1} \sum_{n\in\Omega_T} T_k^n \cos(\omega n \Delta t) = 0, \quad j = 1,$$
$$\frac{\partial J}{\partial aa_j} + \sum_{k=i(j-1)+1}^{i(j+1)} w_{k,j} \sum_{n\in\Omega_T} T_k^n \cos(\omega n \Delta t) = 0, \quad 2 \le j \le M-1,$$
$$\frac{\partial J}{\partial aa_M} + \sum_{k=i(j-1)+1}^{N} w_{k,j} \sum_{n\in\Omega_T} T_k^n \cos(\omega n \Delta t) = 0, \quad j = M,$$
$$\frac{\partial J}{\partial bb_1} + \sum_{k=1}^{i(2)-1} w_{k,1} \sum_{n\in\Omega_T} T_k^n \cos(\omega n \Delta t) = 0, \quad j = 1, \quad (18)$$
$$\frac{\partial J}{\partial bb_j} + \sum_{k=i(j-1)+1}^{i(j+1)} w_{k,j} \sum_{n\in\Omega_T} T_k^n \cos(\omega n \Delta t) = 0, \quad 2 \le j \le M-1,$$
$$\frac{\partial J}{\partial bb_M} + \sum_{k=i(M-1)+1}^{N} w_{k,j} \sum_{n\in\Omega_T} T_k^n \cos(\omega n \Delta t) = 0, \quad j = M,$$

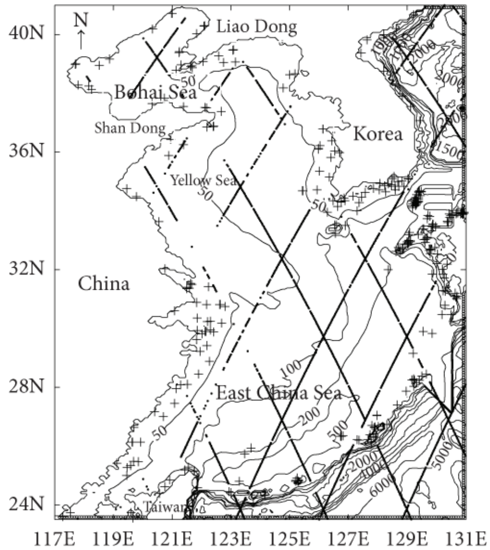

Figure 2: The bathymetric map of the Bohai, Yellow, and East China Seas (contour) and the position of T/P satellite tracks (dot), tidal gauge stations (plus), and open boundaries (open circle). The numbers are the water depth in meter.

where

$$
\begin{aligned}
T_k^n &= -\frac{g\mu_k^n}{\Delta x} \\
&\quad (\text{for GP}\,(k)\ \text{on the right of the area calculated}), \\
T_k^n &= \frac{g\mu_{k_l}^j}{\Delta x} \\
&\quad (\text{for GP}\,(k)\ \text{on the left of the area calculated}), \\
T_k^n &= -\frac{g\nu_k^n}{\Delta y} \\
&\quad (\text{for GP}\,(k)\ \text{under the area calculated}), \\
T_k^n &= \frac{g\nu_k^n}{\Delta y} \\
&\quad (\text{for GP}\,(k)\ \text{above the area calculated}),
\end{aligned} \tag{19}
$$

where μ and ν are the adjoint variables of west-east velocity component u and north-south velocity component v, respectively. The values of μ and ν are computed by running the adjoint model.

3.3.2. Gradients for Fully Space Varying Inversion Strategy. In the second strategy, the OBC is assumed to be fully space varying and the values at every open boundary points (i.e., general points) are taken as control variables. Consequently, the gradients of cost function with respect to the Fourier coefficients at general points $aa_{\mathrm{GP}(k)}$ and $bb_{\mathrm{GP}(k)}$ (aa_k and bb_k for simplicity, $1 \leqslant k \leqslant N$) have to be computed. The gradients are deduced from

$$
\frac{\partial L}{\partial aa_k} = 0, \quad \frac{\partial L}{\partial bb_k} = 0, \quad 1 \le k \le N, \tag{20}
$$

which yields

$$
\begin{aligned}
\frac{\partial J}{\partial aa_k} + \sum_{n\in\Omega_T} T_k^n \cos(\omega n \Delta t) &= 0, \quad 1 \le k \le N, \\
\frac{\partial J}{\partial bb_k} + \sum_{n\in\Omega_T} T_k^n \cos(\omega n \Delta t) &= 0, \quad 1 \le k \le N,
\end{aligned} \tag{21}
$$

where T_k^n can also be computed by using (19).

4. Numerical Experiments and Results Analysis

4.1. Model Settings. The computing area in the present study is the Bohai Sea, the Yellow Sea, and the East China Sea (BYECS), typical marginal shelf seas. The spatial resolution for the model is $1/12^\circ \times 1/12^\circ$. T/P altimeter data and tidal gauge data are assimilated into the tidal model. The bathymetry map of the BYECS, the position of T/P satellite tracks, tidal gauge stations, and the open boundaries are shown in Figure 2. Since the purpose of this paper is to discuss the inversion of OBCs, the bottom friction coefficients are fixed in all the experiments.

The numerical experiments in this work are semi-idealized. Specifically, the coastline, the number, and location of the observations are real. On the contrary, the values of open boundary conditions and observations are artificial. The prescribed open boundary curves are generated by different number of feature points. Apparently, the complexity of open boundary curves is in direct proportion to the number of feature points. For the semi-idealized experiments, only the location of real observations (satellite altimetry and tidal gauge stations) is used and the values of "observations" are obtained by running the dynamic forward model with prescribed open boundary conditions. The advantage of this kind of experiments is that we can obtain a thorough understanding of the "observations." The "observations" generated by the model can be accurate and we can control the quality of the "observations" by adding artificial error. In addition, because the other factors are real, the conclusions based on these semi-idealized experiments can be more useful for referring.

The semi-idealized numerical experiments are run as follows. First a distribution of artificial Fourier coefficients is prescribed and taken as "true values" of open boundary conditions. Then the forward tidal model is run using the "true values" and the simulation results recorded at grid points of T/P satellite tracks and tidal gauge stations are taken as the "observations." Having obtained the "observations", an initial value (taken as zero in this work) of Fourier coefficients is assigned to run the forward model. The differences between simulated values and "observations" will function as the external force to drive the adjoint model. The optimized Fourier coefficients can be obtained through the backward integration of the adjoint equations. The inverse integral time of the adjoint equations is equal to a period of M_2 tide. With the procedures repeated above, the parameters will be optimized continuously and the difference between simulated values and "observations" will be diminished. Meanwhile, the difference between the prescribed and the inverted parameters will also be decreased.

The iteration of optimization will terminate once the following criterion is achieved [21]:

$$\|G\| < \text{eps} \times \max(1, \|X\|), \tag{22}$$

where $\|G\|$ is the L_2 norm of the gradients of cost function with respect to the control variables (i.e., the Fourier coefficients at feature points), eps is a positive variable that determines the accuracy with which the solution is to be found, and $\|X\|$ is the L_2 norm of control variables. Both the values of $\|G\|$ and $\|X\|$ vary along the iterations. For a correct adjoint model and a reasonable method, $\|G\|$ will gradually decrease versus the iteration steps and the inverted values of control variables must gradually approach the prescribed "true values". When using L-BFGS, the number of corrections used in the BFGS update is taken as 5 (usually between 3 and 7, see Alekseev et al. [19]). In the minimization algorithm, the control variables should be scaled to similar magnitudes on the order of unity because within the optimization algorithm convergence, tolerances, and other criteria are based on an implicit definition of small and large [22]. Zou et al. [20] also proved that the efficiency could be greatly improved by a simple scaling. In twin experiments we use 10 to scale the Fourier coefficients [4].

4.2. Modeling Results

4.2.1. Effects of Complexity of Open Boundary Curves. In this section, the semi-idealized experiments (SE) are carried out to calibrate the inversion ability of adjoint model and compare the effectiveness of two strategies developed in Section 3. The prescribed distributions of artificial Fourier coefficients at 173 grid points along the eastern open boundary are inverted. The prescribed distributions (PDs) are designed to be characterized by different numbers of feature points. PDs 1–7 are characterized by 2, 6, 10, 14, 18, 22, and 26 feature points, respectively. The twin experiments are correspondingly indexed with SEa 1–7 for inversion strategy 1 and SEb 1–7 for inversion strategy 2.

The prescribed and inverted distributions of open boundary curves in SEa 1–4 and SEb 1–4 are shown in Figure 3. The prescribed and inverted distributions of open boundary curves in SEa 5-6 and SEb 5-6 are shown in Figure 4. The feature points for prescribed distributions have also been indicated in Figures 3 and 4. Table 1 gives the error statistics for the experiments in this section. The L_2 norm of the gradients of cost function with respect to the control variables versus the iteration steps for the experiments using inversion strategies 1 and 2 are presented in Figures 4(c) and 4(d), respectively. The decrease in data misfit (i.e., cost function) calculated from (3) versus the iteration steps is shown in Figure 5. Note that the values of data misfit and L_2 norm of gradients have been normalized by their values at the first iteration step.

For strategy 1, the values of data misfit can sharply decrease by about 4 orders for all the experiments in about 30 iteration steps. For strategy 2, the values of data misfit can sharply decrease by about 5 orders for SEb 1–5 and by 4 orders for SEb 6-7 in about 60 iteration steps. The decrease in data misfit provides another proof for the inversion ability of the adjoint model and strategies in this work. Correspondingly, the L_2 norms of gradients also decrease by at least 2 orders for inversion strategy 1 and by 3 orders for inversion strategy 2, which demonstrates that the gradients calculated in Section 3.3 can work well with L-BFGS method.

From the decrease in data misfit and gradient it seems as if the effect of inversion strategy 2 is better than that of strategy 1. However, the differences between prescribed and inverted distributions shown in Table 1 indicate that the inversion results of strategy 1 are much better than those of strategy 2. This inconsistency will be explained in Section 4.3. One can find that the adjoint model combined with inversion strategy 1 can reproduce the prescribed distributions of Fourier coefficients perfectly for SEa 1-2 or almost perfectly for SEa 3-4. For SEa 5-6 the inversion is acceptable but largely deviates from perfection. The major trend of the inversion is quite obvious that the effect of inversion is in inverse proportion to the number of feature points which characterizes the complexity of open boundary curves. The inverted open boundary curves shown in Figures 3 and 4 also prove that the inversion using strategy 1 is better than that using strategy 2.

4.2.2. Effects of Data Noises. As we know, the real observations either from satellite altimetry or from tidal gauge stations contain errors (or noises). In this section the effects

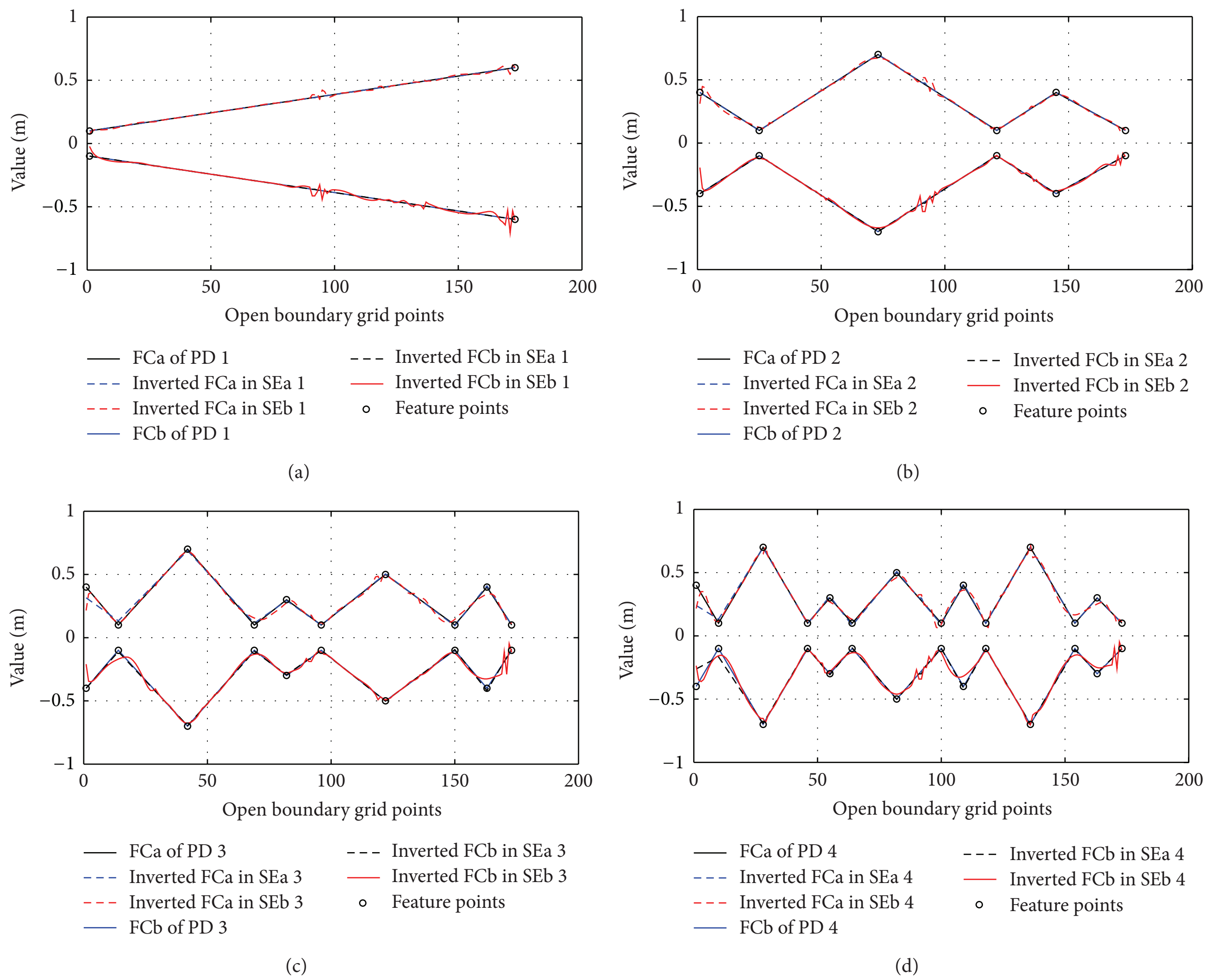

FIGURE 3: The prescribed and inverted distributions of open boundary curves in SEa 1–4 and SEb 1–4. The feature points are indicated by open circles.

of the noises are studied. To do this, we replace each "observation" $\widehat{\zeta}_{i,j}^{n}$ by $(1 + pr_{i,j}^{n})\widehat{\zeta}_{i,j}^{n}$, where $r_{i,j}^{n}$ are uniform random numbers lying in $[-1, 1]$ and p is a factor determining the maximum percentage error. The maximum percentage errors for each prescribed distribution (PDs 1–7) are assigned to 5%, 10%, 15%, and 20%. The corresponding inversion experiments are then indexed with SE_x i.1, SE_x i.2, SE_x i.3, and SE_x i.4, respectively, where $1 \leqslant i \leqslant 7$ and $x = a$ or b. The error statistics for the experiments with P values of 5%, 10%, 15%, and 20% are exhibited in Tables 2, 3, 4, and 5, respectively. The figures are omitted because they are similar to those in Section 4.2.1.

One can find the noises in artificial observations will significantly and negatively influence the inversion of open boundary conditions. It is clear that the inversion using strategy 2 is much more sensitive to the noise than that using strategy 1. For example, when the simplest distribution PD 1 is inverted, the difference between prescribed and inverted values will sharply increase from 0.0101 (Table 1) to 0.0238 (Table 2) for strategy 2 even with a small value of error 5%. When P was increased to 20%, the value of this difference is also increased to 0.0562 (Table 5). However, for strategy 1 the values of this difference are just 0.0011, 0.0011, 0.0032 and 0.0043 under P value of 5%, 10%, 15%, and 20%. Similar results can be found from the inversion results of other distributions. This phenomenon indicates that the effect of ill-posedness of inverse problem will be amplified in the conditions that observations contain noises. In addition, the parameter estimation problems with more control variables will be much more sensitive to data noise and the negative effect of noises can be restricted by reducing the number of control variables.

4.3. Discussions

4.3.1. Rationality of the Adjoint Method (Suggested by an Anonymous Reviewer). The motivation of the present work is to take the open boundary condition as an example to investigate the performance of the adjoint method when applied to ocean modeling and the ill-posedness of relevant

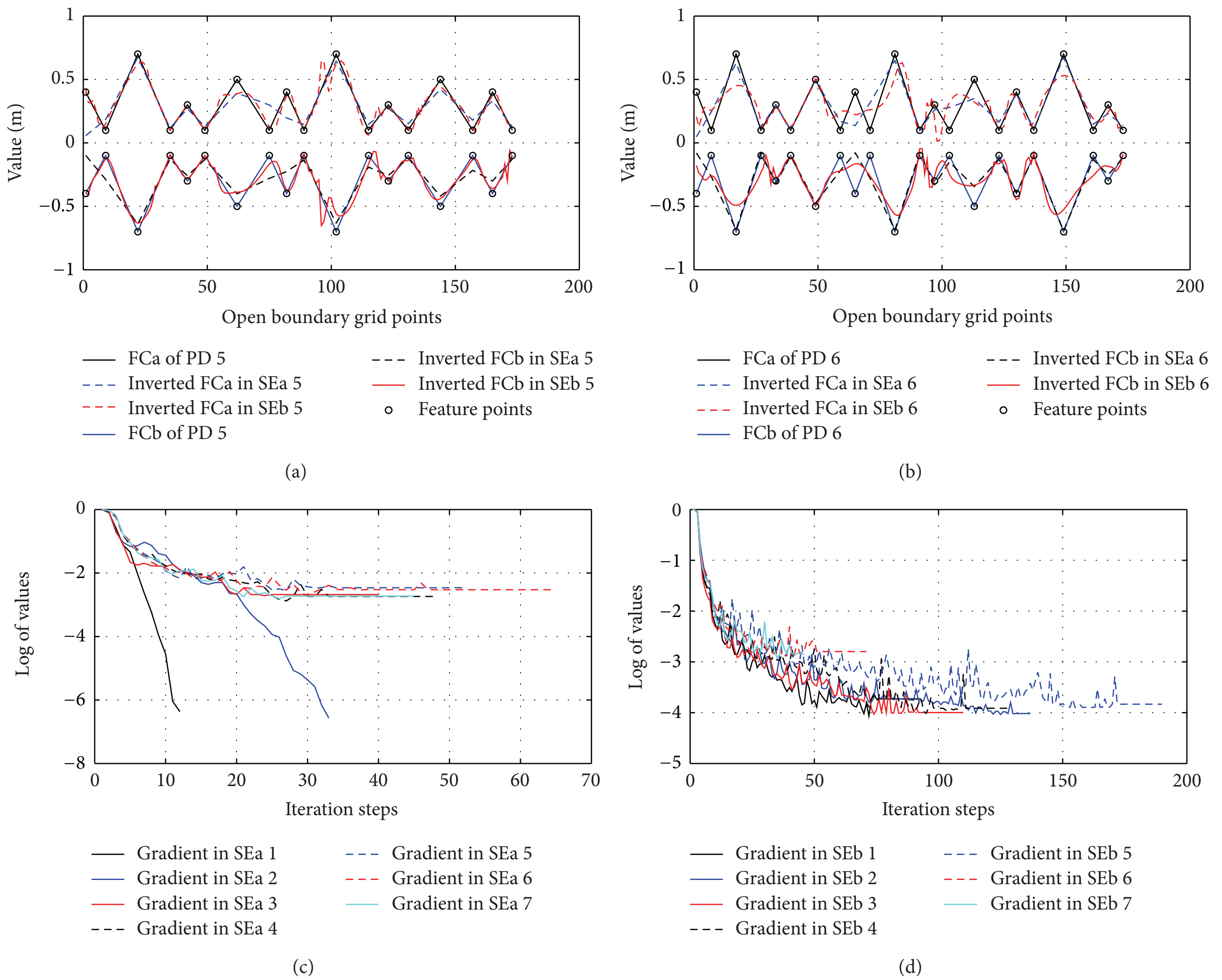

FIGURE 4: (a), (b) The prescribed and inverted distributions of open boundary curves in SEa 5-6 and SEb 5-6. The feature points are indicated by open circles. (c), (d) The L_2 norm of the gradients of cost function with respect to the control variables versus the iteration steps for strategies 1 and 2.

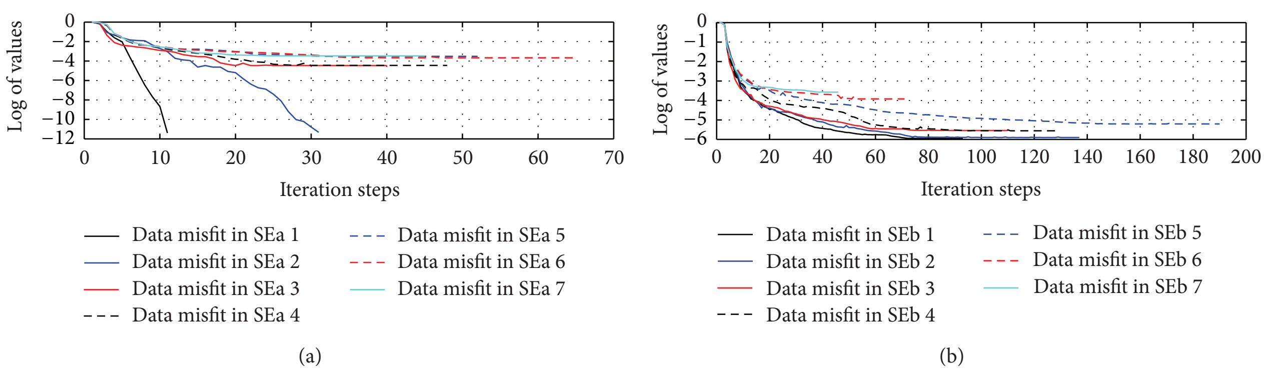

FIGURE 5: Data misfit versus the iteration steps for strategy 1 (a) and strategy 2 (b).

Table 1: Error statistics for SEa 1–7 and SEb 1–7.

Exp.	K_1^a	K_2^a	K_3^a Before	K_3^a After	K_4^a (m) Before	K_4^a (m) After
			Inversion strategy 1			
SEa 1	2	0.00	4979.7808	0.0000	0.3500	0.0000
SEa 2	6	0.00	4229.2929	0.0000	0.3332	0.0000
SEa 3	10	0.00	4549.4140	0.1565	0.3055	0.0059
SEa 4	14	0.00	3966.8884	0.1393	0.3121	0.0091
SEa 5	18	0.00	3546.1967	1.0772	0.3014	0.0334
SEa 6	22	0.00	3319.5297	0.7163	0.3066	0.0451
SEa 7	26	0.00	3776.7236	1.2877	0.3124	0.0737
			Inversion strategy 2			
SEb 1	2	0.00	4979.7808	0.0057	0.3500	0.0101
SEb 2	6	0.00	4229.2929	0.0054	0.3332	0.0125
SEb 3	10	0.00	4549.4140	0.0132	0.3055	0.0152
SEb 4	14	0.00	3966.8884	0.0111	0.3121	0.0194
SEb 5	18	0.00	3546.1967	0.0225	0.3014	0.0472
SEb 6	22	0.00	3319.5297	0.4051	0.3066	0.0662
SEb 7	26	0.00	3776.7236	1.0224	0.3124	0.0783

[a] K_1 is the number of feature points for PDs 1–7 prescribed in semi-idealized experiments. K_2 is the value of maximum percentage error. K_3 is the data misfit before and after assimilation. K_4 is the mean absolute difference between prescribed and inverted Fourier coefficients.

Table 2: Error statistics for SEa 1.1–7.1 and SEb 1.1–7.1.

Exp.	K_1^a	K_2^a	K_3^a Before	K_3^a After	K_4^a (m) Before	K_4^a (m) After
			Inversion strategy 1			
SEa 1.1	2	0.05	5060.1284	4.3569	0.3500	0.0011
SEa 2.1	6	0.05	4306.6660	3.5968	0.3332	0.0007
SEa 3.1	10	0.05	4600.6445	3.9834	0.3055	0.0082
SEa 4.1	14	0.05	4019.1911	3.2996	0.3121	0.0093
SEa 5.1	18	0.05	3614.2876	4.0757	0.3014	0.0443
SEa 6.1	22	0.05	3370.5825	3.4881	0.3066	0.0491
SEa 7.1	26	0.05	3838.0024	4.3227	0.3124	0.0740
			Inversion strategy 2			
SEb 1.1	2	0.05	5060.1284	4.2224	0.3500	0.0238
SEb 2.1	6	0.05	4306.6660	3.4525	0.3332	0.0250
SEb 3.1	10	0.05	4600.6445	3.6353	0.3055	0.0332
SEb 4.1	14	0.05	4019.1911	3.0429	0.3121	0.0337
SEb 5.1	18	0.05	3614.2876	3.0501	0.3014	0.0482
SEb 6.1	22	0.05	3370.5825	2.7539	0.3066	0.0736
SEb 7.1	26	0.05	3838.0024	3.2047	0.3124	0.0833

[a] K_1 is the number of feature points for PDs 1–7 prescribed in semi-idealized experiments. K_2 is the value of maximum percentage error. K_3 is the data misfit before and after assimilation. K_4 is the mean absolute difference between prescribed and inverted Fourier coefficients.

inverse problem. The inverse problems in ocean models are often quite complex. The ocean modeling is not just to solve the partial differential equations which might also be solved by some simple methods like the method of characteristics. A reasonable ocean model should also be related to the field observations (satellite altimetry and tidal gauges in this work). In order to realize a more accurate simulation of ocean dynamics, how to organically combine the numerical ocean model with available observations has already become a problem urgent to be solved. Data assimilation methods have been used widely to solve this problem. Among all data assimilation methods, the adjoint data assimilation method is one of the most effective and powerful approaches developed over the past three decades. It is an advanced data assimilation method and has the advantage of directly assimilating various observations distributed in time and space into the numerical model while maintaining dynamical and physical consistency with the model. The adjoint method

Table 3: Error statistics for SEa 1.2–7.2 and SEb 1.2–7.2.

Exp.	K_1^a	K_2^a	K_3^a Before	K_3^a After	K_4^a (m) Before	K_4^a (m) After
			Inversion strategy 1			
SEa 1.2	2	0.10	5096.1191	17.4292	0.3500	0.0011
SEa 2.2	6	0.10	4329.9121	14.4080	0.3332	0.0013
SEa 3.2	10	0.10	4621.0439	15.3755	0.3055	0.0115
SEa 4.2	14	0.10	4041.4563	12.8185	0.3121	0.0132
SEa 5.2	18	0.10	3633.7822	13.0238	0.3014	0.0438
SEa 6.2	22	0.10	3388.0535	11.9751	0.3066	0.0540
SEa 7.2	26	0.10	3861.5273	13.5251	0.3124	0.0753
			Inversion strategy 2			
SEb 1.2	2	0.10	5096.1191	16.7203	0.3500	0.0343
SEb 2.2	6	0.10	4329.9121	13.8206	0.3332	0.0340
SEb 3.2	10	0.10	4621.0439	14.4797	0.3055	0.0456
SEb 4.2	14	0.10	4041.4563	12.1758	0.3121	0.0485
SEb 5.2	18	0.10	3633.7822	11.9745	0.3014	0.0645
SEb 6.2	22	0.10	3388.0535	11.4183	0.3066	0.0846
SEb 7.2	26	0.10	3861.5273	12.1905	0.3124	0.0902

[a] K_1 is the number of feature points for PDs 1–7 prescribed in semi-idealized experiments. K_2 is the value of maximum percentage error. K_3 is the data misfit before and after assimilation. K_4 is the mean absolute difference between prescribed and inverted Fourier coefficients.

Table 4: Error statistics for SEa 1.3–7.3 and SEb 1.3–7.3.

Exp.	K_1^a	K_2^a	K_3^a Before	K_3^a After	K_4^a (m) Before	K_4^a (m) After
			Inversion strategy 1			
SEa 1.3	2	0.15	5140.9389	39.2166	0.3500	0.0032
SEa 2.3	6	0.15	4360.3886	32.3847	0.3332	0.0018
SEa 3.3	10	0.15	4649.1435	34.2411	0.3055	0.0135
SEa 4.3	14	0.15	4070.1625	28.6868	0.3121	0.0168
SEa 5.3	18	0.15	3659.3095	27.8828	0.3014	0.0446
SEa 6.3	22	0.15	3411.1008	26.0982	0.3066	0.0665
SEa 7.3	26	0.15	3891.3386	28.8848	0.3124	0.0771
			Inversion strategy 2			
SEb 1.3	2	0.15	5140.9389	37.8465	0.3500	0.0449
SEb 2.3	6	0.15	4360.3886	31.0404	0.3332	0.0430
SEb 3.3	10	0.15	4649.1435	32.1405	0.3055	0.0552
SEb 4.3	14	0.15	4070.1625	27.2928	0.3121	0.0569
SEb 5.3	18	0.15	3659.3095	26.6717	0.3014	0.0700
SEb 6.3	22	0.15	3411.1008	25.1515	0.3066	0.0913
SEb 7.3	26	0.15	3891.3386	27.4780	0.3124	0.0963

[a] K_1 is the number of feature points for PDs 1–7 prescribed in semi-idealized experiments. K_2 is the value of maximum percentage error. K_3 is the data misfit before and after assimilation. K_4 is the mean absolute difference between prescribed and inverted Fourier coefficients.

might be complicated and expensive for some simple problems. However, the inverse problems in ocean modeling are often quite complex in contrast with those simple problems. As is known, one advantage of the numerical method over theoretical analysis lies in the disposal of nonlinear terms. The ocean numerical models are usually strongly nonlinear, increasing the complexity of the relevant inverse problem. Therefore, the increased complexity of the inverse problem makes the adjoint method effective. The adjoint method has been proved to be effective and powerful in ocean and atmosphere problems by many works (see the references listed in Section 1). It has been widely applied to meteorological and oceanographic data assimilation, sensitivity studies, and parameter estimation.

4.3.2. Analysis on Ill-Posedness. From the statistics shown in Tables 1–5, we can find an interesting phenomenon. Define the data misfits after assimilation to be $V1_{\mathrm{dm}}$ for inversion strategy 1 and $V2_{\mathrm{dm}}$ for inversion strategy 2. Further define the differences between prescribed and inverted control variables to be $V1_{\mathrm{cv}}$ for inversion strategy 1 and $V2_{\mathrm{cv}}$ for

Table 5: Error statistics for SEa 1.4–7.4 and SEb 1.4–7.4.

Exp.	K_1^a	K_2^a	K_3^a		K_4^a (m)	
			Before	After	Before	After
			Inversion strategy 1			
SEa 1.4	2	0.20	5194.4404	69.7209	0.3500	0.0043
SEa 2.4	6	0.20	4398.0703	57.5559	0.3332	0.0025
SEa 3.4	10	0.20	4684.9663	61.7102	0.3055	0.0169
SEa 4.4	14	0.20	4105.4169	50.8808	0.3121	0.0207
SEa 5.4	18	0.20	3690.9194	48.2412	0.3014	0.0458
SEa 6.4	22	0.20	3439.8129	45.3626	0.3066	0.0711
SEa 7.4	26	0.20	3927.5261	50.4111	0.3124	0.0792
			Inversion strategy 2			
SEb 1.4	2	0.20	5194.4404	67.1112	0.3500	0.0562
SEb 2.4	6	0.20	4398.0703	55.1859	0.3332	0.0493
SEb 3.4	10	0.20	4684.9663	57.6774	0.3055	0.0637
SEb 4.4	14	0.20	4105.4169	48.3631	0.3121	0.0644
SEb 5.4	18	0.20	3690.9194	47.1181	0.3014	0.0755
SEb 6.4	22	0.20	3439.8129	43.9302	0.3066	0.0978
SEb 7.4	26	0.20	3927.5261	48.6330	0.3124	0.1011

[a] K_1 is the number of feature points for PDs 1–7 prescribed in semi-idealized experiments. K_2 is the value of maximum percentage error. K_3 is the data misfit before and after assimilation. K_4 is the mean absolute difference between prescribed and inverted Fourier coefficients.

inversion strategy 2. The values of Vi_{cv} $(i = 1, 2)$ and $Vi_{\mathrm{dm}} (i = 1, 2)$ for all the experiments are plotted in Figure 6. We can find $V1_{\mathrm{dm}}$ are larger than or comparable with $V2_{\mathrm{dm}}$ while $V1_{\mathrm{cv}}$ are greatly smaller than $V2_{\mathrm{cv}}$. Consequently, for all the experiments except SEa 1 and SEa 2, without loss of generality, we can obtain

$$V1_{\mathrm{cv}} < V2_{\mathrm{cv}}, \qquad V1_{\mathrm{dm}} > V2_{\mathrm{dm}}. \tag{23}$$

It is easy to understand that small values of Vi_{cv} $(i = 1, 2)$ indicate more accurate control variables, and small values of Vi_{dm} $(i = 1, 2)$ mean small differences between simulated and observed results. In this work, the open boundary conditions are the only parameters for estimation and other parameters are fixed all the time. Instead of formula (23), we should have expected

$$V1_{\mathrm{cv}} < V2_{\mathrm{cv}}, \quad \text{so} \quad V1_{\mathrm{dm}} < V2_{\mathrm{dm}}, \tag{24}$$

which means a better parameter estimation drives a more accurate simulation. In other words, what we want are small values of V_{dm} and what we need are small values of V_{cv}. Formulas (23) and (24) exactly indicate an inconsistency between the effects of parameter estimation and observation restricted data reproduction.

For PDs 1–7 the numbers of feature points are 2, 6, 10, 14, 18, 22, and 26, respectively. It should be noted that at each feature point the Fourier coefficients include a and b. Therefore the numbers of control variables for inversion are doubled, that is, 4, 12, 20, 28, 36, 44, and 52, respectively. There are a total of 35 semi-idealized experiments in this work. Among these experiments, only SEa 1 and SEa 2 can realize a perfect inversion of control variables. Here we define perfect inversion as follows: the data misfit between observed and simulated values can decrease to zero and the difference between prescribed and inverted control variables can also reach a value of zero. With more control variables and larger data noises, the inversion results will not be exactly equal to the prescribed distributions. In the work of Smedstad and O'Brien [12] where the spatially distributed phase speed in an equatorial Pacific Ocean model was estimated, they could not produce the exact values either, even in the condition that perfect observations were available at every grid of the model. Zhang and Lu [4] put forward the similar viewpoint and it also occurs in the parameter estimation of internal tidal model [23–25]. With identical twin experiments, the "observations" are perfect in the sense that they are produced by the model and thus are consistent with the model physics. From the results of this paper and previous works, we can conclude that ill-posedness has happened in other 33 experiments and the effects of ill-posedness will be amplified by increasing the number of control variables and data noises. Formula (23) obtained in this work provides a concrete evidence that ill-posedness of inverse problem can generate poor parameter inversion results while producing an unreal "good data fitting". For a specific problem, it is necessary and helpful to perform identical semi-idealized experiments in order to find the optimal choices for the number of control variables and inversion strategy.

5. Conclusions

In this work, two strategies for inverting the open boundary conditions with adjoint method are compared by carrying out semi-idealized numerical experiments. In the first strategy, the open boundary curves are assumed to be partly space varying and are generated by linearly interpolating the values at feature points. The feature points are selected by calculating the second-order derivatives of discrete curves and the values

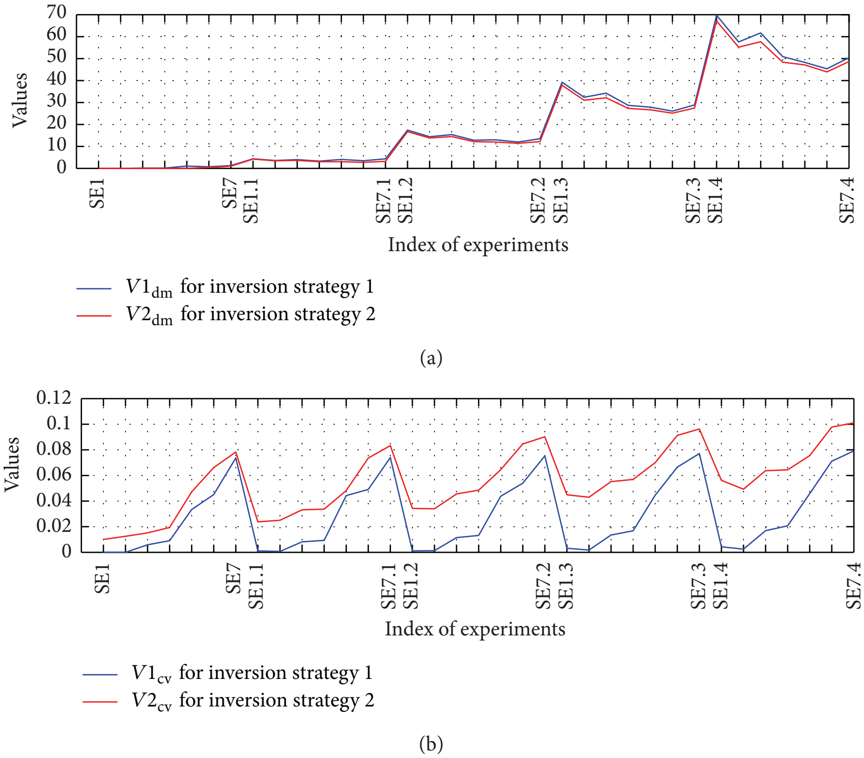

FIGURE 6: (a) The values of Vi_{dm} $(i = 1, 2)$ versus the index of experiments. (b) The values of Vi_{cv} $(i = 1, 2)$ versus the index of experiments.

at selected feature points are taken as control variables to be estimated. The advantage is that most of the variations of the curves can be reproduced by the minimum number of points. In the second strategy, the OBC is assumed to be fully space varying and the values at every open boundary points are taken as control variables.

A series of semi-idealized experiments are carried out to calibrate the inversion ability of adjoint model and compare the effectiveness of two inversion strategies. The results demonstrate that the effect of inversion is in inverse proportion to the number of feature points which characterize the complexity of open boundary curves. The effect of ill-posedness of inverse problem will be amplified in the conditions that observations contain noises. The parameter estimation problems with more control variables will be much more sensitive to data noises and the negative effects of noises can be restricted by reducing the number of control variables. This work provides a concrete evidence that ill-posedness of inverse problem can generate wrong parameter inversion results while producing an unreal "good data fitting". For a specific problem, it is necessary and helpful to perform identical semi-idealized experiments in order to find the optimal choices for the number of control variables and inversion strategy.

Acknowledgments

The authors thank Professor Jorge Nocedal at Northwestern University for sharing the source codes of L-BFGS. Partial support for this research was provided by the National Natural Science Foundation of China through Grants 41206001 and 41076006, the Major State Basic Research Development Program of China through Grant 2013CB956500, the Natural Science Foundation of Jiangsu Province through Grant BK2012315, the Priority Academic Program Development of Jiangsu Higher Education Institutions, and the Fundamental Research Funds for the Central Universities 201261006.

References

[1] W. Munk, "Once again: once again-tidal friction," *Progress in Oceanography*, vol. 40, no. 1, pp. 7–35, 1997.

[2] J. Zhang, P. Wang, and J. Hughes, "EOF analysis of water level variations for microtidal and mangrove-covered Frog Creek system, west-central Florida," *Journal of Coastal Research*, vol. 28, no. 5, pp. 1279–1288, 2012.

[3] A. Zhang, E. Wei, and B. B. Parker, "Optimal estimation of tidal open boundary conditions using predicted tides and adjoint data assimilation technique," *Continental Shelf Research*, vol. 23, no. 11, pp. 1055–1070, 2003.

[4] J. Zhang and X. Lu, "Inversion of three-dimensional tidal currents in marginal seas by assimilating satellite altimetry," *Computer Methods in Applied Mechanics and Engineering*, vol. 199, no. 49–52, pp. 3125–3136, 2010.

[5] I. S. Strub, J. Percelay, M. T. Stacey, and A. M. Bayen, "Inverse estimation of open boundary conditions in tidal channels," *Ocean Modelling*, vol. 29, no. 1, pp. 85–93, 2009.

[6] Z. Guo, A. Cao, and X. Lu, "Inverse estimation of open boundary conditions in the Bohai Sea," *Mathematical Problemsin Engineering*, vol. 2012, Article ID 628061, p. 9, 2012.

[7] J. Zhang and X. Lu, "Parameter estimation for a three-dimensional numerical barotropic tidal model with adjoint method," *International Journal for Numerical Methods in Fluids*, vol. 57, no. 1, pp. 47–92, 2008.

[8] G. I. Marchuk, "Formulation of the theory of perturbations for complicated models," *Applied Mathematics and Optimization*, vol. 2, no. 1, pp. 1–33, 1975.

[9] E. Kazantsev, "Sensitivity of a shallow-water model to parameters," *Nonlinear Analysis: Real World Applications*, vol. 13, no. 3, pp. 1416–1428, 2012.

[10] I. M. Navon, "Practical and theoretical aspects of adjoint parameter estimation and identifiability in meteorology and oceanography," *Dynamics of Atmospheres and Oceans*, vol. 27, no. 1–4, pp. 55–79, 1998.

[11] W. W.-G. Yeh, "Review of parameter identification procedures in groundwater hydrology: the inverse problem," *Water Resources Research*, vol. 22, no. 2, pp. 95–108, 1986.

[12] O. M. Smedstad and J. J. O'Brien, "Variational data assimilation and parameter estimation in an equatorial Pacific ocean model," *Progress in Oceanography*, vol. 26, no. 2, pp. 179–241, 1991.

[13] S. K. Das and R. W. Lardner, "On the estimation of parameters of hydraulic models by assimilation of periodic tidal data," *Journal of Geophysical Research*, vol. 96, pp. 15187–15196, 1991.

[14] S. K. Das and R. W. Lardner, "Variational parameter estimation for a two-dimensional numerical tidal model," *International Journal for Numerical Methods in Fluids*, vol. 15, no. 3, pp. 313–327, 1992.

[15] D. S. Ullman and R. E. Wilson, "Model parameter estimation from data assimilation modeling: temporal and spatial variability of the bottom drag coefficient," *Journal of Geophysical Research C: Oceans*, vol. 103, no. 3, pp. 5531–5549, 1998.

[16] A. W. Heemink, E. E. A. Mouthaan, M. R. T. Roest, E. A. H. Vollebregt, K. B. Robaczewska, and M. Verlaan, "Inverse 3D shallow water flow modelling of the continental shelf," *Continental Shelf Research*, vol. 22, no. 3, pp. 465–484, 2002.

[17] X. Lu and J. Zhang, "Numerical study on spatially varying bottom friction coefficient of a 2D tidal model with adjoint method," *Continental Shelf Research*, vol. 26, no. 16, pp. 1905–1923, 2006.

[18] J. Zhang, X. Lu, P. Wang, and Y. P. Wang, "Study on linear and nonlinear bottom friction parameterizations for regional tidal models using data assimilation," *Continental Shelf Research*, vol. 31, no. 6, pp. 555–573, 2011.

[19] A. K. Alekseev, I. M. Navon, and J. L. Steward, "Comparison of advanced large-scale minimization algorithms for the solution of inverse ill-posed problems," *Optimization Methods & Software*, vol. 24, no. 1, pp. 63–87, 2009.

[20] X. Zou, I. M. Navon, and J. Sela, "Control of gravitational oscillations in variational data assimilation," *Monthly Weather Review*, vol. 121, no. 1, pp. 272–289, 1993.

[21] D. C. Liu and J. Nocedal, "On the limited memory BFGS method for large scale optimization," *Mathematical Programming*, vol. 45, no. 3, pp. 503–528, 1989.

[22] I. M. Navon, X. Zou, J. Derber, and J. Sela, "Variational data assimilation with an adiabatic version of the NMC spectral model," *Monthly Weather Review*, vol. 120, no. 7, pp. 1433–1446, 1992.

[23] A. Cao, H. Chen, J. Zhang, and X. Lv, "Optimization of open boundary conditions in a 3D internal tidal model with the adjoint method around Hawaii," *Abstract and Applied Analysis*, vol. 2013, Article ID 950926, 11 pages, 2013.

[24] H. Chen, C. Miao, and X. Lv, "Estimation of open boundary conditions for an internal tidal model with adjoint method: a comparative study on optimization methods," *Mathematical Problems in Engineering*, vol. 2013, Article ID 802136, 12 pages, 2013.

[25] H. Chen, A. Cao, J. Zhang, C. Miao, and X. Lv, "Estimation of spatially varying open boundary conditions for a numerical internal tidal model with adjoint method," *Mathematics and Computers in Simulation*, 2013.

Hindawi Publishing Corporation
Abstract and Applied Analysis
Volume 2013, Article ID 136483, 10 pages
http://dx.doi.org/10.1155/2013/136483

Research Article

Decoupling the Stationary Navier-Stokes-Darcy System with the Beavers-Joseph-Saffman Interface Condition

Yong Cao,[1] Yuchuan Chu,[1] Xiaoming He,[2] and Mingzhen Wei[3]

[1] *Department of Mechanical Engineering & Automation, Harbin Institute of Technology, Shenzhen Graduate School, Shenzhen, Guangdong 518055, China*
[2] *Department of Mathematics and Statistics, Missouri University of Science and Technology, Rolla, MO 65409, USA*
[3] *Department of Geological Science and Engineering, Missouri University of Science and Technology, Rolla, MO 65409, USA*

Correspondence should be addressed to Xiaoming He; hex@mst.edu

Received 5 April 2013; Accepted 31 July 2013

Academic Editor: R. K. Bera

This paper proposes a domain decomposition method for the coupled stationary Navier-Stokes and Darcy equations with the Beavers-Joseph-Saffman interface condition in order to improve the efficiency of the finite element method. The physical interface conditions are directly utilized to construct the boundary conditions on the interface and then decouple the Navier-Stokes and Darcy equations. Newton iteration will be used to deal with the nonlinear systems. Numerical results are presented to illustrate the features of the proposed method.

1. Introduction

The Stokes-Darcy model has been extensively studied in the recent years due to its wide range of applications in many natural world problems and industrial settings, such as the subsurface flow in karst aquifers, oil flow in vuggy porous media, industrial filtrations, and the interaction between surface and subsurface flows [1–8]. Since the problem domain naturally consists of two different physical subdomains, several different numerical methods have been developed to decouple the Stokes and Darcy equations [6, 9–26]. For other works on the numerical methods and analysis of the Stokes-Darcy model, we refer the readers to [27–45].

Recently the more physically valid Navier-Stokes-Darcy model has attracted scientists' attention, and several coupled finite element methods have been studied for it [46–51]. On the other hand, the advantages of the domain decomposition methods (DDMs) in parallel computation and natural preconditioning have motivated the development of different DDMs for solving the Stoke-Darcy model [6, 10–18, 21, 22]. In this paper, we will develop a domain decomposition method for the Navier-Stokes-Darcy model based on Robin boundary conditions constructed from the interface conditions. This physics-based DDM is different from the traditional ones in the sense that they focus on decomposing different physical domains by directly utilizing the given physical interface conditions.

The rest of paper is organized as follows. In Section 2, we introduce the Navier-Stokes-Darcy model with the Beavers-Joseph-Saffman interface condition. In Section 3, we recall the coupled weak formulation and the corresponding coupled finite element method for the Navier-Stokes-Darcy model. In Section 4, a parallel domain decomposition method and its finite element discretization are proposed to decouple the Navier-Stokes-Darcy system by using the Robin-type boundary conditions constructed from the physical interface conditions. Finally, in Section 5, we present a numerical example to illustrate the features of the proposed method.

2. Stationary Navier-Stokes-Darcy Model

In this section we introduce the following coupled Navier-Stokes-Darcy model on a bounded domain $\Omega = \Omega_m \cup \Omega_c \subset \mathbb{R}^d$, $(d = 2, 3)$; see Figure 1. In the porous media region Ω_m, the flow is governed by the Darcy system

$$\vec{u}_m = -\mathbb{K}\nabla\phi_m,$$
$$\nabla \cdot \vec{u}_m = f_m. \tag{1}$$

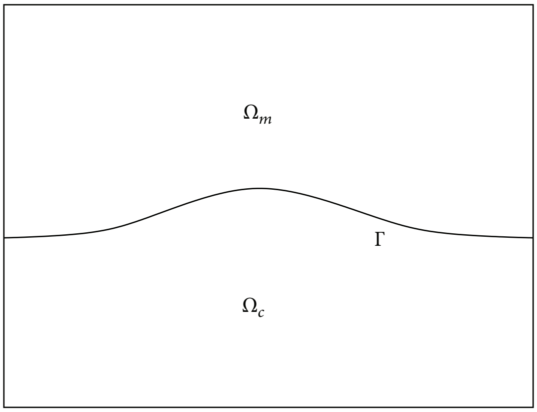

Figure 1: A sketch of the porous median domain Ω_m, fluid domain Ω_c, and the interface Γ.

Here, $\vec{u}_m$ is the fluid discharge rate in the porous media, $\mathbb{K}$ is the hydraulic conductivity tensor, f_m is a sink/source term, and ϕ_m is the hydraulic head defined as $z + (p_m/\rho g)$, where p_m denotes the dynamic pressure, z the height, ρ the density, and g the gravitational acceleration. We will consider the following second-order formulation, which eliminates $\vec{u}_m$ in the Darcy system:

$$-\nabla \cdot (\mathbb{K}\nabla\phi_m) = f_m. \tag{2}$$

In the fluid region Ω_c, the fluid flow is assumed to be governed by the Navier-Stokes equations:

$$\vec{u}_c \cdot \nabla\vec{u}_c - \nabla \cdot \mathbb{T}(\vec{u}_c, p_c) = \vec{f}_c, \tag{3}$$

$$\nabla \cdot \vec{u}_c = 0, \tag{4}$$

where $\vec{u}_c$ is the fluid velocity, p_c is the kinematic pressure, $\vec{f}_c$ is the external body force, ν is the kinematic viscosity of the fluid, $\mathbb{T}(\vec{u}_c, p_c) = 2\nu\mathbb{D}(\vec{u}_c) - p_c\mathbb{I}$ is the stress tensor, and $\mathbb{D}(\vec{u}_c) = (\nabla\vec{u}_c + \nabla^T\vec{u}_c)/2$ is the deformation tensor.

Let $\Gamma = \overline{\Omega}_m \cap \overline{\Omega}_c$ denote the interface between the fluid and porous media regions. On the interface Γ, we impose the following three interface conditions:

$$\vec{u}_c \cdot \vec{u}_c = -\vec{u}_m \cdot \vec{n}_m, \tag{5}$$

$$-\vec{u}_c \cdot (\mathbb{T}(\vec{u}_c, p_c) \cdot \vec{n}_c) = g(\phi_m - z), \tag{6}$$

$$-\boldsymbol{\tau}_j \cdot (\mathbb{T}(\vec{u}_c, p_c) \cdot \vec{n}_c) = \frac{\alpha\nu\sqrt{\mathbf{d}}}{\sqrt{\operatorname{trace}(\prod)}}\boldsymbol{\tau}_j \cdot \vec{u}_c, \tag{7}$$

where $\vec{n}_c$ and $\vec{n}_m$ denote the unit outer normal to the fluid and the porous media regions at the interface Γ, respectively, $\boldsymbol{\tau}_j$ $(j = 1, \dots, d-1)$ denote mutually orthogonal unit tangential vectors to the interface Γ, and $\prod = \mathbb{K}\nu/g$. The third condition (7) is referred to as the Beavers-Joseph-Saffman (BJS) interface condition [52–55].

In this paper, for simplification, we assume that the hydraulic head ϕ_m and the fluid velocity $\vec{u}_c$ satisfy the homogeneous Dirichlet boundary condition except on Γ, that is, $\phi_m = 0$ on the boundary $\partial\Omega_m/\Gamma$ and $\vec{u}_c = 0$ on the boundary $\partial\Omega_c/\Gamma$.

3. Coupled Weak Formulation and Finite Element Method

In this section we will recall the coupled weak formulation and the corresponding coupled finite element method for the Navier-Stokes-Darcy model with Beavers-Joseph-Saffman condition. Let $(\cdot,\cdot)_D$ denote the L^2 inner product on the domain D ($D = \Omega_c$ or Ω_m) and let $\langle\cdot,\cdot\rangle$ denote the L^2 inner product on the interface Γ or the duality pairing between $(H_{00}^{1/2}(\Gamma))'$ and $H_{00}^{1/2}(\Gamma)$ [5]. Define the spaces

$$\begin{aligned} X_c &= \left\{\vec{v} \in \left[H^1(\Omega_c)\right]^d \mid \vec{v} = 0 \text{ on } \frac{\partial\Omega_c}{\Gamma}\right\}, \\ Q_c &= L^2(\Omega_c), \\ X_m &= \left\{\psi \in H^1(\Omega_m) \mid \psi = 0 \text{ on } \frac{\partial\Omega_m}{\Gamma}\right\}, \end{aligned} \tag{8}$$

the bilinear forms

$$\begin{aligned} a_m(\phi_m, \psi) &= (\mathbb{K}\nabla\phi_m, \nabla\psi)_{\Omega_m}, \\ a_c(\vec{u}_c, \vec{v}) &= 2\nu(\mathbb{D}(\vec{u}_c), \mathbb{D}(\vec{v}))_{\Omega_c}, \\ b_c(\vec{v}, q) &= -(\nabla \cdot \vec{v}, q)_{\Omega_c}, \end{aligned} \tag{9}$$

and the projection onto the tangent space on Γ:

$$P_\tau\vec{u} = \sum_{j=1}^{d-1}(\vec{u} \cdot \boldsymbol{\tau}_j)\boldsymbol{\tau}_j. \tag{10}$$

With these notations, the weak formulation of the coupled Navier-Stokes-Darcy model with BJS interface condition is given as follows [46–51]: find $(\vec{u}_c, p_c, \phi_m) \in X_c \times Q_c \times X_m$ such that

$$\begin{aligned} &(\vec{u}_c \cdot \nabla\vec{u}_c, \vec{v})_{\Omega_c} + a_c(\vec{u}_c, \vec{v}) + b_c(\vec{v}, p_c) \\ &\quad - b_c(\vec{u}_c, q) + a_m(\phi_m, \psi) \\ &\quad + \langle g\phi_m, \vec{v} \cdot \vec{n}_c\rangle - \langle\vec{u}_c \cdot \vec{n}_c, \psi\rangle \\ &\quad + \frac{\alpha\nu\sqrt{\mathbf{d}}}{\sqrt{\operatorname{trace}(\prod)}}\langle P_\tau\vec{u}_c, P_\tau\vec{v}\rangle \\ &= (f_m, \psi)_{\Omega_m} + (\vec{f}_c, \vec{v})_{\Omega_c} \\ &\quad + \langle gz, \vec{v} \cdot \vec{n}_c\rangle, \quad \forall(\vec{v}, q, \psi) \in X_c \times Q_c \times X_m. \end{aligned} \tag{11}$$

Assume that we have in hand regular subdivisions of Ω_m and Ω_c into finite elements with mesh size h. Then one can define finite element spaces $X_{mh} \subset X_m$, $X_{ch} \subset X_c$ and

$Q_{ch} \subset Q_c$. We assume that X_{ch} and Q_{ch} satisfy the inf-sup condition [56, 57]

$$\inf_{0 \neq q_h \in Q_{ch}} \sup_{0 \neq \vec{v}_h \in X_{ch}} \frac{b_c(\vec{v}_h, q_h)}{\|\vec{v}_h\|_1 \|q_h\|_0} > \gamma, \tag{12}$$

where $\gamma > 0$ is a constant independent of h. This condition is needed in order to ensure that the spatial discretizations of the Navier-Stokes equations used here are stable. See [56, 57] for more details of finite element spaces X_{mh}, X_{ch}, and Q_{ch} that satisfy (12). One example is the Taylor-Hood element pair that we use in the numerical experiments; for that pair, X_{ch} consists of continuous piecewise quadratic polynomials and Q_{ch} consists of continuous piecewise linear polynomials.

Then a coupled finite element method with Newton iteration for the coupled Navier-Stokes-Darcy model is given as follows [46]: find $(\vec{u}_{c,h}, p_{c,h}, \phi_{m,h}) \in X_{ch} \times Q_{ch} \times X_{mh}$ in the following procedure.

(1) The initial value $\vec{u}_{c,h}^0$ is chosen.

(2) For $m = 0, 1, 2, \ldots, M$, solve

$$\begin{aligned}
&\left(\vec{u}_{c,h}^{m+1} \cdot \nabla \vec{u}_{c,h}^{m}, \vec{v}_h\right)_{\Omega_c} + \left(\vec{u}_{c,h}^{m} \cdot \nabla \vec{u}_{c,h}^{m+1}, \vec{v}_h\right)_{\Omega_c} \\
&\quad + a_c\left(\vec{u}_{c,h}^{m+1}, \vec{v}_h\right) + b_c\left(\vec{v}_h, p_{c,h}^{m+1}\right) \\
&\quad - b_c\left(\vec{u}_{c,h}^{m+1}, q_h\right) + a_m\left(\phi_{m,h}^{m+1}, \psi_h\right) \\
&\quad + \left\langle g\phi_{m,h}^{m+1}, \vec{v}_h \cdot \vec{n}_c\right\rangle - \left\langle \vec{u}_{c,h}^{m+1} \cdot \vec{n}_c, \psi_h\right\rangle \\
&\quad + \frac{\alpha\nu\sqrt{\mathbf{d}}}{\sqrt{\operatorname{trace}(\prod)}} \left\langle P_\tau \vec{u}_{c,h}^{m+1}, P_\tau \vec{v}_h\right\rangle \\
&= \left(\vec{u}_{c,h}^{m} \cdot \nabla \vec{u}_{c,h}^{m}, \vec{v}_h\right)_{\Omega_c} + \left(f_m, \psi_h\right)_{\Omega_m} \\
&\quad + \left(\vec{f}_c, \vec{v}_h\right)_{\Omega_c} + \left\langle gz, \vec{v}_h \cdot \vec{n}_c\right\rangle, \\
&\forall \left(\vec{v}_h, q_h, \psi_h\right) \in X_{ch} \times Q_{ch} \times X_{mh}.
\end{aligned} \tag{13}$$

(3) Set $\vec{u}_{c,h} = \vec{u}_{c,h}^{m+1}$, $p_{c,h} = \vec{p}_{c,h}^{m+1}$, and $\phi_{m,h} = \phi_{m,h}^{M+1}$.

4. Physics-Based Domain Decomposition Method

The coupled finite element method may end up with a huge algebraic system, which combines all parts from the Navier-Stokes equations, Darcy equation, and interface conditions together into one sparse matrix. Hence it is often impractical to directly apply this method to large-scale real world applications. In order to develop a more efficient numerical method in this section, we will directly utilize the three physical interface conditions to construct a physics-based parallel domain decomposition method to decouple the Navier-Stokes and Darcy equations.

Let us first consider the following Robin condition for the Darcy system: for a given constant $\gamma_p > 0$ and a given function η_p defined on Γ,

$$\gamma_p \mathbb{K} \nabla \widehat{\phi}_m \cdot \vec{n}_m + g\widehat{\phi}_m = \eta_p, \quad \text{on } \Gamma. \tag{14}$$

Then, the corresponding weak formulation for the Darcy part is given by the following: for $\eta_p \in L^2(\Gamma)$, find $\widehat{\phi}_m \in X_m$ such that

$$\begin{aligned}
&a_m\left(\widehat{\phi}_m, \psi\right) + \left\langle \frac{g\widehat{\phi}_m}{\gamma_p}, \psi\right\rangle \\
&\quad = \left(f_m, \psi\right)_{\Omega_m} + \left\langle \frac{\eta_p}{\gamma_p}, \psi\right\rangle, \quad \forall \psi \in X_m.
\end{aligned} \tag{15}$$

Second, we can propose the following two Robin-type conditions for the Navier-Stokes equations: for a given constant $\gamma_f > 0$ and given functions η_f and $\vec{\eta}_{f\tau}$ defined on Γ,

$$\begin{aligned}
&\vec{n}_c \cdot \left(\mathbb{T}\left(\widehat{\vec{u}}_c, \widehat{p}_c\right) \cdot \vec{n}_c\right) + \gamma_f \widehat{\vec{u}}_c \cdot \vec{n}_c = \eta_f, \quad \text{on } \Gamma, \\
&-P_\tau\left(\mathbb{T}\left(\widehat{\vec{u}}_c, p_c\right) \cdot \vec{n}_c\right) = \frac{\alpha\nu\sqrt{\mathbf{d}}}{\sqrt{\operatorname{trace}(\prod)}} P_\tau \widehat{\vec{u}}_c, \quad \text{on } \Gamma.
\end{aligned} \tag{16}$$

Then, the corresponding weak formulation for the Navier-Stokes equation is given by the following: for $\eta_f \in L^2(\Gamma)$, find $(\widehat{\vec{u}}_c, \widehat{p}_c) \in X_c \times Q_c$ such that

$$\begin{aligned}
&\left(\widehat{\vec{u}}_c \cdot \nabla \widehat{\vec{u}}_c, \vec{v}\right)_{\Omega_c} + a_c\left(\widehat{\vec{u}}_c, \vec{v}\right) + b_c\left(\vec{v}, \widehat{p}_c\right) \\
&\quad - b_c\left(\widehat{\vec{u}}_c, q\right) + \gamma_f \left\langle \widehat{\vec{u}}_c \cdot \vec{n}_c, \vec{v} \cdot \vec{u}_c\right\rangle \\
&\quad + \frac{\alpha\nu\sqrt{\mathbf{d}}}{\sqrt{\operatorname{trace}(\prod)}} \left\langle P_\tau \widehat{\vec{u}}_c, P_\tau \vec{v}\right\rangle \\
&= \left(\vec{f}_c, \vec{v}\right)_{\Omega_c} + \left\langle \eta_f, \vec{v} \cdot \vec{n}_c\right\rangle, \quad \forall (\vec{v}, q) \in X_c \times Q_c.
\end{aligned} \tag{17}$$

Our next step is to show that, for appropriate choices of γ_f, γ_p, η_f, and η_p, the solutions of the coupled system (11) are equivalent to the solutions of the decoupled equations (15) and (17), and hence we may solve the latter system instead of the former.

Lemma 1. *Let $(\phi_m, \vec{u}_c, p_c)$ be the solution of the coupled Navier-Stokes-Darcy system* (11) *and let $(\widehat{\phi}_m, \widehat{\vec{u}}_c, \widehat{p}_c)$ be the solution of the decoupled Navier-Stokes and Darcy equations* (15) *and* (17) *with Robin boundary conditions at the interface. Then, $(\widehat{\phi}_m, \widehat{\vec{u}}_c, \widehat{p}_c) = (\phi_m, \vec{u}_c, p_c)$ if and only if γ_f, γ_p, η_f, $\vec{\eta}_{f\tau}$, and η_p satisfy the following compatibility conditions:*

$$\eta_p = \gamma_p \widehat{\vec{u}}_c \cdot \vec{n}_c + g\widehat{\phi}_m, \tag{18}$$

$$\eta_f = \gamma_f \widehat{\vec{u}}_c \cdot \vec{n}_c - g\widehat{\phi}_m + gz. \tag{19}$$

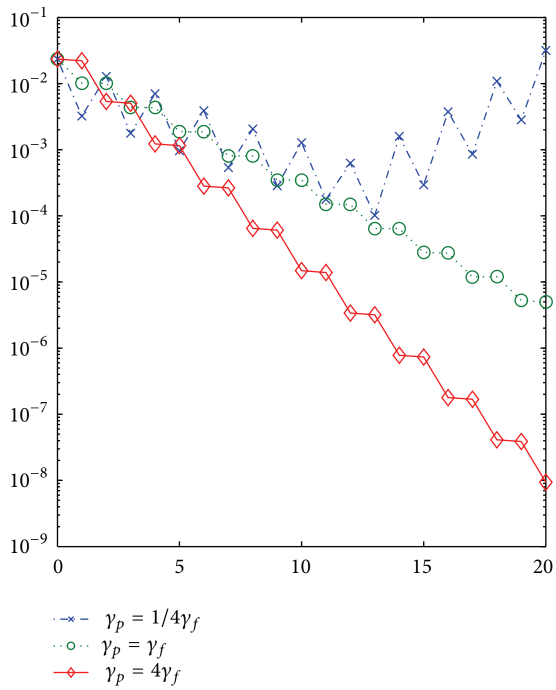

(a)

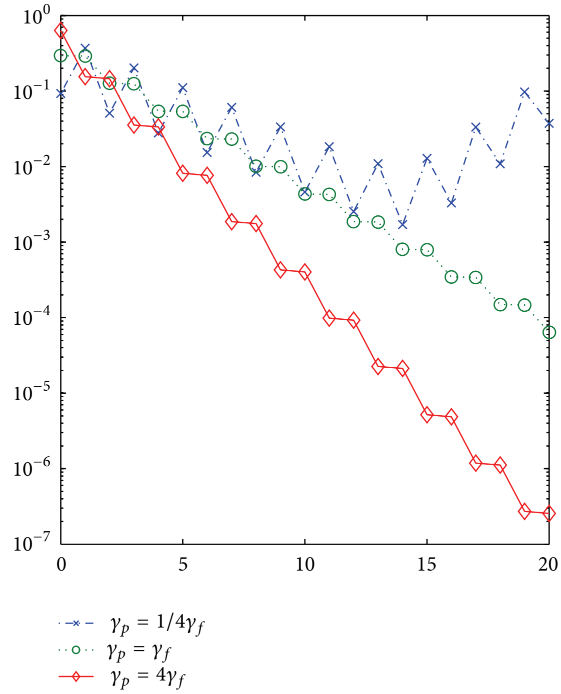

(b)

FIGURE 2: Convergence for the velocity of the free flow (a) and the hydraulic head of the porous medium flow (b) versus the iteration counter m for the parallel DDM with BJS interface condition.

TABLE 1: Errors of the finite element method for the steady Navier-Stokes-Darcy model with BJS interface condition.

h	$\|\vec{u}_h - \vec{u}\|_0$	$\|\vec{u}_h - \vec{u}\|_1$	$\|p_h - p\|_0$	$\|\phi_h - \phi\|_0$	$\|\phi_h - \phi\|_1$
1/8	1.367×10^{-3}	6.147×10^{-2}	8.002×10^{-3}	6.940×10^{-4}	2.452×10^{-2}
1/16	1.687×10^{-4}	1.577×10^{-2}	8.559×10^{-4}	8.687×10^{-5}	6.187×10^{-3}
1/32	2.086×10^{-5}	3.978×10^{-3}	9.506×10^{-5}	1.089×10^{-5}	1.553×10^{-3}
1/64	2.594×10^{-6}	9.974×10^{-4}	1.121×10^{-5}	1.363×10^{-6}	3.890×10^{-4}
1/128	3.235×10^{-7}	2.496×10^{-4}	1.363×10^{-6}	1.705×10^{-7}	9.733×10^{-5}

Proof. Adding (15) and (17) together, we obtain the following: given $\eta_p, \eta_f \in L^2(\Gamma)$, find $(\widehat{\phi}_m, \widehat{u}_f, \widehat{p}_c) \in X_m \times X_c \times Q_c$ such that

$$\begin{aligned}
&\left(\widehat{\vec{u}}_c \cdot \nabla\widehat{\vec{u}}_c, \vec{v}\right)_{\Omega_c} + a_c\left(\widehat{\vec{u}}_c, \vec{v}\right) + b_c\left(\vec{v}, \widehat{p}_c\right) \\
&\quad - b_c\left(\widehat{\vec{u}}_c, q\right) + a_m\left(\widehat{\phi}_m, \psi\right) + \gamma_f\left\langle \widehat{\vec{u}}_c \cdot \vec{n}_c, \vec{v} \cdot \vec{n}_c \right\rangle \\
&\quad + \left\langle \frac{g\widehat{\phi}_m}{\gamma_p}, \psi \right\rangle + \frac{\alpha\nu\sqrt{\mathbf{d}}}{\sqrt{\operatorname{trace}(\prod)}}\left\langle P_\tau \widehat{\vec{u}}_c, P_\tau \vec{v} \right\rangle \\
&= \left(f_m, \psi\right)_{\Omega_m} + \left(\vec{f}_c, \vec{v}\right)_{\Omega_c} + \left\langle \eta_f, \vec{v} \cdot \vec{n}_c \right\rangle \\
&\quad + \left\langle \frac{\eta_p}{\gamma_p}, \psi \right\rangle, \quad \forall\left(\vec{v}, q, \psi\right) \in X_m \times X_c \times Q_c.
\end{aligned} \tag{20}$$

For the necessity of the lemma, we pick $\psi = 0$ and $\vec{v}$ such that $P_\tau \vec{v} = 0$ in (11) and (20); then by subtracting (20) from (11), we get

$$\begin{gathered}
\left\langle \eta_f - \gamma_f \vec{v}_f \cdot \vec{n}_c + g\phi_m - gz, \vec{v} \cdot \vec{n}_c \right\rangle = 0, \\
\forall \vec{v} \in X_c \quad \text{with } P_\tau \vec{v} = 0,
\end{gathered} \tag{21}$$

which implies (19). The necessity of (18) can be derived in a similar fashion.

As for the sufficiency of the lemma, by substituting the compatibility conditions (18)-(19), we easily see that $(\widehat{\phi}_m, \widehat{\vec{u}}_c, \widehat{p}_c)$ solves the coupled Navier-Stokes-Darcy system (11), which completes the proof. □

Now we use the decoupled weak formulation constructed above to propose a physics-based parallel domain decomposition method with Newton iteration as follows.

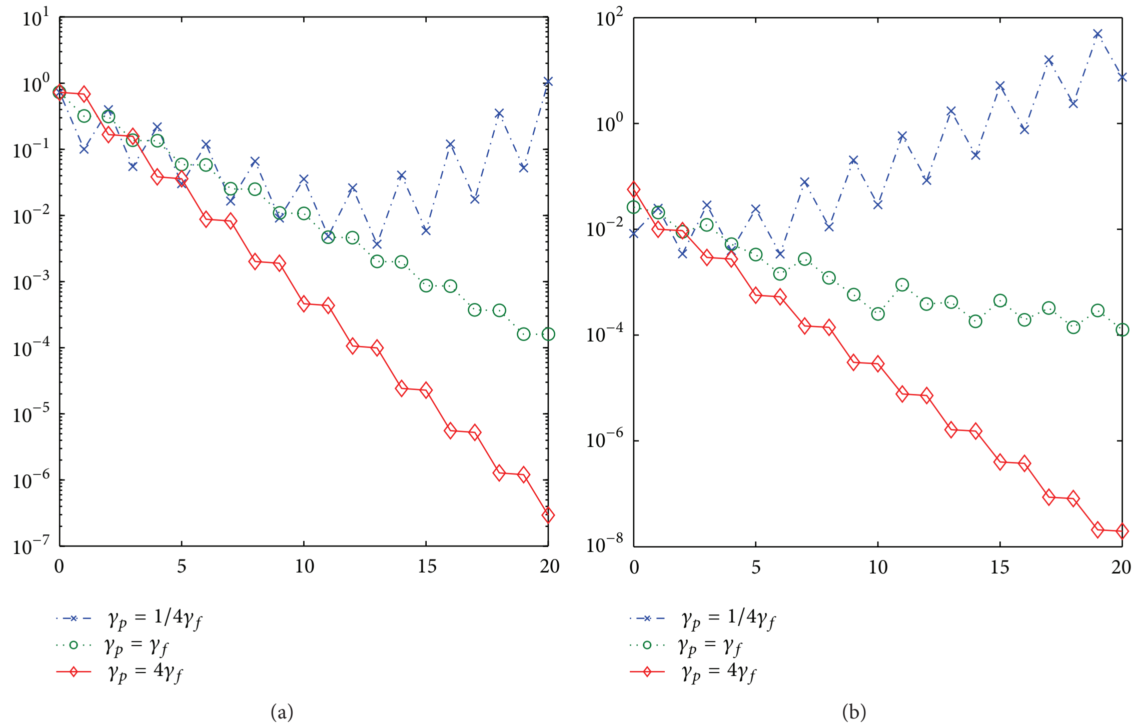

FIGURE 3: Convergence for the pressure of the free flow (a) and η_f (b) versus the iteration counter m for the parallel DDM with BJS interface condition.

(1) Initial values η_p^0 and η_f^0 are guessed. They may be taken to be zero.

(2) For $k = 0, 1, 2, \ldots$, independently solve the Darcy and Navier-Stokes equations constructed above. More precisely, $\phi_m^k \in X_m$ is computed from

$$a_m(\phi_m^k, \psi) + \left\langle \frac{g\phi_m^k}{\gamma_p}, \psi \right\rangle = \left\langle \frac{\eta_p^k}{\gamma_p}, \psi \right\rangle + (f_m, \psi)_{\Omega_m}, \quad \forall \psi \in X_m, \tag{22}$$

and $\vec{u}_c^k \in X_c$ and $p_c^k \in Q_c$ are computed from the following Newton iteration.

(i) Initial value $\vec{u}_c^{k,0}$ is chosen for the Newton iteration. For instance, it may be taken to be $\vec{u}_c^{0,0} = 0$ and $\vec{u}_c^{k,0} = \vec{u}_c^{k-1}$ for $k = 1, 2, \ldots$.

(ii) For $m = 0, 1, 2, \ldots, M$, solve

$$\begin{aligned} &\left(\vec{u}_c^{k,m+1} \cdot \nabla \vec{u}_c^{k,m}, \vec{v}\right)_{\Omega_c} + \left(\vec{u}_c^{k,m} \cdot \nabla \vec{u}_c^{k,m+1}, \vec{v}\right)_{\Omega_c} \\ &\quad + a_c\left(\vec{u}_c^{k,m+1}, \vec{v}\right) + b_c\left(\vec{v}, p_c^{k,m+1}\right) \\ &\quad - b_c\left(\vec{u}_c^{k,m+1}, q\right) + \gamma_f \left\langle \vec{u}_c^{k,m+1} \cdot \vec{n}_c, \vec{v} \cdot \vec{n}_c \right\rangle \\ &\quad + \frac{\alpha\nu\sqrt{\mathbf{d}}}{\sqrt{\operatorname{trace}(\prod)}} \left\langle P_\tau \vec{u}_c^{k,m+1}, P_\tau \vec{v} \right\rangle \\ &= \left(\vec{u}_c^{k,m} \cdot \nabla \vec{u}_c^{k,m}, \vec{v}\right)_{\Omega_c} + \left\langle \eta_f^k, \vec{v} \cdot \vec{n}_c \right\rangle + \left(\vec{f}_c, \vec{v}\right)_{\Omega_c}, \\ &\qquad \forall (\vec{v}, q, \psi) \in X_c \times Q_c \times X_m. \end{aligned} \tag{23}$$

(iii) Set $\vec{u}_c^k = \vec{u}_c^{k,M+1}$ and $p_c^k = p_c^{k,M+1}$.

(3) η_p^{k+1} and η_f^{k+1} are updated in the following manner:

$$\begin{aligned} \eta_f^{k+1} &= \frac{\gamma_f}{\gamma_p}\eta_p^k - \left(1 + \frac{\gamma_f}{\gamma_p}\right) g\phi_m^k + gz, \\ \eta_p^{k+1} &= -\eta_f^k + \left(\gamma_f + \gamma_p\right) \vec{u}_c^k \cdot \vec{n}_c + gz. \end{aligned} \tag{24}$$

Then the corresponding domain decomposition finite element method is proposed as follows.

(1) Initial values $\eta_{p,h}^0$ and $\eta_{f,h}^0$ are guessed. They may be taken to be zero.

(2) For $k = 0, 1, 2, \ldots$, independently solve the Darcy and Navier-Stokes equations with the Robin boundary conditions on the interface, which are constructed previously. More precisely, $\phi_{m,h}^k \in X_{mh}$ is computed from

$$\begin{aligned} &a_m\left(\phi_{m,h}^k, \psi_h\right) + \left\langle \frac{g\phi_{m,h}^k}{\gamma_p}, \psi_h \right\rangle \\ &= \left\langle \frac{\eta_{p,h}^k}{\gamma_p}, \psi_h \right\rangle + (f_m, \psi_h)_{\Omega_m}, \quad \forall \psi_h \in X_{mh}, \end{aligned} \tag{25}$$

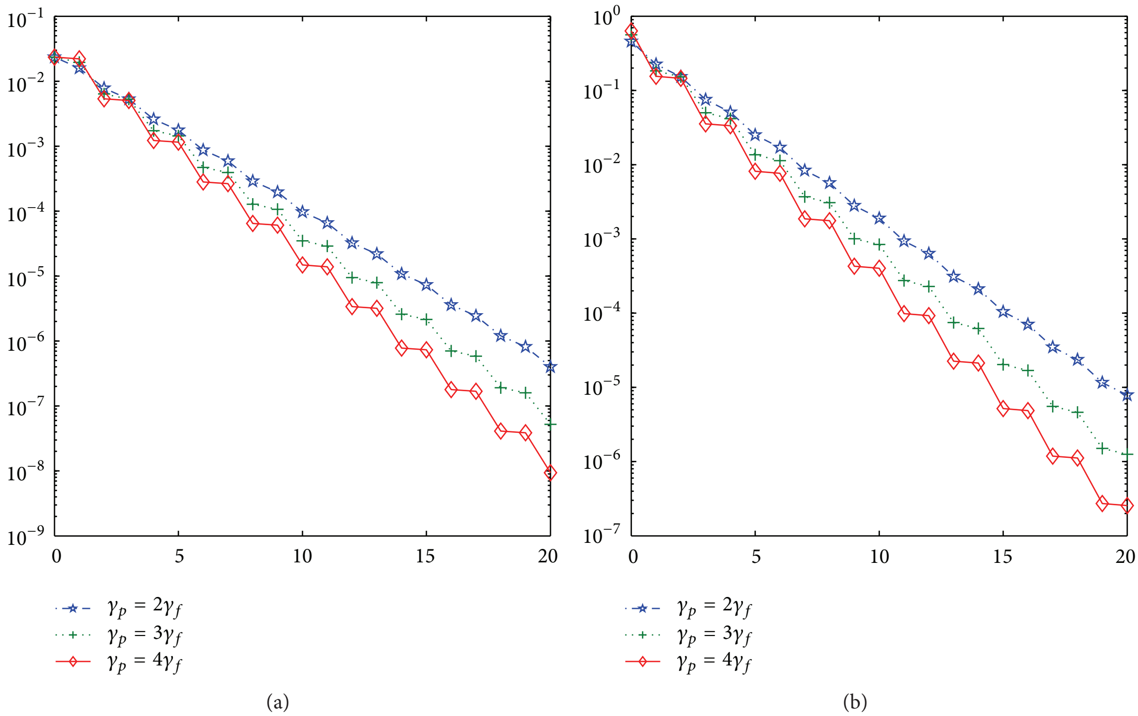

FIGURE 4: Geometric convergence rate of the velocity of the free flow (a) and the hydraulic head of the porous medium flow (b) for the parallel DDM with BJS interface condition.

and $\vec{u}_{c,h}^{k} \in X_{ch}$ and $p_{c,h}^{k} \in Q_{ch}$ are computed from the following Newton iteration.

(i) Initial value $\vec{u}_{c,h}^{k,0}$ is chosen for the Newton iteration. For instance, it may be taken to be $\vec{u}_{c,h}^{0,0} = 0$ and $\vec{u}_{c,h}^{k,0} = \vec{u}_{c,h}^{k-1}$ for $k = 1, 2, \ldots$.

(ii) For $m = 0, 1, 2, \ldots, M$, solve

$$\begin{aligned}
&\left(\vec{u}_{c,h}^{k,m+1} \cdot \nabla \vec{u}_{c,h}^{k,m}, \vec{v}_h\right)_{\Omega_c} + \left(\vec{u}_{c,h}^{k,m} \cdot \nabla \vec{u}_{c,h}^{k,m+1}, \vec{v}_h\right)_{\Omega_c} \\
&\quad + a_c\left(\vec{u}_{c,h}^{k,m+1}, \vec{v}_h\right) + b_c\left(\vec{v}_h, p_c^{k,m+1}\right) - b_c\left(\vec{u}_{c,h}^{k,m+1}, q_h\right) \\
&\quad + \gamma_f \left\langle \vec{u}_{c,h}^{k,m+1} \cdot \vec{n}_c, \vec{v}_h \cdot \vec{n}_c \right\rangle \\
&\quad + \frac{\alpha\nu\sqrt{\mathbf{d}}}{\sqrt{\operatorname{trace}\left(\prod\right)}} \left\langle P_\tau \vec{u}_{c,h}^{k,m+1}, P_\tau \vec{v}_h \right\rangle \\
&= \left(\vec{u}_{c,h}^{k,m} \cdot \nabla \vec{u}_{c,h}^{k,m}, \vec{v}_h\right)_{\Omega_c} + \left\langle \eta_{f,h}^{k}, \vec{v}_h \cdot \vec{n}_c \right\rangle + \left(\vec{f}_c, \vec{v}_h\right)_{\Omega_c}, \\
&\qquad \forall \left(\vec{v}_h, q_h, \psi_h\right) \in X_{ch} \times Q_{ch} \times X_{mh}.
\end{aligned} \tag{26}$$

(iii) Set $\vec{u}_{c,h}^{k} = \vec{u}_{c,h}^{k,m+1}$ and $p_{c,h}^{k} = p_{c,h}^{k,M+1}$.

(3) $\eta_{p,h}^{k+1}$ and $\eta_{f,h}^{k+1}$ are updated in the following manner:

$$\begin{aligned}
\eta_{f,h}^{k+1} &= \frac{\gamma_f}{\gamma_p}\eta_{p,h}^{k} - \left(1 + \frac{\gamma_f}{\gamma_p}\right) g\phi_{m,h}^{k} + gz, \\
\eta_{p,h}^{k+1} &= -\eta_{f,h}^{k} + \left(\gamma_f + \gamma_p\right) \vec{u}_{c,h}^{k} \cdot \vec{n}_c + gz.
\end{aligned} \tag{27}$$

5. Numerical Example

Example 1. Consider the model problem (2)–(6) with the BJS interface condition (7) on $\Omega = [0, \pi] \times [-1, 1]$ with $\Omega_m = [0, \pi] \times [0, 1]$ and $\Omega_c = [0, \pi] \times [-1, 0]$. Choose $(\alpha\nu\sqrt{\mathbf{d}}/\sqrt{\operatorname{trace}(\prod)}) = 1$, $\nu = 1$, $g = 1$, $z = 0$, and $\mathbb{K} = K\mathbb{I}$, where $\mathbb{I}$ is the identity matrix and $K = 1$. The boundary condition data functions and the source terms are chosen such that the exact solution is given by

$$\begin{aligned}
\phi_m &= \left(e^{y} - e^{-y}\right) \sin(x)\, e^{t}, \\
\vec{u}_c &= \left[\frac{K}{\pi} \sin(2\pi y) \cos(x)\, e^{t},\right. \\
&\qquad \left.\left(-2K + \frac{K}{\pi^2}\sin^2(\pi y)\right) \sin(x)\, e^{t}\right]^T, \\
p_c &= 0.
\end{aligned} \tag{28}$$

We divide Ω_m and Ω_c into rectangles of height $h = 1/N$ and width πh, where N is a positive integer, and then subdivide each rectangle into two triangles by drawing a diagonal. The Taylor-Hood element pair is used for the Navier-Stokes equations, and the quadratic finite element is used for the second-order formulation of the Darcy equation.

For the coupled finite element method of the steady Navier-Stokes-Darcy model with BJS interface condition,

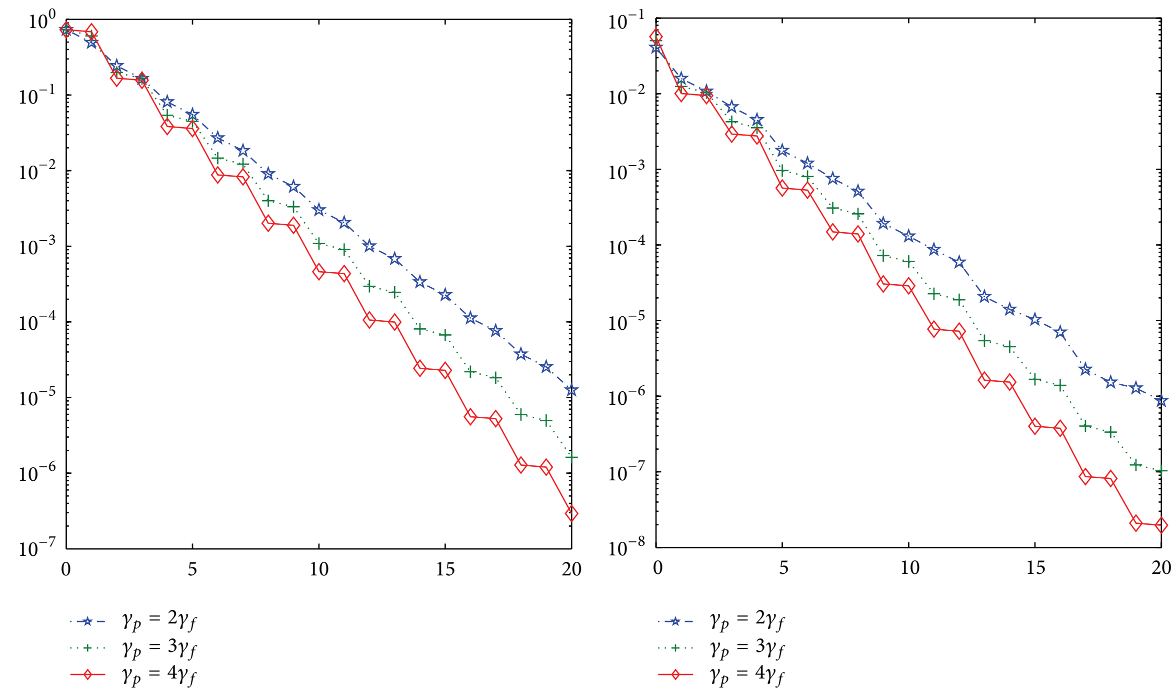

(a) (b)

FIGURE 5: Geometric convergence rate of the pressure of the free flow (a) and η_f (b) versus the iteration counter m for the parallel DDM with BJS interface condition.

TABLE 2: L^2 errors in velocity and hydraulic head for the parallel DDM with BJS interface condition.

	L^2 velocity errors	$e(i)/e(i-4)$	L^2 hydraulic head errors	$e(i)/e(i-4)$
$e(0)$	2.342×10^{-2}		6.338×10^{-1}	
$e(4)$ $(i = 4)$	1.225×10^{-3}	0.0523	3.337×10^{-2}	0.0527
$e(8)$ $(i = 8)$	6.450×10^{-5}	0.0527	1.756×10^{-3}	0.0526
$e(12)$ $(i = 12)$	3.395×10^{-6}	0.0526	9.246×10^{-5}	0.0527
$e(16)$ $(i = 16)$	1.787×10^{-7}	0.0526	4.868×10^{-6}	0.0527
$e(20)$ $(i = 20)$	9.409×10^{-9}	0.0527	2.562×10^{-7}	0.0526

Table 1 provides errors for different choices of h. Using linear regression, the errors in Table 1 satisfy

$$\|\vec{u}_{c,h} - \vec{u}_c\|_0 \approx 0.714h^{3.011}, \qquad |\vec{u}_{c,h} - \vec{u}_c|_1 \approx 3.867h^{1.987},$$
$$\|p_{c,h} - p_c\|_0 \approx 5.123h^{3.129},$$
$$\|\phi_{m,h} - \phi_m\|_0 \approx 0.354h^{2.998}, \qquad |\phi_{m,h} - \phi_m|_1 \approx 1.556h^{1.995}. \tag{29}$$

These rates of convergence are consistent with the approximation capability of the Taylor-Hood element and quadratic element, which is third order with respect to L^2 norm of $\vec{u}_c$ and ϕ_m, second order with respect to H^1 norm of $\vec{u}_c$ and ϕ_m, and second order with respect to L^2 norms of p_c. In particular, the third-order convergence rate of p_c observed above, which is better than the approximation capability of the linear element, is mainly due to the special analytic solution $p = 0$.

For the parallel DDM with $\nu = 1$, $K = 1$, $\gamma_f = 0.3$, and $h = 1/32$, Figures 2 and 3 show the L^2 errors of hydraulic head, velocity, pressure, and η_f. We can see that the parallel domain decomposition method is convergent for $\gamma_f \le \gamma_p$. Moreover, Figures 4 and 5 show that a smaller γ_f/γ_p leads to faster convergence.

Then Tables 2 and 3 list some L^2 errors in velocity, hydraulic head, pressure, and η_f for the parallel domain decomposition method with $\gamma_f = 0.3$ and $\gamma_p = 1.2$. The data in these two tables indicate the geometric convergence rate $\sqrt{\gamma_f/\gamma_p}$ since all the error ratios are less than $(\sqrt{\gamma_f/\gamma_p})^4 = (\sqrt{1/4})^4 = 0.0625$.

Finally, for the preconditioning feature of the domain decomposition method, Table 4 shows the number of iterations M is independent of the grid size h. Here, we set $\gamma_S = 0.3$, $\gamma_D = 1.2$, $\nu = 1$, and $K = 1$. Let ϕ_h^k, $\vec{u}_h^k$, and p_h^k denote the finite element solutions of ϕ_D^k, $\vec{u}_S^k$, and p_S^k at the kth step

Table 3: L^2 errors in pressure and η_f for the parallel DDM with BJS interface condition.

	L^2 velocity errors	$e(i)/e(i-4)$	L^2 hydraulic head errors	$e(i)/e(i-4)$
$e(0)$	7.268×10^{-1}		5.668×10^{-2}	
$e(4)$ $(i = 4)$	3.826×10^{-2}	0.0526	2.752×10^{-3}	0.0486
$e(8)$ $(i = 8)$	2.014×10^{-3}	0.0526	1.399×10^{-4}	0.0508
$e(12)$ $(i = 12)$	1.060×10^{-4}	0.0526	7.233×10^{-6}	0.0517
$e(16)$ $(i = 16)$	5.579×10^{-6}	0.0526	3.767×10^{-7}	0.0521
$e(20)$ $(i = 20)$	2.937×10^{-7}	0.0526	1.969×10^{-8}	0.0523

Table 4: The iteration counter M versus the grid size h for both the parallel Robin-Robin domain decomposition method with BJS interface condition.

h	1/8	1/16	1/32	1/64
M	19	19	19	19

of the domain decomposition algorithm. The criterion used to stop the iteration, that is, to determine the value M, is $\|\vec{u}_h^k - \vec{u}_h^{k-1}\|_0 + \|\phi_h^k - \phi_h^{k-1}\|_0 + \|p_h^k - p_h^{k-1}\|_0 < \varepsilon$, where the tolerance $\varepsilon = 10^{-5}$.

6. Conclusions

In this paper, a parallel physics-based domain decomposition method is proposed for the stationary Navier-Stokes-Darcy model with the BJS interface condition. This method is based on the Robin boundary conditions constructed from the three physical interface conditions. Moreover, it is convergent with geometric convergence rates if the relaxation parameter is selected properly. The number of iteration steps is independent of the grid size due to the natural preconditioning advantage of the domain decomposition methods.

Acknowledgments

This work is partially supported by DOE Grant DE-FE0009843, National Natural Science Foundation of China (11175052).

References

[1] T. Arbogast and D. S. Brunson, "A computational method for approximating a Darcy-Stokes system governing a vuggy porous medium," *Computational Geosciences*, vol. 11, no. 3, pp. 207–218, 2007.

[2] T. Arbogast and M. S. M. Gomez, "A discretization and multigrid solver for a Darcy-Stokes system of three dimensional vuggy porous media," *Computational Geosciences*, vol. 13, no. 3, pp. 331–348, 2009.

[3] T. Arbogast and H. L. Lehr, "Homogenization of a Darcy-Stokes system modeling vuggy porous media," *Computational Geosciences*, vol. 10, no. 3, pp. 291–302, 2006.

[4] Y. Cao, M. Gunzburger, X. Hu, F. Hua, X. Wang, and W. Zhao, "Finite element approximations for Stokes-Darcy flow with Beavers-Joseph interface conditions," *SIAM Journal on Numerical Analysis*, vol. 47, no. 6, pp. 4239–4256, 2010.

[5] Y. Cao, M. Gunzburger, F. Hua, and X. Wang, "Coupled Stokes-Darcy model with Beavers-Joseph interface boundary condition," *Communications in Mathematical Sciences*, vol. 8, no. 1, pp. 1–25, 2010.

[6] M. Discacciati, *Domain decomposition methods for the coupling of surface and groundwater flows [Ph.D. thesis]*, École Polytechnique Fédérale de Lausanne, Lausanne, Switzerland, 2004.

[7] V. J. Ervin, E. W. Jenkins, and S. Sun, "Coupled generalized nonlinear Stokes flow with flow through a porous medium," *SIAM Journal on Numerical Analysis*, vol. 47, no. 2, pp. 929–952, 2009.

[8] M. Moraiti, "On the quasistatic approximation in the Stokes-Darcy model of groundwater-surface water flows," *Journal of Mathematical Analysis and Applications*, vol. 394, no. 2, pp. 796–808, 2012.

[9] I. Babuška and G. N. Gatica, "A residual-based a posteriori error estimator for the Stokes-Darcy coupled problem," *SIAM Journal on Numerical Analysis*, vol. 48, no. 2, pp. 498–523, 2010.

[10] Y. Cao, M. Gunzburger, X. He, and X. Wang, "Robin-Robin domain decomposition methods for the steady-state Stokes-Darcy system with the Beavers-Joseph interface condition," *Numerische Mathematik*, vol. 117, no. 4, pp. 601–629, 2011.

[11] Y. Cao, M. Gunzburger, X.-M. He, and X. Wang, "Parallel, non-iterative, multi-physics domain decomposition methods for time-dependent Stokes-Darcy systems," *Mathematics of Computation*. In press.

[12] W. Chen, M. Gunzburger, F. Hua, and X. Wang, "A parallel Robin-Robin domain decomposition method for the Stokes-Darcy system," *SIAM Journal on Numerical Analysis*, vol. 49, no. 3, pp. 1064–1084, 2011.

[13] M. Discacciati, "Iterative methods for Stokes/Darcy coupling," in *Domain Decomposition Methods in Science and Engineering*, vol. 40 of *Lecture Notes in Computational Science and Engineering*, pp. 563–570, Springer, Berlin, Germany, 2005.

[14] M. Discacciati, E. Miglio, and A. Quarteroni, "Mathematical and numerical models for coupling surface and groundwater flows," *Applied Numerical Mathematics*, vol. 43, no. 1-2, pp. 57–74, 2002, 19th Dundee Biennial Conference on Numerical Analysis (2001).

[15] M. Discacciati and A. Quarteroni, "Analysis of a domain decomposition method for the coupling of Stokes and Darcy equations," in *Numerical Mathematics and Advanced Applications*, pp. 3–20, Springer, Milan, Italy, 2003.

[16] M. Discacciati and A. Quarteroni, "Convergence analysis of a subdomain iterative method for the finite element approximation of the coupling of Stokes and Darcy equations," *Computing and Visualization in Science*, vol. 6, no. 2-3, pp. 93–103, 2004.

[17] M. Discacciati, A. Quarteroni, and A. Valli, "Robin-Robin domain decomposition methods for the Stokes-Darcy coupling," *SIAM Journal on Numerical Analysis*, vol. 45, no. 3, pp. 1246–1268, 2007.

[18] W. Feng, X. He, Z. Wang, and X. Zhang, "Non-iterative domain decomposition methods for a non-stationary Stokes-Darcy model with Beavers-Joseph interface condition," *Applied Mathematics and Computation*, vol. 219, no. 2, pp. 453–463, 2012.

[19] G. N. Gatica, S. Meddahi, and R. Oyarzúa, "A conforming mixed finite-element method for the coupling of fluid flow with porous media flow," *IMA Journal of Numerical Analysis*, vol. 29, no. 1, pp. 86–108, 2009.

[20] G. N. Gatica, R. Oyarzúa, and F.-J. Sayas, "A residual-based a posteriori error estimator for a fully-mixed formulation of the Stokes-Darcy coupled problem," *Computer Methods in Applied Mechanics and Engineering*, vol. 200, no. 21-22, pp. 1877–1891, 2011.

[21] R. H. W. Hoppe, P. Porta, and Y. Vassilevski, "Computational issues related to iterative coupling of subsurface and channel flows," *Calcolo*, vol. 44, no. 1, pp. 1–20, 2007.

[22] B. Jiang, "A parallel domain decomposition method for coupling of surface and groundwater flows," *Computer Methods in Applied Mechanics and Engineering*, vol. 198, no. 9–12, pp. 947–957, 2009.

[23] W. Layton, H. Tran, and X. Xiong, "Long time stability of four methods for splitting the evolutionary Stokes-Darcy problem into Stokes and Darcy subproblems," *Journal of Computational and Applied Mathematics*, vol. 236, no. 13, pp. 3198–3217, 2012.

[24] W. J. Layton, F. Schieweck, and I. Yotov, "Coupling fluid flow with porous media flow," *SIAM Journal on Numerical Analysis*, vol. 40, no. 6, pp. 2195–2218, 2002.

[25] L. Shan, H. Zheng, and W. J. Layton, "A decoupling method with different subdomain time steps for the nonstationary Stokes-Darcy model," *Numerical Methods for Partial Differential Equations*, vol. 29, no. 2, pp. 549–583, 2013.

[26] M. Mu and X. Zhu, "Decoupled schemes for a non-stationary mixed Stokes-Darcy model," *Mathematics of Computation*, vol. 79, no. 270, pp. 707–731, 2010.

[27] C. Bernardi, T. C. Rebollo, F. Hecht, and Z. Mghazli, "Mortar finite element discretization of a model coupling Darcy and Stokes equations," *Mathematical Modelling and Numerical Analysis*, vol. 42, no. 3, pp. 375–410, 2008.

[28] Y. Boubendir and S. Tlupova, "Stokes-Darcy boundary integral solutions using preconditioners," *Journal of Computational Physics*, vol. 228, no. 23, pp. 8627–8641, 2009.

[29] W. Chen, P. Chen, M. Gunzburger, and N. Yan, "Superconvergence analysis of FEMs for the Stokes-Darcy system," *Mathematical Methods in the Applied Sciences*, vol. 33, no. 13, pp. 1605–1617, 2010.

[30] C. D'Angelo and P. Zunino, "Robust numerical approximation of coupled Stokes' and Darcy's flows applied to vascular hemodynamics and biochemical transport," *Mathematical Modelling and Numerical Analysis*, vol. 45, no. 3, pp. 447–476, 2011.

[31] M.-F. Feng, R.-S. Qi, R. Zhu, and B.-T. Ju, "Stabilized Crouzeix-Raviart element for the coupled Stokes and Darcy problem," *Applied Mathematics and Mechanics*, vol. 31, no. 3, pp. 393–404, 2010.

[32] J. Galvis and M. Sarkis, "Balancing domain decomposition methods for mortar coupling Stokes-Darcy systems," in *Domain Decomposition Methods in Science and Engineering XVI*, vol. 55 of *Lecture Notes in Computational Science and Engineering*, pp. 373–380, Springer, Berlin, Germany, 2007.

[33] J. Galvis and M. Sarkis, "Non-matching mortar discretization analysis for the coupling Stokes-Darcy equations," *Electronic Transactions on Numerical Analysis*, vol. 26, pp. 350–384, 2007.

[34] J. Galvis and M. Sarkis, "FETI and BDD preconditioners for Stokes-Mortar-Darcy systems," *Communications in Applied Mathematics and Computational Science*, vol. 5, pp. 1–30, 2010.

[35] G. N. Gatica, R. Oyarzúa, and F.-J. Sayas, "Convergence of a family of Galerkin discretizations for the Stokes-Darcy coupled problem," *Numerical Methods for Partial Differential Equations. An International Journal*, vol. 27, no. 3, pp. 721–748, 2011.

[36] G. Kanschat and B. Rivière, "A strongly conservative finite element method for the coupling of Stokes and Darcy flow," *Journal of Computational Physics*, vol. 229, no. 17, pp. 5933–5943, 2010.

[37] T. Karper, K.-A. Mardal, and R. Winther, "Unified finite element discretizations of coupled Darcy-Stokes flow," *Numerical Methods for Partial Differential Equations*, vol. 25, no. 2, pp. 311–326, 2009.

[38] S. Khabthani, L. Elasmi, and F. Feuillebois, "Perturbation solution of the coupled Stokes-Darcy problem," *Discrete and Continuous Dynamical Systems B*, vol. 15, no. 4, pp. 971–990, 2011.

[39] M. Mu and J. Xu, "A two-grid method of a mixed Stokes-Darcy model for coupling fluid flow with porous media flow," *SIAM Journal on Numerical Analysis*, vol. 45, no. 5, pp. 1801–1813, 2007.

[40] S. Münzenmaier and G. Starke, "First-order system least squares for coupled Stokes-Darcy flow," *SIAM Journal on Numerical Analysis*, vol. 49, no. 1, pp. 387–404, 2011.

[41] B. Rivière, "Analysis of a discontinuous finite element method for the coupled Stokes and Darcy problems," *Journal of Scientific Computing*, vol. 22-23, pp. 479–500, 2005.

[42] B. Rivière and I. Yotov, "Locally conservative coupling of Stokes and Darcy flows," *SIAM Journal on Numerical Analysis*, vol. 42, no. 5, pp. 1959–1977, 2005.

[43] H. Rui and R. Zhang, "A unified stabilized mixed finite element method for coupling Stokes and Darcy flows," *Computer Methods in Applied Mechanics and Engineering*, vol. 198, no. 33–36, pp. 2692–2699, 2009.

[44] S. Tlupova and R. Cortez, "Boundary integral solutions of coupled Stokes and Darcy flows," *Journal of Computational Physics*, vol. 228, no. 1, pp. 158–179, 2009.

[45] J. M. Urquiza, D. N'Dri, A. Garon, and M. C. Delfour, "Coupling Stokes and Darcy equations," *Applied Numerical Mathematics*, vol. 58, no. 5, pp. 525–538, 2008.

[46] L. Badea, M. Discacciati, and A. Quarteroni, "Numerical analysis of the Navier-Stokes/Darcy coupling," *Numerische Mathematik*, vol. 115, no. 2, pp. 195–227, 2010.

[47] M. Cai, M. Mu, and J. Xu, "Numerical solution to a mixed Navier-Stokes/Darcy model by the two-grid approach," *SIAM Journal on Numerical Analysis*, vol. 47, no. 5, pp. 3325–3338, 2009.

[48] A. Çeşmelioğlu and B. Rivière, "Analysis of time-dependent Navier-Stokes flow coupled with Darcy flow," *Journal of Numerical Mathematics*, vol. 16, no. 4, pp. 249–280, 2008.

[49] A. Çeşmelioğlu and B. Rivière, "Primal discontinuous Galerkin methods for time-dependent coupled surface and subsurface flow," *Journal of Scientific Computing*, vol. 40, no. 1–3, pp. 115–140, 2009.

[50] P. Chidyagwai and B. Rivière, "On the solution of the coupled Navier-Stokes and Darcy equations," *Computer Methods in Applied Mechanics and Engineering*, vol. 198, no. 47-48, pp. 3806–3820, 2009.

[51] V. Girault and B. Rivière, "DG approximation of coupled Navier-Stokes and Darcy equations by Beaver-Joseph-Saffman interface condition," *SIAM Journal on Numerical Analysis*, vol. 47, no. 3, pp. 2052–2089, 2009.

[52] G. Beavers and D. Joseph, "Boundary conditions at a naturally permeable wall," *Journal of Fluid Mechanics*, vol. 30, pp. 197–207, 1967.

[53] W. Jäger and A. Mikelić, "On the interface boundary condition of Beavers, Joseph, and Saffman," *SIAM Journal on Applied Mathematics*, vol. 60, no. 4, pp. 1111–1127, 2000.

[54] I. P. Jones, "Low Reynolds number flow past a porous spherical shell," *Proceedings of the Cambridge Philosophical Society*, vol. 73, pp. 231–238, 1973.

[55] P. Saffman, "On the boundary condition at the interface of a porous medium," *Studies in Applied Mathematics*, vol. 1, pp. 77–84, 1971.

[56] V. Girault and P.-A. Raviart, *Finite Element Methods for Navier-Stokes Equations. Theory and Algorithms*, vol. 5 of *Springer Series in Computational Mathematics*, Springer, Berlin, Germany, 1986.

[57] M. D. Gunzburger, *Finite Element Methods for Viscous Incompressible Flows. A Guide to Theory, Practice, and Algorithms*, Computer Science and Scientific Computing, Academic Press, Boston, Mass, USA, 1989.

Hindawi Publishing Corporation
Abstract and Applied Analysis
Volume 2013, Article ID 597807, 8 pages
http://dx.doi.org/10.1155/2013/597807

Research Article

A New Integro-Differential Equation for Rossby Solitary Waves with Topography Effect in Deep Rotational Fluids

Hongwei Yang,[1] Qingfeng Zhao,[1] Baoshu Yin,[2,3] and Huanhe Dong[1]

[1] *Information School, Shandong University of Science and Technology, Qingdao 266590, China*
[2] *Institute of Oceanology, China Academy of Sciences, Qingdao 266071, China*
[3] *Key Laboratory of Ocean Circulation and Wave, Chinese Academy of Sciences, Qingdao 266071, China*

Correspondence should be addressed to Baoshu Yin; baoshuyin@126.com

Received 7 May 2013; Accepted 2 September 2013

Academic Editor: Rasajit Bera

From rotational potential vorticity-conserved equation with topography effect and dissipation effect, with the help of the multiple-scale method, a new integro-differential equation is constructed to describe the Rossby solitary waves in deep rotational fluids. By analyzing the equation, some conservation laws associated with Rossby solitary waves are derived. Finally, by seeking the numerical solutions of the equation with the pseudospectral method, by virtue of waterfall plots, the effect of detuning parameter and dissipation on Rossby solitary waves generated by topography are discussed, and the equation is compared with KdV equation and BO equation. The results show that the detuning parameter α plays an important role for the evolution features of solitary waves generated by topography, especially in the resonant case; a large amplitude nonstationary disturbance is generated in the forcing region. This condition may explain the blocking phenomenon which exists in the atmosphere and ocean and generated by topographic forcing.

1. Introduction

Among the many wave motions that occur in the ocean and atmosphere, Rossby waves play one of the most important roles. They are largely responsible for determining the ocean's response to atmospheric and other climate changes [1]. In the past decades, the research on nonlinear Rossby solitary waves had been given much attention in the mathematics and physics, and some models had been constructed to describe this phenomenon. Based upon the pioneering work of Long [2] and Benney [3] on barotropic Rossby waves, there had been remarkably exciting developments [4–11] and formed classical solitary waves theory and algebraic solitary waves theory. The so-called classical solitary waves indicate that the evolution of solitary waves is governed by the Korteweg-de Vries (KdV) type model, while the behavior of solitary waves is governed by the Benjamin-Ono (BO) model, it is called algebraic solitary waves. After the KdV model and BO model, a more general evolution model for solitary waves in a finite-depth fluid was given by Kubota, and the model was called intermediate long-wave (ILW) model [12, 13]. Many mathematicians solved the above models by all kinds of method and got a series of results [14–19]. We note that most of the previous researches about solitary waves were carried out in the zonal area and could not be applied directly to the spherical earth, and little attention had been focused on the solitary waves in the rotational fluids [20]. Furthermore, as everyone knows the real oceanic and atmospheric motion is a forced and dissipative system. Topography effect as a forcing factor has been studied by many researchers [21–25]; on the other hand, dissipation effect must be considered in the oceanic and atmospheric motion; otherwise, the motion would grow explosively because of the constant injecting of the external forcing energy. Our aim is to construct a new model to describe the Rossby solitary waves in rotational fluid with topography effect and dissipation effect. It has great difference from the previous researches.

In this paper, from rotational potential vorticity-conserved equation with topography effect and dissipation effect, with the help of the multiple-scale method, we will first construct a new model to describe Rossby solitary waves in deep rotational fluids. Then we will analyse the conservation relations of the model and derive the conservation laws of Rossby solitary waves. Finally, the model is solved by the pseudospectral method [26]. Based on the waterfall plots, the effect of detuning parameter and dissipation on Rossby solitary waves generated by topography are discussed, the model is compared with KdV model and BO model, and some conclusions are obtained.

2. Mathematics Model

According to [27], taking plane polar coordinates (r, θ), r pointing to lower latitude is positive and the positive rotation is counter-clockwise, and then the rotational potential vorticity-conserved equation including topography effect and turbulent dissipation is, in the nondimensional form, given by

$$\left[\frac{\partial}{\partial t}+\left(\frac{1}{r}\frac{\partial \Psi}{\partial r}\frac{\partial}{\partial \theta}-\frac{1}{r}\frac{\partial \Psi}{\partial \theta}\frac{\partial}{\partial r}\right)\right] \times\left[\frac{1}{r}\frac{\partial}{\partial r}\left(r\frac{\partial \Psi}{\partial r}\right)+\frac{1}{r^2}\frac{\partial^2 \Psi}{\partial \theta^2}+h(r,\theta)\right]+\frac{\beta}{r}\frac{\partial \Psi}{\partial \theta} = -\lambda_0\left[\frac{1}{r}\frac{\partial}{\partial r}\left(r\frac{\partial \Psi}{\partial r}\right)+\frac{1}{r^2}\frac{\partial^2 \Psi}{\partial \theta^2}\right]+Q, \quad (1)$$

where Ψ is the dimensionless stream function; $\beta = (\omega_0/R_0)\cos\phi_0(L^2/U)$, in which R_0 is the Earth's radius, ω_0 is the angular frequency of the Earth's rotation, ϕ_0 is the latitude, L and U are the characteristic horizontal length and velocity scales, $h(r,\theta)$ expresses the topography effect, $\lambda_0[(1/r)(\partial/\partial r)(r(\partial\Psi/\partial r))+(1/r^2)(\partial^2\Psi/\partial\theta^2)]$ denotes the vorticity dissipation which is caused by the Ekman boundary layer and λ_0 is a dissipative coefficient, Q is the external source, and the form of Q will be given in the latter.

In order to consider weakly nonlinear perturbation on a rotational flow, we assume

$$\Psi = \int^r (\Omega(r) - c + \varepsilon\alpha)\, r\,dr + \varepsilon\psi(r,\theta,t), \quad (2)$$

where α is a small disturbance in the basic flow and reflects the proximity of the system to a resonate state; c is a constant, which is regarded as a Rossby waves phase speed; ψ denotes disturbance stream function; $\Omega(r)$ expresses the rotational angular velocity. In order to consider the role of nonlinearity, we assume the following type of rotational angular velocity:

$$\Omega(r) = \begin{cases} \omega(r) & r_1 \le r \le r_2, \\ \omega_1 & r > r_2, \end{cases} \quad (3)$$

where ω_1 is constant and $\omega(r)$ is a function of r. For simplicity, $\omega(r)$ is assumed to be smooth across $r = r_2$.

In the domain $[r_1, r_2]$, in order to achieve a balance among topography effect, turbulent dissipation, and nonlinearity and to eliminate the derivative term of dissipation, we assume

$$h(r,\theta) = \varepsilon^2 H(r,\theta), \qquad \lambda_0 = \varepsilon^{3/2}\lambda, \qquad Q = \varepsilon^{3/2}\lambda\frac{1}{r}\frac{\partial}{\partial r}\left[r^2(\omega - c_0 + \varepsilon\alpha)\right]. \quad (4)$$

Substituting (2), (3), and (4) into (1) leads to the following equation for the perturbation stream function ψ:

$$\left[\frac{\partial}{\partial t}+(\omega - c+\varepsilon\alpha)\frac{\partial}{\partial \theta}+\varepsilon\left(\frac{1}{r}\frac{\partial \psi}{\partial r}\frac{\partial}{\partial \theta}-\frac{1}{r}\frac{\partial \psi}{\partial \theta}\frac{\partial}{\partial r}\right)\right] \times\left[\frac{1}{r}\frac{\partial}{\partial r}\left(r\frac{\partial \psi}{\partial r}\right)+\frac{1}{r^2}\frac{\partial^2 \psi}{\partial \theta^2}+\varepsilon H(r,\theta)\right] +\frac{1}{r}\left[\beta-\frac{d}{dr}\left(\frac{1}{r}\frac{dr^2\omega}{dr}\right)\right]\frac{\partial \psi}{\partial \theta} = -\varepsilon^{3/2}\lambda\left[\frac{1}{r}\frac{\partial}{\partial r}\left(r\frac{\partial \psi}{\partial r}\right)+\frac{1}{r^2}\frac{\partial^2 \psi}{\partial \theta^2}\right]. \quad (5)$$

In the domain $[r_2, \infty]$, the parameter β is smaller than that in the domain $[r_1, r_2]$, and we assume $\beta = 0$ for $[r_2, \infty]$. Furthermore, the turbulent dissipation and topography effect are absent in the domain and only consider the features of disturbances generated. Substituting (2) and (3) into (1), we have the following governing equations:

$$\left[\frac{\partial}{\partial t}+(\omega_1 - c+\varepsilon\alpha)\frac{\partial}{\partial \theta}+\varepsilon\left(\frac{1}{r}\frac{\partial \psi}{\partial r}\frac{\partial}{\partial \theta}-\frac{1}{r}\frac{\partial \psi}{\partial \theta}\frac{\partial}{\partial r}\right)\right] \times\left[\frac{1}{r}\frac{\partial}{\partial r}\left(r\frac{\partial \psi}{\partial r}\right)+\frac{1}{r^2}\frac{\partial^2 \psi}{\partial \theta^2}\right] = 0. \quad (6)$$

For (5), we introduce the following stretching transformations:

$$\Theta = \varepsilon^{1/2}\theta, \qquad r = r, \qquad T = \varepsilon^{3/2}t, \quad (7)$$

and the perturbation expansion of $\overline{\psi}$ is in the following form:

$$\overline{\psi} = \psi_1(\Theta, r, T) + \varepsilon\psi_2(\Theta, r, T) + \cdots. \quad (8)$$

Substituting (7) and (8) into (5), comparing the same power of ε term, we can obtain the $\varepsilon^{1/2}$ equation:

$$\mathscr{L}\psi_1 = 0, \quad (9)$$

where the operator $\mathscr{L}$ is defined as

$$\mathscr{L} = \frac{1}{r}\frac{\partial}{\partial \Theta}\left\{(\omega - c)\left[\frac{\partial}{\partial r}\left(r\frac{\partial}{\partial r}\right)\right]+\left[\beta-\frac{d}{dr}\left(\frac{1}{r}\frac{dr^2\omega}{dr}\right)\right]\right\}. \quad (10)$$

Assume the perturbation at boundary $r = r_1$ does not exist, that is,

$$\psi_1 = \psi_2 = \cdots = 0, \quad (11)$$

and the perturbation at boundary $r = r_2$ is determined by (6). For the linear solution to be separable, assuming the solution of (9) in the form:

$$\psi_1 = A(\Theta, T)\,\phi(r), \quad (12)$$

thus $\phi(r)$ should satisfy the following equation:

$$(\omega - c)\frac{d}{dr}\left(r\frac{d\phi(r)}{dr}\right)+\left[\beta-\frac{d}{dr}\left(\frac{1}{r}\frac{dr^2\omega}{dr}\right)\right]\phi(r) = 0. \quad (13)$$

On the other hand, we proceed to the $\varepsilon^{3/2}$ equation:

$$\mathscr{L}\psi_2 + \frac{\omega - c}{r^2}\frac{\partial^3 \psi_1}{\partial \Theta^3} + \left(\frac{\partial}{\partial T} + \alpha\frac{\partial}{\partial \Theta} + \frac{1}{r}\frac{\partial \psi_1}{\partial r}\frac{\partial}{\partial \Theta} - \frac{1}{r}\frac{\partial \psi_1}{\partial \Theta}\frac{\partial}{\partial r} + \lambda\right) \times \left[\frac{1}{r}\frac{\partial}{\partial r}\left(r\frac{\partial \psi_1}{\partial r}\right)\right] + (\omega - c)\frac{\partial H(r,\Theta)}{\partial \Theta} = 0. \quad (14)$$

Multiplying the both sides of (14) by $r\phi/(\omega - c)$ and integrating it with respect to r from r_1 to r_2, employing the boundary conditions (11), we get

$$\begin{aligned}&\frac{\partial}{\partial \Theta} r\left(\phi\frac{\partial}{\partial r}\psi_2 - \frac{d\phi}{dr}\psi_2\right)\Bigg|_{r=r_2} \\ &\quad + A\frac{\partial A}{\partial \Theta}\int_{r_1}^{r_2}\frac{\phi^3}{\omega - c}\frac{d}{dr} \times \left[\frac{\beta - (d/dr)\left((1/r)\left(dr^2\omega/dr\right)\right)}{\phi(\omega - c)}\right]dr \\ &\quad + \left(\frac{\partial A}{\partial T} + \alpha\frac{\partial A}{\partial \Theta} + \lambda A\right)\int_{r_1}^{r_2}\frac{\phi}{\omega - c}\frac{d}{dr}\left(r\frac{d\phi}{dr}\right)dr \\ &\quad + \frac{\partial^3 A}{\partial \Theta^3}\int_{r_1}^{r_2}\frac{\phi^2}{r}dr + \int_{r_1}^{r_2} r\phi\frac{\partial H}{\partial \Theta}dr = 0.\end{aligned} \quad (15)$$

In (15), if the boundary conditions on ϕ and ψ_2 are known, the equation governing the amplitude A will be determined. Assuming the solution of (5) matches smoothly with the solution of (6) at $r = r_2$, we can solve (6) to seek the solution at $r = r_2$.

For (6), we adopt the transformations in the forms:

$$\rho = \theta, \qquad r = r, \qquad T = \varepsilon^{3/2}t, \quad (16)$$

and the perturbation function is shown $\widetilde{\psi}$; then by substituting (16) into (6), we can get the ε^0 equation:

$$(\omega_1 - c)\frac{\partial}{\partial \rho}\left[\frac{1}{r}\frac{\partial}{\partial r}\left(r\frac{\partial \widetilde{\psi}}{\partial r}\right) + \frac{1}{r^2}\frac{\partial^2 \widetilde{\psi}}{\partial \rho^2}\right] = 0. \quad (17)$$

It is easy to find that (17) can reduce to

$$\begin{aligned}&\frac{1}{r}\frac{\partial}{\partial r}\left(r\frac{\partial \widetilde{\psi}}{\partial r}\right) + \frac{1}{r^2}\frac{\partial^2 \widetilde{\psi}}{\partial \rho^2} = 0, \quad r \geq r_2, \\ &\widetilde{\psi} \longrightarrow 0, \quad r \longrightarrow \infty.\end{aligned} \quad (18)$$

Obviously, the solution of (18) is

$$\widetilde{\psi}(\rho, r, T, \varepsilon) = \frac{1}{2\pi}\int_0^{2\pi}\frac{\left(r^2 - r_2^2\right)\widetilde{\psi}\left(\rho', r_2, T, \varepsilon\right)}{r_2^2 - 2r_2 r\cos\left(\rho - \rho'\right) + r^2}d\rho'. \quad (19)$$

Taking the derivative with respect to r for both sides of (19) leads to

$$\frac{\partial \widetilde{\psi}}{\partial r} = \frac{r_2}{\pi}\int_0^{2\pi}\widetilde{\psi}\left(\rho', r_2, T, \varepsilon\right)\frac{\left[2r_2 r - \left(r^2 + r_2^2\right)\cos\left(\rho - \rho'\right)\right]}{\left[r_2^2 - 2r_2 r\cos\left(\rho - \rho'\right) + r^2\right]^2}d\rho'. \quad (20)$$

Because the solution of (5) matches smoothly with the solution of (6) at $r = r_2$, we obtain

$$\psi_1(\Theta, r_2, T) + \varepsilon\psi_2(\Theta, r_2, T) = \widetilde{\psi}(\rho, r_2, T, \varepsilon) + O\left(\varepsilon^2\right), \quad (21)$$

$$\frac{\partial \psi_1}{\partial r}(\Theta, r_2, T) + \varepsilon\frac{\partial \psi_2}{\partial r}(\Theta, r_2, T) = \frac{\partial \widetilde{\psi}}{\partial r}(\rho, r_2, T, \varepsilon) + O\left(\varepsilon^2\right). \quad (22)$$

From (21), we have

$$A(\Theta, T)\phi(r_2) = \widetilde{\psi}(\rho, r_2, T, \varepsilon), \qquad \psi_2(\Theta, r_2, T) = 0. \quad (23)$$

Substituting (23) into (20) leads to

$$\frac{\partial \widetilde{\psi}}{\partial r}(\rho, r_2, T, \varepsilon) = \varepsilon\phi(r_2)\frac{\partial^2 \mathscr{J}(A(\Theta, T))}{\partial \Theta^2}, \quad (24)$$

where $\mathscr{J}(A(\Theta,T)) = (r_2/2\pi)\int_0^{2\pi} A(\Theta', T)\ln|\sin((\Theta - \Theta')/2)|d\Theta'$. Then, based on (22) and (24), we get

$$\phi'(r_2) = 0, \qquad \frac{\partial \psi_2}{\partial r}(\Theta, r_2, T) = \phi(r_2)\frac{\partial^2 \mathscr{J}(A(\Theta, T))}{\partial \Theta^2}. \quad (25)$$

Substituting the boundary conditions (23) and (25) into (15) yields

$$\begin{aligned}&\frac{\partial A}{\partial T} + \alpha\frac{\partial A}{\partial \Theta} + a_1 A\frac{\partial A}{\partial \Theta} + a_2\frac{\partial^3 A}{\partial \Theta^3} \\ &\quad + a_3\frac{\partial^3}{\partial \Theta^3}\mathscr{J}(A(\Theta, T)) + \lambda A = \frac{\partial G}{\partial \Theta}.\end{aligned} \quad (26)$$

Equation (26) can be rewritten as follows:

$$\begin{aligned}&\frac{\partial A}{\partial T} + \alpha\frac{\partial A}{\partial \Theta} + a_1 A\frac{\partial A}{\partial \Theta} + a_2\frac{\partial^3 A}{\partial \Theta^3} \\ &\quad + a_3\frac{\partial^2}{\partial \Theta^2}\mathscr{H}(A(\Theta, T)) + \lambda A = \frac{\partial G}{\partial \Theta},\end{aligned} \quad (27)$$

where $\mathscr{H}(A(\Theta,T)) = (r_2/4\pi)\int_0^{2\pi} A(\Theta', T)\cot((\Theta - \Theta')/2)d\Theta'$ and $a = \int_{r_1}^{r_2}(\phi/(\omega - c))(d/dr)(r(d\phi/dr))dr$, $a_1 = \int_{r_1}^{r_2}(\phi^3/(\omega - c))(d/dr)[\beta - (d/dr)((1/r)(dr^2\omega/dr))/\phi(\omega - c)]dr/a$, $a_2 = \int_{r_1}^{r_2}(\phi^2/r)dr/a$, $a_3 = r_2\phi^2(r_2)/a$, $G = \int_{r_1}^{r_2} r\phi H dr/a$. Equation (27) is an integro-differential equation and λA expresses dissipation effect and has the same physical meaning with the term $\partial^2 A/\partial \Theta^2$ in Burgers equation. When $a_3 = \lambda = H = 0$, the equation degenerates to the KdV equation. When $a_2 = \lambda = H = 0$, the equation degenerates to the so-called rotational BO equation. Here we call (27) forced rotational KdV-BO-Burgers equation. As we know, the forced rotational KdV-BO-Burgers equation as a governing model for Rossby solitary waves is first derived in the paper.

3. Conservation Laws

In this section, the conservation laws are used to explore some features of Rossby solitary waves. In [7], Ono presented four conservation laws of BO equation, and we extend Ono's work to investigate the following questions: Has the rotational KdV-BO-Burgers equation also conservation laws without dissipation effect? Has it four conservation laws or more? How to change of these conservation quantities in the presence of dissipation effect?

In this section, topography effect is ignored; that is, H is taken zero in (27). Based on periodicity condition, we assume that the values of A, A_Θ, $A_{\Theta\Theta}$, $A_{\Theta\Theta\Theta}$ at $\Theta = 0$ equal that at $\Theta = 2\pi$. Then integrating (27) with respect to Θ over $(0, 2\pi)$, we are easy to obtain the following conservation relation:

$$Q_1 = \int_0^{2\pi} A d\Theta = \exp(-\lambda T) \int_0^{2\pi} A(\Theta, 0)\, d\Theta. \tag{28}$$

From (28), it is obvious that Q_1 decreases exponentially with the evolution of time T and the dissipation coefficient λ. By analogy with the KdV equation, Q_1 is regarded as the mass of the solitary waves. This shows that the dissipation effect causes the mass of solitary waves decrease exponentially. When dissipation effect is absent, the mass of the solitary waves is conserved.

In what follows, (27) has another simple conservation law, which becomes clear if we multiply (27) by $A(\Theta, T)$ and carry the integration; by using the property of the operator $\mathscr{H}$: $\int_0^{2\pi} f(\Theta)\mathscr{H}(f(\Theta))d\Theta = 0$, then we get

$$Q_2 = \int_0^{2\pi} A^2 d\Theta = \exp(-2\lambda T) \int_0^{2\pi} A^2(\Theta, 0)\, d\Theta. \tag{29}$$

Similar to the mass Q_1, Q_2 is regarded as the momentum of the solitary waves and is conserved without dissipation. The momentum of the solitary waves also decreases exponentially with the evolution of time T and the increasing of dissipative coefficient λ in the presence of dissipation effect. Furthermore, the rate of decline of momentum is faster than the rate of mass.

Next, we multiply (27) by $(A^2 - (a_3/a_1)\mathscr{H}(A_\Theta))$ and obtain

$$\begin{aligned}
&\left(\frac{1}{3}A^3\right)_T - \frac{a_3}{a_1}\mathscr{H}(A_\Theta) A_T \\
&\quad + (\alpha + a_1 A) A_\Theta \left(A^2 - \frac{a_3}{a_1}\mathscr{H}(A_\Theta)\right) \\
&\quad + a_2 A_{\Theta\Theta\Theta} \left(A^2 - \frac{a_3}{a_1}\mathscr{H}(A_\Theta)\right) \\
&\quad + a_3 \left(A^2 - \frac{a_3}{a_1}\mathscr{H}(A_\Theta)\right)(\mathscr{H}(A))_{\Theta\Theta} \\
&\quad + \lambda \left(A^2 - \frac{a_3}{a_1}\mathscr{H}(A_\Theta)\right) A = 0.
\end{aligned} \tag{30}$$

Then taking the derivative of (27) with respect to Θ and multiplying $(-(2a_2/a_1)A_\Theta + (a_3/a_1)\mathscr{H}(A))$ lead to

$$\begin{aligned}
&\left(-\frac{2a_2}{a_1}A_\Theta + \frac{a_3}{a_1}\mathscr{H}(A)\right) A_{\Theta T} \\
&\quad + \left[\alpha A_{\Theta\Theta} + a_1 (A A_\Theta)_\Theta\right] \left(-\frac{2a_2}{a_1}A_\Theta + \frac{a_3}{a_1}\mathscr{H}(A)\right) \\
&\quad + a_2 A_{\Theta\Theta\Theta\Theta} \left(-\frac{2a_2}{a_1}A_\Theta + \frac{a_3}{a_1}\mathscr{H}(A)\right) \\
&\quad + a_3 \left(-\frac{2a_2}{a_1}A_\Theta + \frac{a_3}{a_1}\mathscr{H}(A)\right)\mathscr{H}(A)_{\Theta\Theta\Theta} \\
&\quad + \lambda A \left(-\frac{2a_2}{a_1}A_\Theta + \frac{a_3}{a_1}\mathscr{H}(A)\right) = 0.
\end{aligned} \tag{31}$$

Adding (30) to (31), by virtue of the property of operator $\mathscr{H}$:

$$\mathscr{H}(A)_{\Theta\Theta} = \mathscr{H}(A_{\Theta\Theta}), \qquad \int_0^{2\pi} u\mathscr{H} v d\Theta = -\int_0^{2\pi} v\mathscr{H} u d\Theta, \tag{32}$$

we have

$$\begin{aligned}
&\left(\frac{1}{3}A^3 - \frac{a_2}{a_1}A_\Theta^2 + \frac{a_3}{a_1}A_\Theta \mathscr{H}(A)\right)_T \\
&\quad + \alpha\left[\frac{1}{3}A^3 - \frac{a_2}{a_1}A_\Theta^2 + \frac{a_3}{a_1}\mathscr{H}(A) A_\Theta\right]_\Theta \\
&\quad + \left(\frac{a_1}{4}A^4\right)_\Theta + \frac{a_3^2}{2a_1}\left[H(A) H(A)_{\Theta\Theta}\right]_\Theta \\
&\quad + \frac{a_2 a_3}{a_1}\left(A_{\Theta\Theta\Theta} H(A) - 2A_\Theta H(A)_{\Theta\Theta}\right)_\Theta \\
&\quad - \frac{2a_2}{a_1}\left(A_\Theta A_{\Theta\Theta\Theta} - \frac{1}{2}A_{\Theta\Theta}^2\right)_\Theta + a_2\left(A^2 A_{\Theta\Theta} - 2AA_\Theta^2\right)_\Theta \\
&\quad + a_3\left[A(A\mathscr{H}(A))_\Theta\right]_\Theta + \lambda\left(A^3 - \frac{a_2}{a_1}A_\Theta^2 + \frac{a_3}{a_1}A_\Theta H(A)\right) \\
&= 0.
\end{aligned} \tag{33}$$

Taking $Q_3 = \int_0^{2\pi}((1/3)A^3 - (a_2/a_1)A_\Theta^2 + (a_3/a_1)A_\Theta\mathscr{H}(A))d\Theta$, we are easy to see that when the dissipation effect is absent, that is, $\lambda = 0$, Q_3 is a conserved quantity and regarded as the energy of the solitary waves. So we can conclude that the energy of solitary waves is conserved without dissipation. By analysing (33), we can find the decreasing trend of energy of solitary waves.

Finally, let us consider a quantity related to the phase of solitary waves:

$$\widetilde{Q}_4 = \frac{d}{dT}\int_0^{2\pi}\Theta A d\Theta, \tag{34}$$

and we can get $d\widetilde{Q}_4/dT = 0$ without dissipation. According [7], we present the velocity of the center of gravity for the ensemble of such waves $Q_4 = \widetilde{Q}_4/Q_1$; by employing $dQ_1/dT = 0$ and $d\widetilde{Q}_4/dT = 0$, we have $dQ_4/dT = 0$, which shows that the velocity of the center of gravity is conserved without dissipation.

After the four conservation relations are given, we can proceed to seek the fifth conservation quantity. In fact, after tedious calculation, we can also verify that

$$Q_5 = \int_0^{2\pi}\left(\frac{1}{4}A^4 - \frac{3a_2}{a_1}AA_\Theta^2 + \frac{9a_2}{a_1^2}A_{\Theta\Theta}^2 + \frac{a_3}{4a_1}A^2\mathscr{H}(A)\right)d\Theta \tag{35}$$

is also conservation quantity. According the idea, we can obtain the sixth conservation quantity Q_6 and the seventh conservation quantity $Q_7\ldots$, so we can guess that, similar to the KdV equation, the rotational KdV-BO-Burgers equation without dissipation also owns infinite conservation laws, but it needs to be verified in the future.

4. Numerical Simulation and Discussion

In this section, we will take into account the generation and evolution feature of Rossby solitary waves under the influence of topography and dissipation, so we need to seek the solutions of forced rotational KdV-BO-Burgers equation. But we know that there is no analytic solution for (27), and here we consider the numerical solutions of (27) by employing the pseudospectral method.

The pseudo-spectral method uses a Fourier transform treatment of the space dependence together with a leap-forg scheme in time. For ease of presentation the spatial period is normalized to $[0, 2\pi]$. This interval is divided into $2N$ points, and then $\Delta T = \pi/N$. The function $A(X,T)$ can be transformed to the Fourier space by

$$\widehat{A}(\nu,T) = FA = \frac{1}{\sqrt{2N}}\sum_{j=0}^{2N-1} A(j\Delta X,T)\,e^{-\pi ij\nu/N}, \qquad \nu = 0,\pm1,\ldots,\pm N. \tag{36}$$

The inversion formula is

$$A(j\Delta X,T) = F^{-1}\widehat{A} = \frac{1}{\sqrt{2N}}\sum_{\nu}\widehat{A}(\nu,T)\,e^{\pi ij\nu/N}. \tag{37}$$

These transformations can use Fast Fourier Transform algorithm to efficiently perform. With this scheme, $\partial A/\partial X$ can be evaluated as $F^{-1}\{i\nu FA\}$, $\partial^3 A/\partial X^3$ as $-iF^{-1}\{\nu^3 FA\}$, $\partial H/\partial X$ as $F^{-1}\{i\nu FH\}$, and so on. Combined with a leap-frog time step, (27) would be approximated by

$$\begin{aligned} &A(X,T+\Delta T) - A(X,T-\Delta T) + i\alpha F^{-1}\{\nu FA\}\Delta T \\ &\quad + ia_1 AF^{-1}\{\nu FA\}\Delta T - a_2 iF^{-1}\left\{\nu^3 FA\right\}\Delta T \\ &\quad - a_3 F^{-1}\left\{\nu^2 F\mathscr{H}(A)\right\}\Delta T + \lambda A = iF^{-1}\{\nu FG\}\Delta T. \end{aligned} \tag{38}$$

The computational cost for (38) is six fast Fourier transforms per time step.

Once the zonal flow $\Omega(r)$ and the topography function $H(r,\Theta)$ as well as dissipative coefficient λ are given, it is easy to get the coefficients of (27) by employing (13). In order to simplify the calculation and to focus attention on the time evolution of the solitary waves with topography effect and dissipation effect and to show the difference among the KdV model, BO model, and rotational KdV-BO model, we take $a_1 = 1$, $a_2 = -1$, and $a_3 = -1$. As an initial condition, we take $A(X,0) = 0$. In the present numerical computation, the topography forcing is taken as $G = e^{-[30(\Theta-\pi)]^2/4}$.

4.1. Effect of Detuning Parameter α and Dissipation. In Figure 1, we consider the effect of detuning parameter α on solitary waves. The evolution features of solitary waves generated by topography are shown in the absence of dissipation with different detuning parameter α. It is easy to find from these waterfall plots that the detuning parameter α plays an important role for the evolution features of solitary waves generated by topography.

When $\alpha > 0$ (Figure 1(a)), a positive stationary solitary wave is generated in the topographic forcing region, and a modulated cnoidal wave-train occupies the downstream region. There is no wave in the upstream region. A flat buffer region exists between the solitary wave in the forcing region and modulated cnoidal wave-train in the downstream. With the detuning parameter α decreasing, the amplitudes of both solitary wave in the forcing region and modulated cnoidal wave-train in the downstream region increase and the modulated cnoidal wave-train closes to the forcing region gradually and the flat buffer region disappears slowly.

Up to $\alpha = 0$ (Figure 1(b)), the resonant case forms. In this case, a large amplitude nonstationary disturbance is generated in the forcing region. To some degree, this condition may explain the blocking phenomenon which exists in the atmosphere and ocean and generated by topographic forcing.

As $\alpha < 0$, from Figure 1(c) we can easy to find that a negative stationary solitary wave is generated in the forcing region, and this is great difference with the former two conditions. Meanwhile, there are both wave-trains in the upstream and downstream region. The amplitude and wavelength of wave-train in the upstream region are larger than those in the downstream regions. Similar to Figure 1(b) and unlike Figure 1(a), the wave-trains in the upstream and downstream regions connect to the forcing region and the flat buffer region disappears.

Figure 2 shows the solitary waves generated by topography in the presence of dissipation with dissipative coefficient $\lambda = 0.3$ and detuning parameter $\alpha = 2.5$. The conditions of $\alpha = 0$ and $\alpha < 0$ are omitted. Compared to Figure 1(a), we will

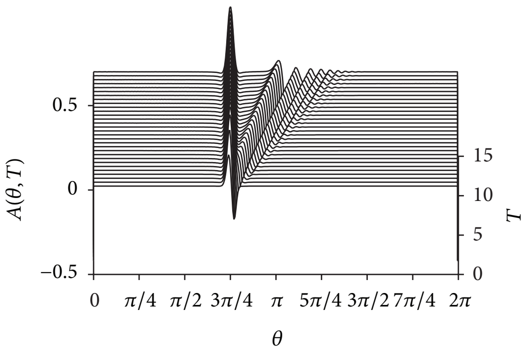

(a) $\alpha = 2.5$

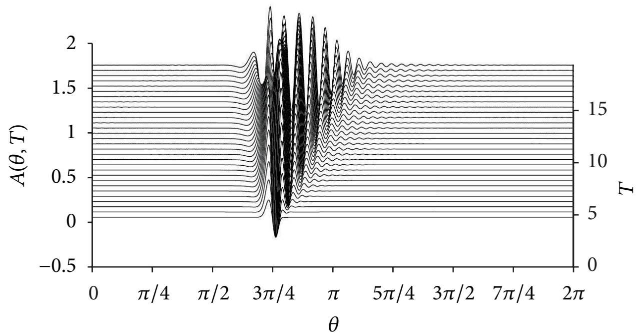

(b) $\alpha = 0$

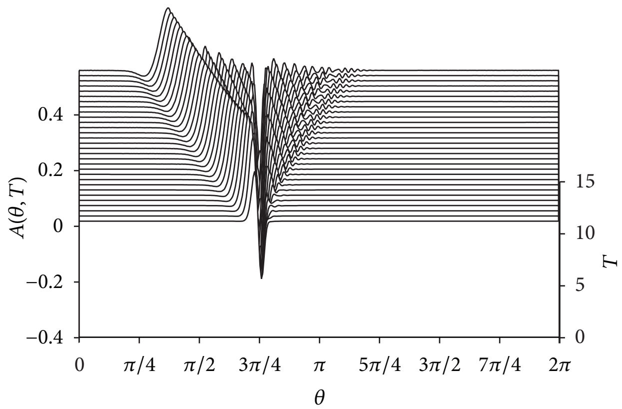

(c) $\alpha = -2.5$

FIGURE 1: Solitary waves generated by topography in the absence of dissipation.

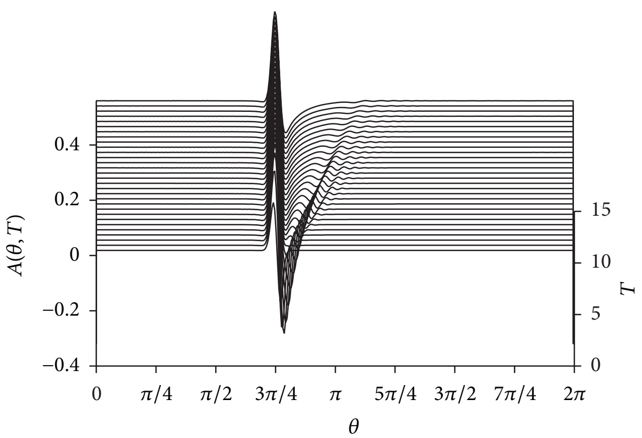

FIGURE 2: Solitary waves generated by topography in the presence of dissipation ($\lambda = 0.3$, $\alpha = 2.5$).

find that there is also a solitary wave generated in the forcing region, but because of dissipation effect the amplitude of solitary wave in the forcing region decreases as the dissipative coefficient λ increases (Figures omitted) and time evolution. Meanwhile, the modulated cnoidal wave-train in the downstream region is dissipated. When λ is big enough, the modulated cnoidal wave-train in the downstream region disappears.

4.2. Comparison of KdV Model, BO Model, and KdV-BO Model. We know that the rotation KdV-BO equation reduces to the KdV equation as $a_3 = 0$ and to the BO equation as $a_2 = 0$, so, in this subsection by comparing Figure 1(a) with Figure 3, we will look for the difference of solitary waves which is described by KdV-BO model, KdV model, and BO model. The role of detuning parameter α and dissipation effect has been studied in the former subsection, so here we only consider the condition of $\lambda = 0$, $\alpha = 2.5$.

At first, we can find that a positive solitary wave is all generated in the forcing region in Figures 1(a), 3(a) and 3(b), but it is stationary in Figures 1(a) and 3(a), and is nonstationary in Figure 3(b). By surveying carefully we find that the amplitude of stationary wave in the forcing region in Figure 1(a) is larger than that in Figure 3(a). Additionally, a modulated cnoidal wave-train is excited in the downstream region in Figures 1(a) and 3(a), and in both downstream and upstream region in Figure 3(b). The amplitude of modulated cnoidal wave-train in downstream region in Figure 3(b) is the largest and in Figure 1(a) is the smallest among the three models. Furthermore, in Figure 3(a) the wave number of modulated cnoidal wave-train is more than that in Figures 1(a) and 3(b). In a word, by the above analysis and comparison, it is easy to find that Figure 1(a) is similar to Figure 3(a) and has great difference with Figure 3(b). This indicates that the term $a_2(\partial^3 A/\partial\Theta^3)$ plays more important role than the term $a_3(\partial^2/\partial\Theta^2)\mathscr{H}(A)$ in rotational KdV-BO equation.

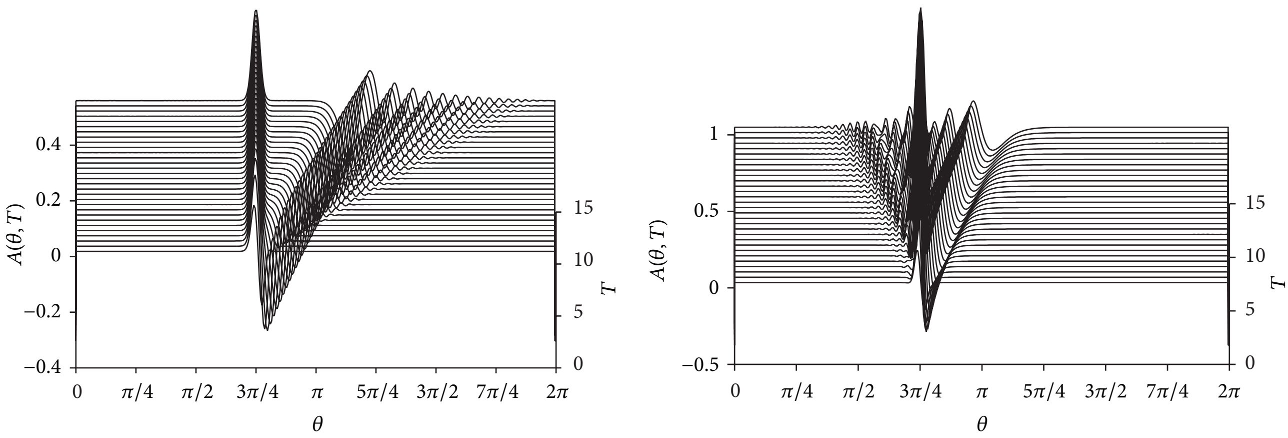

(a) KdV model ($a_3 = 0, \alpha = 2.5, \lambda = 0$)

(b) BO model ($a_2 = 0, \alpha = 2.5, \lambda = 0$)

FIGURE 3: Comparison of KdV model, Bo model, and KdV-BO model.

5. Conclusions

In this paper, we presented a new model: rotational KdV-BO-Burgers model to describe the Rossby solitary waves generated by topography with the effect of dissipation in deep rotational fluids. By analysis and computation, five conservation quantities of KdV-BO-Burgers model were derived and corresponding four conservation laws of Rossby solitary waves were obtained; that is, mass, momentum, energy, and velocity of the center of gravity of Rossby solitary waves are conserved without dissipation effect. Further, we presented that the rotational KdV-BO-Burgers equation owns infinite conservation quantities in the absence of dissipation effect. Detailed numerical results obtained using pseudospectral method are presented to demonstrate the effect of detuning parameter α and dissipation. By comparing the KdV model, BO model, and KdV-BO model, we drew the conclusion that the term $a_2(\partial^3 A/\partial\Theta^3)$ plays more important role than the term $a_3(\partial^2/\partial\Theta^2)\mathscr{H}(A)$ in rotational KdV-BO equation. More problems on KdV-BO-Burgers equation such as the analytical solutions, integrability, and infinite conservation quantities are not studied in the paper due to limited space. In fact, there are many methods carried out to solve some equations with special nonhomogenous terms [28] as well as multiwave solutions and other form solution [29, 30] of homogenous equation. These researches have important value for understanding and realizing the physical phenomenon described by the equation and deserve to carry out in the future.

Acknowledgments

This work was supported by Innovation Project of Chinese Academy of Sciences (no. KZCX2-EW-209), National Natural Science Foundation of China (nos. 41376030 and 11271107), Nature Science Foundation of Shandong Province of China (no. ZR2012AQ015), Science and Technology plan project of the Educational Department of Shandong Province of China (no. J12LI03), and SDUST Research Fund (no. 2012KYTD105).

References

[1] S. G. H. Philander, "Forced oceanic waves," *Reviews of Geophysics and Space Physics*, vol. 16, no. 1, pp. 15–46, 1978.

[2] R. R. Long, "Solitary waves in the westerlies," *Journal of the Atmospheric Sciences*, vol. 21, pp. 197–200, 1964.

[3] D. J. Benney, "Long non-linear waves in fluid flows," *Journal of Mathematical Physics*, vol. 45, pp. 52–63, 1966.

[4] L. G. Redekopp, "On the theory of solitary Rossby waves," *Journal of Fluid Mechanics*, vol. 82, no. 4, pp. 725–745, 1977.

[5] J. I. Yano and Y. N. Tsujimura, "The domain of validity of the KdV-type solitary Rossby waves in the shallow water BETA-plane model," *Dynamics of Atmospheres and Oceans*, vol. 11, no. 2, 1987.

[6] S. Jian and Y. Lian-Gui, "Modified KdV equation for solitary rossby waves with β effect in barotropic fluids," *Chinese Physics B*, vol. 18, no. 7, pp. 2873–2877, 2009.

[7] H. Ono, "Algebraic solitary waves in stratified fluids," vol. 39, no. 4, pp. 1082–1091, 1975.

[8] R. Grimshaw, "Slowly varying solitary waves in deep fluids," *Proceedings of the Royal Society A*, vol. 376, no. 1765, pp. 319–332, 1981.

[9] L. Dehai and J. Liren, "Algebraic rossby solitary wave and blocking in the atmosphere," *Advances in Atmospheric Sciences*, vol. 5, no. 4, pp. 445–454, 1988.

[10] L. Meng and K. L. Lv, "Dissipation and algebraic solitary long-waves excited by localized topography," *Chinese Journal of Computational Physics*, vol. 19, pp. 159–167, 2002.

[11] X. B. Su, G. Wei, and S. Q. Dai, "Two-dimensional algebraic solitary wave and its vertical structure in stratified fluid," *Applied Mathematics and Mechanics*, vol. 26, no. 10, pp. 1255–1265, 2005.

[12] T. Kubota, D. R. S. Ko, and L. D. Dobbs, "Weakly-nonlinear, long internal gravity waves in stratified fluids of finite depth," *Journal of Hydronautics*, vol. 12, no. 4, pp. 157–165, 1978.

[13] Q. P. Zhou, "Second-order solitary waves in stratified fluids of finite depth," *Science China Mathematics*, vol. 10, pp. 924–934, 1984.

[14] W. X. Ma, "Complexiton solutions to the Korteweg-de Vries equation," *Physics Letters A*, vol. 301, no. 1-2, pp. 35–44, 2002.

[15] W.-X. Ma, "Wronskians, generalized Wronskians and solutions to the Korteweg-de Vries equation," *Chaos, Solitons & Fractals*, vol. 19, no. 1, pp. 163–170, 2004.

[16] W.-X. Ma and Y. You, "Solving the Korteweg-de Vries equation by its bilinear form: wronskian solutions," *Transactions of the American Mathematical Society*, vol. 357, no. 5, pp. 1753–1778, 2005.

[17] T. C. Xia, H. Q. Zhang, and Z. Y. Yan, "New explicit and exact travelling wave solutions for a class of nonlinear evolution equations," *Applied Mathematics and Mechanics*, vol. 22, no. 7, pp. 788–793, 2001.

[18] H.-Y. Wei and T.-C. Xia, "Self-consistent sources and conservation laws for nonlinear integrable couplings of the Li soliton hierarchy," *Abstract and Applied Analysis*, vol. 2013, Article ID 598570, 10 pages, 2013.

[19] S. I. A. El-Ganaini, "New exact solutions of some nonlinear systems of partial differential equations using the first integral method," *Abstract and Applied Analysis*, vol. 2013, Article ID 693076, 13 pages, 2013.

[20] D. H. Luo, "Nonlinear schrödinger equation in the rotational atmosphere and atmospheric blocking," *Acta Meteor Sinica*, vol. 48, pp. 265–274, 1990.

[21] O. E. Polukhina and A. A. Kurkin, "Improved theory of nonlinear topographic Rossby waves," *Oceanology*, vol. 45, no. 5, pp. 607–616, 2005.

[22] L. G. Yang, C. J. Da, J. Song, H. Q. Zhang, H. L. Yang, and Y. J. Hou, "Rossby waves with linear topography in barotropic fluids," *Chinese Journal of Oceanology and Limnology*, vol. 26, no. 3, pp. 334–338, 2008.

[23] J. Song and L.-G. Yang, "Force solitary Rossby waves with beta effect and topography effect in stratified flows," *Acta Physica Sinica*, vol. 59, no. 5, pp. 3309–3314, 2010.

[24] H.-W. Yang, B.-S. Yin, D.-Z. Yang, and Z.-H. Xu, "Forced solitary Rossby waves under the influence of slowly varying topography with time," *Chinese Physics B*, vol. 20, no. 12, Article ID 120203, 2011.

[25] H. W. Yang, Y. L. Shi, B. S. Yin, and Q. B. Wang, "Forced ILW-Burgers equation as a model for Rossby solitary waves generated by topography in finite depth fluids," *Journal of Applied Mathematics*, vol. 2012, Article ID 491343, 17 pages, 2012.

[26] B. Fornberg, *A Practical Guide to Pseudospectral Methods*, Cambridge University Press, Cambridge, UK, 1996.

[27] J. Pedlosky, *Geophysical Fluid Dynamics*, Springer, New York, NY, USA, 1979.

[28] W. X. Ma and B. Fuchssteiner, "Explicit and exact solutions to a Kolmogorov-Petrovskii-Piskunov equation," *International Journal of Non-Linear Mechanics*, vol. 31, no. 3, pp. 329–338, 1996.

[29] M. G. Asaad and W.-X. Ma, "Pfaffian solutions to a (3 + 1)-dimensional generalized B-type Kadomtsev-Petviashvili equation and its modified counterpart," *Applied Mathematics and Computation*, vol. 218, no. 9, pp. 5524–5542, 2012.

[30] B. G. Zhang, "Analytical and multishaped solitary wave solutions for extended reduced ostrovsky equation," *Abstract and Applied Analysis*, vol. 2013, Article ID 670847, 8 pages, 2013.

Hindawi Publishing Corporation
Abstract and Applied Analysis
Volume 2013, Article ID 614874, 14 pages
http://dx.doi.org/10.1155/2013/614874

Research Article

A One Step Optimal Homotopy Analysis Method for Propagation of Harmonic Waves in Nonlinear Generalized Magnetothermoelasticity with Two Relaxation Times under Influence of Rotation

S. M. Abo-Dahab,[1,2] Mohamed S. Mohamed,[1,3] and T. A. Nofal[1,4]

[1] *Mathematics Department, Faculty of Science, Taif University, P.O. Box 888, Saudi Arabia*
[2] *Mathematics Department, Faculty of Science, South Valley University, Qena 83523, Egypt*
[3] *Mathematics Department, Faculty of Science, Al-Azhar University, Nasr City 11884, Cairo, Egypt*
[4] *Mathematics Department, Faculty of Science, Minia University, Minia, Egypt*

Correspondence should be addressed to Mohamed S. Mohamed; m_s_mohamed2000@yahoo.com

Received 1 May 2013; Revised 2 June 2013; Accepted 4 June 2013

Academic Editor: Santanu Saha Ray

The aim of this paper is to apply OHAM to solve numerically the problem of harmonic wave propagation in a nonlinear thermoelasticity under influence of rotation, thermal relaxation times, and magnetic field. The problem is solved in one-dimensional elastic half-space model subjected initially to a prescribed harmonic displacement and the temperature of the medium. The HAM contains a certain auxiliary parameter which provides us with a simple way to adjust and control the convergence region and rate of convergence of the series solution. This optimal approach has a general meaning and can be used to get fast convergent series solutions of the different type of nonlinear fractional differential equation. The displacement and temperature are calculated for the models with the variations of the magnetic field, relaxation times, and rotation. The results obtained are displayed graphically to show the influences of the new parameters.

1. Introduction

In the past recent years, much attention has been devoted to simulate some real-life problems which can be described by nonlinear coupled differential equations using reliable and more efficient methods. Nonlinear partial differential equations are useful in describing various phenomena in disciplines. The nonlinear coupled systems of partial differential equations often appear in the study of circled fuel reactor, high-temperature hydrodynamics, and thermoelasticity problems, see [1–4]. From the analytical point of view, a lot of work has been done for such systems. With the rapid development of nanotechnology, there appears an ever increasing interest of scientists and researchers in this field of science. Nanomaterials, because of their exceptional mechanical, physical, and chemical properties, have been the main topic of research in many scientific publications. Wave generation in nonlinear thermoelasticity problems has gained a considerable interest for its utilitarian aspects in understanding the nature of interaction between the elastic and thermal fields as well as the system of PDEs for its applications. A lot of applications were paid on existence, uniqueness, and stability of the solution of the problem, see [5–7].

Recently, much attention has been devoted to numerical methods, which do not require discretization of space-time variables or linearization of the nonlinear equations, among the homotopy analysis methods. Since most of the nonlinear FDEs cannot be solved exactly, approximate and numerical methods must be used. Some of the recent analytical methods for solving nonlinear problems include the homotopy analysis method HAM [8–14]. The HAM, first proposed in 1992 by Liao [8], has been successfully applied to solve many problems in physics and science. This method is applied to solve linear and nonlinear systems.

The homotopy perturbation method HPM has the merits of simplicity and easy execution. The homotopy perturbation method was first proposed by He [15]. Unlike the traditional numerical methods, the HPM does not need discretization and linearization. Most perturbation methods assume that a small parameter exists, but most nonlinear problems have no small parameter at all. Many new methods have been proposed to eliminate the small parameter. Recently, the applications of homotopy theory among scientists appeared, and the homotopy theory became a powerful mathematical tool, when it is successfully coupled with perturbation theory.

Recently, Gepreel et al. [16] investigated the homotopy perturbation method and variational iteration method for harmonic waves propagation in nonlinear magnetothermoelasticity with rotation. Abd-Alla and Abo-Dahab [17] investigated the effect of rotation and initial stress on an infinite generalized magnetothermoelastic diffusion body with a spherical cavity. Abo-Dahab and Mohamed [18] studied the influence of magnetic field and hydrostatic initial stress on reflection phenomena of P (Primary) and SV (Shear Vertical) waves from a generalized thermoelastic solid half space. Abd-Alla and Mahmoud [19] investigated the magnetothermoelastic problem in rotating non-homogeneous orthotropic hollow cylinder under the hyperbolic heat conduction model. Abd-Alla et al. [20] studied the thermal stresses effect in a non-homogeneous orthotropic elastic multilayered cylinder. Abd-Alla et al. [21] studied the generalized magnetothermoelastic Rayleigh waves in a granular medium under the influence of a gravity field and initial stress. Abd-Alla and Abo-Dahab [22] investigated the time-harmonic sources in a generalized magnetothermoviscoelastic continuum with and without energy dissipation.

In the present paper, investigation is devoted for solving numerically the problem of harmonic wave propagation in a nonlinear thermoelasticity under influence of magnetic field, thermal relaxation times, and rotation. The problem is solved in one-dimensional elastic half-space model subjected initially to a prescribed harmonic displacement and the temperature of the medium.

The HAM contains a certain auxiliary parameter which provides us with a simple way to adjust and control the convergence region and rate of convergence of the series solution. The h-curve of the third-order approximate solutions is displayed graphically to show the interval that the exact and approximate solutions take the same values. The displacement and temperature are calculated for the methods with the variations of the magnetic field and rotation. The results obtained are displayed graphically to show the influences of the new parameters.

2. A One-Step Optimal Homotopy Analysis Method for PDEs

To describe the basic ideas of the HAM, we consider the following general nonlinear differential equation:

$$N\left[u\left(x,t\right)\right]=0, \tag{1}$$

where N is a nonlinear operator for this problem, x and t denote independent variables, and $u(x,t)$ is an unknown function.

By means of the HAM, one first constructs the following zero-order deformation equation:

$$\left(1-q\right)\mathscr{L}\left(\phi\left(x,t;q\right)-u_0\left(x,t\right)\right)=qhH\left(t\right)N\left[\phi\left(x,t;q\right)\right], \tag{2}$$

where $q\in[0,1]$ is the embedding parameter, $h\neq 0$ is an auxiliary parameter, $H(t)\neq 0$ is an auxiliary function, $\mathscr{L}$ is an auxiliary linear operator, and $u_0(x,t)$ is an initial guess. Obviously, when $q=0$ and $q=1$, it holds

$$\phi\left(x,t;0\right)=u_0\left(x,t\right),\qquad \phi\left(x,t;1\right)=u\left(x,t\right). \tag{3}$$

Liao [8, 9] expanded $\phi(x,t;q)$ in Taylor series with respect to the embedding parameter q, as follows:

$$\phi\left(x,t;q\right)=u_0\left(x,t\right)+\sum_{m=1}^{\infty}u_m\left(x,t\right)q^m, \tag{4}$$

where

$$u_m\left(x,t\right)=\frac{1}{m!}\left.\frac{\partial^m\phi\left(x,t;q\right)}{\partial q^m}\right|_{q=0}. \tag{5}$$

Assume that the auxiliary linear operator, the initial guess, the auxiliary parameter h, and the auxiliary function $H(t)$ are selected such that the series (4) is convergent at $q=1$; then we have from (4)

$$u\left(x,t\right)=u_0\left(x,t\right)+\sum_{m=1}^{\infty}u_m\left(x,t\right). \tag{6}$$

Let us define the vector

$$\vec{u}_n\left(x,t\right)=\left\{u_0\left(x,t\right),u_1\left(x,t\right),u_2\left(x,t\right),\ldots,u_n\left(x,t\right)\right\}. \tag{7}$$

Differentiating (2) m times with respect to q, then setting $q=0$ and dividing then by $m!$, we have the following mth-order deformation equation:

$$\mathscr{L}\left(u_m\left(x,t\right)-\varkappa_m u_{m-1}\left(x,t\right)\right)=hH\left(t\right)\mathscr{R}_m\left(\vec{u}_{m-1}\right), \tag{8}$$

where

$$\begin{gathered}\mathscr{R}_m\left(\vec{u}_{m-1}\right)=\frac{1}{(m-1)!}\left.\frac{\partial^{m-1}\mathscr{N}\left[\phi\left(x,t;q\right)\right]}{\partial q^{m-1}}\right|_{q=0},\\ \varkappa_m=\begin{cases}0, & m\leq 1,\\ 1, & m>1.\end{cases}\end{gathered} \tag{9}$$

Applying the integral operator on both sides of (8), we have

$$u_m\left(x,t\right)=\varkappa_m u_{m-1}\left(x,t\right)+h\int_0^t H\left(t\right)\mathscr{R}_m\left(\vec{u}_{m-1}\right)dt, \tag{10}$$

where the mth-order deformation equation (8) can be easily solved, especially by means of symbolic computation software such as Mathematica, Maple, and MathLab. The convergence of the homotopy analysis method for solving these equations is discussed in [23].

Abbasbandy and Jalili [24] and Turkyilmazoglu [25–29] applied the homotopy analysis method to nonlinear ODEs and suggested the so-called optimization method to find out the optimal convergence control parameters by minimum of the square residual error integrated in the whole region having physical meaning. Their approach is based on the square residual error.

Let $\Delta(h)$ denote the square residual error of the governing equation (1) and express it as

$$\Delta(h) = \int_{\Omega} \left(N\left[\tilde{u}_n(t)\right]\right)^2 d\Omega, \tag{11}$$

where

$$\tilde{u}_m(t) = u_0(t) + \sum_{k=1}^{m} u_k(t); \tag{12}$$

the optimal value of h is given by a nonlinear algebraic equation:

$$\frac{d\Delta(h)}{dh} = 0. \tag{13}$$

3. Application of HAM on the Nonlinear Magnetothermoelastic with Rotation Equations

In this section, we use the homotopy analysis method to calculate the approximate solutions of the following nonlinear magnetothermoplastic model with rotation equations

$$\begin{aligned}
&(1+\sigma_1)u_{tt} + \Omega u_t - u_{xx}\left(1-\sigma_2+2\gamma u_x+3\delta u_x^2\right) \\
&\qquad - \beta_1(1-i\omega\tau_2)\theta_x - \beta_2(\theta u_x)_x = 0, \\
&\left(\theta(1-i\omega\tau_1) - a u_x(1-i\omega\delta\tau_1) - \frac{1}{2}b u_x^2\right)_t \\
&\qquad - \left[(1+\alpha u_x)\theta_x\right]_x = 0,
\end{aligned} \tag{14}$$

where σ_1, σ_2, Ω, γ, β_1, β_2, a, b, and α are arbitrary constants with the initial conditions

$$\begin{aligned}
u(x,0) = \theta(x,0) &= A(1-\cos(x)), \\
u_t(x,0) = \theta_t(x,0) &= 0,
\end{aligned} \tag{15}$$

where A is an arbitrary constant and the boundary conditions

$$\begin{aligned}
u(0,t) = \theta(0,t) &= 0, \\
u_t(0,t) = \theta_t(0,t) &= 0.
\end{aligned} \tag{16}$$

To demonstrate the effectiveness of the method, we consider the system of nonlinear initial-value problem (14) with the initial conditions (15) and the boundary conditions (16) by choosing the linear operators

$$\begin{aligned}
\mathscr{L}_1\left[\phi_1(x,t;q)\right] &= \frac{\partial^2\phi_1(x,t;q)}{\partial t^2}, \\
\mathscr{L}_2\left[\phi_2(x,t;q)\right] &= \frac{\partial\phi_2(x,t;q)}{\partial t},
\end{aligned} \tag{17}$$

with the property $\mathscr{L}_1[c_1 + c_2 t] = 0$, $\mathscr{L}_2[c_3]$, where c_i, ($i = 1, 2, 3$) are the integral constants and the nonlinear operators are defined as

$$\begin{aligned}
N_1[\phi_1,\phi_2] &= (1+\sigma_1)\frac{\partial^2\phi_1}{\partial t^2} + \Omega\frac{\partial\phi_1}{\partial t} - \frac{\partial^2\phi_1}{\partial x^2} \\
&\quad \times\left(1-\sigma_2+2\gamma\frac{\partial\phi_1}{\partial x}+3\delta\left(\frac{\partial\phi_1}{\partial x}\right)^2\right) - \beta_1\frac{\partial\phi_2}{\partial x} \\
&\quad + i\omega\tau_2\beta_1\frac{\partial\phi_2}{\partial x} - \beta_2\frac{\partial}{\partial x}\left(\phi_2\frac{\partial\phi_1}{\partial x}\right), \\
N_2[\phi_1,\phi_2] &= \frac{\partial}{\partial t}\left((1-i\omega\tau_1)\phi_2 - a(1-i\omega\tau_1\delta)\frac{\partial\phi_1}{\partial x}\right. \\
&\quad \left. -\frac{1}{2}b\left(\frac{\partial\phi_1}{\partial x}\right)^2 - \frac{\partial}{\partial x}\left(1+\alpha\frac{\partial\phi_1}{\partial x}\right)\frac{\partial\phi_2}{\partial x}\right).
\end{aligned} \tag{18}$$

Choosing $H_i(t) = 1$ for $i = 1, 2$, the zeroth-order deformation equations are

$$\begin{aligned}
&(1-q)\mathscr{L}_1\left[\phi_1(x,t;q) - u_0(x,t)\right] \\
&\qquad = qh_1N_1\left[\phi_1(x,t;q),\phi_2(x,t;q)\right], \\
&(1-q)\mathscr{L}_2\left[\phi_2(x,t;q) - v_0(x,t)\right] \\
&\qquad = qh_2N_2\left[\phi_1(x,t;q),\phi_2(x,t;q)\right],
\end{aligned} \tag{19}$$

where

$$\begin{aligned}
\phi_1(x,t;0) &= u_0(x,t), \qquad \phi_1(x,t;1) = u(x,t), \\
\phi_2(x,t;0) &= v_0(x,t), \qquad \phi_2(x,t;1) = \theta(x,t).
\end{aligned} \tag{20}$$

Then, the mth-order deformation equations become

$$\begin{aligned}
\mathscr{L}_1\left[u_m(x,t) - \varkappa_m u_{m-1}(x,t)\right] &= h_1\mathscr{R}_{1m}\left(\vec{u}_{m-1},\vec{\theta}_{m-1}\right), \\
\mathscr{L}_2\left[\theta_m(x,t) - \varkappa_m \theta_{m-1}(x,t)\right] &= h_2\mathscr{R}_{2m}\left(\vec{u}_{m-1},\vec{\theta}_{m-1}\right),
\end{aligned} \tag{21}$$

where

$$\begin{aligned}
&\mathscr{R}_{1m}\left(\vec{u}_{m-1},\vec{\theta}_{m-1}\right)\\
&\quad=\frac{\partial^2 u_{m-1}}{\partial t^2}\\
&\qquad+\frac{1}{1+\sigma_1}\Bigg(\Omega(u_{m-1})_t-(u_{m-1})_{xx}+\sigma_2(u_{m-1})_{xx}\\
&\qquad\qquad-2\gamma\sum_{j=0}^{m-1}\left(u_j\right)_{xx}\left(u_{m-1-j}\right)_x\\
&\qquad\qquad-3\delta\sum_{i=0}^{m-1}\sum_{j=0}^{i}\left(u_j\right)_x\left(u_{i-j}\right)_x\left(u_{m-1-i}\right)_{xx}\\
&\qquad\qquad-\beta_2\sum_{j=0}^{m-1}\left(\theta_j\right)_x\left(u_{m-1-j}\right)_x-\beta_1\left(\theta_{m-1}\right)_x\\
&\qquad\qquad-\beta_2\sum_{j=0}^{m-1}\left(\theta_j\right)\left(u_{m-1-j}\right)_{xx}+i\omega\tau_2\beta_1\theta_{m-1}\Bigg),\\
&\mathscr{R}_{2m}\left(\vec{u}_{m-1},\vec{\theta}_{m-1}\right)\\
&\quad=\frac{\partial\theta_{m-1}}{\partial t}+\frac{1}{1-i\omega\tau_1}\Bigg(-a(u_{m-1})_{xt}\\
&\qquad\qquad-\frac{1}{2}b\sum_{j=0}^{m-1}\left(u_j\right)_{xt}\left(u_{m-1-j}\right)_{xt}\\
&\qquad\qquad-\left(\theta_{m-1}\right)_{xx}\\
&\qquad\qquad-\alpha\sum_{j=0}^{m-1}\left(\theta_{m-1-j}\right)_x\left(u_j\right)_{xx}\\
&\qquad\qquad-\alpha\sum_{j=0}^{m-1}\left(\theta_{m-1-j}\right)_{xx}\left(u_j\right)_x\\
&\qquad\qquad-\left(\theta_{m-1}\right)_{xx}+ai\omega\tau_1\delta(u_{m-1})_{xt}\Bigg).
\end{aligned}\tag{22}$$

For simplicity, we suppose $h_1 = h_2$; the system (21) has the following general solutions:

$$\begin{aligned}
u_m(x,t)&=\varkappa_m u_{m-1}(x,t)+h\iint_0^t\mathscr{R}_{1m}\left(\vec{u}_{m-1},\vec{\theta}_{m-1}\right)dt\,dt,\\
\theta_m(x,t)&=\varkappa_m\theta_{m-1}(x,t)+h\int_0^t\mathscr{R}_{2m}\left(\vec{u}_{m-1},\vec{\theta}_{m-1}\right)dt.
\end{aligned}\tag{23}$$

In this case, where u_0 and θ_0 are constants, the general solution of (23) is taking the following form:

$$\begin{aligned}
u(x,t)&=u_0(x,t)+\sum_{m=1}^{\infty}u_m(x,t),\\
\theta(x,t)&=\theta_0(x,t)+\sum_{m=1}^{\infty}\theta_m(x,t).
\end{aligned}\tag{24}$$

The problems above can be readily solved by symbolic computation packages such as Mathematica. Thereupon, successive solving of these problems yields

$$\begin{aligned}
u_0(x,0)&=A(1-\cos(x)),\\
\theta_0(x,0)&=A(1-\cos(x)),\\
u_1(x,t)&=\frac{Aht^2}{4(1+\sigma_1)}\Big(2A\beta_2(-\cos(x)+\cos(2x))\\
&\qquad+\cos(x)\Big(-2-3A^2\delta\\
&\qquad\qquad+3A^2\delta\cos(2x)\\
&\qquad\qquad-4A\gamma\sin(x)+2\sigma_2\Big)\\
&\qquad+2i\sin(x)\beta_1\left(i+\omega\tau_2\right)\Big),\\
\theta_1(x,t)&=\frac{Aht\cos(x)(1+2A\alpha\sin(x))}{-1+i\omega\tau_1},\\
u_2(x,t)&\\
&=\frac{Aht^2}{4(1+\sigma_1)}\\
&\quad\times\Big(2A\beta_2(-\cos(x)+\cos(2x))+\cos(x)\\
&\qquad\times\Big(-2-3A^2\delta+3A^2\delta\cos(2x)\\
&\qquad\quad-4A\gamma\sin(x)+2\sigma_2\Big)\\
&\qquad+2i\sin(x)\beta_1\left(i+\omega\tau_2\right)\Big)\\
&\quad+\frac{1}{384(1+\sigma_1)^2}\\
&\quad\times\Big(Ah^2t^4\Big(-135A^4\delta^2\cos(5x)\\
&\qquad+240A^3\delta\gamma\sin(4x)-16A^2\\
&\qquad\times(2\cos(x)-5\cos 2(x)+3\cos(3x))\\
&\qquad\times\beta_2^2-96A\gamma\sin(2x)\\
&\qquad\times\left(1+2A^2\delta-\sigma_2\right)+3A^2\cos(3x)\\
&\qquad\times\left(48\delta+63A^2\delta^2+32\gamma^2-48\delta\sigma_2\right)
\end{aligned}$$

$$
\begin{aligned}
&+ 8A\beta_2 \Big(-2\left(2+3A^2\delta\right)\cos(x) \\
&\quad + 10\cos(2x) \\
&\quad + A\,(3A\delta\,(3\cos(2x) \\
&\qquad + 6\cos(3x) \\
&\qquad - 7\cos(4x)) \\
&\quad - 2\gamma\,(\sin(x) \\
&\qquad + 6\sin(2x) \\
&\qquad - 9\sin(3x))) \\
&\quad + 2\,(2\cos(x) \\
&\qquad - 5\cos(2x))\,\sigma_2\Big) \\
&- 2\cos(x)\Big(8 + A^2 \\
&\quad \times\left(3\delta\left(8+9A^2\delta\right)\right. \\
&\qquad \left.+16\gamma^2\right) \\
&\quad + 8\sigma_2\left(-2-3A^2\delta+\sigma_2\right)\Big) \\
&+ 4i\beta_1\,(4\sin(x) \\
&\quad + A\left(-8\gamma\cos(2x)\right. \\
&\qquad + 3A\delta\,(\sin(x) \\
&\qquad - 3\sin(3x))) \\
&\quad - 4\sin(x)\,(A\,(-1 + 2\cos(x)) \\
&\qquad \times\beta_2 + \sigma_2)) \\
&\times\left(i+\omega\tau_0\right)\Big)\Big) \\
&- \frac{1}{24\left(1+\sigma_1\right)^2\left(i+\omega\tau_1\right)} \\
&\times\Big(Ah^2t^3\Big(-2-3A^2\delta+3A^2\delta\cos(2x) \\
&\quad -4A\gamma\sin(x)+2\sigma_2\Big) \\
&\quad \times\left(i+\omega\tau_1\right) + 2A\beta_2 \\
&\quad \times\left(iA\alpha\sin(x)\left(1+\sigma_1\right) - 3Ai\alpha\sin(3x)\right. \\
&\qquad \times\left(1+\sigma_1\right) + 2\Omega\cos(x)\left(i+\omega\tau_1\right) \\
&\qquad \left.- 2i\cos(2x)\left(1+\Omega+\sigma_1-i\Omega\omega\tau_1\right)\right) \\
&\quad + 4\beta_1\left(i+\omega\tau_2\right) \\
&\quad \times\left(-2A\alpha\cos(2x)\left(1+\sigma_1\right)\right. \\
&\qquad \left.+ \sin(x)\left(1+\Omega+\sigma_1-i\omega\Omega\tau_1\right)\right)\Big),
\end{aligned}
$$

$$
\begin{aligned}
\theta_2(x,t) &= \frac{Ah\,(1+h)\,t\cos(x)\,(1+2A\alpha\sin(x))}{-1+i\omega\tau_1} \\
&+ \frac{A^2h^2t^3\alpha}{6\left(1+\sigma_1\right)\left(i+\omega\tau_1\right)} \\
&\times\Big(-\frac{1}{2}i\,\Big(2A\gamma\cos(x) - 6A\gamma\cos(3x) \\
&\qquad - 9A^2\delta\sin(4x) \\
&\qquad + 2A\,(\sin(x)+\sin(2x) \\
&\qquad\quad - 3\sin(3x))\,\beta_2 \\
&\qquad + 2\sin(2x)\left(1+3A^2\delta-\sigma_2\right)\Big) \\
&\quad + \cos(2x)\,\beta_1\left(i+\omega\tau_2\right) \\
&\quad + \frac{1}{8\left(i+\omega\tau_1\right)} \\
&\quad \times\Big(iAh^2t^2 \\
&\qquad \times\Big(\frac{a}{1+\sigma_1} \\
&\qquad\quad \times(-4\sin(x) \\
&\qquad\qquad + A\,(8\nu\cos(2x) \\
&\qquad\qquad\quad - 3A\delta\,(\sin(x) \\
&\qquad\qquad\qquad - 3\sin(3x))) \\
&\qquad\qquad + 4\sin(x)\left(A\,(-1+4\cos(x))\right. \\
&\qquad\qquad\qquad \left.\times\beta_2+\sigma_2\right) \\
&\qquad\qquad + 4\cos(x)\,\beta_1\left(1-i\omega\tau_2\right)) \\
&\qquad\quad + \frac{ia\omega\delta_1}{1+\sigma_1}\,(4\sin(3x) \\
&\qquad\qquad + A\,(-8\nu\cos(x) \\
&\qquad\qquad\quad + 3A\delta\,(\sin(x) \\
&\qquad\qquad\qquad - 3\sin(3x))) \\
&\qquad\qquad - 4\sin(x)\,(A\,(-1 \\
&\qquad\qquad\qquad + 4\cos(x)) \\
&\qquad\qquad\qquad \times\beta_2+\sigma_2) \\
&\qquad\qquad + 4i\cos(x)\,\beta_1\left(i+\omega\tau_2\right)) \\
&\qquad \times\tau_1 - \frac{1}{i+\omega\tau_1} \\
&\qquad \times 4i\Big(\Big(1+A^2 \\
&\qquad\quad + \alpha^2\cos(x) + A\alpha
\end{aligned}
$$

Table 1: The optimal values of h at third-order approximate solutions of (14) when $x = 1.0$, $t = 1.0$, for $\delta = 1$, $\sigma_1 = 0.2$, $\sigma_2 = 0.1$, $\Omega = 0.1$, and $\omega = 0.02$.

τ_1	τ_2	Optimal value of h	Minimum value
		$u(1,1)$	
1	0	−0.95623	1.37312×10^{-3}
0	1	−0.97543	7.9675×10^{-7}
		$\theta(1,1)$	
1	0	−0.95623	1.3242×10^{-2}
0	1	−0.97543	2.1432×10^{-5}

Table 2: The optimal values of h at 5th-order approximate solutions of (14) when $x = 1.0$, $t = 1.0$, for $\delta = 1$, $\sigma_1 = 0.2$, $\sigma_2 = 0.1$, $\Omega = 0.1$, and $\omega = 0.02$.

τ_1	τ_2	Optimal value of h	Minimum value
		$u(1,1)$	
1	0	−0.990321	1.37312×10^{-7}
0	1	−0.995339	7.9675×10^{-9}
		$\theta(1,1)$	
1	0	−0.990321	1.3242×10^{-4}
0	1	−0.995339	2.1432×10^{-6}

$$\times (-3A \times \alpha \cos(3x) + 5 \sin(2x)))\Big)\Big). \quad (25)$$

Now we make calculations for the results obtained by the HAM using the Mathematica software package with the following arbitrary constants:

$$a = 0.5, \quad A = 0.001, \quad b = 0.5, \quad \alpha = 1,$$
$$\beta_1 = 0.5, \quad \beta_2 = 0.05, \quad \gamma = 1, \quad \delta = 0.8, \quad (26)$$
$$\Omega = 1, \quad \sigma_1 = 0.2, \quad \sigma_2 = 0.1.$$

To investigate the influence of h on the convergence of the solution series given by the HAM, we first plot the so-called h-curves of $u(1,1)$ and $\theta(1,1)$. According to the h-curves, it is easy to discover the valid region of h. We used 3 terms in evaluating the approximate solution $u(x,t) \cong \sum_{i=0}^{2} u_i(x,t)$ and $\theta(x,t) \cong \sum_{i=0}^{2} \theta_i(x,t)$. Note that the solution series contains the auxiliary parameter h which provides us with a simple way to adjust and control the convergence of the solution series. In general, by means of the so-called h-curve that is, a curve of a versus h. As pointed by Liao [8] and Turkyilmazoglu [25], the valid region of h is a horizontal line segment. Therefore, it is straightforward to choose an appropriate range for h which ensures the convergence of the solution series (Tables 1 and 2). We sketch the h-curve of $u(1,1)$ and $\theta(1,1)$ in Figure 1, which shows that the solution series is convergent when $-1.45 < h < -0.5$.

4. Discussion

In order to gain physical insight, the temperature T and radial displacement u have been discussed by assigning numerical values to the parameter encountered in the problem in which the numerical results are displayed with the graphical illustrations in 2D and 3D formats. The variations are shown in Figures 1–15, with the view of illustrating the theoretical results obtained in the preceding sections; a numerical result is calculated for the homotopy analysis method.

Figures 1 and 2 display the h-curve of the third-order approximate solutions (14) when $x = 1.0$, $t = 1.0$; it is concluded that the displacement $u(1,1)$ and temperature $\theta(1,1)$ increase with increasing the values of h to their maxima and then decrease with the high values of h; also, it is shown that $u(1,1)$ is convergent when $-0.9 < h < -0.6$ and $\theta(1,1)$ is convergent when $-0.6 < h < -0.4$.

Figures 2–7 show the variations of the radial displacement and temperature with respect to axial x, respectively, for different values of the time t, rotation Ω, and sensitive parts of the magnetic fields σ_1 and σ_2. In both figures, it is clear that the radial displacement and temperature have a zero value only in a bounded region of space. It is observed from Figure 3 that the displacement u and the temperature θ start from their maximum values, decrease, and increase periodically with an increase of the coordinate x; also, it is obvious that their values take the minimum values and increases with the increasing values of the time t. From Figure 4, one can see that u and θ decrease with an increase of the rotation Ω. It is shown that the components of the displacement u and the temperature θ start from the minimum values near zero, increase, and then decrease periodically with the coordinate x; it is clear also that there is a slight increase with an increase of the sensitive parts of the magnetic field (see, Figures 5 and 6). It is shown that the increasing of the coordinate x sensitive an increasing and decreasing on them periodically due to appearance of the pairs (cos, sin) in the initial condition and the approximate solutions; it is also clear that the components begin from their minimum values and increase absolutely with the variation of the time t. The variations of the rotation and magnetic field tend to slightly affect the displacement and the temperature.

From Figures 7 and 8 (GL model), it is clear that the displacement component and temperature if the rotation and magnetic field are vanish, take larger values than the corresponding values with the rotation and magnetic field effects.

Figures 9, 10, and 11 show the variations of the displacement and temperature with respect to the time t with LS and GL models; it is shown that the radial displacement and the temperature increase with an increase of t that takes a slight change with the rotation Ω if $\sigma_1 = \sigma_2 = 0$, σ_1 if $\Omega = \sigma_2 = 0$, and σ_2 if $\Omega = \sigma_1 = 0$.

Figures 12 and 13 show clearly the variations of the displacement and temperature in the presence and absence of the rotation and sensitive magnetic field; it is observed that u and θ in presence of the parameters are smaller than the

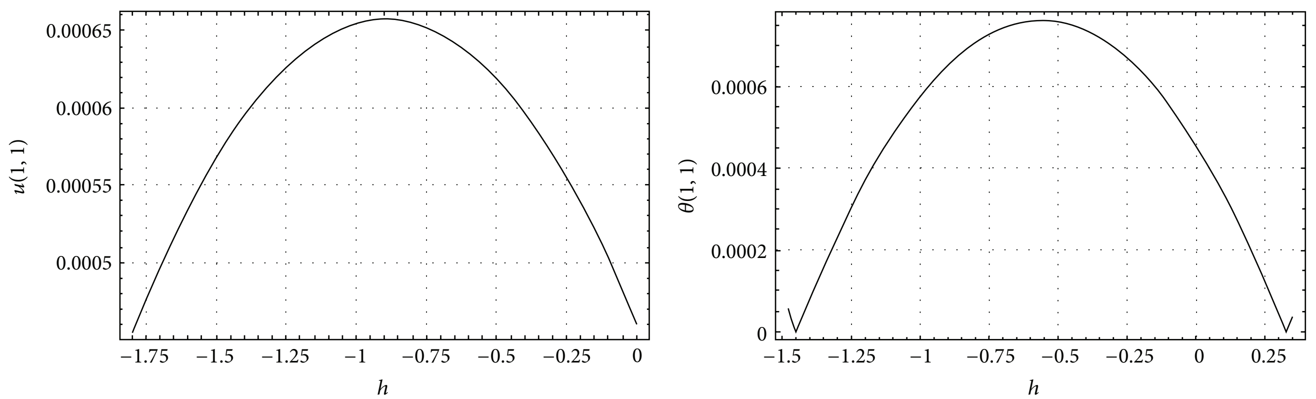

(a) (b)

Figure 1: The h-curve of the third-order approximate solutions of (14) when $x = 1.0$, $t = 1.0$; for LS model when $\tau_2 = 0$, $\tau_1 = 1$, $\delta = 1$, $\sigma_1 = 0.2$, $\sigma_2 = 0.1$, $\Omega = 0.1$, and $\omega = 0.02$.

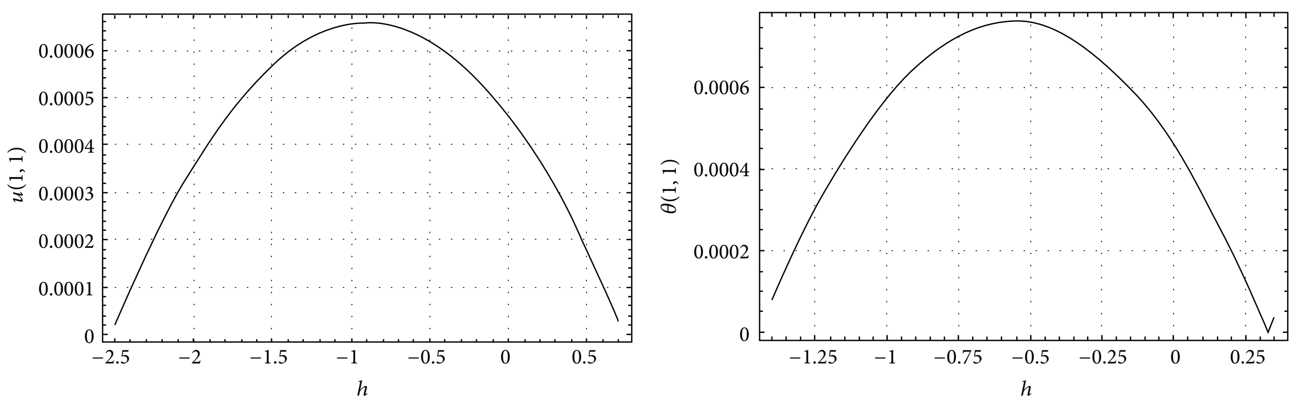

(a) (b)

Figure 2: The h-curve of the third-order approximate solutions of (14) when $x = 1.0$, $t = 1.0$; for GL model when $\tau_2 = 0.2$, $\tau_1 = 0.1$, $\delta = 0$, $\sigma_1 = 0.2$, $\sigma_2 = 0.1$, $\Omega = 0.1$, and $\omega = 0.02$.

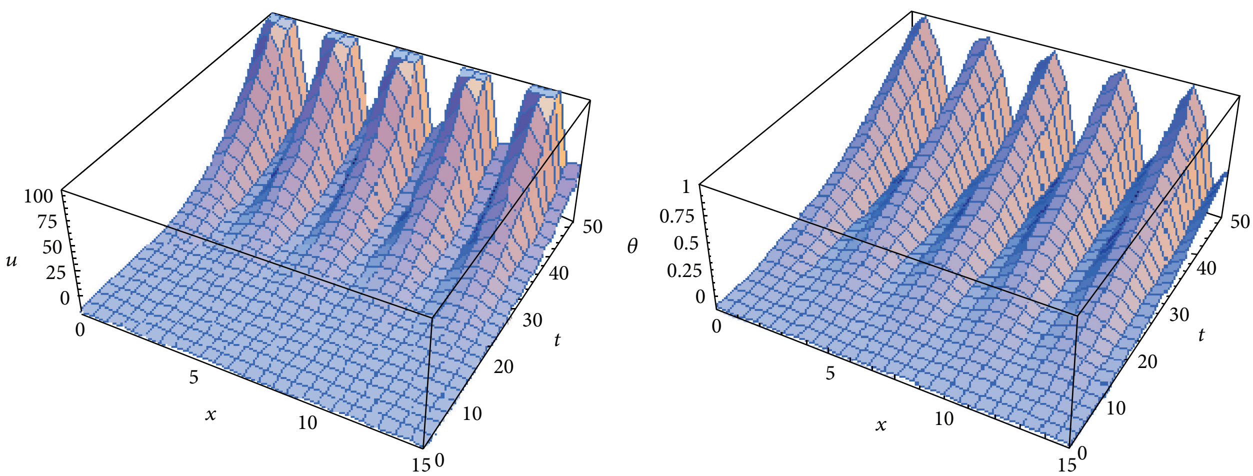

(a) (b)

Figure 3: Variations of the displacement u and the temperature θ for various values of the x-axis and time t when $\tau_2 = 0$, $\tau_1 = 0.1$, $\delta = 1$, $\sigma_1 = 0.2$, $\sigma_2 = 0.1$, $\Omega = 0.1$, and $\omega = 0.02$.

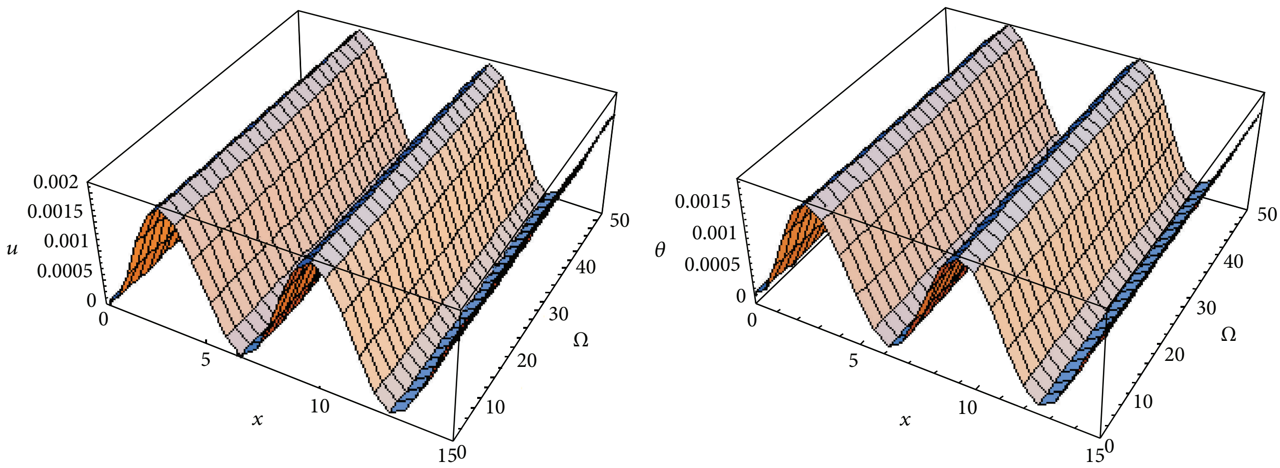

(a) (b)

Figure 4: Variations of the displacement u and the temperature θ for various values of the x-axis and rotation Ω when $t = 0.1$, $\tau_2 = 0$, $\tau_1 = 0.1$, $\delta = 1$, $\sigma_1 = 0.2$, $\sigma_2 = 0.1$, and $\omega = 0.02$.

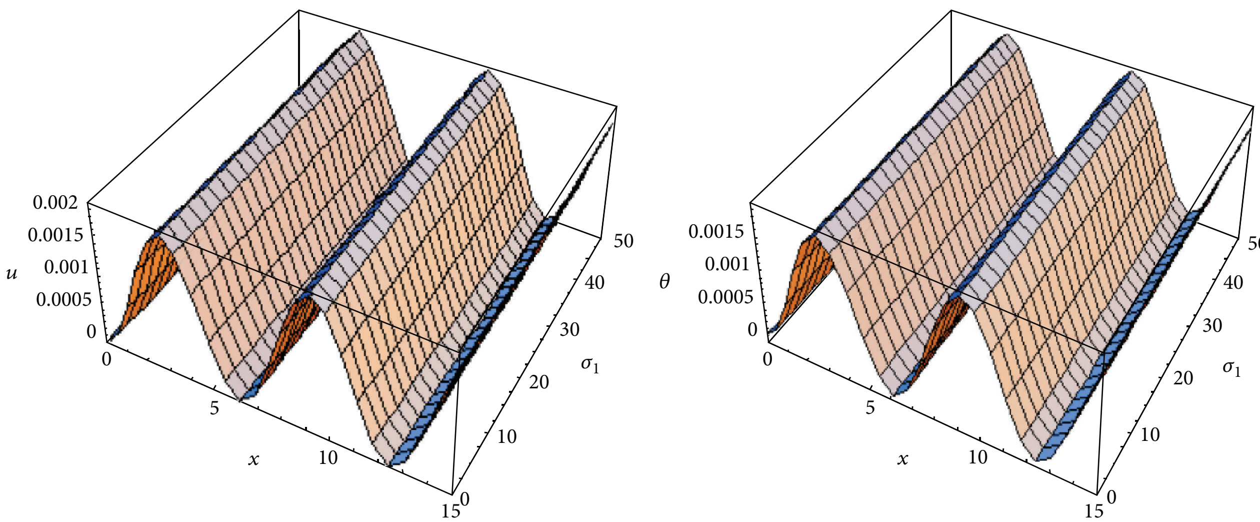

(a) (b)

Figure 5: Variations of the displacement u and the temperature θ for various values of the x-axis and magnetic field σ_1 when $t = 0.1$, $\tau_2 = 0$, $\tau_1 = 0.1$, $\delta = 1$, $\sigma_2 = 0.1$, $\Omega = 0.1$, and $\omega = 0.02$.

corresponding values in the absence of σ_1, σ_2, and Ω, but there is a slight change for LS and GL models.

Finally, Figures 14 and 15 show the variations of the displacement and the temperature with respect to the time t for different values of $\beta = 0.5, 0.005$ and with and without rotation and magnetic field effects, respectively. It is obvious that the radial displacement and the temperature increase with an increase of t; the displacement increases with an increase of β parameter, but the temperature is not affected by β. Is also seen that the radial displacement and the temperature take large values with the rotation and magnetic field effects. Also, it is concluded that takes large values for LS comparing with those in GL model, vice versa for the temperature.

It is obvious that if the rotation and the sensitive part of the magnetic field are neglected, the approximate solutions obtained by HAM agree with the results obtained by Sweilam and Khader [1], taking into consideration VIM. Finally, it is obvious that the displacement takes large values if there are no rotation, thermal relaxation times, and sensitive part of the magnetic field parameters compared with the corresponding value with the rotation and magnetic fields parameters.

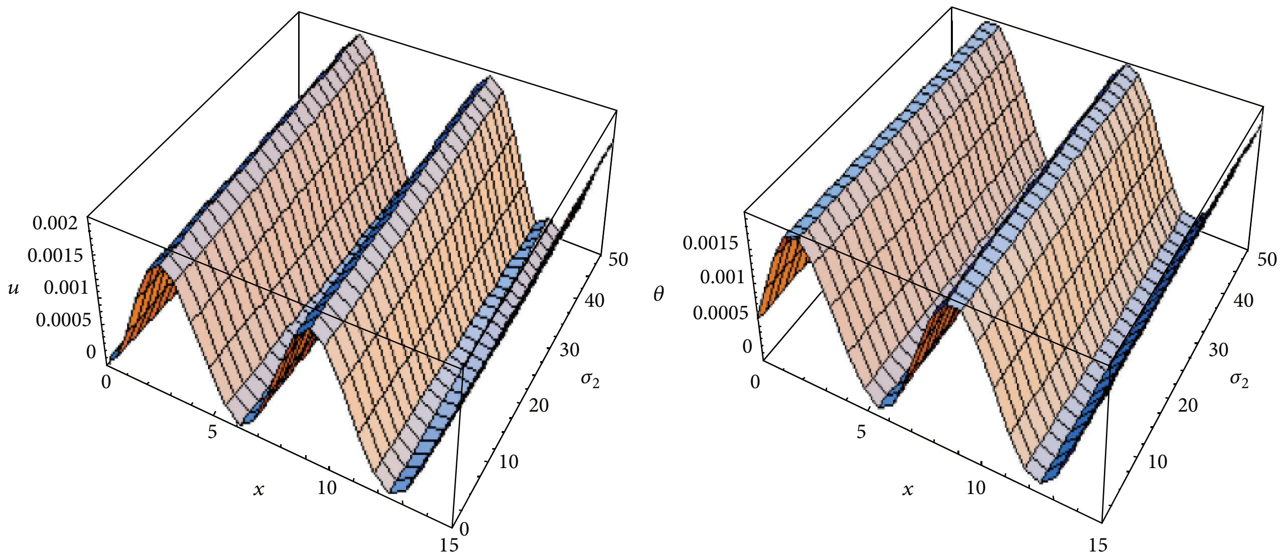

(a) (b)

FIGURE 6: Variations of the displacement u and temperature θ for various values of the x-axis and magnetic field σ_2 when $t = 0.1$, $\tau_2 = 0$, $\tau_1 = 0.1$, $\delta = 1$, and $\omega = 0.02$.

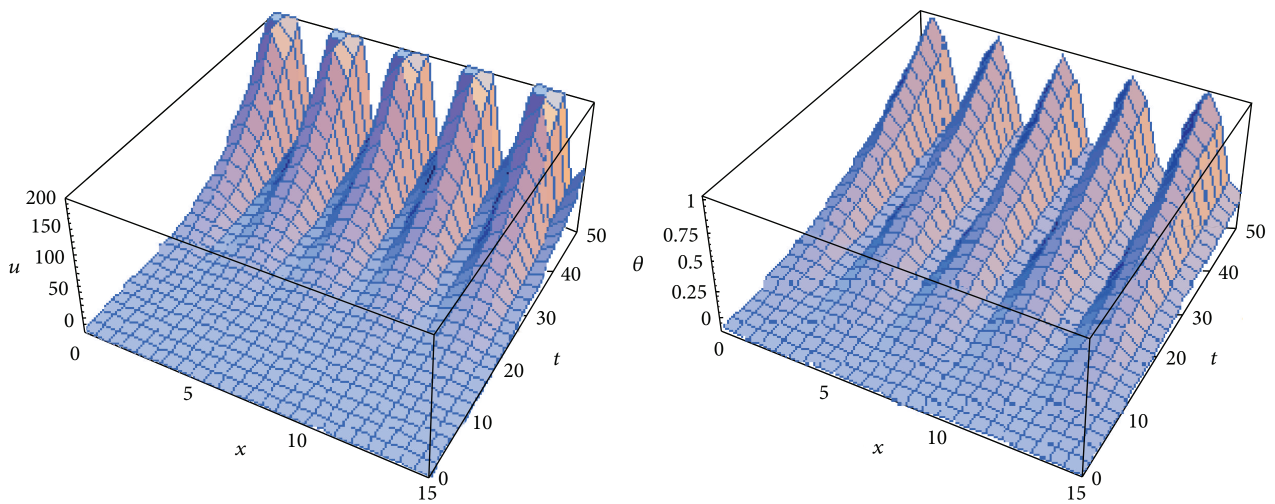

(a) (b)

FIGURE 7: Variations of the displacement u and the temperature θ for various values of the x-axis and time t when $\Omega = \sigma_1 = \sigma_2 = 0$, $\tau_2 = 0.2$, $\tau_1 = 0.1$, $\delta = 1$, and $\omega = 0.02$.

The results indicate that the effect of the rotation and the magnetic field on the radial displacement and the temperature is very pronounced.

5. Conclusion

Due to the complicated nature of the governing equations of the magnetothermoelastic , the finished works in this field are unfortunately limited. The method used in this study provides a quite successful in dealing with such problems. This method gives numerical solutions in the elastic medium without any restrictions on the actual physical quantities that appear in the governing equations of the considered problem. Important phenomena are observed in these computations.

(i) The homotopy analysis method has been successfully applied to obtain the numerical solutions of the nonlinear equation with initial conditions. The reliability of this method and reduction in computations give

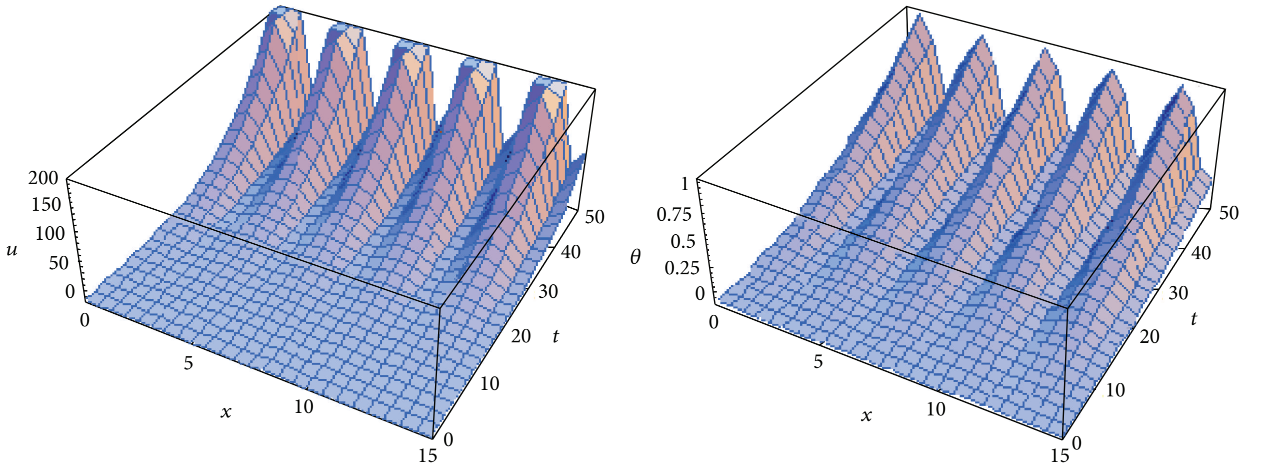

(a) (b)

FIGURE 8: Variations of the displacement u and the temperature θ for various values of the x-axis and time t when $\Omega = \sigma_1 = \sigma_2 = 0$, $\tau_2 = 0.2$, $\tau_1 = 0.1$, $\delta = 0$, and $\omega = 0.02$.

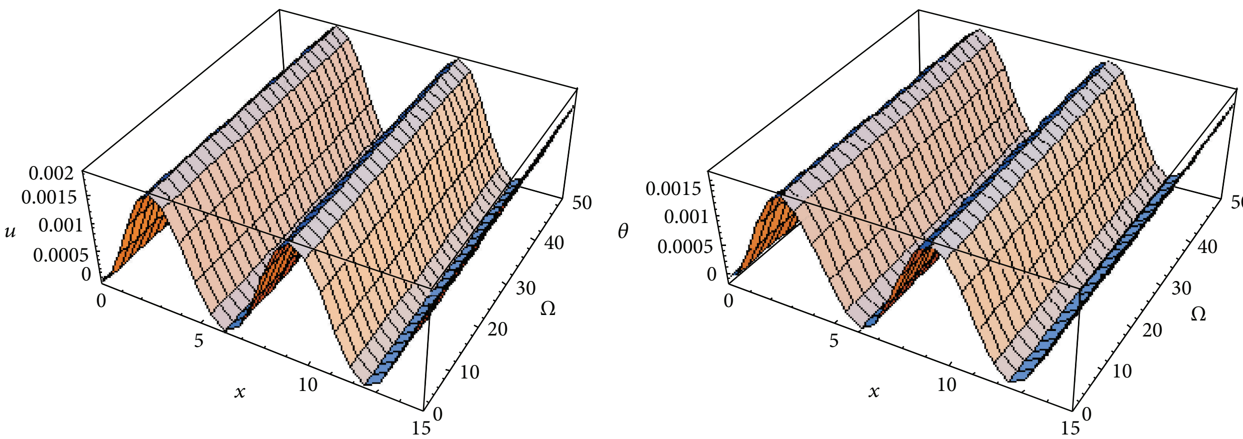

(a) (b)

FIGURE 9: Variations of the displacement u and the temperature θ for various values of the x-axis and rotation Ω when $\sigma_1 = \sigma_2 = 0$, $t = 0.1$, $\tau_2 = 0.2$, $\tau_1 = 0.1$, $\delta = 0$, and $\omega = 0.02$.

this method a wider applicability. HAM contains a certain auxiliary parameter h which provides us with a simple way to adjust and control the convergence region and rate of convergence of the series solution. It was also demonstrated that the Adomian decomposition method, homotopy perturbation method, and variational iteration method are specialcases of. HAM is clearly a very efficient and powerful technique for finding the numerical solutions of the proposed equation. It therefore provides more realistic series solutions that generally converge very rapidly in real physical problems. HAM provides us with a convenient way of controlling the convergence of approximation series, which is a fundamental qualitative difference in analysis between HAM and other methods. The illustrative examples suggest that HAM is a powerful method for nonlinear problems in science and engineering. Mathematica has been used for computations in this paper.

(ii) It was found that for large values of time the large and the generalization give numerical results. The case is quite different when we consider small values of rotation and magnetic field. The coupled theory predicts infinite speeds of wave propagation. The solutions obtained in the context of generalized thermoelasticity theory, however, exhibit the behavior of finite speeds of wave propagation.

(iii) By comparing Figures 1–15 for thermoelastic medium with presence and absence of the rotation and

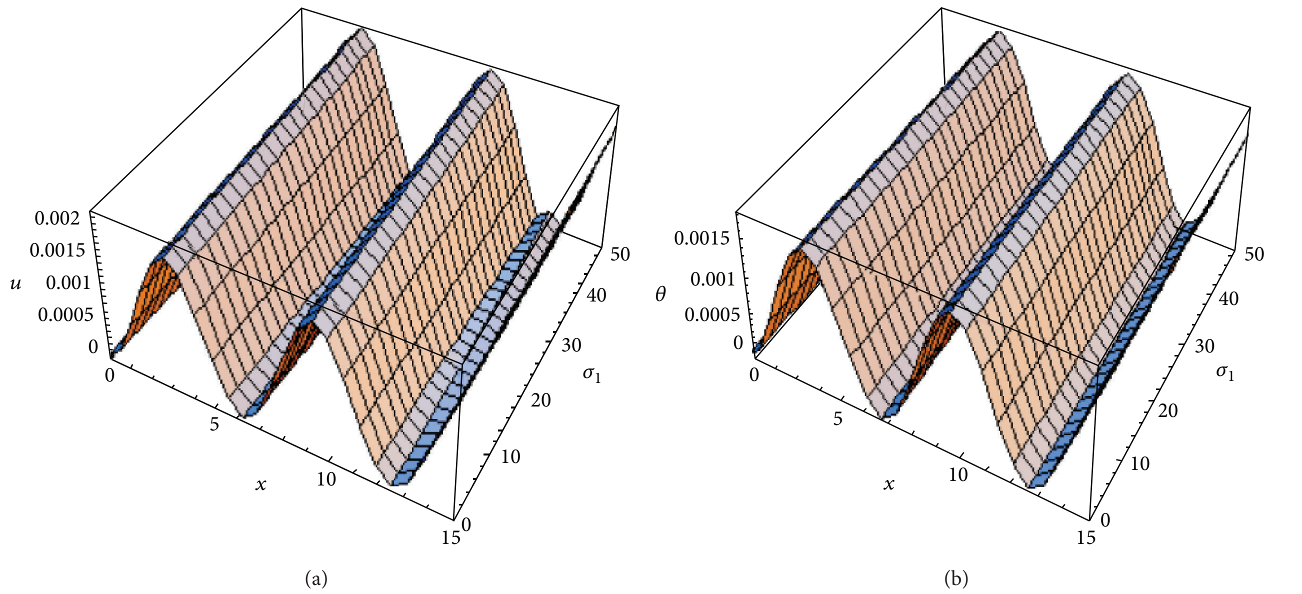

Figure 10: Variations of the displacement u and the temperature θ for various values of the x-axis and magnetic field σ_1 when $\Omega = \sigma_2 = 0$, $t = 0.1$, $\tau_2 = 0.2$, $\tau_1 = 0.1$, $\delta = 0$, and $\omega = 0.02$.

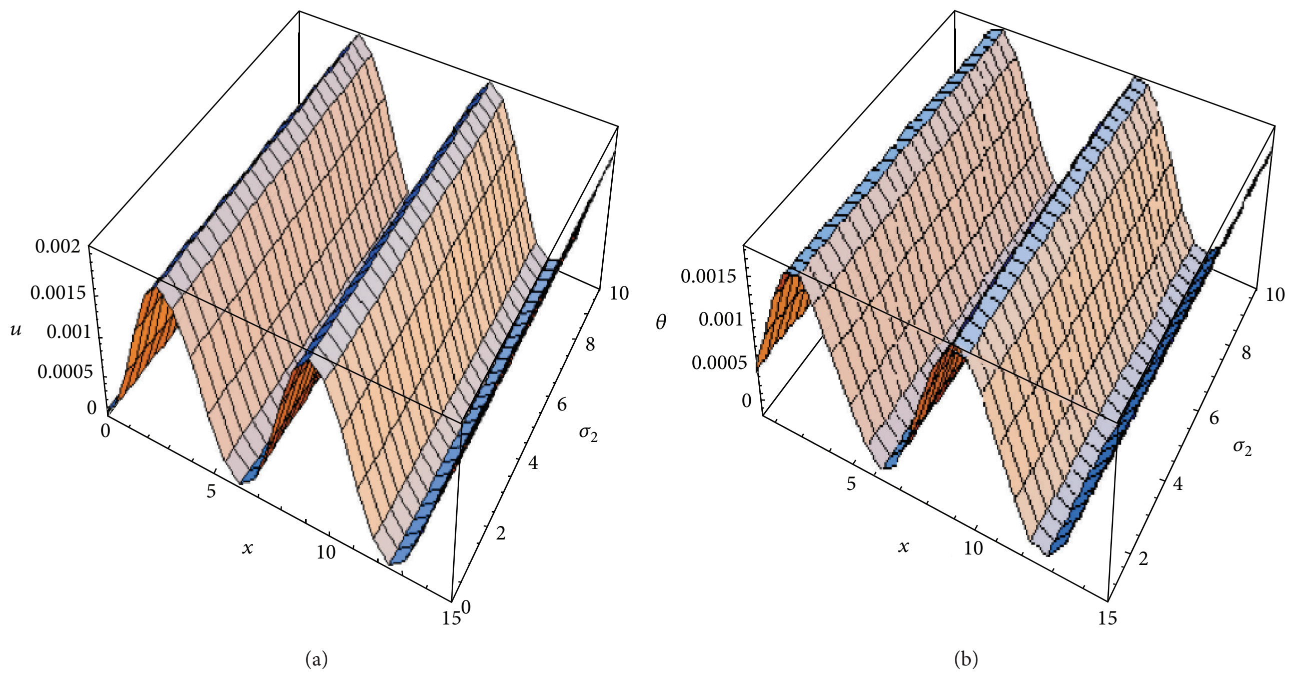

Figure 11: Variations of the displacement u and the temperature θ for various values of the x-axis and magnetic field σ_2 when $\Omega = \sigma_1 = 0$, $t = 0.1$, $\tau_2 = 0.2$, $\tau_1 = 0.1$, $\delta = 0$, and $\omega = 0.02$.

magnetic field, it was found that they have the same behavior in both media. The effect of rotation and sensitive parts of the magnetic field is strongly effective in the displacement and temperature of the propagation of the harmonic waves propagation in nonlinear thermoelasticity.

(iv) The results presented in this paper will be very helpful for researchers concerned with material science, designers of new materials, and low-temperature physicists, as well as for those working on the development of a theory of hyperbolic propagation of hyperbolic thermoelastic. The study of the phenomenon of

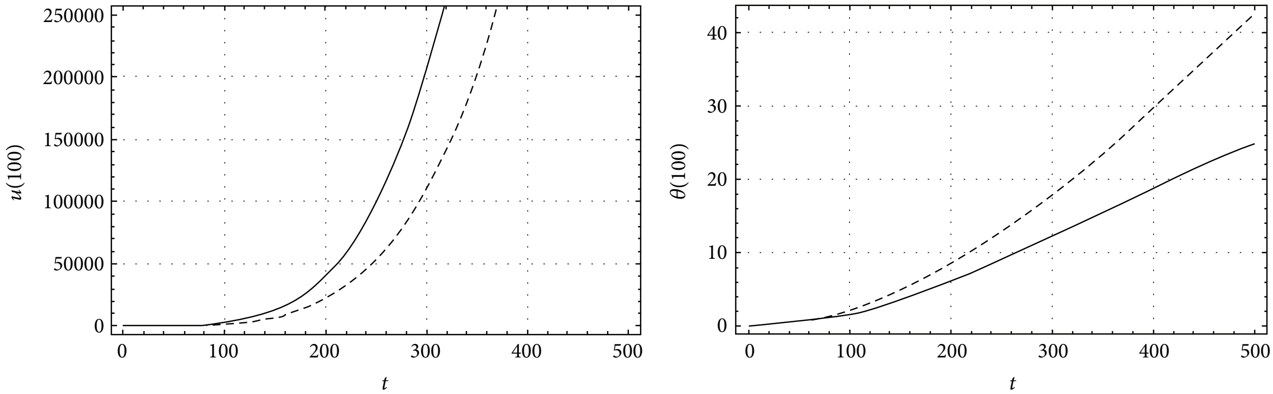

(a) (b)

Figure 12: The displacement as a function of time and the temperature without and with rotation and magnetic field (LS) at $x = 100$, $a = 0.5$, $\beta_1 = 0.5$, $A = 0.001$, $b = 0.5$, $\alpha = 1$, $\beta_2 = 0.05$, $\gamma = 1$, $\delta = 0.8$, $\tau_2 = 0$, $\tau_1 = 0.1$, $\delta = 1$, $\varpi = 0.02$ ($\Omega = \sigma_1 = \sigma_2 = 0$, —), and ($\Omega = 0.1$, $\sigma_1 = 0.2$, $\sigma_2 = 0.1$, - - -).

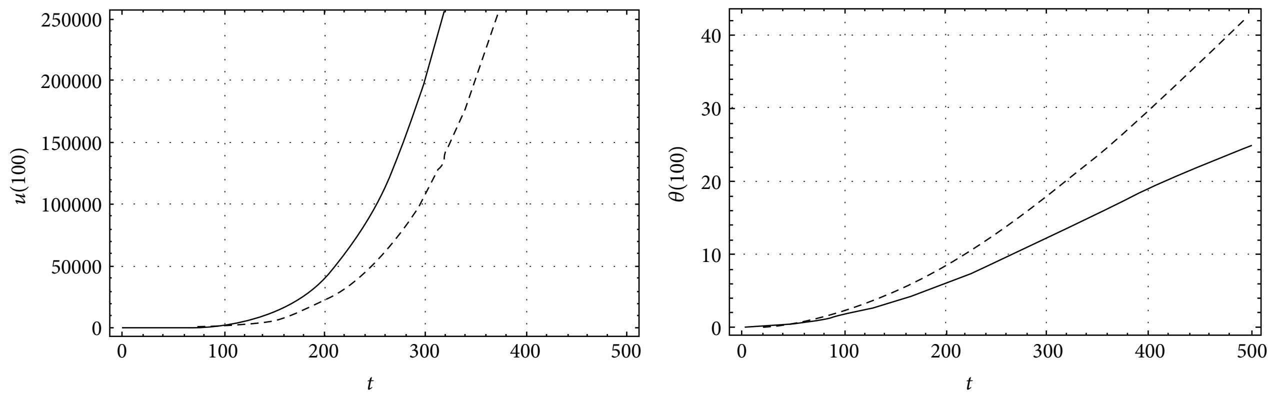

(a) (b)

Figure 13: The displacement as a function of time and the temperature without and with rotation and magnetic field (GL) at $x = 100$, $a = 0.5$, $\beta_1 = 0.5$, $A = 0.001$, $b = 0.5$, $\alpha = 1$, $\beta_2 = 0.05$, $\gamma = 1$, $\delta = 0.8$, $\tau_2 = 0.2$, $\tau_1 = 0.1$, $\delta = 0$, $\varpi = 0.02$ ($\Omega = \sigma_1 = \sigma_2 = 0$, —), and ($\Omega = 0.1$, $\sigma_1 = 0.2$, $\sigma_2 = 0.1$, - - -).

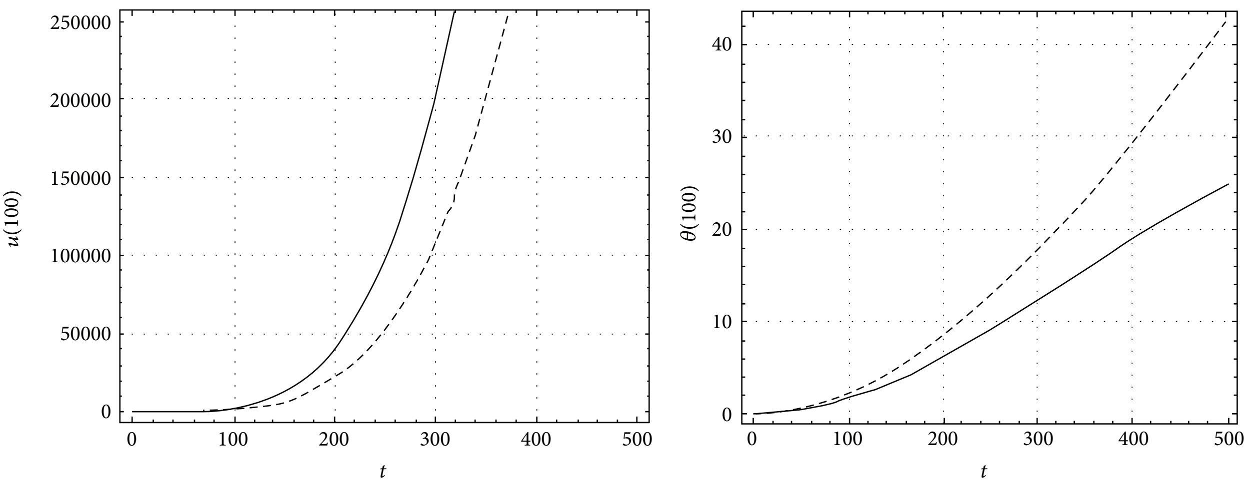

(a) (b)

Figure 14: The displacement as a function of time and the temperature for two values of β_1 (LS) at $x = 100$, $a = 0.5$, $A = 0.001$, $b = 0.5$, $\alpha = 1$, $\beta_2 = 0.05$, $\gamma = 1$, $\delta = 0.8$, $\Omega = 0.1$, $\sigma_1 = 0.2$, $\sigma_2 = 0.1$, $\tau_2 = 0$, $\tau_1 = 0.1$, $\delta = 1$, $\varpi = 0.02$, — $\beta_1 = 0.5$, and - - - $\beta_1 = 0.005$.

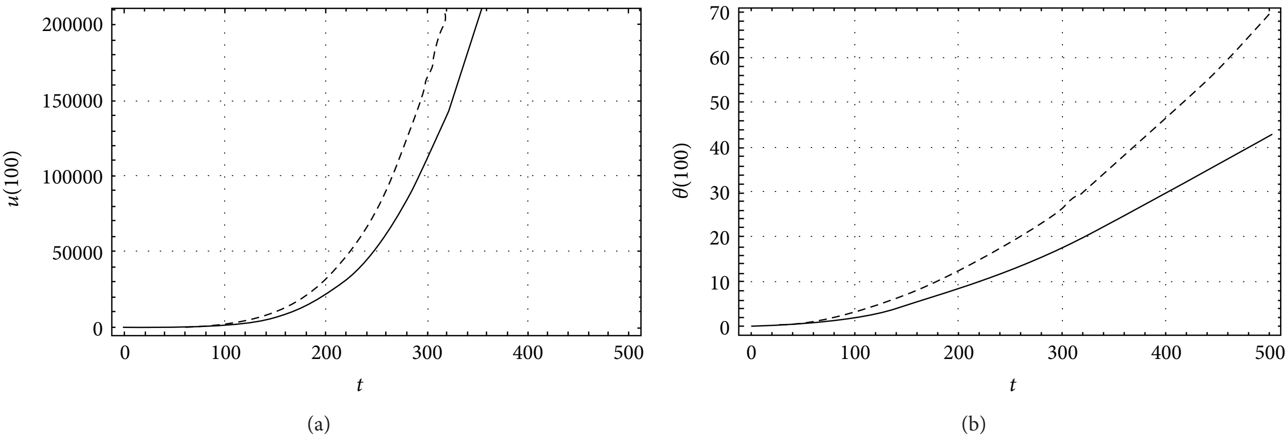

FIGURE 15: The displacement as a function of time and the temperature for two values of β_1 (GL) at $x = 100$, $a = 0.5$, $A = 0.001$, $b = 0.5$, $\alpha = 1$, $\beta_2 = 0.05$, $\gamma = 1$, $\delta = 0.8$, $\Omega = 0.1$, $\sigma_1 = 0.2$, $\sigma_2 = 0.1$, $\tau_2 = 0.2$, $\tau_1 = 0.1$, $\delta = 0$, $\varpi = 0.02$, — $\beta_1 = 0.5$, and - - - $\beta_1 = 0.005$.

rotation and magnetic field is also used to improve the conditions of oil extractions.

References

[1] N. H. Sweilam and M. M. Khader, "Variational iteration method for one dimensional nonlinear thermoelasticity," *Chaos, Solitons & Fractals*, vol. 32, no. 1, pp. 145–149, 2007.

[2] N. H. Sweilam, "Harmonic wave generation in non linear thermoelasticity by variational iteration method and Adomian's method," *Journal of Computational and Applied Mathematics*, vol. 207, no. 1, pp. 64–72, 2007.

[3] H. N. Sweilam, M. M. Khader, and F. R. Al-Bar, "On the numerical simulation of population dynamics with density-dependent migrations and the Allee effects," *Journal of Physics*, vol. 96, no. 1, Article ID 012008, 10 pages, 2008.

[4] N. H. Sweilam, M. M. Khader, and R. F. Al-Bar, "Nonlinear focusing Manakov systems by variational iteration method and adomian decomposition method," *Journal of Physics*, vol. 96, no. 1, Article ID 012164, 7 pages, 2008.

[5] A. N. Abd-Alla, A. F. Ghaleb, and G. A. Maugin, "Harmonic wave generation in nonlinear thermoelasticity," *International Journal of Engineering Science*, vol. 32, no. 7, pp. 1103–1116, 1994.

[6] C. A. De Moura, "A linear uncoupling numerical scheme for the nonlinear coupled thermo-dynamics equations," in *Numerical Methods*, V. Pereyra and A. Reinoze, Eds., vol. 1005 of *Lecture Notes in Mathematics*, pp. 204–211, Springer, Berlin, Germany, 1983.

[7] M. Slemrod, "Global existence, uniqueness, and asymptotic stability of classical smooth solutions in one-dimensional non-linear thermoelasticity," *Archive for Rational Mechanics and Analysis*, vol. 76, no. 2, pp. 97–133, 1981.

[8] S. J. Liao, *The proposed homotopy analysis technique for the solution of nonlinear problem [Ph.D. thesis]*, Shanghai Jiao Tong University, 1992.

[9] S. J. Liao, "An approximate solution technique not depending on small parameters: a special example," *International Journal of Non-Linear Mechanics*, vol. 30, no. 3, pp. 371–380, 1995.

[10] K. M. Hemida and M. S. Mohamed, "Numerical simulation of the generalized Huxley equation by homotopy analysis method," *Journal of Applied Functional Analysis*, vol. 5, no. 4, pp. 344–350, 2010.

[11] K. Hemida and M. S. Mohamed, "Application of homotopy analysis method to fractional order generalized Huxley equation," *Journal of Applied Functional Analysis*, vol. 7, no. 4, pp. 367–372, 2012.

[12] M. S. Mohamed, "Analytic approximations for fractional-order Newton-Leipnik system," *Journal of Advanced Research in Scientific Computing*, vol. 3, no. 2, pp. 56–69, 2011.

[13] M. S. Mohamed and H. A. Ghany, "Analytic approximations for fractional-order hyperchaotic system," *Journal of Advanced Research in Dynamical and Control Systems*, vol. 3, no. 3, pp. 1–12, 2011.

[14] H. A. Ghany and M. S. Mohammed, "White noise functional solutions for Wick-type stochastic fractional KdV-Burgers-Kuramoto equations," *Chinese Journal of Physics*, vol. 50, no. 4, pp. 619–627, 2012.

[15] J.-H. He, "Asymptotology by homotopy perturbation method," *Applied Mathematics and Computation*, vol. 156, no. 3, pp. 591–596, 2004.

[16] K. A. Gepreel, S. M. Abo-Dahab, and T. A. Nofal, "Homotopy perturbation method and variational iteration method for harmonic waves propagation in nonlinear magneto-thermoelasticity with rotation," *Mathematical Problems in Engineering*, vol. 2012, Article ID 827901, 30 pages, 2012.

[17] A. M. Abd-Alla and S. M. Abo-Dahab, "Effect of rotation and initial stress on an infinite generalized gagneto-thermoelastic diffusion body with a spherical cavity," *Journal of Thermal Stresses*, vol. 35, pp. 892–912, 2012.

[18] S. M. Abo-Dahab and R. A. Mohamed, "Influence of magnetic field and hydrostatic initial stress on wave reflection from a generalized thermoelastic solid half-space," *JVC/Journal of Vibration and Control*, vol. 16, no. 5, pp. 685–699, 2010.

[19] A. M. Abd-Alla and S. R. Mahmoud, "Magneto-thermoelastic problem in rotating non-homogeneous orthotropic hollow cylinder under the hyperbolic heat conduction model," *Meccanica*, vol. 45, no. 4, pp. 451–462, 2010.

[20] A. M. Abd-Alla, A. N. Abd-Alla, and N. A. Zeidan, "Thermal stresses in a nonhomogeneous orthotropic elastic multilayered cylinder," *Journal of Thermal Stresses*, vol. 23, no. 5, pp. 413–428, 2000.

[21] A. M. Abd-Alla, S. M. Abo-Dahab, H. A. Hammad, and S. R. Mahmoud, "On generalized magneto-thermoelastic Rayleigh waves in a granular medium under the influence of a gravity field and initial stress," *Journal of Vibration and Control*, vol. 17, no. 1, pp. 115–128, 2011.

[22] A. M. Abd-Alla and S. M. Abo-Dahab, "Time-harmonic sources in a generalized magneto-thermo-viscoelastic continuum with and without energy dissipation," *Applied Mathematical Modelling*, vol. 33, no. 5, pp. 2388–2402, 2009.

[23] M. A. F. Araghia and A. Fallahzadeh, "On the convergence of the Homotopy analysis method for solving the schrodinger equation," *Journal of Applied Sciences Research*, vol. 2, pp. 6076–6083, 2012.

[24] S. Abbasbandy and M. Jalili, "Determination of optimal convergence control parameter value in homotopy analysis method," *Numerical Algorithms*, 2013.

[25] M. Turkyilmazoglu, "Purely analytic solutions of magnetohydrodynamic swirling boundary layer flow over a porous rotating disk," *Computers and Fluids*, vol. 39, no. 5, pp. 793–799, 2010.

[26] M. Turkyilmazoglu, "Numerical and analytical solutions for the flow and heat transfer near the equator of an MHD boundary layer over a porous rotating sphere," *International Journal of Thermal Sciences*, vol. 50, no. 5, pp. 831–842, 2011.

[27] M. Turkyilmazoglu, "Analytic approximate solutions of rotating disk boundary layer flow subject to a uniform suction or injection," *International Journal of Mechanical Sciences*, vol. 52, no. 12, pp. 1735–1744, 2010.

[28] M. Turkyilmazoglu, "Analytic approximate solutions of rotating disk boundary layer flow subject to a uniform vertical magnetic field," *Acta Mechanica*, vol. 218, no. 3-4, pp. 237–245, 2011.

[29] M. Turkyilmazoglu, "A note on the homotopy analysis method," *Applied Mathematics Letters*, vol. 23, no. 10, pp. 1226–1230, 2010.

Hindawi Publishing Corporation
Abstract and Applied Analysis
Volume 2013, Article ID 858597, 13 pages
http://dx.doi.org/10.1155/2013/858597

Research Article

The Effect of Boundary Slip on the Transient Pulsatile Flow of a Modified Second-Grade Fluid

N. Khajohnsaksumeth,[1] B. Wiwatanapataphee,[2] and Y. H. Wu[1]

[1] *Department of Mathematics and Statistics, Curtin University, Perth, WA 6845, Australia*
[2] *Department of Mathematics, Mahidol University, Faculty of Science, Bangkok 10400, Thailand*

Correspondence should be addressed to N. Khajohnsaksumeth; jobscma@yahoo.com
and B. Wiwatanapataphee; benchawan.wiw@mahidol.ac.th

Received 20 May 2013; Accepted 9 August 2013

Academic Editor: Rasajit Bera

We investigate the effect of boundary slip on the transient pulsatile fluid flow through a vessel with body acceleration. The Fahraeus-Lindqvist effect, expressing the fluid behavior near the wall by the Newtonian fluid while in the core by a non-Newtonian fluid, is also taken into account. To describe the non-Newtonian behavior, we use the modified second-grade fluid model in which the viscosity and the normal stresses are represented in terms of the shear rate. The complete set of equations are then established and formulated in a dimensionless form. For a special case of the material parameter, we derive an analytical solution for the problem, while for the general case, we solve the problem numerically. Our subsequent analytical and numerical results show that the slip parameter has a very significant influence on the velocity profile and also on the convergence rate of the numerical solutions.

1. Introduction

In this paper, we study a fluid-structure interaction problem, namely, the effect of boundary slip on the flow of a non-Newtonian fluid through microchannels. This problem has many applications, and in this paper we particularly focus on blood flow in the cardiovascular system.

For the study of blood flow in arteries, two major types of constitutive models have been used. The first type of models is based on the microcontinuum or the structured continuum theories [1–6] in which the balance laws are used to determine the characteristics of blood motion. In the other type of models, blood is considered as a suspension, and its flow is modeled by the non-Newtonian fluid mechanics. Due to the red blood cells (RBC) migration as shown experimentally, blood has been modeled as a two-stage fluid by many researchers [7–9]. The first stage is a peripheral layer which is modeled as a Newtonian viscous fluid, while the other one is a centre core which is modeled as a non-Newtonian fluid. The effect of body acceleration and pulsatile conditions were taken into account under the same problem by Majhi et al. [7, 10]. Later, Massoudi and Phuoc [11] used the (generalized) second-grade fluid constitutive model to describe the shear thinning and normal stress effect, and the behavior of blood flow near the wall is modeled by the Newtonian fluid model, while the behavior of the blood flow at the core is described by the second-grade fluid model.

In all of the above mentioned models, the so-called no-slip boundary condition is used; namely, the velocity of flow relative to the solid is zero on the fluid-solid interface [12]. Although the no-slip condition is supported by many experimental results, the existence of slip of a fluid on the solid surface was also observed by many other researches [13–20]. The Navier slip condition has been used by various researchers to describe boundary slip and is a more general boundary condition, in which the fluid velocity component tangential to the solid surface, relative to the solid surface, is proportional to the shear stress on the fluid-solid interface and the slip length. The surface characteristics constant, slip length, describes the "slipperiness" of the surface. Recently,

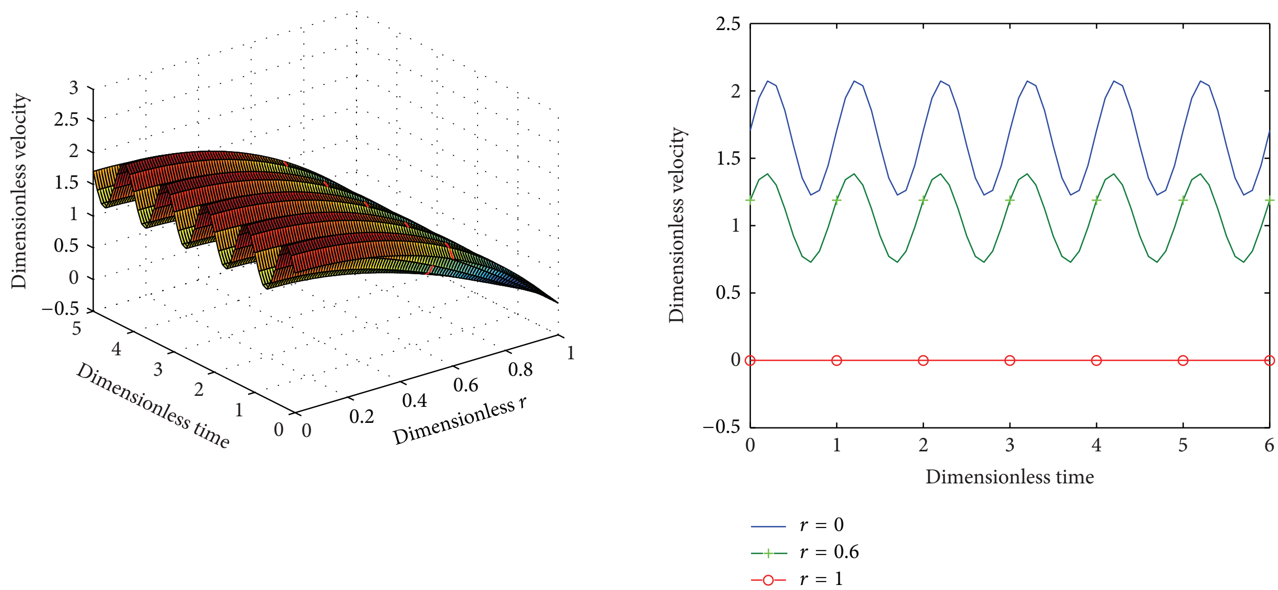

(a)

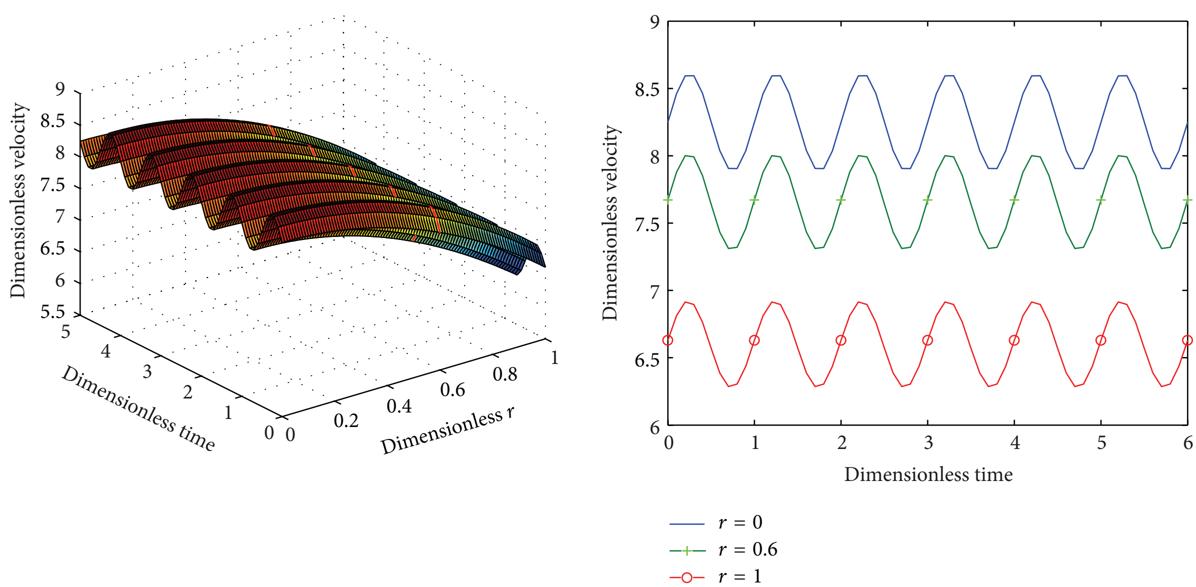

(b)

FIGURE 1: The velocity profile in the small artery with radius 0.15 cm under two different slip parameter values: (a) $l_b = 0$; (b) $l_b = 2$. In the figure, the 3D graphs show the variation of velocity as a function of time and location, while the 2D graphs show the variation of velocity with time at three radial locations including the artery centre ($r = 0$), the interface of inner-outer layer ($r = 0.6$), and the arterial wall ($r = 1$).

we and many other researchers have investigated various flow problems of Newtonian fluids with the traditional no-slip and the Navier slip boundary conditions [12, 20–30], and it is found that the boundary slip and the slip parameter have significant influence on the flow of Newtonian fluids through microchannels and tubes.

Motivated by the above mentioned work, we extend previous work on slip flows of Newtonian fluids [21, 22] to the case involving both Newtonian and non-Newtonian fluid flow in the flow region. The new feature and contribution of this work include establishment of the underlying boundary value problem for the problem, the derivation of an exact solution for a special case, and demonstration of the influence of the slip parameter on the flow profile and flow behavior. The rest of the paper is organized as follows. In Section 2, we present the underlying boundary value problem for the problem in dimensionless form. Then in Section 3, we derive an exact solution for a special case. In Section 4, we investigate numerically the effect of the slip parameter for the general case. Finally, a conclusion is given in Section 5.

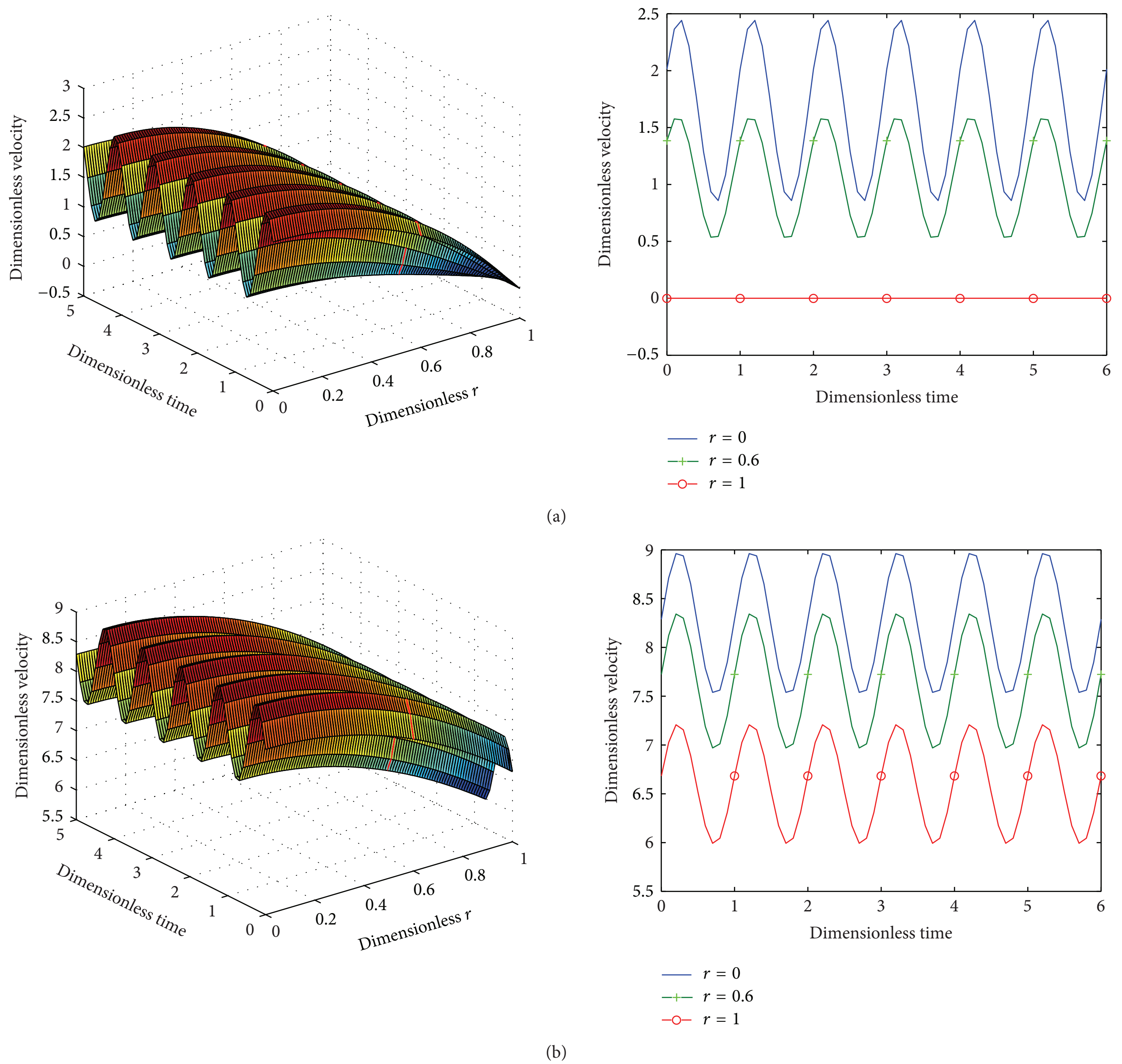

FIGURE 2: The velocity profile in the large artery with radius 0.50 cm under two different slip parameter values: (a) $l_b = 0$; (b) $l_b = 2$. In the figure, the 3D graphs show the variation of velocity as a function of time and location, while the 2D graphs show the variation of velocity with time at three radial locations including the artery centre ($r = 0$), the interface of inner-outer layer ($r = 0.6$), and the arterial wall ($r = 1$).

2. Mathematical Formulation

The flow of a fluid with no thermochemical and electromagnetic effects can be described by the conservation equations of mass and linear momentum; namely,

$$\frac{\partial \rho}{\partial t} + \operatorname{div}(\rho \mathbf{v}) = 0,$$
$$\rho\left(\frac{\partial \mathbf{v}}{\partial t} + \mathbf{v}\cdot\nabla\mathbf{v}\right) = \operatorname{div}\mathbf{T} + \rho\mathbf{b}, \tag{1}$$

where ρ is the density of the fluid, $\partial/\partial t$ is the partial derivative with respect to time, $\mathbf{v}$ is the velocity vector, $\mathbf{b}$ is the body force vector, and $\mathbf{T}$ is the stress tensor.

The stress tensor is related to the velocity gradient by the constitutive equations. For a modified (generalized) second-grade fluid [11, 31, 32], the constitutive equations can be expressed by

$$\mathbf{T} = -p\mathbf{I} + \Pi^{m/2}\left(\mu\mathbf{A}_1 + \alpha_1\mathbf{A}_2 + \alpha_2\mathbf{A}_1^2,\right), \tag{2}$$

where m is a material parameter, $\Pi = (1/2)\operatorname{tr}\mathbf{A}_1^2$ is the second invariant of $\mathbf{A}_1$, p is the fluid pressure, μ is the

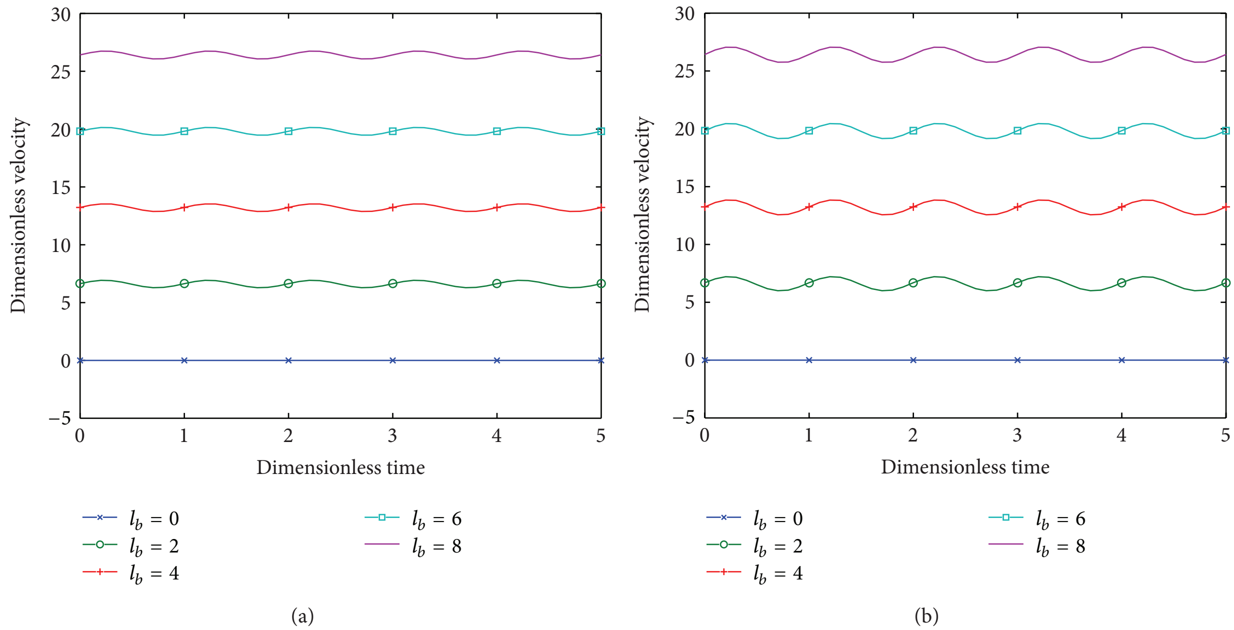

Figure 3: Diagrams showing the velocity profile on the arterial wall with five different slip parameters l_b for two different artery radii (a) $r = 0.15$ cm; (b) $r = 0.5$ cm.

coefficient of viscosity, α_i are material moduli (the normal stress coefficients), and $\mathbf{A_i}$ are the kinematical tensors given by

$$\mathbf{A_1} = \mathbf{L} + \mathbf{L}^T,$$
$$\mathbf{A_2} = \frac{\partial \mathbf{A_1}}{\partial t} + [\text{grad}(\mathbf{A_1})]\,\mathbf{v} + \mathbf{A_1}\mathbf{L} + (\mathbf{L})^T\mathbf{A_1}, \tag{3}$$

in which L is grad $\mathbf{v}$ and the superscript T refers to matrix transposition.

For the axially symmetrical blood flow through a circular tube of radius b, we can assume that $\mathbf{v} = v(r,t)\mathbf{e}_z$, where z is the axial direction and r is the radial direction. Under the periodic body acceleration and a unsteady pulsatile pressure gradient [7, 10], the momentum equation in the z-direction in the cylindrical polar coordinate (r, θ, z) is

$$\rho\frac{\partial v}{\partial t} = -\frac{\partial p}{\partial z} + \rho G + \frac{1}{r}\frac{\partial}{\partial r}\left(rT_{rz}\right). \tag{4}$$

The shear stress T_{rz} for a generalized second-grade fluid can be expressed by

$$T_{rz} = \begin{cases} \mu_1\left|\dfrac{\partial v_1}{\partial r}\right|^m\dfrac{\partial v_1}{\partial r} & 0 \le r \le a, \\ \mu_2\dfrac{\partial v_2}{\partial r} & a \le r \le b. \end{cases} \tag{5}$$

The approximate periodic form of the pressure gradient generated by the heart can be described by

$$-\frac{\partial p}{\partial z} = A_0 + A_1\cos\omega_p t, \tag{6}$$

where $A_0, A_1, \omega_p = 2\pi f_p$, and f_p are the constant component of the pressure gradient, the amplitude of the pressure fluctuation (establishing the systolic and diastolic pressures), the circular frequency, and the frequency of pulse rate, respectively.

The body acceleration G can be approximated by

$$G = A_g\cos\left(\omega_b t + \phi\right), \tag{7}$$

where A_g is the amplitude, $f_b = \omega_b/2\pi$ is the frequency, and ϕ is the lead angle of G with respect to the action of the heart.

Substituting (5)–(7) into (4), the blood flow equation for a modified second-grade fluid in the z-direction, in the inner and outer core, becomes

$$\begin{aligned} \rho_1\frac{\partial v_1}{\partial t} &= A_0 + A_1\cos\omega_p t + \rho A_g\cos\left(\omega_b t + \phi\right) \\ &\quad + \frac{1}{r}\frac{\partial}{\partial r}\left(r\mu_1\left|\frac{\partial v_1}{\partial r}\right|^m\frac{\partial v_1}{\partial r}\right), \quad \text{for } 0 \le r \le a, \\ \rho_2\frac{\partial v_2}{\partial t} &= A_0 + A_1\cos\omega_p t + \rho A_g\cos\left(\omega_b t + \phi\right) \\ &\quad + \frac{1}{r}\frac{\partial}{\partial r}\left(r\mu_2\frac{\partial v_2}{\partial r}\right), \quad \text{for } a \le r \le b. \end{aligned} \tag{8}$$

In order to completely define the problem, boundary and initial conditions are required. In this work, the Navier slip condition is applied. That is, on the solid-fluid interface $r = b$, the axial fluid velocity, relative to the solid surface, is proportional to the shear stress on the interface. As the fluid layer near the wall is modeled as a Newtonian fluid in our model, the shear stress on the boundary is related to the shear

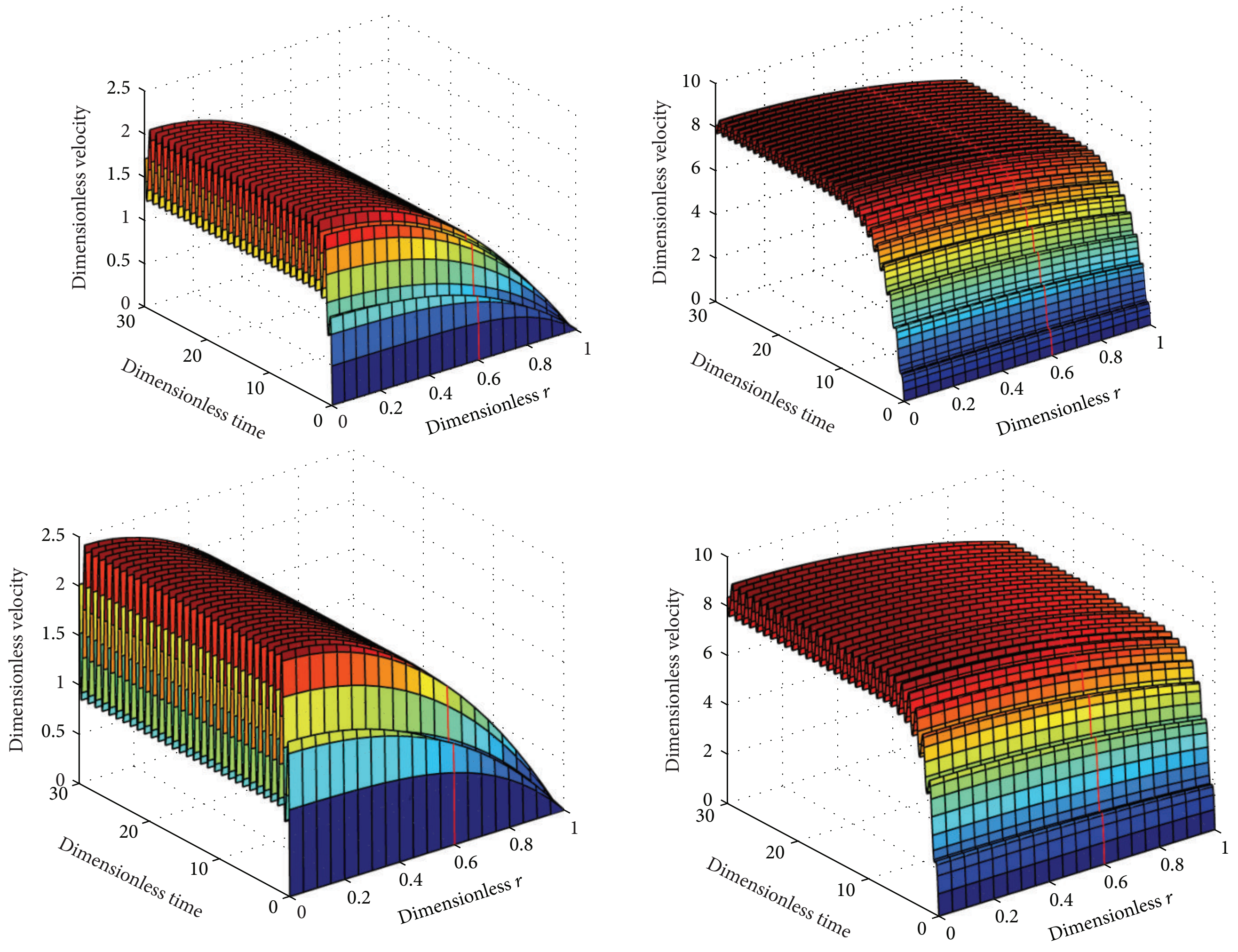

(a)

FIGURE 4: Velocity profiles in arteries with different radii r: (a) $r = 0.15$ cm; (b) $r = 0.5$ cm. In the figure, the graphs on the left column correspond to $l_b = 0$, while the graphs on the right column correspond to $l_b = 2$.

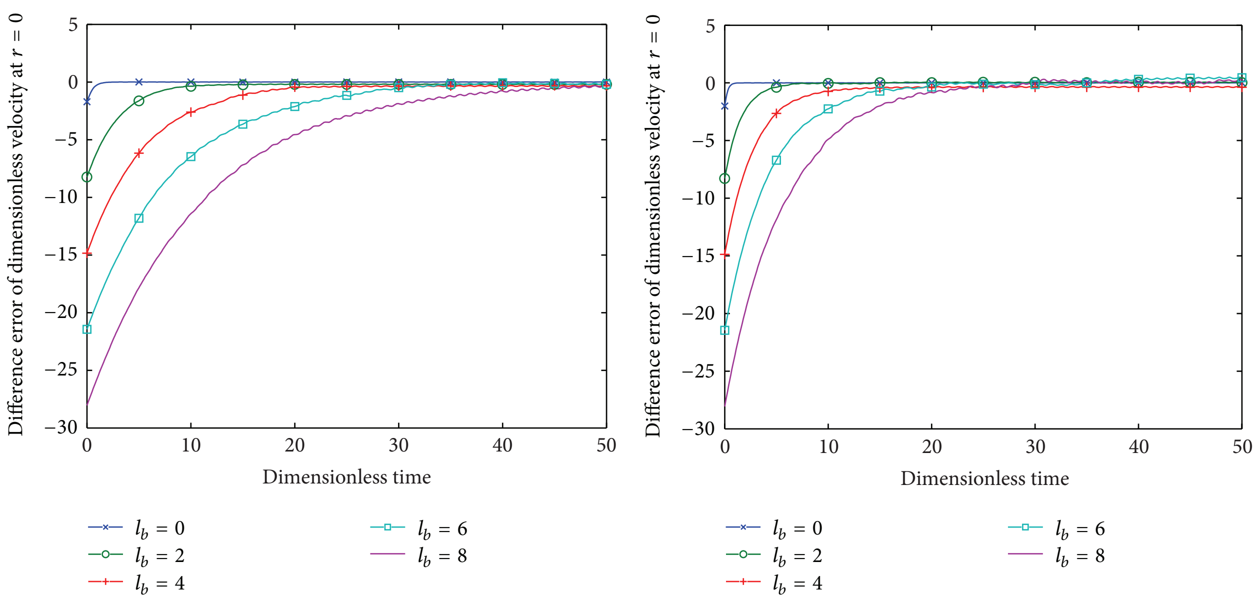

(a) (b)

FIGURE 5: Diagrams showing the convergence of numerical solutions for different slip parameters and artery radii: (a) $r = 0.15$ cm; (b) $r = 0.50$ cm.

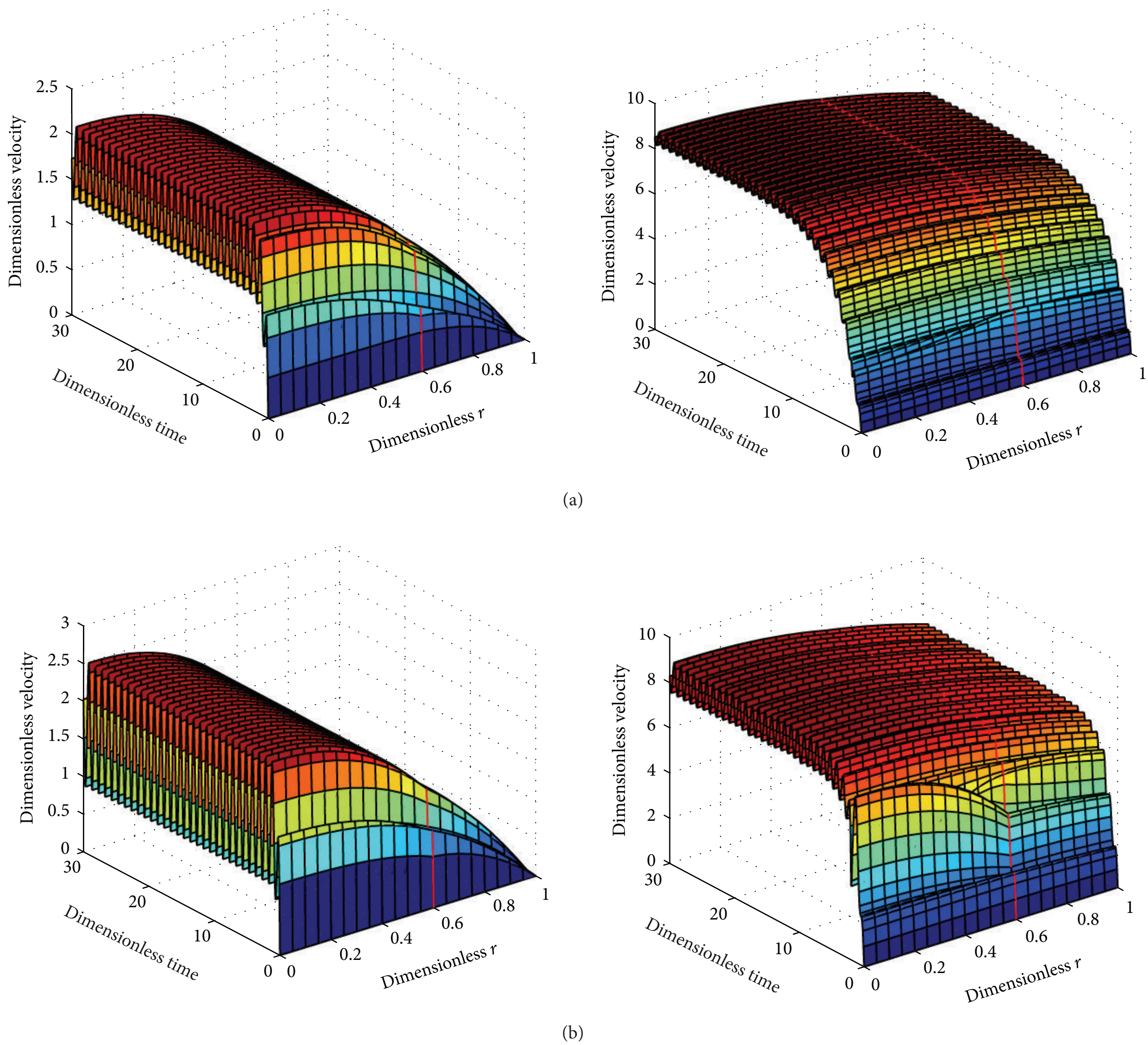

Figure 6: Velocity profiles in arteries with different slip parameters l_b and radii r: (a) $r = 0.15$ cm; (b) $r = 0.50$ cm. In the Figure, the graphs on the left column correspond to $l_b = 0$, while the graphs on the right column correspond to $l_b = 2$.

strain rate by $\sigma_{rz} = \mu_2(\partial v/\partial z)$. Thus, the Navier slip condition can be written as

$$v_2(b,t) + l\frac{\partial v_2}{\partial t}(b,t) = 0, \tag{9}$$

where l is the slip parameter. Moreover, we assume that the slip parameter does not change along the axial direction.

On $r = 0$, the symmetry condition is introduced:

$$\frac{\partial v_1}{\partial r}(0,t) = 0. \tag{10}$$

On the interface between two different fluids, for continuous and smooth behavior of the velocity and shear stresses, we require

$$\begin{gathered} v_1(a,t) = v_2(a,t), \\ \left[\mu_1\left|\frac{\partial v_1}{\partial r}\right|^m \frac{\partial v_1}{\partial r}\right](a,t) = \left[\mu_2\frac{\partial v_2}{\partial r}\right](a,t). \end{gathered} \tag{11}$$

The initial conditions are set to

$$v_1(r,0) = 0 = v_2(r,0), \tag{12}$$

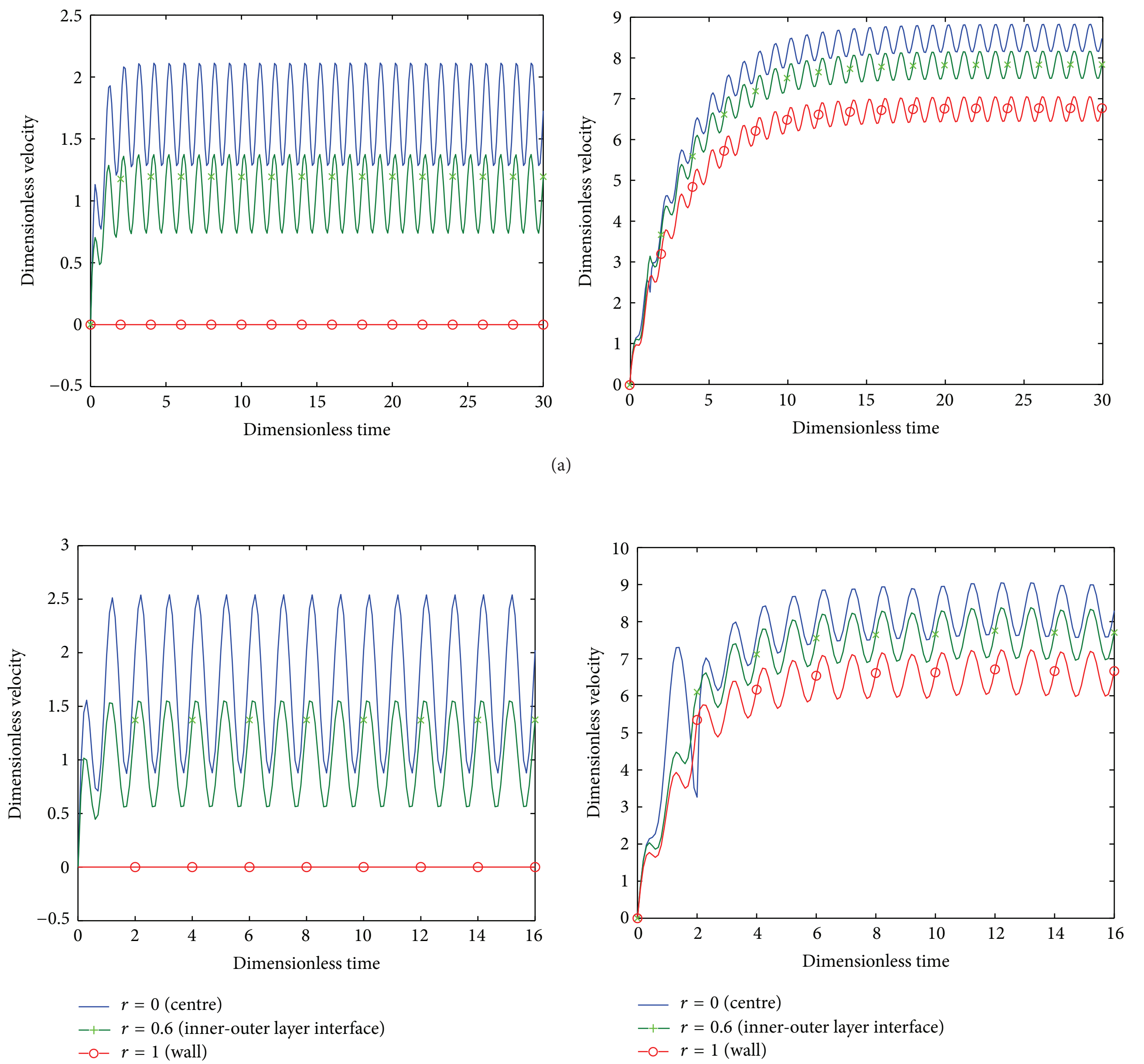

(b)

FIGURE 7: Velocity profiles at three arterial locations (r_1, r_2, r_3): for $m = -1/4$ and under different slip parameters l_b and artery radii (a) $r = 0.15$ cm; (b) $r = 0.50$ cm. In the Figure, the graphs on the left column correspond to $l_b = 0$, while the graphs on the right column correspond to $l_b = 2$.

which is essential for the numerical scheme adopted to estimate the time at which the pulsatile steady state is achieved.

To simplify the equations, we introduce the following nondimensional variables and parameters:

$$\bar{r} = \frac{r}{b}, \qquad \bar{v} = \frac{v}{v_0}, \qquad \bar{t} = \frac{\omega_p}{2\pi} t, \qquad u_0 = \frac{A_0 b^2}{\mu_2},$$

$$e = \frac{A_1}{A_0}, \qquad \omega_r = \frac{\omega_b}{\omega_p}, \qquad r_0 = \frac{a}{b}, \qquad \overline{mu} = \mu\left(\frac{u_0}{b}\right)^m,$$

$$\rho^* = \frac{\rho_1}{\rho_2}, \qquad \mu^* = \frac{\mu_2}{\bar{\mu}},$$

$$C_1 = \frac{A_0 b^2}{\bar{\mu} u_0}, \qquad C_2 = \rho_1 A_g \frac{b^2}{\bar{\mu} u_0} = \frac{\rho_1 A_g}{A_0} B_1,$$

$$\alpha = \frac{\rho_1 \omega_p b^2}{2\pi \bar{\mu}}, \qquad \gamma = \frac{\rho_2 \omega_p b^2}{2\pi \bar{\mu} \mu^*} = \frac{\rho_2 \omega_p b^2 \rho_1}{2\pi \bar{\mu} \mu^* \rho_1} = \alpha \frac{\rho^*}{\mu^*},$$

$$\widehat{C}_1 = \frac{A_0 b^2}{\bar{\mu} u_0 \mu^*} = \frac{C_1}{\mu^*}, \qquad \widehat{C}_2 = \frac{\rho_2 A_g b^2 \rho_1}{\bar{\mu} u_0 \mu^* \rho_1} = C_2 \frac{\rho^*}{\mu^*}. \tag{13}$$

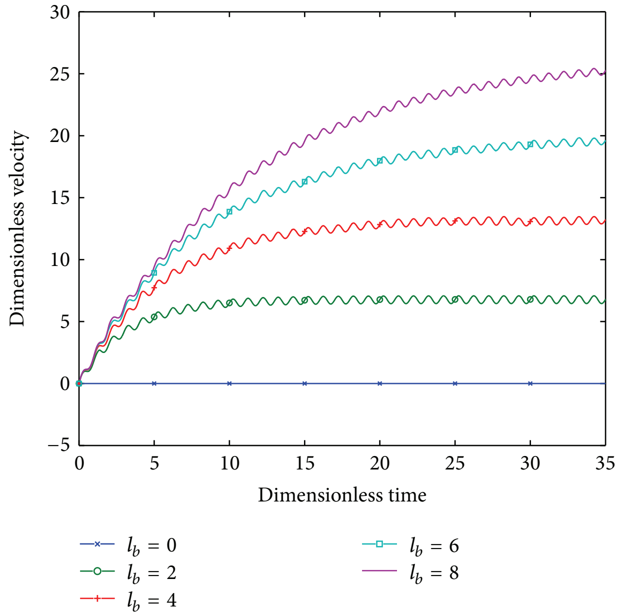

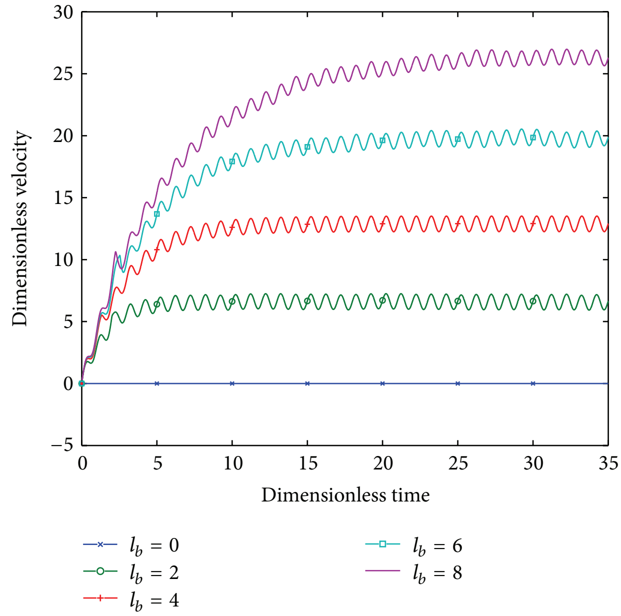

FIGURE 8: Diagrams showing the convergence of numerical results of the fluid velocity on the wall to the steady state pulsatile velocity field under various slip parameters l_b for two different artery radii: (a) $r = 0.15$ cm; (b) $r = 0.50$ cm.

In terms of the nondimensional variables and parameters, (8)–(12) can be written in the form of

$$\begin{aligned}\alpha \frac{\partial \bar{v}_1}{\partial \bar{t}} &= C_1 \left(1 + e \cos 2\pi \bar{t}\right) + C_2 \cos\left(2\pi \omega_r \bar{t} + \phi\right) \\ &\quad + \frac{1}{\bar{r}} \frac{\partial}{\partial \bar{r}} \left[\bar{r} \left|\frac{\partial \bar{v}_1}{\partial \bar{r}}\right|^m \frac{\partial \bar{v}_1}{\partial \bar{r}}\right], \quad \text{for } 0 \le r \le r_0, \\ \gamma \frac{\partial \bar{v}_2}{\partial \bar{t}} &= \overline{C}_1 \left(1 + e \cos 2\pi \bar{t}\right) + \overline{C}_2 \cos\left(2\pi \omega_r \bar{t} + \phi\right) \\ &\quad + \frac{1}{\bar{r}} \frac{\partial}{\partial \bar{r}} \left[\bar{r} \frac{\partial \bar{v}_2}{\partial \bar{r}}\right], \quad \text{for } r_0 \le r \le 1.\end{aligned} \tag{14}$$

The boundary conditions and initial conditions, in dimensionless form, can be expressed by

$$\frac{\partial \bar{v}_1}{\partial \bar{r}} (0, \bar{t}) = 0, \tag{15}$$

$$b\bar{v}_2 (1, t) + l \frac{\partial \bar{v}_2}{\partial \bar{r}} (1, \bar{t}) = 0, \tag{16}$$

$$\bar{v}_1 (r_0, \bar{t}) = \bar{v}_2 (r_0, \bar{t}), \tag{17}$$

$$\left[\left|\frac{\partial \bar{v}_1}{\partial \bar{r}}\right|^m \frac{\partial \bar{v}_1}{\partial \bar{r}}\right] (r_0, \bar{t}) = \left[\mu^* \frac{\partial \bar{v}_2}{\partial \bar{r}}\right] (r_0, \bar{t}), \tag{18}$$

$$\bar{v}_1 (r, 0) = 0 = \bar{v}_2 (r, 0). \tag{19}$$

3. Analytical Solution

For $m = 0$, the model reduces to the linear model with different viscosity in the peripheral layer and the centre core. In this case, (14) have the same form:

$$\begin{aligned}L(v) &= \beta \frac{\partial v}{\partial t} - \frac{1}{r} \frac{\partial v}{\partial r} - \frac{\partial^2 v}{\partial r^2} \\ &= B_1 (1 + e \cos(2\pi t)) + B_2 \cos\left(2\pi \omega_r t + \phi\right).\end{aligned} \tag{20}$$

By the superposition principle, if v_0, v_1, and v_2 are the solution of $L(v) = f(t)$, respectively, for $f(t) = B_1 e^{0ti}$, $B_1 a e^{2\pi t i}$, and $B_2 e^{(2\pi \omega_r t + \phi) i}$, then the complete solution of (20) is $v = \sum_{n=0}^{2} \mathrm{Re}(v_n)$.

To determine v_n, we solve

$$\beta \frac{\partial v_n}{\partial t} = D_n e^{g_n(t) i} + \frac{1}{r} \frac{\partial v_n}{\partial r} + \frac{\partial^2 v_n}{\partial r^2}, \tag{21}$$

where $g_0(t) = 0$, $g_1(t) = 2\pi t$, $g_2(t) = 2\pi \omega_r t + \phi$, $D_0 = B_1$, $D_1 = a B_1$, and $D_2 = B_2$. As (21) admits solutions of the form $v_n = f_n(r) e^{g_n(t) i}$, we have from (21) that

$$\begin{aligned}&\beta g_n'(t) f_n(r) e^{g_n(t) i} i \\ &\quad = D_n e^{g_n(t) i} + \frac{1}{r} f_n'(r) e^{g_n(t) i} + f_n''(r) e^{g_n(t) i}.\end{aligned} \tag{22}$$

Dividing by $e^{g_n(t) i}$ on both sides of (22), we obtain

$$\beta g_n'(t) f_n(r) i = D_n + \frac{1}{r} f_n'(r) + f_n''(r). \tag{23}$$

For $n = 0$, we get

$$f_0''(r) + \frac{1}{r} f_0'(r) = -B_1, \quad (24)$$

which has the general solution: $f_0(r) = (c_1 + c_2 \ln r) - (B_1/4) r^2$.

For $n = 1$, we have

$$f_1''(r) + \frac{1}{r} f_1'(r) - 2\pi\beta i f_1(r) = -eB_1. \quad (25)$$

Let $\overline{\beta}_1^2 = -2\pi\beta i$; then,

$$\frac{1}{\overline{\beta}_1^2} f_1''(r) + \frac{1}{\overline{\beta}_1^2 r} f_1'(r) + f_1(r) = -\frac{eB_1}{\overline{\beta}_1^2}. \quad (26)$$

Let $\hat{r} = \overline{\beta}_1 r$; we have

$$\hat{r}^2 f_1''(\hat{r}) + \hat{r} f_1'(\hat{r}) + \hat{r}^2 f_1(\hat{r}) = -\frac{eB_1}{\overline{\beta}_1^2} \hat{r}^2. \quad (27)$$

The general solution of (27) is

$$f_1(r) = d_1 J_0(\overline{\beta}_1 r) + e_1 Y_0(\overline{\beta}_1 r) - \frac{eB_1}{2\pi\beta} i, \quad (28)$$

where d_1 and e_1 are integration constants and J_0 and Y_0 denote the zero-order Bessel functions of the first kind and the second kind, respectively.

Similarly, for $n = 2$, we have

$$f_2''(r) + \frac{1}{r} f_2'(r) - 2\beta\pi\omega_r f_2(r) i = -B_2, \quad (29)$$

and the general solution is

$$f_2 = d_2 J_0(\overline{\beta}_2 r) + e_2 Y_0(\overline{\beta}_2 r) - \frac{B_2}{2\beta\omega_r\pi} i, \quad (30)$$

where $\overline{\beta}_2^2 = -2\pi\beta\omega_r i$.

Because the boundness of v_1, v_2, c_2, e_1, and e_2 are set to zero, hence, from (14) and the solutions for (20), we have

$$\begin{aligned}
\overline{v}_1 &= \operatorname{Re}\left\{c_1 - \frac{C_1}{4}\overline{r}^2 + \left[d_1 J_0(\beta_1\overline{r}) - \frac{eC_1}{2\pi\alpha} i\right] e^{2\pi\overline{t}i} \right.\\
&\qquad \left. + \left[d_2 J_0(\beta_2\overline{r}) - \frac{C_2}{2\pi\omega_r\alpha} i\right] e^{(2\pi\omega_r\overline{t}+\phi)i}\right\},\\
\overline{v}_2 &= \operatorname{Re}\left\{\hat{c}_1 + \hat{c}_2 \ln\overline{r} - \frac{\overline{C}_1}{4}\overline{r}^2 \right.\\
&\qquad + \left[\hat{d}_1 J_0(\hat{\beta}_1\overline{r}) + \hat{e}_1 Y_0(\hat{\beta}_1\overline{r}) - \frac{e\hat{C}_1}{2\pi\gamma} i\right] e^{2\pi\overline{t}i}\\
&\qquad + \left[\hat{d}_2 J_0(\hat{\beta}_2\overline{r}) + \hat{e}_2 Y_0(\hat{\beta}_2\overline{r}) - \frac{\overline{c}_2 i}{2\pi\omega_r\gamma}\right]\\
&\qquad \left. \times e^{(2\pi\omega_r\overline{t}+\phi)i}\right\},
\end{aligned} \quad (31)$$

where $\hat{\beta}_1^2 = -2\pi\gamma i$, $\hat{\beta}_2^2 = -2\pi\omega_r\gamma i$, $\beta_1^2 = -2\pi\alpha i$, and $\beta_2^2 = -2\pi\omega_r\alpha i$.

As $dJ_0(x)/dx = -J_1(x)$ and $dY_0(x)/dx = -Y_0(x)$, we have

$$\begin{aligned}
\frac{\partial\overline{v}_1}{\partial\overline{r}} &= \operatorname{Re}\left(-\frac{C_1}{2}\overline{r} - d_1\beta_1 J_1(\beta_1\overline{r}) e^{2\pi\overline{t}i}\right.\\
&\qquad \left. - d_2\beta_2 J_1(\beta_2\overline{r}) e^{(2\pi\omega_r\overline{t}+\phi)i}\right),\\
\frac{\partial\overline{v}_2}{\partial\overline{r}} &= \operatorname{Re}\left(\hat{c}_2\frac{1}{\overline{r}} - \frac{\overline{C}_1}{2}\overline{r}\right.\\
&\qquad + \left[-\hat{d}_1\hat{\beta}_1 J_1(\hat{\beta}_1\overline{r}) - \hat{e}_1\hat{\beta}_1 Y_1(\hat{\beta}_1\overline{r})\right] e^{2\pi\overline{t}i}\\
&\qquad \left. + \left[-\hat{d}_2\hat{\beta}_2 J_1(\hat{\beta}_2\overline{r}) - \hat{e}_2\hat{\beta}_2 Y_1(\hat{\beta}_2\overline{r})\right] e^{(2\pi\omega_r\overline{t}+\phi)i}\right).
\end{aligned} \quad (32)$$

Obviously, v_1 satisfies the boundary condition (15) automatically. We now consider the boundary condition (16); namely,

$$\begin{aligned}
\operatorname{Re}&\left[\left(b\hat{c}_1 + l\hat{c}_2 - \left(l + \frac{b}{2}\right)\frac{\overline{C}_1}{2}\right)\right.\\
&+ \left(\left(bJ_0(\hat{\beta}_1) - l\hat{\beta}_1 J_1(\hat{\beta}_1)\right)\hat{d}_1\right.\\
&\qquad \left. + \left(bY_0(\hat{\beta}_1) - l\hat{\beta}_1 Y_1(\hat{\beta}_1)\right)\hat{e}_1 - \frac{eb\overline{C}_1 i}{2\pi\gamma}\right) e^{2\pi\overline{t}i}\\
&+ \left(\hat{d}_2\left(bJ_0(\hat{\beta}_2) - l\hat{\beta}_2 J_1(\hat{\beta}_2)\right)\right.\\
&\qquad + \hat{e}_2\left(bY_0(\hat{\beta}_2) - l\hat{\beta}_2 Y_1(\hat{\beta}_2)\right)\\
&\qquad \left.\left. - \frac{b\overline{C}_2}{2\pi\omega_r\gamma} i\right) e^{(2\pi\omega_r\overline{t}+\phi)i}\right] = 0.
\end{aligned} \quad (33)$$

Further, from boundary conditions (17) and (18), we have

$$\begin{aligned}
\operatorname{Re}&\left[\left(c_1 - \hat{c}_1 - \hat{c}_2 \ln r_0 - \left(C_1 - \hat{C}_1\right)\frac{r_0^2}{4}\right)\right.\\
&+ \left(d_1 J_0(\beta_1 r_0) - \hat{d}_1 J_0(\hat{\beta}_1 r_0) - \hat{e}_1 Y_0(\hat{\beta}_1 r_0)\right.\\
&\qquad \left. - \left(\gamma C_1 - \alpha\overline{C}_1\right)\frac{ei}{2\pi\alpha\gamma}\right) e^{2\pi\overline{t}i}\\
&+ \left(d_2 J_0(\beta_2 r_0) - \hat{d}_2 J_0(\hat{\beta}_2 r_0)\right.\\
&\qquad \left. - \hat{e}_2 Y_0(\hat{\beta}_2 r_0) - \left(\gamma C_2 - \alpha\overline{C}_2\right)\frac{i}{2\pi\omega_r\gamma\alpha}\right)\\
&\left. \times e^{(2\pi\omega_r\overline{t}+\phi)i}\right] = 0,
\end{aligned}$$

$$\operatorname{Re}\left[\left(\left(\mu^*\overline{C}_1 - C_1\right)\frac{r_0}{2} - \mu^*\frac{\widehat{c}_2}{r_0}\right)\right.$$
$$+\left(-d_1\beta_1 J_1(\beta_1 r_0) + \widehat{d}_1\mu^*\widehat{\beta}_1 J_1\left(\widehat{\beta}_1 r_0\right)\right.$$
$$\left.+\widehat{e}_1\mu^*\widehat{\beta}_1 Y_1\left(\widehat{\beta}_1 r_0\right)\right)e^{2\pi\bar{t}i}$$
$$+\left(-d_2\beta_2 J_1(\beta_2 r_0) + \widehat{d}_2\mu^*\widehat{\beta}_2 J_1\left(\widehat{\beta}_2 r_0\right)\right.$$
$$\left.+\widehat{e}_2\mu^*\widehat{\beta}_2 Y_1\left(\widehat{\beta}_2 r_0\right)\right)$$
$$\left.\times e^{(2\pi\omega_r\bar{t}+\phi)i}\right] = 0. \tag{34}$$

As (33)-(34) must be satisfied for any instant of time t, we require that the constant terms and the coefficients of the exponential terms all vanish; namely,

$$b\widehat{c}_1 + l\widehat{c}_2 - \left(l + \frac{b}{2}\right)\frac{\overline{C}_1}{2} = 0,$$
$$c_1 - \widehat{c}_1 - \widehat{c}_2 \ln r_0 - \left(C_1 - \overline{C}_1\right)\frac{r_0^2}{4} = 0,$$
$$\left(\mu^*\overline{C}_1 - C_1\right)\frac{r_0}{2} - \mu^*\frac{\widehat{c}_2}{r_0} = 0,$$
$$\widehat{d}_1\left(bJ_0\left(\widehat{\beta}_1\right) - l\widehat{\beta}_1 J_1\left(\widehat{\beta}_1\right)\right) + \widehat{e}_1\left(bY_0\left(\widehat{\beta}_1\right) - l\widehat{\beta}_1 Y_1\left(\widehat{\beta}_1\right)\right)$$
$$-\frac{eb\overline{C}_1}{2\pi\gamma}i = 0,$$
$$d_1 J_0(\beta_1 r_0) - \widehat{d}_1 J_0\left(\widehat{\beta}_1 r_0\right) - \widehat{e}_1 Y_0\left(\widehat{\beta}_1 r_0\right) - \frac{eC_1}{2\pi\alpha}i$$
$$+\frac{e\overline{C}_1}{2\pi\gamma}i = 0,$$
$$-d_1\beta_1 J_1(\beta_1 r_0) + \widehat{d}_1\mu^*\widehat{\beta}_1 J_1\left(\widehat{\beta}_1 r_0\right) + \widehat{e}_1\mu^*\widehat{\beta}_1 Y_1\left(\widehat{\beta}_1 r_0\right)$$
$$= 0,$$
$$\widehat{d}_2\left(bJ_0\left(\widehat{\beta}_2\right) - l\widehat{\beta}_2 J_1\left(\widehat{\beta}_2\right)\right) + \widehat{e}_2\left(bY_0\left(\widehat{\beta}_2\right) - l\widehat{\beta}_2 Y_1\left(\widehat{\beta}_2\right)\right)$$
$$-\frac{b\overline{C}_2}{2\pi\omega_r\gamma}i = 0,$$
$$d_2 J_0(\beta_2 r_0) - \widehat{d}_2 J_0\left(\widehat{\beta}_2 r_0\right) - \widehat{e}_2 Y_0\left(\widehat{\beta}_2 r_0\right) - \frac{C_1}{2\pi\omega_r\alpha}i$$
$$+\frac{\overline{C}_2}{2\pi\omega_r\gamma}i = 0,$$
$$-d_2\beta_2 J_1(\beta_2 r_0) + \widehat{d}_2\mu^*\widehat{\beta}_2 J_1\left(\widehat{\beta}_2 r_0\right) + \widehat{e}_2\mu^*\widehat{\beta}_2 Y_1\left(\widehat{\beta}_2 r_0\right)$$
$$= 0. \tag{35}$$

Solving the above system of equations yields

$$c_1 = \left(\ln r_0 - \frac{l}{b}\right)\left(\left(\mu^*\overline{C}_1 - C_1\right)\frac{r_0^2}{2\mu^*}\right)$$
$$+\left(\frac{l}{b} + \frac{1 - r_0^2}{2}\right)\frac{\overline{C}_1}{2} + C_1\frac{r_0^2}{4},$$
$$\widehat{c}_1 = -\frac{l}{b}\left(\left(\mu^*\overline{C}_1 - C_1\right)\frac{r_0^2}{2\mu^*}\right) + \left(\frac{l}{b} + \frac{1}{2}\right)\frac{\overline{C}_1}{2},$$
$$\widehat{c}_2 = \left(\mu^*\overline{C}_1 - C_1\right)\frac{r_0^2}{2\mu^*},$$
$$d_1 = \mu^*\left[\left(J_1\left(\widehat{\beta}_1 r_0\right)Y_0\left(\widehat{\beta}_1 r_0\right) - J_0\left(\widehat{\beta}_1 r_0\right)Y_1\left(\widehat{\beta}_1 r_0\right)\right)\right.$$
$$\times\frac{eb\widehat{\beta}_1\overline{C}_1 i}{2\pi\gamma} + \left(\gamma C_1 - \alpha\overline{C}_1\right)$$
$$\times\left[J_1\left(\widehat{\beta}_1 r_0\right)\left(bY_0\left(\widehat{\beta}_1\right) - l\widehat{\beta}_1 Y_1\left(\widehat{\beta}_1\right)\right)\right.$$
$$\left.-Y_1\left(\widehat{\beta}_1 r_0\right)\left(bJ_0\left(\widehat{\beta}_1\right) - l\widehat{\beta}_1 J_1\left(\widehat{\beta}_1\right)\right)\right]$$
$$\left.\times\frac{\widehat{\beta}_1 ei}{2\pi\gamma\alpha}\right] / \left(bJ_0\left(\widehat{\beta}_1\right) - l\widehat{\beta}_1 J_1\left(\widehat{\beta}_1\right)\right)$$
$$\times\left(\beta_1 J_1(\beta_1 r_0)Y_0\left(\widehat{\beta}_1 r_0\right) - \mu^*\widehat{\beta}_1 Y_1\left(\widehat{\beta}_1 r_0\right)J_0(\beta_1 r_0)\right)$$
$$+\left(bY_0\left(\widehat{\beta}_1\right) - l\widehat{\beta}_1 Y_1\left(\widehat{\beta}_1\right)\right)$$
$$\times\left(\mu^*\widehat{\beta}_1 J_0(\beta_1 r_0)J_1\left(\widehat{\beta}_1 r_0\right) - \beta_1 J_1(\beta_1 r_0)J_0\left(\widehat{\beta}_1 r_0\right)\right),$$
$$\widehat{d}_1 = \left[\left(\beta_1 J_1(\beta_1 r_0)Y_0\left(\widehat{\beta}_1 r_0\right)\right.\right.$$
$$\left.-\mu^*\widehat{\beta}_1 Y_1\left(\widehat{\beta}_1 r_0\right)J_0(\beta_1 r_0)\right)$$
$$\times\frac{eb\overline{C}_1}{2\pi\gamma}i + \frac{\left(\gamma C_1 - \alpha\overline{C}_1\right)}{2\pi\gamma\alpha}$$
$$\times\left(bY_0\left(\widehat{\beta}_1\right) - l\widehat{\beta}_1 Y_1\left(\widehat{\beta}_1\right)\right)$$
$$\left.\times e\beta_1 J_1(\beta_1 r_0)i\right] / \left(bJ_0\left(\widehat{\beta}_1\right) - l\widehat{\beta}_1 J_1\left(\widehat{\beta}_1\right)\right)$$
$$\times\left(\beta_1 J_1(\beta_1 r_0)Y_0\left(\widehat{\beta}_1 r_0\right)\right.$$
$$\left.-\mu^*\widehat{\beta}_1 Y_1\left(\widehat{\beta}_1 r_0\right)J_0(\beta_1 r_0)\right)$$
$$+\left(bY_0\left(\widehat{\beta}_1\right) - l\widehat{\beta}_1 Y_1\left(\widehat{\beta}_1\right)\right)$$
$$\times\left(\mu^*\widehat{\beta}_1 J_0(\beta_1 r_0)J_1\left(\widehat{\beta}_1 r_0\right)\right.$$
$$\left.-\beta_1 J_1(\beta_1 r_0)J_0\left(\widehat{\beta}_1 r_0\right)\right),$$
$$\widehat{e}_1 = \left[\left(\mu^*\widehat{\beta}_1 J_0(\beta_1 r_0)J_1\left(\widehat{\beta}_1 r_0\right)\right.\right.$$
$$\left.-\beta_1 J_0\left(\widehat{\beta}_1 r_0\right)J_1(\beta_1 r_0)\right)$$

$$
\begin{aligned}
&\times \frac{eb\overline{C}_1 i}{2\pi\gamma} - \left(bJ_0\left(\widehat{\beta}_1\right) - l\widehat{\beta}_1 J_1\left(\widehat{\beta}_1\right)\right) \\
&\times \left(\gamma C_1 - \alpha\overline{C}_1\right) \\
&\times J_1\left(\beta_1 r_0\right) \left.\frac{\beta_1 e i}{2\pi\alpha\gamma}\right] / \left(bJ_0\left(\widehat{\beta}_1\right) - l\widehat{\beta}_1 J_1\left(\widehat{\beta}_1\right)\right) \\
&\times \left(\beta_1 J_1\left(\beta_1 r_0\right) Y_0\left(\widehat{\beta}_1 r_0\right)\right. \\
&\quad \left. -\mu^* \widehat{\beta}_1 Y_1\left(\widehat{\beta}_1 r_0\right) J_0\left(\beta_1 r_0\right)\right) \\
&+ \left(bY_0\left(\widehat{\beta}_1\right) - l\widehat{\beta}_1 Y_1\left(\widehat{\beta}_1\right)\right) \\
&\times \left(\mu^* \widehat{\beta}_1 J_0\left(\beta_1 r_0\right) J_1\left(\widehat{\beta}_1 r_0\right) - \beta_1 J_1\left(\beta_1 r_0\right) J_0\left(\widehat{\beta}_1 r_0\right)\right),
\end{aligned}
$$

$$
\begin{aligned}
d_2 = \mu^* \Bigg[&\left(J_1\left(\widehat{\beta}_2 r_0\right) Y_0\left(\widehat{\beta}_2 r_0\right) - J_0\left(\widehat{\beta}_2 r_0\right) Y_1\left(\widehat{\beta}_2 r_0\right)\right) \\
&\times \frac{b\widehat{\beta}_2 \overline{C}_1 i}{2\pi\omega_r\gamma} + \left(\gamma C_2 - \alpha\overline{C}_2\right) \\
&\times \left[J_1\left(\widehat{\beta}_2 r_0\right)\left(bY_0\left(\widehat{\beta}_2\right) - l\widehat{\beta}_2 Y_1\left(\widehat{\beta}_2\right)\right)\right. \\
&\quad \left. -Y_1\left(\widehat{\beta}_2 r_0\right)\left(bJ_0\left(\widehat{\beta}_2\right) - l\widehat{\beta}_2 J_1\left(\widehat{\beta}_2\right)\right)\right] \\
&\times \left.\frac{\widehat{\beta}_2 i}{2\pi\omega_r\gamma\alpha}\right] / \left(bJ_0\left(\widehat{\beta}_2\right) - l\widehat{\beta}_2 J_1\left(\widehat{\beta}_2\right)\right) \\
&\times \left(\beta_2 J_1\left(\beta_2 r_0\right) Y_0\left(\widehat{\beta}_2 r_0\right)\right. \\
&\quad \left. -\mu^* \widehat{\beta}_2 Y_1\left(\widehat{\beta}_2 r_0\right) J_0\left(\beta_2 r_0\right)\right) \\
&+ \left(bY_0\left(\widehat{\beta}_2\right) - l\widehat{\beta}_2 Y_1\left(\widehat{\beta}_2\right)\right) \\
&\times \left(\mu^* \widehat{\beta}_2 J_0\left(\beta_2 r_0\right) J_1\left(\widehat{\beta}_2 r_0\right)\right. \\
&\quad \left. -\beta_2 J_1\left(\beta_2 r_0\right) J_0\left(\widehat{\beta}_2 r_0\right)\right),
\end{aligned}
$$

$$
\begin{aligned}
\widehat{d}_2 = \Big[&\left(\beta_2 J_1\left(\beta_2 r_0\right) Y_0\left(\widehat{\beta}_2 r_0\right)\right. \\
&\quad \left. -\mu^* \widehat{\beta}_2 Y_1\left(\widehat{\beta}_2 r_0\right) J_0\left(\beta_2 r_0\right)\right) \\
&\times \frac{b\overline{C}_1}{2\pi\omega_r\gamma} i + \frac{\left(\gamma C_1 - \alpha\overline{C}_1\right)}{2\pi\gamma\alpha\omega_r} \\
&\times \left(bY_0\left(\widehat{\beta}_2\right) - l\widehat{\beta}_2 Y_1\left(\widehat{\beta}_2\right)\right) \\
&\times \beta_2 J_1\left(\beta_2 r_0\right) i\Big] / \left(bJ_0\left(\widehat{\beta}_2\right) - l\widehat{\beta}_2 J_1\left(\widehat{\beta}_2\right)\right) \\
&\times \left(\beta_2 J_1\left(\beta_2 r_0\right) Y_0\left(\widehat{\beta}_2 r_0\right)\right. \\
&\quad \left. -\mu^* \widehat{\beta}_2 Y_1\left(\widehat{\beta}_2 r_0\right) J_0\left(\beta_2 r_0\right)\right) \\
&+ \left(bY_0\left(\widehat{\beta}_2\right) - l\widehat{\beta}_2 Y_1\left(\widehat{\beta}_2\right)\right) \\
&\times \left(\mu^* \widehat{\beta}_2 J_0\left(\beta_2 r_0\right) J_1\left(\widehat{\beta}_2 r_0\right)\right. \\
&\quad \left. -\beta_2 J_1\left(\beta_2 r_0\right) J_0\left(\widehat{\beta}_2 r_0\right)\right),
\end{aligned}
$$

$$
\begin{aligned}
\widehat{e}_2 = \Big[&\left(\mu^* \widehat{\beta}_2 J_0\left(\beta_2 r_0\right) J_1\left(\widehat{\beta}_2 r_0\right)\right. \\
&\quad \left. -\beta_2 J_0\left(\widehat{\beta}_2 r_0\right) J_1\left(\beta_2 r_0\right)\right) \\
&\times \frac{b\overline{C}_1 i}{2\pi\omega_r\gamma} - \left(bJ_0\left(\widehat{\beta}_2\right) - l\widehat{\beta}_2 J_1\left(\widehat{\beta}_2\right)\right) \\
&\times \left(\gamma C_1 - \alpha\overline{C}_1\right) J_1\left(\beta_2 r_0\right) \\
&\times \left.\frac{\beta_2 i}{2\pi\omega_r\alpha\gamma}\right] / \left(bJ_0\left(\widehat{\beta}_2\right) - l\widehat{\beta}_2 J_1\left(\widehat{\beta}_2\right)\right) \\
&\times \left(\beta_2 J_1\left(\beta_2 r_0\right) Y_0\left(\widehat{\beta}_2 r_0\right)\right. \\
&\quad \left. -\mu^* \widehat{\beta}_2 Y_1\left(\widehat{\beta}_2 r_0\right) J_0\left(\beta_2 r_0\right)\right) \\
&+ \left(bY_0\left(\widehat{\beta}_2\right) - l\widehat{\beta}_2 Y_1\left(\widehat{\beta}_2\right)\right) \\
&\times \left(\mu^* \widehat{\beta}_2 J_0\left(\beta_2 r_0\right) J_1\left(\widehat{\beta}_2 r_0\right)\right. \\
&\quad \left. -\beta_2 J_1\left(\beta_2 r_0\right) J_0\left(\widehat{\beta}_2 r_0\right)\right).
\end{aligned} \tag{36}
$$

To show the flow behavior and the effect of the slip parameter, we investigate the velocity profiles in the arteries with different values of the slip parameter under various different conditions. In the first example of investigation, the radius of the artery is taken as $r = b = 0.15$ cm, and the other parameters are set to $A_0 = 698.65\,\text{dyne/cm}^3$, $A_g = 0.5g$, $f_b = f_p = 1.2$, $\phi = 0$, $C_1 = 6.6$, $C_2 = 4.64$, $A_1 = 1.2A_0$, and $\rho_1/\rho_2 = 1$. Figure 1 shows the 3-dimensional velocity profile as a function of time and location and the 2-dimensional velocity profile as a function of time at three different radial locations for two different slip parameters $l = 0$ (no-slip) and $l = 2$. The results show that boundary slip has a very dramatical effect on the fluid flow in the artery. It affects not only the magnitude of the flow velocity significantly, but also the flow pattern and velocity profile on the cross-section of the artery. For the no-slip flow ($l_b = 0$), the pulsatile flow nature gradually disappears toward the arterial wall, while with boundary slip, the flow near the arterial wall also displays a pulsatile nature.

We then investigate whether the above observed flow phenomena associated with boundary slip are affected or not by the radius of the artery, and for this purpose, we consider the fluid flow through an artery with a larger radius $r = 0.5$ cm. The constant pressure gradient is set to $A_0 = 32\,\text{dyne/cm}^3$ in order to achieve a mean velocity magnitude approximately equal to that in the smaller artery, while all other parameters are set to the same values as those used for the smaller radius. Figure 2 shows the velocity profile in the artery for two different slip parameter values including $l_b = 0$ (no-slip) and $l_b = 2$. The 3-dimensional graph shows the variation of the flow velocity with time and radial position, while the 2-dimensional graphs demonstrate the variation of the flow velocity with time at three different radial locations including $r = 0$ (centre), $r = 0.6$ (inner-outer layers interface), and $r = 1$ (arterial wall). From Figures 1 and 2, it is clear that the boundary slip related flow phenomena and behavior observed for the smaller artery also appear in the artery with a larger radius, and further, a more significant pulsatile nature of fluid flow is observed for the larger artery.

To further investigate the effect of the slip parameter on the velocity profile near the artery wall, we show in Figure 3 the velocity of fluid on the artery wall for four different values of the slip parameter including $l_b = 0, 2, 4, 6$, and 8. The results clearly demonstrate that the slip parameter has a very significant effect on the near-wall velocity and that the magnitude of the average wall velocity is proportional to the slip parameter.

4. Numerical Investigation

A numerical scheme, based on the finite different method, is established to solve the underlying boundary value problem for the general case $m \neq 0$, consisting of (14) and boundary condition (15)–(19). To validate the numerical technique, we apply the numerical scheme to generate a series of numerical solutions for the case $m = 0$ and then compare the numerical results with the exact solution derived in Section 3.

Figure 4 presents the velocity profile in the small and large arteries for two different slip parameters $l_b = 0$ (no-slip) and $l_b = 2$ obtained by the numerical technique. The numerical errors between the exact solution and the numerical solution, $E_r = V - U$, are presented in Figure 5 in which V is the exact solution and U is the numerical solution. The results clearly indicate that the numerical solution converges to the exact solution. This shows that a larger slip length has a lower convergence rate.

We then investigate the flow phenomena for the general case $m \neq 0$, and here we consider $m = -1/4$ in the investigation. Figure 6 gives the 3D graph showing the convergence of the transient velocity field to a steady state pulsatile velocity field and also demonstrating the substantial influence of boundary slip on the steady state velocity profile in both magnitude and flow pattern. Figure 7 shows the variations of velocities with time at three arterial locations for different slip parameters and artery radii and also clearly demonstrates the significant effect of boundary slip on the flow through the artery. Figure 8 shows the variation of fluid velocity along the artery wall under different slip parameters and artery radii. The results show that as the slip parameter increases, the time required for achieving convergence results increases, and the magnitude of the average steady state velocity also increases.

5. Conclusion

In this paper, a mathematical model for the transient pulsatile flow of fluids through vessels, taking into account boundary slip and the Fahraeus-Lindqvist effect, is established. For a special case of the underlying boundary value problem, an exact solution for the velocity field has been derived in explicit form, which provides one with an exact analytical method for investigating the flow phenomena under the special case and also a mean for validating the subsequently developed numerical scheme for generating numerical results for the general case. Our analytical and numerical studies show that for the flow of fluids with the Fahraeus-Lindqvist effect, boundary slip has a very significant influence on the magnitude of the mean flow velocity and on the flow pattern and velocity profile on the cross-section. With boundary slip, the boundary layer near the wall also displays significant pulsatile flow nature. The results also show that as the boundary slip length increases, the convergence rate of numerical results to the exact solutions decreases and the time required to achieve the steady state pulsatile flow increases.

References

[1] A. C. Eringen, “Continuum theory of dense rigid suspensions,” *Rheologica Acta*, vol. 30, no. 1, pp. 23–32, 1991.

[2] A. C. Eringen, “A continuum theory of dense suspensions,” *Zeitschrift für Angewandte Mathematik und Physik*, vol. 56, no. 3, pp. 529–547, 2005.

[3] T. Ariman, M. A. Turk, and N. D. Sylvester, “Microcontinuum fluid mechanics—a review,” *International Journal of Engineering Science*, vol. 11, no. 8, pp. 905–930, 1973.

[4] M. A. Turk, N. D. Sylvester, and T. Ariman, “On pulsatile blood flow,” *Transactions of the Society of Rheology*, vol. 17, pp. 1–21, 1973.

[5] L. Debnath, “On a microcontinuum model of pulsatile blood flow,” *Acta Mechanica*, vol. 24, no. 3-4, pp. 165–177, 1976.

[6] G. Ahmadi, “A continuum theory of blood flow,” *Scientia Sinica*, vol. 24, no. 10, pp. 1465–1474, 1981.

[7] S. N. Majhi and L. Usha, “Modelling the Fahraeus-Lindqvist effect through fluids of differential type,” *International Journal of Engineering Science*, vol. 26, no. 5, pp. 503–508, 1988.

[8] K. Haldar and H. I. Andersson, “Two-layered model of blood flow through stenosed arteries,” *Acta Mechanica*, vol. 117, pp. 221–228, 1996.

[9] D. S. Sankar and Y. Yatim, “Comparative analysis of mathematical models for blood flow in tapered constricted arteries,” *Abstract and Applied Analysis*, vol. 2012, Article ID 235960, 34 pages, 2012.

[10] S. N. Majhi and V. R. Nair, “Pulsatile flow of third grade fluids under body acceleration-Modelling blood flow,” *International Journal of Engineering Science*, vol. 32, no. 5, pp. 839–846, 1994.

[11] M. Massoudi and T. X. Phuoc, “Pulsatile flow of blood using a modified second-grade fluid model,” *Computers & Mathematics with Applications*, vol. 56, no. 1, pp. 199–211, 2008.

[12] J. C. Slattery, *Advanced Transport Phenomena*, Cambridge University Press, 1999.

[13] R. Pit, H. Hervet, and L. Léger, “Direct experimental evidence of slip in hexadecane: solid interfaces,” *Physical Review Letters*, vol. 85, no. 5, pp. 980–983, 2000.

[14] R. Tuinier and T. Taniguchi, “Polymer depletion-induced slip near an interface,” *Journal of Physics Condensed Matter*, vol. 17, no. 2, pp. L9–L14, 2005.

[15] B.-Y. Cao, M. Chen, and Z.-Y. Guo, “Velocity slip of liquid flow in nanochannels,” *Acta Physica Sinica*, vol. 55, no. 10, pp. 5305–5310, 2006.

[16] L. Szalmas, “Slip-flow boundary condition for straight walls in thelattice Boltzmann model,” *Physical Review E*, vol. 7306, no. 6, article 6710, 2006.

[17] J. P. Pascal, “Instability of power-law fluid flow down a porous incline,” *Journal of Non-Newtonian Fluid Mechanics*, vol. 133, no. 2-3, pp. 109–120, 2006.

[18] K. C. Sahu, P. Valluri, P. D. M. Spelt, and O. K. Matar, "Linear instability of pressure-driven channel flow of a Newtonian and a Herschel-Bulkley fluid," *Physics of Fluids*, vol. 20, no. 10, Article ID 109902, 2008.

[19] J. Xu and Y. Li, "Boundary conditions at the solid-liquid surface over the multiscale channel size from nanometer to micron," *International Journal of Heat and Mass Transfer*, vol. 50, no. 13-14, pp. 2571–2581, 2007.

[20] Y. Zhu and S. Granick, "Rate-dependent slip of Newtonian liquid at smooth surfaces," *Physical Review Letters*, vol. 87, no. 9, Article ID 096105, pp. 961051–961054, 2001.

[21] Y. H. Wu, B. Wiwatanapataphee, and M. Hu, "Pressure-driven transient flows of Newtonian fluids through microtubes with slip boundary," *Physica A*, vol. 387, no. 24, pp. 5979–5990, 2008.

[22] B. Wiwatanapataphee, Y. H. Wu, M. Hu, and K. Chayantrakom, "A study of transient flows of Newtonian fluids through micro-annuals with a slip boundary," *Journal of Physics A*, vol. 42, no. 6, article 065206, 2009.

[23] G. C. Georgiou and G. Kaoullas, *Newtonian Flow in a Triangularduct with Slip at the Wall*, Mecanica, 2013.

[24] G. Kaoullas and G. C. Georgiou, *Newtonian Poiseuille Flows with Slip and Non-Zero Slip Yield Stress*, Mecanica, 2013.

[25] Y. H. Wu, B. Wiwatanapataphee, and X. Yu, "An enthalpy control volume method for transient mass and heat transport with solidification," *International Journal of Computational Fluid Dynamics*, vol. 18, no. 7, pp. 577–584, 2004.

[26] B. Wiwatanapataphee, "Modelling of non-Newtonian blood flow through stenosed coronary arteries," *Dynamics of Continuous, Discrete & Impulsive Systems B*, vol. 15, no. 5, pp. 619–634, 2008.

[27] S. Amornsamankul, K. Kaorapapong, and B. Wiwatanapataphee, "Three-dimensional simulation of femur bone and implant in femoral canal using finite element method," *International Journal of Mathematics and Computers in Simulation*, vol. 4, no. 4, pp. 171–178, 2010.

[28] Y. H. Wu and B. Wiwatanapataphee, "Modelling of turbulent flow and multi-phase heat transfer under electromagnetic force," *Discrete and Continuous Dynamical Systems B*, vol. 8, no. 3, pp. 695–706, 2007.

[29] H.-B. Lee, I. W. Yeo, and K.-K. Lee, "Water flow and slip on NAPL-wetted surfaces of a parallel-walled fracture," *Geophysical Research Letters*, vol. 34, no. 19, Article ID L19401, 2007.

[30] B. Wiwatanapataphee, D. Poltem, Y. H. Wu, and Y. Lenbury, "Simulation of pulsatile flow of blood in stenosed coronary artery bypass with graft," *Mathematical Biosciences and Engineering*, vol. 3, no. 2, pp. 371–383, 2006.

[31] C. S. Man and Q. K. Sun, "On the significance of normal stress effects in the flow of glaciers," *International Glaciological Society*, pp. 268–273, 1987.

[32] C.-S. Man, "Nonsteady channel flow of ice as a modified second-order fluid with power-law viscosity," *Archive for Rational Mechanics and Analysis*, vol. 119, no. 1, pp. 35–57, 1992.

Hindawi Publishing Corporation
Abstract and Applied Analysis
Volume 2013, Article ID 380484, 9 pages
http://dx.doi.org/10.1155/2013/380484

Research Article

Analytical Solutions of Boundary Values Problem of 2D and 3D Poisson and Biharmonic Equations by Homotopy Decomposition Method

Abdon Atangana[1] and Adem Kılıçman[2]

[1] *Institute for Groundwater Studies, Faculty of Natural and Agricultural Sciences, University of the Free State, Bloemfontein 9300, South Africa*
[2] *Department of Mathematics and Institute for Mathematical Research, University of Putra Malaysia, 43400 Serdang, Selangor, Malaysia*

Correspondence should be addressed to Adem Kılıçman; kilicman@yahoo.com

Received 13 June 2013; Accepted 18 August 2013

Academic Editor: Santanu Saha Ray

The homotopy decomposition method, a relatively new analytical method, is used to solve the 2D and 3D Poisson equations and biharmonic equations. The method is chosen because it does not require the linearization or assumptions of weak nonlinearity, the solutions are generated in the form of general solution, and it is more realistic compared to the method of simplifying the physical problems. The method does not require any corrected function or any Lagrange multiplier and it avoids repeated terms in the series solutions compared to the existing decomposition method including the variational iteration method, the Adomian decomposition method, and Homotopy perturbation method. The approximated solutions obtained converge to the exact solution as N tends to infinity.

1. Introduction

The numerical solution of Poisson equations and biharmonic equations is an important problem in numerical analysis. A vast arrangement of investigating effort has been published on the development of numerical solution of Poisson equations and biharmonic equations. The finite difference schemes of second and fourth order for the solution of Poisson's equation in polar coordinates have been derived by Mittal and Gahlaut [1]. A numerical method to interpolate the source terms of Poisson's equation by using B-spline approximation has been devised by Perrey-Debain and ter Morsche [2]. Sutmann and Steffen [3] proposed compact approximation schemes for the Laplace operator of fourth and sixth order; the schemes are based on a Padé approximation of the Taylor expansion for the discretized Laplace operator. Ge [4] used fourth-order compact difference discretization scheme with unequal mesh sizes in different coordinate directions to solve a 3D Poisson equation on a cubic domain. Gumerov and Duraiswami [5] developed a complete translation theory for the biharmonic equation in three dimensions. Khattar et al. [6] derived a fourth-order finite difference approximation based on arithmetic average discretization for the solution of three-dimensional nonlinear biharmonic partial differential equations on a 19-point compact stencil using coupled approach. Altas et al. [7] used multigrid and preconditioned Krylov iterative methods to solve three-dimensional nonlinear biharmonic partial differential equations. Jeon [8] derived scalar boundary integral equation formulas for both interior and exterior biharmonic equations with the Dirichlet boundary data. A spectral collocation method for numerically solving two-dimensional biharmonic boundary-value problems has been reported in [9]. An indirect radial-basis-function collocation method for numerically solving biharmonic boundary-value problems has been reported in [10]. A high-order boundary integral equation method for the solution of biharmonic equations has been presented in [11]. A Galerkin boundary node method for solving biharmonic problems was developed in [12]. An integral collocation approach based on Chebyshev polynomials for numerically solving biharmonic equations for the case of irregularly shaped domains has been developed by Mai-Duy et al. [13]. A numerical method, based on neural-network-based functions, for solving partial differential equations has been in [14]. Mai-Duy and Tanner [15] presented a collocation method based on a Cartesian grid and a 1D integrated radial basis function scheme for numerically solving partial differential equations in rectangular domains and Haar wavelet presented in [16]. The aim of this paper is to solve these problems via the homotopy decomposition method.

2. Method

In this study we follow the method of [17–20]. In order to illustrate the basic idea of this method we consider a general nonlinear nonhomogeneous partial differential equation with initial conditions of the following form

$$\frac{\partial^m U(x,t)}{\partial t^m} = L(U(x,t)) + N(U(x,t)) + f(x,t), \quad m = 1,2,3,\ldots, \tag{1}$$

subject to the initial conditions

$$\frac{\partial^i U(x,0)}{\partial t^i} = f_m(x), \qquad \frac{\partial^{m-1} U(x,0)}{\partial t^{m-1}} = 0, \quad i = 0,1,2,\ldots,m-2, \tag{2}$$

where f is a known function, N is the general nonlinear differential operator, and L represents a linear differential operator. The method's first step here is to apply the inverse operator $\partial^m/\partial t^m$ of on both sides (1) to obtain

$$\begin{aligned} U(x,t) = {} & \sum_{k=0}^{m-1} \frac{t^k}{k!} \frac{d^k u(x,0)}{dt^k} \\ & + \int_0^t \int_0^{t_1} \cdots \int_0^{t_{m-1}} L(U(x,\tau)) + N(U(x,\tau)) \\ & + f(x,\tau)\, d\tau \cdots dt. \end{aligned} \tag{3}$$

The multi-integrals in (3) can be transformed to

$$\begin{aligned} & \int_0^t \int_0^{t_1} \cdots \int_0^{t_{m-1}} L(U(x,\tau)) + N(U(x,\tau)) + f(x,\tau)\, d\tau \cdots dt_1 \\ & = \frac{1}{(m-1)!} \int_0^t (t-\tau)^{m-1} L(U(x,\tau)) + N(U(x,\tau)) + f(x,\tau)\, d\tau. \end{aligned} \tag{4}$$

So that (3) can be reformulated as

$$\begin{aligned} U(x,t) & = \sum_{k=0}^{m-1} \frac{t^k}{k!} \left\{ \frac{d^k u(x,0)}{dt^k} \right\} \\ & + \frac{1}{(m-1)!} \int_0^t (t-\tau)^{m-1} L(U(x,\tau)) + N(U(x,\tau)) + f(x,\tau)\, d\tau. \end{aligned} \tag{5}$$

Using the homotopy scheme the solution of the previous integral equation is given in a series form as

$$U(x,t,p) = \sum_{n=0}^{\infty} p^n U_n(x,t), \qquad U(x,t) = \lim_{p \to 1} U(x,t,p) \tag{6}$$

and the nonlinear term can be decomposed as

$$NU(r,t) = \sum_{n=1}^{\infty} p^n \mathscr{H}_n(U), \tag{7}$$

where $p \in (0,1]$ is an embedding parameter. $\mathscr{H}_n(U)$ is He's polynomials [21] that can be generated by

$$\mathscr{H}_n(U_0,\ldots,U_n) = \frac{1}{n!} \frac{\partial^n}{\partial p^n} \left[N\left(\sum_{j=0}^{n} p^j U_j(x,t) \right) \right], \quad n = 0,1,2\ldots. \tag{8}$$

The homotopy decomposition method is obtained by the graceful coupling of decomposition method with He's polynomials and is given by

$$\begin{aligned} \sum_{n=0}^{\infty} p^n U_n(x,t) & = T(x,t) + p \frac{1}{(m-1)!} \int_0^t (t-\tau)^{m-1} \\ & \times \left[f(x,\tau) + L\left(\sum_{n=0}^{\infty} p^n U_n(x,\tau) \right) + \sum_{n=0}^{\infty} p^n \mathscr{H}_n(U) \right] d\tau \end{aligned} \tag{9}$$

with

$$T(x,t) = \sum_{k=0}^{m-1} \frac{t^k}{k!} \left\{ \frac{d^k u(x,t)}{dt^k} \mid t = 0 \right\}. \tag{10}$$

Comparing the terms of the same power of p gives the solutions of various orders. The initial guess of the approximation is $T(x,t)$. Some further related results can be seen in [22–25].

Lemma 1 (see [17]). *The complexity of the homotopy decomposition method is of order $O(n)$.*

Proof. The number of computations including product, addition, subtraction, and division are as follows.

In step 2

U_0: 0 because it is obtained directly from the initial conditions

U_1: 3

$\vdots$

U_n: 3.

Now in step 4 the total number of computations is equal to $\sum_{j=0}^{n} U_j(x,t) = 3n = O(n)$. □

3. Solutions of the Main Problems

Problem 1. Consider the following equation

$$\frac{\partial^2 u}{\partial x^2}+\frac{\partial^2 u}{\partial y^2}=\sin(\pi x)\sin(\pi y);$$
$$u(x,y)=0 \text{ along the boundaries,} \quad 0\le x,y\le 1; \tag{11}$$
$$u_x(0,y)=-\frac{\sin(y\pi)}{2\pi}.$$

The exact solution of the previous equation is given as

$$u(x,y)=\frac{\sin(x\pi)\sin(\pi y)}{-2\pi^2}. \tag{12}$$

In the view of the homotopy decomposition method, (11) can be first transformed to

$$\begin{gathered}
u(x,y)=u(0,y)-\frac{\sin(\pi y)}{2\pi}x \\
+\int_0^x (x-\tau)\left[\sin(\pi\tau)\sin(\pi y)-u_{yy}(\tau,y)\right], \\
u(x,y,p)=\sum_{n=0}^{\infty}p^n u_n(x,y).
\end{gathered} \tag{13}$$

Following the decomposition techniques, we obtain the following equation

$$\begin{aligned}
&\sum_{n=0}^{\infty}p^n u_n(x,y) \\
&\quad =T(x,y) \\
&\quad\quad +p\int_0^x (x-\tau)\left[\sin(\pi\tau)\sin(\pi y)\right. \\
&\quad\quad\quad \left.-\frac{\partial^2}{\partial y^2}\left[\sum_{n=0}^{\infty}p^n u_n(x,y)\right]\right].
\end{aligned} \tag{14}$$

Comparing the terms of the same power of p leads to

$$\begin{aligned}
p^0 &: u_0(x,y)=-\frac{\sin(\pi y)}{2\pi}x, \\
p^1 &: u_1(x,y)=\int_0^x (x-\tau)\left[\sin(\pi\tau)\sin(\pi y)-\frac{\partial^2}{\partial y^2}[u_0]\right]d\tau, \\
&\qquad u_1(x,y)=0 \text{ along the boundaries,} \\
p^2 &: u_2(x,y)=\int_0^x (x-\tau)\left[-\frac{\partial^2}{\partial y^2}[u_1]\right]d\tau, \\
p^3 &: u_3(x,y)=\int_0^x (x-\tau)\left[-\frac{\partial^2}{\partial y^2}[u_2]\right]d\tau, \\
p^n &: u_n(x,y)=\int_0^x (x-\tau)\left[-\frac{\partial^2 u_{n-1}}{\partial y^2}\right]d\tau, \\
&\qquad u_n(x,y)=0 \text{ along the boundaries.}
\end{aligned} \tag{15}$$

The following solutions are obtained:

$$\begin{aligned}
u_0(x,y) &= -\frac{\sin(\pi y)}{2\pi}x, \\
u_1(x,y) &= \left[\frac{x}{\pi}-\frac{\pi x^3}{2\times 3!}\right]\sin(\pi y)-\frac{\sin(\pi\tau)\sin(\pi y)}{\pi^2}, \\
u_2(x,y) &= \left[-\frac{x}{\pi}+\frac{\pi x^3}{6}-\frac{\pi^3 x^5}{240}\right]\sin(\pi y)+\frac{\sin(\pi\tau)\sin(\pi y)}{\pi^2}, \\
u_3(x,y) &= \left[\frac{x}{\pi}-\frac{\pi x^3}{6}+\frac{\pi^3 x^5}{120}-\frac{\pi^5 x^7}{10080}\right]\sin(\pi y) \\
&\quad -\frac{\sin(\pi\tau)\sin(\pi y)}{\pi^2}, \\
u_4(x,y) & \\
&= \left[-\frac{x}{\pi}+\frac{\pi x^3}{6}-\frac{\pi^3 x^5}{120}+\frac{\pi^5 x^7}{5040}-\frac{\pi^7 x^9}{725760}\right]\sin(\pi y) \\
&\quad +\frac{\sin(\pi\tau)\sin(\pi y)}{\pi^2}, \\
u_5(x,y) & \\
&= \left[\frac{x}{\pi}-\frac{\pi x^3}{6}+\frac{\pi^3 x^5}{120}-\frac{\pi^5 x^7}{5040}+\frac{\pi^7 x^9}{362880}-\frac{\pi^9 x^{11}}{79833600}\right]\sin(\pi y) \\
&\quad -\frac{\sin(\pi\tau)\sin(\pi y)}{\pi^2}, \\
u_6(x,y) & \\
&= \left[-\frac{x}{\pi}+\frac{\pi x^3}{6}-\frac{\pi^3 x^5}{120}+\frac{\pi^5 x^7}{5040}-\frac{\pi^7 x^9}{362880}\right. \\
&\quad \left.+\frac{\pi^9 x^{11}}{39916800}-\frac{\pi^{11} x^{13}}{12454041600}\right]\sin(\pi y) \\
&\quad +\frac{\sin(\pi\tau)\sin(\pi y)}{\pi^2}, \\
u_7(x,y) & \\
&= \left[\frac{x}{\pi}-\frac{\pi x^3}{6}+\frac{\pi^3 x^5}{120}-\frac{\pi^5 x^7}{5040}+\frac{\pi^7 x^9}{362880}-\frac{\pi^9 x^{11}}{39916800}\right. \\
&\quad \left.+\frac{\pi^{11} x^{13}}{6227020800}-\frac{\pi^{13} x^{15}}{2615348736000}\right]\sin(\pi y) \\
&\quad -\frac{\sin(\pi\tau)\sin(\pi y)}{\pi^2}.
\end{aligned} \tag{16}$$

Table 1: Evaluation of numerical errors for $N = 4$.

x	Y	$u(x, y)$ exact	$u(x, y)$ $N = 4$	Error
0.25	0.25	−0.0253303	−0.0253303	$6.27007 \cdot 10^{-11}$
	0.5	−0.0358224	−0.0358224	$8.86722 \cdot 10^{-11}$
	0.75	−0.0253303	−0.0253303	$6.27007 \cdot 10^{-11}$
	0.95	−0.00560387	−0.00560387	$1.38714 \cdot 10^{-11}$
0.5	0.25	−0.0358224	−0.0358224	$1.26904 \cdot 10^{-11}$
	0.5	−0.0506606	−0.0506604	$1.79469 \cdot 10^{-7}$
	0.75	−0.0358224	−0.0358223	$1.26904 \cdot 10^{-11}$
	0.95	−0.00792506	−0.00792506	$2.80752 \cdot 10^{-8}$
0.75	0.25	−0.0253303	−0.0253195	$1.07646 \cdot 10^{-5}$
	0.5	−0.0358224	−0.0358072	$1.52235 \cdot 10^{-5}$
	0.75	−0.0253303	−0.0253195	$1.07646 \cdot 10^{-5}$
	0.95	−0.00560387	−0.00560148	$2.38148 \cdot 10^{-6}$
0.95	0.25	−0.00560387	−0.00546191	0.000141956
	0.5	−0.00792506	−0.00772431	000200756
	0.75	−0.00560387	−0.00546191	0.000141956
	0.95	−0.00123975	−0.00120835	$3.14051 \cdot 10^{-5}$

In the same manner one can obtain the rest of the components. But for eight terms were computed and the asymptotic solution is given by

$$
\begin{aligned}
u_{N=8}(x, y) &= \left[\frac{x}{2\pi} - \frac{\pi x^3}{2 \times 3!} + \frac{\pi^3 x^5}{2 \times 5!} - \frac{\pi^5 x^7}{2 \times 7!} + \frac{\pi^7 x^9}{2 \times 9!}\right. \\
&\quad \left. - \frac{\pi^9 x^{11}}{2 \times 11!} + \frac{\pi^{11} x^{13}}{2 \times 13!} - \frac{\pi^{13} x^{15}}{2 \times 15!}\right] \sin(\pi y) \\
&\quad - \frac{1}{\pi^2} \sin(x\pi) \sin(y\pi).
\end{aligned} \tag{17}
$$

Therefore in general for any $N > 8$ we have

$$
\begin{aligned}
u_{N=n}(x, y) &= \left[\frac{1}{2\pi^2} \sum_{n=0}^{N} \frac{(-1)^n (x\pi)^{2n+1}}{(2n+1)!}\right] \sin(\pi y) \\
&\quad - \frac{1}{\pi^2} \sin(x\pi) \sin(y\pi), \\
\lim_{N \to \infty} u_N(x, y) &= \frac{1}{2\pi^2} \sin(\pi x) \sin(\pi y) \\
&\quad - \frac{1}{\pi^2} \sin(x\pi) \sin(y\pi) \\
&= -\frac{1}{2\pi^2} \sin(x\pi) \sin(y\pi).
\end{aligned} \tag{18}
$$

This is the exact solution of the problem. Figures 1 and 2 show the comparison of the exact solution and the approximated one for $N = 4$. The approximate solution and the exact solution are compared in Figures 1 and 2, respectively.

The numerical errors for $N = 4$ are evaluated in Table 1.

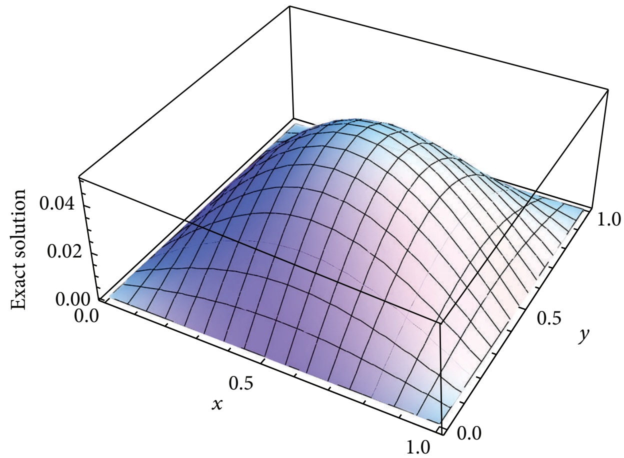

Figure 1: Exact solution.

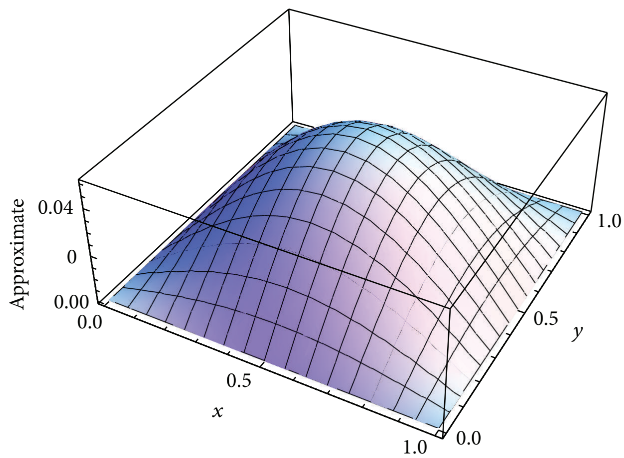

Figure 2: Approximated solution for the 4 first terms.

Problem 2. Consider 3D Poisson equation:

$$
\begin{gathered}
\frac{\partial^2 u}{\partial x^2} + \frac{\partial^2 u}{\partial y^2} + \frac{\partial^2 u}{\partial z^2} = \sin(\pi x) \sin(\pi y) \sin(\pi z), \\
u(x, y, z) = 0 \text{ along the boundaries}, \quad 0 \le x, y \le 1.
\end{gathered} \tag{19}
$$

Following the discussion presented earlier we obtain the following set of integral equations:

$$
\begin{aligned}
p^0 &: u_0(x, y) = -\frac{\sin(\pi y) \sin(\pi z)}{3\pi} x, \\
p^1 &: u_1(x, y) \\
&= \int_0^x (x - \tau) \left[\sin(\pi \tau) \sin(\pi y) \sin(\pi z) - \frac{\partial^2 u_0}{\partial y^2}\right] d\tau, \\
p^n &: u_n(x, y) = \int_0^x (x - \tau) \left[-\frac{\partial^2 u_{n-1}}{\partial y^2}\right] d\tau, \\
&\quad u_n(x, y) = 0 \text{ along the boundaries}, \quad n \ge 2.
\end{aligned} \tag{20}
$$

The following solutions are obtained:

$$u_0(x,y,z) = -\frac{\sin(\pi y)\sin(\pi z)}{3\pi}x,$$

$$u_1(x,y,z) = \left[\frac{1}{\pi}x - \frac{\pi x^3}{9}\right]\sin(\pi y)\sin(\pi z) - \frac{\sin(\pi\tau)\sin(\pi y)\sin(\pi z)}{\pi^2},$$

$$u_2(x,y,z) = \left[-\frac{2}{\pi}x + \frac{\pi x^3}{9} - \frac{\pi^3 x^5}{90}\right]\sin(\pi y)\sin(\pi z) + \frac{2\sin(\pi\tau)\sin(\pi y)\sin(\pi z)}{\pi^2},$$

$$u_3(x,y,z) = \left[\frac{4}{\pi}x - \frac{2\pi x^3}{3} + \frac{\pi^3 x^5}{30} - \frac{\pi^5 x^7}{1890}\right]\sin(\pi y)\sin(\pi z) - \frac{4\sin(\pi\tau)\sin(\pi y)\sin(\pi z)}{\pi^2},$$

$$u_4(x,y,z) = \left[-\frac{8}{\pi}x + \frac{4\pi x^3}{3} - \frac{\pi^3 x^5}{15} + \frac{\pi^5 x^7}{630}\right]\sin(\pi y)\sin(\pi z) + \frac{8\sin(\pi\tau)\sin(\pi y)\sin(\pi z)}{\pi^2},$$

$$u_5(x,y,z) = \left[\frac{16}{\pi}x - \frac{8\pi x^3}{3} + \frac{2\pi^3 x^5}{15} - \frac{\pi^5 x^7}{315} + \frac{\pi^7 x^9}{22680} - \frac{\pi^7 x^{11}}{3742200}\right]\sin(\pi y)\sin(\pi z) - \frac{16\sin(\pi\tau)\sin(\pi y)\sin(\pi z)}{\pi^2}. \tag{21}$$

In the same manner one can obtain the rest of the components. But for six terms were computed and the asymptotic solution is given by

$$u(x,y,z)_{N=6} = \left[\frac{x}{3\pi} - \frac{\pi x^3}{18} + \frac{\pi^3 x^5}{360} - \frac{\pi^5 x^7}{15120} + \frac{\pi^7 x^9}{1088640} - \frac{\pi^9 x^{11}}{119750400}\right]\sin(\pi y)\sin(\pi z) - \frac{2\sin(\pi\tau)\sin(\pi y)\sin(\pi z)}{\pi^2},$$

$$u(x,y,z)_{N=6} = \frac{1}{3\pi^2}\left[\frac{x}{3\pi} - \frac{\pi x^3}{18} + \frac{\pi^3 x^5}{360} - \frac{\pi^5 x^7}{15120} + \frac{\pi^7 x^9}{1088640} - \frac{\pi^9 x^{11}}{119750400}\right]\sin(\pi y)\sin(\pi z) - \frac{2\sin(\pi\tau)\sin(\pi y)\sin(\pi z)}{3\pi^2},$$

$$u(x,y,z)_{N=6} = \frac{1}{3\pi^2}\left[\pi x - \frac{(\pi x)^3}{3!} + \frac{(\pi x)^5}{5!} - \frac{(\pi x)^7}{7!} + \frac{(\pi x)^9}{9!} - \frac{(\pi x)^3}{11!}\right]\sin(\pi y)\sin(\pi z) - \frac{2\sin(\pi\tau)\sin(\pi y)\sin(\pi z)}{3\pi^2}. \tag{22}$$

Therefore, for any $n \geq 6$, the partial sum is given as

$$u_{N=n}(x,y,z) = \frac{1}{3\pi^2}\left[\sum_{k=1}^{N}\frac{(-1)^k(\pi x)^{2k+1}}{(2k+1)!}\right]\sin(\pi y)\sin(\pi z) - \frac{2\sin(\pi\tau)\sin(\pi y)\sin(\pi z)}{3\pi^2}. \tag{23}$$

Thus

$$\begin{aligned} u(x,y,z) &= \lim_{N\to\infty} u_{N=n}(x,y,z) \\ &= \frac{\sin(\pi\tau)\sin(\pi y)\sin(\pi z)}{3\pi^2} - \frac{2\sin(\pi\tau)\sin(\pi y)\sin(\pi z)}{3\pi^2} \\ &= -\frac{\sin(\pi\tau)\sin(\pi y)\sin(\pi z)}{3\pi^2}. \end{aligned} \tag{24}$$

And this is the exact solution to the problem. One can evaluate error committed by choosing the N first terms in the series solutions, in the same manner as in Table 1. The accuracy of the results is estimated by error function

$$R_N(x,y,z) = \left|u_N(x,y,z) - u(x,y,z)\right|. \tag{25}$$

Problem 3. Let us consider the following biharmonic equation

$$\frac{d^4 u(x)}{dx^4} + 4u(x) = 0, \tag{26}$$

for which the exact solution is

$$u(x) = \frac{\operatorname{Exp}[1-x]\cos[x]}{\cos[1]}. \tag{27}$$

The aim of this part is to compare the numerical results obtained via HDM and the method used in [26].

Table 2: Comparison of the HDM and [1] results with the exaction solution for $N = 6$.

x	HDM	Exact	ADM	Err for HDM	Err for ADM
−1.0	7.38906	7.38906	7.38906	$6.78E-16$	$8.88E-16$
−0.6	7.56598	7.56598	7.56598	$4.76E-12$	$7.96E-12$
−0.2	6.02244	6.02244	6.02244	$0.015E-11$	$1.46E-11$
0.2	4.03696	4.03696	4.03696	$0.017E-11$	$1.80E-11$
0.6	2.27883	2.27883	2.27883	$0.015E-11$	$1.46E-11$
1.0	1.0	1.0	1.0	$1.24E-15$	$2.22E-15$

Applying the steps involved in the HDM, we arrive at the following:

$$\begin{aligned}
u_0(x) &= e\operatorname{Sec}(1)\left(1-x+\frac{x^3}{3}\right),\\
u_1(x) &= -e\operatorname{Sec}(1)\left[\frac{x^4}{4}-\frac{x^5}{20}+\frac{x^7}{420}\right],\\
u_2(x) &= -e\operatorname{Sec}(1)\left[-\frac{x^8}{1120}+\frac{x^9}{10080}-\frac{x^{11}}{554400}\right],\\
u_3(x) &= -e\operatorname{Sec}(1)\left[\frac{x^{12}}{2217600}-\frac{x^{13}}{64864800}+\frac{x^{15}}{1135134000}\right],\\
u_4(x) &= -e\operatorname{Sec}(1)\left[-\frac{x^{16}}{16144128000}+\frac{x^{17}}{274450176000}-\frac{x^{19}}{46930980096000}\right],\\
u_5(x) &= -e\operatorname{Sec}(1)\left[\frac{x^{20}}{312873200640000}-\frac{x^{21}}{6570337213440000}+\frac{x^{23}}{1662295315000320000}\right].
\end{aligned} \tag{28}$$

In the same manner, one can obtain the remaining term by using the following recursive formula:

$$u_{n+1}(x) = -\int_0^x (x-t)^3 u_n(t)\,dt. \tag{29}$$

In this paper we consider only the first six terms of the series solution as follows:

$$u_{N=6} = \sum_{n=0}^{5} u_n(x). \tag{30}$$

To access the accuracy of the method used in paper, we compare in Table 2 the numerical results of the above equation, the solution obtained in [26] with the exact solution.

Problem 4. We consider the 2D biharmonic equation

$$\frac{\partial^4 u}{\partial x^4}+2\frac{\partial^4 u}{\partial x^2\partial y^2}+\frac{\partial^4 u}{\partial x^4} = \sin(3\pi x)\sin(3\pi y), \quad 0\le x, y\le 1, \tag{31}$$

subject to the initial conditions:

$$\frac{\partial u(x,y)}{\partial x}\mid(x=0) = \frac{\sin(3\pi y)}{108\pi^3}, \qquad \partial_{x,x}u(0,y)=0, \qquad \partial_{x,x,x}u(0,y) = -\frac{\sin(3\pi y)}{12\pi}. \tag{32}$$

In the view of the homotopy decomposition method, the following integral equations are obtained:

$$\begin{aligned}
p^0 &: u_0(x,y) = \frac{\sin(3\pi y)}{108\pi^3}x-\frac{\sin(3\pi y)}{12\pi}\frac{x^3}{3!},\\
p^1 &: u_1(x,y) = \int_0^x (x-\tau)\left[\sin(\pi\tau)\sin(\pi y)-\frac{\partial^2 u_0}{\partial y^2}-2\frac{\partial^4 u_0}{\partial x^2\partial y^2}\right]d\tau,\\
p^n &: u_n(x,y) = \int_0^x (x-\tau)\left[-\frac{\partial^2 u_{n-1}}{\partial y^2}-2\frac{\partial^4 u_0}{\partial x^2\partial y^2}\right]d\tau,\\
&u_n(x,y)=0 \text{ along the boundaries}, \quad n\ge 2.
\end{aligned} \tag{33}$$

It is worth noting that if the zeroth component $u_0(x,y)$ is defined, then the remaining components $n\ge 1$ can be completely determined such that each term is determined by using the previous terms, and the series solutions are thus entirely determined. Finally, the solution $u(x,y)$ is approximated for $n=4$:

$$\begin{aligned}
u(x,y) &= \sin(3\pi y)\left[\frac{x}{108\pi^3}-\frac{x^3}{72\pi}+\frac{\pi x^5}{160}-\frac{3\pi^3x^7}{2240}+\frac{3\pi^5x^9}{17920}\right.\\
&\left.\quad-\frac{27\pi^7x^{11}}{1971200}+\frac{81\pi^9x^{13}}{102502400}-\frac{81\pi^{11}x^{15}}{7175168000}\right],
\end{aligned} \tag{34}$$

$$\begin{aligned}
u(x,y) &= \frac{\sin(3\pi y)}{324\pi^4}\left[3\pi x-\frac{(3\pi x)^3}{3!}+\frac{(3\pi x)^5}{5!}-\frac{(3\pi x)^7}{7!}+\frac{(3\pi x)^9}{9!}\right.\\
&\left.\quad-\frac{(3\pi x)^{11}}{11!}+\frac{(3\pi x)^{13}}{13!}-\frac{(3\pi x)^{15}}{15!}\right].
\end{aligned} \tag{35}$$

Therefore for any $N\ge 4$ we have the following:

$$u_N(x,y) = \frac{\sin(3\pi y)}{324\pi^4}\sum_{n=0}^{N}\frac{(3\pi x)^{2n+1}}{(2n+1)!}. \tag{36}$$

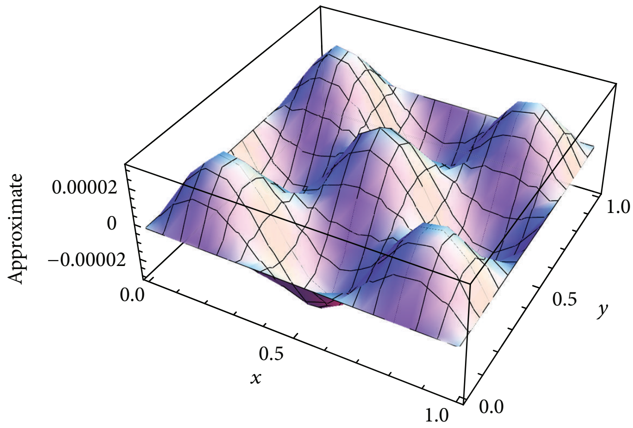

Figure 3: Analytical solution.

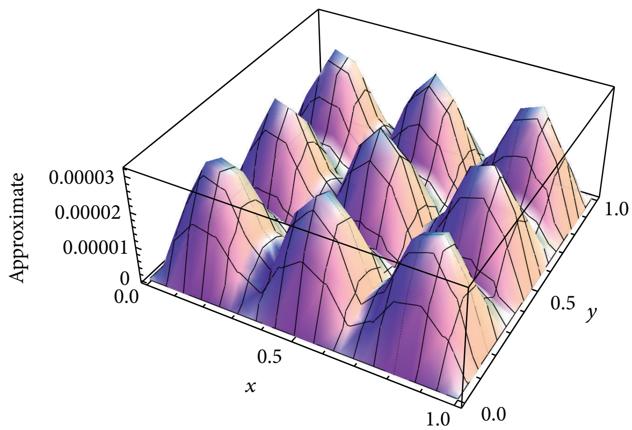

Figure 4: Absolute value of the solution.

Thus

$$\lim_{N\to\infty} u_N(x,y) = \frac{\sin(3\pi y)\sin(3\pi x)}{324\pi^4}. \tag{37}$$

The exact solution of (31) is given by

$$\frac{\sin(3\pi y)\sin(3\pi x)}{324\pi^4} = u(x,y). \tag{38}$$

Figures 3 and 4 are the graphical representation of the previous solution. We have plotted the solution for (31) in Figure 3 and showed absolute value of the solution in Figure 4.

Theorem 2. *Let m be a nonzero natural number and let $(x,y)\in[0,1]\times[0,1]$; then two dimensional biharmonic equation of form*

$$\frac{\partial^4 u}{\partial x^4} + 2\frac{\partial^4 u}{\partial x^2\partial y^2} + \frac{\partial^4 u}{\partial y^4} = \sin(m\pi x)\sin(m\pi y) \tag{39}$$

with $u(x,y)=0$ along the boundaries has an exact solution as follows

$$u(x,y) = \frac{\sin(m\pi x)\sin(m\pi y)}{4m^4\pi^4}. \tag{40}$$

Proof. Use the step of the homotopy decomposition method. □

Problem 5. We consider the 3D biharmonic equation:

$$\begin{gathered}\frac{\partial^4 u}{\partial x^4} + 2\frac{\partial^4 u}{\partial x^2\partial y^2} + 2\frac{\partial^4 u}{\partial x^2\partial z^2} + 2\frac{\partial^4 u}{\partial z^2\partial y^2} + \frac{\partial^4 u}{\partial y^4} + \frac{\partial^4 u}{\partial z^4} \\ = \sin(\pi x)\sin(\pi y)\sin(\pi z), \\ 0\le x,y,z\le 1, \\ u=0, \qquad u_{x,x} = u_{y,y} = u_{z,z} = 0.\end{gathered} \tag{41}$$

In the view of the homotopy decomposition method, the following integral equations are obtained:

$$\begin{aligned} p^0 &: u_0(x,y) = \frac{\sin(3\pi y)}{108\pi^3}x - \frac{\sin(3\pi y)}{12\pi}\frac{x^3}{3!}, \\ p^1 &: u_1(x,y) \\ &= \int_0^x (x-\tau)\left[\sin(\pi\tau)\sin(\pi y)\sin(\pi z) - 2\frac{\partial^4 u_0}{\partial x^2\partial y^2} - 2\frac{\partial^4 u_0}{\partial x^2\partial z^2} - 2\frac{\partial^4 u_0}{\partial z^2\partial y^2} - \frac{\partial^4 u_0}{\partial y^4} - \frac{\partial^4 u_0}{\partial z^4}\right]d\tau, \\ p^n &: u_n(x,y) \\ &= \int_0^x (x-\tau)\left[-2\frac{\partial^4 u_{n-1}}{\partial x^2\partial y^2} - 2\frac{\partial^4 u_{n-1}}{\partial x^2\partial z^2} - 2\frac{\partial^4 u_{n-1}}{\partial z^2\partial y^2} - \frac{\partial^4 u_{n-1}}{\partial y^4} - \frac{\partial^4 u_{n-1}}{\partial z^4}\right]d\tau, \\ & u_n(x,y) = 0 \text{ along the boundaries}, \quad n\ge 2. \end{aligned} \tag{42}$$

Solving the previous integral equations, the series solutions for the first N terms are given as

$$u_N(x,y,z) = \frac{\sin(z\pi)\sin(\pi y)}{9\pi^4}\sum_{n=0}^{N}\frac{(\pi x)^{2n+1}}{(2n+1)!}. \tag{43}$$

Therefore taking the limit at N tending to infinity we obtained

$$u(x,y,z) = \lim_{N\to\infty} u_N(x,y,z) = \frac{\sin(x\pi)\sin(z\pi)\sin(\pi y)}{9\pi^4}. \tag{44}$$

4. Conclusion

In this paper the recent homotopy decomposition [18–21] is used to solve the 2D and 3D Poisson equations and biharmonic equations. The method is chosen because it does not require the linearization or assumptions of weak nonlinearity, the solutions are generated in the form of general solution, and it is more realistic compared to the method of simplifying the physical problems. The method does not require any corrected function any Lagrange multiplier and it avoids repeated terms in the series solutions compared to the existing decomposition method including the variational iteration method and the Adomian decomposition method. The approximated solutions obtained converge to the exact solution as N tends to infinity. The numerical values are presented in Table 1 shows that the method is very efficient and accurate.

Acknowledgment

The authors would like to thank referee(s) for very useful comments regarding the details and their remarks that improved the presentation and the contents of the paper.

References

[1] R. C. Mittal and S. Gahlaut, "High-order finite-difference schemes to solve Poisson's equation in polar coordinates," *IMA Journal of Numerical Analysis*, vol. 11, no. 2, pp. 261–270, 1991.

[2] E. Perrey-Debain and H. G. ter Morsche, "B-spline approximation and fast wavelet transform for an efficient evaluation of particular solutions for Poisson's equation," *Engineering Analysis with Boundary Elements*, vol. 26, no. 1, pp. 1–13, 2002.

[3] G. Sutmann and B. Steffen, "High-order compact solvers for the three-dimensional Poisson equation," *Journal of Computational and Applied Mathematics*, vol. 187, no. 2, pp. 142–170, 2006.

[4] Y. Ge, "Multigrid method and fourth-order compact difference discretization scheme with unequal meshsizes for 3D Poisson equation," *Journal of Computational Physics*, vol. 229, no. 18, pp. 6381–6391, 2010.

[5] N. A. Gumerov and R. Duraiswami, "Fast multipole method for the biharmonic equation in three dimensions," *Journal of Computational Physics*, vol. 215, no. 1, pp. 363–383, 2006.

[6] D. Khattar, S. Singh, and R. K. Mohanty, "A new coupled approach high accuracy numerical method for the solution of 3D non-linear biharmonic equations," *Applied Mathematics and Computation*, vol. 215, no. 8, pp. 3036–3044, 2009.

[7] I. Altas, J. Erhel, and M. M. Gupta, "High accuracy solution of three-dimensional biharmonic equations," *Numerical Algorithms*, vol. 29, no. 1–3, pp. 1–19, 2002.

[8] Y. Jeon, "New indirect scalar boundary integral equation formulas for the biharmonic equation," *Journal of Computational and Applied Mathematics*, vol. 135, no. 2, pp. 313–324, 2001.

[9] N. Mai-Duy and R. I. Tanner, "A spectral collocation method based on integrated Chebyshev polynomials for two-dimensional biharmonic boundary-value problems," *Journal of Computational and Applied Mathematics*, vol. 201, no. 1, pp. 30–47, 2007.

[10] N. Mai-Duy and T. Tran-Cong, "Solving biharmonic problems with scattered-point discretization using indirect radial-basis-function networks," *Engineering Analysis with Boundary Elements*, vol. 30, no. 2, pp. 77–87, 2006.

[11] N. Mai-Duy and R. I. Tanner, "An effective high order interpolation scheme in BIEM for biharmonic boundary value problems," *Engineering Analysis with Boundary Elements*, vol. 29, no. 3, pp. 210–223, 2005.

[12] X. Li and J. Zhu, "A Galerkin boundary node method for biharmonic problems," *Engineering Analysis with Boundary Elements*, vol. 33, no. 6, pp. 858–865, 2009.

[13] N. Mai-Duy, H. See, and T. Tran-Cong, "A spectral collocation technique based on integrated Chebyshev polynomials for biharmonic problems in irregular domains," *Applied Mathematical Modelling*, vol. 33, no. 1, pp. 284–299, 2009.

[14] M. W. M. G. Dissanayake and N. Phan-Thien, "Neural-network-based approximations for solving partial differential equations," *communications in Numerical Methods in Engineering*, vol. 10, no. 3, pp. 195–201, 1994.

[15] N. Mai-Duy and R. I. Tanner, "A collocation method based on one-dimensional RBF interpolation scheme for solving PDEs," *International Journal of Numerical Methods for Heat & Fluid Flow*, vol. 17, no. 2, pp. 165–186, 2007.

[16] Z. Shi, Y.-Y. Cao, and Q.-J. Chen, "Solving 2D and 3D Poisson equations and biharmonic equations by the Haar wavelet method," *Applied Mathematical Modelling*, vol. 36, no. 11, pp. 5143–5161, 2012.

[17] A. Atangana and J. F. Botha, "Analytical solution of the ground water flow equation obtained via homotopy decomposition method," *Journal of Earth Science & Climatic Change*, vol. 3, p. 115, 2012.

[18] A. Atangana and A. Secer, "The time-fractional coupled-Korteweg-de-Vries equations," *Abstract and Applied Analysis*, vol. 2013, Article ID 947986, 8 pages, 2013.

[19] A. Atangana and A. Ahmed, "A generalized version of a low velocity impact between a rigid sphere and a transversely isotropic strain-hardening plate supported by a rigid substrate using the concept of non-integer derivatives," *Abstract Applied Analysisaccepted*, vol. 2013, Article ID 671321, 9 pages, 2013.

[20] A. Atangana and E. Alabaraoye, "Solving system of fractional partial differential equations arisen in the model of HIV infection of $CD4^+$ cells and attractor one-dimensional Keller-Segel equations," *Advance in Difference Equation*, vol. 2013, no. 94, 2013.

[21] S. T. Mohyud-Din, A. Yildirim, and M. M. Hosseini, "Variational iteration method for initial and boundary value problems using He's polynomials," *International Journal of Differential Equations*, vol. 2010, Article ID 426213, 28 pages, 2010.

[22] A. A. Elbeleze, A. Kılıçman, and B. M. Taib, "Homotopy perturbation method for fractional Black-Scholes European option pricing equations using Sumudu transform," *Mathematical Problems in Engineering*, vol. 2013, Article ID 524852, 7 pages, 2013.

[23] A. A. Elbeleze, A. Kılıçman, and B. M. Taib, "Application of homotopy perturbation and variational iteration method for Fredholm integro-differential equation of fractional order," *Abstract and Applied Analysis*, vol. 2012, Article ID 763139, 14 pages, 2012.

[24] A. M. A. El-Sayed and D. Hammad, "A reliable treatment of homotopy perturbation method for solving the nonlinear Klein-Gordon equation of arbitrary (fractional) orders)," *Journal of Applied Mathematics*, vol. 2012, Article ID 581481, 13 pages, 2012.

[25] M. T. Kajani, M. Ghasemi, and E. Babolian, "Comparison between the homotopy perturbation method and the sine-cosine wavelet method for solving linear integro-differential equations," *Computers & Mathematics with Applications*, vol. 54, no. 7-8, pp. 1162–1168, 2007.

[26] A. K. Khalifa, "The decomposition method for one dimensional biharmonic equations," *International Journal of Simulation and Process Modelling*, vol. 2, no. 1-2, 2006.

Hindawi Publishing Corporation
Abstract and Applied Analysis
Volume 2013, Article ID 921879, 12 pages
http://dx.doi.org/10.1155/2013/921879

Research Article

Pattern Dynamics in a Spatial Predator-Prey System with Allee Effect

Gui-Quan Sun,[1,2,3,4] Li Li,[5] Zhen Jin,[1,2] Zi-Ke Zhang,[3] and Tao Zhou[6]

[1] *Complex Sciences Center, Shanxi University, Taiyuan, Shan'xi 030006, China*
[2] *School of Mathematical Sciences, Shanxi University, Taiyuan, Shan'xi 030006, China*
[3] *Institute of Information Economy, Hangzhou Normal University, Hangzhou 310036, China*
[4] *Department of Mathematics, North University of China, Taiyuan, Shan'xi 030051, China*
[5] *Department of Mathematics, Taiyuan Institute of Technology, Taiyuan, Shan'xi 030008, China*
[6] *Web Sciences Center, University of Electronic Science and Technology of China, Chengdu, Sichuan 610054, China*

Correspondence should be addressed to Gui-Quan Sun; gquansun@126.com

Received 9 May 2013; Accepted 22 August 2013

Academic Editor: Rasajit Bera

We investigate the spatial dynamics of a predator-prey system with Allee effect. By using bifurcation analysis, the exact Turing domain is found in the parameters space. Furthermore, we obtain the amplitude equations and determine the stability of different patterns. In Turing space, it is found that predator-prey systems with Allee effect have rich dynamics. Our results indicate that predator mortality plays an important role in the pattern formation of populations. More specifically, as predator mortality rate increases, coexistence of spotted and stripe patterns, stripe patterns, spotted patterns, and spiral wave emerge successively. The results enrich the finding in the spatial predator-prey systems well.

1. Introduction

The Allee effect, named after the ecologist Warder Clyde Allee, has been recognized as an important phenomenon of positive density dependence in low-density population [1–5]. Allee effect can occur whenever fitness of an individual in a small or sparse population decreases as the population size or density also declines [6, 7]. Since the outstanding work of Allee [1], the Allee effect has been regarded as one of the central and highly important issues in the population and community ecology. And its critical importance has widely been realized in the conservation biology that Allee effect is most likely to increase the extinction risk of low-density populations. As a result, studies on Allee effect have received more and more attention from both mathematicians and ecologists.

Long time series of the density of both prey and predator is needed, so it is difficult to analyse their dynamics. As a result, it may provide useful information by constructing mathematical models to investigate the dynamical behaviors of predator-prey systems. There have been a large group of papers on predator-prey systems with Allee effect [8–13]. However, these previous works did not take into account the effect of space.

There are also some works done on spatial predator-prey systems with Allee effect [14–16]. Petrovskii et al. found that the deterministic system with Allee effect can induce patch invasion [14]. Morozov et al. found that the temporal population oscillations can exhibit chaotic dynamics even when the distribution of the species in the space was regular [15]. Moreover, they found that the chaos accompanied with patch invasion even though the environments were heterogeneous [16]. However, their results were obtained by choosing particular initial conditions. Then, it is natural to ask what kind of patterns can be obtained in predator-prey systems with Allee effect by using other initial conditions. To understand that mechanism well, we will investigate a predator-prey system with Allee effect.

Because of the insightful work of many scientists over recent years, we can make research on pattern selection by using the standard multiple scale analysis [17, 18], in which the control parameters and the derivatives are expanded in terms of a small enough parameter. In the neighborhood of the bifurcation points (Hopf and Turing bifurcation points), the critical amplitudes follow the normal forms, and thus their general forms can be obtained from the methods of symmetry-breaking bifurcations.

The paper is organized as follows. In Section 2, we present a predator-prey system with Allee effect and give Turing region in parameters space. In Section 3, by using multiple scale analysis, we obtain amplitude equations. In Section 4, we show the spatial patterns by a series of numerical simulations. Finally, conclusions and discussions are presented in Section 5.

2. A Predator-Prey System with Allee Effect

We consider the following model of two-dimensional spatiotemporal system [14–16, 19]:

$$\frac{\partial H}{\partial T} = F(H) - f(H,P) + D_1 \Delta H, \tag{1a}$$

$$\frac{\partial P}{\partial T} = \kappa f(H,P) - D(P) + D_2 \Delta P, \tag{1b}$$

where $H = H(X,Y,T)$ and $P = P(X,Y,T)$ are densities of prey and predator, respectively, at time T and position (X,Y). The function $F(H)$ represents the intrinsic prey growth, $f(H,P) = f(H)P$ represents predation term, κ is the food utilization coefficient, D_1 and D_2 are diffusion coefficients, and $D(P)$ describes predator mortality.

It is assumed that the predation term is a bilinear form of prey and predator density and predator mortality is a nonlinear function of predator density. As a result, we choose $f(H,P) = HP$ and $D(P) = MP^2$ [20].

When the prey population obeys Allee dynamics, its growth rate can be parameterized as follows [14, 15, 21]:

$$F(H) = \frac{4\omega}{(K - H_0)^2} H (H - H_0)(K - H), \tag{2}$$

where K is the prey-carrying capacity, ω is the maximum per capita growth rate, and H_0 quantifies the intensity of the Allee effect. If $0 < H_0 < K$, $F(H)$ is a strong Allee effect; if $-K < H_0 < 0$, $F(H)$ is a weak Allee effect; if $H_0 \le -K$, the Allee effect is absent.

In order to minimize the number of parameters involved in the model system, it is extremely useful to write the system in a nondimensionalized form. Although there is no unique method of doing this, it is often a good idea to relate the variables to some key relevant parameters. Introducing dimensionless variables

$$u = \frac{H}{K}, \qquad v = \frac{P}{\kappa K}, \qquad t = aT,$$
$$\overline{X} = X\sqrt{\frac{a}{D_1}}, \qquad \overline{Y} = Y\sqrt{\frac{a}{D_1}}, \tag{3}$$

we obtain the following equations:

$$\frac{\partial u}{\partial t} = \gamma u (u - \beta)(1 - u) - uv + \Delta u, \tag{4a}$$

$$\frac{\partial v}{\partial t} = uv - \delta v^2 + \varepsilon \Delta v, \tag{4b}$$

where

$$\beta = \frac{H_0}{K}, \qquad \gamma = \frac{4\omega K}{A\kappa (K - H_0)^2},$$
$$\delta = \frac{M}{a}, \qquad \varepsilon = \frac{D_2}{D_1}. \tag{5}$$

First of all, we need to investigate the dynamics of nonspatial model of systems (4a) and (4b)

$$\frac{du}{dt} = \gamma u (u - \beta)(1 - u) - uv, \tag{6a}$$

$$\frac{dv}{dt} = uv - \delta v^2. \tag{6b}$$

Systems (6a) and (6b) have three boundary equilibrium named $E_0 = (0,0)$, $E_1 = (1,0)$, and $E_2 = (\beta, 0)$ and two interior equilibriums named E_3 and E_4, where

$$E_3 = \left(\frac{\gamma\delta + \gamma\beta\delta - 1 + \sqrt{Q}}{2\gamma\delta}, \frac{\gamma\delta + \gamma\beta\delta - 1 + \sqrt{Q}}{2\gamma\delta^2} \right), \tag{7a}$$

$$E_4 = \left(\frac{\gamma\delta + \gamma\beta\delta - 1 - \sqrt{Q}}{2\gamma\delta}, \frac{\gamma\delta + \gamma\beta\delta - 1 - \sqrt{Q}}{2\gamma\delta^2} \right), \tag{7b}$$

where $Q = (\gamma\delta)^2 - 2(\gamma\delta)^2\beta - 2\gamma\beta\delta + 1$.

From a biological point of view, we are concerned with the dynamics of E_3 and E_4. The Jacobian matrix corresponding to the equilibrium point is that

$$J = \begin{pmatrix} a_{11} & a_{12} \\ a_{21} & a_{22} \end{pmatrix}, \tag{8}$$

where

$$a_{11} = 2\gamma u^* - \gamma\beta - 3\gamma (u^*)^2 + 2\gamma\beta u^*,$$
$$a_{12} = -u^*,$$
$$a_{21} = v^* - \delta,$$
$$a_{22} = u^*. \tag{9}$$

Diffusion-driven instability requires the stable, homogeneous steady state is driven unstable by the interaction of the dynamics and diffusion of the species; and therefore

$$a_{11} + a_{22} < 0,$$
$$a_{11}a_{22} - a_{12}a_{21} > 0. \tag{10}$$

It is found from direct calculations that E_3 is unstable and E_4 is stable. Denote $E_4 = (u^*, v^*)$.

Following the standard linear analysis of the reaction-diffusion equation [22], we consider a perturbation near the steady state:

$$u(\vec{r},t) = u^* + \overline{u}(r,t),$$
$$v(\vec{r},t) = v^* + \overline{v}(r,t), \tag{11}$$

where $\overline{u}(r,t) \ll u^*$, $\overline{v}(r,t) \ll v^*$, and $r = (\overline{X},\overline{Y})$. Assume that

$$\begin{pmatrix} \overline{u}(r,t) \\ \overline{v}(r,t) \end{pmatrix} = \begin{pmatrix} \alpha_1 \\ \alpha_2 \end{pmatrix} e^{\lambda t} e^{i(\kappa_X X + \kappa_Y Y)}, \tag{12}$$

where λ is the growth rate of perturbation in time t, α_1 and α_2 represent the amplitudes, and κ_X and κ_Y are the wave number of the solutions.

The characteristic equation of the systems (4a) and (4b) is

$$(A - \lambda I)\begin{pmatrix} \overline{u} \\ \overline{v} \end{pmatrix} = 0, \tag{13}$$

where

$$A = \begin{pmatrix} a_{11} - \left(\kappa_X^2 + \kappa_Y^2\right) & a_{12} \\ a_{21} & a_{22} - \varepsilon\left(\kappa_X^2 + \kappa_Y^2\right) \end{pmatrix}. \tag{14}$$

As a result, we have characteristic polynomial:

$$\lambda^2 - tr_\kappa \lambda + \Delta_\kappa = 0, \tag{15}$$

$$tr_\kappa = a_{11} + a_{22} - \kappa^2(1+\varepsilon) \overset{\Delta}{=} tr_J - \kappa^2(1+\varepsilon),$$
$$\Delta_\kappa = a_{11}a_{22} - a_{12}a_{21} - \kappa^2(a_{11}\varepsilon + a_{22}) + \kappa^4\varepsilon \tag{16}$$
$$\overset{\Delta}{=} \Delta_J - \kappa^2(a_{11}\varepsilon + a_{22}) + \kappa^4\varepsilon,$$

where $\kappa^2 = \kappa_X^2 + \kappa_Y^2$.

The roots of (15) can be obtained by the following form:

$$\lambda_\kappa = \frac{1}{2}\left(tr_\kappa \pm \sqrt{tr_\kappa^2 - 4\Delta_\kappa}\right). \tag{17}$$

When $\mathrm{Im}(\lambda_\kappa) \neq 0$ and $\mathrm{Re}(\lambda_\kappa) = 0$, Hopf bifurcation will emerge. Then, we have that the critical value of Hopf bifurcation parameter-δ equals

$$\delta_H = \frac{\gamma(\gamma + \beta - 1)}{\gamma^2\beta^2 + \gamma^2 - 2\gamma^2\beta - 1}. \tag{18}$$

When $\kappa^2 = (\kappa_T)^2 = \sqrt{\Delta_J/\varepsilon}$ and $\mathrm{Im}(\lambda_\kappa) = 0$, $\mathrm{Re}(\lambda_\kappa) = 0$, Turing bifurcation will occur. Denote δ_T as the critical value of δ as Turing instability occurs. Since the expression is complicated, we omit it here.

In Figure 1, we show the two critical lines in the parameter space spanned by β and δ. The equilibria that can be found in the region, marked by T (Turing space), are stable with respect to the homogeneous perturbations, but they lose their stability with respect to the perturbations of specific wave numbers κ. In this region, stationary patterns can be observed. To see the effect of parameter δ well, we plot in Figure 2 the dispersion relation corresponding to several values of δ while keeping the other parameters fixed. We see that the available Turing modes shift to higher wave numbers when β decreases.

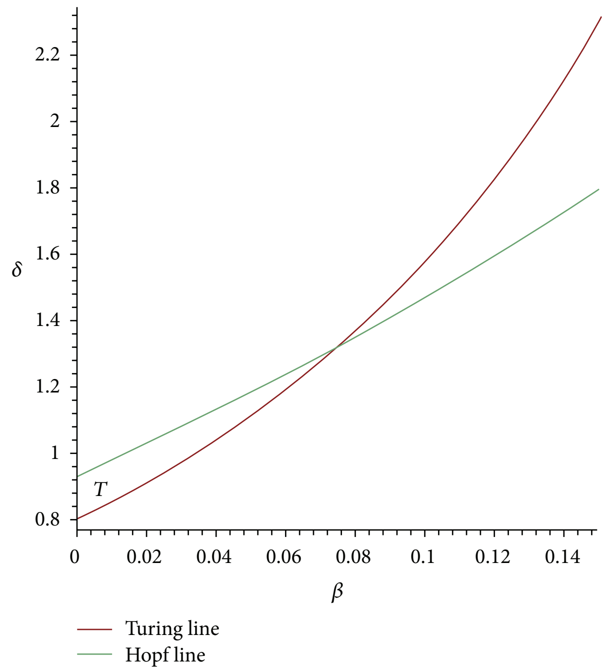

Figure 1: Bifurcation diagram for the systems (4a) and (4b). The green one is the Hopf bifurcation critical line and the red one, Turing bifurcation critical line. The figure shows the Turing space which is marked by T. Parameters values: $\gamma = 1.5$ and $\varepsilon = 0.15$.

3. Spatial Dynamics of Systems (4a) and (4b)

In the following, we use multiple scale analysis to determine the amplitude equations when $|\kappa| = \kappa_T$. Denote δ as the controlled parameters. When the controlled parameter is larger than the critical value of Turing point, the solutions of systems (4a) and (4b) can be expanded as

$$c = c_0 + \sum_{i=1}^{N}\left(A_i \exp(i\kappa_i\vec{r}) + \left(\overline{A}_i \exp(-i\kappa_i\vec{r})\right)\right), \tag{19}$$

with $|\kappa| = \kappa_T$. A_j and the conjugate $\overline{A}_j$ are the amplitudes associated with the modes κ_j and $-\kappa_j$.

Close to onset $\beta = \beta_T$, one has that

$$\frac{\partial A_i}{\partial t} = s_i A_i + F_i\left(A_i, A_j, \ldots\right). \tag{20}$$

Based on the center manifold near the Turing bifurcation point, it can be concluded that amplitude A_j satisfies

$$\frac{\partial A_i}{\partial t} = F_i\left(A_i, \overline{A}_i, A_j, \overline{A}_j, \ldots\right). \tag{21}$$

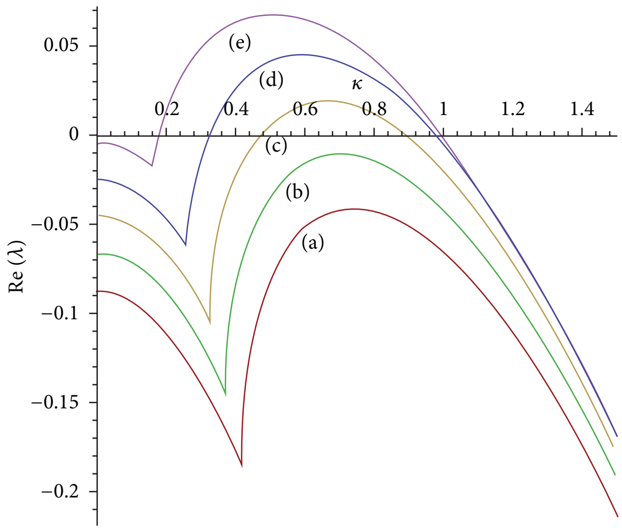

Figure 2: Dispersion relation for different δ. Parameters values: $\beta = 0.02$, $\gamma = 1.5$, and $\varepsilon = 0.15$. (a) $\delta = 1.08$; (b) $\delta = 1.04$; (c) $\delta = 1$; (d) $\delta = 0.96$; and (e) $\delta = 0.92$.

In order to obtain the amplitude equations, we first need to investigate the linearized form of systems (4a) and (4b) at the equilibrium point E_4. By setting $u = u^* + x$ and $v = v^* + y$, we have the following equations:

$$\frac{\partial x}{\partial t} = \left[2\gamma u^* - 3\gamma(u^*)^2 + 2\gamma(u^*)^2\beta - \gamma\beta - v^*\right]x + (\beta\gamma - 3\gamma u^* + \gamma)x^2 - \gamma x^3 - xy + \Delta x, \tag{22a}$$

$$\frac{\partial y}{\partial t} = v^* x + u^* y + xy - 2\delta v^* y - \delta y^2 + \varepsilon\Delta y. \tag{22b}$$

Close to onset $\delta = \delta_T$, the solutions of systems (4a) and (4b) can be expanded as series form:

$$U = U_s + \sum_{j=1}^{3} U_0\left[A_j \exp\left(i\kappa_j \vec{r}\right) + \overline{A}_j \exp\left(-i\kappa_j \vec{r}\right)\right]. \tag{23}$$

System (19) can be expanded as

$$U^* = \sum_{j=1}^{3} U_0\left[A_j \exp\left(i\kappa_j \vec{r}\right) + \overline{A}_j \exp\left(-i\kappa_j \vec{r}\right)\right], \tag{24}$$

where $U_0 = ((a_{11}^*\varepsilon + a_{11}^*)/(2a_{21}^*), 1)^T$ is the eigenvector of the linearized operator.

From the standard multiple scale analysis, up to the third order in the perturbations, the spatiotemporal evolution of the amplitudes can be described as

$$\tau\frac{\partial A_k}{\partial t} = \mu A_k + \sum_{lm} h_{lm} A_l A_m + \sum_{lmn} g_{lmn} A_l A_m A_n. \tag{25}$$

Due to spatial translational symmetry, we have the following equation:

$$\tau\frac{\partial A_k}{\partial t}\exp\left(i\kappa_k r_0\right) = \mu A_k \exp\left(i\kappa_k r_0\right) + \sum_{lm} h_{lm} A_l A_m \exp\left[i\left(\kappa_l + \kappa_m\right) r_0\right] + \sum_{lmn} g_{lmn} A_l A_m A_n \exp\left[i\left(\kappa_l + \kappa_m + \kappa_n\right) r_0\right]. \tag{26}$$

Comparing (25) with (26), one can find that the two equations hold only if $\kappa_k = \kappa_l + \cdots + \kappa_m$. From the center manifold theory, we know that amplitude equations do not include the amplitude with unstable mode. As a result, we have the following equations:

$$\begin{aligned}
\tau_0\frac{\partial A_1}{dt} &= \mu A_1 + h\overline{A}_2\overline{A}_3 - \left(g_1|A_1|^2 + g_2\left(|A_2|^2 + |A_3|^2\right)\right)A_1,\\
\tau_0\frac{\partial A_2}{dt} &= \mu A_2 + h\overline{A}_1\overline{A}_3 - \left(g_1|A_2|^2 + g_2\left(|A_1|^2 + |A_3|^2\right)\right)A_2,\\
\tau_0\frac{\partial A_3}{dt} &= \mu A_3 + h\overline{A}_1\overline{A}_2 - \left(g_1|A_3|^2 + g_2\left(|A_1|^2 + |A_2|^2\right)\right)A_3,
\end{aligned} \tag{27}$$

where $\mu = (\delta_T - \delta)/\delta_T$ and τ_0 is a typical relaxation time.

In the following part, we will give the expressions of τ_0, h, g_1, and g_2. Let

$$X = \begin{pmatrix} x \\ y \end{pmatrix}, \qquad N = \begin{pmatrix} N_1 \\ N_2 \end{pmatrix}. \tag{28}$$

Then systems (4a) and (4b) can be written as:

$$\frac{\partial X}{\partial t} = LX + N, \tag{29}$$

where

$$L = \begin{pmatrix} 2\gamma u^* - 3\gamma(u^*)^2 + 2\gamma\beta(u^*)^2 - \gamma\beta - v^* + \Delta & 0 \\ v^* & u^* - 2\delta v^* + \varepsilon\Delta \end{pmatrix},$$
$$N = \begin{pmatrix} (\beta\gamma - 3\gamma u^* + \gamma) - \gamma x^3 - xy \\ xy - \delta y^2 \end{pmatrix}. \tag{30}$$

We need to investigate the dynamical behavior when δ is close to δ_T, and thus we expand δ as:

$$\delta_T - \delta = \epsilon\delta_1 + \epsilon^2\delta_2 + \epsilon^3\delta_3 + O\left(\epsilon^4\right), \tag{31}$$

where ϵ is a small enough parameter. We expand X and N as the series form of ϵ:

$$X = \begin{pmatrix} x \\ y \end{pmatrix} = \epsilon \begin{pmatrix} x_1 \\ y_1 \end{pmatrix} + \epsilon^2 \begin{pmatrix} x_2 \\ y_2 \end{pmatrix} + \epsilon^3 \begin{pmatrix} x_3 \\ y_3 \end{pmatrix} + \cdots,$$

$$N = \begin{pmatrix} (\beta\gamma - 3\gamma u^* + \gamma)(x_1^2\epsilon^2 + 2x_1x_2\epsilon^3) - \gamma x_1^3\epsilon^3 - x_1y_1\epsilon^2 - (x_2y_1 + x_1y_2)\epsilon^3 + o(\epsilon^4) \\ x_1y_1\epsilon^2 + (x_2y_1 + x_1y_2)\epsilon^3 + o(\epsilon^4) \end{pmatrix}. \tag{32}$$

Linear operator L can be expanded as

$$L = L_T + (\delta_T - \delta) M, \tag{33}$$

where

$$L_T = \begin{pmatrix} a_{11}^* + \Delta & a_{12}^* \\ a_{21}^* & a_{22}^* + \varepsilon\Delta \end{pmatrix}, \qquad M = \begin{pmatrix} b_{11} & b_{12} \\ b_{21} & b_{22} \end{pmatrix}. \tag{34}$$

Let

$$T_0 = t, \qquad T_1 = \epsilon t, \qquad T_2 = \epsilon^2 t, \tag{35}$$

and T_i is a dependent variable. For the derivation of time, we have that

$$\frac{\partial}{\partial t} = \frac{\partial}{\partial T_0} + \epsilon\frac{\partial}{\partial T_1} + \epsilon^2\frac{\partial}{\partial T_2} + o(\epsilon^3). \tag{36}$$

The solutions of systems (4a) and (4b) have the following form:

$$X = \begin{pmatrix} x \\ y \end{pmatrix} = \sum_{i=1}^{3} \begin{pmatrix} A_i^x \\ A_i^y \end{pmatrix} \exp(i\kappa_i\vec{r}) + \cdots. \tag{37}$$

This expression implies that the bases of the solutions have nothing to do with time and the amplitude A is a variable that changes slowly. As a result, one has the following equation:

$$\frac{\partial A}{\partial t} = \epsilon\frac{\partial A}{\partial T_1} + \epsilon^2\frac{\partial A}{\partial T_2} + o(\epsilon^3). \tag{38}$$

Substituting the above equations into (29) and expanding (29) according to different orders of ϵ, we can obtain three equations as follows:

$$\begin{aligned}
\epsilon &: L_T \begin{pmatrix} x_1 \\ y_1 \end{pmatrix} = 0; \\
\epsilon^2 &: L_T \begin{pmatrix} x_2 \\ y_2 \end{pmatrix} = \frac{\partial}{\partial T_1}\begin{pmatrix} x_1 \\ y_1 \end{pmatrix} - \delta_1 M \begin{pmatrix} x_1 \\ y_1 \end{pmatrix} \\
&\quad - \begin{pmatrix} (\beta\gamma - 3\gamma u^* + \gamma) x_1^2 - x_1y_1 \\ x_1y_1 \end{pmatrix}; \\
\epsilon^3 &: L_T \begin{pmatrix} x_3 \\ y_3 \end{pmatrix} = \frac{\partial}{\partial T_1}\begin{pmatrix} x_2 \\ y_2 \end{pmatrix} + \frac{\partial}{\partial T_2}\begin{pmatrix} x_1 \\ y_1 \end{pmatrix} - \delta_1 M \begin{pmatrix} x_2 \\ y_2 \end{pmatrix} \\
&\quad - \delta_2 M \begin{pmatrix} x_1 \\ y_1 \end{pmatrix} - E,
\end{aligned} \tag{39}$$

where

$$E = \begin{pmatrix} 2x_1x_2(\beta\gamma - 3\gamma u^* + \gamma) - \gamma x_1^3 - (x_2y_1 + x_1y_2) \\ x_2y_1 + x_1y_2 \end{pmatrix}. \tag{40}$$

We first consider the case of the first order of ε. Since L_T is the linear operator of the system close to the onset, $(x_1, y_1)^T$ is the linear combination of the eigenvectors that corresponds to the eigenvalue zero. Since that

$$\begin{pmatrix} x \\ y \end{pmatrix} = \sum_{i=1}^{3} \begin{pmatrix} A_i^x \\ A_i^y \end{pmatrix} \exp(i\kappa_i\vec{r}) + \text{c.c.}, \tag{41}$$

we have that

$$(a_{11}^* + \Delta) x_1 + a_{12}^* y_1 = 0, \tag{42a}$$

$$a_{21}^* x_1 + (a_{22}^* + \varepsilon\Delta) y_1 = 0. \tag{42b}$$

As $\varepsilon a_{12}^* = ((a_{22}^* - \varepsilon a_{11}^*)/2a_{21}^*)^2$, we can obtain that $x_1 = (a_{22}^* - \varepsilon a_{11}^*)/(2a_{21}^*)$ by assuming $y_1 = 1$.

Let $R = (a_{11}^*\varepsilon - a_{22}^*)/2a_{21}^*$ then

$$\begin{aligned}
\begin{pmatrix} x_1 \\ y_1 \end{pmatrix} = \begin{pmatrix} R \\ 1 \end{pmatrix} &(W_1 \exp(i\kappa_1\vec{r}) + W_2 \exp(i\kappa_2\vec{r}) \\
&+ W_3 \exp(i\kappa_3\vec{r})) + \text{c.c.},
\end{aligned} \tag{43}$$

where $|\kappa_j| = \kappa_T^*$ and W_j is the amplitude of the mode $\exp(i\kappa_j r)$.

Now, we consider the case of the second order of ε. Note that

$$\begin{aligned}
L_T \begin{pmatrix} x_2 \\ y_2 \end{pmatrix} &= \frac{\partial}{\partial T_1}\begin{pmatrix} x_1 \\ y_1 \end{pmatrix} - \delta_T \begin{pmatrix} b_{11}x_1 + b_{12}y_1 \\ b_{21}x_1 + b_{22}y_1 \end{pmatrix} \\
&\quad - \begin{pmatrix} (\beta\gamma - 3\gamma u^* + \gamma) x_1^2 - x_1y_1 \\ x_1y_1 \end{pmatrix} \\
&= \begin{pmatrix} F_x \\ F_y \end{pmatrix}.
\end{aligned} \tag{44}$$

According to the Fredholm solubility condition, the vector function of the right hand of the above equation must be orthogonal with the zero eigenvectors of operator $\mathbf{L}_c^+$. And the zero eigenvectors of operator $\mathbf{L}_c^+$ are

$$\begin{pmatrix} 1 \\ -\frac{1}{\varepsilon}R \end{pmatrix} \exp(i\kappa_j\vec{r}) + \text{c.c} \quad (j = 1, 2, 3). \tag{45}$$

It can be found from the orthogonality condition that

$$\begin{pmatrix} 1 \\ -\frac{1}{\varepsilon}R \end{pmatrix} \begin{pmatrix} F_x^i \\ F_y^i \end{pmatrix} = 0, \tag{46}$$

where F_x^i and F_y^i represent the coefficients corresponding to $\exp(i\kappa_j r)$ in F_x and F_y.

By investigating $\exp(i\kappa_1\vec{r})$, one has

$$\begin{pmatrix} F_x^1 \\ F_y^1 \end{pmatrix} = \begin{pmatrix} R\dfrac{\partial W_1}{\partial T_1} \\ \dfrac{\partial W_1}{\partial T_1} \end{pmatrix} - \delta_1 \begin{pmatrix} b_{11}RW_1 + b_{12}W_1 \\ b_{21}RW_1 + b_{22}W_1 \end{pmatrix} - \begin{pmatrix} 2R^2(\beta\gamma - 3\gamma u^* + \gamma)\overline{W}_2\overline{W}_3 + 2R\overline{W}_2\overline{W}_3 \\ 2R\overline{W}_2\overline{W}_3 \end{pmatrix}. \tag{47}$$

It can be obtained from the orthogonality condition that

$$\frac{\varepsilon - 1}{\varepsilon}R\frac{\partial W_1}{\partial T_1} = \delta\left(Rb_{11} + b_{22} - \frac{R}{\varepsilon}(Rb_{21} + b_{22})W_1\right) + 2R^2\left(\beta\gamma - 3\gamma u^* + \gamma + \frac{1}{R} - \frac{1}{\varepsilon}\right)\overline{W}_2\overline{W}_3. \tag{48}$$

By using the same methods, one has

$$\begin{pmatrix} x_2 \\ y_2 \end{pmatrix} = \begin{pmatrix} X_0 \\ Y_0 \end{pmatrix} + \sum_{j=1}^{3}\begin{pmatrix} X_j \\ Y_j \end{pmatrix}\exp(i\kappa_j\vec{r}) + \sum_{j=1}^{3}\begin{pmatrix} X_{jj} \\ Y_{jj} \end{pmatrix}\exp(2i\kappa_j\vec{r}) + Q + \text{c.c.}, \tag{49}$$

where

$$Q = \begin{pmatrix} X_{12} \\ Y_{12} \end{pmatrix}\exp(i(\kappa_1 - \kappa_2)\vec{r}) + \begin{pmatrix} X_{23} \\ Y_{23} \end{pmatrix}\exp(i(\kappa_2 - \kappa_3)\vec{r}) + \begin{pmatrix} X_{31} \\ Y_{31} \end{pmatrix}\exp(i(\kappa_3 - \kappa_1)\vec{r}). \tag{50}$$

By solving the sets of the linear equations about $\exp(0)$, $\exp(i\kappa_j\vec{r})$, $\exp(2i\kappa_j\vec{r})$, and $\exp(i(\kappa_j - \kappa_k)\vec{r})$, we obtain that

$$\begin{aligned}
\begin{pmatrix} X_0 \\ Y_0 \end{pmatrix} &= \begin{pmatrix} \dfrac{a_{22}^*\left[-2R^2(\beta\gamma - 3\gamma u^* + \gamma) + 2R\right] + 2Ra_{12}^*}{a_{11}^*a_{22}^* - a_{12}^*a_{21}^*} \\ \dfrac{a_{21}^*\left[2R^2(\beta\gamma - 3\gamma u^* + \gamma) - 2R\right] + 2Ra_{11}^*}{a_{11}^*a_{22}^* - a_{12}^*a_{21}^*} \end{pmatrix} \times \left(|W_1|^2 + |W_2|^2 + |W_3|^2\right), \\
\begin{pmatrix} X_{jj} \\ Y_{jj} \end{pmatrix} &= \begin{pmatrix} \dfrac{(a_{22}^* - 4\varepsilon\kappa_T^2)\left[-R^2(\beta\gamma - 3\gamma u^* + \gamma) + R\right] + Ra_{12}^*}{(a_{11}^* - 4\kappa_T^2)(a_{22}^* - 4\varepsilon\kappa_T^2) - a_{12}^*a_{21}^*} \\ \dfrac{a_{21}^*\left[R^2(\beta\gamma - 3\gamma u^* + \gamma) - 2R\right] - R(a_{11}^* - 4\varepsilon\kappa_T^2)}{(a_{11}^* - 4\kappa_T^2)(a_{22}^* - 4\varepsilon\kappa_T^2) - a_{12}^*a_{21}^*} \end{pmatrix} \times W_j^2, \\
\begin{pmatrix} X_{jk} \\ Y_{jk} \end{pmatrix} &= \begin{pmatrix} \dfrac{(a_{22}^* - 3\varepsilon\kappa_T^2)\left[-2R^2(\beta\gamma - 3\gamma u^* + \gamma) + 2R\right] + 2Ra_{12}^*}{(a_{11}^* - 3\kappa_T^2)(a_{22}^* - 3\varepsilon\kappa_T^2) - a_{12}^*a_{21}^*} \\ \dfrac{a_{21}^*\left[2R^2(\beta\gamma - 3\gamma u^* + \gamma) - 2R\right] - 2R(a_{11}^* - 3\kappa_T^2)}{(a_{11}^* - 3\kappa_T^2)(a_{22}^* - 3\varepsilon\kappa_T^2) - a_{12}^*a_{21}^*} \end{pmatrix} \times W_j\overline{W}_k,
\end{aligned} \tag{51}$$

where $\kappa_T^2 = \sqrt{(a_{11}^*a_{22}^* - a_{12}^*a_{21}^*)/\varepsilon}$.

For the third order of ε, we have that

$$L_T\begin{pmatrix} x_3 \\ y_3 \end{pmatrix} = \frac{\partial}{\partial T_1}\begin{pmatrix} x_2 \\ y_2 \end{pmatrix} + \frac{\partial}{\partial T_2}\begin{pmatrix} x_1 \\ y_1 \end{pmatrix} - \delta_1 M\begin{pmatrix} x_2 \\ y_2 \end{pmatrix} - \delta_2 M\begin{pmatrix} x_1 \\ y_1 \end{pmatrix} - S, \tag{52}$$

where

$$S = \begin{pmatrix} 2x_1x_2(\beta\gamma - 3\gamma u^*) - \gamma x_1^3 - (x_2y_1 + x_1y_2) \\ x_2y_1 + x_1y_2 \end{pmatrix}. \tag{53}$$

Using the Fredholm solubility condition, we can obtain

$$\begin{aligned}
\frac{\varepsilon - 1}{\varepsilon}R\frac{\partial W_1}{\partial T_2} + \frac{\varepsilon - 1}{\varepsilon}R\frac{\partial Y_1}{\partial T_1} &= \delta_2\left[Rb_{11} + b_{12} - \frac{1}{\varepsilon}R(Rb_{21} + b_{22})\right]W_1 \\
&\quad + \delta_1\left[Rb_{11} + b_{12} - \frac{1}{\varepsilon}(Rb_{21} + b_{22})\right]Y_1 + Z,
\end{aligned} \tag{54}$$

where

$$\begin{aligned}
Z = {} & \left[2R^2(\beta\gamma - 3\gamma u^* + \gamma) - 2R - 2\frac{1}{\varepsilon}\right] \\
& \times \left[W_1Y_0 + W - 2Y_{12} + W_3Y_{13} + \overline{W}_1Y_{11} + \overline{W}_2\overline{Y}_3 + \overline{W}_3\overline{Y}_2\right] \\
& - \left(G_1|W_1|^2 + G_2|W_2|^2 + G_3|W_3|^2\right)W_1,
\end{aligned}$$

Table 1: Coefficients for different parameter sets.

β	δ	h	g_1	g_2	μ_1	μ_2	μ_3	μ_4
0.02	0.92	−19.08604	7599.215	6906.578	0.0042531	0	5.770186	0.046076
0.02	0.96	2.1329690	−740.11	−1429.72	−0.000315	0	−0.00708	−0.00611
0.02	1	8.4304106	−207.521	−474.186	−0.015371	0	−0.20741	−0.01250
0.02	1.12	11.304093	−99.3194	−193.856	−0.0655924	0	−1.42005	−0.04391

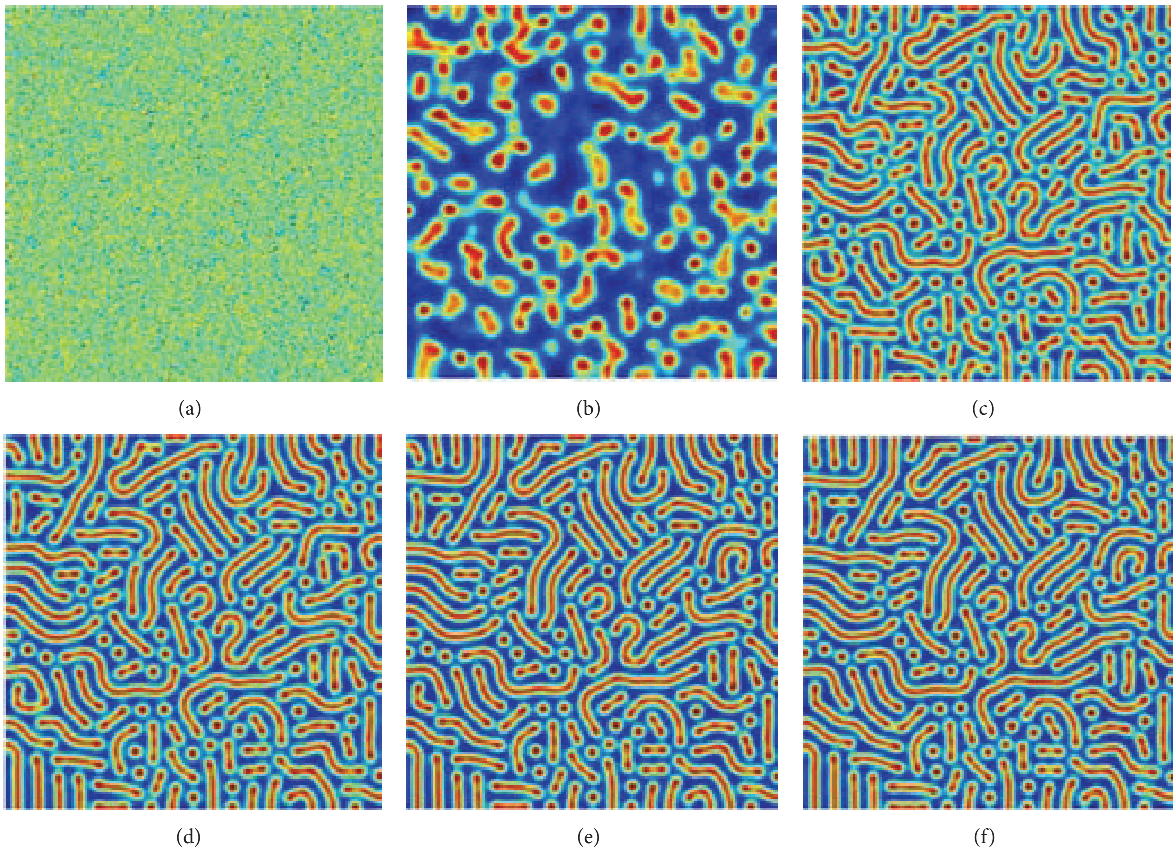

Figure 3: Spatial pattern of prey population at different time. Parameters set: $\gamma = 1.5$, $\varepsilon = 0.15$, and $\delta = 0.92$. (a) $t = 0$; (b) $t = 100$; (c) $t = 200$; (d) $t = 500$; (e) $t = 1000$; and (f) $t = 2000$.

$$G_1 = \left(\frac{1}{\varepsilon}R - 1\right)\left[R\left(y_{11} + y_0\right) + x_{11} + x_0\right] - 2R\left(x_{11} + x_0\right)\left(\beta\gamma - 3\gamma u^* + \gamma\right) + 3\gamma R^3,$$
$$G_2 = \left(\frac{1}{\varepsilon}R - 1\right)\left[R\left(y_{12} + y_0\right) + x_{12} + x_0\right] - 2R\left(x_{12} + x_0\right)\left(\beta\gamma - 3\gamma u^* + \gamma\right) + 6\gamma R^3. \quad (55)$$

By using the same methods, we can obtain the other two equations. The amplitude A_i can be expanded as

$$A_i = \epsilon W_i + \epsilon^2 V_i + o\left(\epsilon^3\right). \quad (56)$$

As a result, we have

$$\tau_0 \frac{\partial A_1}{\partial t} = \mu A_1 + h\overline{A}_2\overline{A}_3 - \left(g_1\left|A_1\right|^2 + g_2\left|A_2\right|^2 + \left|A_3\right|^2\right)A_1. \quad (57)$$

The other two equations can be obtained through the transformation of the subscript of A. By calculations, we obtain the expressions of the coefficients of τ_0, h, g_1, and g_2 as follows:

$$\tau_0 = R\frac{\varepsilon - 1}{\delta_T\left[Rb_{11} + b_{12} - (R/\varepsilon)\left(Rb_{21} + b_{22}\right)\right]},$$
$$h = \frac{\left[2R^2\left(\beta\gamma - 3\gamma u^* + \gamma\right) - 2R - 2\left(R^2/\varepsilon\right)\right]}{\delta_T\left[Rb_{11} + b_{12} - (R/\varepsilon)\left(Rb_{21} + b_{22}\right)\right]},$$
$$g_1 = \frac{G_1}{\delta_T\left[Rb_{11} + b_{12} - (R/\varepsilon)\left(Rb_{21} + b_{22}\right)\right]},$$
$$g_2 = \frac{G_2}{\delta_T\left[Rb_{11} + b_{12} - (R/\varepsilon)\left(Rb_{21} + b_{22}\right)\right]}, \quad (58)$$

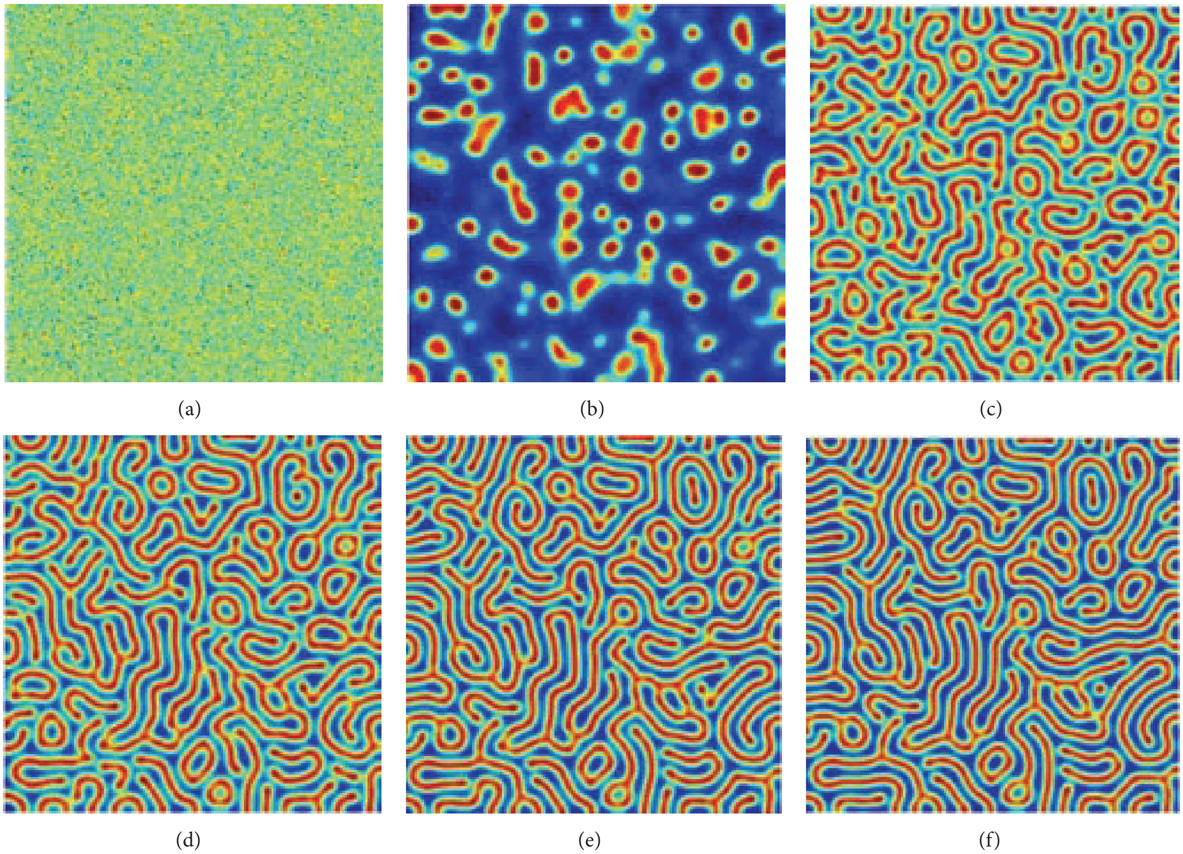

Figure 4: Spatial pattern of prey population at different time. Parameters set: $\gamma = 1.5$, $\varepsilon = 0.15$, and $\delta = 0.96$. (a) $t = 0$; (b) $t = 50$; (c) $t = 100$; (d) $t = 200$; (e) $t = 500$; and (f) $t = 1000$.

where $G_1 = ((R/\varepsilon) - 1)[R(y_0 + y_{11}) + x_0 + x_{11}] - 2R(x_0 + x_{11})(\beta\gamma - 3\gamma u^* + \gamma) + 3\gamma R^3$ and $G_2 = ((R/\varepsilon) - 1)[R(y_0 + y_{12}) + x_0 + x_{12}] - 2R(x_0 + x_{12})(\beta\gamma - 3\gamma u^* + \gamma) + 6\gamma R^3$.

By using substitutions, we have

$$\begin{aligned}
\tau_0 \frac{\partial \varphi}{dt} &= -h \frac{\rho_1^2\rho_2^2 + \rho_1^2\rho_3^2 + \rho_2^2\rho_3^2}{\rho_1\rho_2\rho_3} \sin\varphi, \\
\tau_0 \frac{\partial \rho_1}{dt} &= \mu\rho_1 + h\rho_2\rho_3 \cos\varphi - g_1\rho_1^3 - g_2\left(\rho_2^2\rho_3^2\right)\rho_1, \\
\tau_0 \frac{\partial \rho_2}{dt} &= \mu\rho_2 + h\rho_1\rho_3 \cos\varphi - g_1\rho_2^3 - g_2\left(\rho_1^2\rho_3^2\right)\rho_2, \\
\tau_0 \frac{\partial \rho_3}{dt} &= \mu\rho_3 + h\rho_1\rho_2 \cos\varphi - g_1\rho_3^3 - g_2\left(\rho_1^2\rho_2^2\right)\rho_3,
\end{aligned} \tag{59}$$

where $\varphi = \varphi_1 + \varphi_2 + \varphi_3$. In order to see the relationships between different parameters, we give the values of coefficients for different parameter sets in Table 1.

The dynamical systems (4a) and (4b) possess five kinds of solutions [23] as follows.

(1) The stationary state (O), given by

$$\rho_1 = \rho_2 = \rho_3 = 0, \tag{60}$$

is stable for $\mu < \mu_2 = 0$ and unstable for $\mu > \mu_2$.

(2) Stripe patterns (S), given by

$$\rho_1 = \sqrt{\frac{\mu}{g_1}} \neq 0, \qquad \rho_2 = \rho_3 = 0, \tag{61}$$

are stable for $\mu > \mu_3 = h^2 g_1/(g_2 - g_1)^2$, and unstable for $\mu < \mu_3$.

(3) Hexagon patterns (H_0, H_π) are given by

$$\rho_1 = \rho_2 = \rho_3 = \frac{|h| \pm \sqrt{h^2 + 4\left(g_1 + 2g_2\mu\right)}}{2\left(g_1 + 2g_2\right)}, \tag{62}$$

with $\varphi = 0$ or π, and exist when

$$\mu > \mu_1 = \frac{-h^2}{4\left(g_1 + 2g_2\right)}. \tag{63}$$

The solution $\rho^+ = |h| + \sqrt{h^2 + 4(g_1 + 2g_2\mu)}/2(g_1 + 2g_2)$ is stable only for

$$\mu < \mu_4 = \frac{2g_1 + g_2}{\left(g_2 - g_1\right)^2} h^2, \tag{64}$$

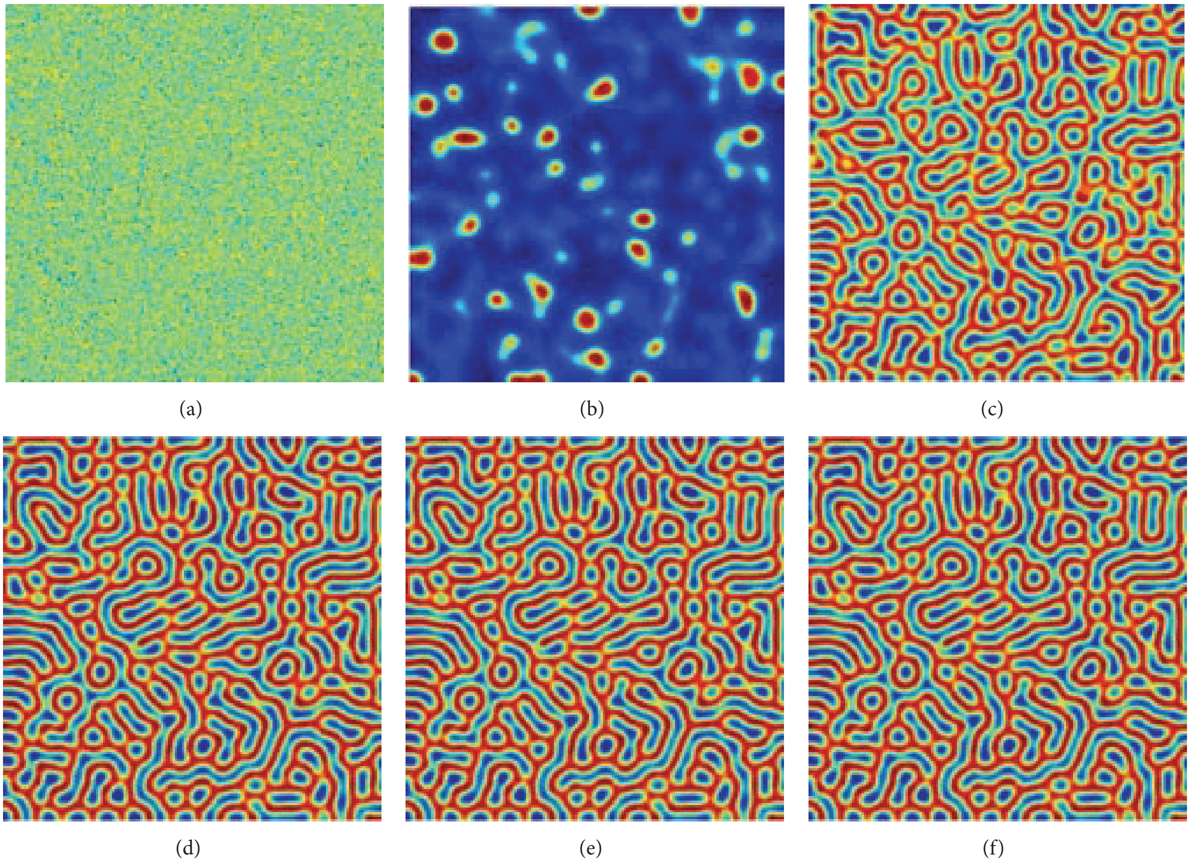

FIGURE 5: Spatial pattern of prey population at different time. Parameters set: $\gamma = 1.5$, $\varepsilon = 0.15$, and $\delta = 1$. (a) $t = 0$; (b) $t = 150$; (c) $t = 300$; (d) $t = 500$; (e) $t = 600$; and (f) $t = 1000$.

and $\rho^- = (|h| - \sqrt{h^2 + 4(g_1 + 2g_2\mu)})/2(g_1 + 2g_2)$ is always unstable.

(4) The mixed states are given by

$$\rho_1 = \frac{|h|}{g_2 - g_1}, \qquad \rho_2 = \rho_3 = \sqrt{\frac{\mu - g_1\rho_1^2}{g_1 + g_2}}, \tag{65}$$

with $g_2 > g_1$. They exist when $\mu > \mu_3$ and are always unstable.

4. Spatial Pattern of Systems (4a) and (4b)

In this section, we perform extensive numerical simulations of the spatially extended systems (4a) and (4b) in two-dimensional spaces. All our numerical simulations employ the zero-flux boundary conditions with a system size of 200×200. The space step is $\Delta H = 1$, and the time step is $\Delta t = 0.00001$.

In Figure 3, we show the spatial pattern of prey population at different time. In the parameter set, $\gamma = 1.5$, $\varepsilon = 0.15$, and $\delta = 0.92$, we find that $\mu \in (\mu_3, \mu_4)$, which means that there is coexistence of spotted and stripe patterns. As shown in this figure, our theoretical results are consistent with the numerical results.

By setting $\gamma = 1.5$, $\varepsilon = 0.15$, and $\delta = 0.96$, one can obtain that $\mu > \mu_4$. In Figure 4, we show the spatial pattern of prey population when t equals 0, 50, 100, 200, 500, and 1000. At the initial time, the prey population shows patched invasion. As time increases, stripe pattern appears and the structure does not change a lot. While keeping other parameters fixed and increasing δ, we find that stripe pattern will occupy the whole space. However, some stripe patterns connect with each other and cause the emergence of spotted patterns which are shown in Figure 5.

Figure 6 shows the evolution of the spatial pattern of prey population at $t = 0$, 100, 300, 500, 1000, and 2000 iterations, with small random perturbation of the stationary solution of the spatially homogeneous systems (4a) and (4b). The corresponding parameters values are $\gamma = 1.5$, $\varepsilon = 0.15$, and $\delta = 1.04$. By the amplitude equations, we can conclude that there are spotted patterns of prey population for this parameter set. In this case, one can see that for the systems (4a) and (4b), the random initial distribution leads to the formation of an irregular transient pattern in the domain. After these forms, it grows slightly and spotted patterns emerge. When the time is large enough, the spotted patterns prevail over the two-dimensional space. As time further increases, the pattern structures of the prey population do not undergo any further changes.

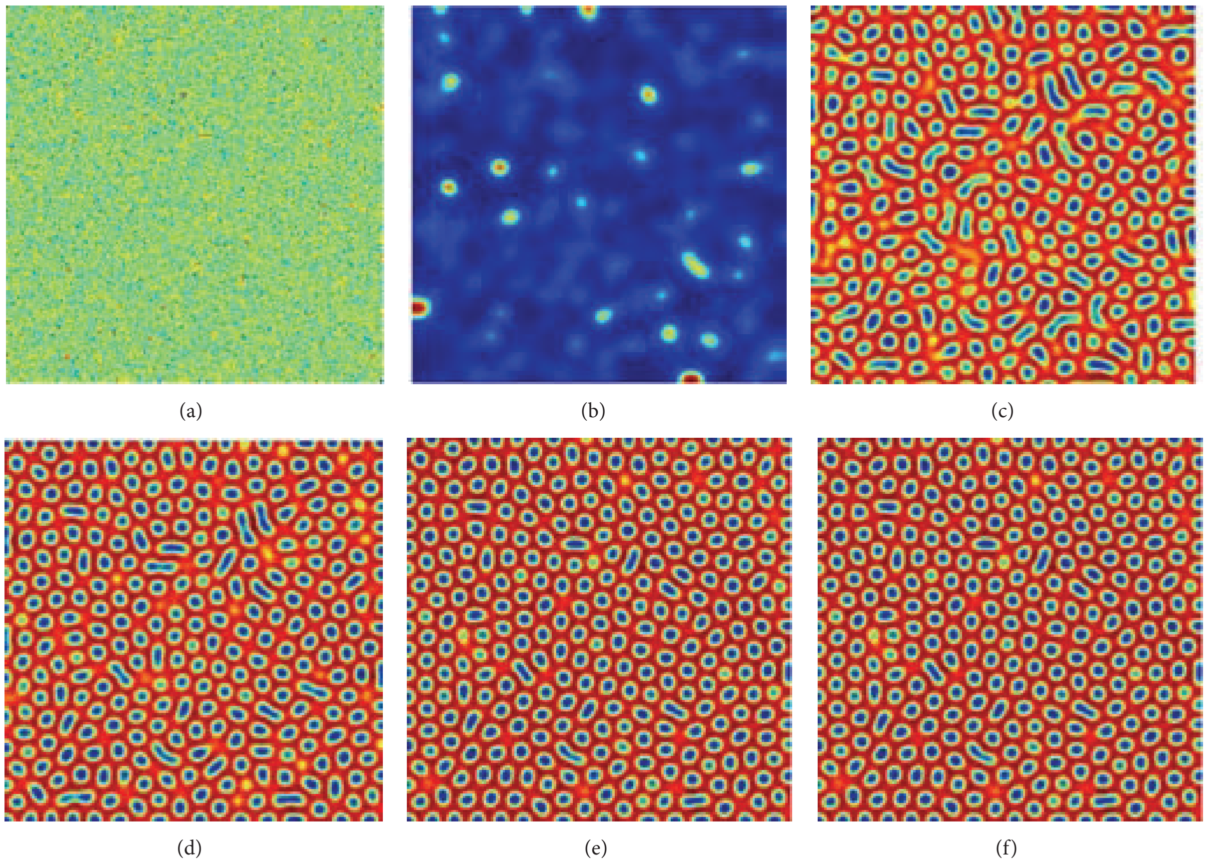

Figure 6: Spatial pattern of prey population at different time. Parameters set: $\gamma = 1.5$, $\varepsilon = 0.15$, and $\delta = 1.04$. (a) $t = 0$; (b) $t = 100$; (c) $t = 300$; (d) $t = 500$; (e) $t = 1000$; and (f) $t = 2000$.

5. Conclusion and Discussion

Allee effect has been paid much attention due to its strong potential impact on population dynamics [24]. In this paper, we investigated the pattern dynamics of a spatial predator-prey systems with Allee effect. Based on the bifurcation analysis, exact Turing pattern region is obtained. By using amplitude equations, the Turing pattern selection of the predator-prey system is well presented. It is found that the predator-prey systems with Allee effect have rich spatial dynamics by performing a series of numerical simulations.

It should be noted that our results were obtained under the assumption that predation is modeled by the bilinear function of the prey and predator densities. However, this function has limitations to describe many realistic phenomena in the biology. By numerical simulations, we find that the system exhibits similar behaviour when the functional response is of other types, such as Holling-II and Holling-III forms.

To compare the spatial dynamics for different parameters, we give the spatial patterns of population u when the parameter values are out of the domain of Turing space. For this parameter set, systems (4a) and (4b) have Hopf bifurcation, and spiral waves occupy the whole domain instead of stationary patterns, which is shown in Figure 7. The stability of spiral wave can be done by using the spectrum theory analysis [25, 26]. In the further study, we will use the spectrum theory to show the stability of spiral wave.

In [15], they found that a spatial predator-prey model with Allee effect and linear death rate could increase the system's complexity and enhance chaos in population dynamics. However, in this paper, we showed that a spatial population model with Allee effect and nonlinear death rate can induce stationary patterns, which is different from the previous results.

From a biological point of view, our results show that predator mortality plays an important role in the spatial invasions of populations. More specifically, low predator mortality will induce stationary patterns (cf. Figures 3–6), and high predator mortality corresponds to travelling patterns (cf. Figure 7). When the populations exhibit wave distribution in space, the dynamics of populations may be accompanied with chaotic properties [27, 28]. If the chaotic behavior occurs, it may lead to the extinction of the population, or the population may be out of control [29, 30]. In that case, we need to find out the best way to control the chaos or change the chaotic behavior.

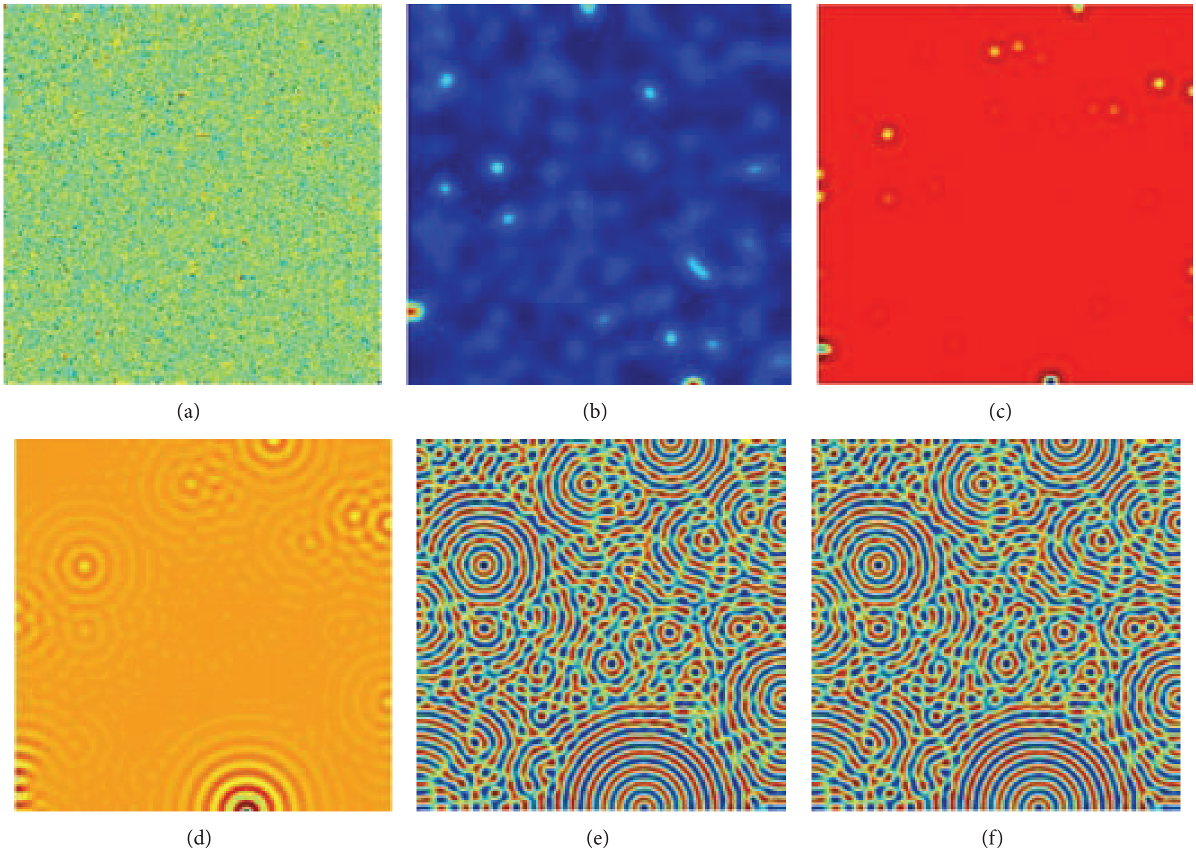

FIGURE 7: Spatial pattern of prey population at different time. Parameters set: $\gamma = 1.5$, $\varepsilon = 0.15$, and $\delta = 1.2$. (a) $t = 0$; (b) $t = 100$; (c) $t = 200$; (d) $t = 300$; (e) $t = 400$; and (f) $t = 500$.

Acknowledgments

This research was partially supported by the National Natural Science Foundation of China under Grant nos. 11301490, 11301491, 11331009, 11147015, 11171314, 11305043, and 11105024; Natural Science Foundation of Shan'xi Province Grant nos. 2012021002-1 and 2012011002-2, the Opening Foundation of Institute of Information Economy, Hangzhou Normal University, Grant no. PD12001003002003; and the specialized research fund for the doctoral program of higher education (preferential development) Grant no. 20121420130001.

References

[1] W. C. Allee, *Animal Aggregations*, University of Chicago Press, 1931.

[2] W. C. Allee and E. Bowen, "Studies in animal aggregations: mass protection against colloidalsilver among goldfishes," *Journal of Experimental Zoology*, vol. 61, pp. 185–207, 1932.

[3] W. C. Allee, O. Emerson, T. Park, and K. Schmidt, *Principles of Animal Ecology*, Saunders, Philadelphia, Pa, USA, 1949.

[4] W. C. Allee, *Cooperation Among Animals*, Henry Shuman, 1951.

[5] W. C. Allee, *The Social Life of Animals*, Beacon Press, 1958.

[6] F. Courchamp, T. Clutton-Brock, and B. Grenfell, "Inverse density dependence and the Allee effect," *Trends in Ecology and Evolution*, vol. 14, no. 10, pp. 405–410, 1999.

[7] P. A. Stephens and W. J. Sutherland, "Consequences of the Allee effect for behaviour, ecology and conservation," *Trends in Ecology and Evolution*, vol. 14, no. 10, pp. 401–405, 1999.

[8] J. Cushing and J. T. Hudson, "Evolutionary dynamics and strong allee effects," *Journal of Biological Dynamics*, vol. 6, pp. 941–958, 2012.

[9] S. N. Elaydi and R. J. Sacker, "Population models with Allee effect: a new model," *Journal of Biological Dynamics*, vol. 4, no. 4, pp. 397–408, 2010.

[10] J. Shi and R. Shivaji, "Persistence in reaction diffusion models with weak Allee effect," *Journal of Mathematical Biology*, vol. 52, no. 6, pp. 807–829, 2006.

[11] J. Wang, J. Shi, and J. Wei, "Predator-prey system with strong Allee effect in prey," *Journal of Mathematical Biology*, vol. 62, no. 3, pp. 291–331, 2011.

[12] A. Verdy, "Modulation of predator-prey interactions by the Allee effect," *Ecological Modelling*, vol. 221, no. 8, pp. 1098–1107, 2010.

[13] V. Méndez, C. Sans, I. Llopis, and D. Campos, "Extinction conditions for isolated populations with Allee effect," *Mathematical Biosciences*, vol. 232, no. 1, pp. 78–86, 2011.

[14] S. V. Petrovskii, A. Y. Morozov, and E. Venturino, "Allee effect makes possible patchy invasion in a predator-prey system," *Ecology Letters*, vol. 5, no. 3, pp. 345–352, 2002.

[15] A. Morozov, S. Petrovskii, and B.-L. Li, "Bifurcations and chaos in a predator-prey system with the Allee effect," *Proceedings of the Royal Society B*, vol. 271, no. 1546, pp. 1407–1414, 2004.

[16] A. Morozov, S. Petrovskii, and B.-L. Li, “Spatiotemporal complexity of patchy invasion in a predator-prey system with the Allee effect,” *Journal of Theoretical Biology*, vol. 238, no. 1, pp. 18–35, 2006.

[17] G. H. Gunaratne, Q. Ouyang, and H. L. Swinney, “Pattern formation in the presence of symmetries,” *Physical Review E*, vol. 50, no. 4, pp. 2802–2820, 1994.

[18] B. Peña and C. Pérez-García, “Stability of Turing patterns in the Brusselator model,” *Physical Review E*, vol. 64, no. 5, part 2, Article ID 056213, 9 pages, 2001.

[19] J. A. Sherratt, “Periodic travelling waves in cyclic predator-prey systems,” *Ecology Letters*, vol. 4, no. 1, pp. 30–37, 2001.

[20] M. Baurmann, T. Gross, and U. Feudel, “Instabilities in spatially extended predator-prey systems: spatio-temporal patterns in the neighborhood of Turing-Hopf bifurcations,” *Journal of Theoretical Biology*, vol. 245, no. 2, pp. 220–229, 2007.

[21] M. A. Lewis and P. Kareiva, “Allee Dynamics and the Spread of Invading Organisms,” *Theoretical Population Biology*, vol. 43, no. 2, pp. 141–158, 1993.

[22] A. M. Turing, “The chemical basis of morphogenesis,” *Philosophical Transactions of the Royal Society B*, vol. 237, pp. 37–72, 1952.

[23] Q. Ouyang, *Pattern Formation in Reaction-Diffusion Systems*, Sci-Tech Education Publishing House, Shanghai, China, 2000.

[24] F. Courchamp, J. Berec, and J. Gascoigne, *Allee Effects in Ecology and Conservation*, Oxford University Press, New York, NY, USA, 2008.

[25] J. D. M. Rademacher, B. Sandstede, and A. Scheel, “Computing absolute and essential spectra using continuation,” *Physica D*, vol. 229, no. 2, pp. 166–183, 2007.

[26] P. Wheeler and D. Barkley, “Computation of spiral spectra,” *SIAM Journal on Applied Dynamical Systems*, vol. 5, no. 1, pp. 157–177, 2006.

[27] M. Pascual, “Diffusion-induced chaos in a spatial predator-prey system,” *Proceedings of the Royal Society B*, vol. 251, no. 1330, pp. 1–7, 1993.

[28] J. A. Sherratt, M. J. Smith, and J. D. M. Rademacher, “Locating the transition from periodic oscillations to spatiotemporal chaos in the wake of invasion,” *Proceedings of the National Academy of Sciences of the United States of America*, vol. 106, no. 27, pp. 10890–10895, 2009.

[29] M. P. Hassell, J. H. Lawton, and R. M. May, “Patterns of dynamical behaviour in single-species populations,” *Journal of Animal Ecology*, vol. 45, pp. 471–486, 1976.

[30] A. A. Berryman and J. A. Millstein, “Are ecological systems chaotic—and if not, why not?” *Trends in Ecology and Evolution*, vol. 4, no. 1, pp. 26–28, 1989.

Hindawi Publishing Corporation
Abstract and Applied Analysis
Volume 2013, Article ID 203875, 6 pages
http://dx.doi.org/10.1155/2013/203875

Research Article

The Analytical Solution of Some Fractional Ordinary Differential Equations by the Sumudu Transform Method

Hasan Bulut,[1] Haci Mehmet Baskonus,[2] and Fethi Bin Muhammad Belgacem[3]

[1] *Department of Mathematics, Firat University, Elazig, Turkey*
[2] *Department of Computer Engineering, Tunceli University, Tunceli, Turkey*
[3] *Department of Mathematics, Faculty of Basic Education, PAAET, Shamiya, Kuwait*

Correspondence should be addressed to Hasan Bulut; hbulut@firat.edu.tr

Received 16 March 2013; Accepted 31 July 2013

Academic Editor: Santanu Saha Ray

We introduce the rudiments of fractional calculus and the consequent applications of the Sumudu transform on fractional derivatives. Once this connection is firmly established in the general setting, we turn to the application of the Sumudu transform method (STM) to some interesting nonhomogeneous fractional ordinary differential equations (FODEs). Finally, we use the solutions to form two-dimensional (2D) graphs, by using the symbolic algebra package Mathematica Program 7.

1. Introduction

The Sumudu transform was first defined in its current shape by Watugala as early as 1993, which he used to solve engineering control problems. Although he might have had ideas for it sooner than that (1989) as some conference proceedings showed, he used it to control engineering problems [1, 2]. Later, Watugala extended in 2002 the Sumudu transform to two variables [3]. The first applications to differential equations and inversion formulae were done by Weerakoon in two papers in 1994 and 1998 [4, 5]. The Sumudu transform was also first defended by Weerakoon against Deakin's definition who claimed that there is no difference between the Sumudu and the Laplace and who reminded Weerakoon that the Sumudu transform is really the Carson or the S-multiplied transform disguised [6, 7]. The applications followed in three consecutive papers by Asiru dealing with the convolution-type integral equations and the discrete dynamic systems [8, 9]. At this point, Belgacem et al. using previous references and connections to the Laplace transform extended the theory and the applications of the Sumudu transform in [10–17] to various applications. In the meantime, subsequent to exchanges between Belgacem and other scholars, the following papers sprang up in the last decade [18–22]. Moreover, the Sumudu transform was also used to solve many ordinary differential equations with integer order [23–29]. The application of STM turns out to be pragmatic in getting analytical solution of the fractional ordinary differential equations fast. Notably, implementations of difference methods such as in the differential transform method (DTM), the Adomian decomposition method (ADM) [30–33], the variational iteration method (VIM) [34–40] empowered us to achieve approximate solutions of various ordinary differential equations. STM [41–44] which is newly submitted to the literature is a suitable technique for solving various kinds of ordinary differential equations with fractional order (FODEs). In this sense, it is estimated that this novel approach that is used to solve homogeneous and nonhomogeneous problems will be particularly valuable as a tool for scientists and applied mathematicians.

2. Fundamental Properties of Fractional Calculus and STM

2.1. Fundamental Facts of the Fractional Calculus. Firstly, we mention some of the fundamental properties of the fractional calculus. Fractional derivatives (and integrals as well) definitions may differ, but the most widely used definitions are those of Abel-Riemann (A-R). Following the nomenclature in [45], a derivative of fractional order in the A-R sense is defined by

$$D^{\alpha}[f(t)] = \begin{cases} \dfrac{1}{\Gamma[m-\alpha]}\dfrac{d}{dt^m}\displaystyle\int_0^t \frac{f(\tau)}{(t-\tau)^{\alpha-m+1}}d\tau, & m-1<\alpha\le m, \\ \dfrac{d^m}{dt^m}f(t), & \alpha = m, \end{cases} \quad (1)$$

where $m \in \mathbb{Z}^{+}$ and $\alpha \in R^{+}$. D^{α} is a derivative operator here, and

$$D^{-\alpha}[f(t)] = \frac{1}{\Gamma[\alpha]}\int_0^t (t-\tau)^{\alpha-1} f(\tau)\,d\tau, \quad 0<\alpha\le 1. \quad (2)$$

On the other hand, according to A-R, an integral of fractional order is defined by implementing the integration operator J^{α} in the following manner:

$$J^{\alpha}[f(t)] = \frac{1}{\Gamma[\alpha]}\int_0^t (t-\tau)^{\alpha-1} f(\tau)\,d\tau, \quad t>0,\ \alpha>0. \quad (3)$$

When it comes to some of the fundamental properties of fractional integration and fractional differentiation, these have been introduced to the literature by Podlubny [46]. Among these, we mention

$$\begin{aligned} J^{\alpha}[t^n] &= \frac{\Gamma[1+n]}{\Gamma[1+n+\alpha]}t^{n+\alpha}, \\ D^{\alpha}[t^n] &= \frac{\Gamma[1+n]}{\Gamma[1+n-\alpha]}t^{n-\alpha}. \end{aligned} \quad (4)$$

Another main definition of the fractional derivative is that of Caputo [46, 47] who defined it by

$$^{C}D^{\alpha}[f(t)] = \begin{cases} \dfrac{1}{\Gamma[m-\alpha]}\displaystyle\int_0^t \frac{f^{(m)}(\tau)}{(t-\tau)^{\alpha-m+1}}d\tau, & m-1<\alpha< m, \\ \dfrac{d^m}{dt^m}f(t), & \alpha = m. \end{cases} \quad (5)$$

A fundamental feature of the Caputo fractional derivative is that [17]

$$J^{\alpha}\left[{}^{C}D^{\alpha}f(t)\right] = f(t) - \sum_{k=0}^{\infty} f^{(k)}(0^{+})\frac{t^k}{k!}. \quad (6)$$

2.2. Fundamental Facts of the Sumudu Transform Method. The Sumudu transform is defined in [1, 2] as follows. Over the set of functions

$$\begin{aligned} A = \{ f(t) \mid \exists M, \tau_1, \tau_2 > 0,& \\ |f(t)| < Me^{|t|/\tau_i}, &\text{if } t \in (-1)^j \times [0,\infty) \}, \end{aligned} \quad (7)$$

the Sumudu transform of $f(t)$ is defined as

$$F(u) = S[f(t)] = \int_0^{\infty} f(ut)\,e^{-t}dt, \quad u \in (-\tau_1, \tau_2). \quad (8)$$

Theorem 1. *If $F(u)$ is the Sumudu transform of $f(t)$, one knows that the Sumudu transform of the derivatives with integer order is given as follows [46–49]:*

$$S\left[\frac{df(t)}{dt}\right] = \frac{1}{u}[F(u) - f(0)]. \quad (9)$$

Proof. Let us take the Sumudu transform [46–49] of $f'(t) = df(t)/dt$ as follows:

$$\begin{aligned} S\left[\frac{df(t)}{dt}\right] &= \int_0^{\infty}\frac{df(ut)}{dt}e^{-t}dt = \lim_{p\to\infty}\int_0^{p}\frac{df(ut)}{dt}e^{-t}dt \\ &= \lim_{p\to\infty}\left[\frac{1}{u}e^{-(t/u)}f(t)\Big|_0^p + \frac{1}{u^2}\int_0^p e^{-(t/u)}f(t)\,dt\right] \\ &= \lim_{p\to\infty}\left[\frac{1}{u}e^{-(t/u)}f(t)\Big|_0^p \right. \\ &\qquad \left. +\frac{1}{u}\left(\frac{1}{u}\int_0^p e^{-(t/u)}f(t)\,dt\right)\right] \\ &= \lim_{p\to\infty}\left[-\frac{1}{u}f(0) + \frac{1}{u}\left(\frac{1}{u}\int_0^p e^{-(t/u)}f(t)\,dt\right)\right] \\ &= -\frac{1}{u}f(0) + \frac{1}{u}F(u). \end{aligned} \quad (10)$$

□

Equation (10) gives us the proof of Theorem 1. When we continue in the same manner, we get the Sumudu transform of the second-order derivative as follows [46–49]:

$$S\left[\frac{d^2f(t)}{dt^2}\right] = \frac{1}{u^2}\left[F(u) - f(0) - u\frac{df(t)}{dt}\Big|_{t=0}\right]. \quad (11)$$

If we go on the same way, we get the Sumudu transform of the n-order derivative as follows:

$$S\left[\frac{d^nf(t)}{dt^n}\right] = u^{-n}\left[F(u) - \sum_{k=0}^{n-1}u^k\frac{d^nf(t)}{dt^n}\Big|_{t=0}\right]. \quad (12)$$

Theorem 2. *If $F(u)$ is the Sumudu transform of $f(t)$, one can take into consideration the Sumudu transform of the Riemann-Liouville fractional derivative as follows [17]:*

$$\begin{aligned} S[D^{\alpha}f(t)] = u^{-\alpha}\left[F(u) - \sum_{k=1}^{n}u^{\alpha-k}\left[D^{\alpha-k}(f(t))\right]_{t=0}\right], \\ -1<n-1\le\alpha<n. \end{aligned} \quad (13)$$

Proof. Let us take the Laplace transform of $f'(t) = df(t)/dt$ as follows:

$$\begin{aligned} L[D^{\alpha}f(t)] &= s^{\alpha}F(s) - \sum_{k=0}^{n-1}s^k\left[D^{\alpha-k-1}(f(t))\right]_{t=0} \\ &= s^{\alpha}F(s) - \sum_{k=0}^{n}s^{k-1}\left[D^{\alpha-k}(f(t))\right]_{t=0}. \end{aligned} \quad (14)$$

Therefore, when we substitute $1/u$ for s, we get the Sumudu transform of fractional order of $f(t)$ as follows:

$$S\left[D^{\alpha} f(t)\right] = u^{-\alpha}\left[F(u) - \sum_{k=1}^{n} u^{\alpha-k}\left[D^{\alpha-k}\left(f(t)\right)\right]_{t=0}\right]. \quad (15)$$

□

Now, we will introduce the improvement form of STM for solving FODEs. We take into consideration a general linear ordinary differential equation with fractional order as follows:

$$\frac{\partial^{\alpha} U(t)}{\partial t^{\alpha}} = \frac{\partial^{2} U(t)}{\partial t^{2}} + \frac{\partial U(t)}{\partial t} + U(t) + c, \quad (16)$$

being subject to the initial condition

$$U(0) = f(0). \quad (17)$$

Then, we will obtain the analytical solutions of some of the fractional ordinary differential equations by using STM. When we take the Sumudu transform of (16) under the terms of (12) and (15), we obtain the Sumudu transform of (16) as follows:

$$\begin{aligned}
S\left[\frac{\partial^{\alpha} U(t)}{\partial t^{\alpha}}\right] &= S\left[\frac{\partial^{2} U(t)}{\partial t^{2}}\right] + S\left[\frac{\partial U(t)}{\partial t}\right] + S\left[U(t)\right] + S\left[c\right],\\
u^{-\alpha}&\left[F(u) - \sum_{k=1}^{n} u^{\alpha-k}\left[D^{\alpha-k}\left(U(t)\right)\right]_{t=0}\right]\\
&= \frac{1}{u^{2}}\left[F(u) - f(0) - u\left.\frac{\partial f(t)}{\partial t}\right|_{t=0}\right]\\
&\quad + \frac{1}{u}\left[F(u) - f(0)\right] + F(u) + c,\\
F(u) &- \sum_{k=1}^{n} u^{\alpha-k}\left[D^{\alpha-k}\left(U(t)\right)\right]_{t=0}\\
&= u^{\alpha-2}\left[F(u) - f(0) - u\left.\frac{\partial U(t)}{\partial t}\right|_{t=0}\right]\\
&\quad + u^{\alpha-1}\left[F(u) - f(0)\right]\\
&\quad + u^{\alpha} F(u) + cu^{\alpha},\\
F(u) &= u^{\alpha-2} F(u) - u^{\alpha-2} U(0)\\
&\quad + \sum_{k=1}^{n} u^{\alpha-k}\left[D^{\alpha-k}\left(U(t)\right)\right]_{t=0} - u^{\alpha-1}\left.\frac{\partial U(t)}{\partial t}\right|_{t=0}\\
&\quad + u^{\alpha-1} F(u) - u^{\alpha-1} f(0)\\
&\quad + u^{\alpha} F(u) + cu^{\alpha},\\
F(u) &- u^{\alpha-2} F(u) - u^{\alpha-1} F(u) - u^{\alpha} F(u)\\
&= -u^{\alpha-2} f(0)\\
&\quad + \sum_{k=1}^{n} u^{\alpha-k}\left[D^{\alpha-k}\left(U(t)\right)\right]_{t=0} - u^{\alpha-1}\left.\frac{\partial U(t)}{\partial t}\right|_{t=0}\\
&\quad - u^{\alpha-1} U(0) + cu^{\alpha},\\
F(u) &= \frac{1}{1 - u^{\alpha-2} - u^{\alpha-1} - u^{\alpha}}\\
&\quad \times \left[g(u) - u^{\alpha-1} U(0) - u^{\alpha-2} U(0) + cu^{\alpha}\right],
\end{aligned} \quad (18)$$

where $g(u)$ is defined by $\sum_{k=1}^{n} u^{\alpha-k}[D^{\alpha-k}(U(t))]_{t=0} - u^{\alpha-1}(\partial U(t)/\partial t)|_{t=0}$. When we take the inverse Sumudu transform of (18) by using the inverse transform table in [11, 17], we get the solution of (16) by using STM as follows:

$$\begin{aligned}
U(t) = S^{-1}&\left[\frac{1}{1 - u^{\alpha-2} - u^{\alpha-1} - u^{\alpha}}\right.\\
&\left.\times\left[g(u) - u^{\alpha-1} U(0) - u^{\alpha-2} U(0) + cu^{\alpha}\right]\right].
\end{aligned} \quad (19)$$

3. Applications of STM to Nonhomogeneous Fractional Ordinary Differential Equations

In this section, we have applied STM to the nonhomogeneous fractional ordinary differential equations as follows.

Example 3. Firstly, we consider the nonhomogeneous fractional ordinary differential equation as follows [50]:

$$\begin{aligned}
D^{\alpha}\left[U(t)\right] = -U(t) &+ \frac{2}{\Gamma[3-\alpha]} t^{2-\alpha} - \frac{1}{\Gamma[2-\alpha]} t^{1-\alpha}\\
&+ t^{2} - t, \quad t > 0,\ 0 < \alpha \leq 1,
\end{aligned} \quad (20)$$

With the initial condition being

$$U(0) = 0. \quad (21)$$

In order to solve (20) by using STM, when we take the Sumudu transform of both sides of (20), we get the Sumudu transform of (20) as follows:

$$\begin{aligned}
S&\left[D^{\alpha} U(t)\right] + S\left[U(t)\right]\\
&= S\left[\frac{2}{\Gamma[3-\alpha]} t^{2-\alpha} - \frac{1}{\Gamma[2-\alpha]} t^{1-\alpha} + t^{2} - t\right],\\
S&\left[D^{\alpha} U(t)\right] + F(u) = S\left[\frac{2}{\Gamma[3-\alpha]} t^{2-\alpha}\right]\\
&\quad - S\left[\frac{1}{\Gamma[2-\alpha]} t^{1-\alpha}\right] + S\left[t^{2}\right] - S\left[t\right],\\
&\frac{F(u)}{u^{\alpha}} - \left.\frac{D^{\alpha-1}\left[U(t)\right]}{u}\right|_{t=0} + F(u) = \frac{2}{\Gamma[3-\alpha]} S\left[t^{2-\alpha}\right]\\
&\quad - \frac{1}{\Gamma[2-\alpha]} S\left[t^{1-\alpha}\right]\\
&\quad + S\left[t^{2}\right] - S\left[t\right],\\
&\frac{F(u)}{u^{\alpha}} + F(u) = \frac{2}{\Gamma[3-\alpha]} u^{2-\alpha}\Gamma[3-\alpha]\\
&\quad - \frac{1}{\Gamma[2-\alpha]} u^{1-\alpha}\Gamma[2-\alpha] + 2u^{2} - u,\\
&\left(1 + \frac{1}{u^{\alpha}}\right) F(u) = 2u^{2-\alpha} - u^{1-\alpha} + 2u^{2} - u,\\
&\left(1 + u^{\alpha}\right) F(u) = 2u^{2} - u + 2u^{2+\alpha} - u^{1+\alpha},\\
&\left(1 + u^{\alpha}\right) F(u) = u(2u - 1) + u^{\alpha} u(2u - 1),\\
&F(u) = (2u - 1)u,\\
&F(u) = 2u^{2} - u.
\end{aligned} \quad (22)$$

When we take the inverse Sumudu transform of (22) by using the inverse transform table in [11], we get the analytical solution of (20) by STM as follows:

$$U(t) = t^2 - t. \tag{23}$$

Remark 4. If we take the corresponding values for some parameters into consideration, then the solution of (20) is in full agreement with the solution of (30) mentioned in [50]. To our knowledge, the analytical solution of FODEs that we find in this paper has been newly submitted to the literature.

Example 5. Secondly, we consider the nonhomogeneous fractional ordinary differential equation as follows [51]:

$$D^{0.5}U(t) + U(t) = t^2 + \frac{\Gamma[3]}{\Gamma[2.5]}t^{1.5}, \quad t > 0, \tag{24}$$

With the initial condition being

$$U(0) = 0. \tag{25}$$

In order to solve (24) by using STM, when we take the Sumudu transform of both sides of (24), we get the Sumudu transform of (24) as follows:

$$S\left[D^{0.5}U(t)\right] + S[U(t)] = S\left[t^2\right] + \frac{\Gamma[3]}{\Gamma[2.5]}S\left[t^{1.5}\right],$$

$$S\left[D^{0.5}U(t)\right] + S[U(t)] = S\left[t^2\right] + 1.50451S\left[t^{1.5}\right],$$

$$\begin{aligned} &\frac{F(u)}{u^{0.5}} - \left.\frac{D^{\alpha-1}[U(t)]}{u}\right|_{t=0} + F(u) \\ &\quad = 2u^2 + 2u^{1.5} \\ &\quad \Longrightarrow \frac{F(u)}{u^{0.5}} + F(u) = 2u^2 + 2u^{1.5}, \end{aligned} \tag{26}$$

$$\left(\frac{1+u^{0.5}}{u^{0.5}}\right)F(u) = 2u^2 + 2u^{1.5}$$

$$\Longrightarrow \left(1+u^{0.5}\right)F(u) = 2u^2 + 2u^{1.5},$$

$$F(u) = \frac{2u^{2.5}}{1+u^{0.5}} + \frac{2u^2}{1+u^{0.5}} = \frac{2u^2\left(1+u^{0.5}\right)}{1+u^{0.5}} = 2u^2.$$

When we take the inverse Sumudu transform of (26) by using the inverse transform table in [48], we get the analytical solution of (24) by using STM as follows:

$$U(t) = t^2. \tag{27}$$

Remark 6. The solution (27) obtained by using the Sumudu transform method for (24) has been checked by the Mathematica Program 7. To our knowledge, the analytical solution that we find in this paper has been newly submitted to the literature.

4. Conclusion and Future Work

Prior to this study, various approaches have been performed to obtain approximate solutions of some fractional differential equations [50, 51]. In this paper, nonhomogeneous fractional ordinary differential equations have been solved by using the Sumudu transform after giving the related formulae for the fractional integrals, the derivatives, and the Sumudu transform of FODEs. The Sumudu technique can be used to solve many types such as initial-value problems and boundary-value problems in applied sciences, engineering fields, aerospace sciences, and mathematical physics. The Sumudu transform method has been used for The discrete fractional calculus in [43]. This technique has been investigated in terms of the double Sumudu transform in [44]. Consequently, this new approach has been implemented with success on interesting fractional ordinary differential equations. As such and pragmatically so, it enriches the library of integral transform approaches. Without a doubt, and based on our findings such as Figures 1 and 2, the STM technique remains direct, robust and valuable tool for solving same fractional differential equations.

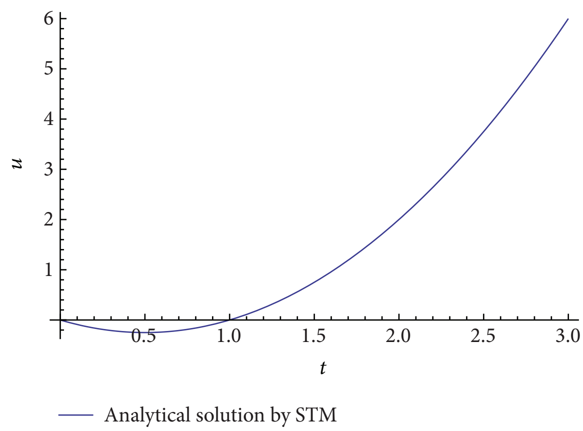

Figure 1: The 2D surfaces of the obtained solution by means of STM for (23) when $0 < t < 3$.

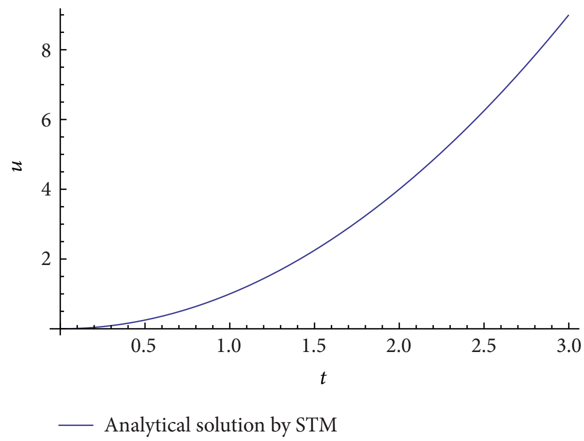

Figure 2: The 2D surfaces of the obtained solution by means of STM for (27) when $0 < t < 3$.

References

[1] G. K. Watugala, "Sumudu transform: a new integral transform to solve differential equations and control engineering

problems," *International Journal of Mathematical Education in Science and Technology*, vol. 24, no. 1, pp. 35–43, 1993.

[2] G. K. Watugala, "Sumudu transform—a new integral transform to solve differential equations and control engineering problems," *Mathematical Engineering in Industry*, vol. 6, no. 4, pp. 319–329, 1998.

[3] G. K. Watugala, "The Sumudu transform for functions of two variables," *Mathematical Engineering in Industry*, vol. 8, no. 4, pp. 293–302, 2002.

[4] S. Weerakoon, "Application of Sumudu transform to partial differential equations," *International Journal of Mathematical Education in Science and Technology*, vol. 25, no. 2, pp. 277–283, 1994.

[5] S. Weerakoon, "Complex inversion formula for Sumudu transform," *International Journal of Mathematical Education in Science and Technology*, vol. 29, no. 4, pp. 618–621, 1998.

[6] M. A. B. Deakin, "The "Sumudu transform" and the Laplace transform," *International Journal of Mathematical Education in Science and Technology*, vol. 28, p. 159, 1997.

[7] S. Weerakoon, "The "Sumudu transform" and the Laplace transform—reply," *International Journal of Mathematical Education in Science and Technology*, vol. 28, no. 1, p. 160, 1997.

[8] M. A. Asiru, "Sumudu transform and the solution of integral equations of convolution type," *International Journal of Mathematical Education in Science and Technology*, vol. 32, no. 6, pp. 906–910, 2001.

[9] M. A. Aşiru, "Further properties of the Sumudu transform and its applications," *International Journal of Mathematical Education in Science and Technology*, vol. 33, no. 3, pp. 441–449, 2002.

[10] F. B. M. Belgacem, A. A. Karaballi, and S. L. Kalla, "Analytical investigations of the Sumudu transform and applications to integral production equations," *Mathematical Problems in Engineering*, no. 3-4, pp. 103–118, 2003.

[11] F. B. M. Belgacem and A. Karaballi, "Sumudu transform fundamental properties investigations and applications," *Journal of Applied Mathematics and Stochastic Analysis*, Article ID 91083, 23 pages, 2006.

[12] F. B. M. Belgacem, "Introducing and analyzing deeper Sumudu properties Sumudu transform fundemantal properties investigations and applications," *Nonlinear Studies Journal*, vol. 1, no. 31, pp. 101–114, 2006.

[13] F. B. M. Belgacem, "Applications of the Sumudu transform to indefinite periodic parabolic problems," in *Proceedings of the International Conference on Nonlinear Problems and Aerospace Applications (ICNPAA '06)*, chapter 6, pp. 51–60, 2006.

[14] M. G. M. Hussain and F. B. M. Belgacem, "Transient solutions of Maxwell's equations based on Sumudu transform," *Progress in Electromagnetics Research*, vol. 74, pp. 273–289, 2007.

[15] F. B. M. Belgacem, "Sumudu applications to Maxwell's equations," *The Plan Index Enquiry and Retrieval System Online*, vol. 5, pp. 355–360, 2009.

[16] F. B. M. Belgacem, "Sumudu transform applications to Bessel functions and equations," *Applied Mathematical Sciences*, vol. 4, no. 73-76, pp. 3665–3686, 2010.

[17] Q. D. Katatbeh and F. B. M. Belgacem, "Applications of the Sumudu transform to fractional differential equations," *Nonlinear Studies*, vol. 18, no. 1, pp. 99–112, 2011.

[18] S. Salinas, A. Jimenez, F. Arteaga, and J. Rodriguez, "Estudio analitico de la transformada de Sumudu y algunas aplicaciones a la teoria de control," *Revista Ingeneria UC*, vol. 11, no. 3, pp. 79–86, 2004 (Spanish).

[19] M. A. Rana, A. M. Siddiqui, Q. K. Ghori, and R. Qamar, "Application of He's homotopy perturbation method to Sumudu transform," *International Journal of Nonlinear Sciences and Numerical Simulation*, vol. 8, no. 2, pp. 185–190, 2007.

[20] A. Tamrabet and A. Kadem, "A combined Walsh function and Sumudu transform for solving the two-dimensional neutron transport equation," *International Journal of Mathematical Analysis*, vol. 1, no. 9-12, pp. 409–421, 2007.

[21] J. M. Tchuenche and N. S. Mbare, "An application of the double Sumudu transform," *Applied Mathematical Sciences*, vol. 1, no. 1–4, pp. 31–39, 2007.

[22] J. Zhang, "Sumudu transform based coefficients calculation," *Nonlinear Studies*, vol. 15, no. 4, pp. 355–372, 2008.

[23] V. B. L. Chaurasia, R. S. Dubey, and F. B. M. Belgacem, "Fractional radial diffusion equation analytical solution via Hankel and Sumudu transforms," *International Journal of Mathematics in Engineering Science and Aerospace*, vol. 3, no. 2, pp. 1–10, 2012.

[24] P. Goswami and F. B. M. Belgacem, "Fractional differential equation solutions through a Sumudu rational," *Nonlinear Studies*, vol. 19, no. 4, pp. 591–598, 2012.

[25] F. B. M. Belgacem, "Introducing and analysing deeper Sumudu properties," *Nonlinear Studies*, vol. 13, no. 1, pp. 23–41, 2006.

[26] F. B. M. Belgacem and R. Silambarasan, "Maxwell's equations solutions by means of the natural transform," *International Journal of Mathematics in Engineering, Science And Aeorospace*, vol. 3, no. 3, pp. 313–323, 2012.

[27] S. K. Alomari, "An estimate of Sumudu transforms for Boehmians," in *Proceedings of the Conference on Mathematical problems in Engineering, Aerospace and Science*, Vienna, Austria, 2012.

[28] H. Bulut, H. M. Baskonus, and S. Tuluce, "The solutions of partial differential equations with variable coefficients by sumudu transform method," *AIP Proceeding*, vol. 1493, p. 91, 2012.

[29] H. Z. Khan and W. A. Khan, "N-transform-properties and applications," *NUST Journal of Engineering Sciences*, vol. 1, no. 1, pp. 127–133, 2008.

[30] G. Adomian, "A review of the decomposition method and some recent results for nonlinear equations," *Mathematical and Computer Modelling*, vol. 13, no. 7, pp. 17–43, 1990.

[31] G. Adomian and R. Rach, "Equality of partial solutions in the decomposition method for linear or nonlinear partial differential equations," *Computers & Mathematics with Applications*, vol. 19, no. 12, pp. 9–12, 1990.

[32] G. Adomian, *Solving Frontier Problems of Physics: The Decomposition Method*, vol. 60 of *Fundamental Theories of Physics*, Kluwer Academic Publishers, Boston, Mass, USA, 1994.

[33] G. Adomian, "A review of the decomposition method in applied mathematics," *Journal of Mathematical Analysis and Applications*, vol. 135, no. 2, pp. 501–544, 1988.

[34] Z.-G. Deng and G.-C. Wu, "Approximate solution of fractional differential equations with uncertainty," *Romanian Journal of Physics*, vol. 56, no. 7-8, pp. 868–872, 2011.

[35] M. A. Abdou and A. A. Soliman, "Variational iteration method for solving Burger's and coupled Burger's equations," *Journal of Computational and Applied Mathematics*, vol. 181, no. 2, pp. 245–251, 2005.

[36] Z. M. Odibat and S. Momani, "Application of variational iteration method to nonlinear differential equations of fractional order," *International Journal of Nonlinear Sciences and Numerical Simulation*, vol. 7, no. 1, pp. 27–34, 2006.

[37] J.-H. He and X.-H. Wu, "Variational iteration method: new development and applications," *Computers & Mathematics with Applications*, vol. 54, no. 7-8, pp. 881–894, 2007.

[38] N. H. Sweilam, "Fourth order integro-differential equations using variational iteration method," *Computers & Mathematics with Applications*, vol. 54, no. 7-8, pp. 1086–1091, 2007.

[39] S. Abbasbandy, "A new application of He's variational iteration method for quadratic Riccati differential equation by using Adomian's polynomials," *Journal of Computational and Applied Mathematics*, vol. 207, no. 1, pp. 59–63, 2007.

[40] A.-M. Wazwaz, "The variational iteration method for exact solutions of Laplace equation," *Physics Letters A*, vol. 363, no. 4, pp. 260–262, 2007.

[41] M. A. Asiru, "Application of the sumudu transform to discrete dynamical systems," *International Journal of Mathematical Education, Science and Technology*, vol. 34, no. 6, pp. 944–949, 2003.

[42] H. Bulut, H. M. Baskonus, and S. Tuluce, "Homotopy perturbation sumudu transform method for heat equations," *Mathematics in Engineering, Science and Aerospace*, vol. 4, no. 1, pp. 49–60, 2013.

[43] F. Jarad and K. Taş, "On Sumudu transform method in discrete fractional calculus," *Abstract and Applied Analysis*, vol. 2012, Article ID 270106, 16 pages, 2012.

[44] V. G. Gupta, B. Shrama, and A. Kiliçman, "A note on fractional Sumudu transform," *Journal of Applied Mathematics*, vol. 2010, Article ID 154189, 9 pages, 2010.

[45] R. C. Mittal and R. Nigam, "Solution of fractional integro-differential equations by adomian decomposition method," *The International Journal of Applied Mathematics and Mechanics*, vol. 4, no. 2, pp. 87–94, 2008.

[46] I. Podlubny, *Fractional Differential Equations*, vol. 198 of *Mathematics in Science and Engineering*, Academic Press, San Diego, Calif, USA, 1999.

[47] M. Caputo, "Linear model of dissipation whose Q is almost frequency independent-II," *Geophysical Journal of the Royal Astronomical Society*, vol. 13, no. 5, pp. 529–539, 1967.

[48] F. B. M. Belgacem and R. Silambarasan, "The Sumudu transform analysis by infinite series," in *Proceedings of the AIP Proceeding*, Vienna, Austria, 2012.

[49] P. Goswami and F. B. M. Belgacem, "Solving special fractional differential equations by the Sumudu transform," in *Proceedings of the AIP Proceeding*, Vienna, Austria, 2012.

[50] Z. M. Odibat and S. Momani, "An algorithm for the numerical solution of differential equations of fractional order," *Journal of Applied Mathematics and Informatics*, vol. 26, no. 1-2, pp. 15–127.

[51] N. J. Ford and A. C. Simpson, "The numerical solution of fractional differential equations: speed versus accuracy," Numerical Analysis Report no. 385, A Report in Association with Chester College, 2003.

Hindawi Publishing Corporation
Abstract and Applied Analysis
Volume 2013, Article ID 414353, 7 pages
http://dx.doi.org/10.1155/2013/414353

Research Article

Improved (G'/G)-Expansion Method for the Space and Time Fractional Foam Drainage and KdV Equations

Ali Akgül,[1,2] Adem Kılıçman,[3] and Mustafa Inc[4]

[1] *Department of Mathematics, Education Faculty, Dicle University, 21280 Diyarbakır, Turkey*
[2] *Department of Mathematics and Statistics, Missouri University of Science and Technology, Rolla, MO 65409-0020, USA*
[3] *Department of Mathematics and Institute for Mathematical Research, University Putra Malaysia, 43400 Serdang, Selangor, Malaysia*
[4] *Department of Mathematics, Science Faculty, Fırat University, 23119 Elazığ, Turkey*

Correspondence should be addressed to Mustafa Inc; minc@firat.edu.tr

Received 10 June 2013; Accepted 17 July 2013

Academic Editor: Santanu Saha Ray

The fractional complex transformation is used to transform nonlinear partial differential equations to nonlinear ordinary differential equations. The improved (G'/G)-expansion method is suggested to solve the space and time fractional foam drainage and KdV equations. The obtained results show that the presented method is effective and appropriate for solving nonlinear fractional differential equations.

1. Introduction

The soliton solutions of nonlinear evolution equations have made a major impact in the flesh. These solitons appear in various areas of physical and biological sciences. They show up in nonlinear optics, plasma physics, fluid dynamics, biochemistry, and mathematical chemistry. Fractional partial differential equations (FPDEs) have received considerable interest in recent years and have been extensively investigated. These equations were applied for many real problems which are modeled in various areas, for example, in mathematical physics [1], fluid and continuum mechanics [2], viscoplastic and viscoelastic flow [3], biology, chemistry, acoustics, and psychology [4, 5]. Some FPDEs do not have exact solutions, so approximation and numerical techniques must be used. There are several approximation and numerical methods. The most commonly used ones are the homotopy perturbation method [6, 7], the Adomian decomposition method [8, 9], the variational iteration method [10–12], the homotopy analysis method [13, 14], the generalized differential transform method [15], the finite difference method [16], and the finite element method [17]. In recent years, some authors have got exact solutions of FPDEs by using analytical methods. S. Zhang and H.-Q. Zhang [18] proposed to solve the nonlinear time fractional biological population model and (4 + 1)-dimensional space-time fractional Fokas equation by using the fractional subequation method. Guo et al. [19] presented the improved subequation method to solve the space-time fractional Whitham-Broer-Kaup and the generalized Hirota-Satsuma coupled KdV equations. Tang et al. [20] used the generalized fractional subequation method to obtain exact solutions of the space-time fractional Gardner equation with variable coefficients. Lu [21] investigated the exact solutions of the nonlinear fractional Klein-Gordon equation, the generalized time fractional Hirota-Satsuma coupled KdV system, and the nonlinear fractional Sharma-Tasso-Olver equation. Bin [22] solved the time-space fractional generalized Hirota-Satsuma coupled KdV equations and the time fractional fifth-order Sawada-Kotera equation by using the (G'/G)-expansion method. Omran and Gepreel [23] used the improved (G'/G)-expansion method to calculate the exact solutions to the time-space fractional foam drainage and KdV equations. In this paper, we will apply the improved (G'/G)-expansion method to obtain the exact solutions for the time-space fractional foam drainage and KdV equations with the modified Riemann-Liouville derivative defined by Jumarie [24–27]:

$$\frac{\partial^{\alpha} u}{\partial t^{\alpha}} = \frac{1}{2} u \frac{\partial^{2\beta} u}{\partial x^{2\beta}} + 2u^{2} \frac{\partial^{\beta} u}{\partial x^{\beta}} + \left(\frac{\partial^{\beta} u}{\partial x^{\beta}}\right)^{2}, \qquad t > 0,\ \alpha > 0,\ \beta \le 1, \tag{1}$$

$$\frac{\partial^\alpha u}{\partial t^\alpha} + \alpha u \frac{\partial^\beta u}{\partial x^\beta} + \frac{\partial^{3\beta} u}{\partial x^{3\beta}} = 0, \quad t > 0, \ \alpha > 0, \ \beta \le 1, \tag{2}$$

where α is arbitrary constant. This paper is organized as follows. In Section 2, we introduce some basic definitions of Jumarie's modified Riemann-Liouville derivative. In Section 3, the main steps of the improved (G'/G)-expansion method are given. In Section 4, we construct the exact solutions of (1) and (2) by the proposed method. Some conclusions are given in Section 5.

2. Preliminaries

There are several definitions for fractional differential equations. These definitions include Riemann-Liouville, Weyl, Grünwald-Letnikov, Riesz, and Jumarie fractional derivatives. The Riemann-Liouville fractional derivative of a constant is not zero. So the fractional derivative is only defined for differentiable function. In order to deal with nondifferentiable functions, Jumarie [24–27] presented a modification of the Riemann-Liouville definition which appears to provide a framework for a fractional calculus. This modification was successfully applied in the probability calculus, fractional Laplace problem, exact solutions of the nonlinear fractional differential equations, and many other types of linear and nonlinear fractional differential equations [28–30].

Definition 1. The Riemann-Liouville fractional integral is defined [31] as

$$\begin{aligned} {}_0I_x^\alpha f(x) &= I^\alpha f(x) \\ &= \frac{1}{\Gamma(\alpha)} \int_0^x f(\xi)(x-\xi)^{\alpha-1} d\xi, \quad \alpha > 0, \\ I^0 f(x) &= f(x). \end{aligned} \tag{3}$$

Definition 2. Jumarie [24–27] defined the fractional derivative in the limit form by

$$f^{(\alpha)}(x) = \lim_{h \to 0} \frac{\Delta^\alpha [f(x) - f(0)]}{h^\alpha}, \tag{4}$$

where $f(x)$ should be a continuous (but not necessarily differentiable) function and $h > 0$ denotes a constant discretization span. So, the modified form of the Riemann-Liouville derivative is defined as

$${}_0D_x^\alpha f(x) = \frac{1}{\Gamma(n-\alpha)} \frac{d^n}{dx^n} \int_0^x (x-\xi)^{(n-\alpha)} [f(\xi) - f(0)], \tag{5}$$

where $x \in [0, 1]$, $n - 1 \le \alpha < n$ and $n \ge 1$.

Lemma 3. *The integral with respect to $(dx)^\alpha$ is defined by Jumarie [24, 25] as follows:*

$$\begin{aligned} &\int_0^x f(\xi)(d\xi)^\alpha = \alpha \int_0^x (x-\xi) f(\xi) d\xi, \quad 0 < \alpha \le 1, \\ &\frac{d^\alpha}{dx^\alpha} \int_0^{u(x)} f(\xi)(d\xi)^\alpha = \Gamma(\alpha+1) f[u(\xi)][u'(\xi)]^\alpha, \\ &\qquad 0 < \alpha \le 1. \end{aligned} \tag{6}$$

Theorem 4. *Assume that the continuous function $f(x)$ has a fractional derivative of order α; then*

$$\begin{aligned} \frac{d^\alpha}{dx^\alpha} I^\alpha f(x) &= f(x), \\ I^\alpha \frac{d^\alpha}{dx^\alpha} f(x) &= f(x) - f(0), \quad 0 < \alpha \le 1, \end{aligned} \tag{7}$$

hold.

3. Description of the Improved (G'/G)-Expansion Method

In this section, we give the description of the improved (G'/G)-expansion method for solving the nonlinear FPDEs as

$$\begin{aligned} &F\left(u, D_t^\alpha u, D_x^\beta u, D_y^\gamma u, D_z^\delta u, D_t^\alpha D_t^\alpha u, \right. \\ &\left. D_t^\alpha D_x^\beta u, D_x^\beta D_x^\beta u, \dots\right) = 0, \\ &0 < \alpha, \beta, \gamma, \delta \le 1, \end{aligned} \tag{8}$$

where u is an unknown function and F is a polynomial of u and its partial fractional derivatives, in which the highest order derivatives and nonlinear terms are involved. We offer an improved (G'/G)-expansion method [32]. The essential steps of this method are described as follows.

Step 1. Li and He [33] and He and Li [34] presented a fractional complex transform to transform fractional differential equations into ordinary differential equations. So, all analytical methods devoted to advanced calculus can be easily dedicated to fractional calculus. The traveling wave variable is given as

$$\begin{aligned} u(x, y, z, t) &= u(\xi), \\ \xi &= \frac{Kx^\beta}{\Gamma(\beta+1)} + \frac{Ny^\gamma}{\Gamma(\gamma+1)} + \frac{Lt^\alpha}{\Gamma(\alpha+1)}, \end{aligned} \tag{9}$$

where K, N, and L are nonzero arbitrary constants. So, (9) is reduced to (10):

$$p\left(u, u', u'', u''', \dots\right) = 0, \tag{10}$$

where $u = u(\xi)$.

Step 2. Suppose that (10) has the solution (11):

$$u(\xi) = \sum_{i=0}^n a_i F^i(\xi), \tag{11}$$

where a_i $(i = 0, 1, \dots, n)$ are real constants to be determined, the balancing number n is a positive integer which can be determined by balancing the highest derivative terms with the highest power nonlinear terms in (10). More precisely, we define the degree of $u(\xi)$ as $D[u(\xi)] = m$, which gives rise to the degrees of other expressions, as follows:

$$\begin{aligned} D\left[\frac{d^q u}{d\xi^q}\right] &= m + q, \\ D\left[u^p \left(\frac{d^q u}{d\xi^q}\right)^s\right] &= mp + s(q+m). \end{aligned} \tag{12}$$

Therefore, we can obtain the value of m in (11).

Step 3. $F(\xi)$ is

$$F(\xi) = \frac{G'(\xi)}{G(\xi)}, \quad (13)$$

where $G(\xi)$ expresses the solution of the following auxiliary ordinary differential equation

$$G(\xi)G''(\xi) = AG^2(\xi) + BG(\xi)G'(\xi) + C[G(\xi)]^2, \quad (14)$$

where the prime denotes derivative with respect to ξ. A, B, and C are real parameters.

Step 4. Substituting (13) into (10), using (14), collecting all terms with the same order of $(G'(\xi)/G(\xi))$ together, and then equating each coefficient of the resulting polynomial to zero, we obtain a set of algebraic equations for a_i $(i = 0, 1, \ldots, n)$, A, B, C, K, N, and L.

Step 5. Using the general solutions of (14), with the aid of Mathematica, we have the following four solutions of (13).

Case 1. If $B \neq 0$ and $\Delta = B^2 + 4A - 4AC \geq 0$, then

$$F(\xi) = \frac{B}{2(1-C)} + \frac{B\sqrt{\Delta}}{2(1-C)} \times \frac{c_1 \exp\left(\left(\sqrt{\Delta}/2\right)\xi\right) + c_2 \exp\left(\left(-\sqrt{\Delta}/2\right)\xi\right)}{c_1 \exp\left(\left(\sqrt{\Delta}/2\right)\xi\right) - c_2 \exp\left(\left(-\sqrt{\Delta}/2\right)\xi\right)}. \quad (15)$$

Case 2. If $B \neq 0$ and $\Delta = B^2 + 4A - 4AC < 0$, then

$$F(\xi) = \frac{B}{2(1-C)} + \frac{B\sqrt{-\Delta}}{2(1-C)} \times \frac{ic_1 \cos\left(\left(\sqrt{-\Delta}/2\right)\xi\right) - c_2 \sin\left(\left(\sqrt{-\Delta}/2\right)\xi\right)}{ic_1 \sin\left(\left(\sqrt{-\Delta}/2\right)\xi\right) + c_2 \cos\left(\left(\sqrt{-\Delta}/2\right)\xi\right)}. \quad (16)$$

Case 3. If $B = 0$ and $\Delta = A(C-1) \geq 0$, then

$$F(\xi) = \frac{\sqrt{\Delta}}{(1-C)} \frac{c_1 \cos\left(\sqrt{\Delta}\xi\right) + c_2 \sin\left(\sqrt{\Delta}\xi\right)}{c_1 \sin\left(\sqrt{\Delta}\xi\right) - c_2 \cos\left(\sqrt{\Delta}\xi\right)}. \quad (17)$$

Case 4. If $B = 0$ and $\Delta = A(C-1) < 0$, then

$$F(\xi) = \frac{\sqrt{-\Delta}}{(1-C)} \frac{ic_1 \cosh\left(\sqrt{-\Delta}\xi\right) - c_2 \sinh\left(\sqrt{-\Delta}\xi\right)}{ic_1 \sinh\left(\sqrt{-\Delta}\xi\right) - c_2 \cosh\left(\sqrt{-\Delta}\xi\right)}, \quad (18)$$

where

$$\xi = \frac{Kx^\beta}{\Gamma(\beta+1)} + \frac{Ny^\gamma}{\Gamma(\gamma+1)} + \frac{Lt^\alpha}{\Gamma(\alpha+1)} \quad (19)$$

and A, B, C, c_1, and c_2 are real parameters.

4. Applications

We use the improved (G'/G)-expansion method on the time-space fractional nonlinear foam drainage equation and the time-space fractional nonlinear KdV equation in this section.

4.1. The Time and Space-Fractional Nonlinear Foam Drainage Equation. We apply the improved (G'/G)-expansion method to construct the exact solutions for the time-space fractional nonlinear foam drainage equation in this subsection. Foams are of great importance in many technological processes and applications. Their properties are subject of intensive studies from practical and scientific points of view [27, 35–37]. Liquid foam is an example of soft matter with a very well-defined structure, described by Joseph Plateau in the 19th century. Foams are common in foods and personal care products such as lotions and creams. They have important applications in food and chemical industries, mineral processing, fire fighting, and structural material sciences [27, 35–37]. This equation is numerically and analytically taken into account by different authors [38–40]. The space-time fractional nonlinear foam drainage equation is solved analytically only by Omran and Gepreel [23]. We can see the fractional complex transform as

$$u(x,t) = u(\xi), \qquad \xi = \frac{Kx^\beta}{\Gamma(\beta+1)} + \frac{Lt^\alpha}{\Gamma(\alpha+1)}, \quad (20)$$

where K and L are constants. So, (20) reduces to (21):

$$-Lu' + \frac{1}{2}K^2uu'' + 2Ku^2u' + K^2\left(u'\right)^2 = 0. \quad (21)$$

Balancing the highest order nonlinear term and the highest order linear term, we get $n = 1$. Thus, we obtain

$$u(\xi) = a_0 + a_1 F(\xi), \qquad F(\xi) = \frac{G'(\xi)}{G(\xi)}, \quad (22)$$

where a_0 and a_1 will be determined constants. Substituting (22) into (21), using (14), collecting all the terms of powers of (G'/G), and setting each coefficient to zero, we have the following system of algebraic equations:

$$\left(\frac{G'}{G}\right)^0 : 2Aa_0^2a_1K + A^2a_1^2K^2 + \frac{1}{2}Aa_0a_1BK^2 - Aa_1L = 0,$$

$$\left(\frac{G'}{G}\right)^1 : 2a_0^2a_1BK - Aa_0a_1K^2 + \frac{5}{2}Aa_1^2BK^2 + \frac{1}{2}a_0a_1B^2K^2 + Aa_0a_1CK^2 - a_1BL = 0,$$

$$\left(\frac{G'}{G}\right)^2 : -2a_0^2a_1K + 2Aa_1^3K + 4a_0a_1^2BK + 2a_0^2a_1CK - 3Aa_1^2K^2 + \frac{3}{2}a_0a_1BK^2 + \frac{3}{2}a_1^2B^2K^2 + 3Aa_1^2CK^2 + \frac{3}{2}a_0a_1BCK^2 + \frac{3}{2}a_1^2B^2K^2 + 3Aa_1^2CK^2 + \frac{3}{2}a_0a_1BCK^2 + a_1L - a_1CL = 0,$$

$$\left(\frac{G'}{G}\right)^3 : -4a_0a_1^2K + 2a_1^3BK + 4a_0a_1^2CK + a_0a_1K^2 - \frac{7}{2}a_1^2BK^2 + 2a_0a_1CK^2 + \frac{7}{2}a_1^2BCK^2 + a_0a_1C^2K^2 = 0,$$
$$\left(\frac{G'}{G}\right)^4 : -2a_1^3K + 2a_1^3CK + 2a_1^2K^2 - 4a_1^2CK^2 + 2a_1^2C^2K^2 = 0. \tag{23}$$

Solving the set of the above algebraic equations, we get the following result:

$$a_0 = \frac{8ABK(C-1)}{B^2+6A-6AC}, \qquad a_1 = K(C-1),$$
$$L = \frac{1}{2}\left(4a_0^2K + a_0BK^2 + 2AK^3 - 2ACK^3\right), \tag{24}$$
$$KB(C-1) \neq 0.$$

Substituting this value in (22) and by Cases 1–4, we obtain the following exponential, hyperbolic and triangular function solutions of (1).

(1) If we choose $B \neq 0$ and $\Delta = B^2 + 4A - 4AC \geq 0$, then the exponential function solutions can be found as

$$u(x,t) = \frac{16ABK(C-1) - KB[\Delta + 2A(C-1)]}{2\Delta + 2A(C-1)} - \frac{KB\sqrt{\Delta}}{2} \times \frac{c_1\exp\left(\left(\sqrt{\Delta}/2\right)\xi\right) + c_2\exp\left(\left(-\sqrt{\Delta}/2\right)\xi\right)}{c_1\exp\left(\left(\sqrt{\Delta}/2\right)\xi\right) - c_2\exp\left(\left(-\sqrt{\Delta}/2\right)\xi\right)}, \tag{25}$$

where

$$\xi = \frac{Kx^\beta}{\Gamma(\beta+1)} + \frac{1}{2}\left(4a_0^2K + a_0BK^2 + 2AK^3 - 2ACK^3\right) \times \frac{t^\alpha}{\Gamma(\alpha+1)}. \tag{26}$$

(2) If we choose $B \neq 0$ and $\Delta = B^2 + 4A - 4AC < 0$, then the triangular function solution will be

$$u(x,t) = \frac{16ABK(C-1) - KB[\Delta + 2A(C-1)]}{2\Delta + 2A(C-1)} - \frac{KB\sqrt{-\Delta}}{2} \times \frac{ic_1\cos\left(\left(\sqrt{-\Delta}/2\right)\xi\right) - c_2\sin\left(\left(\sqrt{-\Delta}/2\right)\xi\right)}{ic_1\sin\left(\left(\sqrt{-\Delta}/2\right)\xi\right) + c_2\cos\left(\left(\sqrt{-\Delta}/2\right)\xi\right)}, \tag{27}$$

where

$$\xi = \frac{Kx^\beta}{\Gamma(\beta+1)} + \frac{1}{2}\left(4a_0^2K + a_0BK^2 + 2AK^3 - 2ACK^3\right) \times \frac{t^\alpha}{\Gamma(\alpha+1)}. \tag{28}$$

(3) If we choose $B = 0$ and $\Delta_1 = A(C-1) \geq 0$, then we get another triangular function solution

$$u(x,t) = -K\sqrt{\Delta_1}\frac{c_1\cos\left(\sqrt{\Delta_1}\xi\right) + c_2\sin\left(\sqrt{\Delta_1}\xi\right)}{c_1\sin\left(\sqrt{\Delta_1}\xi\right) - c_2\cos\left(\sqrt{\Delta_1}\xi\right)}, \tag{29}$$

where $\xi = Kx^\beta/\Gamma(\beta+1) - \Delta_1(K^3t^\alpha/\Gamma(\alpha+1))$.

(4) If we choose $B = 0$ and $\Delta_1 = A(C-1) < 0$, then we obtain the hyperbolic function solution

$$u(x,t) = -K\sqrt{\Delta_1}\frac{ic_1\cosh\left(\sqrt{-\Delta_1}\xi\right) - c_2\sinh\left(\sqrt{-\Delta_1}\xi\right)}{ic_1\sinh\left(\sqrt{-\Delta_1}\xi\right) - c_2\cosh\left(\sqrt{-\Delta_1}\xi\right)}, \tag{30}$$

where $\xi = Kx^\beta/\Gamma(\beta+1) - \Delta_1(K^3t^\alpha/\Gamma(\alpha+1))$.

If we take $c_1 = -c_2$ and $c_1 = c_2$ in (25), respectively, then we get

$$u(x,t) = \frac{16ABK(C-1) - KB[\Delta + 2A(C-1)]}{2\Delta + 2A(C-1)} - \frac{KB\sqrt{\Delta}}{2}\tanh\left(\frac{\sqrt{\Delta}}{2}\xi\right),$$
$$u(x,t) = \frac{16ABK(C-1) - KB[\Delta + 2A(C-1)]}{2\Delta + 2A(C-1)} - \frac{KB\sqrt{\Delta}}{2}\coth\left(\frac{\sqrt{\Delta}}{2}\xi\right). \tag{31}$$

4.2. The Nonlinear Space-Time Fractional KdV Equation. The KdV equation is the most popular soliton equation, and it has been largely investigated. In addition, the space and time fractional KdV equations with initial conditions were widely worked by [27, 38, 39]. Integrating (2) with respect to u and ignoring the integral constants leads to

$$\frac{1}{2}Lu^2 + \frac{1}{6}aKu^3 + \frac{1}{2}K^3(u')^2 = 0. \tag{32}$$

Considering the homogeneous balance between the highest order derivatives and the nonlinear term in (32), we get $n = 2$. So, we can suppose that (32) has the following ansatz:

$$u(\xi) = a_0 + a_1F(\xi) + a_2F^2(\xi), \tag{33}$$

where a_0, a_1, a_2, L, and K are arbitrary constants to be determined later. Substituting (33) and (14), along with (13), into (32) and using Mathematica yields a system of Equations of (G'/G):

$$\begin{aligned}
&\left(\frac{G'}{G}\right)^0 : \frac{1}{3}aa_0^3K + A^2a_1^2K^3 + a_0^2L = 0,\\
&\left(\frac{G'}{G}\right)^1 : \frac{1}{2}aa_0^2a_1K + 2A^2a_1a_2K^3 \\
&\qquad + Aa_1^2BK^3 + a_0a_1L = 0,\\
&\left(\frac{G'}{G}\right)^2 : \frac{1}{2}aa_0a_1^2K + \frac{1}{2}aa_0^2a_2K - Aa_1^2K^3 \\
&\qquad + 2A^2a_2^2K^3 + 4Aa_1a_2BK^3 + \frac{1}{2a_1^2B^2K^3} \\
&\qquad + Aa_1^2CK^3 + \frac{1}{2}a_1^2L + a_0a_2L = 0,\\
&\left(\frac{G'}{G}\right)^3 : \frac{1}{6}aa_1^3K + aa_0a_1a_2K - 4Aa_1a_2K^3 \\
&\qquad - a_1^2BK^3 + 4Aa_2^2BK^3 + 2a_1a_2B^2K^3 \\
&\qquad + 4Aa_1a_2CK^3 + a_1^2BCK^3 + a_1a_2L = 0,\\
&\left(\frac{G'}{G}\right)^4 : \frac{1}{2}a_1^2a_2K + \frac{1}{2}aa_0a_2^2K + \frac{1}{2}a_1^2K^3 \\
&\qquad - 4Aa_2^2K^3 - 4a_1a_2BK^3 + 2a_2^2B^2K^3 \\
&\qquad - a_1^2CK^3 + 4a_1a_2BCK^3 + \frac{1}{2}a_1^2C^2K^3 \\
&\qquad + \frac{1}{2}a_2^2L = 0,\\
&\left(\frac{G'}{G}\right)^5 : \frac{1}{2}aa_1a_2^2K + 2a_1a_2K^3 - 4a_2^2BK^3 \\
&\qquad - 4a_1a_2CK^3 + 4a_2^2BCK^3 + 2a_1a_2C^2K^3 = 0,\\
&\left(\frac{G'}{G}\right)^6 : \frac{1}{6}a_1a_2^2K + 2a_2^2K^3 - 4a_2^2CK^3 \\
&\qquad + 2a_2^2C^2K^3 = 0.
\end{aligned} \tag{34}$$

Solving the set of the above algebraic equations by use of Mathematica, we get the following results:

$$\begin{aligned}
a \neq 0, \quad a_0 &= -\frac{12AK^2}{a}(C-1),\\
a_1 &= \frac{12BK^2}{a}(C-1),\\
a_2 &= -\frac{12K^2}{a}(C-1),\\
L &= -K^3\left(B^2 - 4AC + 4A\right).
\end{aligned} \tag{35}$$

Substituting (35) into (33) and according to (15)–(18), we obtain the following exponential function solutions, hyperbolic function solutions, and triangular function solutions of (2), respectively.

(1) If we choose $B \neq 0$ and $\Delta = B^2 + 4A - 4AC \geq 0$, then the exponential function solution can be found as

$$\begin{aligned}
u(x,t) = {} & \frac{3K^2(\Delta - 2C)}{a(C-1)} - \frac{6CK^2\sqrt{\Delta}}{a(C-1)} \\
& \times \frac{c_1\exp\left(\sqrt{\Delta}\xi/2\right) + c_2\exp\left(\left(-\sqrt{\Delta}/2\right)\xi\right)}{c_1\exp\left(\left(\sqrt{\Delta}/2\right)\xi\right) - c_2\exp\left(\left(-\sqrt{\Delta}/2\right)\xi\right)} \\
& - \frac{6CK^2\Delta}{a(C-1)} \\
& \times \left[\frac{c_1\exp\left(\left(\sqrt{\Delta}/2\right)\xi\right) + c_2\exp\left(-\left(\sqrt{\Delta}/2\right)\xi\right)}{c_1\exp\left(\left(\sqrt{\Delta}/2\right)\xi\right) - c_2\exp\left(-\left(\sqrt{\Delta}/2\right)\xi\right)}\right]^2,
\end{aligned} \tag{36}$$

where $\xi = Kx^\beta/\Gamma(\beta+1) - K^3\Delta(t^\alpha/\Gamma(\alpha+1))$.

(2) If we choose $B \neq 0$ and $\Delta = B^2 + 4A - 4AC < 0$, then the triangular function solution will be

$$\begin{aligned}
u(x,t) = {} & \frac{3K^2(\Delta - 2C)}{a(C-1)} + \frac{6CK^2\sqrt{\Delta}}{a(C-1)} \\
& \times \frac{ic_1\cos\left(\sqrt{-\Delta}\xi/2\right) - c_2\sin\left(\left(\sqrt{-\Delta}/2\right)\xi\right)}{ic_1\sin\left(\left(\sqrt{-\Delta}/2\right)\xi\right) + c_2\cos\left(\left(\sqrt{-\Delta}/2\right)\xi\right)} \\
& + \frac{6CK^2\Delta}{a(C-1)} \\
& \times \left[\frac{ic_1\cos\left(\left(\sqrt{-\Delta}/2\right)\xi\right) - c_2\sin\left(\left(\sqrt{-\Delta}/2\right)\xi\right)}{ic_1\sin\left(\left(\sqrt{-\Delta}/2\right)\xi\right) + c_2\cos\left(\left(\sqrt{-\Delta}/2\right)\xi\right)}\right]^2,
\end{aligned} \tag{37}$$

where $\xi = Kx^\beta/\Gamma(\beta+1) - K^3\Delta(t^\alpha/\Gamma(\alpha+1))$.

(3) If we choose $B = 0$ and $\Delta_1 = A(C-1) \geq 0$, then the triangular function solution is given as

$$\begin{aligned}
u(x,t) = {} & -\frac{12K^2\Delta_1}{a} - \frac{12K^2\Delta_1}{a(C-1)} \\
& \times \left[\frac{c_1\cos\left(\sqrt{\Delta_1}\xi\right) + c_2\sin\left(\sqrt{\Delta_1}\xi\right)}{c_1\sin\left(\sqrt{\Delta_1}\xi\right) - c_2\cos\left(\sqrt{\Delta_1}\xi\right)}\right]^2,
\end{aligned} \tag{38}$$

where $\xi = Kx^\beta/\Gamma(\beta+1) + 4K^3\Delta_1(t^\alpha/\Gamma(\alpha+1))$.

(4) If we choose $B = 0$ and $\Delta_1 = A(C-1) < 0$, then the hyperbolic function solution is given as

$$u(x,t) = -\frac{12K^2\Delta_1}{a} + \frac{12K^2\Delta_1}{a(C-1)} \times \left[\frac{ic_1\cosh\left(\sqrt{-\Delta_1}\xi\right) - c_2\sinh\left(\sqrt{-\Delta_1}\xi\right)}{ic_1\sinh\left(\sqrt{-\Delta_1}\xi\right) - c_2\cosh\left(\sqrt{-\Delta_1}\xi\right)}\right]^2, \quad (39)$$

where $\xi = Kx^\beta/\Gamma(\beta+1) - 4K^3\Delta_1(t^\alpha/\Gamma(\alpha+1))$. Equation (36) can be rewritten at $c_1 = -c_2$; so we get the other hyperbolic function solution of (2):

$$\begin{aligned} u(x,t) = {} & \frac{3K^2(\Delta-2C)}{a(C-1)} - \frac{6CK^2\sqrt{\Delta}}{a(C-1)} \\ & \times \tanh\left[\frac{\sqrt{\Delta}}{2}\left(\frac{Kx^\beta}{\Gamma(\beta+1)} - K^3\Delta\frac{t^\alpha}{\Gamma(\alpha+1)}\right)\right] \\ & + \frac{6CK^2\sqrt{\Delta}}{a(C-1)} \\ & \times \tanh^2\left[\frac{\sqrt{\Delta}}{2}\left(\frac{Kx^\beta}{\Gamma(\beta+1)} - K^3\Delta\frac{t^\alpha}{\Gamma(\alpha+1)}\right)\right]. \end{aligned} \quad (40)$$

Equation (36) becomes

$$\begin{aligned} u(x,t) = {} & \frac{3K^2(\Delta-2C)}{a(C-1)} - \frac{6CK^2\sqrt{\Delta}}{a(C-1)} \\ & \times \coth\left[\frac{\sqrt{\Delta}}{2}\left(\frac{Kx^\beta}{\Gamma(\beta+1)} - K^3\Delta\frac{t^\alpha}{\Gamma(\alpha+1)}\right)\right] \\ & + \frac{6CK^2\sqrt{\Delta}}{a(C-1)} \\ & \times \coth^2\left[\frac{\sqrt{\Delta}}{2}\left(\frac{Kx^\beta}{\Gamma(\beta+1)} - K^3\Delta\frac{t^\alpha}{\Gamma(\alpha+1)}\right)\right] \end{aligned} \quad (41)$$

at $c_1 = c_2$.

Remark 5. Kudryashov et al. [41–44] have showed that every solution, which was obtained when soliton solutions have been found by some analytic methods, is not a new solution. They also showed that these methods are very similar. Furthermore, they mentioned that authors who used these methods should check the obtained results very carefully. The reason for using improved (G'/G)-expansion method in this work is to use nonlinear equation (14) instead of linear equation

$$G'' - \lambda G' - \mu G = 0, \quad (42)$$

which was used in standard (G'/G) method and to obtain lots of different solutions.

5. Conclusion

In this paper, we introduced an improved (G'/G)-expansion method and carried it out to obtain new travelling wave solutions of the space-time fractional foam drainage equation and the space-time fractional KdV equation. This method gives new exact solutions for nonlinear FPDEs. These solutions include the hyperbolic function solution, the exponential function solution, the triangular function solution, and the trigonometric function solution. These solutions are useful to understand the mechanisms of the complicated nonlinear physical phenomena.

References

[1] I. Podlubny, *Fractional Differential Equations*, vol. 198 of *Mathematics in Science and Engineering*, Academic Press, San Diego, Calif, USA, 1999, An introduction to fractional derivatives, fractional differential equations, to methods of their solution and some of their applications.

[2] C. Li, A. Chen, and J. Ye, "Numerical approaches to fractional calculus and fractional ordinary differential equation," *Journal of Computational Physics*, vol. 230, no. 9, pp. 3352–3368, 2011.

[3] X. Yang, "Local fractional integral transforms," *Progress in Nonlinear Science*, no. 4, pp. 1–225, 2011.

[4] S. Momani and Z. Odibat, "A novel method for nonlinear fractional partial differential equations: combination of DTM and generalized Taylor's formula," *Journal of Computational and Applied Mathematics*, vol. 220, no. 1-2, pp. 85–95, 2008.

[5] J. Sabatier, A. Oustaloup, J. C. Trigeasson, and N. Maamri, "A Lyapunov approach to the stability of fractional differential equations," *Signal Processing*, vol. 91, no. 3, pp. 437–445, 2011.

[6] J.-H. He, "Homotopy perturbation technique," *Computer Methods in Applied Mechanics and Engineering*, vol. 178, no. 3-4, pp. 257–262, 1999.

[7] J.-H. He, "Homotopy perturbation method with an auxiliary term," *Abstract and Applied Analysis*, vol. 2012, Article ID 857612, 7 pages, 2012.

[8] V. Daftardar-Gejji and S. Bhalekar, "Solving multi-term linear and non-linear diffusion-wave equations of fractional order by Adomian decomposition method," *Applied Mathematics and Computation*, vol. 202, no. 1, pp. 113–120, 2008.

[9] V. Daftardar-Gejji and H. Jafari, "Solving a multi-order fractional differential equation using Adomian decomposition," *Applied Mathematics and Computation*, vol. 189, no. 1, pp. 541–548, 2007.

[10] J. He, "Variational iteration method for delay differential equations," *Communications in Nonlinear Science and Numerical Simulation*, vol. 2, no. 4, pp. 235–236, 1997.

[11] J. H. He, "Variational iteration method for delay differential equations," *Journal of Computational and Applied Mathematics*, vol. 25, pp. 3–17, 2007.

[12] M. Inc, "The approximate and exact solutions of the space- and time-fractional Burgers equations with initial conditions by variational iteration method," *Journal of Mathematical Analysis and Applications*, vol. 345, no. 1, pp. 476–484, 2008.

[13] S. Liao, "On the homotopy analysis method for nonlinear problems," *Applied Mathematics and Computation*, vol. 147, no. 2, pp. 499–513, 2004.

[14] M. Ganjiani, "Solution of nonlinear fractional differential equations using homotopy analysis method," *Applied Mathematical Modelling*, vol. 34, no. 6, pp. 1634–1641, 2010.

[15] J. Liu and G. Hou, "Numerical solutions of the space- and time-fractional coupled Burgers equations by generalized differential transform method," *Applied Mathematics and Computation*, vol. 217, no. 16, pp. 7001–7008, 2011.

[16] M. Cui, "Compact finite difference method for the fractional diffusion equation," *Journal of Computational Physics*, vol. 228, no. 20, pp. 7792–7804, 2009.

[17] H. Zhan, Q. Huang, and G. Huang, "Finite element solution for the fractional advection-dispersion equation," *Advances in Water Resources*, vol. 31, no. 12, pp. 1578–1589, 2008.

[18] S. Zhang and H.-Q. Zhang, "Fractional sub-equation method and its applications to nonlinear fractional PDEs," *Physics Letters A*, vol. 375, no. 7, pp. 1069–1073, 2011.

[19] S. Guo, L. Mei, Y. Fang, and Z. Qiu, "Compacton and solitary pattern solutions for nonlinear dispersive KdV-type equations involving Jumarie's fractional derivative," *Physics Letters A*, vol. 376, no. 3, pp. 158–164, 2012.

[20] B. Tang, Y. He, L. Wei, and X. Zhang, "A generalized fractional sub-equation method for fractional differential equations with variable coefficients," *Physics Letters A*, vol. 376, no. 38-39, pp. 2588–2590, 2012.

[21] B. Lu, "The first integral method for some time fractional differential equations," *Journal of Mathematical Analysis and Applications*, vol. 395, no. 2, pp. 684–693, 2012.

[22] Z. Bin, "G'/G-expansion method for solving fractional partial differential equations," *Communications in Theoretical Physics*, vol. 58, pp. 623–630, 2012.

[23] S. Omran and K. A. Gepreel, "Exact solutions for nonlinear partial fractional differential equations," *Chinese Physics B*, vol. 21, Article ID 110204, 2012.

[24] G. Jumarie, "Modified Riemann-Liouville derivative and fractional Taylor series of nondifferentiable functions further results," *Computers & Mathematics with Applications*, vol. 51, no. 9-10, pp. 1367–1376, 2006.

[25] G. Jumarie, "New stochastic fractional models for Malthusian growth, the Poissonian birth process and optimal management of populations," *Mathematical and Computer Modelling*, vol. 44, no. 3-4, pp. 231–254, 2006.

[26] J. Guy, "Lagrange characteristic method for solving a class of nonlinear partial differential equations of fractional order," *Applied Mathematics Letters of Rapid Publication*, vol. 19, no. 9, pp. 873–880, 2006.

[27] G. Jumarie, "Table of some basic fractional calculus formulae derived from a modified Riemann-Liouville derivative for non-differentiable functions," *Applied Mathematics Letters of Rapid Publication*, vol. 22, no. 3, pp. 378–385, 2009.

[28] A. Golbabai and K. Sayevand, "Analytical treatment of differential equations with fractional coordinate derivatives," *Computers & Mathematics with Applications*, vol. 62, no. 3, pp. 1003–1012, 2011.

[29] A. Golbabai and K. Sayevand, "Analytical modelling of fractional advection-dispersion equation defined in a bounded space domain," *Mathematical and Computer Modelling*, vol. 53, no. 9-10, pp. 1708–1718, 2011.

[30] A. Golbabai and K. Sayevand, "Solitary pattern solutions for fractional Zakharov-Kuznetsov equations with fully nonlinear dispersion," *Applied Mathematics Letters of Rapid Publication*, vol. 25, no. 4, pp. 757–766, 2012.

[31] K. Sayevand, A. Golbabai, and A. Yildirim, "Analysis of differential equations of fractional order," *Applied Mathematical Modelling*, vol. 36, no. 9, pp. 4356–4364, 2012.

[32] Z. Li, X. Liu, and W. Zhang, "Application of improved G'/G-expansion method to traveling wave solutions of two nonlinear evolution equations," *Advances in Applied Mathematics and Mechanics*, vol. 4, no. 1, pp. 122–131, 2012.

[33] Z. B. Li and J. H. He, "Converting fractional differential equations into partial differential equations," *Thermal Science*, vol. 16, pp. 331–334, 2012.

[34] J. H. He and Z. B. Li, "Application of the fractional complex transform to fractional differential equations," *Nonlinear Science Letters A*, vol. 2, pp. 121–126, 2011.

[35] M. P. Brenner, J. Eggers, S. A. Koehler, and H. A. Stone, "Dynamics of foam drainage," *Physical Review E*, vol. 58, no. 2, pp. 2097–2106, 1998.

[36] S. Hutzler and D. L. Weaire, *The Physics of Foams*, oxford university press, Oxford, UK, 2000.

[37] J. Banhart and W. Brinkers, "Fatigue behavior of aluminum foams," *Journal of Materials Science Letters*, vol. 18, no. 8, pp. 617–619, 1999.

[38] A. Fereidoon, H. Yaghoobi, and M. Davoudabadi, "Application of the homotopy perturbation method for solving the foam drainage equation," *International Journal of Differential Equations*, vol. 2011, Article ID 864023, 13 pages, 2011.

[39] M. A. Helal and M. S. Mehanna, "The tanh method and Adomian decomposition method for solving the foam drainage equation," *Applied Mathematics and Computation*, vol. 190, no. 1, pp. 599–609, 2007.

[40] F. Khani, S. Hamedi-Nezhad, M. T. Darvishi, and S.-W. Ryu, "New solitary wave and periodic solutions of the foam drainage equation using the Exp-function method," *Nonlinear Analysis: Real World Applications*, vol. 10, no. 3, pp. 1904–1911, 2009.

[41] N. A. Kudryashov and M. B. Soukharev, "Popular ansatz methods and solitary wave solutions of the Kuramoto-Sivashinsky equation," *Regular and Chaotic Dynamics*, vol. 14, no. 3, pp. 407–419, 2009.

[42] N. A. Kudryashov, "Seven common errors in finding exact solutions of nonlinear differential equations," *Communications in Nonlinear Science and Numerical Simulation*, vol. 14, no. 9-10, pp. 3507–3529, 2009.

[43] N. A. Kudryashov, "A note on the G'/G-expansion method," *Applied Mathematics and Computation*, vol. 217, no. 4, pp. 1755–1758, 2010.

[44] N. A. Kudryashov and N. B. Loguinova, "Be careful with the Exp-function method," *Communications in Nonlinear Science and Numerical Simulation*, vol. 14, no. 5, pp. 1881–1890, 2009.

Hindawi Publishing Corporation
Abstract and Applied Analysis
Volume 2013, Article ID 932085, 5 pages
http://dx.doi.org/10.1155/2013/932085

Research Article

The Solution to the BCS Gap Equation for Superconductivity and Its Temperature Dependence

Shuji Watanabe

Division of Mathematical Sciences, Graduate School of Engineering, Gunma University, 4-2 Aramaki-machi, Maebashi 371-8510, Japan

Correspondence should be addressed to Shuji Watanabe; shuwatanabe@gunma-u.ac.jp

Received 27 May 2013; Accepted 9 August 2013

Academic Editor: Santanu Saha Ray

From the viewpoint of operator theory, we deal with the temperature dependence of the solution to the BCS gap equation for superconductivity. When the potential is a positive constant, the BCS gap equation reduces to the simple gap equation. We first show that there is a unique nonnegative solution to the simple gap equation, that it is continuous and strictly decreasing, and that it is of class C^2 with respect to the temperature. We next deal with the case where the potential is not a constant but a function. When the potential is not a constant, we give another proof of the existence and uniqueness of the solution to the BCS gap equation, and show how the solution varies with the temperature. We finally show that the solution to the BCS gap equation is indeed continuous with respect to both the temperature and the energy under a certain condition when the potential is not a constant.

1. Introduction

We use the unit $k_B = 1$, where k_B stands for the Boltzmann constant. Let $\omega_D > 0$ and $k \in \mathbb{R}^3$ stand for the Debye frequency and the wave vector of an electron, respectively. Let $h > 0$ be Planck's constant, and set $\hbar = h/(2\pi)$. Let $m > 0$ and $\mu > 0$ stand for the electron mass and the chemical potential, respectively. We denote by $T(\geq 0)$ the absolute temperature, and by x the kinetic energy of an electron minus the chemical potential; that is, $x = \hbar^2|k|^2/(2m) - \mu$. Note that $0 < \hbar\omega_D \ll \mu$.

In the BCS model [1, 2] of superconductivity, the solution to the BCS gap equation (1) is called the gap function. The gap function corresponds to the energy gap between the superconducting ground state and the superconducting first excited state. Accordingly, the value of the gap function (the solution) is nonnegative. We regard the gap function as a function of both T and x and denote it by u; that is, $u : (T, x) \mapsto u(T, x)$ (≥ 0). The BCS gap equation is the following nonlinear integral equation $(0 < \varepsilon \leq x \leq \hbar\omega_D)$:

$$u(T, x) = \int_\varepsilon^{\hbar\omega_D} \frac{U(x, \xi)\, u(T, \xi)}{\sqrt{\xi^2 + u(T, \xi)^2}} \times \tanh \frac{\sqrt{\xi^2 + u(T, \xi)^2}}{2T} d\xi, \tag{1}$$

where $U(\cdot, \cdot) > 0$ is the potential multiplied by the density of states per unit energy at the Fermi surface and is a function of x and ξ. In (1) we introduce $\varepsilon > 0$, which is small enough and fixed $(0 < \varepsilon \ll \hbar\omega_D)$. In the original BCS model, the integration interval is $[0, \hbar\omega_D]$; it is not $[\varepsilon, \hbar\omega_D]$. However, we introduce very small $\varepsilon > 0$ for the following mathematical reasons. In order to show the continuity of the solution to the BCS gap equation with respect to the temperature and in order to show that the transition to a superconducting state is a second-order phase transition, we make the form of the BCS gap equation somewhat easier to handle. So we choose the closed interval $[\varepsilon, \hbar\omega_D]$ as the integration interval in (1).

The integral with respect to ξ in (1) is sometimes replaced by the integral over $\mathbb{R}^3$ with respect to the wave vector k. Odeh [3] and Billard and Fano [4] established the existence and uniqueness of the positive solution to the BCS gap equation in the case $T = 0$. For $T \geq 0$, Vansevenant [5] determined the transition temperature (the critical temperature) and showed that there is a unique positive solution to the BCS gap equation. Recently, Frank et al. [6] gave a rigorous analysis of the asymptotic behavior of the transition temperature at weak coupling. Hainzl et al. [7] proved that the existence of a positive solution to the BCS gap equation is equivalent to the existence of a negative eigenvalue of a certain linear operator to show the existence of a transition temperature. Moreover, Hainzl and Seiringer [8] derived upper and lower bounds on the transition temperature and the energy gap for the BCS gap equation.

Since the existence and uniqueness of the solution were established for each fixed T in the previous literature, the temperature dependence of the solution is not covered. It is well known that studying the temperature dependence of the solution to the BCS gap equation is very important in condensed matter physics. This is because, by dealing with the thermodynamical potential, this study leads to a mathematical proof of the statement that the transition to a superconducting state is a second-order phase transition. So, in condensed matter physics, it is highly desirable to study the temperature dependence of the solution to the BCS gap equation.

When the potential $U(\cdot,\cdot)$ in (1) is a positive constant, the BCS gap equation reduces to the simple gap equation (3). In this case, one assumes in the BCS model that there is a unique nonnegative solution to the simple gap equation (3) and that the solution is of class C^2 with respect to the temperature T (see e.g., [1] and [9, (11.45), page 392]). In this paper, applying the implicit function theorem, we first show that this assumption of the BCS model indeed holds true; we show that there is a unique nonnegative solution to the simple gap equation (3) and that the solution is of class C^2 with respect to the temperature T. We next deal with the case where the potential is not a constant but a function. In order to show how the solution varies with the temperature, we then give another proof of the existence and uniqueness of the solution to the BCS gap equation (1) when the potential is not a constant. More precisely, we show that the solution belongs to the subset V_T (see (12)). Note that the subset V_T depends on T. We finally show that the solution to the BCS gap equation (1) is indeed continuous with respect to both T and x when T satisfies (20) when the potential is not a constant.

Let

$$U(x,\xi)=U_1 \quad \text{at all } (x,\xi)\in[\varepsilon,\hbar\omega_D]^2, \tag{2}$$

where $U_1>0$ is a constant. Then the gap function depends on the temperature T only. So we denote the gap function by Δ_1 in this case; that is, $\Delta_1 : T\mapsto\Delta_1(T)$. Then (1) leads to the simple gap equation

$$1=U_1\int_\varepsilon^{\hbar\omega_D}\frac{1}{\sqrt{\xi^2+\Delta_1(T)^2}}\tanh\frac{\sqrt{\xi^2+\Delta_1(T)^2}}{2T}d\xi. \tag{3}$$

The following is the definition of the temperature $\tau_1>0$.

Definition 1 (see [1]). Consider

$$1=U_1\int_\varepsilon^{\hbar\omega_D}\frac{1}{\xi}\tanh\frac{\xi}{2\tau_1}d\xi. \tag{4}$$

2. The Simple Gap Equation

Set

$$\Delta=\frac{\sqrt{\left(\hbar\omega_D-\varepsilon e^{1/U_1}\right)\left(\hbar\omega_D-\varepsilon e^{-1/U_1}\right)}}{\sinh\left(1/U_1\right)}. \tag{5}$$

Proposition 2 (see [10, Proposition 2.2]). *Let Δ be as in* (5). *Then there is a unique nonnegative solution $\Delta_1 : [0,\tau_1]\to[0,\infty)$ to the simple gap equation* (3) *such that the solution Δ_1 is continuous and strictly decreasing on the closed interval $[0,\tau_1]$:*

$$\begin{aligned}\Delta_1(0)&=\Delta>\Delta_1(T_1)>\Delta_1(T_2)\\&>\Delta_1(\tau_1)=0,\quad 0<T_1<T_2<\tau_1.\end{aligned} \tag{6}$$

Moreover, the solution Δ_1 is of class C^2 on the interval $[0,\tau_1)$ and satisfies

$$\Delta_1'(0)=\Delta_1''(0)=0,\qquad \lim_{T\uparrow\tau_1}\Delta_1'(T)=-\infty. \tag{7}$$

Proof. Setting $Y=\Delta_1(T)^2$ turns (3) into

$$1=U_1\int_\varepsilon^{\hbar\omega_D}\frac{1}{\sqrt{\xi^2+Y}}\tanh\frac{\sqrt{\xi^2+Y}}{2T}d\xi. \tag{8}$$

Note that the right side is a function of the two variables T and Y. We see that there is a unique function $T\mapsto Y$ defined by (8) implicitly, that the function $T\mapsto Y$ is continuous and strictly decreasing on $[0,\tau_1]$, and that $Y=0$ at $T=\tau_1$. We moreover see that the function $T\mapsto Y$ is of class C^2 on the closed interval $[0,\tau_1]$. □

Remark 3. We set $\Delta_1(T)=0$ for $T>\tau_1$.

Remark 4. In Proposition 2, $\Delta_1(T)$ is nothing but $\sqrt{f(T)}$ in [10, Proposition 2.2].

We introduce another positive constant $U_2>0$. Let $0<U_1<U_2$. We assume the following condition on $U(\cdot,\cdot)$:

$$\begin{aligned}&U_1\le U(x,\xi)\\&\quad\le U_2\quad\text{at all } (x,\xi)\in[\varepsilon,\hbar\omega_D]^2,\ U(\cdot,\cdot)\in C\left([\varepsilon,\hbar\omega_D]^2\right).\end{aligned} \tag{9}$$

When $U(x,\xi)=U_2$ at all $(x,\xi)\in[\varepsilon,\hbar\omega_D]^2$, an argument similar to that in Proposition 2 gives that there is a unique nonnegative solution $\Delta_2 : [0,\tau_2]\to[0,\infty)$ to the simple gap equation

$$\begin{aligned}1=U_2\int_\varepsilon^{\hbar\omega_D}&\frac{1}{\sqrt{\xi^2+\Delta_2(T)^2}}\\&\times\tanh\frac{\sqrt{\xi^2+\Delta_2(T)^2}}{2T}d\xi,\quad 0\le T\le\tau_2.\end{aligned} \tag{10}$$

Here, $\tau_2>0$ is defined by

$$1=U_2\int_\varepsilon^{\hbar\omega_D}\frac{1}{\xi}\tanh\frac{\xi}{2\tau_2}d\xi. \tag{11}$$

We again set $\Delta_2(T)=0$ for $T>\tau_2$. A straightforward calculation gives the following.

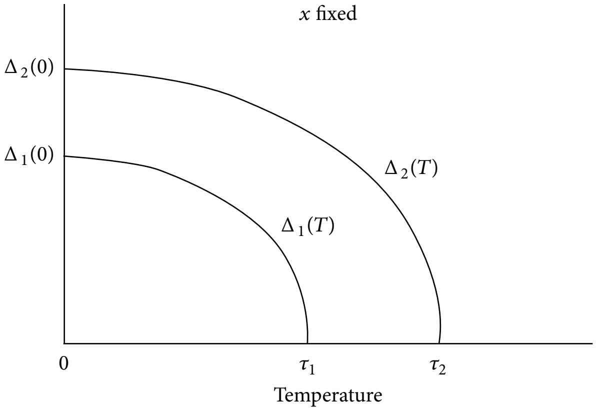

FIGURE 1: The graphs of the functions Δ_1 and Δ_2.

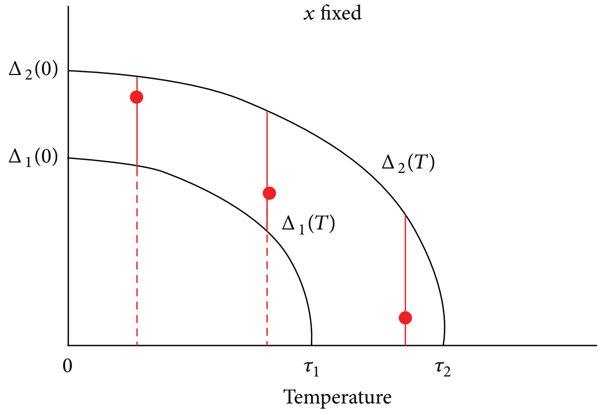

FIGURE 2: For each T, the solution $u_0(T, x)$ lies between $\Delta_1(T)$ and $\Delta_2(T)$.

Lemma 5 ([11, Lemma 1.5]). *(a) The inequality $\tau_1 < \tau_2$ holds. (b) If $0 \le T < \tau_2$, then $\Delta_1(T) < \Delta_2(T)$. If $T \ge \tau_2$, then $\Delta_1(T) = \Delta_2(T) = 0$.*

Note that Proposition 2 and Lemma 5 point out how Δ_1 and Δ_2 depend on the temperature and how Δ_1 and Δ_2 vary with the temperature; see Figure 1.

Remark 6. On the basis of Proposition 2, the present author [10, Theorem 2.3] proved that the transition to a superconducting state is a second-order phase transition under the restriction (2).

3. The BCS Gap Equation

Let $0 \le T \le \tau_2$ and fix T, where τ_2 is that in (11). We consider the Banach space $C[\varepsilon, \hbar\omega_D]$ consisting of continuous functions of x only and deal with the following subset V_T:

$$V_T = \{u(T, \cdot) \in C[\varepsilon, \hbar\omega_D] : \Delta_1(T) \le u(T, x) \le \Delta_2(T) \ \text{ at } x \in [\varepsilon, \hbar\omega_D]\}. \tag{12}$$

Remark 7. The subset V_T depends on T. So we denote each element of V_T by $u(T, \cdot)$; see Figure 1.

As it is mentioned in the introduction, the existence and uniqueness of the solution to the BCS gap equation were established for each fixed T in the previous literature, and the temperature dependence of the solution is not covered. We therefore give another proof of the existence and uniqueness of the solution to the BCS gap equation (1) so as to show how the solution varies with the temperature. More precisely, we show that the solution belongs to V_T.

Theorem 8 (see [11, Theorem 2.2]). *Assume condition (9) on $U(\cdot, \cdot)$. Let $T \in [0, \tau_2]$ be fixed. Then there is a unique nonnegative solution $u_0(T, \cdot) \in V_T$ to the BCS gap equation (1) ($x \in [\varepsilon, \hbar\omega_D]$):*

$$u_0(T, x) = \int_\varepsilon^{\hbar\omega_D} \frac{U(x, \xi)\, u_0(T, \xi)}{\sqrt{\xi^2 + u_0(T, \xi)^2}} \times \tanh \frac{\sqrt{\xi^2 + u_0(T, \xi)^2}}{2T} d\xi. \tag{13}$$

Consequently, the solution is continuous with respect to x and varies with the temperature as follows:

$$\Delta_1(T) \le u_0(T, x) \le \Delta_2(T) \quad \text{at } (T, x) \in [0, \tau_2] \times [\varepsilon, \hbar\omega_D]. \tag{14}$$

Proof. We define a nonlinear integral operator A on V_T by

$$Au(T, x) = \int_\varepsilon^{\hbar\omega_D} \frac{U(x, \xi)\, u(T, \xi)}{\sqrt{\xi^2 + u(T, \xi)^2}} \times \tanh \frac{\sqrt{\xi^2 + u(T, \xi)^2}}{2T} d\xi, \tag{15}$$

where $u(T, \cdot) \in V_T$. Clearly, V_T is a bounded, closed, and convex subset of the Banach space $C[\varepsilon, \hbar\omega_D]$. A straightforward calculation gives that the operator $A : V_T \to V_T$ is compact. Therefore, the Schauder fixed point theorem applies, and hence the operator $A : V_T \to V_T$ has at least one fixed point $u_0(T, \cdot) \in V_T$. Moreover, we can show the uniqueness of the fixed point; see Figure 2. □

The existence of the transition temperature T_c is pointed out in the previous papers [5–8]. In our case, it is defined as follows.

Definition 9. Let $u_0(T, \cdot) \in V_T$ be as in Theorem 8. The transition temperature T_c stemming from the BCS gap equation (1) is defined by

$$T_c = \inf \{T > 0 : u_0(T, x) = 0 \text{ at all } x \in [\varepsilon, \hbar\omega_D]\}. \tag{16}$$

Remark 10. Combining Definition 9 with Theorem 8 implies that $\tau_1 \le T_c \le \tau_2$. For $T > T_c$, we set $u_0(T,x) = 0$ at all $x \in [\varepsilon, \hbar\omega_D]$.

4. Continuity of the Solution with respect to the Temperature

Let $U_0 > 0$ be a constant satisfying $U_0 < U_1 < U_2$. An argument similar to that in Proposition 2 gives that there is a unique nonnegative solution $\Delta_0 : [0,\tau_0] \to [0,\infty)$ to the simple gap equation

$$1 = U_0 \int_\varepsilon^{\hbar\omega_D} \frac{1}{\sqrt{\xi^2 + \Delta_0(T)^2}} \times \tanh \frac{\sqrt{\xi^2 + \Delta_0(T)^2}}{2T} d\xi, \quad 0 \le T \le \tau_0. \tag{17}$$

Here, $\tau_0 > 0$ is defined by

$$1 = U_0 \int_\varepsilon^{\hbar\omega_D} \frac{1}{\xi} \tanh \frac{\xi}{2\tau_0} d\xi. \tag{18}$$

We set $\Delta_0(T) = 0$ for $T > \tau_0$. A straightforward calculation gives the following.

Lemma 11. *(a)* $\tau_0 < \tau_1 < \tau_2$.

(b) If $0 \le T < \tau_0$, *then* $0 < \Delta_0(T) < \Delta_1(T) < \Delta_2(T)$.

(c) If $\tau_0 \le T < \tau_1$, *then* $0 = \Delta_0(T) < \Delta_1(T) < \Delta_2(T)$.

(d) If $\tau_1 \le T < \tau_2$, *then* $0 = \Delta_0(T) = \Delta_1(T) < \Delta_2(T)$.

(e) If $\tau_2 \le T$, *then* $0 = \Delta_0(T) = \Delta_1(T) = \Delta_2(T)$.

Remark 12. Let the functions Δ_k $(k = 0, 1, 2)$ be as above. For each Δ_k, there is the inverse $\Delta_k^{-1} : [0, \Delta_k(0)] \to [0, \tau_k]$. Here,

$$\Delta_k(0) = \frac{\sqrt{\left(\hbar\omega_D - \varepsilon e^{1/U_k}\right)\left(\hbar\omega_D - \varepsilon e^{-1/U_k}\right)}}{\sinh(1/U_k)}, \tag{19}$$

and $\Delta_0(0) < \Delta_1(0) < \Delta_2(0)$.

We introduce another temperature. Let T_1 satisfy $0 < T_1 < \Delta_0^{-1}(\Delta_0(0)/2)$ and

$$\frac{\Delta_0(0)}{4\Delta_2^{-1}(\Delta_0(T_1))} \tanh \frac{\Delta_0(0)}{4\Delta_2^{-1}(\Delta_0(T_1))} > \frac{1}{2}\left(1 + \frac{4\hbar^2\omega_D^2}{\Delta_0(0)^2}\right). \tag{20}$$

Remark 13. Numerically, the temperature T_1 is very small.

Consider the following subset V of the Banach space $C([0,T_1] \times [\varepsilon, \hbar\omega_D])$ consisting of continuous functions of both the temperature T and the energy x:

$$V = \{u \in C([0,T_1] \times [\varepsilon, \hbar\omega_D]) : \Delta_1(T) \le u(T,x) \le \Delta_2(T) \ \text{ at } \ (T,x) \in [0,T_1] \times [\varepsilon, \hbar\omega_D]\}. \tag{21}$$

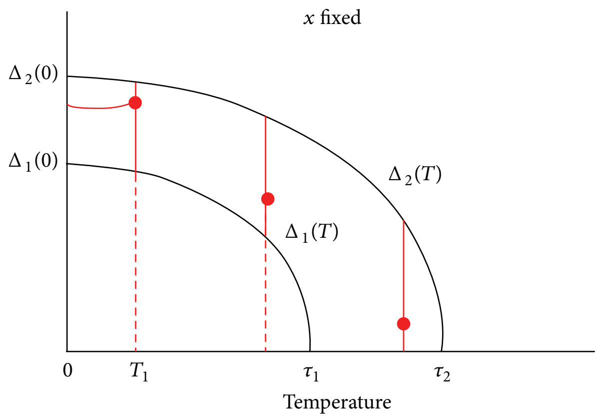

FIGURE 3: The solution u_0 is continuous on $[0,T_1] \times [\varepsilon, \hbar\omega_D]$.

Theorem 14 (see [12, Theorem 1.2]). *Assume* (9). *Let* u_0 *be as in Theorem 8 and* V *as in* (21). *Then* $u_0 \in V$. *Consequently, the gap function* u_0 *is continuous on* $[0,T_1] \times [\varepsilon, \hbar\omega_D]$.

Proof. We define a nonlinear integral operator B on V by

$$Bu(T,x) = \int_\varepsilon^{\hbar\omega_D} \frac{U(x,\xi)\, u(T,\xi)}{\sqrt{\xi^2 + u(T,\xi)^2}} \times \tanh \frac{\sqrt{\xi^2 + u(T,\xi)^2}}{2T} d\xi, \tag{22}$$

where $u \in V$.

Clearly, V is a closed subset of the Banach space $C([0,T_1] \times [\varepsilon, \hbar\omega_D])$. A straightforward calculation gives that the operator $B : V \to V$ is contractive as long as (20) holds true. Therefore, the Banach fixed-point theorem applies, and hence the operator $B : V \to V$ has a unique fixed point $u_0 \in V$. The solution $u_0 \in V$ to the BCS gap equation is thus continuous both with respect to the temperature and with respect to the energy x; see Figure 3. □

Acknowledgment

Shuji Watanabe is supported in part by the JSPS Grant-in-Aid for Scientific Research (C) 24540112.

References

[1] J. Bardeen, L. N. Cooper, and J. R. Schrieffer, "Theory of superconductivity," *Physical Review*, vol. 108, pp. 1175–1204, 1957.

[2] N. N. Bogoliubov, "A new method in the theory of superconductivity. I," *Soviet Physics*, vol. 34, pp. 41–46, 1958.

[3] F. Odeh, "An existence theorem for the BCS integral equation," *Journal of Research and Development*, vol. 8, pp. 187–188, 1964.

[4] P. Billard and G. Fano, "An existence proof for the gap equation in the superconductivity theory," *Communications in Mathematical Physics*, vol. 10, pp. 274–279, 1968.

[5] A. Vansevenant, "The gap equation in superconductivity theory," *Physica D*, vol. 17, no. 3, pp. 339–344, 1985.

[6] R. L. Frank, C. Hainzl, S. Naboko, and R. Seiringer, "The critical temperature for the BCS equation at weak coupling," *The Journal of Geometric Analysis*, vol. 17, no. 4, pp. 559–567, 2007.

[7] C. Hainzl, E. Hamza, R. Seiringer, and J. P. Solovej, "The BCS functional for general pair interactions," *Communications in Mathematical Physics*, vol. 281, no. 2, pp. 349–367, 2008.

[8] C. Hainzl and R. Seiringer, "Critical temperature and energy gap for the BCS equation," *Physical Review B*, vol. 77, Article ID 184517, 2008.

[9] J. M. Ziman, *Principles of the Theory of Solids*, Cambridge University Press, London, UK, 1972.

[10] S. Watanabe, "A mathematical proof that the transition to a superconducting state is a second-order phase transition," *Far East Journal of Mathematical Sciences*, vol. 34, no. 1, pp. 37–57, 2009.

[11] S. Watanabe, "The solution to the BCS gap equation and the second-order phase transition in superconductivity," *Journal of Mathematical Analysis and Applications*, vol. 383, no. 2, pp. 353–364, 2011.

[12] S. Watanabe, "Addendum to 'The solution to the BCS gap equation and the second-order phase transition in superconductivity'," *Journal of Mathematical Analysis and Applications*, vol. 405, no. 2, pp. 742–745, 2013.

Hindawi Publishing Corporation
Abstract and Applied Analysis
Volume 2013, Article ID 490689, 4 pages
http://dx.doi.org/10.1155/2013/490689

Research Article

Numerical Solution for IVP in Volterra Type Linear Integrodifferential Equations System

F. Ghomanjani,[1] A. Kılıçman,[2] and S. Effati[1]

[1] *Department of Mathematics, Ferdowsi University of Mashhad, Mashhad, Iran*
[2] *Department of Mathematics, Universiti Putra Malaysia, 43400 Serdang, Selangor, Malaysia*

Correspondence should be addressed to A. Kılıçman; kilicman@yahoo.com

Received 23 May 2013; Accepted 9 July 2013

Academic Editor: Santanu Saha Ray

A method is proposed to determine the numerical solution of system of linear Volterra integrodifferential equations (IDEs) by using Bezier curves. The Bezier curves are chosen as piecewise polynomials of degree n, and Bezier curves are determined on $[t_0, t_f]$ by $n+1$ control points. The efficiency and applicability of the presented method are illustrated by some numerical examples.

1. Introduction

Integrodifferential equations (IDEs) have been found to describe various kinds of phenomena, such as glass forming process, dropwise condensation, nanohydrodynamics, and wind ripple in the desert (see [1, 2]).

There are several numerical and analytical methods for solving IDEs. Some different methods are presented to solve integral and IDEs in [3, 4]. Maleknejad et al. [5] used rationalized Haar functions method to solve the linear IDEs system. Linear IDEs system has been solved by using Galerkin methods with the hybrid Legendre and block-Pulse functions on interval $[0, 1)$ (see [6]). Yusufoğlu [7] presented an application of He's homotopy perturbation (HPM) method to solve the IDEs system. He's variational iteration method has been used for solving two systems of Volterra integrodifferential equations (see [8]). Arikoglu and Ozkol [9] presented differential transform method (DTM) for integrodifferential and integral equation systems. He's homotopy perturbation (HPM) method was proposed for system of integrodifferential equations (see [10]). A numerical method based on interpolation of unknown functions at distinct interpolation points has been introduced for solving linear IDEs system with initial values (see [11]). Recently, Biazar introduced a new modification of homotopy perturbation method (NHPM) to obtain the solution of linear IDEs system (see [12]). Taylor expansion method has been used for solving IDEs (see [13, 14]). Rashidinia and Tahmasebi developed and modified Taylor series method (TSM) introduced in [15] to solve the system of linear Volterra IDEs.

In the present work, we suggest a technique similar to the one which was used in [16] for solving the system of linear Volterra IDEs in the following form:

$$\sum_{i=1}^{n}\sum_{j=0}^{\alpha_{mi}} p_{mij}(t)\, y_i^{(j)}(t) + \sum_{i=1}^{n}\int_{t_0}^{t}\left(k_{mi}(t,x)\sum_{j=0}^{\alpha_{mi}} y_i^{(j)}(x)\right)dx = f_m(t), \quad m = 1, 2, \dots, n,\ t_0 \le t \le t_f, \tag{1}$$

with the initial conditions

$$y_i^{(0)}(t_0) = c_{i0}, \qquad y_i^{(1)}(t_0) = c_{i1}, \dots, y_i^{(\alpha_{mi}-1)}(t_0) = c_{i(\alpha_{mi}-1)}, \tag{2}$$

where $y_i^{(j)}(t)$ stands for jth-order derivative of $y_i(t)$. $f_m(t)$, $k_{mi}(t,x)$, and $p_{mij}(t)$ are known functions ($m, i = 1, 2, \dots, n$; $j = 0, 1, \dots, \alpha_{mi}$), and t_0, t_f, and c_{ij} ($i = 1, 2, \dots, n$; $j = 0, 1, \dots, \alpha_{mi} - 1$) are appropriate constants.

The current paper is organized as follows. In Section 2, function approximation will be introduced. Numerical examples will be stated in Section 3. Finally, Section 4 will give a conclusion briefly.

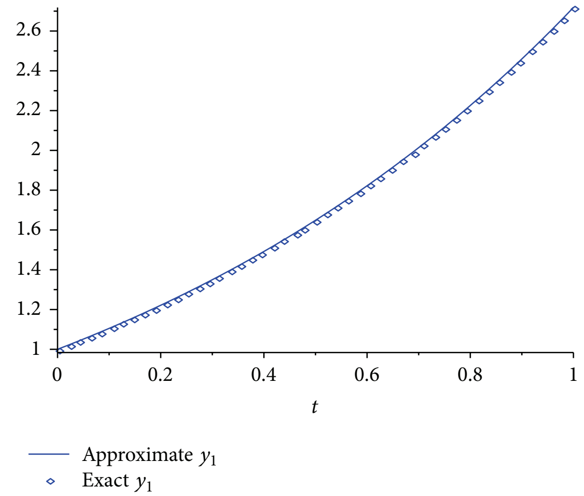

FIGURE 1: The graph of approximated $y_1(t)$ for Example 1.

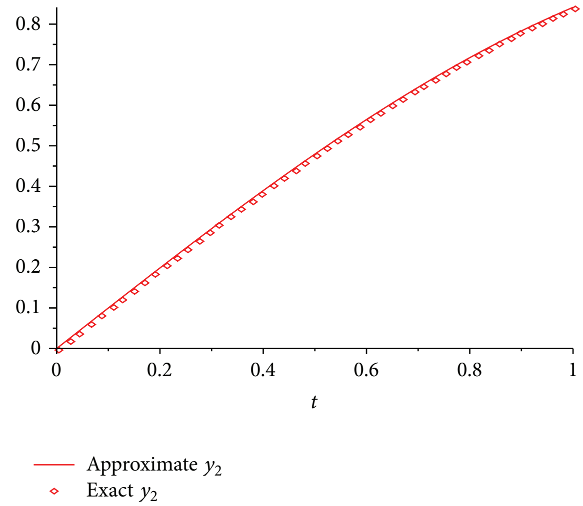

FIGURE 2: The graph of approximated $y_2(t)$ for Example 1.

2. Function Approximation

Our strategy is to use Bezier curves to approximate the solutions $y_i(t)$, for $1 \leq i \leq n$, which are given below. Define the Bezier polynomials of degree N that approximate, respectively, the actions of $y_i(t)$ over the interval $[t_0, t_f]$ as follows:

$$y_i(t) = \sum_{r=0}^{N} a_r^i B_{r,N}\left(\frac{t-t_0}{h}\right), \tag{3}$$

where $h = t_f - t_0$ and a_r is the control point of Bezier curve, and

$$B_{r,N}\left(\frac{t-t_0}{h}\right) = \binom{N}{r}\frac{1}{h^N}\left(t_f - t\right)^{N-r}\left(t-t_0\right)^r \tag{4}$$

is the Bernstein polynomial of degree N over the interval $[t_0, t_f]$ (see [17]). By substituting (3) in (2), $R_m(t)$ can be defined for $t \in [t_0, t_f]$ as

$$\begin{aligned} R_m(t) = &\sum_{i=1}^{n}\sum_{j=0}^{\alpha_{mi}} p_{mij}(t)\, y_i^{(j)}(t) \\ &+ \sum_{i=1}^{n}\int_0^t \left(k_{mi}(t,x)\sum_{j=0}^{\alpha_{mi}} y_i^{(j)}(x)\right)dx - f_m(t), \\ & \qquad m = 1, 2, \ldots, n, \end{aligned} \tag{5}$$

where (2) is satisfied. The convergence was proved in the approximation with Bezier curves when the degree of the approximate solution, N, tends to infinity (see [18]).

Now, the residual function is defined over the interval $[t_0, t_f]$ as follows:

$$R(t) = \int_{t_0}^{t_f}\sum_{m=1}^{n}\left\|R_m(t)\right\|^2 dt, \tag{6}$$

where $\|\cdot\|$ is the Euclidean norm. Our aim is to solve the following problem over the interval $[t_0, t_f]$:

$$\begin{aligned} &\min \quad R(t) \\ &\text{s.t.} \quad y_i^{(0)}(t_0) = c_{i0}, \\ &\qquad y_i^{(1)}(t_0) = c_{i1}, \ldots, y_i^{(\alpha_{mi}-1)}(t_0) = c_{i(\alpha_{m_i}-1)}. \end{aligned} \tag{7}$$

The mathematical programming problem (7) can be solved by many subroutine algorithms, and we used Maple 12 to solve this optimization problem.

Remark 1. In Chapter 1 of [19], it was proved that N satisfies

$$N > \frac{S}{\delta^2\epsilon}, \tag{8}$$

where $S = \|y_i(t)\|$, and because of this reason that $y_i(t)$ is uniformly continuous on $[t_0, t_f]$, we have $s,\ t \in [t_0, t_f]$ that $|t-s| < \delta$ and $-(\epsilon/2) < y_i(t) - y_i(s) < \epsilon/2$, for more details see [19].

3. Applications and Numerical Results

Consider the following examples which can be solved by using the presented method.

Example 1. Consider a system of third-order linear Volterra IDEs on the interval $[0, 1]$ (see [4]):

$$\begin{aligned} &y_1''(t) + t^2 y_1(t) - y_2''(t) \\ &\quad + \int_0^t \left((t-x)\, y_1(x) + y_2(x)\right)dx = g_1(t), \\ &4t^3 y_1'(t) + 6t^2 y_1(t) + y_2'''(t) \\ &\quad + \int_0^t \left(y_1(x) + (t+x)\, y_2(x)\right)dx = g_2(t), \end{aligned} \tag{9}$$

Table 1: Computed errors for Example 1.

t	Absolute error for $y_1(t)$	Absolute error for $y_2(t)$
0.0	0.000000	0.0000000000
0.2	1.4801×10^{-10}	2.2475×10^{-11}
0.4	$0.162735585 \times 10^{-5}$	$3.12780502 \times 10^{-7}$
0.6	$0.251133963 \times 10^{-5}$	$0.1536077787 \times 10^{-5}$
0.8	1.8337×10^{-10}	$0.8864238659 \times 10^{-5}$
1.0	4.5905×10^{-10}	7.897×10^{-12}

Table 2: Computed errors for Example 2.

t	Absolute error for $y_1(t)$	Absolute error for $y_2(t)$
0.0	0.000000	0.0000000000
0.2	3.840×10^{-11}	1.5360×10^{-11}
0.4	$0.5791064832 \times 10^{-3}$	$0.156041748480 \times 10^{-3}$
0.6	$0.17373195072 \times 10^{-2}$	$0.156041748480 \times 10^{-3}$
0.8	$0.69492781056 \times 10^{-2}$	1.5360×10^{-11}
1.0	0.000	0.000

with the initial conditions $y_1(0) = y_1'(0) = 1$, $y_2(0) = y_2''(0) = 0$, and $y_2'(0) = 1$, where

$$g_1(t) = \left(2 + t^2\right) e^t - t - \cos(t) + \sin(t),$$

$$g_2(t) = 7\sin(t) - (1 + 2t)\cos(t) + e^t\left(1 + 4t^2 + 4t^3\right) + t - 1. \tag{10}$$

The exact solution of this system is $y_1(t) = e^t$, $y_2(t) = \sin(t)$.

With $N = 5$, the approximated solutions for $y_1(t)$ and $y_2(t)$ are shown, respectively, in Figures 1 and 2, and the computed errors are shown in Table 1 which show the high accuracy of the proposed method.

Example 2. Consider the following system of linear Volterra IDEs equations as follows (see [4]):

$$\begin{aligned} &-y_1' - \frac{1}{2}ty_1 + \frac{3}{2}y_2 \\ &\quad = \frac{5}{2} - t - \frac{27}{2}t^2 + t^4 + \frac{3}{2}\left(-1 + 2t^2\right) - \frac{1}{2}\left(-3t + 4t^3\right) \\ &\qquad + \int_{-1}^{t} \left(y_1 - 3ty_2\right) dx, \\ &t^2 y_1 + y_2' - ty_2 \\ &\quad = \frac{2}{5} + 3t + 3t^3 - \frac{8}{5}t^5 + t^2\left(-3t + 4t^3\right) \\ &\qquad + \int_{-1}^{t} \left((2t + x)\, y_1 + 3x^2 y_2\right) dx, \end{aligned} \tag{11}$$

under the conditions $y_1(0) = 0$ and $y_2(0) = -1$, with the exact solution $y_1(t) = 4t^3 - 3t$, $y_2(t) = 2t^2 - 1$.

With $N = 5$, the computed errors are shown in Table 2 which show the high accuracy of the proposed method.

4. Conclusions

In this paper, Bernstein's approximation is used to approximate the solution of linear Volterra IDEs. In this method, we approximate our unknown function with Bernstein's approximation. The present results show that Bernstein's approximation method for solving linear Volterra IDEs is very effective and simple, and the answers are trusty, and their accuracy is high, and we can execute this method in a computer simply. The numerical examples support this claim.

Acknowledgment

The authors are very grateful to the referees for their valuable suggestions and comments that improved the paper.

References

[1] T. L. Bo, L. Xie, and X. J. Zheng, "Numerical approach to wind ripple in desert," *International Journal of Nonlinear Sciences and Numerical Simulation*, vol. 8, no. 2, pp. 223–228, 2007.

[2] L. Xu, J. H. He, and Y. Liu, "Electro spun nano-porous spheres with Chinese drug," *International Journal of Nonlinear Sciences and Numerical Simulation*, vol. 8, no. 2, pp. 199–202, 2007.

[3] R. Agarwal and D. O'Regan, *Integral and integro-differential equations theory, methods and applications*, vol. 2, The Gordon and breach science publishers, Singapore, 2000.

[4] J. Rashidinia and A. Tahmasebi, "Taylor series method for the system of linear Volterra integro-differential equations," *The Journal of Mathematics and Computer Science*, vol. 4, no. 3, pp. 331–343, 2012.

[5] K. Maleknejad, F. Mirzaee, and S. Abbasbandy, "Solving linear integro-differential equations system by using rationalized Haar functions method," *Applied Mathematics and Computation*, vol. 155, no. 2, pp. 317–328, 2004.

[6] K. Maleknejad and M. Tavassoli Kajani, "Solving linear integro-differential equation system by Galerkin methods with hydrid functions," *Applied Mathematics and Computation*, vol. 159, no. 3, pp. 603–612, 2004.

[7] E. Yusufoğlu, "An efficient algorithm for solving integro-differential equations system," *Applied Mathematics and Computation*, vol. 192, no. 1, pp. 51–55, 2007.

[8] J. Saberi-Nadjafi and M. Tamamgar, "The variational iteration method: a highly promising method for solving the system of integro-differential equations," *Computers & Mathematics with Applications*, vol. 56, no. 2, pp. 346–351, 2008.

[9] A. Arikoglu and I. Ozkol, "Solutions of integral and integro-differential equation systems by using differential transform method," *Computers & Mathematics with Applications*, vol. 56, no. 9, pp. 2411–2417, 2008.

[10] J. Biazar, H. Ghazvini, and M. Eslami, "He's homotopy perturbation method for systems of integro-differential equations," *Chaos, Solitons & Fractals*, vol. 39, no. 3, pp. 1253–1258, 2009.

[11] E. Yusufoğlu, "Numerical solving initial value problem for Fredholm type linear integro-differential equation system," *Journal of the Franklin Institute*, vol. 346, no. 6, pp. 636–649, 2009.

[12] J. Biazar and M. Eslami, “Modified HPM for solving systems of Volterra integral equations of the second kind,” *Journal of King Saud University*, vol. 23, no. 1, pp. 35–39, 2011.

[13] Y. Huang and X.-F. Li, “Approximate solution of a class of linear integro-differential equations by Taylor expansion method,” *International Journal of Computer Mathematics*, vol. 87, no. 6, pp. 1277–1288, 2010.

[14] A. Karamete and M. Sezer, “A Taylor collocation method for the solution of linear integro-differential equations,” *International Journal of Computer Mathematics*, vol. 79, no. 9, pp. 987–1000, 2002.

[15] A. Tahmasbi and O. S. Fard, “Numerical solution of linear Volterra integral equations system of the second kind,” *Applied Mathematics and Computation*, vol. 201, no. 1-2, pp. 547–552, 2008.

[16] F. Ghomanjani and M. H. Farahi, “The Bezier control points method for solving delay differential equation,” *Intelligent Control and Automation*, vol. 3, no. 2, pp. 188–196, 2012.

[17] J. Zheng, T. W. Sederberg, and R. W. Johnson, “Least squares methods for solving differential equations using Bézier control points,” *Applied Numerical Mathematics*, vol. 48, no. 2, pp. 237–252, 2004.

[18] F. Ghomanjani, M. H. Farahi, and M. Gachpazan, “Bézier control points method to solve constrained quadratic optimal control of time varying linear systems,” *Computational & Applied Mathematics*, vol. 31, no. 3, pp. 433–456, 2012.

[19] M. I. Berenguer, A. I. Garralda-Guillem, and M. Ruiz Galn, “An approximation method for solving systems of Volterra integro-differential equations,” *Applied Numerical Mathematics*, vol. 67, pp. 126–135, 2013.

Hindawi Publishing Corporation
Abstract and Applied Analysis
Volume 2013, Article ID 670847, 8 pages
http://dx.doi.org/10.1155/2013/670847

Research Article

Analytical and Multishaped Solitary Wave Solutions for Extended Reduced Ostrovsky Equation

Ben-gong Zhang

School of Mathematical and Computer Science, Wuhan Textile University, Wuhan 430200, China

Correspondence should be addressed to Ben-gong Zhang; benyan1219@126.com

Received 5 June 2013; Accepted 25 July 2013

Academic Editor: Santanu Saha Ray

We present the analytical and multishaped solitary wave solutions for extended reduced Ostrovsky equation (EX-ROE). The exact solitary (traveling) wave solutions are expressed by three types of functions which are hyperbolic function solution, trigonometric function solution, and rational solution. These results generalized the previous results. Multishape solitary wave solutions such as loop-shaped, cusp-shaped, and hump-shaped can be obtained as well when the special values of the parameters are taken. The (G'/G)-expansion method presents a wide applicability for handling nonlinear partial differential equations.

1. Introduction

The well-known Ostrovsky equation [1]

$$\left(u_t + c_0 u_x + \alpha u u_x + \beta u_{xxx}\right)_x = \gamma u, \tag{1}$$

where c_0 is the velocity of dispersiveness linear waves, α is the nonlinear coefficient, and β and γ are dispersion coefficients, is a model for weakly nonlinear surface and internal waves in a rotating ocean.

For long waves, for which high-frequency dispersion is negligible, $\beta = 0$, and (1) becomes the so-called reduced Ostrovsky equation (ROE) [2]

$$\left(u_t + c_0 u_x + \alpha u u_x\right)_x = \gamma u. \tag{2}$$

Parkes [3] has studied (2) and found its periodic and solitary traveling wave solutions.

In fact, by applying the following transformation [4]:

$$u \longrightarrow \frac{u}{\alpha}, \qquad t \longrightarrow \frac{t}{\sqrt{|\gamma|}}, \qquad x \longrightarrow \frac{(x + c_0 t)}{\sqrt{|\gamma|}} \tag{3}$$

to (2), we obtain the ROE in the neat form

$$\begin{gathered}\frac{\partial}{\partial x}\mathfrak{D}u + \delta u = 0, \\ \text{where } \mathfrak{D} := \frac{\partial}{\partial t} + u\frac{\partial}{\partial x}, \qquad \delta = \frac{\gamma}{|\gamma|} = \pm 1.\end{gathered} \tag{4}$$

Just as it mentioned in [5] and the reference therein, when $\delta = -1$, (4) is referred to the Ostrovsky-Hunter equation (OHE). When $\delta = 1$, (4) is referred to the Vakhnenko equation (VE), which is in order to model the propagation of waves in a relaxing medium [6, 7]. Parkes [3] pointed out that (4) is invariant under the transformation

$$u \longrightarrow -u, \qquad t \longrightarrow -t, \qquad \delta \longrightarrow -\delta, \tag{5}$$

so that the solutions of the OHE and VE are related in a simple way.

The purpose of this paper is to study the extended reduced Ostrovsky equation (EX-ROE):

$$\frac{\partial}{\partial x}\left(\mathfrak{D}^2 u + \frac{1}{2}pu^2 + \beta u\right) + q\mathfrak{D}u = 0, \tag{6}$$

where $\mathfrak{D}$ is defined previous, p, q, and β are arbitrary nonzero constants. It is originally derived by Morrison and Parkes [8] which dubbed it as modified generalized Vakhnenko equation (mGVE) when $p = 2q$. They found that not only does it have loop soliton solutions, hump-like and cusp-like soliton solutions, but it also has N-soliton solutions.

In order to investigate mGVE's N-soliton solution, Morrison and Parkes [8] considered a Hirota-Satsuma-type shallow water wave equation [9] of the form

$$U_{XXT} + pUU_T - qU_X \int_X^{\infty} U_T\left(X', T\right) \mathrm{d}X' + \beta U_T + qU_X = 0, \tag{7}$$

where $p \neq 0$, $q \neq 0$, and β is arbitrary constant. By using the transformation

$$\begin{gathered} x = T + \int_{-\infty}^{X} U_T\left(X', T\right) \mathrm{d}X' + x_0, \\ t = X, \quad u(x,t) = U(X,T), \end{gathered} \tag{8}$$

where x_0 is a constant, (7) yields (6). So (6) and (7) are equivalent to each other under the transformation (8). Specifically, in (7), when $p = 2q$ and $\beta = -1$, it was discussed by Ablowitz et al. [10] and was shown to be integrable by inverse scatting method. When $p = q$ and $\beta = -1$, it was discussed by Hirota and Satsuma [11] and was shown to be integrable using Hirota's bilinear technique. In [12], the authors referred to (6) with $p = q = 1$ and β an arbitrary nonzero constant as the generalized Vakhnenko equation (GVE). In fact, when $p = q$ and $\beta = 0$, (6) can be written as

$$\left(\frac{\partial u}{\partial x} + \mathfrak{D}\right)\left(\frac{\partial}{\partial x}\mathfrak{D}u + pu\right) = 0. \tag{9}$$

Clearly, solutions of the ROE are also solutions of (9) with $p = \pm 1$. So for arbitrary p, q, and β, if we obtain the solutions of EX-ROE, then we can also obtain the solutions of VE, GVE, mGVE, ROE, and OHE by taking the special values of p, q, and β.

The EX-ROE has been studied by several researchers. For example, Liu et al. [13] used Jacobi elliptic function method to obtain exact double periodic wave solutions and solitary wave solutions. Parkes [4] constructed periodic and solitary wave solutions of EX-ROE and gave the categorization of the solutions. Xie and Cai [14] used the bifurcation method of dynamic systems and simulation method of differential equations to get exact compacton and generalized kink wave solutions of EX-ROE. Stepanyants [15] applied the qualitative theory of differential equations to give a full classification of its solutions.

Recently, there are many methods being proposed to study the traveling wave solutions of nonlinear partial differential equations which are derived from physics, for example, [16–27]. As well as these methods, there are still many other methods; we cannot list all of them. Here we will use modified (G'/G)-expansion method to investigate EX-ROE. As a result, three types of traveling wave solutions are were obtained. When the special values of the parameters are taken, they are reduced to some previous results which obtained by an other method.

The rest of the paper is organized as follows. In Section 2, we present a methodology of the modified (G'/G)-expansion method. In Section 3, we apply the method to the extended reduced Ostrovsky equation. In Section 4, some conclusions are given.

2. Description of the Modified (G'/G)-Expansion Method

The (G'/G)-expansion method is first proposed by Wang et al. [28]. The useful (G'/G)-expansion method is then widely used by many authors [29–32]. Then it is modified in [33–35]. The main steps are as follows.

Suppose that a nonlinear equation is given by

$$P_1\left(u, u_t, u_x, u_{tt}, u_{xt}, u_{xx}, \ldots\right) = 0, \tag{10}$$

where $u = u(x,t)$ is an unknown function and P is a polynomial in $u = u(x,t)$ and its partial derivatives, in which the highest-order derivatives and nonlinear terms are involved. In the following we give the main steps of the (G'/G)-expansion method.

Step 1. The traveling wave variable $u(x,t) = u(\xi)$, $\xi = x - ct$, where c is a constant, permits us to reduce (10) to an ODE for $u = u(\xi)$ in the form

$$P_2\left(u, -cu', u', c^2u'', -cu'', u'', \ldots\right) = 0. \tag{11}$$

Step 2. Suppose that the solution of (10) can be expressed by a polynomial in (G'/G) as follows:

$$\begin{aligned} u(\xi) = {} & \alpha_{-m}\left(\frac{G'}{G}\right)^{-m} + \alpha_{-(m-1)}\left(\frac{G'}{G}\right)^{-(m-1)} + \cdots \\ & + \alpha_{m-1}\left(\frac{G'}{G}\right)^{m-1} + \alpha_m\left(\frac{G'}{G}\right)^{m}, \end{aligned} \tag{12}$$

where $G = G(\xi)$ satisfies the second-order linear ordinary differential equation (LODE) in the form

$$G'' + \lambda G' + \mu G = 0, \tag{13}$$

where $\alpha_{-m}, \ldots, \alpha_m$, λ, and μ are constants to be determined later. The unwritten part in (12) is also a polynomial in (G'/G), but the degree of which is generally equal to or less than $m-1$. The positive integer m can be determined by considering the homogeneous balance between the highest-order derivatives and nonlinear terms appearing in (11).

Step 3. Substituting (12) into (11) and using (13), collecting all terms with the same order of (G'/G) together, and then equating each coefficient of the resulting polynomial to zero yields a set of algebraic equations for $\alpha_m, \alpha_{m-1}, \ldots, \alpha_{-m}$, c, λ, and μ.

Step 4. Since the general solutions of (13) have been well known for us, then substituting $\alpha_m, \alpha_{m-1}, \ldots, \alpha_{-m}$ and c and the general solutions of (13) into (12) we have more traveling wave solutions of the nonlinear differential equation (10).

The main idea of (G'/G)-expansion method is to use an integrable ODE to expand a solution to a nonlinear partial differential equation (PDE) as a polynomial or rational function of the solution of the ODE. However, such an idea was also presented in [36–38]. The method used in this paper can be also thought of as the application of transformed rational function method used in [37] in some sense. Maybe the similar results can be obtained by using these very closely related methods. We plan to further study the EX-ROE in near future by using the methods proposed in [36–38]. We hope we can find much more interesting properties and new phenomenon of this equation.

3. Exact Traveling Wave Solutions of the Extended Reduced Ostrovsky Equation

In this section, we will use the (G'/G)-expansion method to the extended reduced Ostrovsky equation to get exact traveling wave solutions.

First, in order to get traveling wave solutions, we need some transformation. Recall that in Section 1 we have stated that EX-ROE is equivalent to a Hirota-Satsuma-type shallow water wave equation (7) under the transformation of (8). So here we introduce a new variable W defined by

$$U = W_X. \tag{14}$$

Substituting (14) into (7) yields

$$W_{XXXT} + pW_XW_{XT} + qW_{XX}W_T + \beta W_{XT} + qW_{XX} = 0. \tag{15}$$

Now giving the traveling wave transformation $W(X,T) = W(\xi)$, $\xi = X - cT$, where c is wave speed. Substituting them into (15) and integrating once, we have

$$c_1 + cW_{3\xi} + \frac{1}{2}c\left(p+q\right)W_\xi^2 + \left(c\beta - q\right)W_\xi = 0, \tag{16}$$

where c_1 is integral constant that is to be determined later.

Considering the homogeneous balance between $W_{3\xi}$ and W_ξ^2, we have

$$m + 3 = 2m + 2 \Longrightarrow m = 1. \tag{17}$$

We suppose that

$$W\left(\xi\right) = \alpha_{-1}\left(\frac{G'}{G}\right)^{-1} + \alpha_0 + \alpha_1\left(\frac{G'}{G}\right), \tag{18}$$

where the $G = G(\xi)$ satisfies the second-order LODE,

$$G'' + \lambda G' + \mu G = 0, \tag{19}$$

and α_{-1}, α_0, α_1, λ, and μ are constants to be determined later.

By using (18) and (19), it is derived that

$$\begin{aligned} W_\xi = {} & \mu\alpha_{-1}\left(\frac{G'}{G}\right)^{-2} + \lambda\alpha_{-1}\left(\frac{G'}{G}\right)^{-1} + \alpha_{-1} \\ & - \alpha_1\mu - \lambda\alpha_1\left(\frac{G'}{G}\right) - \alpha_1\left(\frac{G'}{G}\right)^2, \end{aligned} \tag{20}$$

$$\begin{aligned} W_\xi^2 = {} & \mu^2\alpha_{-1}^2\left(\frac{G'}{G}\right)^{-4} + 2\lambda\alpha_{-1}^2\mu\left(\frac{G'}{G}\right)^{-3} \\ & + \left(2\alpha_{-1}^2\mu + \lambda^2\alpha_{-1}^2 - 2\mu\alpha_{-1}\alpha\_1\right)\left(\frac{G'}{G}\right)^{-2} \\ & + \left(2\lambda\alpha_{-1}^2 - 4\mu\lambda\alpha_{-1}\alpha_1\right)\left(\frac{G'}{G}\right)^{-1} + \alpha_{-1}^2 - 4\mu\alpha_{-1}\alpha_1 \\ & - 2\lambda^2\alpha_{-1}\alpha_1 + \alpha_1^2\mu^2 + 2\lambda\alpha_1^2\mu\left(\frac{G'}{G}\right) \\ & + \left(2\alpha_1^2\mu + \lambda^2\alpha_1^2\right)\left(\frac{G'}{G}\right)^2 + 2\lambda\alpha_1^2\left(\frac{G'}{G}\right)^3 + \alpha_1^2\left(\frac{G'}{G}\right)^4, \end{aligned} \tag{21}$$

$$\begin{aligned} W_{3\xi} = {} & 6\alpha_{-1}\mu^3\left(\frac{G'}{G}\right)^{-4} + 12\alpha_{-1}\lambda\mu^2\left(\frac{G'}{G}\right)^{-3} \\ & - \left(8\mu^2\alpha_{-1} + 7\alpha_{-1}\lambda^2\mu\right)\left(\frac{G'}{G}\right)^{-2} \\ & - \left(8\alpha_{-1}\lambda\mu + \alpha_{-1}\lambda^3\right)\left(\frac{G'}{G}\right)^{-1} \\ & - \left(2\alpha_{-1}\mu + \lambda^2\alpha_{-1}\right) - \left(2\alpha_1\mu^2 + \lambda^2\alpha_1\mu\right) \\ & - \left(8\alpha_1\lambda\mu + \alpha_1\lambda^3\right)\left(\frac{G'}{G}\right) - \left(8\mu\alpha_1 + 7\alpha_1\lambda^2\right)\left(\frac{G'}{G}\right)^2 \\ & - 12\alpha_1\lambda\left(\frac{G'}{G}\right)^3 - 6\alpha_1\left(\frac{G'}{G}\right)^4. \end{aligned} \tag{22}$$

By substituting (20)–(22) into (16) and collecting all terms with the same power of (G'/G) together, the left-hand sides of (16) are converted into the polynomials in (G'/G). Equating the coefficients of the polynomials to zero yields a set of simultaneous algebraic equations for α_{-1}, α_0, α_1, λ, c, c_1, and μ as follows (denote A for (G'/G)):

$$A^{-4}: 6c\alpha_{-1}\mu^3 + \frac{c\left(p+q\right)\mu^2\alpha_{-1}^2}{2} = 0,$$

$$A^{-3}: 12c\lambda\mu^2\alpha_{-1} + c\left(p+q\right)\lambda\mu\alpha_{-1}^2 = 0,$$

$$
\begin{aligned}
A^{-2}&: (q - c\beta)\,\mu\alpha_{-1}\\
&\quad - \frac{c(p+q)\left(\lambda^2\alpha_{-1}^2 + 2\mu\lambda_{-1}^2 - 2\mu^2\alpha_1\alpha_{-1}\right)}{2}\\
&\quad - c\left(7\lambda^2\mu\alpha_{-1} + 8\mu^2\alpha_{-1}\right) = 0,\\
A^{-1}&: (c\beta - q)\,\lambda\alpha_{-1}\lambda + c(p+q)\left(\lambda\alpha_{-1}^2 - 2\lambda\mu\alpha\alpha_{-1}\right)\\
&\quad + c\left(\lambda^3\alpha_{-1} + 8\lambda\mu\alpha_{-1}\right) = 0,\\
A^{0}&: c_1 + c\left(\lambda^2\alpha_{-1} + 2\mu\alpha_{-1}\right)\\
&\quad - \frac{c\left(2\alpha_1\mu^2 + \lambda^2\alpha_1\mu\right) + c(p+q)\alpha_{-1}^2}{2}\\
&\quad - 2c\mu\alpha\alpha_{-1}(p+q) + \frac{c\alpha_1^2\mu^2(p+q)}{2} - (c\beta - q)\,\mu\alpha_1\\
&\quad - c\lambda^2\alpha_1\alpha_{-1}(p+q) + \alpha_{-1}(c\beta - q) = 0,\\
A^{1}&: (q - c\beta)\,\alpha_1\lambda + c(p+q)\left(\lambda\mu\alpha_1^2 - 2\lambda\alpha_1\alpha_{-1}\right)\\
&\quad - c\left(\lambda^3\alpha_1 + 8\lambda\mu\alpha_1\right) = 0,\\
A^{2}&: (q - c\beta)\,\alpha_1 + c(p+q)\\
&\quad \times\left(\lambda^2\alpha_1^2 + 2a\alpha_1^2\mu - 2\alpha_1\alpha_{-1} - c\left(7\lambda^2\alpha_1 + 8\mu\alpha_1\right)\right)\\
&= 0,\\
A^{3}&: -12c\lambda\alpha_1 + c(p+q)\,\lambda\alpha_1^2 = 0,\\
A^{4}&: -6c\alpha_1 + \frac{c(p+q)\,\alpha_1^2}{2} = 0.
\end{aligned}
\tag{23}
$$

Solving the algebraic equations above yields

$$
\alpha_1 = \frac{12}{(p+q)}, \quad c = \frac{q}{(\beta + \lambda^2 - 4\mu)}, \quad c_1 = 0, \quad \alpha_{-1} = 0, \tag{24}
$$

or

$$
\alpha_{-1} = -\frac{12\mu}{(p+q)}, \quad c = \frac{q}{(\beta + \lambda^2 - 4\mu)}, \quad c_1 = 0, \quad \alpha_1 = 0. \tag{25}
$$

Substituting system (24) and (25) into (18), we have the formula of the solutions of (15) as follows:

$$
W(X,T) = W(\xi) = \frac{12}{(p+q)}\left(\frac{G'}{G}\right) + \alpha_0, \tag{26}
$$

or

$$
W(X,T) = W(\xi) = -\frac{12\mu}{(p+q)}\left(\frac{G'}{G}\right)^{-1} + \alpha_0, \tag{27}
$$

where G satisfies (19), $\xi = X - qT/(\beta + \lambda^2 - 4\mu)$, and α_0 is an arbitrary constant.

Since the general solutions $G = G(\xi)$ (hence $G' = dG/d\xi$) of ODE (19) have been known for us, substituting the solutions of (19) into (24) and (25), we have the general traveling wave solutions of (15) as follows.

Case 1. When $\lambda^2 - 4\mu > 0$, then we have the following exact traveling wave solution of (15):

$$
\begin{aligned}
&W_1(X,T)\\
&\quad = W_1(\xi) = \frac{6\sqrt{\lambda^2 - 4\mu}}{p+q}\\
&\qquad \times\Bigg(\Bigg(A_1\cosh\left(\frac{1}{2}\sqrt{\lambda^2 - 4\mu}\xi\right)\\
&\qquad\qquad + A_2\sinh\left(\frac{1}{2}\sqrt{\lambda^2 - 4\mu}\xi\right)\Bigg)\\
&\qquad\qquad \times\Bigg(A_1\sinh\left(\frac{1}{2}\sqrt{\lambda^2 - 4\mu}\xi\right)\\
&\qquad\qquad\quad + A_2\cosh\left(\frac{1}{2}\sqrt{\lambda^2 - 4\mu}\xi\right)\Bigg)^{-1}\Bigg)\\
&\qquad - \frac{6\lambda}{(p+q) + \alpha_0}
\end{aligned}
\tag{28}
$$

or

$$
\begin{aligned}
&W_2(X,T)\\
&\quad = W_2(\xi)\\
&\quad = -24\mu \times \Bigg((p+q)\\
&\qquad \times\Bigg(\sqrt{\lambda^2 - 4\mu}\\
&\qquad\quad \times\Bigg(\Bigg(A_1\cosh\left(\frac{1}{2}\sqrt{\lambda^2 - 4\mu}\xi\right)\\
&\qquad\qquad + A_2\sinh\left(\frac{1}{2}\sqrt{\lambda^2 - 4\mu}\xi\right)\Bigg)\\
&\qquad\qquad \times\Bigg(A_1\sinh\left(\frac{1}{2}\sqrt{\lambda^2 - 4\mu}\xi\right)\\
&\qquad\qquad\quad + A_2\cosh\left(\frac{1}{2}\sqrt{\lambda^2 - 4\mu}\xi\right)\Bigg)^{-1}\Bigg)\\
&\qquad - \lambda\Bigg)\Bigg)^{-1} + \alpha_0,
\end{aligned}
\tag{29}
$$

where $\xi = X - qT/(\beta + \lambda^2 - 4\mu)$ and α_0, A_1, A_2 are arbitrary constants.

Case 2. When $\lambda^2 - 4\mu < 0$, then we have the following exact traveling wave solution of (15):

$$\begin{aligned}
&W_3(X,T) \\
&= W_3(\xi) = \frac{6\sqrt{4\mu-\lambda^2}}{p+q} \\
&\quad \times \left(\left(-A_1 \sin\left(\frac{1}{2}\sqrt{4\mu-\lambda^2}\xi\right) + A_2 \cos\left(\frac{1}{2}\sqrt{4\mu-\lambda^2}\xi\right)\right)\right. \\
&\qquad \times \left(A_1 \cos\left(\frac{1}{2}\sqrt{4\mu-\lambda^2}\xi\right)\right. \\
&\qquad\qquad \left.\left.+A_2 \sin\left(\frac{1}{2}\sqrt{4\mu-\lambda^2}\xi\right)\right)^{-1}\right) \\
&\quad - \frac{6\lambda}{(p+q)+\alpha_0}
\end{aligned} \tag{30}$$

or

$$\begin{aligned}
&W_4(X,T) \\
&\quad = W_4(\xi) \\
&\quad = -24\mu \\
&\qquad \times \left((p+q)\left(\sqrt{\lambda^2-4\mu}\right.\right. \\
&\qquad\qquad \times \left(\left(-A_1 \sin\left(\frac{1}{2}\sqrt{4\mu-\lambda^2}\xi\right)\right.\right. \\
&\qquad\qquad\quad \left.+A_2 \cos\left(\frac{1}{2}\sqrt{4\mu-\lambda^2}\xi\right)\right) \\
&\qquad\qquad \times \left(A_1 \cos\left(\frac{1}{2}\sqrt{4\mu-\lambda^2}\xi\right)\right. \\
&\qquad\qquad\quad \left.\left.+A_2 \sin\left(\frac{1}{2}\sqrt{4\mu-\lambda^2}\xi\right)\right)^{-1}\right) \\
&\qquad\qquad\quad \left.\left.-\lambda\right)\right)^{-1} + \alpha_0,
\end{aligned} \tag{31}$$

where $\xi = X - qT/(\beta + \lambda^2 - 4\mu)$ and α_0, A_1, A_2 are arbitrary constants.

Case 3. When $\lambda^2 - 4\mu = 0$, then we have the following exact rational solution of (15):

$$W_5(X,T) = W_5(\xi) = \frac{12}{p+q}\left(\frac{A_2}{A_1 + A_2\xi}\right) - \frac{6\lambda}{(p+q)} + \alpha_0 \tag{32}$$

or

$$W_6(X,T) = W_6(\xi) = -\frac{24\mu(A_1 + A_2\xi)}{(p+q)\left[2A_2 - \lambda(A_1 + A_2\xi)\right]} + \alpha_0, \tag{33}$$

where $\xi = X - qT/(\beta + \lambda^2 - 4\mu)$ and α_0, A_1, A_2 are arbitrary constants.

Now we will show how to get exact traveling wave solutions of (6). From (8) and (14), the solution of EX-ROE (6) is given in parametric form, with T as the parameter, by

$$u(x,t) = U(t,T), \qquad x = \theta(t,T), \tag{34}$$

where

$$\theta(X,T) = T + W(X,T) + x_0. \tag{35}$$

So by using (8), (14), (34), (35), (28), and (29), we obtain a parameterized hyperbolic-function-type traveling wave solution of (6) as follows:

$$\begin{aligned}
&u_1(x,t) \\
&\quad = 3\left(A_2^2 - A_1^2\right)\left(\lambda^2 - 4\mu\right) \\
&\qquad \times \left(\vphantom{\frac{1}{2}}(p+q)\right. \\
&\qquad\quad \times \left(A_1 \sinh\left(\frac{1}{2}\sqrt{\lambda^2-4\mu}\xi\right)\right. \\
&\qquad\qquad \left.\left.+A_2 \cosh\left(\frac{1}{2}\sqrt{\lambda^2-4\mu}\xi\right)\right)^2\right)^{-1}, \\
&\qquad\qquad x = T + W_1(t,T) + x_0,
\end{aligned} \tag{36}$$

or

$$\begin{aligned}
&u_2(x,t) \\
&= -12\mu\left(A_2^2 - A_1^2\right)\left(\lambda^2 - 4\mu\right) \\
&\quad \times \left(\vphantom{\frac{1}{2}}(p+q)\right. \\
&\qquad \times \left[\left(A_1\sqrt{\lambda^2-4\mu} - A_2\lambda\right)\cosh\left(\frac{1}{2}\sqrt{\lambda^2-4\mu}\xi\right)\right. \\
&\qquad\quad + \left(A_2\sqrt{\lambda^2-4\mu} - A_1\lambda\right) \\
&\qquad\quad \left.\left.\times \sinh\left(\frac{1}{2}\sqrt{\lambda^2-4\mu}\xi\right)\right]^2\right)^{-1}, \\
&\qquad\quad x = T + W_2(t,T) + x_0,
\end{aligned} \tag{37}$$

where $\xi = t - qT/(\beta + \lambda^2 - 4\mu)$ and x_0 is an arbitrary constant.

By using (8), (14), (34), (35), (30), and (31), we obtain a parameterized trigonometric-function-type traveling wave solution of (6) as follows:

$$\begin{aligned} &u_3(x,t) \\ &= -3\left(A_2^2 + A_1^2\right)\left(\lambda^2 - 4\mu\right) \\ &\quad \times \left((p+q) \right. \\ &\quad\quad \times \left(A_1 \cos\left(\frac{1}{2}\sqrt{\lambda^2 - 4\mu}\xi\right) \right. \\ &\quad\quad\quad \left. \left. + A_2 \sin\left(\frac{1}{2}\sqrt{\lambda^2 - 4\mu}\xi\right)\right)^2 \right)^{-1}, \\ &\quad x = T + W_3(t,T) + x_0, \end{aligned} \tag{38}$$

or

$$\begin{aligned} &u_4(x,t) \\ &= -12\mu\left(A_2^2 - A_1^2\right)\left(\lambda^2 - 4\mu\right) \\ &\quad \times \left((p+q) \right. \\ &\quad\quad \times \left[\left(-A_2\sqrt{\lambda^2 - 4\mu} + A_1\lambda\right)\cos\left(\frac{1}{2}\sqrt{\lambda^2 - 4\mu}\xi\right) \right. \\ &\quad\quad\quad + \left(A_1\sqrt{\lambda^2 - 4\mu} + A_2\lambda\right) \\ &\quad\quad\quad \left. \left. \times \sin\left(\frac{1}{2}\sqrt{\lambda^2 - 4\mu}\xi\right)\right]^2 \right)^{-1}, \\ &\quad x = T + W_4(t,T) + x_0, \end{aligned} \tag{39}$$

where $\xi = t - qT/(\beta + \lambda^2 - 4\mu)$ and x_0 is an arbitrary constant.

By using (8), (14), (34), (35), (32), and (33), we obtain a parameterized rational-type traveling wave solution of (6) as follows:

$$\begin{aligned} u_5(x,t) &= -\frac{12A_2^2}{(p+q)\left(A_1 + A_2\xi\right)^2}, \\ x &= T + W_5(t,T) + x_0, \end{aligned} \tag{40}$$

or

$$\begin{aligned} u_6(x,t) &= -\frac{48\mu A_2^2}{(p+q)\left(\lambda A_1 + (-2 + \lambda\xi) A_2\right)^2}, \\ x &= T + W_6(t,T) + x_0, \end{aligned} \tag{41}$$

where $\xi = t - qT/(\beta + \lambda^2 - 4\mu)$ and x_0 is an arbitrary constant. To our knowledge, these solutions are presented for the first time; they are new exact solutions of EX-ROE.

If we take $A_1 = 0$, $\mu = 0$, $A_2 \neq 0$ and $\lambda > 0$, then (36) yields the following solitary wave solution of (6):

$$\begin{aligned} u(x,t) &= \frac{3\lambda^2}{p+q}\operatorname{sech}^2\left[\frac{1}{2}\lambda\left(t - \frac{q}{\beta + \lambda^2}T\right)\right], \\ x &= T + \frac{6\lambda}{(p+q)}\tanh\left[\frac{1}{2}\lambda\left(t - \frac{q}{\beta + \lambda^2}T\right)\right] + x_0. \end{aligned} \tag{42}$$

Now we will give some discussion of the solitary wave solution (42). Let $\lambda = 2k$, $x_0 = 0$; the solution (42) is reduced to the solution of (3.26) in [13] after correcting some minor errors [4]. Now from (35), we introduce a new variable:

$$\chi = x - \nu t = -\nu(X - cT) + \frac{6\lambda}{p+q}\tanh\left[\frac{1}{2}\lambda(X - cT)\right] + x_0, \tag{43}$$

where $\nu = 1/c = (\lambda^2 + \beta)/q$. In [8], the authors considered EX-ROE with $p = 2q$, $\beta \neq 0$ as mGVE and obtained 1-soliton solution. In fact, if we take $p = 2q$, $\lambda = 2k$, the solitary wave solution (42) with (43) is reduced to the soliton solution (4.4) and (4.5) in [8]. From the above we can see that the solitary wave solution (3.26) in [4] and the 1-soliton solution of mGVE are just a special case of the solution (42) in this paper.

4. Multishaped Solitary Wave Solutions

In [8, 13], the authors showed that the solutions of (4.4) and (4.5), (3.26) and (3.28) may be of different types, namely, loops, cusps, or humps for different values of parameters β, k, p. Here we also show that by choosing different values of the parameters β, λ, p, q, different shape wave solutions can be obtained. As it is stated in Section 1, (9) reduces to VE when $p = q = 1$, $\beta = 0$. Taking solution (42) with (43), for example, let $p = q = 1$, $\beta = 0$, $\lambda = 2k$; then it is reduced to one-loop soliton solution (3.4) and (3.5) in [39]. On the other hand, because the solutions of OHE and VE are connected in a particularly simple way, if we take $p = q = -1$, $\beta = 0$, $\lambda = 2k$ in (42), we can obtain one-loop soliton solution of OHE.

From above analysis, one can clearly see that the solutions obtained in this paper are generalized for the previous results because here we only take the special case $A_1 = 0$, $\mu = 0$, $A_2 \neq 0$, $\lambda > 0$ and give special discussion of solution (42). We conclude that if we take different values of the parameters A_1, A_2, λ, μ, p, q, abundancy of types of exact solutions can be obtained from solutions (36), (38), and (40). Here we omit the detailed discussion.

Instead, we give some discussion about solution (37). Science from this solution, multishaped solitary wave solutions can be obtained. Suppose $A_1 \neq 0$, $\mu < 0$, $A_2 = 0$, $\lambda = 0$; we reduce solution (37) to

$$\begin{aligned} u(x,t) &= \frac{12\mu}{p+q}\operatorname{sech}^2\left[\sqrt{-\mu}\left(t - \frac{q}{\beta - 4\mu}T\right)\right], \\ x &= T + \frac{24\sqrt{-\mu}}{(p+q)}\tanh\left[\sqrt{-\mu}\left(t - \frac{q}{\beta - 4\mu}T\right)\right] + x_0. \end{aligned} \tag{44}$$

We show that for different values of β, μ, and p, the solution (44) may be of different types. It also owns the property of

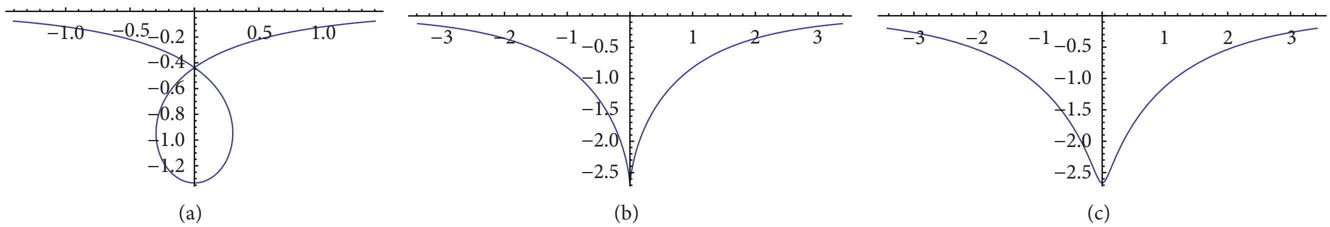

Figure 1: The profile of solution (44) with $p = 3$, $q = 1.5$, $t = 0$, and $x_0 = 0$. For (a) loop-shaped $\beta = 0.005$, $\mu = -0.5$, (b) cusp-shaped $\beta = 0.05$, $\mu = -1$, and (c) hump-shaped $\beta = 0.5$, $\mu = -1$.

being loop-shaped, cusp-shaped and hump-shaped, as shown in Figure 1.

5. Conclusion

In this paper, we use (G'/G)-expansion method to study extended reduced Ostrovsky equation. Several pairs of generalized traveling wave solutions are given directly. These solutions extend the previous results to more general cases. At the same time, multishaped wave solutions can be obtained if the different parameters values are chosen. These explicit solitary wave solutions own the property of being loop-shaped, cusp-shaped, and hump-shaped. These exact traveling wave solutions are also helpful to further study this nonlinear equation which has their physical meaning. The method used in this paper has more advantages. It is direct and concise. Much tedious algebraic calculations can be finished by computer program such as MATHEMATICA and MAPLE. Many well-known nonlinear wave equations can be handled by this method.

Acknowledgment

The authors thank anonymous referees for valuable suggestions and comments which improve this paper readability and convincibility. This paper is supported by the Starting Research Founding of Wuhan Textile University.

References

[1] L. A. Ostrovsky, "Nonlinear internal waves in a rotating ocean," *Oceanology*, vol. 18, pp. 119–125, 1978.

[2] Y. A. Stepanyants, "On stationary solutions of the reduced Ostrovsky equation: periodic waves, compactons and compound solitons," *Chaos, Solitons & Fractals*, vol. 28, no. 1, pp. 193–204, 2006.

[3] E. J. Parkes, "Explicit solutions of the reduced Ostrovsky equation," *Chaos, Solitons & Fractals*, vol. 31, no. 3, pp. 602–610, 2007.

[4] E. J. Parkes, "Periodic and solitary travelling-wave solutions of an extended reduced Ostrovsky equation," *SIGMA*, vol. 4, article 053, pp. 1–17, 2008.

[5] J. P. Boyd, "Ostrovsky and Hunter's generic wave equation for weakly dispersive waves: matched asymptotic and pseudospectral study of the paraboloidal travelling waves (corner and near-corner waves)," *European Journal of Applied Mathematics*, vol. 16, no. 1, pp. 65–81, 2005.

[6] V. A. Vakhnenko, "Solitons in a nonlinear model medium," *Journal of Physics A*, vol. 25, no. 15, pp. 4181–4187, 1992.

[7] V. O. Vakhnenko, "High-frequency soliton-like waves in a relaxing medium," *Journal of Mathematical Physics*, vol. 40, no. 4, pp. 2011–2020, 1999.

[8] A. J. Morrison and E. J. Parkes, "The N-soliton solution of the modified generalised Vakhnenko equation (a new nonlinear evolution equation)," *Chaos, Solitons & Fractals*, vol. 16, no. 1, pp. 13–26, 2003.

[9] A. Espinosa and J. Fujioka, "Hydrodynamic foundation and Painlevé analysis of Hirota-Satsuma-type equations," *Journal of the Physical Society of Japan*, vol. 63, no. 4, pp. 1289–1294, 1994.

[10] M. J. Ablowitz, D. J. Kaup, A. C. Newell, and H. Segur, "The inverse scattering transform-Fourier analysis for nonlinear problems," vol. 53, no. 4, pp. 249–315, 1974.

[11] R. Hirota and J. Satsuma, "N-soliton solutions of model equations for shallow water waves," vol. 40, no. 2, pp. 611–612, 1976.

[12] A. J. Morrison and E. J. Parkes, "The N-soliton solution of a generalised Vakhnenko equation," *Glasgow Mathematical Journal*, vol. 43A, pp. 65–90, 2001, Integrable systems: linear and nonlinear dynamics (Islay, 1999).

[13] Y. Liu, Z. Li, and K. Wang, "Symbolic computation of exact solutions for a nonlinear evolution equation," *Chaos, Solitons & Fractals*, vol. 31, no. 5, pp. 1173–1180, 2007.

[14] S. Xie and J. Cai, "Exact compacton and generalized kink wave solutions of the extended reduced Ostrovsky equation," *Communications in Nonlinear Science and Numerical Simulation*, vol. 14, no. 9-10, pp. 3561–3573, 2009.

[15] Y. A. Stepanyants, "Solutions classification to the extended reduced Ostrovsky equation," *SIGMA*, vol. 4, article 073, pp. 1–19, 2008.

[16] M. Song, "Application of bifurcation method to the generalized Zakharov equations," *Abstract and Applied Analysis*, vol. 2012, Article ID 308326, 8 pages, 2012.

[17] M. Song, S. A. Bouthina, and A. Biswas, "Topological soliton solution and bifurcation analysis of the Klein-Gordon-Zakharov equation in (1 + 1)-dimensions with power law nonlinearity," *Journal of Applied Mathematics*, vol. 2013, Article ID 972416, 7 pages, 2013.

[18] A. Biswas and M. Song, "Soliton solution and bifurcation analysis of the Zakharov-Kuznetsov-Benjamin-Bona-Mahoney equation with power law nonlinearity," *Communications in Nonlinear Science and Numerical Simulation*, vol. 18, pp. 1676–1683, 2013.

[19] M. Song, C. Yang, and B. Zhang, "Exact solitary wave solutions of the Kadomtsov-Petviashvili-Benjamin-Bona-Mahony equation," *Applied Mathematics and Computation*, vol. 217, no. 4, pp. 1334–1339, 2010.

[20] B.-G. Zhang, Z.-R. Liu, and Q. Xiao, "New exact solitary wave and multiple soliton solutions of quantum Zakharov-Kuznetsov equation," *Applied Mathematics and Computation*, vol. 217, no. 1, pp. 392–402, 2010.

[21] B.-G. Zhang, S.-Y. Li, and Z.-R. Liu, "Homotopy perturbation method for modified Camassa-Holm and Degasperis-Procesi equations," *Physics Letters A*, vol. 372, no. 11, pp. 1867–1872, 2008.

[22] J. Li and F. Chen, "Exact travelling wave solutions and their dynamical behavior for a class coupled nonlinear wave equations," *Discrete and Continuous Dynamical Systems. Series B*, vol. 18, no. 1, pp. 163–172, 2013.

[23] J. Li, "Existence of exact families of traveling wave solutions for the sixth-order Ramani equation and a coupled Ramani equation," *International Journal of Bifurcation and Chaos in Applied Sciences and Engineering*, vol. 22, no. 1, Article ID 1250002, 2 pages, 2012.

[24] C. Pan and Z. Liu, "Further results on the traveling wave solutions for an integrable equation," *Journal of Applied Mathematics*, Article ID 681383, 6 pages, 2013.

[25] Z. Liu and Y. Liang, "The explicit nonlinear wave solutions and their bifurcations of the generalized Camassa-Holm equation," *International Journal of Bifurcation and Chaos in Applied Sciences and Engineering*, vol. 21, no. 11, pp. 3119–3136, 2011.

[26] H.-T. Chen, S.-H. Yang, and W.-X. Ma, "Double sub-equation method for complexiton solutions of nonlinear partial differential equations," *Applied Mathematics and Computation*, vol. 219, no. 9, pp. 4775–4781, 2013.

[27] W.-X. Ma and Y. Liu, "Invariant subspaces and exact solutions of a class of dispersive evolution equations," *Communications in Nonlinear Science and Numerical Simulation*, vol. 17, no. 10, pp. 3795–3801, 2012.

[28] M. Wang, X. Li, and J. Zhang, "The (G'/G)-expansion method and travelling wave solutions of nonlinear evolution equations in mathematical physics," *Physics Letters A*, vol. 372, no. 4, pp. 417–423, 2008.

[29] M. Wang, J. Zhang, and X. Li, "Application of the (G'/G)-expansion to travelling wave solutions of the Broer-Kaup and the approximate long water wave equations," *Applied Mathematics and Computation*, vol. 206, no. 1, pp. 321–326, 2008.

[30] D. D. Ganji and M. Abdollahzadeh, "Exact traveling solutions of some nonlinear evolution equation by (G'/G)-expansion method," *Journal of Mathematical Physics*, vol. 50, no. 1, Article ID 013519, p. 10, 2009.

[31] Y.-B. Zhou and C. Li, "Application of modified G'/G-expansion method to traveling wave solutions for Whitham-Broer-Kaup-like equations," *Communications in Theoretical Physics*, vol. 51, no. 4, pp. 664–670, 2009.

[32] H. Zhang, "New application of the (G'/G)-expansion method," *Communications in Nonlinear Science and Numerical Simulation*, vol. 14, pp. 3220–3225, 2009.

[33] S. Zhang, J. L. Tong, and W. Wang, "A generalized (G'/G)-expansion method for the mKdV equation with variable coefficients," *Physics Letters A*, vol. 372, pp. 2254–2257, 2008.

[34] J. Zhang, X. Wei, and Y. Lu, "A generalized (G'/G)-expansion method and its applications," *Physics Letters A*, vol. 372, no. 20, pp. 3653–3658, 2008.

[35] W. A. Li, H. Chen, and G. C. Zhang, "The (ω/g)-expansion method and its application to Vakhnenko equation," *Chinese Physics B*, vol. 18, pp. 400–405, 2009.

[36] W. X. Ma and B. Fuchssteiner, "Explicit and exact solutions to a Kolmogorov-Petrovskii-Piskunov equation," *International Journal of Non-Linear Mechanics*, vol. 31, no. 3, pp. 329–338, 1996.

[37] W.-X. Ma and J.-H. Lee, "A transformed rational function method and exact solutions to the 3 + 1 dimensional Jimbo-Miwa equation," *Chaos, Solitons & Fractals*, vol. 42, no. 3, pp. 1356–1363, 2009.

[38] W.-X. Ma and Z. Zhu, "Solving the $(3+1)$-dimensional generalized KP and BKP equations by the multiple exp-function algorithm," *Applied Mathematics and Computation*, vol. 218, no. 24, pp. 11871–11879, 2012.

[39] V. O. Vakhnenko and E. J. Parkes, "The two loop soliton solution of the Vakhnenko equation," *Nonlinearity*, vol. 11, no. 6, pp. 1457–1464, 1998.

Hindawi Publishing Corporation
Abstract and Applied Analysis
Volume 2013, Article ID 268902, 5 pages
http://dx.doi.org/10.1155/2013/268902

Research Article

New Exact Solutions for a Generalized Double Sinh-Gordon Equation

Gabriel Magalakwe and Chaudry Masood Khalique

International Institute for Symmetry Analysis and Mathematical Modelling, Department of Mathematical Sciences, North-West University, Mafikeng Campus, Private Bag X 2046, Mmabatho 2735, South Africa

Correspondence should be addressed to Chaudry Masood Khalique; masood.khalique@nwu.ac.za

Received 26 June 2013; Revised 15 July 2013; Accepted 15 July 2013

Academic Editor: Santanu Saha Ray

We study a generalized double sinh-Gordon equation, which has applications in various fields, such as fluid dynamics, integrable quantum field theory, and kink dynamics. We employ the Exp-function method to obtain new exact solutions for this generalized double sinh-Gordon equation. This method is important as it gives us new solutions of the generalized double sinh-Gordon equation.

1. Introduction

It is well known that finding exact travelling wave solutions of nonlinear partial differential equations (NLPDEs) is useful in many scientific applications such as fluid mechanics, plasma physics, and quantum field theory. Due to these applications many researchers are investigating exact solutions of NLPDEs since they play a vital role in the study of nonlinear physical phenomena. Finding exact solutions of such NLPDEs provides us with a better understanding of the physical phenomena that these NLPDEs describe. Several techniques have been presented in the literature to find exact solutions of the NLPDEs. These include the homogeneous balance method, the Weierstrass elliptic function expansion method, the F-expansion method, the (G'/G)-expansion method, the Exp-function method, the tanh function method, the extended tanh function method, and the Lie group method [1–10].

In this work, we study one such NLPDE, namely, the generalized double sinh-Gordon equation:

$$u_{tt} - ku_{xx} + 2\alpha \sinh(nu) + \beta \sinh(2nu) = 0, \quad n \geq 1, \tag{1}$$

which appears in many scientific applications [11–13]. It should be noted that when $k = a$, $\alpha = (1/2)b$, and $\beta = 0$, (1) becomes the generalized sinh-Gordon equation [14, 15]. Furthermore, if $n = a = 1$ and $b = 2$, (1) reduces to the sinh-Gordon equation [16].

Many authors have studied the generalized double sinh-Gordon equation (1). Travelling waves solutions of (1) were obtained in [11] by using the tanh function method and the variable separable method. In [12] the method of bifurcation theory of dynamical system was used to prove the existence of periodic wave, solitary wave, kink and antikink wave, and unbounded wave solutions of (1). It should be noted that solutions obtained in [12] were different the ones obtained in [11]. Recently, solitary and periodic waves solutions of (1) were found in [13] by employing (G'/G)-expansion method. It is further shown in [13] that solutions obtained by using the (G'/G)-expansion method are more general than those given in [11], which were obtained by tanh function method.

In this paper, we employ an entirely different method, known as the Exp-function method, to obtain new exact solutions of the generalized sinh-Gordon equation (1). The paper is structured as follows. In Section 2, we obtain exact solutions of the generalized double sinh-Gordon equation (1) with the help of the Exp-function method. In Section 3 we present concluding remarks.

2. Exact Solutions of (1) Using Exp-Function Method

In this section we employ the Exp-function method to solve the generalized double sinh-Gordon equation (1). This method was introduced by He and Wu [17]. The Exp-function method results in the travelling wave solution based on the assumption that the solution can be expressed in the following form:

$$H(z) = \frac{\sum_{n=-c}^{d} a_n \exp(nz)}{\sum_{m=-p}^{q} b_m \exp(mz)}, \quad (2)$$

where c, d, p, and q are positive integers that can be determined and a_n and b_m are unknown constants. According to Exp-function method, we introduce the travelling wave substitution $u(x,t) = W(z)$, where $z = x - ct$. Then (1) transforms to the nonlinear ordinary differential equation:

$$\left(c^2 - k\right) W''(z) + 2\alpha \sinh(nW(z)) + \beta \sinh(2nW(z)) = 0. \quad (3)$$

Further, using the transformation $W(z) = (1/n)\ln(H(z))$ on (3), we obtain

$$2\left(c^2 - k\right) H(z) H''(z) - 2\left(c^2 - k\right) H'(z)^2 + 2\alpha n H(z)^3 - 2\alpha n H(z) + \beta n H(z)^4 - \beta n = 0. \quad (4)$$

We assume that the solution of (4) can be expressed as

$$H(z) = \frac{a_c \exp(cz) + \cdots + a_{-d}\exp(-dz)}{b_p \exp(pz) + \cdots + b_{-q}\exp(-qz)}. \quad (5)$$

The values of c and d, p and q can be determined by balancing the linear term of the highest order with the highest order of nonlinear term in (4), that is, HH'' and H^4. By straight forward calculation, we have

$$HH'' = \frac{c_1 \exp[(2c+3p)z] + \cdots}{c_2 \exp[5pz] + \cdots},$$
$$H^4 = \frac{c_3 \exp[4cz] + \cdots}{c_4 \exp[4pz] + \cdots} = \frac{c_3 \exp[(4c+p)z] + \cdots}{c_4 \exp[5pz] + \cdots}, \quad (6)$$

where c_i are coefficients only for simplicity. Balancing the highest order of Exp-function in (6), we have $2c+3p = 4c+p$, which yields $c = p$. Similarly, we balance the lowest order in (4) to determine values of d and q. We have

$$HH'' = \frac{\cdots + s_1 \exp[-(2d+3q)z]}{\cdots + s_2 \exp[-5qz]},$$
$$H^4 = \frac{\cdots + s_3 \exp[4dz]}{\cdots + s_4 \exp[-4qz]} = \frac{\cdots + s_3 \exp[-(4d+q)z]}{\cdots + s_4 \exp[-5qz]}, \quad (7)$$

where s_i are coefficients only for simplicity. Balancing the lowest order of Exp-function in (7), we have $2d+3q = 4d+q$, which yields $d = q$. For simplicity, we first set $c = p = 1$ and $d = q = 1$. then (5) reduces to

$$H(z) = \frac{a_1 \exp(z) + a_0 + a_{-1}\exp(-z)}{b_1 \exp(z) + b_0 + b_{-1}\exp(-z)}. \quad (8)$$

Inserting (8) into (4) and using Maple, we obtain

$$\frac{1}{B}\left[C_4 \exp(4z) + C_3 \exp(3z) + C_2 \exp(2z) + C_1 \exp(z) + C_0 + C_{-1}\exp(-z) + C_{-2}\exp(-2z) + C_{-3}\exp(-3z) + C_{-4}\exp(-4z)\right] = 0, \quad (9)$$

where

$$B = \left(b_1 \exp(z) + b_0 + b_{-1}\exp(-z)\right)^4,$$

$$C_4 = 2\alpha a_1^3 b_1 n - \beta b_1^4 n + \beta a_1^4 n - 2\alpha a_1 b_1^3 n,$$

$$\begin{aligned} C_3 = {} & -2a_1^2 b_0 b_1 c^2 + 2a_1 a_0 b_1^2 c^2 + 6\alpha a_0 a_1^2 b_1 n \\ & - 6\alpha a_1 b_0 b_1^2 n + 2a_1^2 b_0 b_1 k - 2a_0 a_1 b_1^2 k \\ & + 2\alpha a_1^3 b_0 n - 2a_0 a_1 b_1^2 k + 2\alpha a_1^3 b_0 n \\ & + 4\beta a_0 a_1^3 n - 2\alpha a_0 b_1^3 n - 4\beta b_0 b_1^3 n, \end{aligned}$$

$$\begin{aligned} C_2 = {} & 4\beta a_{-1} a_1^3 n - 8a_1^2 b_{-1} b_1 c^2 + 8a_{-1} a_1 b_1^2 c^2 \\ & + 8a_1^2 b_{-1} b_1 k - 8a_{-1} a_1 b_1^2 k + 2\alpha a_1^3 b_{-1} n \\ & - 2\alpha a_{-1} b_1^3 n - 4\beta b_{-1} b_1^3 n + 6\alpha a_0 a_1^2 b_0 n \\ & + 6\alpha a_0^2 a_1 b_1 n - 6\alpha a_1 b_0^2 b_1 n - 6\beta b_0^2 b_1^2 n \\ & + 6\alpha a_{-1} a_1^2 b_1 n - 6\alpha a_1 b_1^2 b_{-1} n + 6\beta a_0^2 a_1^2 n \\ & - 6\alpha a_0 b_0 b_1^2 n, \end{aligned}$$

$$\begin{aligned} C_1 = {} & -2a_0^2 b_0 b_1 c^2 + 2a_0 a_1 b_0^2 c^2 + 2a_0^2 b_0 b_1 k \\ & - 2a_0 a_1 b_0^2 k - 2a_1^2 b_0 b_{-1} c^2 + 2a_{-1} a_0 b_1^2 c^2 \\ & - 2a_0 a_{-1} b_1^2 k + 2\alpha a_0^3 b_1 n + 4\beta a_0^3 a_1 n - 2\alpha a_1 b_0^3 n \\ & - 4\beta b_0^3 b_1 n + 12a_{-1} a_1 b_0 b_1 c^2 - 12a_{-1} a_1 b_0 b_1 k \\ & + 12a_0 a_1 b_{-1} b_1 k + 6\alpha a_0^2 a_1 b_0 n - 6\alpha a_0 b_0^2 b_1 n \\ & + 12\alpha a_{-1} a_0 a_1 b_1 n - 12\alpha a_1 b_{-1} b_0 b_1 n \\ & + 6\alpha a_{-1} a_1^2 b_0 n - 6\alpha a_0 b_{-1} b_1^2 n - 6\alpha a_{-1} b_0 b_1^2 n \\ & + 6\alpha a_0 a_1^2 b_{-1} n + 12\beta a_{-1} a_0 a_1^2 n - 12\beta b_{-1} b_0 b_1^2 n \\ & + 2a_1^2 b_0 b_{-1} k - 12a_0 a_1 b_{-1} b_1 c^2, \end{aligned}$$

$$\begin{aligned}
C_0 ={}& 2\alpha a_0^3 b_0 n - 2\alpha a_0 b_0^3 n + \beta a_0^4 n \\
&+ 6\alpha a_{-1} a_1^2 b_{-1} n + 6\alpha a_0^2 a_1 b_{-1} n + 6\alpha a_{-1}^2 a_1 b_1 n \\
&+ 6\alpha a_{-1} a_0^2 b_1 n + 12\beta a_{-1} a_0^2 a_1 n - 6\alpha a_1 b_{-1}^2 b_1 n \\
&- 6\alpha a_1 b_{-1} b_0^2 n - 6\alpha a_{-1} b_{-1} b_1^2 n - \beta b_0^4 n \\
&- 6\alpha a_{-1} b_0^2 b_1 n - 12\beta b_{-1} b_0^2 b_1 n + 8 a_{-1} a_1 b_0^2 c^2 \\
&- 8 a_0^2 b_{-1} b_1 c^2 - 8 a_{-1} a_1 b_0^2 k + 8 a_0^2 b_{-1} b_1 k \\
&+ 6\beta a_{-1}^2 a_1^2 n - 6\beta b_{-1}^2 b_1^2 n + 12\alpha a_{-1} a_0 a_1 b_0 n \\
&- 12\alpha a_0 b_{-1} b_0 b_1 n, \\
C_{-1} ={}& 12\alpha a_{-1} a_0 a_1 b_{-1} n - 12\alpha a_{-1} b_{-1} b_0 b_1 n \\
&+ 2 a_{-1} a_0 b_0^2 c^2 - 2 a_0^2 b_{-1} b_0 c^2 + 2 a_0^2 b_{-1} b_0 k \\
&- 2 a_{-1} a_0 b_0^2 k + 2 a_0 a_1 b_{-1}^2 c^2 - 2 a_{-1}^2 b_0 b_1 c^2 \\
&- 2 a_0 a_1 b_{-1}^2 k + 2 a_{-1}^2 b_0 b_1 k + 2\alpha a_0^3 b_{-1} n \\
&+ 4\beta a_{-1} a_0^3 n - 2\alpha a_{-1} b_0^3 n - 4\beta b_{-1} b_0^3 n \\
&+ 12 a_{-1} a_1 b_{-1} b_0 c^2 - 12 a_{-1} a_0 b_{-1} b_1 c^2 \\
&- 12 a_{-1} a_1 b_{-1} b_0 k + 12 a_{-1} a_0 b_{-1} b_1 k \\
&+ 6\alpha a_{-1} a_0^2 b_0 n - 6\alpha a_0 b_{-1} b_0^2 n + 6\alpha a_{-1}^2 a_1 b_0 n \\
&+ 6\alpha a_{-1}^2 a_0 b_1 n + 12\beta a_{-1}^2 a_0 a_1 n - 6\alpha a_1 b_{-1}^2 b_0 n \\
&- 6\alpha a_0 b_{-1}^2 b_1 n - 12\beta b_{-1}^2 b_0 b_1 n, \\
C_{-2} ={}& 2\alpha a_{-1}^3 b_1 n + 8 a_{-1} a_1 b_{-1}^2 c^2 + 8 a_{-1}^2 b_{-1} b_1 k \\
&- 8 a_{-1} a_1 b_{-1}^2 k + 4\beta a_{-1}^3 a_1 n - 4\beta b_{-1}^3 b_1 n \\
&- 2\alpha a_1 b_{-1}^3 n - 8 a_{-1}^2 b_{-1} b_1 c^2 + 6\alpha a_{-1} a_0^2 b_{-1} n \\
&+ 6\alpha a_{-1}^2 a_0 b_0 n - 6\alpha a_0 b_{-1}^2 b_0 n + 6\alpha a_{-1}^2 a_1 b_{-1} n \\
&- 6\alpha a_{-1} b_{-1}^2 b_1 n + 6\beta a_{-1}^2 a_0^2 n - 6\beta b_{-1}^2 b_0^2 n \\
&- 6\alpha a_{-1} b_{-1} b_0^2 n, \\
C_{-3} ={}& 6\alpha a_0 a_{-1}^2 b_{-1} n - 6\alpha a_{-1} b_{-1}^2 b_0 n \\
&- 2 a_{-1}^2 b_{-1} b_0 c^2 + 2 a_{-1} a_0 b_{-1}^2 c^2 \\
&+ 2 a_{-1}^2 b_0 b_{-1} k - 2 a_{-1} a_0 b_{-1}^2 k \\
&+ 2\alpha a_{-1}^3 b_0 n + 4\beta a_0 a_{-1}^3 n \\
&- 2\alpha a_0 b_{-1}^3 n - 4\beta b_0 b_{-1}^3 n, \\
C_{-4} ={}& \beta a_{-1}^4 n - \beta b_{-1}^4 n + 2\alpha a_{-1}^3 b_{-1} n - 2\alpha a_{-1} b_{-1}^3 n.
\end{aligned} \tag{10}$$

Equating the coefficients of $\exp(z)$ in (9) to zero, we obtain a set of algebraic equations:

$$\begin{gathered}
C_4 = 0, \quad C_3 = 0, \quad C_2 = 0, \quad C_1 = 0, \quad C_0 = 0, \\
C_{-1} = 0, \quad C_{-2} = 0, \quad C_{-3} = 0, \quad C_{-4} = 0.
\end{gathered} \tag{11}$$

Solving the system (11) with the help of Maple, we obtain the following three cases.

Case 1. We have the following:

$$\begin{gathered}
a_{-1} = b_{-1}, \qquad a_0 = -b_0, \qquad a_1 = b_1, \qquad \beta = \frac{\alpha b_0^2 - 4\alpha b_1 b_{-1}}{4 b_1 b_{-1}}, \\
k = \frac{\alpha b_0^2 n + 2 b_{-1} b_1 c^2}{2 b_{-1} b_1}.
\end{gathered} \tag{12}$$

Case 2. We have the following:

$$\begin{gathered}
a_{-1} = \frac{b_{-1} b_1}{a_1}, \qquad a_0 = 0, \qquad b_0 = 0, \qquad \alpha = \frac{-\beta\left(a_1^2 + b_1^2\right)}{2 a_1 b_1}, \\
k = \frac{-2\beta a_1^2 b_1^2 n + \beta a_1^4 n + \beta b_1^4 n + 8 a_1^2 b_1^2 c^2}{8 a_1^2 b_1^2}.
\end{gathered} \tag{13}$$

Case 3. We have the following:

$$\begin{gathered}
a_{-1} = -\phi b_1, \qquad b_{-1} = -\phi a_1, \qquad \alpha = \frac{-\beta\left(a_1^2 + b_1^2\right)}{2 a_1 b_1}, \\
k = \frac{-2\beta a_1^2 b_1^2 n + \beta a_1^4 n + \beta b_1^4 n + 2 a_1^2 b_1^2 c^2}{2 a_1^2 b_1^2},
\end{gathered} \tag{14}$$

where $\phi = (-a_0 a_1^2 b_0 + a_0^2 a_1 b_1 + a_1 b_0^2 b_1 - a_0 b_0 b_1^2)/(a_1 - b_1)^2 (a_1 + b_1)^2$.

Substituting values from (12) into (8), we obtain

$$H(z) = \frac{b_1 \exp(z) - b_0 + b_{-1} \exp(-z)}{b_1 \exp(z) + b_0 + b_{-1} \exp(-z)}. \tag{15}$$

As a result one of the solutions of (1) is given by

$$u_1(x, t) = \frac{1}{n} \ln\left(\frac{b_1 \exp(z) - b_0 + b_{-1} \exp(-z)}{b_1 \exp(z) + b_0 + b_{-1} \exp(-z)}\right), \tag{16}$$

where $z = x - ct$, $\beta = (\alpha b_0^2 - 4\alpha b_1 b_{-1})/4 b_1 b_{-1}$, and $k = (\alpha b_0^2 n + 2 b_{-1} b_1 c^2)/2 b_{-1} b_1$.

As a special case, if we choose $b_0 = 2$ and $b_{-1} = b_1 = 1$ in (16), then we get $\beta = 0$, $k = 2\alpha n + c^2$ and obtain the solution of the generalized sinh-Gordon equation as

$$u_1(x, t) = \frac{1}{n} \ln\left(\tanh^2\left[\left(\frac{1}{2}\right)(x - ct)\right]\right), \tag{17}$$

which is the solution obtained in [14, 15].

Now substituting the values from (13) (Case 2) into (8) results in the second solution of (1) as

$$u_2(x,t) = \frac{1}{n}\ln\left(\frac{a_1\exp(z) + (b_{-1}b_1/a_1)\exp(-z)}{b_1\exp(z) + b_{-1}\exp(-z)}\right), \quad (18)$$

with $z = x - ct$, $\alpha = -\beta(a_1^2 + b_1^2)/2a_1b_1$, and $k = (-2\beta a_1^2b_1^2n + \beta a_1^4n + \beta b_1^4n + 8a_1^2b_1^2c^2)/8a_1^2b_1^2$.

The third solution of (1) is obtained by using the values from (14) (Case 3) and substituting them into (8). Consequently, it is given by

$$u_3(x,t) = \frac{1}{n}\ln\left(\frac{a_1\exp(z) + a_0 - b_1\phi\exp(-z)}{b_1\exp(z) + b_0 - a_{-1}\phi\exp(-z)}\right), \quad (19)$$

where $z = x - ct, \phi = (-a_0a_1^2b_0 + a_0^2a_1b_1 + a_1b_0^2b_1 - a_0b_0b_1^2)/(a_1 - b_1)^2(a_1 + b_1)^2$, $\alpha = -\beta(a_1^2 + b_1^2)/2a_1b_1$, and $k = (-2\beta a_1^2b_1^2n + \beta a_1^4n + \beta b_1^4n + 2a_1^2b_1^2c^2)/2a_1^2b_1^2$.

To construct more solutions of (1), we now set $c = p = 2$ and $d = q = 2$. Then (5) reduces to

$$\begin{aligned} H(z) = {} & (a_2\exp(2z) + a_1\exp(z) + a_0 + a_{-1}\exp(-z) \\ & + a_{-2}\exp(-2z)) \\ & \times (b_2\exp(z) + b_1\exp(z) + b_0 \\ & + b_{-1}\exp(-z) + b_{-2}\exp(-2z))^{-1}. \end{aligned} \quad (20)$$

Proceeding as above, we obtain the following three solutions of (1):

$$\begin{aligned} u_4(x,t) = {} & \frac{1}{n}\ln\left(a_2\exp(2z) + \left(\frac{a_{-1}b_1}{b_{-1}}\right)\exp(z)\right. \\ & \left. + \left(\frac{a_{-1}b_0}{b_{-1}}\right) + a_{-1}\exp(-z)\right) \\ & \times\left(\frac{a_2b_{-1}}{a_{-1}}\exp(z) + b_1\exp(z)\right. \\ & \left. + b_0 + b_{-1}\exp(-z)\right)^{-1}, \end{aligned} \quad (21)$$

where $z = x - ct$, $\alpha = -\beta(a_{-1}^2 + b_{-1}^2)/2a_{-1}b_{-1}$,

$$u_5(x,t) = \frac{1}{n}\ln\left(\frac{a_2\exp(2z) + a_1\exp(z) + b_0}{-a_2\exp(z) + b_1\exp(z) + b_0}\right), \quad (22)$$

with $z = x - ct$, $\beta = \alpha(b_1^2 + 4a_2b_0)/4a_2b_0$, and $k = (\alpha nb_1^2 + 2a_2b_0c^2)/2a_2b_0$, and

$$u_6(x,t) = \frac{1}{n}\ln\left(\frac{a_2\exp(2z) - b_0 + b_{-2}\exp(-2z)}{a_2\exp(2z) + b_0 + b_{-2}\exp(-2z)}\right), \quad (23)$$

where $z = x - ct$, $\alpha = -(8a_2b_{-2}(c^2 - k)/b_0^2n)$, and $\beta = 2(4a_2b_{-2}c^2 - 4a_2b_{-2}k - b_0^2c^2 + b_0^2k)/b_0^2n$.

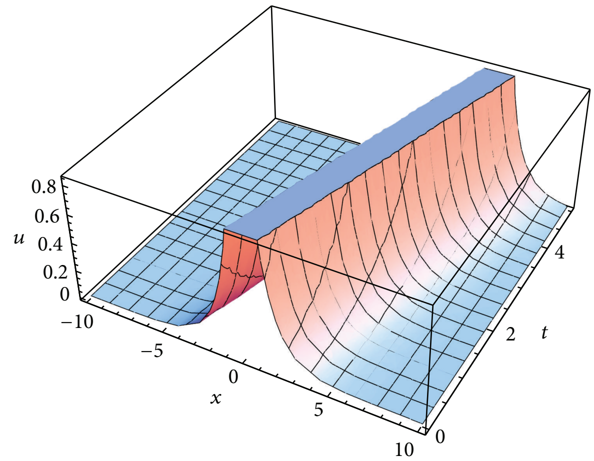

Figure 1: Profile of solution (16).

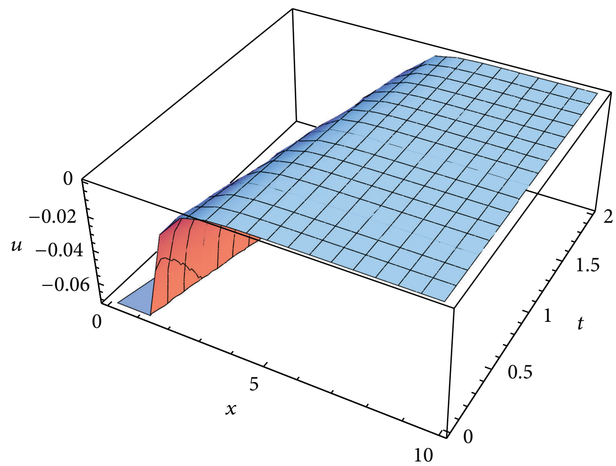

Figure 2: Profile of solution (23).

By taking $n = 2$, $b_{-1} = -1$, $b_0 = 2$, $c = 1$, and $b_1 = -1$ in the solution (16), we have its profile given in Figure 1.

By taking $n = 3$, $b_{-2} = 1$, $b_0 = 2$, $c = 1$, and $a_1 = 1$ in the solution (23), we have its profile given in Figure 2.

3. Concluding Remarks

In this paper we obtained new exact solutions of the generalized double sinh-Gordon equation (1) using the Exp-function method. We presented six different solutions of (1). Earlier, the tanh function, the bifurcation, and the (G'/G)-expansion methods [11–13] were employed to obtain exact solutions of (1). The solutions obtained in this paper were new and were different from the ones obtained in [11–13]. By taking special values of the constants, we also retrieved the solution of the generalized sinh-Gordon equation, which was obtained in [14, 15]. The Exp-function method is very simple and straightforward method for solving nonlinear partial differential equations. Indeed this has some pronounced merit as compared to the other methods. The correctness of the solutions obtained here has been verified by substituting them back into (1).

Acknowledgments

Gabriel Magalakwe would like to thank SANHARP, NRF, and North-West University, Mafikeng Campus, South Africa, for their financial support.

References

[1] M. Wang, Y. Zhou, and Z. Li, "Application of a homogeneous balance method to exact solutions of nonlinear equations in mathematical physics," *Physics Letters A*, vol. 216, no. 1–5, pp. 67–75, 1996.

[2] Y. Chen and Z. Yan, "The Weierstrass elliptic function expansion method and its applications in nonlinear wave equations," *Chaos, Solitons and Fractals*, vol. 29, no. 4, pp. 948–964, 2006.

[3] M. Wang and X. Li, "Applications of F-expansion to periodic wave solutions for a new Hamiltonian amplitude equation," *Chaos, Solitons and Fractals*, vol. 24, no. 5, pp. 1257–1268, 2005.

[4] M. Wang, X. Li, and J. Zhang, "The(G', G)-expansion method and travelling wave solutions of nonlinear evolution equations in mathematical physics," *Physics Letters A*, vol. 372, no. 4, pp. 417–423, 2008.

[5] S. Zhang, "Application of Exp-function method to high-dimensional nonlinear evolution equation," *Chaos, Solitons and Fractals*, vol. 38, no. 1, pp. 270–276, 2008.

[6] H. Zhi and H. Zhang, "Applications of the combined tanh function method with symmetry method to the nonlinear evolution equations," *Applied Mathematics and Computation*, vol. 188, no. 1, pp. 385–393, 2007.

[7] D.-S. Li and H.-Q. Zhang, "A further extended tanh-function method and new soliton-like solutions to the integrable Broer-Kaup (BK) equations in $(2+1)$ dimensional spaces," *Applied Mathematics and Computation*, vol. 147, no. 2, pp. 537–545, 2004.

[8] G. W. Bluman and S. Kumei, *Symmetries and Differential Equations*, vol. 81 of *Applied Mathematical Sciences*, Springer, New York, NY, USA, 1989.

[9] P. J. Olver, *Applications of lie Groups to Differential Equations*, vol. 107 of *Graduate Texts in Mathematics*, Springer, Berlin, Germany, 2nd edition, 1993.

[10] N. H. Ibragimov, *CRC Handbook of Lie Group Analysis of Differential Equations*, vol. 1–3, CRC Press, Boca Raton, Fla, USA, 1994–1996.

[11] A. M. Wazwaz, "Exact solutions to the double sinh-Gordon equation by the tanh method and a variable separated ODE method," *Computers and Mathematics with Applications*, vol. 50, no. 10–12, pp. 1685–1696, 2005.

[12] S. Tang and W. Huang, "Bifurcations of travelling wave solutions for the generalized double sinh-Gordon equation," *Applied Mathematics and Computation*, vol. 189, no. 2, pp. 1774–1781, 2007.

[13] H. Kheiri and A. Jabbari, "Exact solutions for the double sinh-Gordon and the generalized form of the double sinh-Gordon equations by (G'/G)-expansion method," *Turkish Journal of Physics*, vol. 34, no. 2, pp. 73–82, 2010.

[14] A.-M. Wazwaz, "Exact solutions for the generalized sine-Gordon and the generalized sinh-Gordon equations," *Chaos, Solitons and Fractals*, vol. 28, no. 1, pp. 127–135, 2006.

[15] K. Parand, J. A. Rad, and A. Rezaei, "Application of Exp-function method for class of nonlinear PDE's in mathematical physics," *Journal of Applied Mathematics & Informatics*, vol. 29, pp. 763–779, 2011.

[16] A.-M. Wazwaz, "The tanh method: exact solutions of the sine-Gordon and the sinh-Gordon equations," *Applied Mathematics and Computation*, vol. 167, no. 2, pp. 1196–1210, 2005.

[17] J.-H. He and X.-H. Wu, "Exp-function method for nonlinear wave equations," *Chaos, Solitons and Fractals*, vol. 30, no. 3, pp. 700–708, 2006.

Hindawi Publishing Corporation
Abstract and Applied Analysis
Volume 2013, Article ID 278097, 6 pages
http://dx.doi.org/10.1155/2013/278097

Research Article

Optimal Homotopy Asymptotic Method for Solving the Linear Fredholm Integral Equations of the First Kind

Mohammad Almousa and Ahmad Ismail

School of Mathematical Sciences, Universiti Sains Malaysia (USM), 11800 Gelugor, Penang, Malaysia

Correspondence should be addressed to Mohammad Almousa; mohammadalmousa12@yahoo.com

Received 20 April 2013; Accepted 16 June 2013

Academic Editor: Santanu Saha Ray

The aim of this study is to present the use of a semi analytical method called the optimal homotopy asymptotic method (OHAM) for solving the linear Fredholm integral equations of the first kind. Three examples are discussed to show the ability of the method to solve the linear Fredholm integral equations of the first kind. The results indicated that the method is very effective and simple.

1. Introduction

Integral equations of the first kind arise in several applications. These include applications in biology, chemistry, physics, and engineering. In recent years, much work has been carried out by researchers in mathematics and engineering in applying and analyzing novel numerical and semi analytical methods for obtaining solutions of integral equations of the first kind. Among these are the homotopy analysis method [1], operational Tau method [2], homotopy perturbation method [3], Adomian decomposition [3], quadrature rule [4], and automatic augmented Galerkin algorithms [5].

In this study, we develop the optimal homotopy asymptotic method (OHAM), which was proposed by Marinca et al. [6, 7], for solving the linear Fredholm integral equations of the first kind. This method is characterized by it is convergence criteria which are more flexible than other methods.

The general form of the linear Fredholm integral equations of the first kind is

$$f(s) = \int_a^b K(s,t)\, g(t)\, dt, \tag{1}$$

where a and b are constant and the functions $k(s,t)$ and $f(s)$ are known.

It should be noted that OHAM has been applied to the nonlinear Fredholm integral equations of the second kind by [8].

2. Application of OHAM to the Linear Fredholm Integral Equations of the First Kind

In this section, we formulate the optimal homotopy asymptotic method (OHAM) for solving the linear Fredholm integral equations of the first kind following the procedure as outlined in [6, 7] and other papers. Let us consider a form of the linear Fredholm integral equation of the first kind:

$$f(s) - \int_a^b K(x,t)\, g(t)\, dt = 0. \tag{2}$$

Using OHAM, we can obtain a family of equations as follows:

$$\begin{aligned}(1-p)&\left[L(g(s,p)) + f(s)\right] \\ &= H(p)\left[L(g(s,p)) + f(s) + N(g(s,p))\right],\end{aligned} \tag{3}$$

where $p \in [0,1]$ is an embedding parameter, $g(s,p)$ is unknown function, and $H(p)$ is an (nonzero) auxiliary function for $p \neq 0$ and $H(0) = 0$ and given as $H(p) = \sum_{j=1}^{m} c_j p^j$ where c_j, $j = 1, 2, \ldots$, are auxiliary constants, and when $p = 0$ and $p = 1$ it holds that

$$g(s,0) = g_0(s), \qquad g(s,1) = g(s), \tag{4}$$

respectively. For obtaining the approximate solution, we use Taylor's series expansion about p as follows:

$$g\left(s,p,c_j\right)=g_0\left(s\right)+\sum_{m=1}^{\infty}g_m\left(s,c_j\right)p^m,\quad j=1,2,\ldots. \tag{5}$$

If the series (5) convergence occurs when $p=1$, one has

$$g\left(s,1,c_j\right)=g_0\left(s\right)+\sum_{m=1}^{\infty}g_m\left(s,c_j\right),\quad j=1,2,\ldots. \tag{6}$$

Substituting (5) in (3) and equating the coefficients of like powers of p, we get as follows:

$$\begin{aligned}
O\left(p^0\right)&: g_0\left(s\right)=-f\left(s\right),\\
O\left(p^1\right)&: g_1\left(s\right)=-c_1\int_a^b K\left(s,t\right)g_0\left(t\right)dt,\\
O\left(p^2\right)&: g_2\left(s\right)=\left(1+c_1\right)g_1\left(s\right)-c_1\int_a^b K\left(s,t\right)g_1\left(t\right)dt\\
&\quad-c_2\int_a^b K\left(s,t\right)g_0\left(t\right)dt,\\
O\left(p^i\right)&: g_i\left(s\right)=\left(1+c_1\right)g_{i-1}\left(s\right)+\sum_{j=2}^{i-1}c_jg_{i-j}\left(s\right)\\
&\quad-\sum_{k=1}^{i}c_k\int_a^b K\left(s,t\right)g_{i-k}\left(t\right)dt.
\end{aligned} \tag{7}$$

For finding the constants $c_1,c_2,c_3,\ldots$, we can get the result of the mth-order approximations as follows:

$$g^m\left(s,c_j\right)=g_0\left(s\right)+\sum_{k=1}^{m}g_k\left(s,c_j\right),\quad j=1,2,\ldots,m. \tag{8}$$

If we substitute (8) into (1) we obtain the residual equation

$$R\left(s,c_j\right)=L\left(g^m\left(s,c_j\right)\right)+f\left(s\right)-\int_a^b K\left(s,t\right)g^m\left(t,c_j\right)dt. \tag{9}$$

If $R(s,c_j)=0$, then $g^m(s,c_j)$ will be the exact solution. The least squares method can be used to determine $c_1,c_2,c_3,\ldots$. At first we consider the functional

$$J\left(c_j\right)=\int_a^b R^2\left(s,c_j\right)ds. \tag{10}$$

By using Galerkin's method we get the following system:

$$\frac{\partial J}{\partial c_j}=2\int_a^b R\left(s,c_j\right)\frac{\partial R}{\partial c_j}ds, \tag{11}$$

and then minimizing it to obtain the values of $c_1,c_2,\ldots,m$, we have

$$\frac{\partial J}{\partial c_1}=\frac{\partial J}{\partial c_2}=\cdots=\frac{\partial J}{\partial c_m}=0. \tag{12}$$

With these constants, the approximate solution is determined.

3. Numerical Examples and Discussion

In this section, three examples of the linear Fredholm integral equations of the first kind were solved to show the efficiency of the present method. Maple software with long format and double accuracy was used to carry out the computations.

Example 1. We consider the following equation [9]:

$$\frac{1}{2}\sin\left(s\right)=\int_0^{\pi/2}\frac{2}{\pi}\sin\left(s\right)\sin\left(t\right)g\left(t\right)dt, \tag{13}$$

for which the exact solution is $g(s)=\sin(s)$. Applying OHAM to the linear Fredholm integral equation of first kind yields

$$\begin{aligned}
L\left(g\left(s,p\right)\right)&=g\left(s\right),\\
N\left(g\left(s,p\right)\right)&=-\int_0^{\pi/2}\frac{2}{\pi}\sin\left(s\right)\sin\left(t\right)g\left(t\right)dt,\\
f\left(s\right)&=\frac{1}{2}\sin\left(s\right)
\end{aligned} \tag{14}$$

which satisfies

$$\begin{aligned}
&\left(1-p\right)\left[\left(g_0\left(s\right)+pg_1\left(s\right)+p^2g_2\left(s\right)+\cdots\right)+\frac{1}{2}\sin\left(s\right)\right]\\
&=\left(pc_1+p^2c_2+p^3c_3+\cdots\right)\\
&\quad\times\left[\left(g_0\left(s\right)+pg_1\left(s\right)+p^2g_2\left(s\right)+\cdots\right)+\frac{1}{2}\sin\left(s\right)\right.\\
&\quad-\int_0^{\pi/2}\frac{2}{\pi}\sin\left(s\right)\sin\left(t\right)\left(g_0\left(t\right)+pg_1\left(t\right)\right.\\
&\quad\left.\left.+p^2g_2\left(t\right)+\cdots\right)dt\right].
\end{aligned} \tag{15}$$

Now we use (7) to obtain a series of problems:

$$\begin{aligned}
O\left(p^0\right)&: g_0\left(s\right)=-\frac{1}{2}\sin\left(s\right),\\
O\left(p^1\right)&: g_1\left(s\right)=-c_1\int_0^{\pi/2}\frac{2}{\pi}\sin\left(s\right)\sin\left(t\right)g_0\left(t\right)dt,\\
O\left(p^2\right)&: g_2\left(s\right)=\left(1+c_1\right)g_1\left(s\right)\\
&\quad-c_1\int_0^{\pi/2}\frac{2}{\pi}\sin\left(s\right)\sin\left(t\right)g_1\left(t\right)dt\\
&\quad-c_2\int_0^{\pi/2}\frac{2}{\pi}\sin\left(s\right)\sin\left(t\right)g_0\left(t\right)dt.
\end{aligned} \tag{16}$$

Hence the solutions are

$$\begin{aligned}
O\left(p^0\right)&: g_0\left(s\right)=-\frac{1}{2}\sin\left(s\right),\\
O\left(p^1\right)&: g_1\left(s\right)=\frac{1}{4}c_1\sin\left(s\right),\\
O\left(p^2\right)&: g_2\left(s\right)=\frac{1}{4}\left(1+c_1\right)c_1\sin\left(s\right)\\
&\quad-\frac{1}{8}c_1^2\sin\left(s\right)+\frac{1}{4}c_2\sin\left(s\right).
\end{aligned} \tag{17}$$

By substituting $g_0(s)$, $g_1(s)$, and $g_3(s)$ solutions in (6), we obtain

$$\begin{aligned} g(s) = &-\frac{1}{2}\sin(s) + \frac{1}{4}c_1\sin(s) \\ &+ \frac{1}{4}(1+c_1)c_1\sin(s) \\ &- \frac{1}{8}c_1^2\sin(s) + \frac{1}{4}c_2\sin(s). \end{aligned} \tag{18}$$

For the calculations of the constants c_1 and c_2, the use of the technique mentioned in (8)–(12) yields

$$c_1 = 6.000000004, \quad c_2 = -24.00000002. \tag{19}$$

Substituting values in (18), the final solution becomes

$$g(s) = \sin(s). \tag{20}$$

This is the exact solution.

Table 1 shows some numerical results of these solutions calculated according to the present method.

The exact solution, OHAM solution and absolute error of this example are shown in Figure 1.

Example 2. We consider the following equation [10]:

$$\frac{1}{4}s^2 = \int_0^1 \frac{5}{2}s^2t^2 g(t)\,dt, \tag{21}$$

for which the exact solution is $g(s) = (1/2)s^2$. Applying OHAM to the linear Fredholm integral equation of first kind yields

$$\begin{aligned} L(g(s,p)) &= g(s), \\ N(g(s,p)) &= -\int_0^1 \frac{5}{2}s^2t^2 g(t)\,dt, \\ f(s) &= \frac{1}{4}s^2 \end{aligned} \tag{22}$$

which satisfies

$$\begin{aligned} &(1-p)\left[\left(g_0(s) + pg_1(s) + p^2g_2(s) + \cdots\right) + \frac{1}{4}s^2\right] \\ &\quad = \left(pc_1 + p^2c_2 + p^3c_3 + \cdots\right) \\ &\qquad \times \Bigg[\left(g_0(s) + pg_1(s) + p^2g_2(s) + \cdots\right) + \frac{1}{4}s^2 \\ &\qquad\quad - \int_0^1 \frac{5}{2}s^2t^2\left(g_0(t) + pg_1(t) + p^2g_2(t) + \cdots\right)dt\Bigg]. \end{aligned} \tag{23}$$

Table 1: Numerical results of Example 1.

s	g_{exact}	g_{OHAM}	$\lvert g_{\text{exact}} - g_{\text{OHAM}}\rvert$
0	0	0	0
0.1	0.09983341665	0.09983341665	0
0.2	0.1986693308	0.1986693308	0
0.3	0.2955202067	0.2955202067	0
0.4	0.3894183423	0.3894183423	0
0.5	0.4794255386	0.4794255386	0
0.6	0.5646424734	0.5646424734	0
0.7	0.6442176872	0.6442176872	0
0.8	0.7173560909	0.7173560909	0
0.9	0.7833269096	0.7833269096	0
1.0	0.8414709848	0.8414709848	0

Now we use (7) to obtain a series of problems:

$$\begin{aligned} O\left(p^0\right) &: g_0(s) = -\frac{1}{4}s^2, \\ O\left(p^1\right) &: g_1(s) = -c_1\int_0^1 \frac{5}{2}s^2t^2 g_0(t)\,dt, \\ O\left(p^2\right) &: g_2(s) = (1+c_1)\ g_1(s) \\ &\quad -c_1\int_0^1 \frac{5}{2}s^2t^2 g_1(t)\,dt - c_2\int_0^1 \frac{5}{2}s^2t^2 g_0(t)\,dt. \end{aligned} \tag{24}$$

Hence the solutions are

$$\begin{aligned} O\left(p^0\right) &: g_0(s) = -\frac{1}{4}s^2, \\ O\left(p^1\right) &: g_1(s) = \frac{1}{8}c_1s^2, \\ O\left(p^2\right) &: g_2(s) = \frac{1}{8}(1+c_1)c_1s^2 - \frac{1}{16}c_1^2s^2 + \frac{1}{8}c_2s^2. \end{aligned} \tag{25}$$

By substituting $g_0(s)$, $g_1(s)$, and $g_3(s)$ solutions in (6), we obtain

$$g(s) = -\frac{1}{4}s^2 + \frac{1}{8}c_1s^2 + \frac{1}{8}(1+c_1)\ c_1s^2 - \frac{1}{16}c_1^2s^2 + \frac{1}{8}c_2s^2. \tag{26}$$

For the calculations of the constants $c_1$and c_2, the use of the technique mentioned in (8)–(12) yields

$$c_1 = 6, \quad c_2 = -24. \tag{27}$$

Substituting values in (26), the final solution becomes

$$g(s) = \frac{1}{2}s^2. \tag{28}$$

This is the exact solution.

Table 2 shows some numerical results of these solutions calculated according to the present method.

The exact solution, OHAM solution and absolute error of this example are shown in Figure 2.

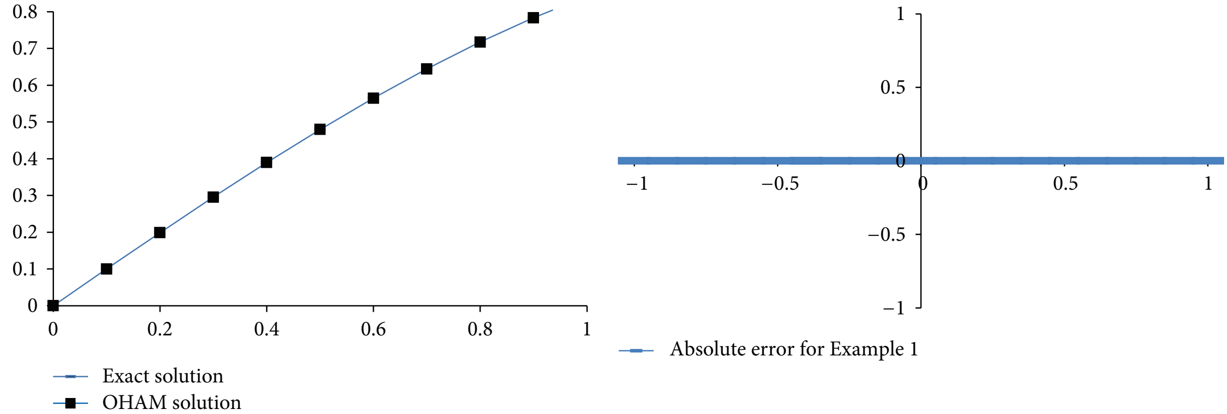

(a) Results for Example 1 (b) Absolute error for Example 1

FIGURE 1

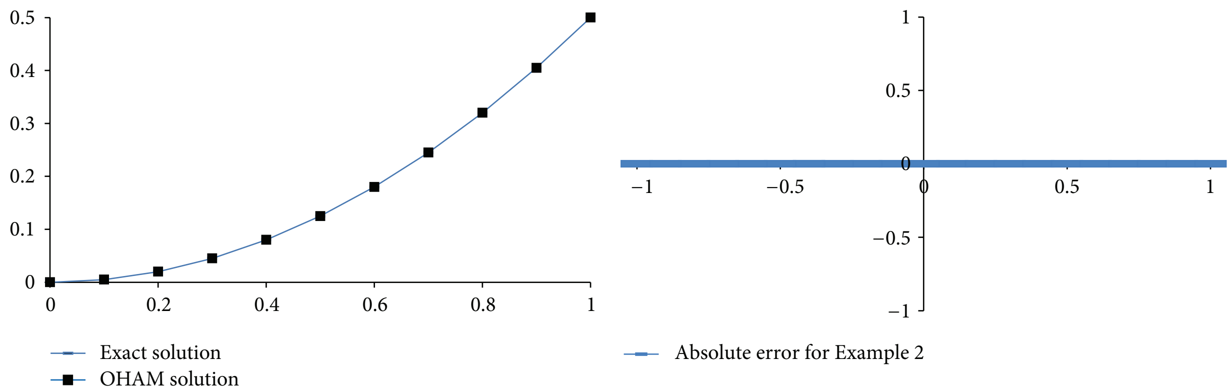

(a) Results for Example 2 (b) Absolute error for Example 2

FIGURE 2

TABLE 2: Numerical results of Example 2.

s	g_{exact}	g_{OHAM}	$\lvert g_{\text{exact}} - g_{\text{OHAM}} \rvert$
0	0	0	0
0.1	0.005	0.005	0
0.2	0.02	0.02	0
0.3	0.045	0.045	0
0.4	0.08	0.08	0
0.5	0.125	0.125	0
0.6	0.18	0.18	0
0.7	0.245	0.245	0
0.8	0.32	0.32	0
0.9	0.405	0.405	0
1.0	0.5	0.5	0

Example 3. We consider the following equation [9]:

$$\frac{1}{2}s^2 = \int_0^1 2s^2 t \; g(t)\, dt, \tag{29}$$

for which the exact solution is $g(s) = (1/2)s^2$. Applying OHAM to the linear Fredholm integral equation of first kind yields

$$\begin{gathered} L(g(s,p)) = g(s), \\ N(g(s,p)) = -\int_0^1 2s^2 t \; g(t)\, dt, \\ f(s) = \frac{1}{2}s^2 \end{gathered} \tag{30}$$

which satisfies

$$\begin{aligned} &(1-p)\left[\left(g_0(s) + pg_1(s) + p^2 g_2(s) + \cdots\right) + \frac{1}{2}s^2\right] \\ &= \left(pc_1 + p^2 c_2 + p^3 c_3 + \cdots\right) \\ &\quad \times \left[\left(g_0(s) + pg_1(s) + p^2 g_2(s) + \cdots\right) + \frac{1}{2}s^2\right. \\ &\quad \left. - \int_0^1 2s^2 t\left(g_0(t) + pg_1(t) + p^2 g_2(t) + \cdots\right) dt\right]. \end{aligned} \tag{31}$$

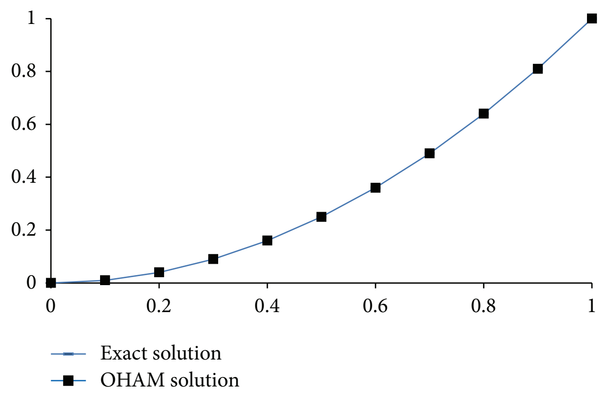

(a) Results for Example 3

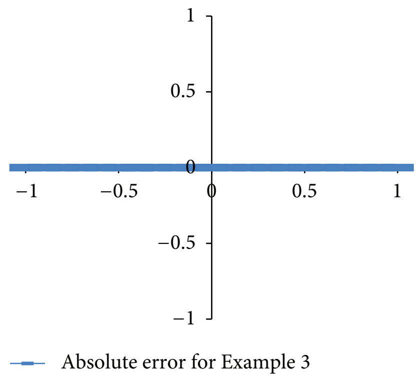

(b) Absolute error for Example 3

FIGURE 3

Now we use (7) to obtain a series of problems:

$$\begin{aligned} O\left(p^0\right) &: g_0(s) = -\frac{1}{2}s^2, \\ O\left(p^1\right) &: g_1(s) = -c_1\int_0^1 2s^2 t g_0(t)\,dt, \\ O\left(p^2\right) &: g_2(s) \\ &= (1+c_1)\,g_1(s) - c_1\int_0^1 2s^2 t g_1(t)\,dt \\ &\quad - c_2\int_0^1 2s^2 t g_0(t)\,dt. \end{aligned} \tag{32}$$

Hence the solutions are

$$\begin{aligned} O\left(p^0\right) &: g_0(s) = -\frac{1}{2}s^2, \\ O\left(p^1\right) &: g_1(s) = \frac{1}{4}c_1 s^2, \\ O\left(p^2\right) &: g_2(s) = \frac{1}{4}(1+c_1)\,c_1 s^2 - \frac{1}{8}c_1^2 s^2 + \frac{1}{4}c_2 s^2. \end{aligned} \tag{33}$$

By substituting $g_0(s)$, $g_1(s)$, and $g_3(s)$ solutions in (6), we obtain

$$\begin{aligned} g(s) = &-\frac{1}{2}s^2 + \frac{1}{4}c_1 s^2 + \frac{1}{4}(1+c_1)\,c_1 s^2 \\ &- \frac{1}{8}c_1^2 s^2 + \frac{1}{4}c_2 s^2. \end{aligned} \tag{34}$$

For the calculations of the constants c_1 and c_2, the use of the technique mentioned in (8)–(12) yields

$$c_1 = 6, \quad c_2 = -24. \tag{35}$$

Substituting values in (34), the final solution becomes

$$g(s) = s^2. \tag{36}$$

This is the exact solution.

TABLE 3: Numerical results of Example 3.

s	g_{exact}	g_{OHAM}	$\lvert g_{\text{exact}} - g_{\text{OHAM}}\rvert$
0	0	0	0
0.1	0.01	0.01	0
0.2	0.04	0.04	0
0.3	0.09	0.09	0
0.4	0.16	0.16	0
0.5	0.25	0.25	0
0.6	0.36	0.36	0
0.7	0.49	0.49	0
0.8	0.64	0.64	0
0.9	0.81	0.81	0
1.0	1.0	1.0	0

Table 3 shows some numerical results of these solutions calculated according to the present method.

The exact solution, OHAM solution and absolute error of this example are shown in Figure 3.

4. Conclusions

In this paper, we presented the application of the OHAM in solving the linear Fredholm integral equations of the first kind. This method was tested on three different examples. This method proved to be an accurate and efficient technique for finding approximate solutions for the linear Fredholm integral equations of the first kind.

References

[1] A. Adawi, F. Awawdeh, and H. Jaradat, "A numerical method for solving linear integral equations," *International Journal of Contemporary Mathematical Sciences*, vol. 4, no. 9–12, pp. 485–496, 2009.

[2] M. H. AliAbadi and S. Shahmorad, "A matrix formulation of the tau method for Fredholm and Volterra linear integro-differential equations," *The Korean Journal of Computational & Applied Mathematics*, vol. 9, no. 2, pp. 497–507, 2002.

[3] S. Abbasbandy, "Numerical solutions of the integral equations: homotopy perturbation method and Adomian's decomposition method," *Applied Mathematics and Computation*, vol. 173, no. 1, pp. 493–500, 2006.

[4] F. Mirzaee, "Numerical solution for Volterra integral equations of the first kind via quadrature rule," *Applied Mathematical Sciences*, vol. 6, no. 17–20, pp. 969–974, 2012.

[5] S. Abbasbandy and E. Babolian, "Automatic augmented Galerkin algorithms for linear first kind integral equations: non-singular and weak-singular kernels," *Bulletin of the Iranian Mathematical Society*, vol. 21, no. 1, pp. 35–62, 1995.

[6] V. Marinca and N. Herişanu, "Application of optimal homotopy asymptotic method for solving nonlinear equations arising in heat transfer," *International Communications in Heat and Mass Transfer*, vol. 35, no. 6, pp. 710–715, 2008.

[7] N. Herişanu, V. Marinca, T. Dordea, and G. Madescu, "A new analytical approach to nonlinear vibration of an electrical machine," *Proceedings of the Romanian Academy. Series A*, vol. 9, no. 3, pp. 229–236, 2008.

[8] M. S. Hashmi, N. Khan, and S. Iqbal, "Optimal homotopy asymptotic method for solving nonlinear Fredholm integral equations of second kind," *Applied Mathematics and Computation*, vol. 218, no. 22, pp. 10982–10989, 2012.

[9] A. Sulaiman and I. Hassan, "Successive approximation method (S.A.M.) for solving integral equation of the first kind with symmetric kernel," *Journal of Education and Sciences*, vol. 21, no. 4, pp. 149–159, 2008.

[10] A. J. Mohammed and J. I. Mustafa, "Construction of a new technique in Aitken extrapolation method for solving Fredholm integral equation of the first kind with iterated kernel," *Journal of Education and Sciences*, vol. 21, no. 2, pp. 143–149, 2008.

Hindawi Publishing Corporation
Abstract and Applied Analysis
Volume 2013, Article ID 929478, 10 pages
http://dx.doi.org/10.1155/2013/929478

Research Article

Numerical Study of Two-Dimensional Volterra Integral Equations by RDTM and Comparison with DTM

Reza Abazari[1] and Adem Kılıçman[2]

[1] *Young Researchers and Elite Club, Ardabil Branch, Islamic Azad University, Ardabil, Iran*
[2] *Department of Mathematics and Institute of Mathematical Research, University Putra Malaysia (UPM), 43400 Serdang, Malaysia*

Correspondence should be addressed to Reza Abazari; abazari-r@uma.ac.ir

Received 17 April 2013; Accepted 10 June 2013

Academic Editor: Santanu Saha Ray

The two-dimensional Volterra integral equations are solved using more recent semianalytic method, the reduced differential transform method (the so-called RDTM), and compared with the differential transform method (DTM). The concepts of DTM and RDTM are briefly explained, and their application to the two-dimensional Volterra integral equations is studied. The results obtained by DTM and RDTM together are compared with exact solution. As an important result, it is depicted that the RDTM results are more accurate in comparison with those obtained by DTM applied to the same Volterra integral equations. The numerical results reveal that the RDTM is very effective, convenient, and quite accurate compared to the other kind of nonlinear integral equations. It is predicted that the RDTM can be found widely applicable in engineering sciences.

1. Introduction

Mathematical modeling of many problems in science, engineering, physics, and other disciplines leads to linear and nonlinear integrodifferential equations (IDE). The great use of mathematical models including integrodifferential equations is one of the main reasons obtaining the solutions of this kind of problems (see, e.g., [1–3] and the references therein). So, it is very important to get some information about the analytical solutions of these problems because these solutions give significant information about the character of the modeled event. But, in some cases, it is more difficult to obtain analytical solutions of these models. These are usually difficult to solve analytically, and in many cases the solution must be approximated. To approximate the solutions of these models, in recent years several numerical approaches have been proposed.

In this paper, we consider the following Volterra type of integral equation [4, 5]:

$$u(x,t) - \int_0^t \int_0^x K(x,t,y,z,u(y,z))\,dy\,dz = f(x,t), \quad (1)$$

where K and f are continuous functions and K has the following form:

$$K(x,t,y,z,u(y,z)) = \sum_{i=0}^{m} p_i(x,t)\,q_i(y,z,u(y,z)). \quad (2)$$

The one-dimensional Volterra type of integral equation has been solved by many numerical methods, such as collocation methods [1], Taylor-series expansion methods [2], Gauss-type quadratures method [3], spectral methods [6], Chebyshev polynomial method [7], Tau method [8], sine-cosine wavelets method [9], Monte Carlo method [10], and Haar functions method [11].

But in two-dimensional cases, a small amount of work has been done (see, e.g., [12–14]). Very recently, Tari et al. in [4] employed the classic differential transform method for solving two-dimensional Volterra type of integral equations (1), and Jang in [5] improved the proofs of the presented theorems by Tari et al. in [4]. They derived fundamental properties of the differential transforms of some kernel functions K in Volterra integral equations.

However, the classic differential transform method, introduced by Zhou [15], is based on the definition of the differential transform, which is a Taylor series. Thus, it requires a cumbersome calculation to obtain the basic properties of the differential transforms. Some of DTM applications are mentioned in [16–21].

Recently, Keskin and Oturanç introduced a reduced form of DTM as reduced DTM (RDTM) and applied it to approximate some PDE [22] and factional PDEs [23]. More recently, Abazari and Ganji [24] extended RDTM to study the partial differential equation with proportional delay in t and shrinking in x and showed that, as a special advantage of RDTM rather than DTM, the reduced differential transform recursive equations produce exactly all the Poisson series coefficients of solutions based on the initial condition as weighted function, whereas the differential transform recursive equations produce exactly all the Taylor series coefficients of solutions.

Here, we suggest the RDTM, for the approximating of the solutions of the two-dimensional Volterra integral equations (1) with the same kernel functions in [4, 5]. In order to demonstrate the effectiveness of the RDTM, the illustrative examples for the same kernel function of references [5] are presented. These examples show that the RDTM produces exactly all the Poisson series coefficients (see Remark 5) of the exact solutions, whereas, the classic DTM produces exactly all the Taylor series coefficients of the exact solutions. As an important result, notwithstanding the simplicity and robustness of RDTM, it is depicted that the RDTM results are more accurate in comparison with those obtained by classic DTM.

2. Basic Definitions

With reference to the articles [16–21], the basic definitions of two-dimensional differential transform method (DTM) and their reduced form (RDTM) are introduced in the following two subsections, respectively.

2.1. Two-Dimensional DTM. Consider a function of two variables $w(x,t)$, and suppose that it can be represented as a product of two single-variable functions, that is, $w(x,t) = f(x)g(t)$. On the basis of the properties of the one-dimensional differential transform, the function $w(x,t)$ can be represented as

$$w(x,t) = \sum_{i=0}^{\infty} F(i)\, x^i \sum_{j=0}^{\infty} G(j)\, t^j = \sum_{i=0}^{\infty}\sum_{j=0}^{\infty} W(i,j)\, x^i t^j, \quad (3)$$

where $W(i,j) = F(i)G(j)$ is called the spectrum of $w(x,t)$.

The basic definitions and operations for two-dimensional differential transform are introduced as follows.

Definition 1. If $w(x,t)$ is analytic and continuously differentiable with respect to time t in the domain of interest, then

$$W(m,n) = \frac{1}{m!n!}\left[\frac{\partial^{m+n}}{\partial x^m \partial t^n} w(x,t)\right]_{\substack{x=x_0\\ t=t_0}}, \quad (4)$$

where the spectrum function $W(m,n)$ is the transformed function, which is also called T-function in brief.

The differential inverse transform of $W(k,h)$ is defined as

$$w(x,t) = \sum_{m=0}^{\infty}\sum_{n=0}^{\infty} W(m,n)\,(x-x_0)^m (t-t_0)^n. \quad (5)$$

Combining (4) and (5), it can be obtained that

$$w(x,t) = \sum_{m=0}^{\infty}\sum_{n=0}^{\infty} \frac{1}{m!n!}\left[\frac{\partial^{m+n}}{\partial x^m \partial t^n} w(x,t)\right]_{\substack{x=x_0\\ t=t_0}} \times (x-x_0)^m (t-t_0)^n. \quad (6)$$

When (x_0, t_0) are taken as $(0,0)$, then (5) can be expressed as

$$w(x,t) = \sum_{m=0}^{\infty}\sum_{n=0}^{\infty} W(m,n)\, x^m t^n. \quad (7)$$

In real applications, the function $w(x,t)$ is represented by a finite series of (7) that can be written as

$$w_{M,N}(x,t) = \sum_{m=0}^{M}\sum_{n=0}^{N} W(m,n)\, x^m t^n + R_{M,N}(x,t), \quad (8)$$

and (7) implies that $R_{M,N}(x,t) = \sum_{m=M+1}^{\infty}\sum_{n=N+1}^{\infty} W(m,n) x^m t^n$ is negligibly small. Usually, the values of M and N are decided by convergency of the series coefficients.

From the above definitions, it can be found that the concept of the two-dimensional differential transform is derived from the two-dimensional Taylor series expansion. With (4) and (5), the fundamental mathematical operations performed using the two-dimensional differential transform may be readily obtained, and these are listed in Table 1. (See [4, 5, 15, 16].)

Recently, Jang [5] extended the two-dimensional DTM on (1) as follows.

Theorem 2. *Assume that $U(m,n)$, $V(m,n)$, $H(m,n)$, and $G(m,n)$ are the differential transforms of the functions $u(x,t)$, $v(x,t)$, $h(x,t)$, and $g(x,t)$, respectively; then we have the following:*

(a) *if $g(x,t) = \int_0^t \int_0^x u(y,z)\,dy\,dz$, then*

$$G(m,0) = G(0,n) = 0, \quad m,n = 0,1,\ldots,$$
$$G(m,n) = \frac{1}{mn} U(m-1,n-1), \quad m,n = 1,2,\ldots, \quad (9)$$

Table 1: The fundamental operations of two-dimensional differential transform method.

Original function	Transformed function
$w(x,t) = u(x,t) \pm v(x,t)$	$W(m,n) = U(m,n) \pm V(m,n)$
$w(x,t) = c\, u(x,t)$	$W(m,n) = c\, U(m,n)$
$w(x,t) = \dfrac{\partial}{\partial x} u(x,t)$	$W(m,n) = (m+1)U(m+1,n)$
$w(x,t) = \dfrac{\partial}{\partial t} u(x,t)$	$W(m,n) = (m+1)U(m,n+1)$
$w(x,t) = \dfrac{\partial^{r+s}}{\partial x^r \partial t^s} u(x,t)$	$W(m,n) = \dfrac{(m+r)!(n+s)!}{m!n!} U(m+r,n+s)$
$w(x,t) = u(x,t)v(x,t)$	$W(m,n) = \sum_{r=0}^{m} \sum_{s=0}^{n} U(r,n-s)V(m-r,s)$
$w(x,t) = x^{\alpha} t^{\beta}$	$W(m,n) = \delta(m-\alpha, n-\beta) = \begin{cases} 1 & m=\alpha, n=\beta \\ 0 & \text{otherwise} \end{cases}$

(b) *if* $g(x,t) = \int_0^t \int_0^x u(y,z)v(y,z)dy\,dz$, *then*

$$G(m,0) = G(0,n) = 0, \quad m,n = 0,1,\ldots,$$
$$G(m,n) = \frac{1}{mn}\sum_{\ell=0}^{n-1}\sum_{k=0}^{m-1} U(k,\ell)\, V(m-k-1, n-\ell-1), \quad m,n = 1,2,\ldots, \tag{10}$$

(c) *if* $g(x,t) = h(x,t) \int_0^t \int_0^x u(y,z)dy\,dz$, *then*

$$G(m,0) = G(0,n) = 0, \quad m,n = 0,1,\ldots,$$
$$G(m,n) = \frac{1}{mn}\sum_{\ell=0}^{n-1}\sum_{k=0}^{m-1} H(k,\ell)\, \frac{V(m-k-1, n-\ell-1)}{(m-k)(n-\ell)}, \quad m,n = 1,2,\ldots. \tag{11}$$

Proof. See [5]. □

Theorem 3. *Assume that* $U(m,n)$, $V(m,n)$, *and* $G(m,n)$ *are the differential transforms of the functions* $u(x,t)$, $v(x,t)$, *and* $g(x,t)$, *respectively; then we have the following:*

(a) *if* $g(x,t) = \int_0^t \int_0^x (u(y,z)/v(y,z))dy\,dz$, *then*

$$G(m,0) = G(0,n) = 0, \quad m,n = 0,1,\ldots,$$
$$\sum_{\ell=0}^{n-1}\sum_{k=0}^{m-1} (m-k+1)(n-\ell+1)\, V(k,\ell)\, G(m-k+1, n-\ell+1) = U(m,n), \tag{12}$$

(b) *if* $g(x,t) = (1/v(x,t)) \int_0^t \int_0^x u(y,z)dy\,dz$, *then*

$$G(m,0) = G(0,n) = 0, \quad m,n = 0,1,\ldots,$$
$$\sum_{\ell=0}^{n-1}\sum_{k=0}^{m-1} V(k,\ell)\, G(m-k+1, n-\ell+1) = \frac{1}{(m+1)(n+1)} U(m,n). \tag{13}$$

Proof. See [5]. □

2.2. Two-Dimensional Reduced DTM (RDTM). Consider a function of two variables $w(x,t)$, and suppose that it can be represented as a product of two single-variable functions, that is, $w(x,t) = f(x)g(t)$. Based on the properties of one-dimensional differential transform, the function $w(x,t)$ can be represented as

$$w(x,t) = \sum_{i=0}^{\infty} F(i)\, x^i \sum_{j=0}^{\infty} G(j)\, t^j = \sum_{i=0}^{\infty}\sum_{j=0}^{\infty} W(i,j)\, x^i t^j, \tag{14}$$

where $W(i,j) = F(i)G(j)$ is called the spectrum of $w(x,t)$.

Remark 4. The poisson function series generates a multivariate Taylor series expansion of the input expression w, with respect to the variables X, to order n, using the variable weights W.

Remark 5. The relationship introduced in (14) is the poisson series form of the input expression $w(x,t)$, with respect to the variables x and t, to order N, using the variable weights $W_k(x)$.

Similarly on previous section, the basic definitions of two-differential reduced differential transformation are introduced as follows.

Definition 6. If $w(x,t)$ is analytical function in the domain of interest, then the spectrum function

$$W_k(x) = \frac{1}{k!}\left[\frac{\partial^k}{\partial t^k} w(x,t)\right]_{t=t_0} \quad (15)$$

is the reduced transformed function of $w(x,t)$.

Similarly on previous sections, the lowercase $w(x,t)$ respects the original function while the uppercase $W_k(x)$ stands for the reduced transformed function. The differential inverse transform of $W_k(x)$ is defined as

$$w(x,t) = \sum_{k=0}^{\infty} W_k(x)(t-t_0)^k. \quad (16)$$

Combining (15) and (16), it can be obtained that

$$w(x,t) = \sum_{k=0}^{\infty}\frac{1}{k!}\left[\frac{\partial^k}{\partial t^k} w(x,t)\right]_{t=t_0}(t-t_0)^k. \quad (17)$$

In real applications, the function $w(x,t)$ is represented by a finite series of (16), around $t_0 = 0$, and can be written as

$$w_n(x,t) = \sum_{k=0}^{n} W_k(x)t^k + R_n(x,t), \quad (18)$$

and (18) implies that $R_n(x,t) = \sum_{k=n+1}^{\infty} W_k(x)t^k$ is negligibly small. Usually, the values of n and m are decided by convergency of the series coefficients. From the above proposition, it can be found that the concept of the reduced two-dimensional differential transform is derived from the two-dimensional differential transform method. With (15) and (16), the fundamental mathematical operations performed by reduced two-dimensional differential transform can readily be obtained and listed in Table 2.

Similarly on previous subsection, we can extend the RDTM on Volterra integral equations (1) as follow.

Theorem 7. *Assume that $U_k(x)$, $V_k(x)$, $H_k(x)$, and $W_k(x)$ are the reduced differential transforms of the functions $u(x,t)$, $v(x,t)$, $h(x,t)$, and $w(x,t)$, respectively; then we have the following:*

(a) *if $w(x,t) = \int_{t_0}^{t}\int_{x_0}^{x} u(y,z)v(y,z)dy\,dz$, then*

$$W_k(x) = \frac{1}{k}\int_{x_0}^{x}\left(\sum_{r=0}^{k-1} U_r(y)V_{k-r-1}(y)\right)dy, \quad k = 1, 2, \ldots, \quad (19)$$

(b) *if $w(x,t) = h(x,t)\int_{t_0}^{t}\int_{x_0}^{x} u(y,z)dy\,dz$, then*

$$W_k(x) = \sum_{r=0}^{k}\frac{1}{k-r}H_r(x)\int_{x_0}^{x} U_{k-r-1}(y)\,dy, \quad k = 1, 2, \ldots. \quad (20)$$

Proof. (a) According to the fundamental operations of two-dimensional RDTM listed in Table 2 and from Leibnitz formula, we get

$$\begin{aligned}\frac{\partial^k}{\partial t^k} w(x,t) &= \frac{\partial^k}{\partial t^k}\left(\int_{t_0}^{t}\int_{x_0}^{x} u(y,z)v(y,z)\,dy\,dz\right)\\ &= \int_{x_0}^{x}\frac{\partial^{k-1}}{\partial t^{k-1}}\{u(y,t)v(y,t)\}\,dy\\ &= \int_{x_0}^{x}\left\{\sum_{r=0}^{k-1}\binom{k-1}{r}\frac{\partial^r}{\partial t^r}u(y,t)\right.\\ &\qquad\left.\times\frac{\partial^{k-r-1}}{\partial t^{k-r-1}}v(y,t)\right\}dy,\end{aligned} \quad (21)$$

therefore

$$\begin{aligned}\left[\frac{\partial^k}{\partial t^k} w(x,t)\right]_{t=t_0} &= \int_{x_0}^{x}\left\{\sum_{r=0}^{k-1}\binom{k-1}{r} r!\,(k-r-1)!\right.\\ &\qquad\left.\times U_r(y)V_{k-r-1}(y)\right\}dy\\ &= (k-1)!\int_{x_0}^{x}\left\{\sum_{r=0}^{k-1}U_r(y)V_{k-r-1}(y)\right\}dy,\end{aligned} \quad (22)$$

and then, from using (15), for $k = 1, 2, \ldots$, we get

$$W_k(x) = \frac{1}{k}\int_{x_0}^{x}\left\{\sum_{r=0}^{k-1}U_r(y)V_{k-r-1}(y)\right\}dy. \quad (23)$$

(b) Analogous to part (a), we get

$$\begin{aligned}\frac{\partial^k}{\partial t^k} w(x,t) &= \frac{\partial^k}{\partial t^k}\left(h(x,t)\int_{t_0}^{t}\int_{x_0}^{x} u(y,z)\,dy\,dz\right)\\ &= \sum_{r=0}^{k}\binom{k}{r}\frac{\partial^r}{\partial t^r}h(x,t)\int_{x_0}^{x}\frac{\partial^{k-r-1}}{\partial t^{k-r-1}}u(y,t)\,dy,\end{aligned} \quad (24)$$

TABLE 2: The fundamental operations of two-dimensional RDTM.

Original function	Reduced transformed function
$w(x,t) = u(x,t) \pm v(x,t)$	$W_k(x) = U_k(x) \pm V_k(x)$
$w(x,t) = \dfrac{\partial}{\partial x}u(x,t)$	$W_k(x) = \dfrac{\partial}{\partial x}U_k(x)$
$w(x,t) = \dfrac{\partial}{\partial t}u(x,t)$	$W_k(x) = (k+1)U_{k+1}(x)$
$w(x,t) = \dfrac{\partial^{r+s}}{\partial x^r \partial t^s}u(x,t)$	$W_k(x) = \dfrac{(k+s)!}{k!}\dfrac{\partial^r}{\partial x^r}U_{k+s}(x)$
$w(x,t) = u(x,t)v(x,t)$	$W_k(x) = \sum_{r=0}^{k} U_r(x)V_{k-r}(x)$
$w(x,t) = x^m t^n$	$W_k(x) = x^m\delta(k-n) = \begin{cases} x^m & k=n \\ 0 & \text{otherwise} \end{cases}$

therefore

$$\left[\frac{\partial^k}{\partial t^k} w(x,t)\right]_{t=t_0} = \sum_{r=0}^{k}\binom{k}{r} r!\,(k-r-1)!\,H_r(x) \times \int_{x_0}^{x} U_{k-r-1}(y)\,dy, = \sum_{r=0}^{k}\frac{k!}{k-r}H_r(x)\int_{x_0}^{x} U_{k-r-1}(y)\,dy, \tag{25}$$

and then from using (15), for $k = 1, 2, \ldots$, we get

$$W_k(x) = \sum_{r=0}^{k}\frac{1}{k-r}H_r(x)\int_{x_0}^{x} U_{k-r-1}(y)\,dy. \tag{26}$$

□

Theorem 8. *Assume that $U_k(x)$, $V_k(x)$, and $W_k(x)$ are the reduced differential transforms of the functions $u(x,t)$, $v(x,t)$, and $w(x,t)$, respectively; then we have the following:*

(a) *if $w(x,t) = \int_{t_0}^{t}\int_{x_0}^{x}(u(y,z)/v(y,z))\,dy\,dz$, then*

$$U_k(x) = \sum_{r=0}^{k}(r+1)\frac{\partial W_{r+1}(x)}{\partial x}V_{k-r}(y), \quad k = 0,1,2,\ldots, \tag{27}$$

(b) *if $w(x,t) = (1/v(x,t))\int_{t_0}^{t}\int_{x_0}^{x}u(y,z)\,dy\,dz$, then*

$$k\sum_{r=0}^{k}W_r(x)V_{k-r}(x) = \int_{x_0}^{x}U_{k-1}(y)\,dy, \quad k = 1,2,\ldots. \tag{28}$$

Proof. (a) By following the same manner as in the Theorem 7, we get

$$u(x,t) = \frac{\partial^2 w(x,t)}{\partial x\,\partial t}v(x,t), \tag{29}$$

then

$$\frac{\partial^k}{\partial t^k}u(x,t) = \frac{\partial^k}{\partial t^k}\left(\frac{\partial^2 w(x,t)}{\partial x\,\partial t}v(x,t)\right) = \sum_{r=0}^{k}\binom{k}{r}\frac{\partial^{r+2}}{\partial x\,\partial t^{r+1}}w(x,t)\,\frac{\partial^{k-r}}{\partial t^{k-r}}v(y,t), \tag{30}$$

therefore

$$k!U_k(x) = \sum_{r=0}^{k}\binom{k}{r}(r+1)!\,(k-r)!\frac{\partial W_{r+1}}{\partial x}(x)\,V_{k-r}(x), \tag{31}$$

and then from using (15), for $k = 0, 1, 2, \ldots$, we get

$$U_k(x) = \sum_{r=0}^{k}(r+1)\frac{\partial W_{r+1}}{\partial x}(x)\,V_{k-r}(x). \tag{32}$$

(b) Analogous to part (a), we get

$$w(x,t)\,v(x,t) = \int_{t_0}^{t}\int_{x_0}^{x}u(y,z)\,dy\,dz, \tag{33}$$

then

$$\frac{\partial^k}{\partial t^k}\{w(x,t)\,v(x,t)\} = \int_{x_0}^{x}\frac{\partial^{k-1}}{\partial t^{k-1}}u(y,t)\,dy, \tag{34}$$

therefore

$$\sum_{r=0}^{k}\binom{k}{r}\frac{\partial^r}{\partial t^r}w(x,t)\,\frac{\partial^{k-r}}{\partial t^{k-r}}v(x,t) = \int_{x_0}^{x}\frac{\partial^{k-1}}{\partial t^{k-1}}u(y,t)\,dy, \tag{35}$$

and then from using (15), for $k = 1, 2, \ldots$, we get

$$k!\sum_{r=0}^{k} W_r(x) V_{k-r}(x) = (k-1)! \int_{x_0}^{x} U_{k-1}(y)\, dy, \quad (36)$$

and therefore

$$k\sum_{r=0}^{k} W_r(x) V_{k-r}(x) = \int_{x_0}^{x} U_{k-1}(y)\, dy. \quad (37)$$

□

3. Numerical Results of DTM and RDTM

In this section, the reduced differential transform technique is described to solve a class of Volterra integral equations (1) with kernel functions of (2). In order to demonstrate the effectiveness of the RDTM, the illustrative examples for the same kernel function of [5] are presented. In each example, the numerical results of DTM, RDTM, and their comparisons with exact solution are given in separate tables. The results of the test examples show that the RDTM results are more powerful than DTM results.

Example 9. In the first example, consider the following two-dimensional Volterra integral equation [5]:

$$\begin{aligned} u(x,t) &- \int_0^t \int_0^x \frac{u(y,z)}{2+\sin(y+z)} dy\, dz \\ &= (x-t)(4+2\sin(x+t)-xt). \end{aligned} \quad (38)$$

(a) *DTM*: Jang [5] solved this equation by using DTM and obtained the following five-term DTM solution:

$$\begin{aligned} u_{5,5}(x,t) &= \left(4x+2x^2-\frac{x^4}{3}\right)+\left(-4-\frac{2x^3}{3}+\frac{x^5}{15}\right)t \\ &+\left(-2+\frac{x^4}{12}\right)t^2+\left(\frac{2x}{3}-\frac{x^5}{180}\right)t^3 \\ &+\left(\frac{1}{3}-\frac{x^2}{12}\right)t^4+\left(-\frac{x}{15}+\frac{x^3}{180}\right)t^5. \end{aligned} \quad (39)$$

(b) *RDTM*: from Volterra integral equation (38), it is easy to see that the $u(x,0) = x(4+2\sin(x))$, and therefore RDTM version is

$$U_0(x) = x(4+2\sin(x)). \quad (40)$$

By applying the RDTM properties listed in Theorem 8, on Volterra integral equation (38), for $k = 0, 1, 2, \ldots$, we get

$$\begin{aligned} U_k(x) &= \sum_{r=0}^{k} (r+1) \frac{d}{dx} \\ &\times \Bigg\{ U_{r+1}(x) \\ &\quad - \sum_{\ell=0}^{r+1} (x\delta_{\ell,0}-\delta_{\ell,1}) \\ &\quad \times \left[4\delta_{r+1-\ell,0} + \frac{2\sin(x+((r+1-\ell)\pi/2))}{(r+1-\ell)!} \right. \\ &\quad \left. -x\delta_{r+1-\ell,1} \right] \Bigg\} \\ &\times \left\{ 2\delta_{k-r,0} + \sin\left(x+\frac{(k-r)\pi}{2}\right) \right\}, \end{aligned} \quad (41)$$

where $U_i(x)$ is the reduced differential transform of $u(x,t)$. After expanding the RDTM recurrence equations (41), with initial value of (40), for $k = 0, 1, 2, 3, 4$, the first five terms of $U_k(x)$ are obtained as follows:

$$\begin{aligned} U_1(x) &= 2x\cos(x) - 4 - 2\sin(x), \\ U_2(x) &= -x\sin(x) - 2\cos(x), \\ U_3(x) &= \sin(x) - \frac{1}{3}x\cos(x), \\ U_4(x) &= \frac{1}{3}\cos(x) + \frac{1}{12}x\sin(x), \\ U_5(x) &= \frac{1}{60}x\cos(x) - \frac{1}{12}\sin(x). \end{aligned} \quad (42)$$

In the same manner, the rest of the components can be obtained by using the recursive equations (41). Substituting the quantities (41) in (18), the approximation solution of Volterra integral equation (38) in the Poisson series form is

$$\begin{aligned} U_5(x,t) &= 2x(2+\sin(x)) + (2x\cos(x)-4-2\sin(x))t \\ &+(-x\sin(x)-2\cos(x))t^2+\left(\sin(x)-\frac{x\cos(x)}{3}\right)t^3 \\ &+\left(\frac{\cos(x)}{3}+\frac{x\sin(x)}{12}\right)t^4 \\ &+\left(\frac{x\cos(x)}{60}-\frac{\sin(x)}{12}\right)t^5, \end{aligned} \quad (43)$$

which is the same as the first five terms of the Poisson series of the exact solution $u(x,t) = 2(x-t)(2+\sin(x+t))$.

TABLE 3: Comparisons of the exact solution $u(x,t) = 2(x-t)(2+\sin(x+t))$, with $U_{5,5}(x,t)$ obtained by classic DTM [5] and $U_5(x,t)$ obtained by RDTM at some test points (x,t) in Example 9.

x	t	$u(x,t)$	Classic DTM [5]		Reduced DTM	
			$U_{5,5}(x,t)$	$\lvert u(x,t)-U_{5,5}(x,t)\rvert$	$U_5(x,t)$	$\lvert u(x,t)-U_5(x,t)\rvert$
0.2	0.1	+0.4591040413	+0.4591115320	7.4906677321$e-06$	+0.4591040577	1.6393507773$e-08$
	0.4	−1.0258569894	−1.0257575253	9.9464024681$e-05$	−1.0257906614	6.6327927673$e-05$
	0.7	−2.7833269096	−2.7813944067	1.9325029608$e-03$	−2.7814532650	1.8736446239$e-03$
	1	−4.6912625375	−4.6755840000	1.5678537548$e-02$	−4.6756686352	1.5593902330$e-02$
0.5	0.1	+2.0517139787	+2.0516661667	4.7812049361$e-05$	+2.0517139939	1.5172903822$e-08$
	0.4	+0.5566653819	+0.5573213333	6.5595140784$e-04$	+0.5567258924	6.0510490391$e-05$
	0.7	−1.1728156344	−1.1698785000	2.9371343869$e-03$	−1.1711316158	1.6840186272$e-03$
	1	−2.9974949866	−2.9817708333	1.5724153271$e-02$	−2.9836944470	1.3800539634$e-02$
0.8	0.1	+3.8966576735	+3.8929643413	3.6933321451$e-03$	+3.8966576865	1.3025739598$e-08$
	0.4	+2.3456312688	+2.3439851520	1.6461167738$e-03$	+2.3456822669	5.0998086549$e-05$
	0.7	+0.5994989973	+0.6014245867	1.9255893459$e-03$	+0.6008906123	1.3916149372$e-03$
	1	−1.1895390524	−1.1754026667	1.4136385685$e-02$	−1.1783733000	1.1165752332$e-02$
1	0.1	+5.2041732481	+5.1881855000	1.5987748111$e-02$	+5.2041732592	1.1127633925$e-08$
	0.4	+3.5825396760	+3.5680853333	1.4454342653$e-02$	+3.5825824990	4.2822997450$e-05$
	0.7	+1.7949988863	+1.7840151667	1.0983719605$e-02$	+1.7961453619	1.1464756153$e-03$
	1	+0.0000000000	−0.0000000000	−0.0000000000	+0.0090050384	9.0050384311$e-03$

The numerical results obtained with RDTM are presented in Table 3, in comparison with the classic DTM solution of [5] and the exact solution $u(x,t) = 2(x-t)(2+\sin(x+t))$, for some points of the intervals $0 \le x \le 1$ and $0 \le t \le 1$.

Example 10. In the second example, consider the following two-dimensional Volterra integral equation [5]:

$$u(x,t) - 2\int_0^t \int_0^x e^{y-z} u(y,z)\,dy\,dz = \sin(x+t)\left(e^{x-t}+1\right) - e^{-t}\sin(t) - e^{x}\sin(x). \tag{44}$$

(a) *DTM*: the approximation solution of this equation is also obtained by DTM in [5] as follows:

$$\begin{aligned} u_{5,5}(x,t) &= \left(x - \frac{x^3}{6} + \frac{x^5}{120}\right) + \left(1 - \frac{x^2}{2} + \frac{x^4}{24}\right)t \\ &\quad + \left(-\frac{x}{2} + \frac{x^3}{24} - \frac{x^5}{240}\right)t^2 + \left(-\frac{1}{6} + \frac{x^2}{12} - \frac{x^4}{144}\right)t^3 \\ &\quad + \left(\frac{x}{24} - \frac{x^3}{144} + \frac{x^5}{2880}\right)t^4 \\ &\quad + \left(\frac{1}{120} - \frac{x^2}{240} + \frac{x^4}{2880}\right)t^5. \end{aligned} \tag{45}$$

(b) *RDTM*: it is easy to see that the $u(x,0) = \sin(x)$, and therefore RDTM version is

$$U_0(x) = \sin(x). \tag{46}$$

By applying the RDTM on nonlinear Volterra integral equation (44), for $k = 1, 2, \ldots$, we get

$$\begin{aligned} U_k(x) &- \left\{ \sum_{r=0}^{k} \frac{\sin(x + r\pi/2)}{r!} \left(\frac{(-1)^{k-r} e^x}{(k-r)!} + \delta_{k-r,0} \right) \right. \\ &\quad \left. - \sum_{r=0}^{k} \frac{(-1)^r \sin((k-r)\pi/2)}{r!\,(k-r)!} - \delta_{k,0} e^x \sin(x) \right\} \\ &= \frac{2}{k} \int_0^x \left\{ \sum_{r=0}^{k-1} e^y \frac{(-1)^r}{r!} U_{k-r-1}(y) \right\} dy, \end{aligned} \tag{47}$$

where $U_i(x)$ is the reduced differential transform of $u(x,t)$. After expanding the RDTM recurrence equations (47), with initial value of (46), for $k = 1, 2, 3, 4, 5$, the first five terms of $U_k(x)$ are obtained as follows:

$$\begin{aligned} U_1(x) &= \cos(x), \\ U_2(x) &= -\frac{1}{2}\sin(x), \end{aligned}$$

TABLE 4: Comparisons of the exact solution $u(x,t) = \sin(x+t)$, with $U_{5,5}(x,t)$ obtained by classic DTM [5] and $U_5(x,t)$ obtained by reduced DTM at some test points (x,t) in Example 10.

x	t	$u(x,t)$	Classic DTM [5]		Reduced DTM	
			$U_{5,5}(x,t)$	$\lvert u(x,t) - U_{5,5}(x,t)\rvert$	$U_5(x,t)$	$\lvert u(x,t) - U_5(x,t)\rvert$
0.2	0.1	0.2955202067	0.2955202184	$1.1688660428e-08$	0.2955202070	$2.9532337686e-10$
	0.4	0.5646424734	0.5646439552	$1.4818049646e-06$	0.5646439183	$1.4448767682e-06$
	0.7	0.7833269096	0.7833750550	$4.8145422517e-05$	0.7833749959	$4.8086256376e-05$
	1	0.9320390860	0.9325020000	$4.6291403277e-04$	0.9325019239	$4.6283789648e-04$
0.5	0.1	0.5646424734	0.5646461680	$3.6945737146e-06$	0.5646424741	$6.8315986201e-10$
	0.4	0.7833269096	0.7833397500	$1.2840372517e-05$	0.7833299139	$3.0042708277e-06$
	0.7	0.9320390860	0.9321460859	$1.0699997027e-04$	0.9321309857	$9.1899716402e-05$
	1	0.9974949866	0.9983398437	$8.4485714595e-04$	0.9983208230	$8.2583639762e-04$
0.8	0.1	0.7833269096	0.7834038828	$7.6973172517e-05$	0.7833269106	$1.0099717729e-09$
	0.4	0.9320390860	0.9322215424	$1.8245643277e-04$	0.9320433813	$4.2953023213e-06$
	0.7	0.9974949866	0.9978859380	$3.9095139595e-04$	0.9976224907	$1.2750404846e-04$
	1	0.9738476309	0.9752880000	$1.4403691218e-03$	0.9749626963	$1.1150653929e-03$
1	0.1	0.8912073601	0.8915382743	$3.3091424412e-04$	0.8912073612	$1.1792198329e-09$
	0.4	0.9854497300	0.9861662222	$7.1649223376e-04$	0.9854546786	$4.9486333631e-06$
	0.7	0.9916648105	0.9928385451	$1.1737346864e-03$	0.9918098802	$1.4506974814e-04$
	1	0.9092974268	0.9118055556	$2.5081287299e-03$	0.9105512242	$1.2537973843e-03$

$$U_3(x) = -\frac{1}{6}\cos(x),$$
$$U_4(x) = \frac{1}{24}\sin(x),$$
$$U_5(x) = -\frac{1}{120}\cos(x). \tag{48}$$

In the same manner, the rest of the components were obtained by using the recursive equations (47). Substituting the quantities (48) in (18), the approximation solution of Volterra integral equation (44) in the Poisson series form is

$$U_5(x,t) = \sin(x) + \cos(x)t - \frac{\sin(x)}{2}t^2 - \frac{\cos(x)}{6}t^3 + \frac{\sin(x)}{24}t^4 - \frac{\cos(x)}{120}t^5, \tag{49}$$

which is the same as the first five terms of the Poisson series of the exact solution $u(x,t) = \sin(x+t)$. The numerical results obtained with reduced DTM are presented in Table 4, in comparison with the classic DTM solution of [5] and the exact solution $u(x,t) = \sin(x+t)$, for some points of the intervals $0 \le x \le 1$ and $0 \le t \le 1$.

Example 11. In the third example, consider the following two-dimensional Volterra integral equation [5]:

$$u(x,t) - e^{t-x}\int_0^t\int_0^x u(y,z)\,dy\,dz = \sinh(x+t)\left(e^{t-x}+1\right) - e^{t-x}(\sinh(x) - \sinh(t)). \tag{50}$$

(a) *DTM*: the approximation solution of this equation is also obtained by DTM in [5] as follows

$$u_{5,5}(x,t) = \left(-x - \frac{x^3}{6} - \frac{x^5}{120}\right) + \left(1 + \frac{x^2}{2} + \frac{x^4}{24}\right)t + \left(-\frac{x}{2} - \frac{x^3}{12} - \frac{x^5}{240}\right)t^2 + \left(\frac{1}{6} + \frac{x^2}{12} + \frac{x^4}{144}\right)t^3 + \left(-\frac{x}{24} - \frac{x^3}{144} - \frac{x^5}{2880}\right)t^4 + \left(\frac{1}{120} + \frac{x^2}{240} + \frac{x^4}{2880}\right)t^5. \tag{51}$$

(b) *RDTM*: it is easy to see that the $u(x,0) = -\sinh(x)$, and therefore RDTM version is

$$U_0(x) = -\sinh(x). \tag{52}$$

Table 5: Comparisons of the exact solution $u(x,t) = \sinh(t-x)$, with $U_{5,5}(x,t)$ obtained by classic DTM [5] and $U_5(x,t)$ obtained by reduced DTM at some test points (x,t) in Example 11.

x	t	$u(x,t)$	Classic DTM [5]		Reduced DTM	
			$U_{5,5}(x,t)$	$\lvert u(x,t)-U_{5,5}(x,t)\rvert$	$U_5(x,t)$	$\lvert u(x,t)-U_5(x,t)\rvert$
0.2	0.1	−0.1001667500	−0.1001667561	6.0968226301e − 09	−0.1001667498	2.5944103810e − 10
	0.4	+0.2013360025	+0.2013367851	7.8252557270e − 07	+0.2013368189	8.1631586063e − 07
	0.7	+0.5210953055	+0.5211116472	1.6341756253e − 05	+0.5211117115	1.6406043554e − 05
	1	+0.8881059822	+0.8881853333	7.9351145710e − 05	+0.8881854339	7.9451747271e − 05
0.5	0.1	−0.4107523258	−0.4107529453	6.1950968455e − 07	−0.4107523251	7.0149602793e − 10
	0.4	−0.1001667500	−0.1001714167	4.6666468226e − 06	−0.1001641445	2.6055545215e − 06
	0.7	+0.2013360025	+0.2013887643	5.2761781823e − 05	+0.2014033478	1.7345289013e − 05
	1	+0.5210953055	+0.5215820313	4.8672575625e − 04	+0.5216052465	5.0994098756e − 04
0.8	0.1	−0.7585837018	−0.7585783977	5.3041062001e − 06	−0.7585837006	1.2071608158e − 09
	0.4	−0.4107523258	−0.4108535808	1.0125499718e − 04	−0.4107476947	4.6310571234e − 06
	0.7	−0.1001667500	−0.1002690359	1.4228584682e − 04	−0.1000423588	1.2439120515e − 04
	1	+0.2013360025	+0.2019546667	6.1866412557e − 04	+0.2023226727	9.8667016118e − 04
1	0.1	−1.0265167257	−1.0264561563	6.0569458175e − 05	−1.0265167241	1.6018943949e − 09
	0.4	−0.6366535821	−0.6370106667	3.5708451843e − 04	−0.6366473802	6.2019846800e − 06
	0.7	−0.3045202934	−0.3051720521	6.5175863619e − 04	−0.3043519610	1.6833243259e − 04
	1	+0.0000000000	−0.0000000000	−0.0000000000	+0.0013512390	1.3512390404e − 03

By applying the RDTM on nonlinear Volterra integral equation (50), for $k = 1, 2, \ldots$, we get

$$\sum_{r=0}^{k}\left\{U_r(x)+\frac{\delta_{r,0}\left(1+e^{-x}\right)}{2}+\frac{1}{2r!}\left(1+(-1)^r e^x-\left(1+2^r\right)\left(e^{-x}+e^{-2x}\right)\right)\right\}\left\{\frac{(-1)^{k-r}}{(k-r)!}e^x\right\}=\frac{1}{k}\int_0^x U_{k-r}(y)\,dy, \tag{53}$$

where $U_i(x)$ is the reduced differential transform of $u(x,t)$. After expanding the RDTM recurrence equations (53), with initial value of (52), for $k = 1, 2, 3, 4, 5$, the first five terms of $U_k(x)$ are obtain as follows:

$$\begin{aligned}U_1(x)&=\cosh(x),\\ U_2(x)&=-\frac{1}{2}\sinh(x),\\ U_3(x)&=\frac{1}{6}\cosh(x),\\ U_4(x)&=\frac{1}{24}\sinh(x),\\ U_5(x)&=\frac{1}{120}\cosh(x).\end{aligned} \tag{54}$$

In the same manner, the rest of the components were obtained by using the recursive equations (47). Substituting the quantities (48) in (18), the approximation solution of Volterra integral equation (44) in the Poisson series form is

$$U_5(x,t)=-\sinh(x)+\cosh(x)\,t-\frac{\sinh(x)}{2}t^2+\frac{\cosh(x)}{6}t^3-\frac{\sinh(x)}{24}t^4+\frac{\cosh(x)}{120}t^5, \tag{55}$$

which is same as the first five terms of the Poisson series of the exact solution $u(x,t) = \sinh(t-x)$. The numerical results obtained with reduced DTM are presented in Table 5, in comparison with the classic DTM solution of [5] and the exact solution $u(x,t) = \sinh(t-x)$, for some points of the intervals $0 \le x \le 1$ and $0 \le t \le 1$.

4. Conclusions

In this study, we presented the definition and operation of both two-dimensional differential transformation method (DTM) and their reduced form, the so-called reduced-DTM (RDTM) for finding the solutions of a class of Volterra integral equations. For illustration purposes, we consider three different examples. It is worth pointing out that both DTM and RDTM have convergence for the solutions; actually, the accuracy of the series solution increases when the number of terms in the series solution is increased. From the computational process of DTM and RDTM, we find that the RDTM is easier to apply. In other words, it is obvious that DTM has very complicated computational process rather than RDTM.

The RDTM reduces the computational difficulties of the DTM and all the calculations can be made with simple manipulations MATLAB. Actually, as a special advantage of RDTM rather than DTM, the reduced differential transform recursive equations produce exactly all the Poisson series coefficients of solutions, whereas the differential transform recursive equations produce exactly all the Taylor series coefficients of solutions. The reliability of the RDTM and the reduction in the size of computational domain give this method a wider applicability. For small value of x, t, in Tables 3, 4, and 5, we find that the RDTM has a smaller error than DTM. Also, for large values of x, t, we may increase the accuracy of the series solution by computing more terms, which is quite easy using MATLAB.

References

[1] H. Brunner, *Collocation Methods for Volterra Integral and Related Functional Differential Equations*, vol. 15 of *Cambridge Monographs on Applied and Computational Mathematics*, Cambridge University Press, Cambridge, UK, 2004.

[2] P. Huabsomboon, B. Novaprateep, and H. Kaneko, "On Taylor-series expansion methods for the second kind integral equations," *Journal of Computational and Applied Mathematics*, vol. 234, no. 5, pp. 1466–1472, 2010.

[3] H. Kaneko and Y. Xu, "Gauss-type quadratures for weakly singular integrals and their application to Fredholm integral equations of the second kind," *Mathematics of Computation*, vol. 62, no. 206, pp. 739–753, 1994.

[4] A. Tari, M. Y. Rahimi, S. Shahmorad, and F. Talati, "Solving a class of two-dimensional linear and nonlinear Volterra integral equations by the differential transform method," *Journal of Computational and Applied Mathematics*, vol. 228, no. 1, pp. 70–76, 2009.

[5] B. Jang, "Comments on "Solving a class of two-dimensional linear and nonlinear Volterra integral equations by the differential transform method"," *Journal of Computational and Applied Mathematics*, vol. 233, no. 2, pp. 224–230, 2009.

[6] Y.-J. jiang, "On spectral methods for Volterra-type integro-differential equations," *Journal of Computational and Applied Mathematics*, vol. 230, no. 2, pp. 333–340, 2009.

[7] A. Akyüz-Daşcıoğlu and M. Sezer, "Chebyshev polynomial solutions of systems of higher-order linear Fredholm-Volterra integro-differential equations," *Journal of the Franklin Institute. Engineering and Applied Mathematics*, vol. 342, no. 6, pp. 688–701, 2005.

[8] S. M. Hosseini and S. Shahmorad, "Numerical solution of a class of integro-differential equations by the tau method with an error estimation," *Applied Mathematics and Computation*, vol. 136, no. 2-3, pp. 559–570, 2003.

[9] M. T. Kajani, M. Ghasemi, and E. Babolian, "Numerical solution of linear integro-differential equation by using sine-cosine wavelets," *Applied Mathematics and Computation*, vol. 180, no. 2, pp. 569–574, 2006.

[10] R. Farnoosh and M. Ebrahimi, "Monte Carlo method for solving Fredholm integral equations of the second kind," *Applied Mathematics and Computation*, vol. 195, no. 1, pp. 309–315, 2008.

[11] K. Maleknejad and F. Mirzaee, "Numerical solution of integro-differential equations by using rationalized Haar functions method," *Kybernetes*, vol. 35, no. 10, pp. 1735–1744, 2006.

[12] K. E. Atkinson, *The Numerical Solution of Integral Equations of the Second Kind*, vol. 4 of *Cambridge Monographs on Applied and Computational Mathematics*, Cambridge University Press, Cambridge, UK, 1997.

[13] H. Guoqiang and W. Jiong, "Extrapolation of Nystrom solution for two dimensional nonlinear Fredholm integral equations," *Journal of Computational and Applied Mathematics*, vol. 134, no. 1-2, pp. 259–268, 2001.

[14] G. Han and R. Wang, "Richardson extrapolation of iterated discrete Galerkin solution for two-dimensional Fredholm integral equations," *Journal of Computational and Applied Mathematics*, vol. 139, no. 1, pp. 49–63, 2002.

[15] J. K. Zhou, *Differential Transformation and Its Application for Electrical CircuIts*, Huazhong University Press, Wuhan, China, 1986.

[16] R. Abazari and A. Borhanifar, "Numerical study of the solution of the Burgers and coupled Burgers equations by a differential transformation method," *Computers & Mathematics with Applications*, vol. 59, no. 8, pp. 2711–2722, 2010.

[17] A. Borhanifar and R. Abazari, "Exact solutions for non-linear Schrödinger equations by differential transformation method," *Journal of Applied Mathematics and Computing*, vol. 35, no. 1-2, pp. 37–51, 2011.

[18] A. Borhanifar and R. Abazari, "Numerical study of nonlinear Schrödinger and coupled Schrödinger equations by differential transformation method," *Optics Communications*, vol. 283, no. 10, pp. 2026–2031, 2010.

[19] R. Abazari and M. Abazari, "Numerical simulation of generalized Hirota-Satsuma coupled KdV equation by RDTM and comparison with DTM," *Communications in Nonlinear Science and Numerical Simulation*, vol. 17, no. 2, pp. 619–629, 2012.

[20] R. Abazari, "Solution of Riccati types matrix differential equations using matrix differential transform method," *Journal of Applied Mathematics & Informatics*, vol. 27, pp. 1133–1143, 2009.

[21] R. Abazari and R. Abazari, "Numerical study of some coupled PDEs by using differential transformation method," *World Academy of Science, Engineering and Technology*, vol. 66, pp. 52–59, 2010.

[22] Y. Keskin and G. Oturanç, "Reduced differential transform method for partial differential equations," *International Journal of Nonlinear Sciences and Numerical Simulation*, vol. 10, no. 6, pp. 741–749, 2009.

[23] Y. Keskin and G. Oturanç, "The reduced differential transform method: a new approach to factional partial differential equations," *Nonlinear Science Letters A*, vol. 1, pp. 207–217, 2010.

[24] R. Abazari and M. Ganji, "Extended two-dimensional DTM and its application on nonlinear PDEs with proportional delay," *International Journal of Computer Mathematics*, vol. 88, no. 8, pp. 1749–1762, 2011.

Hindawi Publishing Corporation
Abstract and Applied Analysis
Volume 2013, Article ID 161873, 13 pages
http://dx.doi.org/10.1155/2013/161873

Research Article

A Pressure-Stabilized Lagrange-Galerkin Method in a Parallel Domain Decomposition System

Qinghe Yao and Qingyong Zhu

School of Engineering, Sun Yat-Sen University, 510275 Guangzhou, China

Correspondence should be addressed to Qingyong Zhu; mcszqy@mail.sysu.edu.cn

Received 30 April 2013; Accepted 14 June 2013

Academic Editor: Santanu Saha Ray

A pressure-stabilized Lagrange-Galerkin method is implemented in a parallel domain decomposition system in this work, and the new stabilization strategy is proved to be effective for large Reynolds number and Rayleigh number simulations. The symmetry of the stiffness matrix enables the interface problems of the linear system to be solved by the preconditioned conjugate method, and an incomplete balanced domain preconditioner is applied to the flow-thermal coupled problems. The methodology shows good parallel efficiency and high numerical scalability, and the new solver is validated by comparing with exact solutions and available benchmark results. It occupies less memory than classical product-type solvers; furthermore, it is capable of solving problems of over 30 million degrees of freedom within one day on a PC cluster of 80 cores.

1. Introduction

The Lagrange-Galerkin method raises wide concern about the finite-element simulation of fluid dynamics. Based on the approximation of the material derivative along the trajectory of fluid particle, the method is natural in the simulation to physical phenomena, and it is demonstrated to be unconditionally stable for a wide class of problems [1–5]. A number of researches about the Lagrange-Galerkin method were done in the case of single processor element (PE) (cf. [6–8]); the symmetry of the matrices and good stability of the scheme were reported; using a numerical integration based on a division of each element, Rui and Tabata [9] developed a second scheme for convection-diffusion problem; Massarotti et al. [10] used a second-order characteristic curve method, and a special iteration was used to keep the symmetry of the stiffness matrix. The Lagrange-Galerkin method uses an implicit time discretization, and therefore an element searching algorithm is necessary to implement it. The element searching may become very expensive when the geometry is complicated or the mesh size is very small. Due to its doubtable efficiency and feasibility for complex simulations in the case of single PE, rare research has been done to implement it in parallel, by which the enormous computation power enables us to solve more challenging simulation problems.

The present study is concentrated on improving the solvability of the Lagrange-Galerkin method on large scale and complex problems by domain decompositions. Piecewise linear interpolations are thus employed for velocity, pressure, and temperature; therefore, the so-called inf-sup condition [11] should be satisfied, which is the first difficulty to be overcome in this work. Stabilization methods for incompressible flow problems were reported by many researchers (cf. [12–15]). Park and Sung proposed a stabilization for Rayleigh-Bénard convection by using feedback control [16]; for consistently stabilized finite element methods, Barth et al. classified the stabilization techniques and studied influence of the stabilization parameter in convergence [17]; Bochev et al. stated the requirements on choice of stabilization parameter if time step and mesh are allowed to vary independently [18]. As far as we know, it may not be enough to investigate what stabilization techniques are efficient for nonsteady and nonlinear flow problems approximated by Lagrange-Galerkin methods in a domain decomposition system, where the interface problem can be solved by preconditioned conjugate gradient (PCG) method. In this paper, a pressure-stabilization method, which keeps the symmetry of the linear system and is effective for high Reynolds number and Rayleigh number simulations, is introduced to implement the Lagrange-Galerkin method in a domain decomposition system.

The element searching algorithm in a domain decomposition system using unstructured grids is the second difficulty to implement the Lagrange-Galerkin method in a domain decomposition system (cf. [5, 19]). Minev et al. reported an optimized binary searching algorithm for single PE by storing the necessary data structures in a way similar to the CSR compact storage format; however, the element information data is stored distributedly in the domain decomposition system by the skyline format, and a different way needs to be found to overcome the extra difficulty caused by the parallel computing algorithm. This step is critical, in the sense that it can be very computationally expensive and can thus make the entire algorithm impractical.

The remainder of this paper is organized as follows: in Section 2, the formula of the governing equation and the pressure-stabilization Lagrange-Galerkin method is described; Section 3 focuses on the parallel implementation of this scheme. Numerical results and comparisons with classical asymmetric product type methods in [20] are shown in Section 4. Conclusions are drawn in Section 5.

2. Formulation

2.1. The Governing Equations. Let Ω be a three-dimensional polyhedral domain with the boundary $\partial\Omega$. The conservation equations of mass and momentum are governed by

$$\begin{aligned}
&\frac{\partial u}{\partial t} + (u\cdot\nabla)\,u - 2\nu\nabla\cdot D(u) + \nabla p = f^{\text{buoyancy}} \quad \text{in } \Omega\times(0,\bar{t}),\\
&\nabla\cdot u = 0 \quad \text{in } \Omega\times(0,\bar{t}),\\
&u = \hat{u} \quad \text{on } \Gamma_1\times(0,\bar{t}),\\
&\sum_{j=0}^{3}\sigma_{ij}n_j = 0 \quad \text{on } \frac{\partial\Omega}{\Gamma_1\times(0,\bar{t})},\\
&u = u_0 \quad \text{in } \Omega, \text{ at } t=0,
\end{aligned}\tag{1}$$

where $\Gamma_1\subset\partial\Omega$ and

$$f^{\text{buoyancy}} = \beta\,(T_r - T)\,g \tag{2}$$

is the gravity force per unit mass derived on the basis of Boussinesq approximation. g is the gravity [m/s^2], β, T, and T_r are the thermal expansion coefficient [$1/K$], the temperature [K], and the reference temperature [K], and u, t, ν, and p are velocity vector [m/s], time [s], kinematic viscosity coefficient [m^2/s], and kinematic pressure [m^2/s^2], respectively. σ_{ij} is the stress tensor [N/m^2] defined by

$$\begin{aligned}
&\sigma_{ij}(u,p) \equiv -p\delta_{ij} + 2\nu D_{ij}(u),\\
&D_{ij}(u) \equiv \frac{1}{2}\left(\frac{\partial u_i}{\partial x_j} + \frac{\partial u_j}{\partial x_i}\right), \quad i,j = 1,2,3,
\end{aligned}\tag{3}$$

with the Kronecker delta δ_{ij}.

The fluid is assumed to be incompressible according to Boussinesq approximation, and the density is assumed to be constant except in the gravity force term where it depends on temperature according to the indicated linear law; see (2). The energy equation is

$$\begin{aligned}
&\frac{\partial T}{\partial t} + u\cdot\nabla T - a\Delta T = S \quad \text{in } \Omega\times(0,\bar{t}),\\
&T = \hat{T} \quad \text{on } \Gamma_2\times(0,\bar{t}),\\
&a\frac{\partial T}{\partial n} = 0 \quad \text{on } \frac{\partial\Omega}{\Gamma_2\times(0,\bar{t})},\\
&T = T_0 \quad \text{in } \Omega, \text{ at } t=0,
\end{aligned}\tag{4}$$

where $\Gamma_2\subset\partial\Omega$, a is the thermal diffusion coefficient [m^2/s], and S is the source term with the unit of [K/s].

2.2. The Lagrange-Galerkin Finite-Element Method. Some preliminaries are arranged for the derivation of a finite element scheme of (1) and (4). Let the subscript h denote the representative length of the triangulation, and let $\mathfrak{I}_h \equiv \{K\}$ denote a triangulation of Ω consisting of tetrahedral elements. Given that g is a vector valued function on Γ_1, the finite element spaces are as follows:

$$\begin{aligned}
&X_h \equiv \left\{v_h \in C^0\left(\overline{\Omega}\right)^3;\, v_h\big|_K \in P_1(K)^3, \forall K\in\mathfrak{I}_h\right\},\\
&M_h \equiv \left\{q_h \in C^0\left(\overline{\Omega}\right);\, q_h\big|_K \in P_1(K), \forall K\in\mathfrak{I}_h\right\},\\
&V_h(g) \equiv \left\{v_h\in X_h;\, v_h(P) = g(P), \forall P\in\Gamma_1\right\},\\
&\Theta_h(b) \equiv \left\{\theta_h\in M_h;\, \theta_h(P) = b(P), \forall P\in\Gamma_2\right\},\\
&V_h \equiv V_h(0),\ \Theta_h \equiv \Theta_h(0),\ Q_h = M_h.
\end{aligned}\tag{5}$$

Let $(\cdot,\cdot)$ defines the L_2 inner product; the continuous bilinear forms a and b are introduced by

$$\begin{aligned}
&a(u,v) \equiv 2\nu\,(D(u), D(v)),\\
&b(u,v) \equiv -(\nabla\cdot u, q),
\end{aligned}\tag{6}$$

respectively.

Let Δt be the time increment, and let $N_{\bar{t}} \equiv [\bar{t}/\Delta t]$ be the total step number. Let the superscript n denote the time step; a finite element approximation of (1) is described as follows: find $\{(u_h^n, p_h^n)\}_{n=1}^{N_{\bar{t}}} \in V_h(g)\times Q_h$, such that for $(v_h, q_h)\in V_h\times Q_h$,

$$\begin{aligned}
&\left(\frac{u_h^n - u_h^{n-1}\circ X_1\left(u_h^{n-1},\Delta t\right)}{\Delta t}, v_h\right) + a\left(u_h^n, v_h\right)\\
&\quad + b\left(v_h, p_h^n\right) = \left(f^n, v_h\right),\\
&b\left(u_h^n, q_h\right) = 0,
\end{aligned}\tag{7}$$

where $X_1(\cdot,\cdot)$ denotes a first-order approximation of a particle's position [5], and the notation $\circ$ denotes the composition of functions.

For the purpose of large scale computation, a piecewise equal-order interpolation for velocity and pressure is used, as can be seen from (5). Pressure stabilization is thus needed to keep the necessary link between V_h and Q_h. A penalty Galerkin least-squares (GLS) stabilization method for pressure is proved in [12] to hold the same asymptotic error estimates as the method of Hughes et al. [21] and it is computationally cheap. For P1/P1 elements, the stabilization is reduced to

$$\sum_{K\in\mathfrak{T}_h} \delta_K h_K^2 (\nabla p_h^n, -\nabla q_h)_K, \tag{8}$$

which does no modification to the momentum equation because of vanishing of the second-order derivate term. Here, h_K denotes the maximum diameter of an element K. Unlike [6, 12], where a constant δ (>0) is used as the stabilization parameter, an element-wise stabilization parameter

$$\delta_K = \begin{cases} \alpha, \\ \text{for } \log_{10}\left[\operatorname{Max}\left\{\left\|\nabla p_h^{n-1}\right\|_2\right\}_{i=1}^4\right] \le 1, \\ \alpha \times \log_{10}\left[\operatorname{Max}\left\{\left\|\nabla p_h^{n-1}\right\|_2\right\}_{i=1}^4\right], \\ \qquad\qquad\qquad\text{otherwise} \end{cases} \tag{9}$$

is used in this work, where ∇p_h^{n-1} is gradient of the FEM approximated pressure at t^{n-1} and i is the number of the nodal point in a tetrahedral element. Since α is very important to balance the accuracy and convergence of the scheme, it is discussed in Section 4.1. The localized stabilization parameter is designed to be adaptive to the pressure gradient, and thus it has a better control on the pressure field.

By adding (8) to (7), a pressure-stabilized FEM scheme for Navier-Stokes problems is achieved. The nonsteady iteration loops for solving (1) and (4) and then reads the following.

Step 1. Compute the particle's coordinates by

$$X_1\left(u_h^{n-1}, \Delta t\right) \equiv x - u_h^{n-1}\Delta t, \tag{10}$$

and search the element holding the particle at t^{n-1}.

Step 2. Find T_h^n by

$$\left(\frac{T_h^n - T_h^{n-1} \circ X_1\left(u_h^{n-1}, \Delta t\right)}{\Delta t}, \theta_h\right) + \left(a\nabla T_h^n, \nabla\theta_h\right) = \left(S^n, \theta_h\right). \tag{11}$$

Step 3. Find (u_h^n, p_h^n) by

$$\begin{aligned} &\left(\frac{u_h^n - u_h^{n-1} \circ X_1\left(u_h^{n-1}, \Delta t\right)}{\Delta t}, v_h\right) + a_0\left(u_h^n, v_h\right) \\ &\quad + b\left(v_h, p_h^n\right) + b\left(u_h^n, q_h\right) \\ &\quad + \sum_{K\in\mathfrak{T}_h} \delta_K h_K^2 (\nabla p_h^n, -\nabla q_h)_K \\ &= \left(f^n, v_h\right) + \left(\beta\left(T_r - T_h^n\right) g, v_h\right). \end{aligned} \tag{12}$$

Step 4. Compute the relative error by a $H^1 \times L^2 \times H^1$ norm defined by

$$\begin{aligned} \|(u, p, T)\|_{H^1\times L^2\times H^1} \equiv{}& \frac{1}{\sqrt{\text{Re}}}\|u\|_{H^1(\Omega)^3} \\ &+ \|p\|_{L^2} + \|T\|_{H^1(\Omega)}, \end{aligned} \tag{13}$$

where Re denotes the Reynolds number, and set

$$\begin{aligned} \text{diff} ={}& \frac{\left\|\left(u^n, p^n, T^n\right) - \left(u^{n-1}, p^{n-1}, T^{n-1}\right)\right\|_{H^1\times L^2\times H^1}}{\left\|\left(u^{n-1}, p^{n-1}, T^{n-1}\right)\right\|_{H^1\times L^2\times H^1}} \\ &\le \text{Err}_{\text{NS}} \end{aligned} \tag{14}$$

as the steady-state criterion; if (14) is satisfied or the number of loops reaches the maximum, then stop the iteration; otherwise, repeat Steps 1–3.

As can be seen from Steps 2 and 3, both (1) and (4) are approximated by the Lagrange-Galerkin method, and the searching algorithm only needs to be performed once in a nonsteady loop. It can also be seen that the solver is also flexible, and it can solve pure Navier-Stokes problems by setting the body force in (2) to external force and omitting Step 2.

3. Implementation

3.1. A Parallel Domain Decomposition System. To begin with the parallel domain decomposition method, the domain decomposition is introduced briefly as follows. The whole domain is decomposed into a number of *subdomains* without overlapping, and the solution of each *subdomain* is superimposed on the equation of the inner boundary of the *subdomains*. By static condensation, the linear system

$$K\overline{u} = \overline{f} \tag{15}$$

is written as

$$\begin{aligned} &\begin{bmatrix} K_{II}^{(1)} & 0 & \cdots & 0 & K_{IB}^{(1)}R_B^{(1)} \\ 0 & \ddots & & \vdots & \vdots \\ \vdots & & \ddots & \vdots & \vdots \\ 0 & \cdots & \cdots & K_{II}^{(N)} & K_{IB}^{(N)}R_B^{(N)} \\ R_B^{(1)T}K_{IB}^{(1)T} & \cdots & \cdots & R_B^{(N)T}K_{IB}^{(N)T} & K_{BB} \end{bmatrix} \begin{bmatrix} \overline{u}_I^{(1)} \\ \vdots \\ \vdots \\ \overline{u}_I^{(N)} \\ \overline{u}_B \end{bmatrix} \\ &= \begin{bmatrix} \overline{f}_I^{(1)} \\ \vdots \\ \vdots \\ \overline{f}_I^{(N)} \\ \overline{f}_B \end{bmatrix}, \end{aligned} \tag{16}$$

where K is the stiffness matrix, $\overline{u}$ denotes the unknowns (u and p), and $\overline{f}$ is the force vector. R is the restriction operator consists of 0-1 matrix. The superscripts (N) means the

Nth *subdomain*, and subscript I and B relate to the element of the inner boundary, and interface boundary respectively.

From (16), it can be observed that the interface problems

$$\sum_{i=1}^{N} R_B^{(i)^T} \left(K_{BB}^{(i)} - K_{IB}^{(i)^T} K_{II}^{(i)^{-1}} K_{IB}^{(i)} \right) R_B^{(i)} \overline{u}_B = \sum_{i=1}^{N} R_B^{(i)^T} \left(\overline{f}_B^{(i)} - K_{IB}^{(i)^T} K_{II}^{(i)^{-1}} \overline{f}_I^{(i)} \right) \tag{17}$$

and the inner problems

$$\overline{u}_I^{(i)} = K_{II}^{(i)^{-1}} \left(\overline{f}_I^{(i)} - K_{IB}^{(i)^T} R_B^{(i)} \overline{u}_B \right), \quad i = 1, \ldots, N \tag{18}$$

can be solved separately [22]. In this work, the interface problems are solved first iteratively, and the inner problems are then solved by substituting $\overline{u}_B$ in to (18).

The Lagrange-Galerkin method keeps the symmetry of the stiffness matrix, and the GLS pressure-stabilization term in (8) also produces a symmetric matrix; therefore, K is symmetric in (15), and a PCG method is employed to get the u_I in (18), and to avoid drawback of the classical domain decomposition method, such as Neumann-Neumann and diagonal-scaling, a balanced domain decomposition preconditioner is used to prevent the growing of condition number with the number of *subdomains*. An identity matrix is chosen as the coarse matrix, and the coarse problem is solved incompletely by omitting the *fill-ins* in some sensitive places during the Cholesky factorization. By using this inexact balanced domain decomposition preconditioning, the coarse matrix is sparser and thus easier to be solved; therefore, the new solver is expected to have better solvability on large scale computation models.

3.2. The Lagrange-Galerkin Method in Parallel. The element searching algorithm requires a global-wise element information to determine the position of one particle in the previous time step. However, in the parallel domain decomposition system, the whole domain is split into several *parts* one processor element (PE) works only on the current *part,* and it does not contain any element information of other *parts*. Each *part* is further divided into many *subdomains,* and the domain decomposition is performed by the PE in charge of the *part*. This parallelity causes a computational difficulty: for each time step, the particle is not limited within one *part*; therefore, exchanging the data between different PEs is necessary, which demands the PEs to communicate in the *subdomain*-wise computation.

In order to know the position of a particle at t^{n-1}, a neighbour elements list is created at the beginning of the analysis. Based on the information of neighbour elements and the coordinates calculated by (10), it is possible to find the element holding this particle at t^{n-1}. A 2-dimensional searching algorithm is present as follows (λ_i is the barycentric coordinates, and $ne(\lambda_i)$ is the neighbour element; see Figure 1):

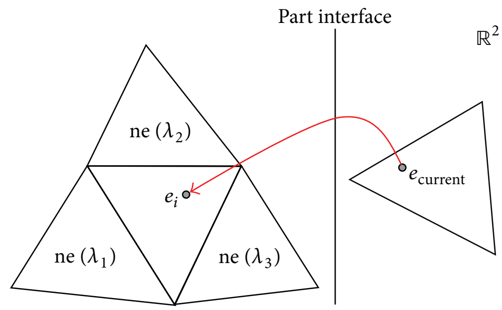

Figure 1: A searching algorithm.

(1) initialize: $e_0 = e_{\text{current}}$;

(2) iterate $i = 0, 1, \ldots$, Maxloops;

If $\lambda_1, \lambda_2, \lambda_3 > 0$, return e_i;

else if $ne(\text{Min}\{\lambda_1, \lambda_2, \lambda_3\}) \neq$ boundary

$e_{i+1} = ne(\text{Min}\{\lambda_1, \lambda_2, \lambda_3\})$;

else break;

(3) return e_i.

The request of the old solutions, which is the u_h^{n-1} in (10), is relatively trivial when using single PEs or simply solving the problem parallel using symmetric multiprocessing; however, in the domain decomposition system, the particle is not limited within one *part*; it may pass the interface of different *parts*, as can be seen from Figure 1. Because one PE only has the elements information that belongs to the current *part*, communications between PEs are necessary. However, the number of total elements in one *subdomain* may be different, which means that some point to point communication techniques, such as MPI_Send/MPI_Recv or MPI_Sendrecv in MPICH, cannot be used in element wise computation. In the previous research [23], a global variable to store all the old solutions is constructed. This method maintains a high computation speed but costs a huge memory usage. To reduce the memory consumption, a request-response system is used in this work. In the computation, the searching algorithm is performed first, and the element that contains the current particle in the previous time step is thus known; therefore, the PE to get u_h^{n-1} from is also known. However, as the sender does not know which PE requires message from itself, the receiver has to send its request to the sender first; after the request is detected, the sender sends the message to the receiver. The procedure is as follows:

(1) by scanning all the particles in the current *subdomain*, an array including all the data that is needed by the current PE is sent to all the other PEs.

(2) All PEs check if there is any request to itself. If it exists, PEs will prepare an array of the needed data and send it.

(3) The current PE receives the data sent by other PEs.

Data transferred by MPI communication should be packaged properly to avoid the overflow of MPI buffer in case

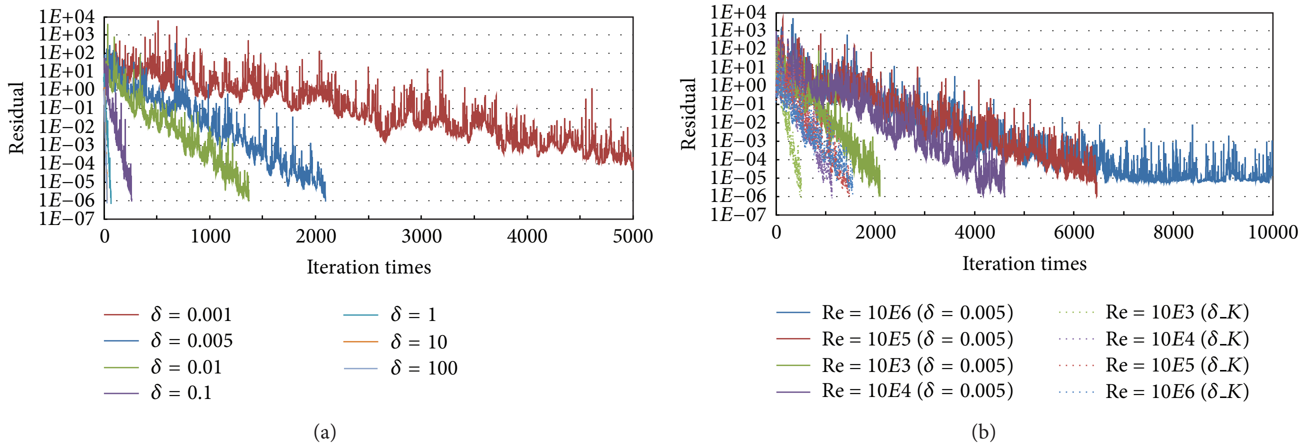

FIGURE 2: Convergence of (a) different constant δ at Re $= 10^3$; (b) different Re for $\delta = 0.005$ and localized δ_K.

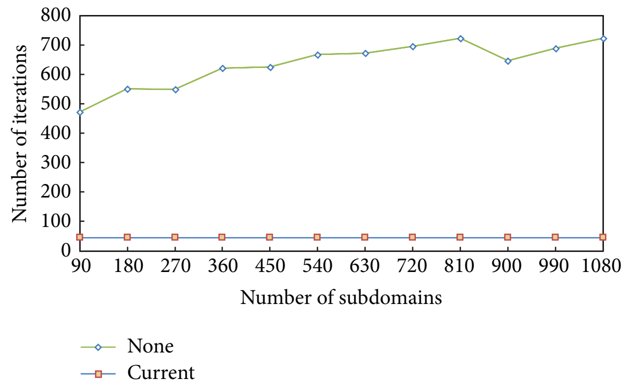

FIGURE 3: Numerical scalability.

of large-scale computation. Nonblocking communication is employed, and as the 3 steps are performed subsequently, thus the computation time and communication time will be overlapped.

4. Numerical Results and Discussion

The parallel efficiency of new solver is firstly evaluated in this section, and to validate the scheme, exact solutions and available benchmark results classical computational models are compared. The CG convergence is judged by Euclidian norm with a tolerance of 10^{-6}, and for nonsteady iteration, $\mathrm{Err}_{\mathrm{NS}} = 10^{-4}$ is set as the criterion, using the $H^1 \times L^2 \times H^1$ norm defined in (13). For pure Navier-Stokes problems, a similar $H^1 \times L^2$ norm, which is related to velocity and pressure, is employed to judge the steady state.

4.1. Efficiency Test. The BDD serious preconditioners were employed in this work; they are very efficient, and their iteration numbers are about 1âĄĎ10 of the normal domain decomposition preconditioners (cf. [23]). The inexact preconditioner mentioned in Section 3 also shows good convergence and is more suitable for large scale computations [24]. It was set as the default preconditioner for all the following computations of this research.

The penalty methods are not consistent since the substitution of an exact solution into the discrete equations (12) leaves a residual that is proportional to the penalty parameter (cf. [17]); therefore, δ_K should be determined carefully. Numerical experiments of a lid-driven cavity flow were tested, and the mesh size was $62 \times 62 \times 62$. The total degrees of freedom (DOF) are 1,000,188, and the results are given by Figure 2. For the purpose of higher accuracy, δ_K is expected to be small; however, the convergence turns worse when δ_K goes small, as can be seen from Figure 2(a). In Figure 2(b), a constant $\delta = 0.005$ is used for different Reynolds numbers, and no convergence is achieved within 10000 PCG loops for Re $= 10^6$; and the comparison shows that the δ_K performs much better than a constant $\delta = 0.005$ when α is set to 0.005.

The parallel efficiency is assessed firstly by freezing the mesh size of test problem and refining the domain decomposition by decreasing the subdomain size and therefore increasing the number of subdomains; the comparison of the numerical scalability of the current scheme with and without the preconditioner is assessed by Figure 3. It can be seen that with the preconditioning technique, the iterative procedure

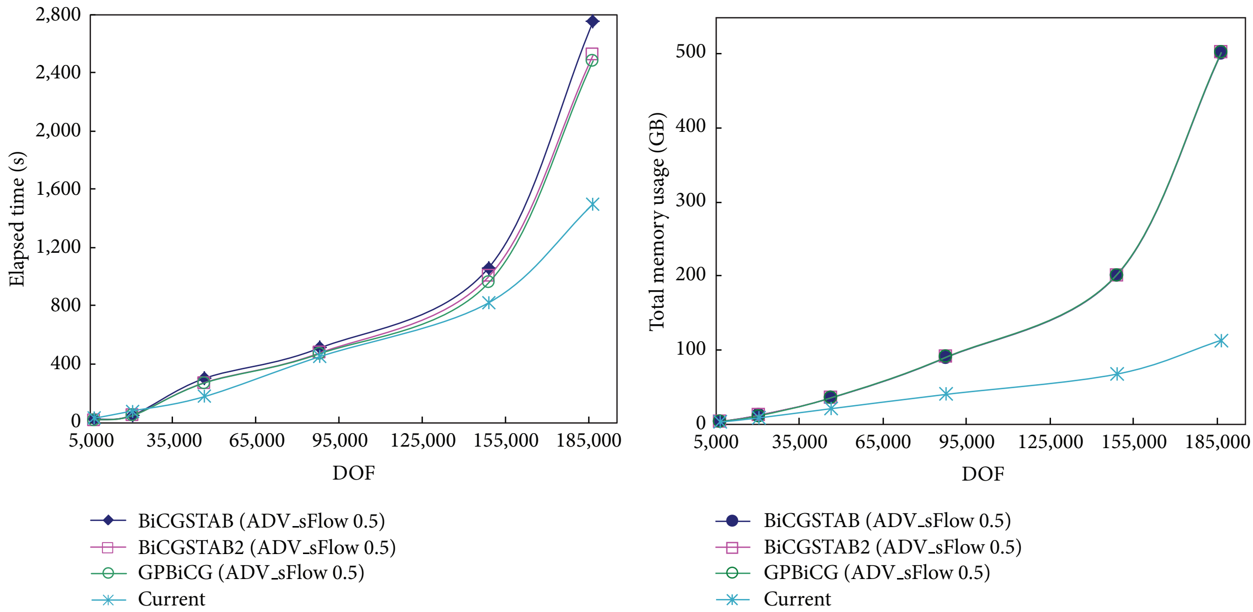

(a) (b)

Figure 4: Time and memory usages.

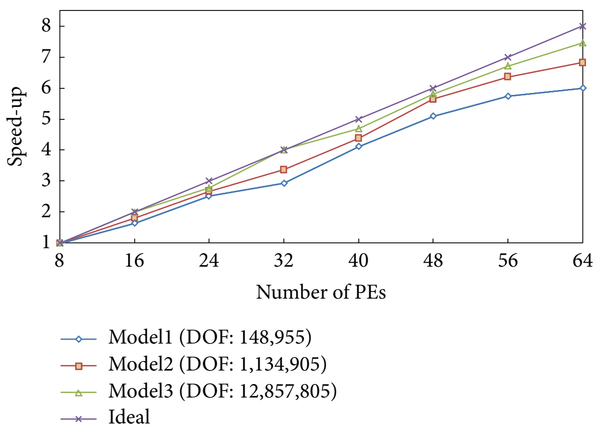

Figure 5: Numerical scalability.

of current scheme converges rapidly, and the convergence is independent of the number of subdomains.

Based on the paralyzed Lagrange-Galerkin method, the new solver makes a symmetric stiffness matrix, therefore only the lower/upper triangular matrix needs to be saved. Moreover, nonblocking MPI communication is used instead of constructing global arrays to keep the old solutions, and the current solver is expected to reduce the memory consumption without sacrificing the computation speed. The usage of time and memory of solving the thermal driven cavity problem by different solvers is compared, and the results are given by Figure 4.

The test problem was solved by the new solver and the ADV_sFlow 0.5 [25], which contains some nonsymmetric product-type solvers like GPBiCG, BiCGSTAB, and BiCGSTAB2 [20]. The ADV_sFlow 0.5 employed a domain decomposition system similar to the work; however, no precondition technique is used because of the non-symmetry of the stiffness matrix in (15). The comparisons of elapsed time and memory occupation of the new solver and that of product-type solvers in ADV_sFlow 0.5 are show in Figures 4(a) and 4(b). As can be seen, the current scheme reduces the demand of computation time and memory consumption remarkably, and it is more suitable for large scale problems than product-type solvers.

The parallel scalability of the searching algorithm is also a concern for us, as it characterizes the ability of an algorithm to deliver larger speed-up using a larger number of PEs. To know this, the number of *subdomains* in one part is fixed, and computations on the test problem of various mesh sizes are performed by the new scheme. The speed-up is shown in Figure 5. Three models were tested by the searching algorithm. With an increase in the mesh size of the computation model, the parallel scalability of the searching algorithm tends to be better. An explanation to this is that when the DOF increase, the number of elements in one subdomain is also increasing; therefore, the searching algorithm is accelerated more efficiently. However, too many elements in one subdomain will occupy more memory, and a trade-off strategy is necessary for parameterization.

4.2. Validation Tests. In this section, a variety of test problems have been presented in order to prove the capability of the parallel Lagrange-Galerkin algorithm. Benchmarks test of

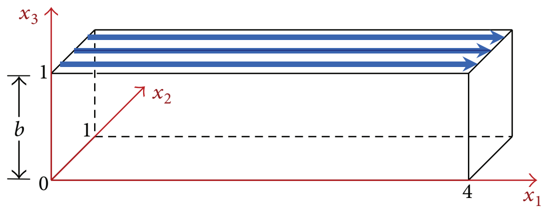

FIGURE 6: A plane Couette flow model.

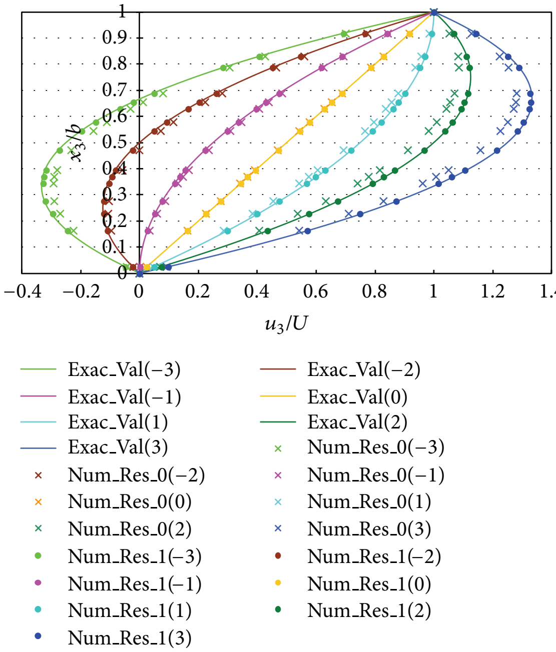

FIGURE 7: Numerical results versus exact solutions.

Navier-Stokes problems are in Sections 4.2.1, 4.2.2, and 4.2.3, and flow-thermal coupled problems are in Sections 4.2.4 and 4.2.5.

4.2.1. A Plane Couette Flow. The solver for Navier-Stokes equations in (1) was first tested with a 3D plane Couette flow. Under ideal conditions, the model is of infinite length; therefore, 4 times of the height is used as the length of the model see Figure 6. A constant velocity $(\hat{u}, 0, 0)$ is applied on the upper horizontal face, and no-slip conditions are set on the lower horizontal face. A pressure gradient is imposed along x_1 for all the faces as essential boundary conditions.

An unstructured 3D mesh was generated by ADVENTURE_TetMesh [25], and the local density around the plane of $x_1 = 2$, where the data was picked from, was enriched. The total DOF is around 1,024,000. The so-called Brinkman number [26] is believed to be the dominating parameter of the flow, and a serious of numerical experiments is done at various Brinkman number. To simulate the infinity length better, the exact solution is enforced on both the left face $(x_1 = 0)$ and the right face $(x_1 = 4)$ as Dirichlet boundary conditions. The comparisons between the computation results and exact solutions are given by Figure 7. Dotted lines are used to present the results, and they are named as "Num_Res_1(B)," where B stands for the Brinkman number. Crossed lines in Figure 7 present the computation results with no exact solutions setting on the left and right faces, and they are named as "Num_Res_0(B)."

It can be seen form Figure 7 that both of these two sets of computation results show good agreement with the exact solution, and dotted lines are closer to the exact solution, representing a better simulation to the ideal condition (cf. [27, 28]).

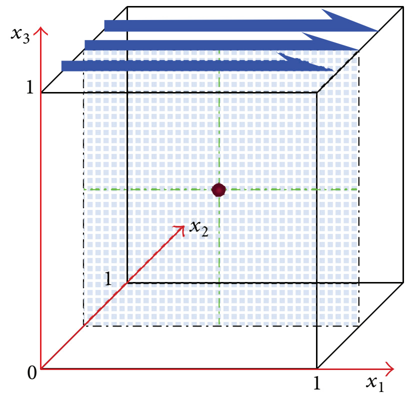

FIGURE 8: A lid-driven cavity model.

4.2.2. A Lid-Driven Cavity. The Navier-Stokes problems solver was then verified by a lid-driven cavity flow. The ideal gas flows over the upper face of the cube, and no-slip conditions are applied to all other faces, as in Figure 8.

All the faces of the cube were set with Dirichlet boundary conditions, and a zero reference pressure was at the centre of the cube to keep the simulation stable. The pressure profiles of the scheme using localized stabilization parameter in (9) and the scheme using constant $(\delta = 1)$ parameter are compared, and the results are show in Figure 9.

Figure 9(a) shows the pressure counters of the scheme with the localized stabilization parameter in (9) and the Figure 9(b), shows scheme with a constant parameter. The model was run at $\mathrm{Re} = 10^4$, and oscillations are viewed in Figure 9(b); however, the isolines in Figure 9(a) is quite smooth, showing that the pressure-stabilization term has a better control on the pressure field at high Reynolds number.

The model was run at different Reynolds numbers with a $128 \times 128 \times 128$ mesh to test the solvability of the new scheme. As shown in Figure 10, when the Reynolds number increases, the eddy at right bottom of plane x_1x_3 vanishes, while the eddy at the left bottom appears due to the increasing in the speed, and the flow goes more likely around the wall. The primary eddy goes lower and lower when Reynolds number becomes higher, and the particle is no longer limited to a single side of the cavity; it can pass from one side to the other, and back again violating the mirror symmetry, as is seen from other planes of Figure 10. Similar 3D results for high Reynolds number were reported by [29], and the solvability of the new solver for high Reynolds number was confirmed.

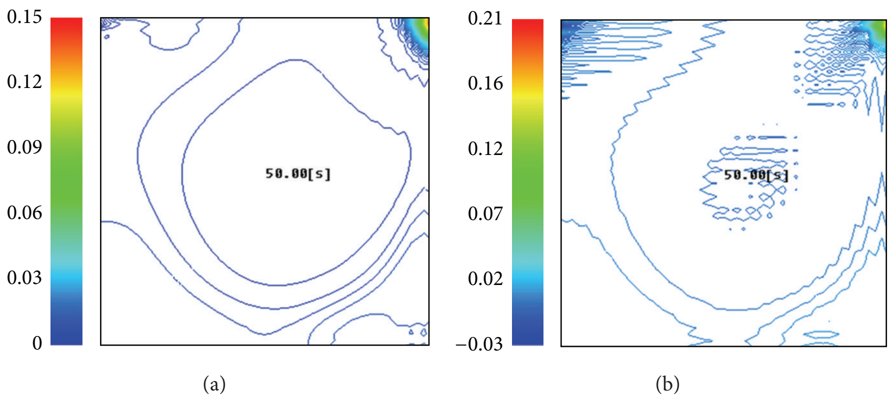

FIGURE 9: Pressure counters ($Re = 10^4$).

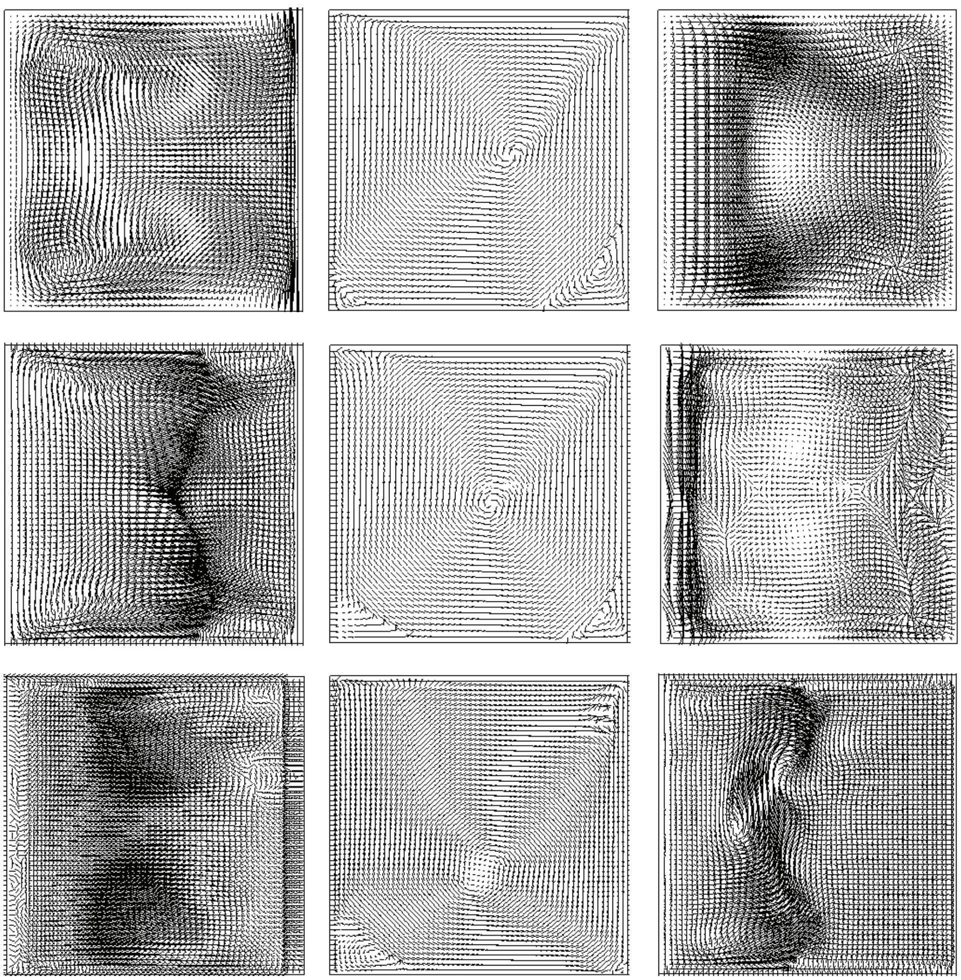

FIGURE 10: Velocity and pressure profiles for different Reynolds number: Re = 1,000 (top), Re = 3,200 (middle), and Re = 12,000 (bottom) along different middle planes: plane x_1x_2 (left), plane x_1x_3 (middle), and plane x_2x_3 (right).

4.2.3. Backward Facing Step. The solver for Navier-Stokes equations was then tested with backward facing step, the fluid considered was air. The problem definition is shown in Figure 11, and the height of the step h is the characteristic length. An unstructured 3D mesh was generated with 419,415 nodal points and 2,417,575 tetrahedral elements, and the local density of mesh was increased around the step.

A laminar flow is considered to enter the domain at inlet section, the inlet velocity profile is parabolic, and the Reynolds number is based on the average velocity at the inlet.

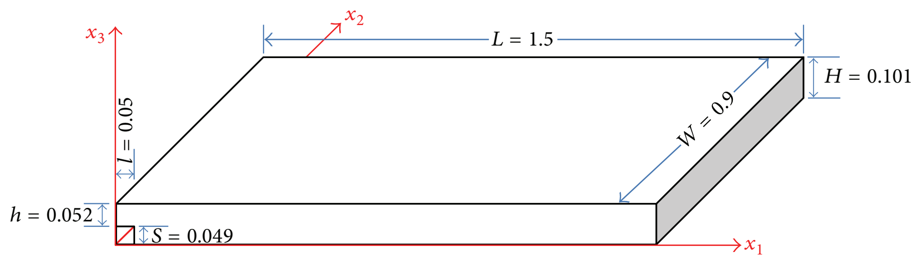

FIGURE 11: Backward facing steps.

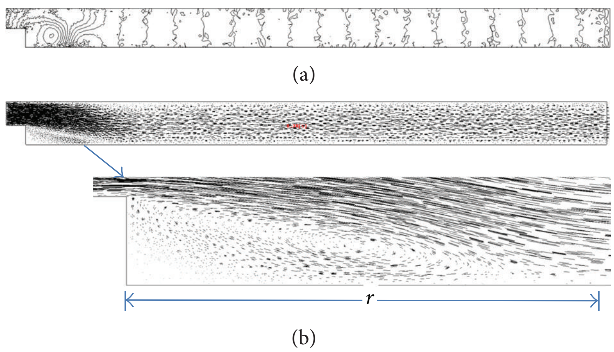

FIGURE 12: Pressure counters (a) and velocity vectors (b) (Re = 200).

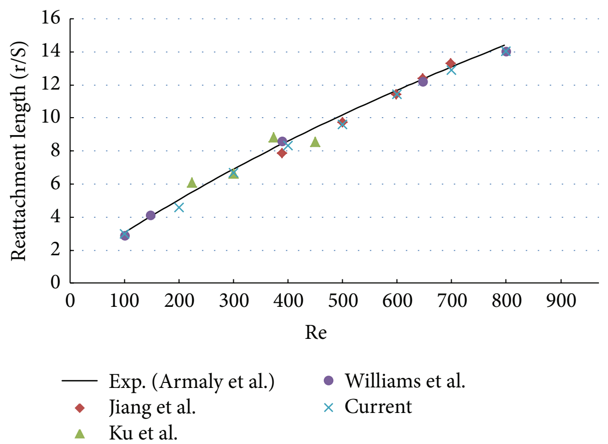

FIGURE 13: Primary reattachment lengths.

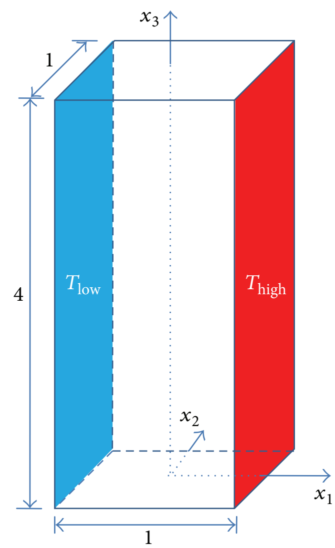

FIGURE 14: The model of infinite plates.

The total length of the domain is 30 times the step height, so that the zero pressure is set at the outlet. A full 3D simulation of the step geometry for $100 \le \text{Re} \le 800$ is present in this paper, and the primary reattachment lengths are predicted.

To determine the reattachment length, the position of the zero-mean-velocity line was measured. The points of detachment and reattachment were taken as the extrapolated zero-velocity line down the wall. The pressure contour in Figure 12(a) confirms the success of the pressure-stabilization method; velocity vectors and the primary attachment are demonstrated in Figure 12(b); similar results have been documented by many, like in [10, 30].

The comparison of primary reattachment length between current results and other available benchmark results are show in Figure 13. It is seen that the agreement is excellent at different Rayleigh numbers (cf. [31, 32]).

4.2.4. Natural Convection of Flat Plates. In order to test the coupled solver of Navier-Stokes equations and the convection-diffusion equation, the third application model was the natural convection between two infinite flat plates. The geometry is given in 3-dimensional by Figure 14. No-slip boundary conditions applied on the left and right vertical walls. The temperature on the left wall is assumed to be lower and set at $5[K]$; the right wall is set at $6[K]$. An unstructured 3D mesh about 1 million tetrahedral elements was generated, and the local grid density around the mid-plane was enriched.

The model was run at the size of $20 \times 20 \times 80$ to get the numerical solutions, and it was compared with the exact solutions in Figure 15. To simulate the infinity length of the plate better, the exact solution is enforced on both the upper face ($x_3 = 4$) and the lower face ($x_3 = 0$) as what is done in Section 4.2.1, and the results are present by a dotted line ("Num_Res_1") in Figure 12. And the model without exact solution set as boundary is named as "Num_Res_0" in Figure 15.

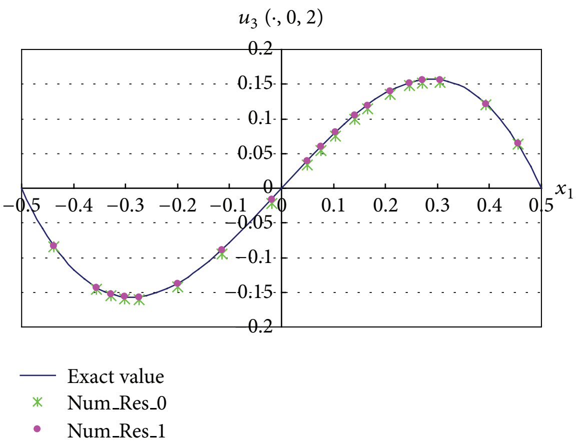

FIGURE 15: Numerical results versus exact solutions.

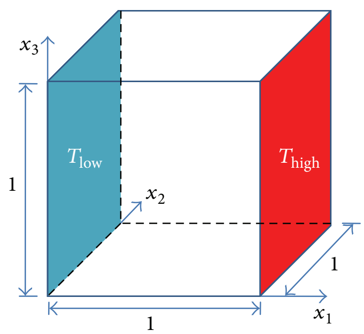

FIGURE 16: A thermal-driven cavity.

With the parameter setting of $\nu = 0.5$, $T_r = 5.5$, $\beta = 1.0$, and $a = 1$, the numerical experiment was performed. Results of the profile on $u_3(\cdot, 0, 2)$, which are believed by many to be very sensitive, are shown in Figure 15. Both "Num_Res_0" and "Num_Res_1" are in great agreement with the exact solutions, and "Num_Res_1" is closer to the exact solution, producing a better simulation to the ideal condition. Similar results have been documented in [33].

4.2.5. Thermal-Driven Cavity. The new solver is also applied to a 3-dimensional nonlinear thermal driven cavity flow problem, which is cavity full of ideal gas; see Figure 16.

No-slip boundary conditions are assumed to prevail on all the walls of the cavity. Both the horizontal walls are assumed to be thermally insulated, and the left and right sides are kept at different temperatures. The cube is divided into $120 \times 120 \times 120$ small cubes, and each small cube contains six tetrahedral elements. The time step is set to 0.01 s, with $\mathrm{Pr} = 0.71$ and $\mathrm{Ra} = 10^4$; the steady state is achieved after 0.39 s, as in Figure 17.

Figures 17(a) and 17(b) show the contour of vorticity and the velocity vectors at the steady stage, respectively, from the front view. The temperature contour is shown in Figure 17(c), and pressure profiles are show in Figure 17(d). The previous results convince us of the success in solving flow-thermal coupled problems described by (1) and (4). Similar three-dimensional results can also be found in [33, 34]. The pressure profile in Figure 17(d) is smooth and symmetric, implying that the stabilization item in (8) works well.

In order to further validate the new solver, a comparison of temperature and velocity profiles of the current solver and other benchmark results was made. The centreline velocity results $w(\cdot, 0.5, 0.5)$ and the temperature results $T(\cdot, 0.5, 0.5)$, which are believed to be very sensitive in this simulation, are present in diagrams (a) and (b) of Figure 18, respectively. The velocity results share close resemblance to that of the ADV_sFlow 0.5, and they both show the more end-wall effects compared with the results of 2D case. The three temperature results show good agreement with each other, and the line representing the current results is the smoothest, as the mesh is the finest among the three. Similar results have been reported by other researchers (cf. [10, 33, 34]).

Thermal convection problems are believed to be dominated by two dimensionless numbers by many researchers, the Prandtl number and the Rayleigh number. To acquaint ourselves with the solvability of the new solver and to challenge applications of higher difficulty, a wide range of Rayleigh numbers from 10^3 to 10^7 is studied with $\mathrm{Pr} = 0.71$, and the results for the steady-state solution are presented in Figure 19. Dimensionless length is used and the variation of Rayleigh number is determined by changing the characteristic length of the model.

The local Nusselt number ($\mathrm{Nu} = \partial T/\partial x_1$) is a concern of many researchers, as they are sensitive to the mesh size. In Figure 19, the diagram (a) and the diagram (b) represent the local Nusselt number at the hot wall and the cold wall, respectively. Similar results can also be found in [10, 30, 35, 36]. The capability of the solver based on domain decomposed Lagrange-Galerkin scheme for high Rayleigh number is also confirmed by this figure.

The new solver enables the simulation of large scale problems, thus models of Rayleigh number up to 10^7 can be run on small PC cluster. In this simulation, an unstructured mesh of 30,099,775 DOF is generated, the time step, is 0.01 s and it takes about 24 hours to finish, using the a small Linux cluster of 64 PEs (64 cores@2.66 GHz).

5. Conclusions

A pressure-stabilized Lagrange-Galerkin method is implemented in a domain decomposition system in this research. By using localized stabilization parameter, the new scheme shows better control in the pressure field than constant stabilization parameter; therefore it has good solvability at high Reynolds number and high Rayleigh number. The reliability and accuracy of the present numerical results are validated by comparing with the exact solutions and recognized numerical results. Based on a domain decomposition method, the element searching algorithm shows good numerical scalability and parallel efficiency. The new solver reduces the memory consumption and is faster than classical product-type solvers. It is able to solve large scale problems of over 30 million degrees of freedom within one day by a small PC cluster.

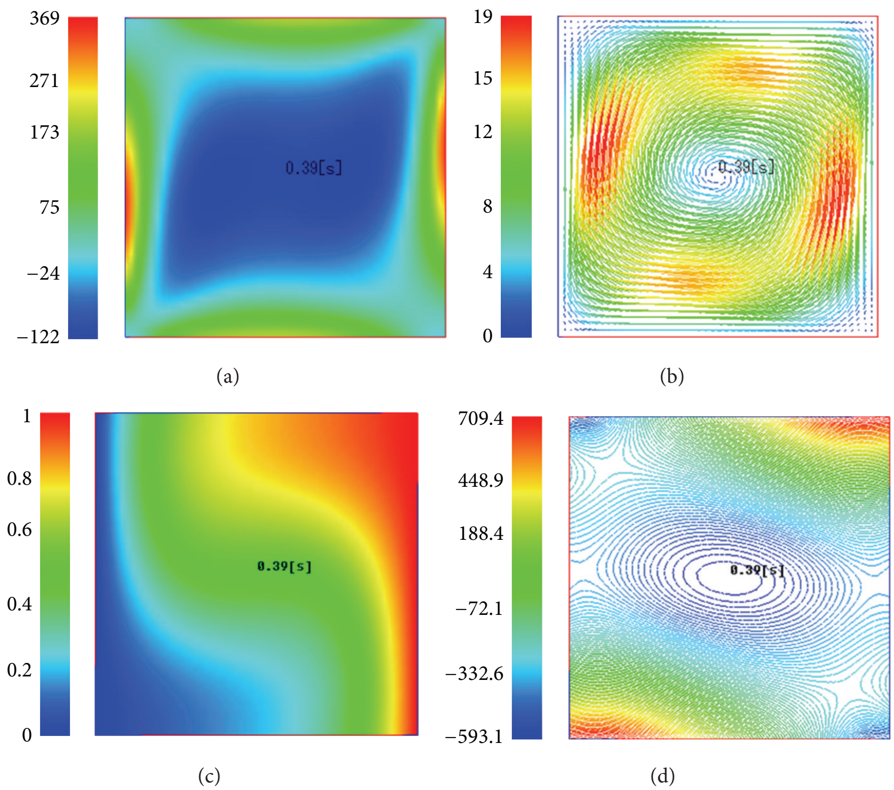

FIGURE 17: Steady state of the thermal-driven cavity (Ra = 10^4).

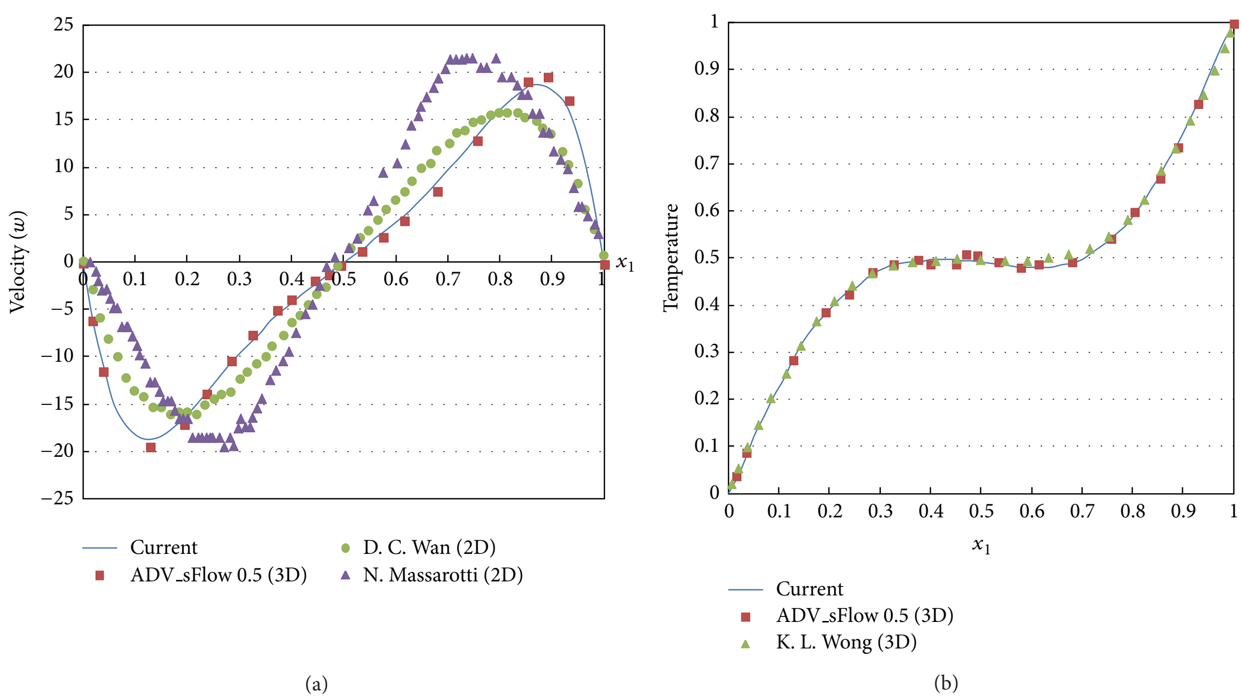

FIGURE 18: Centerline temperature velocity profiles of the symmetry plane (Ra = 10^4).

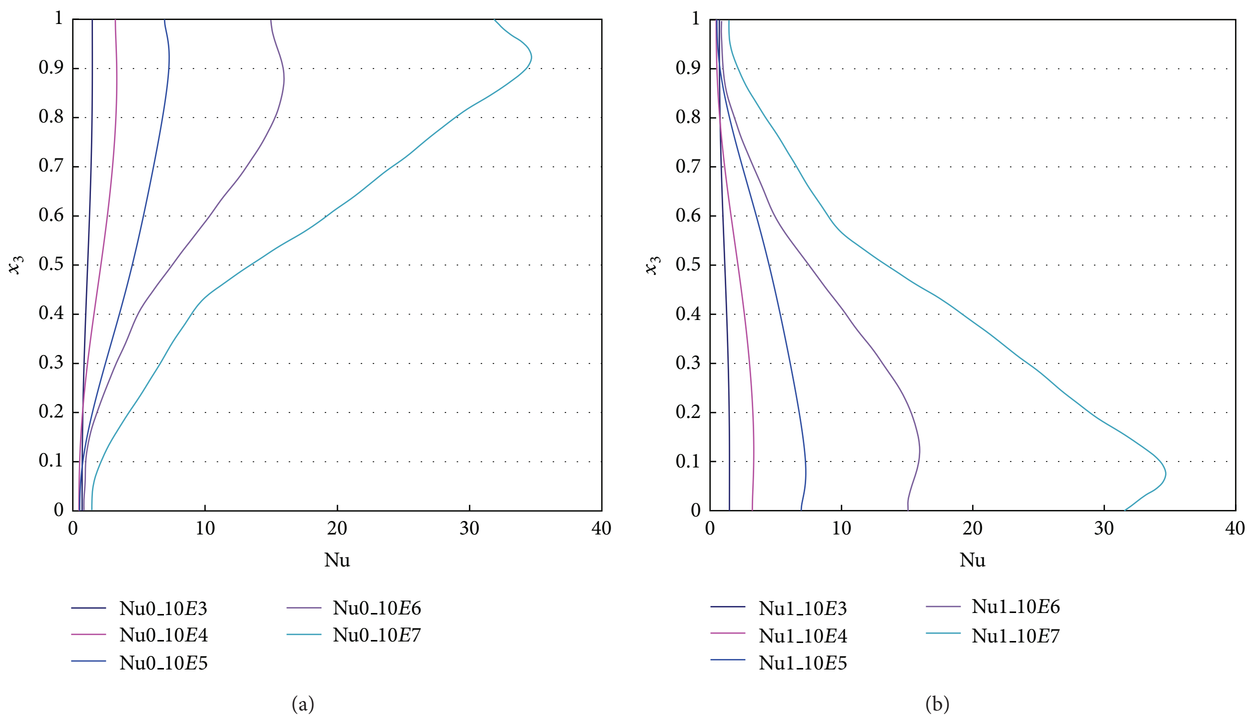

FIGURE 19: Local Nusselt number along the hot wall (a) and the cold wall (b).

Acknowledgments

This work was supported by the National Science Foundation of China (NSFC), Grants 11202248, 91230114, and 11072272; the China Postdoctoral Science Foundation, Grant 2012M521646, and the Guangdong National Science Foundation, Grant S2012040007687.

References

[1] M. Bercovier, O. Pironneau, and V. Sastri, "Finite elements and characteristics for some parabolic-hyperbolic problems," *Applied Mathematical Modelling*, vol. 7, no. 2, pp. 89–96, 1983.

[2] J. Douglas Jr. and T. F. Russell, "Numerical methods for convection-dominated diffusion problems based on combining the method of characteristics with finite element or finite difference procedures," *SIAM Journal on Numerical Analysis*, vol. 19, no. 5, pp. 871–885, 1982.

[3] O. Pironneau, "On the transport-diffusion algorithm and its applications to the Navier-Stokes equations," *Numerische Mathematik*, vol. 38, no. 3, pp. 309–332, 1982.

[4] T. F. Russell, "Time stepping along characteristics with incomplete iteration for a Galerkin approximation of miscible displacement in porous media," *SIAM Journal on Numerical Analysis*, vol. 22, no. 5, pp. 970–1013, 1985.

[5] O. Pironneau, *Finite Element Methods for Fluids*, John Wiley & Sons, Chichester, UK, 1989.

[6] H. Notsu, "Numerical computations of cavity flow problems by a pressure stabilized characteristic-curve finite element scheme," in *Japan Society for Computational Engineering and Science*, 2008.

[7] H. Notsu and M. Tabata, "A combined finite element scheme with a pressure stabilization and a characteristic-curve method for the Navier-Stokes equations," *Transactions of the Japan Society for Industrial and Applied Mathematics*, vol. 18, no. 3, pp. 427–445, 2008.

[8] M. Tabata and S. Fujima, "Robustness of a characteristic finite element scheme of second order in time increment," in *Computational Fluid Dynamics 2004*, pp. 177–182, 2006.

[9] H. Rui and M. Tabata, "A second order characteristic finite element scheme for convection-diffusion problems," *Numerische Mathematik*, vol. 92, no. 1, pp. 161–177, 2002.

[10] N. Massarotti, P. Nithiarasu, and O. C. Zienkiewicz, "Characteristic-based split (CBS) algorithm for incompressible flow problems with heat transfer," *International Journal of Numerical Methods for Heat and Fluid Flow*, vol. 11, no. 3, p. 278, 2001.

[11] F. Brezzi and M. Fortin, *Mixed and Hybrid Finite Element Methods*, vol. 15 of *Springer Series in Computational Mathematics*, Springer, New York, NY, USA, 1991.

[12] F. Brezzi and J. Douglas Jr., "Stabilized mixed methods for the Stokes problem," *Numerische Mathematik*, vol. 53, no. 1-2, pp. 225–235, 1988.

[13] H. Jia, D. Liu, and K. Li, "A characteristic stabilized finite element method for the non-stationary Navier-Stokes equations," *Computing*, vol. 93, no. 1, pp. 65–87, 2011.

[14] H. Kanayama, D. Tagami, T. Araki, and H. Kume, "A stabilization technique for steady flow problems," *International Journal of Computational Fluid Dynamics*, vol. 18, no. 4, pp. 297–301, 2004.

[15] C. R. Dohrmann and P. B. Bochev, "A stabilized finite element method for the Stokes problem based on polynomial pressure projections," *International Journal for Numerical Methods in Fluids*, vol. 46, no. 2, pp. 183–201, 2004.

[16] H. M. Park and M. C. Sung, "Stabilization of two-dimensional Rayleigh-Bénard convection by means of optimal feedback control," *Physica D*, vol. 186, no. 3-4, pp. 185–204, 2003.

[17] T. Barth, P. Bochev, M. Gunzburger, and J. Shadid, "A taxonomy of consistently stabilized finite element methods for the Stokes problem," *SIAM Journal on Scientific Computing*, vol. 25, no. 5, pp. 1585–1607, 2004.

[18] P. B. Bochev, M. D. Gunzburger, and R. B. Lehoucq, "On stabilized finite element methods for the Stokes problem in the small time step limit," *International Journal for Numerical Methods in Fluids*, vol. 53, no. 4, pp. 573–597, 2007.

[19] G. C. Buscaglia and E. A. Dari, "Implementation of the Lagrange-Galerkin method for the incompressible Navier-Stokes equations," *International Journal for Numerical Methods in Fluids*, vol. 15, no. 1, pp. 23–26, 1992.

[20] H. A. van der Vorst, *Iterative Krylov Methods for Large Linear Systems*, vol. 13 of *Cambridge Monographs on Applied and Computational Mathematics*, Cambridge University Press, Cambridge, UK, 2003.

[21] T. J. R. Hughes, L. P. Franca, and M. Balestra, "A new finite element formulation for computational fluid dynamics. V. Circumventing the Babuška-Brezzi condition: a stable Petrov-Galerkin formulation of the Stokes problem accommodating equal-order interpolations," *Computer Methods in Applied Mechanics and Engineering*, vol. 59, no. 1, pp. 85–99, 1986.

[22] A. Toselli and O. Widlund, *Domain Decomposition Methods—Algorithms and Theory*, vol. 34 of *Springer Series in Computational Mathematics*, Springer, Berlin, Germany, 2005.

[23] Q. Yao, H. Kanayama, H. Notsu, and M. Ogino, "Balancing domain decomposition for non-stationary incompressible flow problems using a characteristic-curve method," *Journal of Computational Science and Technology*, vol. 4, pp. 121–135, 2010.

[24] Q. H. Yao and Q. Y. Zhu, "Investigation of the contamination control in a cleaning room with a moving Agv by 3D large-scale simulation," *Journal of Applied Mathematics*, vol. 2013, Article ID 570237, 10 pages, 2013.

[25] "Adventure Project," http://adventure.sys.t.u-tokyo.ac.jp/.

[26] C. W. Hall, *Laws and Models: Science, Engineering, and Technology*, CRC Press, 2000.

[27] R. S. Brodkey and H. C. Hershey, *Basic Concepts in Transport Phenomena*, Brodkey, 2001.

[28] S. M. Richardson, *Fluid Mechanics*, Hemisphere, 1989.

[29] E. Hachem, B. Rivaux, T. Kloczko, H. Digonnet, and T. Coupez, "Stabilized finite element method for incompressible flows with high Reynolds number," *Journal of Computational Physics*, vol. 229, no. 23, pp. 8643–8665, 2010.

[30] M. T. Manzari, "An explicit finite element algorithm for convection heat transfer problems," *International Journal of Numerical Methods for Heat and Fluid Flow*, vol. 9, no. 8, pp. 860–877, 1999.

[31] N. A. Malamataris, "A numerical investigation of wall effects in three-dimensional, laminar flow over a backward facing step with a constant aspect and expansion ratio," *International Journal for Numerical Methods in Fluids*, vol. 71, pp. 1073–1102, 2013.

[32] P. T. Williams and A. J. Baker, "Numerical simulations of laminar flow over a 3D backward-facing step," *International Journal for Numerical Methods in Fluids*, vol. 24, no. 11, pp. 1159–1183, 1997.

[33] H. Kanayama, K. Komori, and D. Sato, "Development of a Thermal Convection Solver with Hierarchical Domain Decomposition Method," in *Proceedings of the 8th World Congress on Computational Mechanics and the 5th European Congress on Computational Methods in Applied Sciences and Engineering*, Venice, Italy, 2008.

[34] K. L. Wong and A. J. Baker, "A 3D incompressible Navier-Stokes velocity-vorticity weak form finite element algorithm," *International Journal for Numerical Methods in Fluids*, vol. 38, no. 2, pp. 99–123, 2002.

[35] G. de Vahl Davis, "Natural convection of air in a square cavity: a bench mark numerical solution," *International Journal for Numerical Methods in Fluids*, vol. 3, no. 3, pp. 249–264, 1983.

[36] G. de Vahl Davis and I. P. Jones, "Natural convection in square cavity: a comparison exercise," *International Journal for Numerical Methods in Fluids*, vol. 3, no. 3, pp. 227–248, 1983.

Hindawi Publishing Corporation
Abstract and Applied Analysis
Volume 2013, Article ID 769102, 10 pages
http://dx.doi.org/10.1155/2013/769102

Research Article

A Note on the Triple Laplace Transform and Its Applications to Some Kind of Third-Order Differential Equation

Abdon Atangana

Institute for Groundwater Studies, Faculty of Natural and Agricultural Sciences, University of the Free State, Bloemfontein 9300, South Africa

Correspondence should be addressed to Abdon Atangana; abdonatangana@yahoo.fr

Received 25 March 2013; Accepted 20 May 2013

Academic Editor: R. K. Bera

We introduced a relatively new operator called the triple Laplace transform. We presented some properties and theorems about the relatively new operator. We examine the triple Laplace transform of some function of three variables. We make use of the operator to solve some kind of third-order differential equation called "Mboctara equations."

1. Introduction

The topic of partial differential equations is one of the most important subjects in mathematics and other sciences. The behaviour of the solution very much depends essentially on the classification of PDEs therefore the problem of classification for partial differential equations is very natural and well known since the classification governs the sufficient number and the type of the conditions in order to determine whether the problem is well posed and has a unique solution. The Laplace transform has been intensively used to solve nonlinear and linear equations [1–7]. The Laplace transform is used frequently in engineering and physics; the output of a linear time invariant system can be calculated by convolving its unit impulse response with the input signal. Performing this calculation in Laplace space turns the convolution into a multiplication; the latter is easier to solve because of its algebraic form. The Laplace transform can also be used to solve differential equations and is used extensively in electrical engineering [1–7]. The Laplace transform reduces a linear differential equation to an algebraic equation, which can then be solved by the formal rules of algebra. The original differential equation can then be solved by applying the inverse Laplace transform. The English electrical engineer Oliver Heaviside first proposed a similar scheme, although without using the Laplace transform, and the resulting operational calculus is credited as the Heaviside calculus. Recently Kılıçman et al. [8–11] extended the Laplace transform to the concept of double Laplace transform. This new operator has been intensively used to solve some kind of differential equation [11] and fractional differential equations. The aim of this work is to extend the Laplace transform to the triple Laplace transform. We will start with the definition of the triple Laplace transform.

2. Definitions and Theorems

Definition 1. Let f be a continuous function of three variables; then, the triple Laplace transform of $f(x,y,t)$ is defined by

$$\begin{aligned} L_{x,y,t}\left[f(x,y,t)\right] &= F(p,s,k)\iiint_0^{\infty}\exp[-px]\exp[-sy] \\ &\quad\times\exp[-kt]\,f(x,y,t)\,dx\,dy\,dt, \end{aligned} \tag{1}$$

where, $x, y, t > 0$ and p, s, k are Laplace variables, and

$$\begin{aligned} &f(x,y,t) \\ &= \frac{1}{2\pi i}\int_{\alpha-i\infty}^{\alpha+i\infty}e^{px} \\ &\qquad\times\left[\frac{1}{2\pi i}\int_{\beta-i\infty}^{\beta+i\infty}e^{sy}\right. \end{aligned}$$

$$\times\left[\frac{1}{2\pi i}\int_{\mu-i\infty}^{\mu+i\infty}e^{kt}\right.$$
$$\left.\left.\left.\times F(p,s,k)\,dk\right]ds\right]dp \tag{2}$$

is the inverse triple Laplace transform.

Property 2. Assuming that the continuous function $f(x,y,t)$ is triple Laplace transformable, then,

$$\begin{aligned}
&L_{t,y,x}\left[\frac{\partial^3 f(x,y,t)}{\partial x\partial y\partial t}\right]\\
&\quad= pskF(p,s,k) - psF(p,s,0) - psF(p,0,k)\\
&\qquad+ pF(p,0,0) - skF(0,s,k) + sF(0,s,0)\\
&\qquad+ kF(0,0,k) - F(0,0,0),\\
&L_{x,x,t}\left[\frac{\partial^3 f(x,y,t)}{\partial t\partial x^2}\right]\\
&\quad= kp^2F(p,y,k) - pkF(0,y,k) - \frac{\partial F(0,y,k)}{\partial x}\\
&\qquad- p^2F(p,y,0) + pF(0,y,0) + \frac{\partial F(0,y,0)}{\partial x},\\
&L_{xxx}\left[\frac{\partial^3 f(x,y,t)}{\partial x^3}\right]\\
&\quad= p^3F(p,y,t) - p^2F(0,y,t)\\
&\qquad- p\frac{\partial F(0,y,t)}{\partial x} - \frac{\partial^2 F(0,y,t)}{\partial x^2}.
\end{aligned} \tag{3}$$

3. Uniqueness and Existence of the Triple Laplace Transform

In this section, we will study the uniqueness and existence of triple Laplace transform. First of all, let $f(x,y,t)$ be a continuous function on the interval $[0,\infty)$ which is of exponential order, that is, for some $a,b,c\in R$. Consider

$$\sup_{x,y,t>0}\left|\frac{f(x,y,t)}{\exp[ax+by+ct]}\right|<0. \tag{4}$$

Under the previous condition, the triple Laplace transform,

$$\begin{aligned}F(p,s,k) = \iiint_0^\infty &\exp[-px]\exp[-sy]\\ &\times\exp[-kt]\,f(x,y,t)\,dx\,dy\,dt,\end{aligned} \tag{5}$$

exists for all $p>a$, $s>b$, and $k>c$ and is in actuality infinitely differentiable with respect to $p>a$, $s>b$ and $k>c$. All functions in this study are assumed to be of exponential order. The following theorem shows that $f(x,y,t)$ can be uniquely obtained from $F(p,s,t)$.

Theorem 3. *Let $f(x,y,t)$ and $g(x,y,t)$ be continuous functions defined for $x,y,t\geq 0$ and having Laplace transforms, $F(p,s,k)$ and $G(p,s,k)$, respectively. If $F(p,s,k)=G(p,s,k)$, then $f(x,y,t)=g(x,y,t)$.*

Proof. From the definition of the inverse Laplace transform, if α, β, and μ are sufficiently large, then the integral expression, by

$$\begin{aligned}
f(x,y,t) &= \frac{1}{2\pi i}\int_{\alpha-i\infty}^{\alpha+i\infty}e^{px}\\
&\quad\times\left[\frac{1}{2\pi i}\int_{\beta-i\infty}^{\beta+i\infty}e^{sy}\right.\\
&\quad\times\left[\frac{1}{2\pi i}\int_{\mu-i\infty}^{\mu+i\infty}e^{kt}\right.\\
&\quad\left.\left.\times F(p,s,k)\,dk\right]ds\right]dp,
\end{aligned} \tag{6}$$

for the triple inverse Laplace transform, can be used to obtain

$$\begin{aligned}
f(x,y,t) &= \frac{1}{2\pi i}\int_{\alpha-i\infty}^{\alpha+i\infty}e^{px}\\
&\quad\times\left[\frac{1}{2\pi i}\int_{\beta-i\infty}^{\beta+i\infty}e^{sy}\right.\\
&\quad\times\left[\frac{1}{2\pi i}\int_{\mu-i\infty}^{\mu+i\infty}e^{kt}\right.\\
&\quad\left.\left.\times F(p,s,k)\,dk\right]ds\right]dp.
\end{aligned} \tag{7}$$

By hypothesis, we have that $F(p,s,k) = G(p,s,k)$. then replacing this in the previous expression, we have the following:

$$\begin{aligned}
f(x,y,t) &= \frac{1}{2\pi i}\int_{\alpha-i\infty}^{\alpha+i\infty}e^{px}\\
&\quad\times\left[\frac{1}{2\pi i}\int_{\beta-i\infty}^{\beta+i\infty}e^{sy}\right.\\
&\quad\times\left[\frac{1}{2\pi i}\int_{\mu-i\infty}^{\mu+i\infty}e^{kt}\right.\\
&\quad\left.\left.\times G(p,s,k)\,dk\right]ds\right]dp,
\end{aligned} \tag{8}$$

which boil down to

$$f(x,y,t) = \frac{1}{2\pi i}\int_{\alpha-i\infty}^{\alpha+i\infty} e^{px} \times \left[\frac{1}{2\pi i}\int_{\beta-i\infty}^{\beta+i\infty} e^{sy} \times \left[\frac{1}{2\pi i}\int_{\mu-i\infty}^{\mu+i\infty} e^{kt} \times G(p,s,k)\,dk\right] ds\right] dp, = g(x,y,t), \quad (9)$$

and this proves the uniqueness of the triple Laplace transform. □

Theorem 4. *If, at the point (p,s,k), the integrals*

$$F_1(p,s,k) = \iiint_0^\infty \exp[-px]\exp[-sy] \times \exp[-kt]\, f_1(x,y,t)\,dx\,dy\,dt$$
$$F_2(p,s,k) = \iiint_0^\infty \exp[-px]\exp[-sy] \times \exp[-kt]\, f_2(x,y,t)\,dx\,dy\,dt \quad (10)$$

are convergent and in addition if

$$F_3(p,s,k) = \iiint_0^\infty \exp[-px]\exp[-sy] \times \exp[-kt]\, f_3(x,y,t)\,dx\,dy\,dt \quad (11)$$

is absolutely convergent, then, the following expression:

$$F(p,s,k) = F_1(p,s,k)\,F_2(p,s,k)\,F_3(p,s,k) \quad (12)$$

is the Laplace transform of the function

$$f(x,y,t) = \int_0^t\int_0^y\int_0^x f_3(x-(x_1+\rho), y-(y_1+\sigma), t-(t_1+\tau))\, f_2(x_1-\rho, y_1-\sigma, t_1-\tau) \times f_1(\rho,\sigma,\tau)\,d\rho\,d\sigma\,d\tau, \quad (13)$$

and the integral

$$F(p,s,k) = \iiint_0^\infty \exp[-px]\exp[-sy] \times \exp[-kt]\, f(x,y,t)\,dx\,dy\,dt \quad (14)$$

is convergent at the point (p,s,k); for the readers who are interested, they can see the proof in [11, 12].

Theorem 5. *A function $f(x,y,t)$ which is continuous on $[0,\infty)$ and satisfies the growth condition (4) can be recovered from only $F(p,s,k)$ as*

$$f(x,y,t) = \lim_{\substack{n_1\to\infty\\ n_2\to\infty\\ n_3\to\infty}} \frac{(-1)^{n_1+n_2+n_3}}{n_1!n_2!n_3!}\left(\frac{n_1}{x}\right)^{n_1+1}\left(\frac{n_2}{y}\right)^{n_2+1} \times \left(\frac{n_3}{t}\right)^{n_3+1} X^{n_1+n_2+n_3}\left[\frac{n_1}{x},\frac{n_2}{y},\frac{n_3}{t}\right]. \quad (15)$$

Evidently, the main difficulty in using Theorem 5 for computing the inverse Laplace transform is the repeated symbolic differentiation of $F(p,s,k)$.

Let us see how Theorem 5 can be applicable. Let us consider the following functions:

$$f(x,y,t) = \exp[-ax-by-ct]. \quad (16)$$

Naturally the triple Laplace transform of the previous function is given later as

$$F(p,s,k) = \frac{1}{(p-a)(s-b)(k-c)}. \quad (17)$$

Now applying the high-order mixed derivative to the previous expression, we obtain the following:

$$\frac{\partial^{n_1+n_2+n_3}[F(p,s,k)]}{\partial p^{n_1}\partial s^{n_2}\partial k^{n_3}} = n_1!n_2!n_3!(-1)^{n_1+n_2+n_3} \times (a+P)^{-1-n_1}(s+b)^{-1-n_2}(c+k)^{-1-n_3}. \quad (18)$$

Applying Theorem 5 in the previous expression, we obtain the following result:

$$f(x,y,t) = \lim_{\substack{n_1\to\infty\\ n_2\to\infty\\ n_3\to\infty}} \frac{{n_1}^{1+n_1}{n_2}^{1+n_2}{n_3}^{1+n_3}}{x^{n_1+1}y^{n_2+1}t^{n_3+1}}\left(a+\frac{n_1}{x}\right)^{-n_1-1} \times \left(b+\frac{n_2}{y}\right)^{-n_2-1}\left(c+\frac{n_3}{t}\right)^{-n_3-1}. \quad (19)$$

Making a change of variable in the previous expression, we obtain the following simplified result:

$$f(x,y,t) = \lim_{\substack{n_1\to\infty\\ n_2\to\infty\\ n_3\to\infty}} \left(1+\frac{an_1}{x}\right)^{-n_1-1}\left(1+\frac{bn_2}{y}\right)^{-n_2-1} \times \left(1+\frac{cn_3}{t}\right)^{-n_3-1}. \quad (20)$$

Using together, the application of logarithm and the L'Hôpital's rule on the previous expression, we arrive at the following result:

$$\ln(f(x,y,t)) = -ax-by-ct \Longrightarrow f(x,y,t) = \exp[-ax-by-ct]. \quad (21)$$

4. Some Properties of Triple Laplace Transform

In this section, we present some properties of the triple Laplace transform. Note that these properties follow from those of the double Laplace transform introduced by Kılıçman and Eltayeb [8]. The properties of the triple Laplace transform will enable us to find further transform pairs $\{f(x,y,t), F(p,s,k)\}$:

(i)
$$F(p+a,s+b,k+d) = L_{x,y,t}\left[e^{-ax-yb-ct}f(x,y,t)\right](p,s,k). \tag{22}$$

We will present the proof

$$\begin{aligned}
&L_{x,y,t}\left[e^{-ax-yb-ct}f(x,y,t)\right](p,s,k)\\
&\quad=\iiint_0^\infty \exp[-px]\exp[-sy]\exp[-kt]\exp[-ax]\\
&\qquad\times\exp[-by]\exp[-ct]\,f(x,y,t)\,dx\,dy\,dt,\\
&\int_0^\infty \exp[-px]\exp[-ax]\\
&\quad\times\left(\iint_0^\infty \exp[-sy]\exp[-kt]\exp[-by]\right.\\
&\qquad\left.\times\exp[-ct]\,f(x,y,t)\,dt\,dy\right)dt.
\end{aligned} \tag{23}$$

Note that the integral inside the bracket satisfies the properties of the double Laplace transform and is given as [11]

$$\begin{aligned}
&\left(\iint_0^\infty \exp[-sy]\exp[-kt]\exp[-by]\exp[-ct]\right.\\
&\quad\left.\times f(x,y,t)\,dt\,dy\right) = F(x,s+b,k+d).
\end{aligned} \tag{24}$$

Thus

$$\begin{aligned}
&\int_0^\infty \exp[-px]\exp[-ax]\,F(x,s+b,k+d)\,dt\\
&\quad= F(p+a,s+b,k+d),
\end{aligned} \tag{25}$$

and this completes the proof.

(ii) The following can also be observed:

$$\frac{1}{\alpha\beta\gamma}F\left(\frac{p}{\alpha},\frac{s}{\beta},\frac{k}{\gamma}\right) = L_{x,y,t}\left[f(\alpha x,\beta y,\gamma t)\right](p,s,k). \tag{26}$$

We will present the proof

$$\begin{aligned}
&L_{x,y,t}\left[f(\alpha x,\beta y,\gamma t)\right](p,s,k)\\
&\quad=\iiint_0^\infty \exp[-px]\exp[-sy]\exp[-kt]\\
&\qquad\times f(\alpha x,\beta y,\gamma t)\,dx\,dy\,dt,\\
&\int_0^\infty \exp[-px]\left(\iint_0^\infty \exp[-sy]\exp[-kt]\right.\\
&\qquad\left.\times f(\alpha x,\beta y,\gamma t)\,dy\,dt\right)dx.
\end{aligned} \tag{27}$$

Note that the double integral inside the bracket satisfies the property of the double Laplace transform as [11]

$$\begin{aligned}
&\left(\iint_0^\infty \exp[-sy]\exp[-kt]\,f(\alpha x,\beta y,\gamma t)\,dy\,dt\right)\\
&\quad=\frac{1}{\beta\gamma}F\left(\alpha x,\frac{s}{\beta},\frac{k}{\gamma}\right).
\end{aligned} \tag{28}$$

Thus

$$\begin{aligned}
&L_{x,y,t}\left[f(\alpha x,\beta y,\gamma t)\right](p,s,k)\\
&\quad=\int_0^\infty \exp[-px]\frac{1}{\beta\gamma}F\left(\alpha x,\frac{s}{\beta},\frac{k}{\gamma}\right)dx\\
&\quad=\frac{1}{\alpha\beta\gamma}F\left(\frac{p}{\alpha},\frac{s}{\beta},\frac{k}{\gamma}\right),
\end{aligned} \tag{29}$$

and this completes the proof.

(iii) The following property can also be observed:

$$\begin{aligned}
&\frac{\partial^{n+m+v}\left[F(p,s,k)\right]}{\partial p^n\partial s^n\partial k^v}\\
&\quad= L_{x,y,t}\left[(-1)^{n+m+v}x^n y^m t^v f(x,y,t)\right](p,s,k).
\end{aligned} \tag{30}$$

We will present the proof

$$\begin{aligned}
F(p,s,k) = {}&\iiint_0^\infty \exp[-px]\exp[-sy]\exp[-kt]\\
&\times f(x,y,t)\,dx\,dy\,dt.
\end{aligned} \tag{31}$$

Then,

$$\begin{aligned}
&\frac{\partial^{n+m+v}\left[F(p,s,k)\right]}{\partial p^n\partial s^n\partial k^v}\\
&\quad=\frac{\partial^{n+m+v}}{\partial p^n\partial s^n\partial k^v}\left(\iiint_0^\infty \exp[-px]\exp[-sy]\right.\\
&\qquad\left.\times\exp[-kt]\,f(x,y,t)\,dx\,dy\,dt\right).
\end{aligned} \tag{32}$$

Now making use of the convergence properties of the improper integral involved, we can interchange the operation of differentiation and integration and differentiate with respect to p, s, and k under the integral sign. Thus, we arrive at the following expression:

$$\begin{aligned} &\frac{\partial^{n+m+v}\left[F(p,s,k)\right]}{\partial p^n \partial s^n \partial k^v} \\ &\quad = \frac{\partial^n}{\partial p^n}\int_0^\infty \exp\left[-px\right] \\ &\qquad \times \left(\frac{\partial^{m+v}}{\partial s^n \partial k^v}\iint_0^\infty \exp\left[-sy\right]\exp\left[-kt\right] \right. \\ &\qquad\qquad \left. \times f(x,y,t)\,dy\,dt\right) dx. \end{aligned} \tag{33}$$

Note that the expression in the bracket satisfies the property of the double Laplace transform as [11]

$$\begin{aligned} &\frac{\partial^{m+v}}{\partial s^n \partial k^v}\iint_0^\infty \exp\left[-sy\right]\exp\left[-kt\right] f(x,y,t)\,dy\,dt \\ &\quad = L_{y,t}\left[(-1)^{m+v} y^m t^v f(x,y,t)\right](s,k). \end{aligned} \tag{34}$$

Thus

$$\begin{aligned} &\frac{\partial^{n+m+v}\left[F(p,s,k)\right]}{\partial p^n \partial s^n \partial k^v} \\ &\quad = \frac{\partial^n}{\partial p^n}\int_0^\infty \exp\left[-px\right] \\ &\qquad \times \left(L_{y,t}\left[(-1)^{m+v} y^m t^v f(x,y,t)\right](s,k)\right) dx. \end{aligned} \tag{35}$$

And finally, we obtain

$$\begin{aligned} &\frac{\partial^{n+m+v}\left[F(p,s,k)\right]}{\partial p^n \partial s^n \partial k^v} \\ &\quad = L_{x,y,t}\left[(-1)^{n+m+v} x^n y^m t^v f(x,y,t)\right](p,s,k), \end{aligned} \tag{36}$$

and this completes the proof.

Now using the previous three properties, we will show the proof of Theorem 5.

Proof of Theorem 5. Let us define the set of functions depending on parameters m, n, and v as

$$h_{m,n,v}(x,y,t) = \frac{m^{m+1} n^{n+1} v^{v+1}}{m!n!v!} x^m y^n t^v e^{-mx-ny-vt}. \tag{37}$$

It worth noting that the previous function is a kind of three-dimensional density of probability, and it therefore follows that

$$\iiint_0^\infty h_{m,n,v}(x,y,t)\,dx\,dy\,dt = 1. \tag{38}$$

In addition of this, we will have that

$$\lim_{\substack{m\to\infty\\ n\to\infty\\ v\to\infty}} \iiint_0^\infty h_{m,n,v}(x,y,t)\,\psi(x,y,t)\,dx\,dy\,dt = \psi(1,1,1), \tag{39}$$

where $\psi(x,y,t)$ is any continuous function. Let $\Psi(p,s,k)$ denote the triple Laplace transform of the continuous function $\psi(x,y,t)$. However, if one defines the function $M(x,y,t) = f(x\alpha, y\beta, t\gamma)$, making use of the second property established in (29), we arrive at the following:

$$\frac{1}{\alpha\beta\gamma}F\left(\frac{p}{\alpha},\frac{s}{\beta},\frac{k}{\gamma}\right) = L_{x,y,t}\left[f(\alpha x, \beta y, \gamma t)\right](p,s,k). \tag{40}$$

Here if one applies the third property, in particular by replacing $p = m/x$, $s = n/y$, $k = v/t$ as follows:

$$L_{xyt}(M(x,y,t)) = \frac{1}{\alpha\beta\gamma}F\left(\frac{p}{\alpha},\frac{s}{\beta},\frac{k}{\gamma}\right), \tag{41}$$

$$\begin{aligned} &\frac{\partial^{n+m+v}\left[L_{xyt}(M(x,y,t))\right]}{\partial p^n \partial s^n \partial k^v} \\ &\quad = \frac{\partial^{n+m+v}\left[(1/\alpha\beta\gamma)F(p/\alpha, s/\beta, k/\gamma)\right]}{\partial p^n \partial s^n \partial k^v} \\ &\quad = \frac{1}{\alpha^{m+1}\beta^{n+1}\gamma^{v+1}} \\ &\qquad \times \frac{\partial^{n+m+v}\left[F(p/\alpha, s/\beta, k/\gamma)\right]}{\partial p^n \partial s^n \partial k^v}. \end{aligned} \tag{42}$$

Now let us put $\psi(x,y,t) = e^{-px-sy-kt}M(x,y,t)$. Now if we make use of (38), we obtain the following

$$\begin{aligned} &\psi(1,1,1) = e^{-p-s-k}M(1,1,1) = e^{-p-s-k}f(\alpha,\beta,\gamma) \\ &\quad = \lim_{\substack{m\to\infty\\ n\to\infty\\ v\to\infty}} \frac{m^{m+1} n^{n+1} v^{v+1}}{m!n!v!} \iiint_0^\infty x^m y^n t^v e^{-px-sy-kt} \\ &\qquad\qquad \times e^{-mx-ny-vt}\Psi(x,y,t)\,dx\,dy\,dt \\ &\quad = \lim_{\substack{m\to\infty\\ n\to\infty\\ v\to\infty}} \frac{m^{m+1} n^{n+1} v^{v+1}}{m!n!v!} L_{xyt}\left[x^m y^n t^v e^{-mx-ny-vt}\Psi(x,y,t)\right]. \end{aligned} \tag{43}$$

Now taking into account properties (i) and (ii), (42) together with the function $M(x,y,t)$, we arrive at the following:

$$\begin{aligned} &L_{xyt}\left[x^m y^n t^v e^{-mx-ny-vt}\Psi(x,y,t)\right] \\ &\quad = (-1)^{m+n+v}\frac{\partial^{n+m+v}\left[L_{xyt}\left(e^{-mx-ny-kt}\Psi(x,y,t)\right)(p,s,k)\right]}{\partial p^n \partial s^n \partial k^v} \\ &\quad = (-1)^{m+n+v}\frac{1}{\alpha^m\beta^n\gamma^v} \\ &\qquad \times \frac{\partial^{n+m+v}\left[L_{xyt}(\Psi(x,y,t))(p+m, s+n, k+v)\right]}{\partial p^n \partial s^n \partial k^v} \\ &\quad = (-1)^{m+n+v}\frac{1}{\alpha^m\beta^n\gamma^v} \\ &\qquad \times\left(\left(\partial^{n+m+v}\left[L_{xyt}\left(f(\alpha x, \beta y, \gamma t)\right)\right.\right.\right. \\ &\qquad\qquad \left.\left.\left.\times\left(\frac{p+m}{\alpha},\frac{s+n}{\beta},\frac{k+v}{\gamma}\right)\right]\right)\left(\partial p^n \partial s^n \partial k^v\right)^{-1}\right) \end{aligned}$$

$$= (-1)^{m+n+v} \times \frac{1}{\alpha^m \beta^n \gamma^v} \frac{\partial^{n+m+v} \left[F\left((p+m)/\alpha, (s+n)/\beta, (k+v)/\gamma\right)\right]}{\partial p^n \partial s^n \partial k^v}. \tag{44}$$

Now observe that from (44) with the fact that $f(\alpha, \beta, t) = \psi(1,1,1)e^{p+s+k}$, we arrive at the following:

$$\begin{aligned} f(\alpha, \beta, t) &= e^{p+s+k} \lim_{\substack{m\to\infty \\ n\to\infty \\ v\to\infty}} \frac{m^{m+1} n^{n+1} v^{v+1}}{m!n!v!} \\ &\quad \times \left(\frac{m}{\alpha}\right)^{m+1} \left(\frac{n}{\beta}\right)^{n+1} \left(\frac{v}{\gamma}\right)^{v+1} \\ &\quad \times \frac{\partial^{n+m+v} \left[F\left((p+m)/\alpha, (s+n)/\beta, (k+v)/\gamma\right)\right]}{\partial p^n \partial s^n \partial k^v}. \end{aligned} \tag{45}$$

The previously mentioned is true for any p, s, k in the complete space, in particular, for $p = 0$, $s = 0$, $k = 0$, and in this case Theorem 5 is covered. □

5. Application to Third-Order Partial Differential Equation

In this section, we present the application of this operator for solving some kind of third-order partial differential equations.

Example 1. consider the following third-order partial differential equation:

$$\partial_{xyt} u(x, y, t) + u(x, y, t) = 0. \tag{46}$$

The previous equation is called the Mboctara equation and is subjected to the following boundaries and initial conditions:

$$\begin{aligned} &u(x, y, 0) = e^{x+y}, \qquad u(x, 0, t) = e^{x-t}, \\ &u(0, y, t) = e^{y-t}, \qquad u(x, y, 1) = e^{x+y-1}. \end{aligned} \tag{47}$$

Now applying the triple Laplace transform on both sides of (46), we obtain the following:

$$pskU(p, s, k) + U(p, s, k) = G(p, s, k). \tag{48}$$

Here

$$\begin{aligned} G(p, s, k) = {} & psU(p, s, 0) + psU(p, 0, k) - pU(p, 0, 0) \\ & + skU(0, s, k) - sU(0, s, 0) - kU(0, 0, k) \\ & + U(0, 0, 0). \end{aligned} \tag{49}$$

Factorising the right side of equation (49), we obtain the following:

$$U(p, s, k) = \frac{G(p, s, k)}{1 + psk}. \tag{50}$$

Now applying the inverse triple Laplace transform on the previous equation we obtain the following solution:

$$u(x, y, t) = L_{xyt}^{-1}\left[\frac{G(p, s, k)}{1 + psk}\right] = e^{x+y-t}. \tag{51}$$

This is the exact solution for Mboctara equation.

Example 2. Let us consider the following nonhomogeneous Mboctara equation

$$\partial_{xyt} u(x, y, t) + u(x, y, t) = -e^{x-2y+t} \tag{52}$$

subjected to the following initial and boundaries conditions:

$$\begin{aligned} &u(x, 0, 0) = e^{x}, \quad \partial_t u(x, 0, t) = e^{x+t}, \quad \partial_x u(x, 0, t) = e^{x+t}, \\ &u(0, 0, 0) = 1, \quad u(x, 0.5, t) = e^{x+t-1}. \end{aligned} \tag{53}$$

Now applying the triple Laplace transform on both sides of (52), we obtain the following:

$$\begin{aligned} &pskU(p, s, k) + U(p, s, k) \\ &\quad = G(p, s, k) - \frac{1}{(1+p)(2+s)(1+k)}. \end{aligned} \tag{54}$$

Factorising the right side of (54), we obtain the following:

$$U(p, s, k) = \frac{G(p, s, k) - 1/(1+p)(2+s)(1+k)}{1 + psk}. \tag{55}$$

Now applying the inverse triple Laplace transform on the previous equation, we obtain the following solution

$$\begin{aligned} u(x, y, t) &= L_{xyt}^{-1}\left[\frac{G(p, s, k) - 1/(1+p)(2+s)(1+k)}{1 + psk}\right] \\ &= e^{x-2y+t}. \end{aligned} \tag{56}$$

This is the exact solution for nonhomogeneous Mboctara equation.

Example 3. Let us consider the following nonhomogeneous Mboctara equation

$$\begin{aligned} \partial_{xyt} u(x, y, t) + u(x, y, t) = {} & \cos(x)\cos(y)\cos(-t) \\ & - \sin(x)\sin(y)\sin(-t), \end{aligned} \tag{57}$$

subjected to the following initial and boundaries conditions:

$$\begin{aligned} &u(x, y, 0) = \cos(x)\cos(y), \\ &\partial_t u(x, y, 0) = \partial_x u(0, y, t) = \partial_y u(x, 0, t) = 0, \\ &u\left(x, \frac{\pi}{2}, t\right) = u\left(x, y, \frac{\pi}{2}\right) = u\left(\frac{\pi}{2}, y, t\right) = 0. \end{aligned} \tag{58}$$

Table 1: Table of triple Laplace transform for some function of three variables.

Functions $f(x, y, t)$	Triple laplace transform $F(p, s, k)$
abc	$\dfrac{abc}{psk}$
xyt	$\dfrac{1}{p^2 s^2 k^2}$
$x^n y^m t^v$, n, m, v are natural numbers	$k^{-1-v} s^{-1-m} p^{-n-1} \Gamma(1+n)\Gamma(1+m)\Gamma(1+v)$
$x^n y^m t^v e^{-ax-by-ct}$	$(k+c)^{-1-v}(s+b)^{-1-m}(p+a)^{-n-1}\Gamma(1+n)\Gamma(1+m)\Gamma(1+v)$
$e^{-ax-by-ct}$	$\dfrac{1}{(a+p)(b+s)(c+k)}$
$\cos(x)\cos(y)\cos(t)$	$\dfrac{ksp}{(1+p^2)(1+s^2)(1+k^2)}$
$\sin(x)\sin(y)\sin(t)$	$\dfrac{1}{(1+p^2)(1+s^2)(1+k^2)}$
$\sin(x+y+t)$	$\dfrac{-1+ps+k(p+s)}{(1+p^2)(1+s^2)(1+k^2)}$
$\cos(x+y+t)$	$-\dfrac{k+p+s-kps}{(1+p^2)(1+s^2)(1+k^2)}$
$\sqrt{xyt}$	$\dfrac{\pi\sqrt{\pi}}{8^3\sqrt{ksp}}$
$e^{ax+yb+ct}\sinh(ax)\sinh(by)\sinh(ct)$	$\dfrac{(b)(c)(a)}{(-2ap+p^2)(-2bs+s^2)(-2ck+k^2)}$
$e^{ax+yb+ct}\cosh(ax)\cosh(by)\cosh(ct)$	$\dfrac{(b-s)(c-k)(a-p)}{(-2ap+p^2)(-2bs+s^2)(-2ck+k^2)}$
$\mathrm{Erf}\left[\dfrac{a}{2\sqrt{x}}\right]\mathrm{Erf}\left[\dfrac{b}{2\sqrt{y}}\right]\mathrm{Erf}\left[\dfrac{c}{2\sqrt{t}}\right]$	$\dfrac{e^{-\sqrt{c^2}k-\sqrt{b^2}s}}{kps}\left(-1+e^{-\sqrt{c^2}k}\right)\left(1-e^{-\sqrt{a^2}p}\right)\left(-1+e^{-\sqrt{b^2}s}\right)$
$\dfrac{\sin(ax)}{x}\dfrac{\sin(by)}{y}\dfrac{\sin(ct)}{t}$	$\arctan\left(\dfrac{\sqrt{a^2}}{p}\right)\arctan\left(\dfrac{\sqrt{b^2}}{s}\right)\arctan\left(\dfrac{\sqrt{c^2}}{k}\right)$
$\dfrac{\cos(ax)}{x^n}\dfrac{\cos(by)}{y^m}\dfrac{\cos(ct)}{t^v}$	$k^{-1+v}\left(1+\dfrac{b^2}{s^2}\right)^{1/2(-1+m)} s^{-1+m}\cos[ct]\cos\left((-1+m)\arctan\left[\dfrac{\sqrt{b^2}}{s}\right]\right)\Gamma(1-m)\Gamma(1-v)$ $\times\left(1+\dfrac{a^2}{p^2}\right)^{1/2(-1+n)} p^{-1+n}\cos\left((n-1)\arctan\left(\dfrac{\lvert a\rvert}{p}\right)\right)\Gamma(1-n)$
$\dfrac{\sin(ax)}{x^n}\dfrac{\sin(by)}{y^m}\dfrac{\sin(ct)}{t^v}$	$k^{-1+v}\left(1+\dfrac{b^2}{s^2}\right)^{1/2(-1+m)} s^{-1+m}\Gamma(1-m)\Gamma(1-v)\left(1+\dfrac{a^2}{p^2}\right)^{1/2(-1+n)}$ $\times p^{-1+n}\Gamma(1-n)\,\mathrm{sign}(a)\sin\left((n-1)\arctan\left(\dfrac{\lvert a\rvert}{p}\right)\right)\Gamma(1-n)$
$J_n(x)J_n(y)J_n(t)$	$8^{-n}(ksp)^{-1-n}\,\mathrm{Hypergeometric2}F1\left(\dfrac{1+n}{2},\dfrac{2+n}{2},-\dfrac{1}{k^2}\right)$ $\mathrm{Hypergeometric2}F1\left(\dfrac{1+n}{2},\dfrac{2+n}{2},-\dfrac{1}{s^2}\right)$ $[\mathrm{Hypergeometric2}F1\left(\dfrac{1+n}{2},\dfrac{2+n}{2},-\dfrac{1}{p^2}\right)$
$I_n(x)I_n(y)I_n(t)$	$8^{-n}(ksp)^{-1-n}\,\mathrm{Hypergeometric2}F1\left(\dfrac{1+n}{2},\dfrac{2+n}{2},1+n,\dfrac{1}{k^2}\right)$ $\mathrm{Hypergeometric2}F1\left(\dfrac{1+n}{2},\dfrac{2+n}{2},1+n,\dfrac{1}{s^2}\right)$ $\mathrm{Hypergeometric2}F1\left(\dfrac{1+n}{2},\dfrac{2+n}{2},1+n,\dfrac{1}{p^2}\right)$

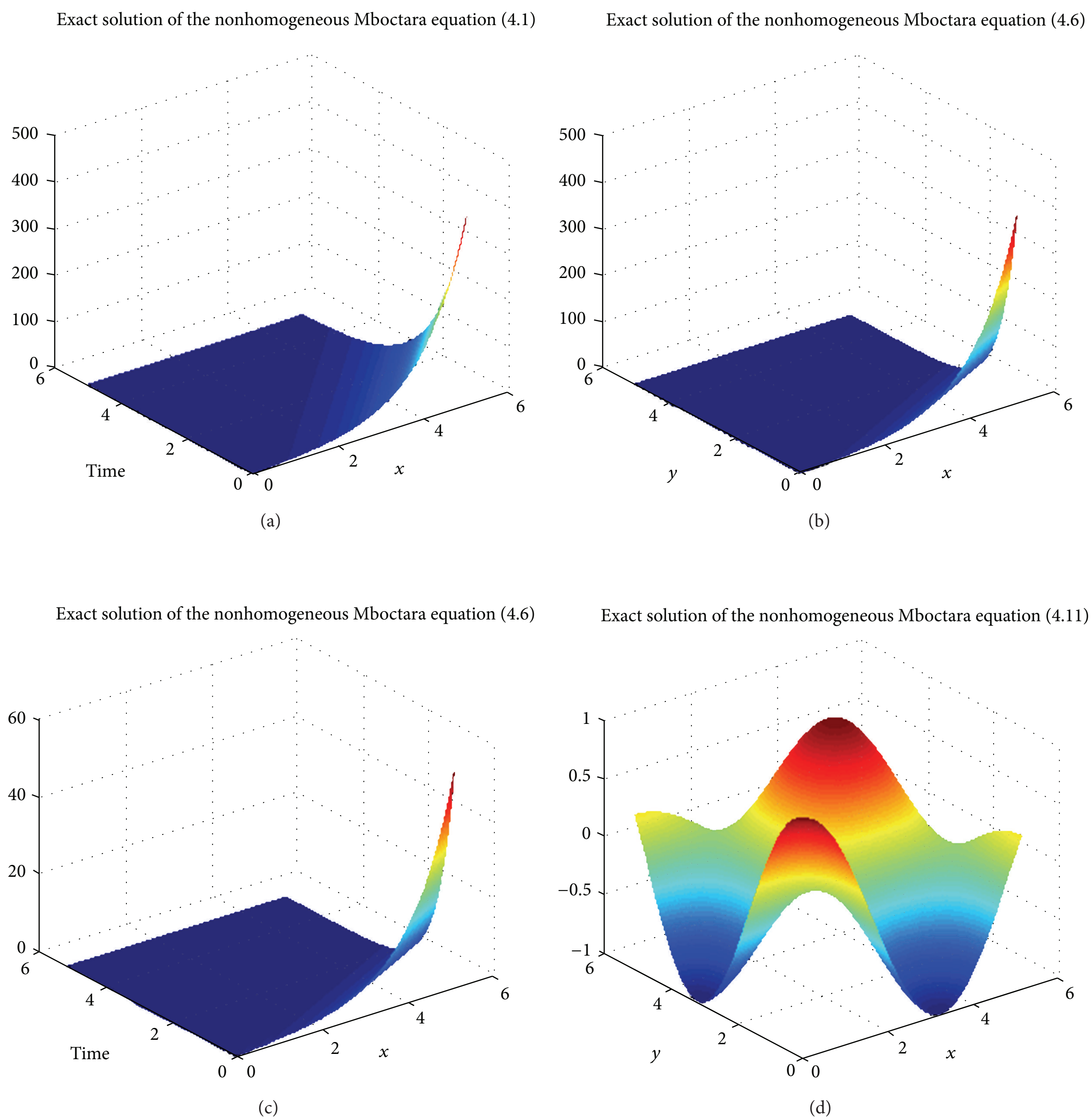

FIGURE 1: Numerical simulation of the exact solutions of the Homogeneous and non-homogeneous Mboctara equations.

Now applying the triple Laplace transform on both sides of (57), we obtain the following:

$$\begin{aligned} &pskU(p,s,k)+U(p,s,k)\\ &\quad = G(p,s,k)+\frac{ksp}{(1+p^2)(1+s^2)(-1+k^2)}\\ &\qquad -\frac{1}{(1+p^2)(1+s^2)(-1+k^2)}. \end{aligned} \tag{59}$$

Factorising the right side of (59), we obtain the following:

$$\begin{aligned} U(p,s,k) &= \frac{G(p,s,k)}{1+psk}+\frac{ksp/(1+p^2)(1+s^2)(-1+k^2)}{1+psk}\\ &\quad -\frac{1/(1+p^2)(1+s^2)(-1+k^2)}{1+psk}. \end{aligned} \tag{60}$$

Now applying the inverse triple Laplace transform on the previous equation, we obtain the following solution:

$$\begin{aligned}
&u(x,y,t) \\
&= L_{xyt}^{-1}\left[\frac{G(p,s,k)}{1+psk}+\frac{ksp/\left(1+p^2\right)\left(1+s^2\right)\left(-1+k^2\right)}{1+psk}\right. \\
&\qquad\left.-\frac{1/\left(1+p^2\right)\left(1+s^2\right)\left(-1+k^2\right)}{1+psk}\right] \\
&= \cos(x)\cos(y)\cos(-t).
\end{aligned} \tag{61}$$

This is the exact solution for nonhomogeneous Mboctara equation.

Example 4. consider the following nonlinear nonhomogeneous with variable coefficient Mboctara equation:

$$\begin{aligned}
&e^{x+y+t}\partial_{xyt}u(x,y,t)-3u^2(x,y,t)+e^{x+y+t}u(x,y,t) \\
&\qquad = e^{2x+2y+2t}, \\
&u_x(x,y,0)=e^{x+y}, \qquad u(0,0,0)=1, \\
&u(1,0,0)=e, \qquad \partial_{xyt}u(0,0,0)=1.
\end{aligned} \tag{62}$$

Now applying the triple Laplace transform on both sides of (62) and then using the properties of the triple Laplace transform and after factorising as in the previous examples and taking the inverse triple Laplace transform, we obtain the following as an exact solution of this type of Mboctara equation:

$$u(x,y,t)=e^{x+y+t}. \tag{63}$$

The numerical simulations of the exact solutions of the Mboctara equation are depicted in Figure 1(a) (4.1), Figure 1(b) (4.6), Figure 1(c) (4.6) and Figure 1(d) (4.11), respectively.

6. Triple Laplace Transform of Some Functions of Three Variables

In this section, we examine the triple Laplace transform of some functions in Table 1:

$$\begin{aligned}
&L_{xyt}\left(Y_n(x)Y_n(y)Y_n(t)\right) \\
&= 8^{-n}(ksp)^{-1-n}Csc^3[n\pi] \\
&\quad\times\left(-\left(4k^2\right)^n \text{Hypergeometric2}F1\right. \\
&\qquad\times\left(\frac{1+n}{2},\frac{2+n}{2},1-n,-\frac{1}{k^2}\right) \\
&\qquad+\cos(n\pi)\,\text{Hypergeometric2}F1 \\
&\qquad\left.\times\left(\frac{1+n}{2},\frac{2+n}{2},1+n,-\frac{1}{k^2}\right)\right) \\
&\quad\times\left(-\left(4s^2\right)^n \text{Hypergeometric2}F1\right. \\
&\qquad\times\left(\frac{1+n}{2},\frac{2+n}{2},1-n,-\frac{1}{s^2}\right) \\
&\qquad+\cos(n\pi)\,\text{Hypergeometric2}F1 \\
&\qquad\left.\times\left(\frac{1+n}{2},\frac{2+n}{2},1+n,-\frac{1}{s^2}\right)\right) \\
&\quad\times\left(-\left(4p^2\right)^n \text{Hypergeometric2}F1\right. \\
&\qquad\times\left(\frac{1+n}{2},\frac{2+n}{2},1-n,-\frac{1}{p^2}\right) \\
&\qquad+\cos(n\pi)\,\text{Hypergeometric2}F1 \\
&\qquad\left.\times\left(\frac{1+n}{2},\frac{2+n}{2},1+n,-\frac{1}{p^2}\right)\right).
\end{aligned} \tag{64}$$

7. Conclusion

This work presents the definition of the triple Laplace transform. Some triple Laplace transform is presented in Table 1. Some theorems and properties of this new relatively new operator are presented. Applications of the new operator, for solving some kind of third-order partial differential equations called Mboctara equation, are presented. Numerical solutions of the Mboctara equation are given.

References

[1] G. L. Lamb Jr., *Introductory Applications of Partial Differential Equations with Emphasis on Wave Propagation and Diffusion*, John Wiley & Sons, New York, NY, USA, 1995.

[2] U. T. Myint, *Differential Equations of Mathematical Physics*, American Elsevier, New York, NY, USA, 1980.

[3] C. Constanda, *Solution Techniques for Elementary Partial Differential Equations*, Chapman & Hall/CRC, New York, NY, USA, 2002.

[4] D. G. Duffy, *Transform Methods for Solving Partial Differential Equations*, CRC Press, New York, NY, USA, 2004.

[5] A. Babakhani and R. S. Dahiya, "Systems of multi-dimensional Laplace transforms and a heat equation," in *Proceedings of the 16th Conference on Applied Mathematics*, vol. 7 of *ElectronicJournal of Differential Equations*, pp. 25–36, University of Central Oklahoma, Edmond, Okla, USA, 2001.

[6] Y. A. Brychkov, H. -J. Glaeske, A. P. Prudnikov, and V. K. Tuan, *Multidimensional Integral Transformations*, Gordon and Breach Science Publishers, Philadelphia, Pa, USA, 1992.

[7] A. Atangana and A. Kilicman, "A possible generalization of acoustic wave equation using the concept of perturbed derivative order," *Mathematical Problems in Engineering*, vol. 2013, Article ID 696597, 6 pages, 2013.

[8] A. Kılıçman and H. Eltayeb, "A note on the classifications of hyperbolic and elliptic equations with polynomial coefficients," *Applied Mathematics Letters*, vol. 21, no. 11, pp. 1124–1128, 2008.

[9] H. Eltayeb, A. Kılıçman, and P. Ravi Agarwal, "An analysis on classifications of hyperbolic and elliptic PDEs," *Mathematical Sciences*, vol. 6, article 47, 2012.

[10] H. Eltayeb and A. Kılıçman, "A note on double laplace transform and telegraphic equations," *Abstract and Applied Analysis*, vol. 2013, Article ID 932578, 6 pages, 2013.

[11] A. Kılıçman and H. E. Gadain, "On the applications of Laplace and Sumudu transforms," *Journal of the Franklin Institute*, vol. 347, no. 5, pp. 848–862, 2010.

[12] R. P. Kanwal, *Generalized Functions Theory and Applications*, Birkhäauser, Boston, Mass, USA, 2004.

Hindawi Publishing Corporation
Abstract and Applied Analysis
Volume 2013, Article ID 759801, 8 pages
http://dx.doi.org/10.1155/2013/759801

Research Article

Approximate Solution of Tuberculosis Disease Population Dynamics Model

Abdon Atangana[1] and Necdet Bildik[2]

[1] *Institute for Groundwater Studies, University of the Free State, P.O. Box 9300, Bloemfontein, South Africa*
[2] *Department of Mathematics, Faculty of Art & Sciences, Celal Bayar University, Muradiye Campus, 45047 Manisa, Turkey*

Correspondence should be addressed to Abdon Atangana; abdonatangana@yahoo.fr

Received 22 March 2013; Accepted 2 June 2013

Academic Editor: R. K. Bera

We examine possible approximate solutions of both integer and noninteger systems of nonlinear differential equations describing tuberculosis disease population dynamics. The approximate solutions are obtained via the relatively new analytical technique, the homotopy decomposition method (HDM). The technique is described and illustrated with numerical example. The numerical simulations show that the approximate solutions are continuous functions of the noninteger-order derivative. The technique used for solving these problems is friendly, very easy, and less time consuming.

1. Introduction

Tuberculosis, MTB, or TB (short for tubercle bacillus) is a common and in many cases lethal, infectious disease caused by various strains of *Mycobacterium*, usually *Mycobacterium Tuberculosis* [1]. Tuberculosis typically attacks the lungs, but can also affect other parts of the body. It is spread through the air when people who have an active TB infection cough, sneeze, or otherwise transmit their saliva through the air [2]. Most infections are asymptomatic and latent, but about one in ten latent infections eventually progresses to active disease which, if left untreated, kills more than 50% of those so infected. Interested reader can find more about this model in [3–7].

Based on the standard SIRS model, the model population was compartmentalised into the susceptible (S) and the infected (I) which is further broken down into latently infected (I_L) and actively infected (I_A) while the recovered subpopulation is ploughed back into the susceptible group due to the possibility of reinfection after successful treatment of the earlier infection. The model monitors the temporary dynamics in the population of susceptible people (t), TB latently infected people $I_L(t)$, and TB actively infected people $I_A(t)$ as captured in the model system of ordinary differential equations that follows.

$$\begin{aligned}
\frac{dS(t)}{dt} &= \nu f N - \alpha I_A S(t) + \delta S(t) + T_A I_A(t) + T_L I_L(t), \\
\frac{dI_L(t)}{dt} &= (1-P)\alpha I_A S(t) - \beta_A I_L(t) - T_L I_L(t) - \delta I_L(t), \\
\frac{dI_A(t)}{dt} &= P\alpha I_A S(t) + \beta_A I_L(t) - T_A I_A(t) - \delta I_A(t) - \varepsilon I_A(t)
\end{aligned} \tag{1}$$

subject to the initial conditions

$$S(0) = N, \qquad I_L(0) \geq 0, \qquad I_A(0) \geq 0, \tag{2}$$

where N is the total number of new people in the location of interest; S is the number of susceptible people in the location; I_L is the number of TB latently infected people; I_A is the number of TB actively infected people; ν is the probability that a susceptible person is not vaccinated; f is the efficient rate of vaccines; T_L is the success rate of latent T_B therapy; T_A is the active TB treatment cure rate; α is the TB instantaneous incidence rate per susceptible; δ is humans natural death rate; P is the proportion of infection instantaneously degenerating into active TB; ε is the TB-induced death rate; and β_A is the breakdown rate from latent to active TB. The equilibrium analysis of the model was studied in [8]. Equation (1) together with (2) does not have an exact solution and is usually solved numerically.

The purpose of this paper is to derive approximate analytical solutions for the standard form as well as the fractional version of (1) together with (2) using the relatively new analytical technique, the homotopy decomposition method (HDM).

The paper is structured as follows. In Section 2, we present the basic ideal of the homotopy decomposition method for solving partial differential equations. We present the application of the HDM for system Tuberculosis disease population dynamics model in Section 3. In Section 4, we present the application of the HDM for system of fractional Tuberculosis disease population dynamics model. The conclusions are then given finally in Section 5.

2. Fundamental Information about Homotopy Decomposition Method

To demonstrate the elementary notion of this technique, we consider a universal nonlinear nonhomogeneous partial differential equation with initial conditions of the following form [9–13].

$$\frac{\partial^m U(x,t)}{\partial t^m} = L(U(x,t)) + N(U(x,t)) + f(x,t), \quad m = 1,2,3\ldots, \tag{3}$$

focused on the primary condition

$$\frac{\partial^i U(x,0)}{\partial t^i} = y_i(x), \qquad \frac{\partial^{m-1} U(x,0)}{\partial t^{m-1}} = 0, \quad i = 0,1,2,\ldots,m-2, \tag{4}$$

where m is the order of the derivative, where f is an identified function, N is the common nonlinear differential operator, L denotes a linear differential operator, and m is the order of the derivative. The procedures first stage here is to apply the inverse operator $\partial^m/\partial t^m$ on both sides of (3) to obtain

$$\begin{aligned} U(x,t) &= \sum_{k=0}^{m-1} \frac{t^k}{k!} \frac{d^k u(x,0)}{dt^k} \\ &\quad + \int_0^t \int_0^{t_1} \cdots \int_0^{t_{m-1}} L(U(x,\tau)) \\ &\quad + N(U(x,\tau)) + f(x,\tau)\, d\tau \cdots dt. \end{aligned} \tag{5}$$

The multi-integral in (3) can be transformed to

$$\begin{aligned} &\int_0^t \int_0^{t_1} \cdots \int_0^{t_{m-1}} L(U(x,\tau)) \\ &\quad + N(U(x,\tau)) + f(x,\tau)\, d\tau \cdots dt \\ &= \frac{1}{(m-1)!} \int_0^t (t-\tau)^{m-1} L(U(x,\tau)) \\ &\quad + N(U(x,\tau)) + f(x,\tau)\, d\tau \end{aligned} \tag{6}$$

so that (3) can be reformulated as

$$\begin{aligned} U(x,t) &= \sum_{k=0}^{m-1} \frac{t^k}{k!} y_i(x) \\ &\quad + \frac{1}{(m-1)!} \int_0^t (t-\tau)^{m-1} L(U(x,\tau)) \\ &\quad + N(U(x,\tau)) + f(x,\tau)\, d\tau. \end{aligned} \tag{7}$$

Using the homotopy scheme, the solution of the aforementioned integral equation is given in series form as

$$\begin{aligned} U(x,t,p) &= \sum_{n=0}^{\infty} p^n U_n(x,t), \\ U(x,t) &= \lim_{p\to 1} U(x,t,p), \end{aligned} \tag{8}$$

and the nonlinear term can be decomposed as

$$NU(r,t) = \sum_{n=1}^{\infty} p^n \mathscr{H}_n(U), \tag{9}$$

where $p \in (0,1]$ is an implanting parameter. $\mathscr{H}_n(U)$ is the polynomials that can be engendered by

$$\mathscr{H}_n(U_0,\ldots,U_n) = \frac{1}{n!} \frac{\partial^n}{\partial p^n} \left[N\left(\sum_{j=0}^{n} p^j U_j(x,t) \right) \right], \quad n = 0,1,2\ldots. \tag{10}$$

The homotopy decomposition method is obtained by the combination of decomposition method with Abel integral and is given by

$$\begin{aligned} &\sum_{n=0}^{\infty} p^n U_n(x,t) \\ &\quad = T(x,t) + p \frac{1}{(m-1)!} \\ &\quad \times \int_0^t (t-\tau)^{m-1} \left[f(x,\tau) + L\left(\sum_{n=0}^{\infty} p^n U_n(x,\tau) \right) \right. \\ &\quad \left. + \sum_{n=0}^{\infty} p^n \mathscr{H}_n(U) \right] d\tau \end{aligned} \tag{11}$$

with

$$T(x,t) = \sum_{k=0}^{m-1} \frac{t^k}{k!} y_i(x). \tag{12}$$

Relating the terms of same powers of p, this gives solutions of various orders. The initial guess of the approximation is $T(x,t)$ that is actually the Taylor series of the exact solution of order m. Note that this initial guess insures the uniqueness of the series decompositions [9].

3. Application of the HDM to the Model with Integer-Order Derivative

In this section, we employ this method for deriving the set of the mathematical equations describing the tuberculosis disease population dynamics model.

Resulting from the steps involved in the HDM method, we reach at the following integral equations that are very simple to solve:

$$p^0: \; S_0(t) = S(0),$$
$$p^0: \; I_{L0}(t) = I_L(0),$$
$$p^0: \; I_{A0}(t) = I_A(0),$$
$$p^1: S_1(t) = \int_0^t (\nu f N - \alpha I_{A0} S_0(\tau) + \delta S_0(\tau) + T_A I_{A0}(\tau) + T_L I_{L0}(\tau))\, d\tau, \quad S_1(0) = 0,$$
$$p^1: I_{L1}(t) = \int_0^t ((1-P)\alpha I_{A0} S_0(\tau) - \beta_A I_{L0}(\tau) - T_L I_L 0(\tau) - \delta I_{L0}(\tau))\, d\tau, \quad I_{L1}(0) = 0,$$
$$p^1: I_{A1}(t) = \int_0^t (P\alpha I_{A0} S_0(\tau) + \beta_A I_{L0}(\tau) - T_A I_{A0}(\tau) - \delta I_{A0}(\tau) - \varepsilon I_{A0}(\tau))\, d\tau, \quad I_{A1}(0) = 0,$$
$$\vdots$$
$$p^n: S_n(t) = \int_0^t \left(\nu f N - \alpha \sum_{j=0}^{n-1} I_{Aj} S_{n-j-1}(\tau) + \delta S_{n-1}(\tau) + T_A I_{A(n-1)}(\tau) + T_L I_{L(n-1)}(\tau)\right) d\tau,$$
$$S_{n-1}(0) = 0,$$
$$p^n: I_{Ln}(t) = \int_0^t \left((1-P)\alpha \sum_{j=0}^{n-1} I_{Aj} S_{n-j-1}(\tau) - \beta_A I_{L(n-1)}(\tau) - T_L I_{L(n-1)}(\tau) - \delta I_{L(n-1)}(\tau)\right) d\tau,$$
$$I_{Ln}(0) = 0$$
$$p^n: I_{An}(t) = \int_0^t \left(P\alpha \sum_{j=0}^{n-1} I_{Aj} S_{n-j-1}(\tau) + \beta_A I_{L(n-1)}(\tau) - T_A I_{A(n-1)}(\tau) - \delta I_{A(n-1)}(\tau) - \varepsilon I_{A(n-1)}(\tau)\right) d\tau, \quad I_{An}(0) = 0. \tag{13}$$

Integrating the previous, we obtain the following components:

$$S_0(t) = S(0); \qquad I_{L0}(t) = I_L(0);$$
$$I_{A0}(t) = I_A(0),$$
$$S_1(t) = (\nu f N - \alpha I_{A0} S_0 + \delta S_0 + T_A I_{A0} + T_L I_{L0})\, t,$$
$$I_{L1}(t) = ((1-P)\alpha I_{A0} S_0 - \beta_A I_{L0} - T_L I_L 0 - \delta I_{L0})\, t,$$
$$I_{A1}(t) = (P\alpha I_{A0} S_0 + \beta_A I_{L0} - T_A I_{A0} - \delta I_{A0} - \varepsilon I_{A0})\, t. \tag{14}$$

For simplicity, let us put

$$a = (\nu f N - \alpha I_{A0} S_0 + \delta S_0 + T_A I_{A0} + T_L I_{L0}),$$
$$b = ((1-P)\alpha I_{A0} S_0 - \beta_A I_{L0} - T_L I_L 0 - \delta I_{L0}),$$
$$c = (P\alpha I_{A0} S_0 + \beta_A I_{L0} - T_A I_{A0} - \delta I_{A0} - \varepsilon I_{A0}),$$
$$S_2(t) = \frac{1}{2} t^2 (b T_A + c T_L - a I_{A0}\alpha - b S_0 \alpha + a\delta) = \frac{t^2}{2} a_1,$$
$$I_{L2}(t) = \frac{1}{2} t^2 (-c T_L + a I_{A0}\alpha - a I_{A0} P\alpha + b S_0 \alpha - c\beta_A - c\delta) = \frac{t^2}{2} b_1,$$
$$I_{A2}(t) = \frac{1}{2} t^2 (a I_{A0} P\alpha + b P\alpha S_0 - b T_A + c\beta_A - b\delta - b\varepsilon) = c_1 \frac{t^2}{2}. \tag{15}$$

In general, we obtain the following recursive formulas:

$$S_n(t) = \frac{t^n}{n!} a_n,$$
$$I_{Ln}(t) = \frac{t^n}{n!} b_n, \tag{16}$$
$$I_{An}(t) = c_n \frac{t^n}{n!},$$

where a_n, b_n, and c_n depend on the fixed set of empirical parameters. It therefore follows that the approximate solution of the system (1) is given as

$$S_N(t) = \sum_{n=0}^{N} \frac{t^n}{n!} a_n,$$
$$I_{LN}(t) = \sum_{n=0}^{N} \frac{t^n}{n!} b_n, \qquad (17)$$
$$I_{AN}(t) = \sum_{n=0}^{N} \frac{t^n}{n!} c_n.$$

If for instance one supposes that the total number of new people in the location of interest is $N = 100$; the initial number of susceptible people in the location is $S(0) = 96$; the initial number of TB latently infected people is $I_L(0) = 3$; the initial number of TB actively infected people is $I_A(0) = 1$; the probability that a susceptible person is not vaccinated is $v = 0.5$; the efficient rate of vaccines is $f = 0.5$; the success rate of latent TB therapy is $T_L = 0.8$; the active TB treatment cure rate is $T_A = 0.74$; the TB instantaneous incidence rate per susceptible is $\alpha = 0.41$; humans natural death rate is $\delta = 1/(366 \times 70)$; the proportion of infection instantaneously degenerating into active TB is $P = 0.0197$; the TB-induced death rate is $\varepsilon = 0.0735$; and the breakdown rate from latent to active TB is $\beta_A = 0.01$, then the following approximate solution is obtained as a result of the first 8 terms of the series decomposition:

$$\begin{aligned} S(t) &= 96 - 11.2162t + 62.1069t^2 - 29.5924t^3 - 149.2t^4 \\ &\quad + 48.3455t^5 - 20.6378t^6 + 15.5857t^7 + \cdots \\ I_L(t) &= 3 + 36.8527t - 62.9161t^2 - 797.302t^3 + 151.174t^4 \\ &\quad - 48.8926t^5 + 20.7629t^6 - 15.6036t^7 + \cdots \\ I_A(t) &= 1 - 0.706394t + 0.252053t^2 - 0.252832t^3 \\ &\quad - 1.96203t^4 + 0.573666t^5 - 0.131459t^6 \\ &\quad + 0.0190148t^7 + \cdots . \end{aligned} \qquad (18)$$

If in addition we assume that no new person migrates or is born in this area, we obtain the following figures. The approximate solutions of the main problem are depicted in Figures 1, 2, and 3, respectively.

Figure 1 shows that, if there is migration or newborn in the location of interest, the number of susceptible people will vanish as time goes, because of the natural death rate and due to TB. Note that any person that is latently infected is removed from the set of susceptible. Figure 2 indicates that the number of people that are latently infected will increase up to a certain time and then vanish as time goes. The number of susceptible people, will become latently infected since some are not vaccinated against the TB and finally will vanish due to. Figure 3 indicates that the number of TB actively infected people will also vanish because of the natural death rate and the death due to TB.

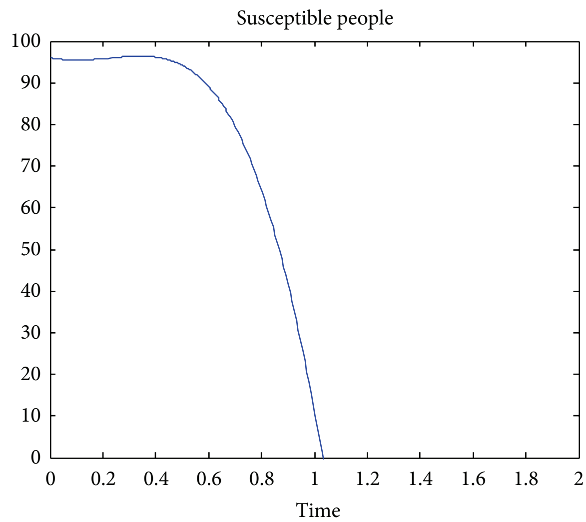

FIGURE 1: Approximate solution for the number of susceptible people in the location.

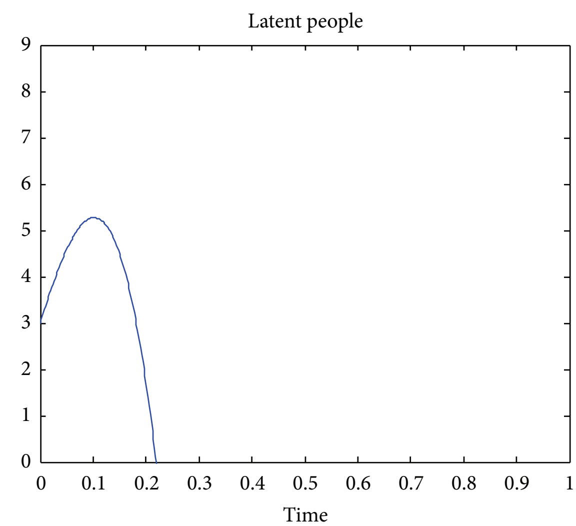

FIGURE 2: Approximate solution for the number of TB latently infected people.

4. Application of the HDM to the Model with Noninteger-Order Derivative

Fractional calculus has been used to model physical and engineering processes, which are found to be best described by fractional differential equations. It is worth noting that the standard mathematical models of integer-order derivatives, including nonlinear models, do not work adequately in many cases. In the recent years, fractional calculus has played a very important role in various fields such as mechanics, electricity, chemistry, biology, economics, notably control theory, and signal and image processing. Major topics

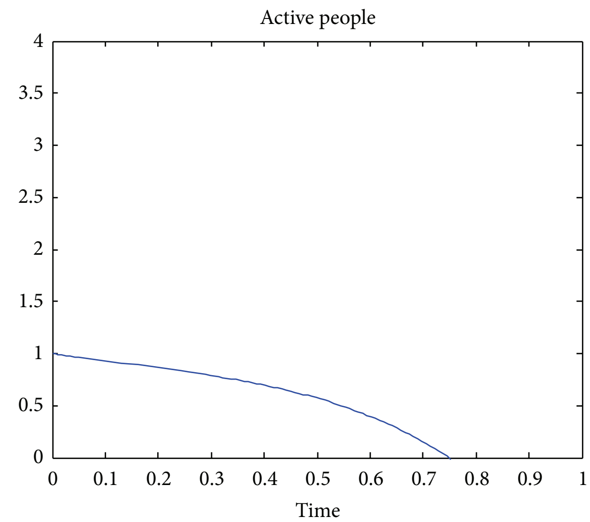

FIGURE 3: Approximate solution for the number of TB actively infected people.

include anomalous diffusion; vibration and control; continuous time random walk; Levy statistics, fractional Brownian motion; fractional neutron point kinetic model; power law; Riesz potential; fractional derivative and fractals; computational fractional derivative equations; nonlocal phenomena; history-dependent process; porous media; fractional filters; biomedical engineering; fractional phase-locked loops, and groundwater problem (see [14–21]).

4.1. Properties and Definitions

Definition 1. A real function $f(x), x > 0$, is said to be in the space C_μ, $\mu \in \mathbb{R}$, if there exists a real number $p > \mu$, such that $f(x) = x^p h(x)$, where $h(x) \in C[0,\infty)$, and it is said to be in space C_μ^m if $f^{(m)} \in C_\mu$, $m \in \mathbb{N}$.

Definition 2. The Riemann-Liouville fractional integral operator of order $\alpha \geq 0$, of a function $f \in C_\mu$, $\mu \geq -1$, is defined as

$$J^\alpha f(x) = \frac{1}{\Gamma(\alpha)} \int_0^x (x-t)^{\alpha-1} f(t)\, dt, \quad \alpha > 0,\ x > 0$$
$$J^0 f(x) = f(x). \tag{19}$$

Properties of the operator can be found in [14–16]. We mention only the following: for $f \in C_\mu$, $\mu \geq -1$, $\alpha, \beta \geq 0$, and $\gamma > -1$,

$$J^\alpha J^\beta f(x) = J^{\alpha+\beta} f(x),$$
$$J^\alpha J^\beta f(x) = J^\beta J^\alpha f(x)\, J^\alpha x^\gamma = \frac{\Gamma(\gamma+1)}{\Gamma(\alpha+\gamma+1)} x^{\alpha+\gamma}. \tag{20}$$

Lemma 3. *If $m-1 < \alpha \leq m$, $m \in \mathbb{N}$, and $f \in C_\mu^m$, $\mu \geq -1$, then*

$$D^\alpha J^\alpha f(x) = f(x),$$
$$J^\alpha D_0^\alpha f(x) = f(x) - \sum_{k=0}^{m-1} f^{(k)}(0^+) \frac{x^k}{k!}, \quad x > 0. \tag{21}$$

Definition 4 (partial derivatives of fractional order). Assume now that $f(\mathbf{x})$ is a function of n variables x_i $i = 1, \ldots, n$ also of class C on $D \in \mathbb{R}_n$. We define partial derivative of order α for f respect to x_i the function

$$a\partial_{\underline{\mathbf{x}}}^\alpha f = \frac{1}{\Gamma(m-\alpha)} \int_a^{x_i} (x_i - t)^{m-\alpha-1} \partial_{x_i}^m f(x_j)\Big|_{x_j=t} dt. \tag{22}$$

where $\partial_{x_i}^m$ is the usual partial derivative of integer-order m.

4.2. Approximate Solution of Fractional Version.

The system of equations under investigation here is given as

$$\begin{aligned}
\frac{d^\mu S(t)}{dt^\mu} &= \nu f N - \alpha I_A S(t) + \delta S(t) \\
&\quad + T_A I_A(t) + T_L I_L(t), \quad 0 < \mu \leq 1, \\
\frac{d^\eta I_L(t)}{dt^\eta} &= (1-P)\alpha I_A S(t) - \beta_A I_L(t) \\
&\quad - T_L I_L(t) - \delta I_L(t), \quad 0 < \eta \leq 1, \\
\frac{d^\upsilon I_A(t)}{dt^\upsilon} &= P\alpha I_A S(t) + \beta_A I_L(t) - T_A I_A(t) \\
&\quad - \delta I_A(t) - \varepsilon I_A(t), \quad 0 < \upsilon \leq 1.
\end{aligned} \tag{23}$$

Following the discussion presented earlier, we arrive at the following equations:

$$p^0: \ S_0(t) = S(0),$$
$$p^0: \ I_{L0}(t) = I_L(0),$$
$$p^0: \ I_{A0}(t) = I_A(0),$$

$$\begin{aligned}
p^1 &: S_1(t) \\
&= \frac{1}{\Gamma(\mu)} \int_0^t (t-\tau)^{\mu-1} \\
&\quad \times \left(\nu f N - \alpha I_{A0} S_0(\tau) + \delta S_0(\tau) \right. \\
&\quad \left. + T_A I_{A0}(\tau) + T_L I_{L0}(\tau)\right) d\tau, \\
&\quad S_1(0) = 0,
\end{aligned}$$

$$\begin{aligned}
p^1 &: I_{L1}(t) \\
&= \frac{1}{\Gamma(\eta)} \int_0^t (t-\tau)^{\eta-1} \\
&\quad \times \left((1-P)\alpha I_{A0} S_0(\tau) - \beta_A I_{L0}(\tau) \right. \\
&\quad \left. - T_L I_L 0(\tau) - \delta I_{L0}(\tau)\right) d\tau, \\
&\quad I_{L1}(0) = 0,
\end{aligned}$$

$$\begin{aligned}
p^1 &: I_{A1}(t) \\
&= \frac{1}{\Gamma(\upsilon)} \int_0^t (t-\tau)^{\upsilon-1} \\
&\quad \times \left(P\alpha I_{A0} S_0(\tau) + \beta_A I_{L0}(\tau) \right. \\
&\quad \left. - T_A I_{A0}(\tau) - \delta I_{A0}(\tau) - \varepsilon I_{A0}(\tau)\right) d\tau, \\
&\quad I_{A1}(0) = 0,
\end{aligned}$$

$$
\begin{aligned}
p^n: S_n(t) &= \frac{1}{\Gamma(\mu)} \int_0^t (t-\tau)^{\mu-1} \\
&\quad \times \left(\nu f N - \alpha \sum_{j=0}^{n-1} I_{Aj} S_{n-j-1}(\tau) + \delta S_{n-1}(\tau) \right. \\
&\quad \left. + T_A I_{A(n-1)}(\tau) + T_L I_{L(n-1)}(\tau) \right) d\tau, \\
& S_{n-1}(0) = 0, \\
p^n: I_{Ln}(t) &= \frac{1}{\Gamma(\eta)} \int_0^t (t-\tau)^{\eta-1} \\
&\quad \times \left((1-P)\alpha \sum_{j=0}^{n-1} I_{Aj} S_{n-j-1}(\tau) - \beta_A I_{L(n-1)}(\tau) \right. \\
&\quad \left. - T_L I_{L(n-1)}(\tau) - \delta I_{L(n-1)}(\tau) \right) d\tau, \\
& I_{Ln}(0) = 0, \\
p^n: I_{An}(t) &= \frac{1}{\Gamma(\upsilon)} \int_0^t (t-\tau)^{\upsilon-1} \\
&\quad \times \left(P\alpha \sum_{j=0}^{n-1} I_{Aj} S_{n-j-1}(\tau) + \beta_A I_{L(n-1)}(\tau) \right. \\
&\quad - T_A I_{A(n-1)}(\tau) - \delta I_{A(n-1)}(\tau) \\
&\quad \left. - \varepsilon I_{A(n-1)}(\tau) \right) d\tau, \\
& I_{An}(0) = 0.
\end{aligned} \tag{24}
$$

Integrating the previous, we obtain the following components:

$$
\begin{aligned}
& S_0(t) = S(0); \qquad I_{L0}(t) = I_L(0); \\
& I_{A0}(t) = I_A(0), \\
& S_1(t) = -\frac{11.2162 t^{\mu}}{\Gamma(1+\mu)}; \\
& I_{L1}(t) = \frac{36.8527 t^{\eta}}{\Gamma(1+\eta)}, \\
& I_{A1}(t) = -\frac{0.706394 t^{\upsilon}}{\Gamma(1+\upsilon)}, \\
& S_2(t) = t^{\mu} \left(\frac{29.4822 t^{\eta}}{\Gamma(1+\eta+\mu)} + \frac{4.59822 t^{\mu}}{\Gamma(1+2\mu)} + \frac{27.2809 t^{\upsilon}}{\Gamma(1+\upsilon+\mu)} \right), \\
& I_{L2}(t) = -t^{\eta} \left(\frac{29.8522 t^{\eta}}{\Gamma(1+2\eta)} + \frac{4.58965 t^{\mu}}{\Gamma(1+\eta+\mu)} + \frac{27.7492 t^{\upsilon}}{\Gamma(1+\upsilon+\mu)} \right), \\
& I_{A2}(t) = t^{\upsilon} \left(\frac{0.368527 t^{\eta}}{\Gamma(1+\eta+\upsilon)} - \frac{0.00901337 t^{\mu}}{\Gamma(1+\upsilon+\mu)} + \frac{0.520184 t^{\upsilon}}{\Gamma(1+2\upsilon)} \right), \\
& S_3(t) = t^{\mu} \left(-\frac{3.24846 t^{\mu+\upsilon} \Gamma(1+\mu+\upsilon)}{\Gamma(1+\mu)\Gamma(1+\upsilon)\Gamma(1+2\mu+\upsilon)} \right. \\
& \qquad - \frac{0.298522 t^{2\eta}}{\Gamma(1+2\eta+\upsilon)} - \frac{15.7583 t^{\eta+\mu}}{\Gamma(1+\eta+2\mu)} \\
& \qquad - \frac{1.88509 t^{2\mu}}{\Gamma(1+3\mu)} - \frac{36.4319 t^{\eta+\upsilon}}{\Gamma(1+\mu+\upsilon+\eta)} \\
& \qquad \left. - \frac{10.836 t^{\mu+\upsilon}}{\Gamma(1+2\mu+\upsilon)} - \frac{20.0895 t^{2\upsilon}}{\Gamma(1+\mu+2\upsilon)} \right), \\
& I_{L3}(t) = t^{\eta} \left(-\frac{1148.5 t^{2\eta}}{\Gamma(1+3\eta)} - \frac{164.513 t^{\eta+\mu}}{\Gamma(1+2\eta+\mu)} + \frac{1.88158 t^{2\mu}}{\Gamma(1+\eta+2\mu)} \right. \\
& \qquad - \frac{1067.59 t^{\eta}}{\Gamma(1+2\eta+\upsilon)} + \frac{11.1633 t^{\mu+\upsilon}}{\Gamma(1+\eta+\mu+\upsilon)} \\
& \qquad \left. + \frac{3.2421 t^{\mu+\upsilon} \Gamma(1+\mu+\upsilon)}{\Gamma(1+\mu)\Gamma(1+\upsilon)\Gamma(1+\eta+\mu+\upsilon)} \right), \\
& I_{A3}(t) = t^{\upsilon} \left(\frac{0.00636699 t^{\mu+\upsilon} \Gamma(1+\mu+\upsilon)}{\Gamma(1+\mu)\Gamma(1+\upsilon)\Gamma(1+2\upsilon+\mu)} \right. \\
& \qquad - \frac{0.298522 t^{2\eta}}{\Gamma(1+2\eta+\upsilon)} - \frac{0.0222046 t^{\eta+\mu}}{\Gamma(1+\eta+2\mu)} \\
& \qquad + \frac{0.00369513 t^{2\mu}}{\Gamma(1+3\mu)} - \frac{0.548873 t^{\eta+\upsilon}}{\Gamma(1+\mu+2\upsilon)} \\
& \qquad \left. + \frac{0.0285603 t^{\mu+\upsilon}}{\Gamma(1+\mu+2\upsilon)} - \frac{0.38306 t^{2\upsilon}}{\Gamma(1+3\upsilon)} \right).
\end{aligned} \tag{25}
$$

The remaining terms can be obtained in the same manner. But here only few terms of the series solutions are considered, and the asymptotic solution is given as

$$
\begin{aligned}
S(t) &= S_0(t) + S_1(t) + S_2(t) + S_3(t) + \cdots, \\
I_L(t) &= I_{L0}(t) + I_{L1}(x,t) + I_{L2}(x,t) + I_{L3}(x,t) + \cdots, \\
I_A(t) &= I_{A0}(t) + I_{A1}(x,t) + I_{A2}(x,t) + I_{A3}(x,t) + \cdots.
\end{aligned} \tag{26}
$$

The following figures show the simulated solutions for different values of the fractional order derivatives. The approximate

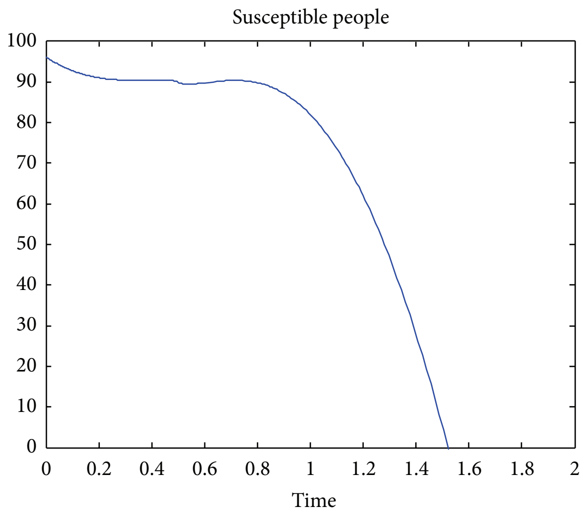

FIGURE 4: Approximate for $\mu = 0.45$, $\eta = 0.7$, and $\upsilon = 0.85$.

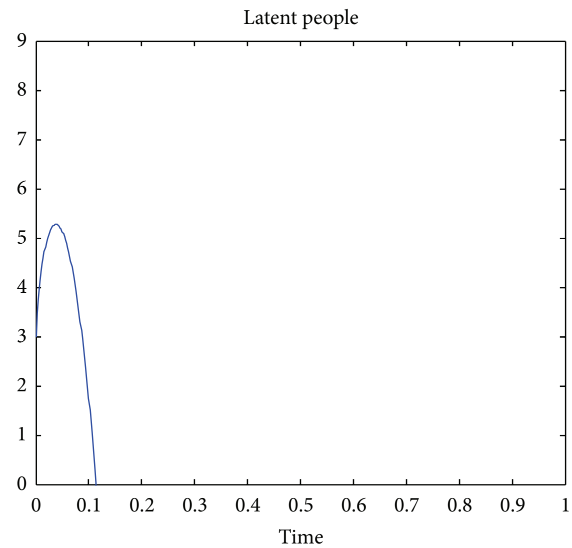

FIGURE 5: Approximate for $\mu = 0.45$, $\eta = 0.7$, and $\upsilon = 0.85$.

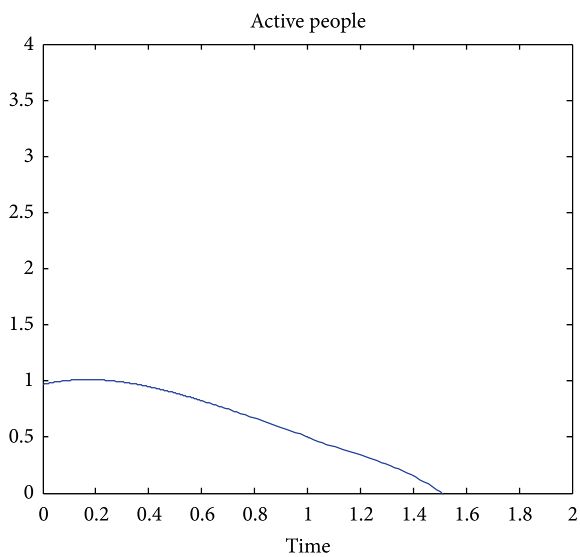

FIGURE 6: Approximate for $\mu = 0.45$, $\eta = 0.7$, and $\upsilon = 0.85$.

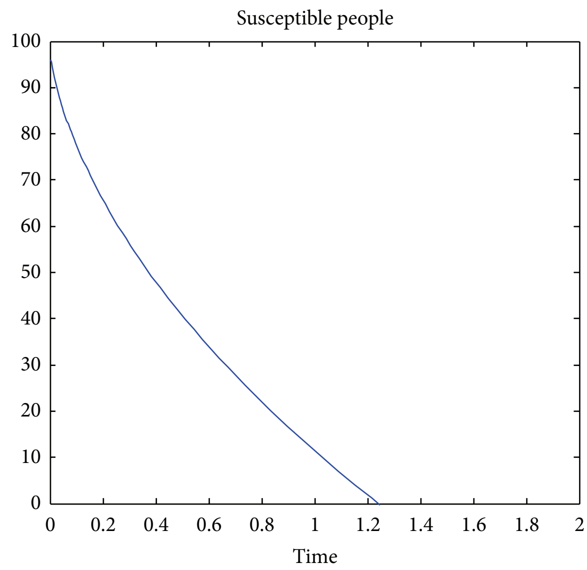

FIGURE 7: Approximate for $\mu = 0.045$, $\eta = 0.5$, and $\upsilon = 0.085$.

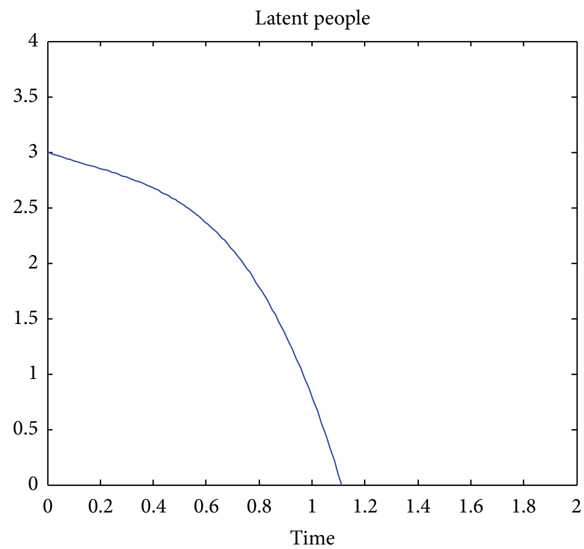

FIGURE 8: Approximate for $\mu = 0.045$, $\eta = 0.5$, and $\upsilon = 0.085$.

solutions of the main problem are depicted in Figures 4, 5, 6, 7, 8, and 9, respectively.

The numerical simulations show that the approximate solutions are continuous functions of the noninteger-order derivative. It is worth noting that the standard mathematical models of integer-order derivatives, including nonlinear models, do not work adequately in many cases. It is therefore advisable to use the fractional model for describing this problem.

5. Conclusion

The tuberculosis model was examined for the case of integer- and noninteger-order derivatives. Both systems of nonlinear equations were solved with an iterative analytical model

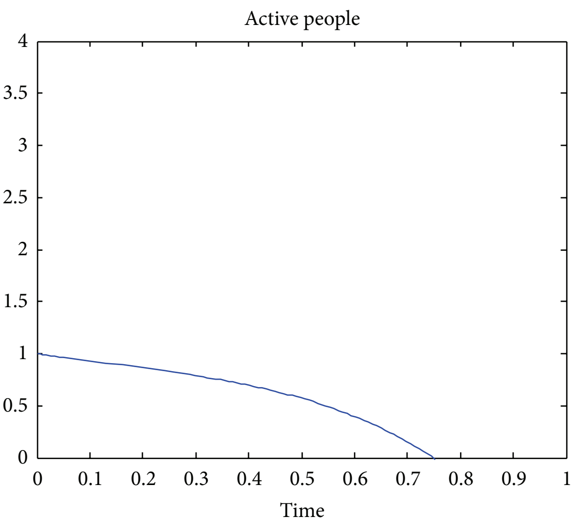

FIGURE 9: Approximate for $\mu = 0.045$, $\eta = 0.5$, and $\upsilon = 0.085$.

called the homotopy decomposition model method. The basic characters of the relatively new technique are presented in detail. The approximate solutions of the noninteger case are increasing continuous functions of the fractional order derivative. The technique used for solving these problems is friendly, very easy, and less time consuming. The numerical solutions in both cases display the biological behaviour of the real world situation.

References

[1] V. Kumar, A. K. Abbas, N. Fausto, and R. N. Mitchell, *Robbins Basic Pathology*, Saunders Elsevier, 8th edition, 2007.

[2] A. Konstantinos, *Testing For Tuberculosis*, vol. 33, Australian Prescriber, 2010.

[3] K. G. Castro, "Global tuberculosis challenges," *Emerging Infectious Disease*, vol. 4, no. 3, pp. 408–409, 1998.

[4] C. Dye, Z. Fengzengb, S. Scheele et al., "Evaluating the impact of tuberculosis control number of deathsprevented by short-course chemotherapy in China," *International Journal of Epidemiology*, vol. 29, no. 3, pp. 558–564, 2000.

[5] L. Gammaitoni and M. C. Nucci, "Using a mathematical model to evaluate the efficacy of TB control measures," *Emerging Infectious Diseases*, vol. 3, no. 3, pp. 335–342, 1997.

[6] C. J. Murray and J. A. Salomon, *Using Mathematical Models To Evaluate Global Tuberculosis Control Strategies—A Paper Presented at the Centre For Population and Development Studies*, Harvard University, Cambridge, Mass, USA, 1998.

[7] World health Organization, *WHO: Tuberculosis Fact Sheet*, 2007.

[8] O. K. Koriko and T. T. Yusuf, "Mathematical model to simulate tuberculosis disease population dynamics," *American Journal of Applied Sciences*, vol. 5, no. 4, pp. 301–306, 2008.

[9] D. Baleanu, K. Diethelm, E. Scalas, and J. J. Trujillo, *Fractional Calculus Models and Numerical Methods Series on Complexity, Nonlinearity and Chaos*, World Scientific, 2012.

[10] A. Atangana, A. Ahmed, and N. Belic, "A generalized version of a low velocity impact between a rigid sphere and a transversely isotropic strain-hardening plate supported by a rigid substrate using the concept of non-integer derivatives," *Abstract Applied Analysis*, vol. 2013, Article ID 671321, 9 pages, 2013.

[11] A. Atangana and J. F. Botha, "Analytical solution of the groundwater flow equation obtained via homotopy decomposition method," *Journal of Earth Science & Climatic Change*, vol. 3, p. 115, 2012.

[12] A. Atangana and E. Alabaraoye, "Solving a system of fractional partial differential equations arising in the model of HIV infection of $CD4^+$ cells and attractor one-dimensional Keller-Segel equations," *Advances in Difference Equations*, vol. 2013, p. 94, 2013.

[13] A. Atangana and A. Secer, "Time-fractional coupled- the korteweg-de vries equations," *Abstract Applied Analysis*, vol. 2013, Article ID 947986, 8 pages, 2013.

[14] K. B. Oldham and J. Spanier, *The Fractional Calculus*, Academic Press, New York, NY, USA, 1974.

[15] I. Podlubny, *Fractional Differential Equations*, Academic Press, New York, NY, USA, 1999.

[16] A. A. Kilbas, H. M. Srivastava, and J. J. Trujillo, *Theory and Applications of Fractional Differential Equations*, Elsevier Science B.V., Amsterdam, The Netherlands, 2006.

[17] A. Atangana and A. Secer, "A note on fractional order derivatives and Table of fractional derivative of some specials functions," *Abstract Applied Analysis*, vol. 2013, Article ID 279681, 2013.

[18] M. Caputo, "Linear models of dissipation whose Q is almost frequency independent, part II," *Geophysical Journal International*, vol. 13, no. 5, pp. 529–539, 1967.

[19] S. G. Samko, A. A. Kilbas, and O. I. Marichev, *Fractional Integrals and Derivatives: Theory and Applications*, Gordon and Breach, Yverdon, Switzerland, 1993.

[20] D. Baleanu, K. Diethelm, E. Scalas, and J. J. Trujillo, *Fractional Calculus*, Series on Complexity, Nonlinearity and Chaos, World Scientific, 2012, Models and numerical methods.

[21] A. Atangana and A. Kılıçman, "A possible generalization of acoustic wave equation using the concept of perturbed derivative order," *Mathematical Problems in Engineering*, vol. 2013, Article ID 696597, 6 pages, 2013.

Hindawi Publishing Corporation
Abstract and Applied Analysis
Volume 2013, Article ID 580461, 10 pages
http://dx.doi.org/10.1155/2013/580461

Research Article

A Rectangular Mixed Finite Element Method with a Continuous Flux for an Elliptic Equation Modelling Darcy Flow

Xindong Li and Hongxing Rui

School of Mathematics, Shandong University, Jinan 250100, China

Correspondence should be addressed to Hongxing Rui; hxrui@sdu.edu.cn

Received 26 March 2013; Accepted 29 May 2013

Academic Editor: Santanu Saha Ray

We introduce a mixed finite element method for an elliptic equation modelling Darcy flow in porous media. We use a staggered mesh where the two components of the velocity and the pressure are defined on three different sets of grid nodes. In the present mixed finite element, the approximate velocity is continuous and the conservation law still holds locally. The LBB consistent condition is established, while the *L2* error estimates are obtained for both the velocity and the pressure. Numerical examples are presented to confirm the theoretical analysis.

1. Introduction

We consider the discretization technique for the elliptic problem modelling the flow in saturated porous media, or the classical Darcy flow problem, including a system of mass conservation law and Darcy's law [1, 2]. The most popular numerical methods for this elliptic equation focus on mixed finite element methods, since by this kind of methods the original scalar variable, called pressure, and its vector flux, named Darcy velocity, can be approximated simultaneously and maintain the local conservation. The classical theory for the mixed finite element, which includes the LBB consistent condition, the existence and uniqueness of the approximate solution, and the error estimate, has been established. Some mixed finite element methods such as RT mixed finite element and BDM mixed finite element are introduced (as in [3–6]), which satisfy the consistent condition and have optimal order error estimate [7, 8]. Give some stabilized mixed finite methods by adding to the classical mixed formulation some least squares residual forms of the governing equations.

By using the abovementioned mixed finite element methods, the approximate velocity is continuous in the normal direction and discontinuous in the tangential direction on the edges of the element. This is reasonable for the case of heterogenous permeability, yet it is desirable that the flux be continuous in some applications [9]. In particular, when we track the characteristic segment using the approximate velocity, the discontinuities of the velocity may introduce some difficulties when the characteristic line cross the edges of element. While applying mass-conservative characteristic finite element method to the coupled system of compressible miscible displacement in porous media, the continuous flux is crucial [10]. A brief description of this point will be found at the last part of this paper.

To overcome this disadvantage, Arbogast and Wheeler [11] introduced a mixed finite element method with an approximate velocity continuous in both the normal direction and the tangential direction, which was got by adding some freedom to the RT mixed finite element. In this paper, we introduced a mixed finite element method with an approximate velocity continuous in all directions. It is based on rectangular mesh and uses continuous piecewise bilinear functions to approximate the velocity components and uses piecewise constant functions to approximate the pressure. We obtain the element by improving a kind of element for Stokes equation and Navier-Stokes equation given by Han [12], Han and Wu [13], and Han and Yan [14]. By using this mixed finite element, we can get continuous velocity vector and maintain the local conservation. Comparing to the mixed finite element method in [11], we need less degrees of freedom for the same convergence rate. The LBB consistent condition and *L*2 error estimates of velocity and pressure are also established.

The outline of the rest of this paper is organized as follows. In Sections 2 and 3, we recall the model problem and weak formulation for the mixed finite element method and then establish the discrete inf-sup consistent condition and $L2$ error estimates for the velocity and the pressure in Section 4. In Section 5, we present some numerical examples which verify the efficiency of the proposed mixed finite element method. A valuable application of this method to mass-conservative characteristic (MCC) scheme for the coupled compressible miscible displacement in porous media closes the paper in Section 6.

2. The Mixed Finite Formulation for Darcy Equation

The mathematical model for viscous flow in porous media includes Darcy's law and conservation law of mass, written as follows:

$$\begin{aligned} &u = -\frac{\kappa}{\mu}\nabla p \quad &&\text{on } \Omega \text{ (Darcy's law)} \\ &\operatorname{div} u = \phi \quad &&\text{on } \Omega \text{ (mass conservation)} \\ &u \cdot n = 0 \quad &&\text{on } \Gamma, \end{aligned} \tag{1}$$

where $\kappa > 0$ is the permeability, $\mu > 0$ is the viscosity, and ϕ is the volumetric flow rate source or sink. Γ is the boundary of Ω, and n is the unit outward normal vector to Γ. The variable $u = (u_1, u_2)$ is the Darcy velocity vector, and p is the pressure. The source ϕ must satisfy the consistency constraint

$$\int_\Omega \phi d\Omega = 0. \tag{2}$$

Let $L^2(\Omega)$ be the space of square integrable function in Ω with inner product $(\cdot,\cdot)$ and norm $\|\cdot\|$. We use the notation of the Hilbert space

$$H(\operatorname{div},\Omega) = \left\{u \in \left[L^2(\Omega)\right]^2; \operatorname{div} u \in L^2(\Omega)\right\}, \tag{3}$$

with norm

$$\|u\|_{H(\operatorname{div},\Omega)} = \{\|u\|^2 + \|\operatorname{div} u\|^2\}^{1/2}. \tag{4}$$

Define the following subspaces of $H(\operatorname{div},\Omega)$ and $L^2(\Omega)$:

$$\begin{gathered} V = H_0(\operatorname{div},\Omega) = \{u \in H(\operatorname{div},\Omega) : u\cdot n = 0 \text{ on } \Gamma\}, \\ S = \left\{q \mid q \in L^2(\Omega) : \int_\Omega q d\Omega = 0\right\}. \end{gathered} \tag{5}$$

The classical weak variational formulation of Problem (1) is as follows: find $(u, p) \in V \times S$, such that

$$\begin{aligned} &a(u,v) - b(v,p) = 0 \quad \forall v \in V, \\ &b(u,q) = (\phi,q) \quad \forall q \in S. \end{aligned} \tag{6}$$

Here,

$$a(u,v) = \int_\Omega \frac{\mu}{\kappa} u\cdot v dx \qquad b(v,q) = \int_\Omega q \operatorname{div} v dx. \tag{7}$$

The following discussion and discrete analysis are related to the weak form (6). Let V_0 be a closed subspace of V via

$$V_0 = \{v \in V : b(v,q) = 0, \forall q \in S\}. \tag{8}$$

For the bilinear forms $a(u,v)$ and $b(v,q)$, we have the standard result.

Lemma 1. *The bilinear form $a(u,v)$ is bounded on $V \times V$ and coercive on V_0, and the bilinear form $b(v,q)$ is bound on $V \times S$. Namely,*

(1) *there exist two constants $C_1 > 0$ and $\alpha > 0$ such that*

$$\begin{aligned} |a(u,v)| &\le C_1 \|u\|_{H(\operatorname{div},\Omega)} \|v\|_{H(\operatorname{div},\Omega)} \quad \forall u,v \in V, \\ a(u,u) &\ge \alpha \|u\|^2_{H(\operatorname{div},\Omega)} \quad \forall u \in V_0, \end{aligned} \tag{9}$$

(2) *there is a constant $C_2 > 0$ such that*

$$|b(v,q)| \le C_2 \|q\|_{0,\Omega} \|v\|_{H(\operatorname{div},\Omega)} \quad \forall q \in S, v \in V. \tag{10}$$

For the space V and S, the Ladyzhenskaya-Babuška-Brezzi(L-B-B) condition holds; see [15, 16], for example.

Lemma 2. *There is a constant $\beta > 0$ such that*

$$\sup_{v\in V} \frac{b(v,q)}{\|v\|_{H(\operatorname{div},\Omega)}} \ge \beta \|q\|_{0,\Omega}, \quad \forall q \in S. \tag{11}$$

It is clear that there exists a unique solution $(u, p) \in V \times S$ to the Problem (6).

3. Finite Element Discretization

In this section, we present the mixed finite element based on rectangular mesh for the Darcy flow problem.

In [13], Han and Wu introduced a mixed finite element for Stokes problem and then extended to solve the Navier-Stokes problem [14]. Based on this element, we introduced the new mixed finite element with a continuous flux approximation for Darcy flow problem.

For simplicity, we suppose that the domain Ω is a unit square, and the mixed finite element discussed here can be easily generalized to the case when the domain Ω is a rectangular.

Let N be a given integer and $h = 1/N$. We construct the finite-dimensional subspaces of S and V by introducing three different quadrangulations τ_h, τ_h^1, τ_h^2 of Ω.

First, we divide Ω into uniform squares

$$\begin{aligned} T_{i,j} = \{(x,y) : x_{i-1} \le x \le x_i, y_{j-1} \le y \le y_j\}, \\ i,j = 1,\dots,N, \end{aligned} \tag{12}$$

where $x_i = ih$ and $y_j = jh$. The corresponding quadrangulation is denoted by τ_h. See Figure 1(a).

$$\tau_{i,j} = \{T_{i,j} : i,j = 1,\dots,N\}. \tag{13}$$

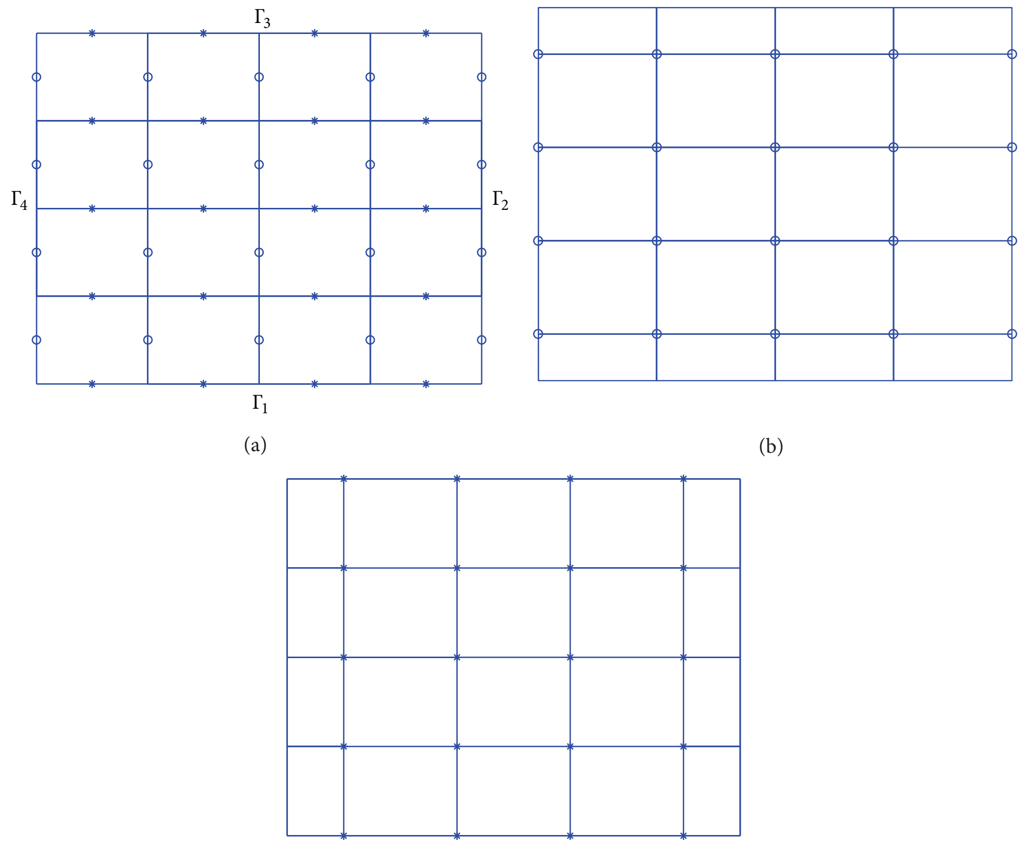

FIGURE 1: Quadrangulations: (a)τ_h, (b)τ_h^1, and (c) τ_h^2.

Then, for all $T_{i,j} \in \tau_h$, we connect all the neighbor midpoints of the vertical sides of $T_{i,j}$ by straight segments if the neighbor midpoints have the same vertical coordinate. Then, Ω is divided into squares and rectangles. The corresponding quadrangulation is denoted by τ_h^1 (see Figure 1(b)). Similarly, for all $T_{i,j} \in \tau_h$, we connect all the neighbor midpoints of the horizontal sides of $T_{i,j}$ by straight line segments if the neighbor midpoints have the same horizontal coordinate. Then, we obtained the third quadrangulation of Ω, which is denoted by τ_h^2 (see Figure 1(c)).

Based on the quadrangulation τ_h, we define the piecewise constant functional space used to approximate the pressure

$$S_h := \left\{ q_h : q_h|_T = \text{constant}, \ \forall T \in \tau_h; \int_\Omega q_h dx = 0 \right\}. \tag{14}$$

S_h is a subspace of S.

Furthermore, using the quadrangulations τ_h^1 and τ_h^2, we construct a subspace of V. Denote by $\Gamma_1, \Gamma_2, \Gamma_3$, and Γ_4 the south, right, north, and left sides on the boundary of Ω. Set

$$\begin{aligned} V_h^1 &= \left\{ v_h \in C^{(0)}\left(\overline{\Omega}\right) : v_h|_{T^1} \in Q_{1,1}\left(T^1\right) \forall T^1 \in \tau_h^1, \right. \\ &\qquad \left. v_h = 0 \ \text{ on } \Gamma_2 \cup \Gamma_4 \right\}, \\ V_h^2 &= \left\{ v_h \in C^{(0)}\left(\overline{\Omega}\right) : v_h|_{T^2} \in Q_{1,1}\left(T^2\right) \forall T^2 \in \tau_h^2, \right. \\ &\qquad \left. v_h = 0 \ \text{ on } \Gamma_1 \cup \Gamma_3 \right\}, \end{aligned} \tag{15}$$

where $Q_{1,1}$ denotes the piecewise bilinear polynomial space with respect to the variables x and y. Let

$$V_h = V_h^1 \times V_h^2. \tag{16}$$

Obviously, V_h is a subspace of V.

Using the subspaces V_h and S_h instead of V and S in the variational Problem (6), we obtain the discrete problem: find $(u_h, p_h) \in V_h \times S_h$, such that

$$\begin{aligned} a\left(u_h, v_h\right) - b\left(v_h, p_h\right) &= 0 \quad \forall v_h \in V_h, \\ b\left(u_h, q_h\right) &= \left(\phi, q_h\right) \quad \forall q_h \in S_h. \end{aligned} \tag{17}$$

4. Convergence Analysis and Error Estimate

In this section, we give the corresponding convergence analysis and error estimate. Firstly, we define an interpolating for the following analysis.

For the quadrangulation τ_h, we divided the edges of all squares into two sets. The first one denoted by L_V contains all vertical edges, and the second one denoted by L_H contains all horizontal edges. We define the interpolation operator

$\Pi : V \to V_h$ by $\Pi u = (\Pi_h^1 u_1, \Pi_h^2 u_2) \in V_h^1 \times V_h^2$, which satisfy the following:

$$\begin{aligned} \int_l \Pi_h^1 u_1 ds &= \int_l u_1 ds \quad \forall l \in L_{V'}, \\ \int_l \Pi_h^2 u_2 ds &= \int_l u_2 ds \quad \forall l \in L_{H'}, \end{aligned} \tag{18}$$

where $L_{V'}$ is a set of edges of elements got by bisecting the most bottom element edges and the most top element edges of L_V and $L_{H'}$ are got by bisecting the most left element edges and the most right element edges of L_H. See Figures 2 and 3.

Lemma 3. *For any $u \in V$, the interpolating $\Pi u \in V_h$ is uniquely determined by* (18).

Proof. It is easy to see that (18) is equivalent to an equation of $AX = B$, where A is a matrix and X, B are vectors. Direct calculation shows that

$$A = h * \operatorname{diag}\{A_1, A_1, \ldots\}, \tag{19}$$

and the form of submatrix A_1 is as follows

$$\begin{pmatrix} \frac{1}{4} & \frac{1}{4} & 0 & 0 & 0 & \cdots & 0 & 0 & 0 & 0 \\ 0 & \frac{3}{8} & \frac{1}{8} & 0 & 0 & \cdots & 0 & 0 & 0 & 0 \\ 0 & \frac{1}{8} & \frac{3}{4} & \frac{1}{8} & 0 & \cdots & 0 & 0 & 0 & 0 \\ 0 & 0 & \frac{1}{8} & \frac{3}{4} & \frac{1}{8} & \cdots & 0 & 0 & 0 & 0 \\ \cdots & \cdots & \cdots & \cdots & \cdots & \cdots & \cdots & \cdots & \cdots \\ 0 & 0 & 0 & 0 & 0 & \cdots & \frac{1}{8} & \frac{3}{4} & \frac{1}{8} & 0 \\ 0 & 0 & 0 & 0 & 0 & \cdots & 0 & \frac{1}{8} & \frac{3}{8} & 0 \\ 0 & 0 & 0 & 0 & 0 & \cdots & 0 & 0 & \frac{1}{4} & \frac{1}{4} \end{pmatrix}. \tag{20}$$

We can see that the matrix is invertible and the equation is solvable, and therefore X can be uniquely determined. □

Assume that the solution (u, p) of Problem (6) has the following smoothness properties:

$$u \in V' := V \bigcap H^2((\Omega))^2, \qquad p \in S \bigcap H^1(\Omega). \tag{21}$$

Then, we should give the following lemma about the properties of the interpolations defined in (18).

Lemma 4. (i) *There exist two constants C_3 and C_4 independent of h, such that*

$$|u - \Pi u|_{i,2,\Omega} \le C_3 h^{j-i} |u|_{j,2,\Omega}, \quad i = 0, 1, \ i \le j \le 2, \tag{22}$$

$$\inf_{q_h \in S_h} \|p - q_h\| \le C_4 h |p|_{1,\Omega}. \tag{23}$$

(ii) *There exists a constant C_5 independent of h such that*

$$\|\Pi u\|_{H(\mathrm{div},\Omega)} \le C_5 \|u\|_{1,\Omega} \quad \forall u \in V. \tag{24}$$

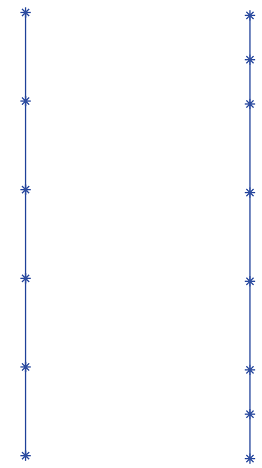

Some edges on L_V Corresponding edges on $L_{V'}$

(a) (b)

Figure 2: Some edges on L_V and corresponding edges on $L_{V'}$.

(iii) *For any $u \in V$, we have that*

$$\int_\Omega q_h \operatorname{div}(u - \Pi u)\, dx = 0, \quad \forall q_h \in S_h. \tag{25}$$

Proof. The estimates (22), (23), and (24) follow from Definition (18) and the approximation theory; see [1], for example.

For (25), based on Green formulation, we know that

$$\begin{aligned} \int_\Omega q_h \operatorname{div}(u - \Pi u)\, dx &= \sum_{T \in \tau_h} \int_T q_h \operatorname{div}(u - \Pi u)\, dx \\ &= \sum_{T \in \tau_h} \int_{\partial T} q_h (u - \Pi u) \cdot \vec{n} ds \\ &\quad - \sum_{T \in \tau_h} \int_T \nabla q_h \cdot (u - \Pi u)\, dx \\ &= \sum_{l \in L_V} \int_l q_h \left(u_1 - \Pi_h^1 u_1\right) n_1 ds \\ &\quad + \sum_{l \in L_H} \int_l q_h \left(u_2 - \Pi_h^2 u_2\right) n_2 ds \\ &= \sum_{l \in L_{V'}} \int_l q_h \left(u_1 - \Pi_h^1 u_1\right) n_1 ds \\ &\quad + \sum_{l \in L_{H'}} \int_l q_h \left(u_2 - \Pi_h^2 u_2\right) n_2 ds \\ &= 0. \end{aligned} \tag{26}$$

Here, $\vec{n} = (n_1, n_2)$, and we use (18) for the last step. The proof is completed. □

Some edges on L_H Corresponding edges on $L_{H'}$

(a) (b)

Figure 3: Some edges on L_H and corresponding edges on $L_{H'}$.

Theorem 5. *The discrete Inf-sup condition is valid; namely, there is a constant $\beta \geq 0$, such that*

$$\sup_{v_h \in V_h} \frac{b(v_h, q_h)}{\|v_h\|_{H(\mathrm{div},\Omega)}} \geq \beta \|q_h\|, \quad \forall q_h \in S_h. \tag{27}$$

Proof. From the process above, we obtain that $b(v, q_h) = b(\Pi v, q_h)$, any $v \in V, q_h \in S_h$. For any $p_h \in S_h$, there exists $v \in (H_0^1(\Omega))^2$, such that

$$\nabla \cdot v = q_h, \qquad \|v\|_{1,\Omega} \leq C_6 \|q_h\|, \tag{28}$$

where C_6 is a constant independent of q_h; then we obtain

$$\begin{aligned}
\sup_{v_h \in V_h} \frac{b(v_h, q_h)}{\|v_h\|_{H(\mathrm{div},\Omega)}} &\geq \frac{b(\Pi v, q_h)}{\|\Pi v\|_{H(\mathrm{div},\Omega)}} \\
&= \frac{b(v, q_h)}{\|\Pi v\|_{H(\mathrm{div},\Omega)}} \\
&= \frac{\|q_h\|_0^2}{\|\Pi v\|_{H(\mathrm{div},\Omega)}}.
\end{aligned} \tag{29}$$

Using Lemma 4, we have that

$$\sup_{v_h \in V_h} \frac{b(v_h, q_h)}{\|v_h\|_{H(\mathrm{div},\Omega)}} \geq \frac{1}{C_5} \frac{\|q_h\|_0^2}{\|v\|_{1,\Omega}} \geq \frac{1}{C_5 C_6} \|q_h\|. \tag{30}$$

Taking $\beta = 1/C_5 C_6$, we complete the proof of (27). □

With the analysis technique presented by Arbogast and Wheeler [11], we consider the numerical analysis of the mixed finite element presented in this paper. Recall the RT_0 mixed element spaces $V_h' \times S_h'$ [3, 5, 6] based on the partition τ_h

$$V_h' = Q_{1,0}(\tau_h) \times Q_{0,1}(\tau_h), \qquad S_h' = S_h. \tag{31}$$

Define the interpolation operator $\Pi' : V \to V_h'$ by the following equations:

$$\begin{aligned}
\int_l \Pi' u_1 ds &= \int_l u_1 ds \quad \forall l \in L_V, \\
\int_l \Pi' u_2 ds &= \int_l u_2 ds \quad \forall l \in L_H.
\end{aligned} \tag{32}$$

Denote by $P_S : S \to S_h$ the L^2 projection operator and by $P_{V'} : V \to V_h'$ the $(L^2(\Omega))^2$ vector projection operator. The following properties of the projections hold:

$$\begin{aligned}
\|p - P_S p\|_0 &\leq Ch|p|_1 \\
\|u - P_{V'} u\|_0 &\leq Ch\|u\|_1.
\end{aligned} \tag{33}$$

Then, we have an important property about the operator Π'.

Lemma 6. *For any $u \in Q_{1,1}(\tau_h^1) \times Q_{1,1}(\tau_h^2)$, there holds the equivalence $\Pi' u = P_{V'} u$; namely,*

$$(u - \Pi' u, v) = 0, \quad \forall v \in V_h'. \tag{34}$$

Proof. As the definition of V_h' is based on each element T, we focus our discussion on arbitrary element $e \subset \tau_h, e = [x_0, x_0 + h] \times [y_0, y_0 + h]$. Firstly, we consider the x-component (see Figure 4). The analysis for y-component is similar.

For a function $U_1 \in V_h^1$, on an element e, it is uniquely given by its node values $u_i, i = 1, \ldots, 6$. As U_1 is a continuous bilinear function on each of the two parts as shown in Figure 4. Then, from (32), we know that $\Pi' u_1 = a + bx$ is given by

$$\begin{aligned}
\int_{l_1} (a + bx) ds &= (a + bx_0) * h = (u_1 + 2u_3 + u_5) * \frac{h}{4} \\
\int_{l_2} (a + bx) ds &= (a + b(x_0 + h)) * h = (u_2 + 2u_4 + u_6) * \frac{h}{4}.
\end{aligned} \tag{35}$$

We deduce that

$$\begin{aligned}
a &= \frac{u_1 + 2u_3 + u_5 - 4bx_0}{4}, \\
b &= ((u_2 - u_1) + 2(u_4 - u_3) + (u_6 - u_5)) * \frac{1}{4h}.
\end{aligned} \tag{36}$$

It is clear that we just need to verify (34) for both $v = 1$ and $v = x$.

We first consider $v = 1$. Denote by φ_i the node basis function at the point i, which implies that $\varphi_i(x_j) = \delta_{i,j}$, which has the value 1 if and only if $i = j$; otherwise, it is zero. By direct calculation, we can get the basis, for example,

$$\varphi_1 = \frac{1}{4}\left(2 - \frac{2}{h}x + \frac{2}{h}x_0\right)\left(2 - \frac{4}{h}y + \frac{4}{h}y_0\right), \tag{37}$$

so

$$\begin{aligned}
\int_e U_1 dx\, dy &= \int_{x_0}^{x_0+h} \int_{y_0}^{y_0+\frac{h}{2}} (u_1\varphi_1 + u_2\varphi_2 + u_3\varphi_3 + u_4\varphi_4) dx\, dy \\
&\quad + \int_{x_0}^{x_0+h} \int_{y_0+h/2}^{y_0+h} (u_3\varphi_3 + u_4\varphi_4 + u_5\varphi_5 + u_6\varphi_6) dx\, dy \\
&= \frac{h^2}{8}(u_1 + u_2 + u_3 + u_4) + \frac{h^2}{8}(u_3 + u_4 + u_5 + u_6) \\
&= \frac{h^2}{8}(u_1 + u_2 + 2u_3 + 2u_4 + u_5 + u_6).
\end{aligned} \tag{38}$$

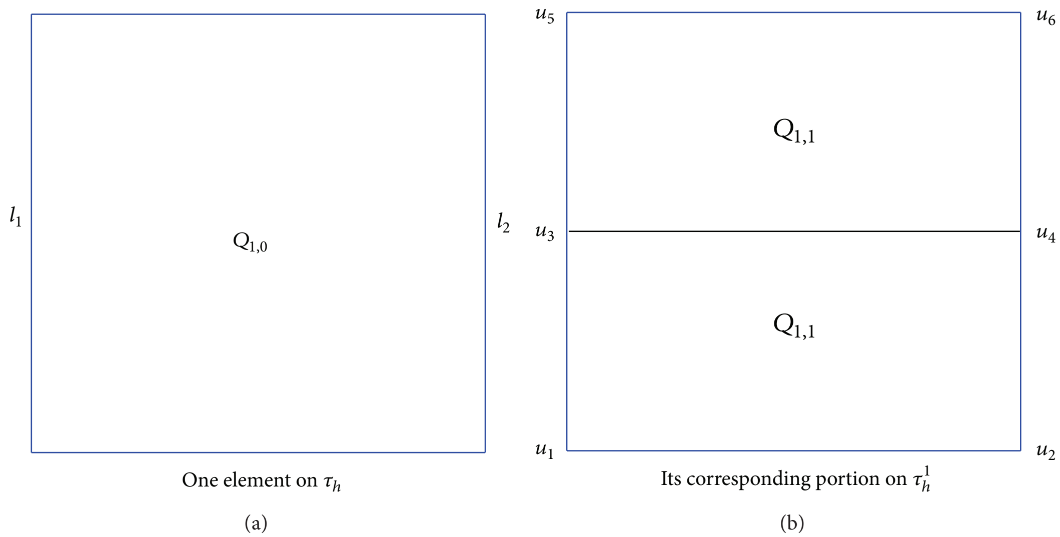

FIGURE 4: An element on τ_h and its corresponding portion on τ_h^1.

By direct computation, we can easily see that $\int_e \Pi' U_1 dx\,dy$ has the same value, so

$$\int_e \Pi' U_1 dx\,dy = \int_e U_1 dx\,dy. \tag{39}$$

When $v = x$, we have that

$$\begin{aligned}\int_e \Pi' U_1 * x dx\,dy &= \int_{x_0}^{x_0+h}\int_{y_0}^{y_0+h} ax + bx^2 dx\,dy \\ &= a\left(x_0 h^2 + \frac{h^3}{2}\right) \\ &\quad + b\left(x_0^2 h^2 + x_0 h^3 + \frac{1}{3}h^4\right),\end{aligned} \tag{40}$$

where a, b are defined in (36). Next, we compare the coefficients of u_i in (40) with the coefficients in $\int_e U_1 * x dx\,dy$,

$$\begin{aligned}\int_e \varphi_1 * x dx\,dy &= \int_{y_0}^{y_0+h/2}\int_{x_0}^{x_0+h} \varphi * x dx\,dy \\ &= \frac{h}{2}\int_{x_0}^{x_0+h} \frac{1}{4}\left(2x - \frac{2}{h}x^2 + \frac{2}{h}x_0 x\right) \\ &= \frac{1}{24}h^3 + \frac{1}{8}x_0 h^2 = k_1,\end{aligned} \tag{41}$$

which determine k_1 as the coefficient of u_1. With similar computation, we obtain that

$$\begin{aligned} k_5 &= k_1, \qquad k_2 = k_6 = \frac{x_0 h^2}{8} + \frac{h^3}{12}, \\ k_3 &= \frac{x_0 h^2}{4} + \frac{h^3}{12}, \qquad k_4 = \frac{x_0 h^2}{4} + \frac{h^3}{6}.\end{aligned} \tag{42}$$

Comparing with (40), we can find that (34) is true with $v = x$.

So, we certify the lemma. □

Theorem 7. *If (u, p) satisfy (6) and (u_h, p_h) satisfy (17), then there exists a positive constant C independent of h such that the following error estimates hold:*

$$\begin{aligned}\|u - u_h\|_0 &\le Ch\|u\|_1, \\ \|p - p_h\|_0 &\le Ch\left(\|u\|_1 + \|p\|_1\right).\end{aligned} \tag{43}$$

Proof. First, we focus on the error $u - u_h$. From (6), (17), (18), and (32), we derive that

$$b(u, q_h) = b(u_h, q_h) = b(\Pi u, q_h) = b(\Pi' u, q_h), \quad \forall q_h \in S_h. \tag{44}$$

Let $v = \Pi' v_h$ in (6); then

$$a(u, \Pi' v_h) - b(\Pi' v_h, p) = 0. \tag{45}$$

Namely,

$$a(P_{v'} u, v_h) - (P_s \nabla \cdot v_h, p) = a(P_{v'} u, v_h) - b(v_h, P_s p) = 0. \tag{46}$$

Here, we used the property $\nabla \cdot \Pi' v = P_s \nabla \cdot v$. Subtracting from (17), we get that

$$a(P_{v'} u - u_h, v_h) - b(v_h, P_s p - p_h) = 0. \tag{47}$$

Take

$$v_h = \Pi u - u_h, \qquad q_h = P_s p - p_h. \tag{48}$$

Then

$$a(P_{v'} u - u_h, \Pi u - u_h) - b(\Pi u - u_h, P_s p - p_h) = 0. \tag{49}$$

Due to (44), we find that

$$b(\Pi u - u_h, P_s p - p_h) = 0. \tag{50}$$

Now, we analyze the error $u - u_h$ based on the equations above

$$\begin{aligned} a&(u-u_h, u-u_h) \\ &= a(u-u_h, u-\Pi u) + a(u-u_h, \Pi u - u_h) \\ &= a(u-u_h, u-\Pi u) + a(u-P_{v'}u, \Pi u - u_h) \\ &\quad + a(P_{v'}u - u_h, \Pi u - u_h) \\ &\le \epsilon_1 \|u-u_h\|_0^2 + \frac{1}{\epsilon_1}\|u-\Pi u\|_0^2 \\ &\quad + \epsilon_2 \|\Pi u - u\|_0^2 + \frac{1}{\epsilon_2}\|u - P_{v'}u\|_0^2 \\ &\quad + \epsilon_3 \|u-u_h\|_0^2 + \frac{1}{\epsilon_3}\|u-P_{v'}u\|_0^2, \end{aligned} \tag{51}$$

where $\epsilon_i > 0, i = 1, 2, 3$ are positive constants. Take the value of $\epsilon_1 = \epsilon_3 = \mu/4\kappa, \epsilon_2 = 1$, and combining with (22) and (33), we conclude that

$$\|u - u_h\|_0 \le Ch\|u\|_1. \tag{52}$$

We also can obtain a higher order error estimate for $\|P_s p - p_h\|$. Consider the classical duality argument. Let ϕ be the solution of the following elliptical problem:

$$\Delta\phi = P_s p - p_h, \qquad \frac{\partial \phi}{\partial n} = 0. \tag{53}$$

By the elliptic regularity, the estimate holds: $|\phi|_{H^2} \le C\|P_s p - p_h\|_0$. So

$$\begin{aligned} &\|P_s p - p_h\|_0^2 \\ &= (P_s p - p_h, \nabla\cdot\nabla\phi) \\ &= (P_s p - p_h, \nabla\cdot\Pi\nabla\phi) \\ &= a(P_{v'}u - u_h, \Pi\nabla\phi) \\ &= a(P_{v'}u - u_h, \Pi\nabla\phi - P_{v'}\nabla\phi) + a(P_{v'}u - u_h, P_{v'}\nabla\phi) \\ &= a(P_{v'}u - u_h, \Pi\nabla\phi - P_{v'}\nabla\phi) + a(P_{v'}u - u, P_{v'}\nabla\phi) \\ &\quad + a(u-u_h, P_{v'}\nabla\phi) \\ &= a(P_{v'}u - u_h, \Pi\nabla\phi - P_{v'}\nabla\phi) + a(u-u_h, P_{v'}\nabla\phi - \nabla\phi) \\ &\quad + a(u-u_h, \nabla\phi). \end{aligned} \tag{54}$$

Now, we estimate the right hand terms of the above inequality. From (33), (22), and (52), we have

$$\begin{aligned} a(P_{v'}u - u_h, \Pi\nabla\phi - P_{v'}\nabla\phi) &= a(P_{v'}u - u, \Pi\nabla\phi - \nabla\phi) \\ &\quad + a(u-u_h, \Pi\nabla\phi - \nabla\phi) \\ &\quad + a(P_{v'}u - u, \nabla\phi - P_{v'}\nabla\phi) \\ &\quad + a(u-u_h, \nabla\phi - P_{v'}\nabla\phi) \\ &\le Ch^2\|u\|_1 \mid \phi|_{H^2} \\ &\le Ch^2\|u\|_1 \mid \|P_s p - p_h\|_0. \end{aligned} \tag{55}$$

It is easy to see that

$$\begin{aligned} a&(u-u_h, P_{v'}\nabla\phi - \nabla\phi) \le Ch^2\|u\|_1|\phi|_{H^2} \\ &\qquad\qquad \le Ch^2\|u\|_1\|P_s p - p_h\|_0, \\ a&(u-u_h, \nabla\phi) \\ &= a(u-\Pi u, \nabla\phi) + a(\Pi u - u_h, \nabla\phi - P_{v'}\nabla\phi) \\ &\quad + a(\Pi u - u_h, P_{v'}\nabla\phi) \\ &\le C\left(h^2|u|_2\|\phi\|_2 + h^2|u|_1\|\phi\|_2\right) \\ &\le Ch^2\|u\|_2\|P_s p - p_h\|_0. \end{aligned} \tag{56}$$

Here, we used the fact that $a(\Pi u - u_h, P_{v'}\nabla\phi) = 0$ which is got from the Green formulation and (44).

Combining the above inequalities, we conclude that

$$\begin{aligned} \|p - p_h\|_0 &\le \|p - P_s p\|_0 + \|P_s p - p_h\|_0 \\ &\le Ch\left(\|u\|_1 + \|p\|_0\right). \end{aligned} \tag{57}$$

We complete the proof. □

It is worth mentioning that we analyze this mixed finite element method in a direct way as it is not straightforward to apply the classical inf-sup theory. We just have the coercivity property for $a(u_h, v_h)$ on the normal L_2 space, not in the subspace of $v_{0h} = \{v_h \in V_h : b(v_h, q_h) = 0, \forall q_h \in S_h\}$, and the same issue also occurs in [11]. The problem is that testing $(\nabla\cdot v, w)$ by $w \in W_h$ does not control the full divergence of V, and it does not occur when this method is applied to Stokes or Navier-Stokes equations (as in [13, 14]). As a result, we just obtain a convergence rate of $\|u - u_h\|_0$. Failing to obtain convergence rate of $\|u - u_u\|_{H(\mathrm{div},\Omega)}$ is a weak point of this proposed mixed formulation compared to the classical Raviart-Thomas mixed method. But the significance of continuous flux applied to mass conservation can be found in Section 6.

5. Numerical Examples

In this section, we present some numerical results for the model Problem (1). For simplicity, we assume that the domain

Table 1: Three numerical test cases.

Case	Coefficient μ/κ	True solution u	True solution p
1	1	$\begin{pmatrix} x^2y - x^4y \\ xy^4 - xy^2 \end{pmatrix}$	$(x-1/2)(y-1/2)$
2	$\begin{pmatrix} e^{2xy^2} & 0 \\ 0 & \dfrac{1}{x+y} \end{pmatrix}$	$\begin{pmatrix} x^2y - x^4y \\ xy^4 - xy^2 \end{pmatrix}$	$(x-1/2)(y-1/2)$
3	$\begin{pmatrix} e^{2xy^2} & 0 \\ 0 & \dfrac{1}{x+y} \end{pmatrix}$	$\begin{pmatrix} e^{-xy} \\ x^2\cos y \end{pmatrix}$	ye^x

is a unit square $\Omega = [0,1]\times[0,1]$ and the test cases are summarized in Table 1. We can choose the boundary conditions and the right hand terms according to the analytical solutions.

We compare our method to the formulation constructed by Arbogast and Wheeler [11]. Its corresponding discrete finite element spaces are

$$\begin{aligned}\overline{V}_h &= \Big\{v_h \in \left(C^{(0)}\left(\overline{\Omega}\right)\right)^2 : v_h|_T \in Q_{1,2}(T) \\ &\qquad \times Q_{2,1}(T), \forall\, T \in \tau_h\Big\},\\ \overline{S}_h &= \Big\{q_h : q_h|_T = \text{constant}, \\ &\qquad \forall T \in \tau_h; \int_\Omega q_h dx = 0\Big\}.\end{aligned} \tag{58}$$

The results of the error estimate with various norms are listed in Table 2, while the corresponding convergence rates of the presented method are shown in Table 3.

Close results of numerical errors for both formulations are shown in Table 2. From Table 3, we can see that p converges to p_h as $O(h)$ and $P_s p - p_h$ as $O(h^2)$ for our formulation, which both agree with the theorem. From the examples, we can observe that u_h converges to u somewhat better than expected, and it appears that on the uniform grid we attain $O(h^{3/2})$ superconvergence in the L^2 norm which is similar to the tests of Arbogast's formulation [11]. Yet, the degrees of freedom of our method are less than Arbogast's scheme. As in the case of $64 * 64$, the degrees of freedom of Arbogast's scheme are 20866 and 12676 for our formulation. The convergence rate of $\|u-u_h\|_{H(\mathrm{div},\Omega)}$ is first order, but here we cannot give the corresponding analysis.

6. A Valuable Application

In this section, we briefly show an application of the proposed mixed finite element method to the miscible displacement of one incompressible fluid by another in porous media. The model is as follows:

$$\begin{gathered}\mu(C)K^{-1}u + \nabla p = \gamma(C)\nabla d, \quad (x,t)\in\Omega\times J,\\ \phi\frac{\partial C}{\partial t} + \nabla\cdot(uC) - \nabla\cdot(D(u)\nabla C) = \widetilde{C}q, \quad (x,t)\in\Omega\times J,\\ \nabla\cdot u = g, \quad (x,t)\in\Omega\times J,\\ u\cdot n = g_1, \quad (x,t)\in\partial\Omega\times J,\\ C(x,0) = C_0(x), \quad x\in\Omega,\end{gathered} \tag{59}$$

where $\gamma(C)$ and d are the gravity coefficient and vertical coordinate, $\phi(x)$ is the porosity of the rock, and $\widetilde{C}q$ represents a known source. $D(x,u)$ is the molecular diffusion and mechanical dispersion coefficient. For convenience, we denote that $f = \widetilde{C}q$ and $a(C) = \mu(C)K^{-1}$. Let $\chi : (0,T] \to R^2$ be the solution of the ordinary differential equation

$$\begin{gathered}\frac{d\chi}{d\tau} = \frac{\mathbf{u}(\chi(x,t;\tau),\tau)}{\phi(x)},\\ \chi(x,t;t) = x.\end{gathered} \tag{60}$$

Let $V = H(\mathrm{div},\Omega)$, $S = L_0^2(\Omega)$, $M = H^1(\Omega)$; then, we derive the entire weak formulation for the model: find $(\mathbf{u},p,C)\in V\times S\times M$, such that

$$\begin{gathered}(a(C)u,v) - (p,\nabla\cdot v) = (\gamma(C)\nabla d,\mathbf{v}), \quad \forall\mathbf{v}\in V,\\ \left(\phi(x)\frac{dC(\chi,\tau)}{d\tau} + gC, w\right) + (D\nabla C,\nabla w) = (f,w), \\ \forall w\in M,\\ (\nabla\cdot u,\varphi) = (g,\varphi), \quad \forall\varphi\in S.\end{gathered} \tag{61}$$

Let Δt be the time step for both concentration and pressure; define

$$M_h = \left\{v_h \in C^{(0)}\left(\overline{\Omega}\right) : v_h|_T \in Q_{1,1}(T),\ \forall T\in\tau_h\right\}. \tag{62}$$

Combing with the new characteristic finite element method which preserves the mass balance proposed by Rui and Tabata [10], the approximate characteristic line of χ is defined as

$$\chi^n(x) = x - \frac{u_h^n}{\phi(x)}\Delta t. \tag{63}$$

We obtain the corresponding full-discrete mass-conservative characteristic (MCC) scheme: find $(u_h,p_h,C_h)\in V_h\times S_h\times M_h$, such that

$$\begin{gathered}\left(a\left(C_h^n\right)u_h^n,v_h\right) - \left(p_h,\nabla\cdot v_h\right)\\ = \left(\gamma\left(C_h^n\right)\nabla d, v_h\right), \quad \forall v_h\in V_h\\ \left(\frac{\phi C_h^n - \left(\phi C_h^{n-1}\right)\circ\chi^n\gamma^n}{\Delta t},\varphi_h\right) + \left(D\left(u_h^n\right)\nabla C_h^n,\nabla\varphi_h\right)\\ = \left(f,\varphi_h\right), \quad \forall\varphi_h\in M_h\\ \left(\nabla\cdot u_h^n, q_h\right) = \left(g,q_h\right), \quad \forall q_h\in S_h\\ C_h^0 = \widetilde{C}^0,\end{gathered} \tag{64}$$

where

$$\begin{aligned}\gamma^n &= \det\left(\frac{\partial\chi^n}{\partial x}\right)\\ &= 1 - \frac{\nabla\cdot u_h^n}{\phi}\Delta t + u_h^n\frac{\nabla\phi}{\phi^2}\Delta t\\ &\quad + \nabla\left(\frac{u_{h,1}^n}{\phi}\right)\cdot\mathrm{curl}\left(\frac{u_{h,2}^n}{\phi}\right)\Delta t^2.\end{aligned} \tag{65}$$

Table 2: The numerical error for fm. 1 (our formulation) and fm. 2 (Arbogast's formulation).

Case	Mesh	$\|u-u_h\|$		$\|\nabla\cdot(u-u_h)\|$		$\|p-p_h\|$		$\|P_sp-p_h\|$	
		fm. 1	fm. 2	fm. 1	fm. 2	fm. 1	fm. 2	fm. 1	fm. 2
1	4	$4.90e-2$	$5.67e-2$	$3.06e-1$	$3.24e-1$	$2.93e-2$	$2.93e-2$	$4.53e-3$	$4.17e-3$
	8	$1.78e-2$	$2.05e-2$	$1.53e-1$	$1.62e-1$	$1.47e-2$	$1.47e-2$	$1.24e-3$	$1.20e-3$
	16	$6.45e-3$	$7.37e-3$	$7.67e-2$	$8.13e-2$	$7.37e-3$	$7.37e-3$	$3.18e-4$	$3.15e-4$
	32	$2.31e-3$	$2.64e-3$	$3.84e-2$	$4.07e-2$	$3.68e-3$	$3.68e-3$	$8.01e-5$	$7.98e-5$
	64	$8.25e-4$	$9.38e-4$	$1.92e-2$	$2.03e-2$	$1.84e-3$	$1.84e-3$	$2.01e-5$	$2.01e-5$
2	4	$4.70e-2$	$5.47e-2$	$2.99e-1$	$3.22e-1$	$2.95e-2$	$2.94e-2$	$5.42e-3$	$4.97e-3$
	8	$1.72e-2$	$1.99e-2$	$1.53e-1$	$1.63e-1$	$1.47e-2$	$1.47e-2$	$1.54e-3$	$1.48e-3$
	16	$6.25e-3$	$7.19e-3$	$7.75e-2$	$8.27e-2$	$7.37e-3$	$7.37e-3$	$4.04e-4$	$3.98e-4$
	32	$2.25e-3$	$2.58e-3$	$3.89e-2$	$4.15e-2$	$3.68e-3$	$3.68e-3$	$1.03e-4$	$1.02e-4$
	64	$8.08e-4$	$9.21e-4$	$1.95e-2$	$2.08e-2$	$1.84e-3$	$1.84e-3$	$2.59e-5$	$2.58e-5$
3	4	$9.65e-2$	$1.09e-1$	$4.14e-1$	$4.67e-1$	$1.49e-1$	$1.49e-1$	$7.39e-3$	$6.21e-3$
	8	$3.79e-2$	$4.31e-2$	$2.16e-1$	$2.46e-1$	$7.44e-2$	$7.44e-2$	$2.14e-3$	$1.89e-3$
	16	$1.42e-2$	$1.62e-2$	$1.11e-1$	$1.28e-1$	$3.72e-2$	$3.72e-2$	$5.72e-4$	$5.19e-4$
	32	$5.19e-3$	$5.91e-3$	$5.63e-2$	$6.51e-2$	$1.86e-2$	$1.86e-2$	$1.47e-4$	$1.35e-4$
	64	$1.87e-3$	$2.13e-3$	$2.84e-2$	$3.28e-2$	$9.31e-3$	$9.31e-3$	$3.72e-5$	$3.44e-5$

Table 3: The corresponding convergence rates of fm. 1 and fm. 2.

Case	Mesh	$\|u-u_h\|$		$\|\nabla\cdot(u-u_h)\|$		$\|p-p_h\|$		$\|P_sp-p_h\|$	
		fm. 1	fm. 2	fm. 1	fm. 2	fm. 1	fm. 2	fm. 1	fm. 2
1	8	1.459	1.468	0.997	1.001	0.995	0.993	1.875	1.795
	16	1.468	1.476	0.998	0.995	0.999	0.999	1.961	1.934
	32	1.479	1.484	1.000	0.998	1.000	1.000	1.987	1.978
	64	1.486	1.489	1.000	1.000	1.000	1.000	1.996	1.993
2	8	1.449	1.457	0.968	0.978	0.999	0.996	1.817	1.742
	16	1.462	1.471	0.983	0.984	1.001	1.001	1.930	1.901
	32	1.471	1.479	0.993	0.993	1.001	1.000	1.976	1.960
	64	1.480	1.485	0.997	0.997	1.000	1.000	1.989	1.984
3	8	1.347	1.340	0.942	0.924	0.998	0.997	1.787	1.708
	16	1.416	1.414	0.957	0.945	0.999	0.999	1.906	1.870
	32	1.452	1.452	0.979	0.973	1.000	1.000	1.959	1.942
	64	1.472	1.473	0.990	0.986	1.000	1.000	1.983	1.975

We can see that the continuous flux is indispensable for γ^n. Let $\varphi_h = 1$ in (64), and summing it up from $n = 1$ to N, we get the mass balance

$$\int_\Omega \phi C_h^N dx = \int_\Omega \phi C_h^0 dx + \Delta t \sum_{n=1}^{N} \int_\Omega f^n dx. \tag{66}$$

Here, we just give numerical example to show the feasibility of this application, and the theoretical analysis of stability, mass balance, and convergence of this discrete scheme will be discussed in the future. Firstly, we define compute mass error and relative mass error as follows:

$$\begin{aligned} \text{compute mass error}: & \int_\Omega \phi C_h^N dx \\ & - \left(\int_\Omega \phi C_h^0 dx + \Delta t \sum_{n=1}^{N} \int_\Omega f^n dx\right), \\ \text{relative mass error}: & \frac{\int_\Omega \phi C_h^N dx - \int_\Omega \phi C^N dx}{\int_\Omega \phi C^N dx}. \end{aligned} \tag{67}$$

Now, we select $\mu(C) = C$, and the following analytical solution of the problem is

$$\begin{aligned} u(x,y,t) &= \left(e^x + t, e^y + t\right), \\ p(x,y,t) &= e^{-t}\left(x^2 + y^2\right), \\ C(x,y,t) &= e^{-t}\left(\left(x - \frac{1}{2}\right)^2 + \left(y - \frac{1}{2}\right)^2\right). \end{aligned} \tag{68}$$

The error results with different norms of this numerical simulation can be listed in Tables 4 and 5, and at last we give a mass error to check the mass conservation in Table 6.

As can be seen from Tables 4 and 5, we conjecture that almost all the convergence rates are true in general. From Table 6 we find that mass balance is right as computational mass error resulting from computer is inevitable and nearly invariable for different meshes, while the relative mass error decreases as was expected. The corresponding theoretical analysis about this system will be considered in the future work.

Table 4: Numerical error and convergence rate ($\Delta t = Ch$).

Mesh	5×5		10×10		20×20		40×40	
Norm type	Error	Rate	Error	Rate	Error	Rate	Error	Rate
$\|u\|_{l^2(L^2)}$	$1.83e-4$	—	$7.10e-5$	1.36	$3.38e-5$	1.07	$1.65e-5$	1.03
$\|u\|_{l^\infty(L^2)}$	$1.29e-2$	—	$5.19e-3$	1.31	$2.64e-3$	0.97	$1.37e-3$	0.95
$\|p\|_{l^2(L^2)}$	$1.33e-3$	—	$6.67e-4$	1.00	$3.33e-4$	1.00	$1.67e-4$	1.00
$\|p\|_{l^\infty(L^2)}$	$9.43e-2$	—	$4.71e-2$	1.00	$2.35e-2$	1.00	$1.18e-2$	1.00
$\|C\|_{l^2(H^1)}$	$2.32e-3$	—	$1.16e-3$	1.01	$5.78e-4$	1.00	$2.88e-4$	1.00
$\|C\|_{l^\infty(H^1)}$	$1.63e-1$	—	$8.18e-2$	1.00	$4.11e-2$	0.99	$2.05e-2$	0.99

Table 5: Numerical error and convergence rate ($\Delta t = Ch^2$).

Mesh	5×5		10×10		20×20		40×40	
Norm type	Error	Rate	Error	Rate	Error	Rate	Error	Rate
$\|C\|_{l^2(L^2)}$	$8.48e-5$	—	$2.13e-5$	1.995	$5.37e-6$	1.986	$1.36e-6$	1.971
$\|C\|_{l^\infty(L^2)}$	$1.34e-2$	—	$3.37e-3$	1.989	$8.56e-4$	1.978	$2.21e-4$	1.952

Table 6: Mass error for concentration C ($\Delta t = Ch$).

Mesh	5×5	10×10	20×20	40×40
Compute mass error	$1.209e-3$	$1.243e-3$	$1.269e-3$	$1.284e-3$
Relative mass error	$2.068e-2$	$5.427e-3$	$1.487e-3$	$4.371e-4$

Acknowledgment

The work is supported by the National Natural Science Foundation of China Grant no. 11171190.

References

[1] P. G. Ciarlet, *The Finite Element Method for Elliptic Problems*, North-Holland, Amsterdam, The Netherlands, 1977.

[2] V. Girault and P.-A. Raviart, *Finite Element Approximations of the Navier-Stokes Equations*, vol. 749, Springer, New York, NY, USA, 1979.

[3] F. Brezzi, J. Douglas, Jr., R. Durán, and M. Fortin, "Mixed finite elements for second order elliptic problems in three variables," *Numerische Mathematik*, vol. 51, no. 2, pp. 237–250, 1987.

[4] F. Brezzi, J. Douglas,, M. Fortin, and L. D. Marini, "Efficient rectangular mixed finite elements in two and three space variables," *Mathematical Modelling and Numerical Analysis*, vol. 21, no. 4, pp. 581–604, 1987.

[5] F. Brezzi and M. Fortin, *Mixed and Hybrid Finite Element Methods*, vol. 15 of *Springer Series in Computational Mathematics*, Springer, New York, NY, USA, 1991.

[6] P.-A. Raviart and J. M. Thomas, "A mixed finite element method for 2nd order elliptic problems," in *Mathematical Aspects of the FEM*, vol. 606 of *Lecture Notes in Mathematics*, pp. 292–315, Springer, 1977.

[7] M. R. Correa and A. F. D. Loula, "Unconditionally stable mixed finite element methods for Darcy flow," *Computer Methods in Applied Mechanics and Engineering*, vol. 197, no. 17-18, pp. 1525–1540, 2008.

[8] A. Masud and T. J. R. Hughes, "A stabilized mixed finite element method for Darcy flow," *Computer Methods in Applied Mechanics and Engineering*, vol. 191, no. 39-40, pp. 4341–4370, 2002.

[9] J. Bear, *Dynamics of Fluids in Porous Media*, Dover, New York, NY, USA, 1972.

[10] H. Rui and M. Tabata, "A mass-conservative characteristic finite element scheme for convection-diffusion problems," *Journal of Scientific Computing*, vol. 43, no. 3, pp. 416–432, 2010.

[11] T. Arbogast and M. F. Wheeler, "A family of rectangular mixed elements with a continuous flux for second order elliptic problems," *SIAM Journal on Numerical Analysis*, vol. 42, no. 5, pp. 1914–1931, 2005.

[12] H. D. Han, "An economical finite element scheme for Navier-Stokes equations," *Journal of Computational Mathematics*, vol. 5, no. 2, pp. 135–143, 1987.

[13] H. Han and X. Wu, "A new mixed finite element formulation and the MAC method for the Stokes equations," *SIAM Journal on Numerical Analysis*, vol. 35, no. 2, pp. 560–571, 1998.

[14] H. Han and M. Yan, "A mixed finite element method on a staggered mesh for Navier-Stokes equations," *Journal of Computational Mathematics*, vol. 26, no. 6, pp. 816–824, 2008.

[15] I. Babuška, "Error-bounds for finite element method," *Numerische Mathematik*, vol. 16, pp. 322–333, 1971.

[16] F. Brezzi, "On the existence, uniqueness and approximation of saddle-point problems arising from Lagrangian multipliers," vol. 8, no. 2, pp. 129–151, 1974.